

---

**PROCEEDINGS**  
from the  
**SECOND U.S. - JAPAN WORKSHOP**  
**ON LIQUEFACTION, LARGE GROUND DEFORMATION**  
**AND THEIR EFFECTS ON LIFELINES**

held at the  
Grand Island Holiday Inn  
Grand Island, New York  
on September 26-28  
and Cornell University  
Ithaca, New York  
on September 29, 1989

Technical Report NCEER-89-0032

Edited by: T.D. O'Rourke<sup>1</sup> and M. Hamada<sup>2</sup>  
December 1, 1989

NCEER Contract Number 88-6009A

NSF Master Contract Number ECE 86-07591

- 1 Professor, School of Civil and Environmental Engineering, Cornell University  
2 Professor, Faculty of Marine Science and Technology, Tokai University

NATIONAL CENTER FOR EARTHQUAKE ENGINEERING RESEARCH  
State University of New York at Buffalo  
Red Jacket Quadrangle, Buffalo, NY 14261

---



REPORT DOCUMENTATION PAGE	1. REPORT NO. NCEER-89-0032	2.	3. Recipient's Accession No. <b>PB 90 209388/AS</b>				
4. Title and Subtitle Proceedings from the Second U.S.-Japan Workshop on Liquefaction, Large Ground Deformation and Their Effects on Lifelines - September 26-29, 1989			5. Report Date December 1, 1989				
7. Author(s) T.D. O'Rourke and M. Hamada			6.				
9. Performing Organization Name and Address			8. Performing Organization Rept. No.				
12. Sponsoring Organization Name and Address National Center for Earthquake Engineering Research State University of New York at Buffalo Red Jacket Quadrangle Buffalo, New York 14261			10. Project/Task/Work Unit No.				
15. Supplementary Notes This workshop was conducted at the Grand Island Holiday Inn, Grand Island, New York and at Cornell University, Ithaca, New York. It was partially funded by the National Science Foundation under Grant No. ECE 86-07591.			11. Contract(C) or Grant(G) No. (C) 88-6009A (G) ECE 86-07591				
16. Abstract (Limit: 200 words) The US-Japan Research Program on Liquefaction, Large Ground Deformation, and Their Effects on Lifeline Facilities focuses on permanent ground deformations caused by earthquakes, with emphasis on liquefaction-induced soil movements and their effects on lifelines. The papers delivered at this workshop deal primarily with liquefaction and ground deformation. There are case studies and examples of analytical and physical modeling. Also covered are soil-structure interaction of pile foundations, waterfront facilities, and buried pipelines; plus the assessment of damage potential and earthquake countermeasures for lifelines both in the United States and Japan.			13. Type of Report & Period Covered Technical Report				
14.							
<table border="0"> <tr> <td data-bbox="125 1587 819 1774"> <b>17. Document Analysis</b>    <b>a. Descriptors</b>  SEISMIC RESISTANT DESIGN.  SEISMIC HAZARD MITIGATION.  EARTHQUAKE ENGINEERING.  GROUND DEFORMATION.  COSTAL FACILITIES.  <b>b. Identifiers/Open-Ended Terms</b> </td> <td data-bbox="819 1587 1584 1774"> LIQUEFACTION            STRUCTURAL DYNAMICS  LIFELINES  PIPELINES  UNITED STATES  JAPAN </td> </tr> <tr> <td colspan="2" data-bbox="125 1944 1584 1976"> <b>c. COSATI Field/Group</b> </td> </tr> </table>				<b>17. Document Analysis</b> <b>a. Descriptors</b> SEISMIC RESISTANT DESIGN. SEISMIC HAZARD MITIGATION. EARTHQUAKE ENGINEERING. GROUND DEFORMATION. COSTAL FACILITIES. <b>b. Identifiers/Open-Ended Terms</b>	LIQUEFACTION            STRUCTURAL DYNAMICS LIFELINES PIPELINES UNITED STATES JAPAN	<b>c. COSATI Field/Group</b>	
<b>17. Document Analysis</b> <b>a. Descriptors</b> SEISMIC RESISTANT DESIGN. SEISMIC HAZARD MITIGATION. EARTHQUAKE ENGINEERING. GROUND DEFORMATION. COSTAL FACILITIES. <b>b. Identifiers/Open-Ended Terms</b>	LIQUEFACTION            STRUCTURAL DYNAMICS LIFELINES PIPELINES UNITED STATES JAPAN						
<b>c. COSATI Field/Group</b>							
18. Availability Statement  Release Unlimited		19. Security Class (This Report) Unclassified	21. No. of Pages 517				
		20. Security Class (This Page) Unclassified	22. Price A22				



## PREFACE: 1989 LOMA PRIETA EARTHQUAKE

On October 17, 1989 an earthquake of magnitude,  $M_s = 7.1$ , struck the Santa Cruz Mountains and San Francisco Bay Area of California. The earthquake occurred during national television broadcasting of the World Series, in San Francisco, thereby attracting live media coverage, the likes of which are unparalleled in the history of earthquake observations.

Soil liquefaction in response to the 1989 Loma Prieta earthquake occurred over a broad and extensive region, with severe consequences for structures and buried lifelines at many locations.

Perhaps the most graphic example of the consequences of soil liquefaction was found in the Marina area of San Francisco where two to four story structures collapsed and a major fire erupted without the immediate benefit of water. Liquefaction-induced ground movements ruptured the municipal water supply at over one hundred locations within the Marina, and liquefaction in the South of Market area broke water mains and hydrants operated by the fire department. These breaks in the fire department's network, combined with breaks in the municipal supply, resulted in the loss of pipeline water to the Marina. Luckily, the threat of ground deformation had been recognized. Portable hose tenders had been acquired by the fire department only two years earlier to contend with just such an emergency. As a result, water pumped by the fire boat from the bay was conveyed by the portable hosing to control and extinguish the fire.

Elsewhere, liquefaction resulted in settlement and lateral ground deformation along the East Bay at Alameda and Treasure Islands. Runways were disrupted at Oakland Airport by liquefaction-induced movements, and the Port of Oakland sustained significant damage. In the southern earthquake area, lateral spreading damaged the highway bridge across the Pajaro River into Watsonville and caused a bridge collapse across Struve Slough. Lateral spreading in excess of 1 m severely damaged the California State Marine Laboratory.

The Second US-Japan Workshop on Liquefaction, Large Ground Deformation, and Their Effects on Lifeline Facilities was held only two and a half weeks before the earthquake. Virtually all the papers and discussions presented at this workshop deal expressly with liquefaction and ground deformation, which had severe repercussions on lifelines during the 1989 Loma Prieta earthquake. It is timely, then, that the proceedings of this workshop should be published during a period when public awareness of earthquake hazards has been heightened, and engineering and research investigations are being pursued to clarify the conditions which caused liquefaction damage in the San Francisco Bay and adjacent areas.

We hope that the contents of these proceedings will provide guidance in forthcoming earthquake studies. We also hope that the case history and research findings in these proceedings will help set an agenda for future research and international collaboration.

T. D. O'Rourke  
October 31, 1989



# TABLE OF CONTENTS

	<u>Page</u>
Preface: 1989 Loma Prieta Earthquake. . . . .	iii
Table of Contents. . . . .	v
US-Japan Cooperative Research Program and Workshops. . . . .	ix
Acknowledgments. . . . .	xi
I. RESEARCH ORGANIZATION	
The Current Status of Research Works Related to Large Ground Displacement in Japan <i>K. Kubo</i>	1
II. CASE STUDIES OF LIQUEFACTION AND LARGE GROUND DEFORMATION	
Liquefaction-Induced Ground Displacement During the 1948. Fukui Earthquake <i>M. Hamada, K. Wakamatsu, and S. Yasuda</i>	6
Effects of Ground Failure on Water Supply and Fire Following. Earthquake: The 1906 San Francisco Earthquake <i>C. Scawthorn and T.D. O'Rourke</i>	16
Liquefaction Induced Ground Displacement During the 1923. Kanto Earthquake <i>K. Wakamatsu, M. Hamada, S. Yasuda, and I. Morimoto</i>	36
A Case Study of Large Ground Deformation During the 1971 San. Fernando Earthquake <i>T.D. O'Rourke, B.L. Roth, and M. Hamada</i>	50
Liquefaction Induced Permanent Ground Displacements in Niigata. City <i>S. Yasuda, M. Hamada, K. Wakamatsu, and I. Morimoto</i>	67
Lateral Spreading Field Experiments by the U.S. Geological. Survey <i>T.L. Holzer, M.J. Benett, and T.L. Youd</i>	82
Liquefaction and Ground Failure in Ferland, Quebec triggered. by the 1988 Saguenay Earthquake <i>M. Tuttle, T. Law, L. Seeber, and K. Jacob</i>	102
Large Ground Deformations induced by the 1985 Earthquake in Port Facilities in Chile <i>C.J. Poran and J.A. Rodriguez</i>	118
III. ANALYTICAL AND PHYSICAL MODELING OF LIQUEFACTION AND GROUND DEFORMATION	
Analytical Solution of Permanent Displacement of Ground Caused by Liquefaction	131

<i>I. Towhata, K. Yamada, H. Kubo, and M. Kikuta</i>	
Pore Pressure and Acceleration Response of Wildlife Site . . . . .	145
during the 1987 Earthquake	
<i>R. Dobry, A.-W. Elgamal, and M. Baziar</i>	
Initial Stress and Residual Deformation - Effective Stress . . . . .	161
Analysis of Anchored Sheet Pile Quaywall	
<i>S. Iai and T. Kameoka</i>	
An Analysis of Earthquake Data Observed at the Wildlife . . . . .	176
Liquefaction Array Site, Imperial County, California	
<i>C.M. Keane and J.H. Prevost</i>	
Spatial Severity of Liquefaction . . . . .	193
<i>M. Shinozuka and K. Ohtomo</i>	
Finite Displacement Analysis on Liquefaction-Induced Large . . . . .	207
Permanent Ground Displacements	
<i>N. Yoshida</i>	
Centrifuge Modeling of Large Ground Motions and Their Effects . . . . .	218
on Structures	
<i>R.S. Steedman</i>	
Study of Effect of Clay Layers on Liquefaction of Sand Deposits . . . . .	233
Using Small-Scale Models	
<i>A.-W. Elgamal, R. Dobry, and K. Adalier</i>	
Some Observations on the Mechanics of Post-Liquefaction . . . . .	246
Deformations	
<i>G.R. Martin</i>	

IV. SOIL-STRUCTURE INTERACTION OF PILE FOUNDATIONS, WATERFRONT FACILITIES, AND BURIED PIPELINES

Seismic Response Analysis of Pile Foundation-Structure . . . . .	262
Systems taking into account Nonlinear Behavior of Ground	
<i>T. Tazoh and K. Shimizu</i>	
Vibration Failure Tests of Piles . . . . .	284
<i>T. Tazoh, K. Shimizu, and T. Hirose</i>	
Lateral Spreading Effects on Pile Foundations . . . . .	295
<i>F. Miura, H.E. Stewart, and T.D. O'Rourke</i>	
Seismic Stability of Waterfront Tied-Back Walls . . . . .	308
<i>G. Neelakantan, M. Budhu, and R. Richards, Jr.</i>	
Liquefaction Analysis of Seawall during 1983 Nipponkai-Chubu . . . . .	322
Earthquake	
<i>Y. Fujii, M. Hatanaka, T. Shiomi, and Y. Tanaka</i>	
Approximate Analysis Procedures for Permanent Ground Deformation . . . . .	336
Effects on Buried Pipelines	
<i>M.J. O'Rourke</i>	
Parametric Study on Flexibility of Buried Pipeline Subject to . . . . .	348
Large Ground Displacement	
<i>T. Kobayashi, H. Nakane, N. Suzuki, and M. Ishikawa</i>	
Relieving Seismic Stresses Locked in Gas Pipelines . . . . .	363
<i>J.D. McNorgan</i>	
Effects of Large Ground Deformation on Buried Water Pipes of . . . . .	370
Power Plant	
<i>H. Suzuki, M. Satoh, and S. Fukui</i>	
Effects of Liquefaction-Induced Ground Movement on Pipeline . . . . .	386
<i>M. Miyajima and M. Kitaura</i>	



On Beam Mode of Buckling of Buried Pipelines. . . . .	401
<i>T. Ariman and B.J. Lee</i>	
Modeling of Permanent Ground Deformation for Buried Pipelines . . . . .	413
<i>N. Suzuki, T. Kobayashi, H. Nakane, and M. Ishikawa</i>	
Model Vibration Test of Framed Foundation-Ground Systems. . . . .	426
During Liquefaction	
<i>M. Yoshikawa and M. Arano</i>	
V. ASSESSMENT OF DAMAGE POTENTIAL AND EARTHQUAKE COUNTERMEASURES FOR LIFELINES	
Liquefaction Severity Index Attenuation for the Eastern United. . . . .	438
States	
<i>T.L. Youd, D.M. Perkins, and W.G. Turner</i>	
Liquefaction Disaster Mitigation for Civil Engineering Structure. . . . .	453
in Japan	
<i>T. Iwatate, Y. Nozawa, and S. Gotoh</i>	
Countermeasures to Mitigate Damage to Pipelines . . . . .	468
<i>J. Isenberg and E. Richardson</i>	
WORKING GROUP SESSIONS . . . . .	483
CLOSING REMARKS. . . . .	497
WORKSHOP PARTICIPANTS. . . . .	498



## US-JAPAN COOPERATIVE RESEARCH PROGRAM AND WORKSHOPS

The US-Japan Research Program on Liquefaction, Large Ground Deformation, and Their Effects on Lifeline Facilities focuses on permanent ground deformations caused by earthquakes, with emphasis on liquefaction-induced soil movements and their effects on lifelines. Currently, there is a growing recognition in the civil and earthquake engineering communities of the importance of large ground deformations, yet our understanding of the mechanisms of movement and our ability to predict magnitude and distribution of displacements are limited and in need of substantial improvement. Permanent ground movements are known to have been the most troublesome source of subsurface structural damage during previous earthquakes. Both U.S. and Japanese researchers have worked in this subject area, and it was recognized that considerable benefits will result from a cooperative effort to collect case history data and recommend analytical and design methods on the basis of a careful data review.

The program was initiated formally in 1988 with the signing of a Memorandum of Understanding between the Japanese and U.S. sides. The document was signed at a ceremony during a workshop in Tokyo, Japan by K. Kubo, Professor Emeritus of Tokyo University, and M. Shinozuka, Sollenberger Professor of Civil Engineering of Princeton University. Professor Kubo signed on behalf of the Association for the Development of Earthquake Prediction (ADEP), the Japanese sponsoring agency. Professor Shinozuka signed on behalf of Robert L. Ketter, then Director of the National Center for Earthquake Engineering Research (NCEER), the U.S. sponsoring agency.

The research program concentrates on case histories of both ground deformations and ground movement effects on lifeline facilities. The case histories are being collected in two volumes and will be published as a joint US-Japan effort. The U.S. earthquakes included in the case history summary are: 1906 San Francisco, 1964 Alaska, 1971 San Fernando, and 1979 Imperial Valley earthquakes. The Japanese earthquakes included in the case history summary are: 1923 Kanto, 1948 Fukui, 1964 Niigata, and 1983 Nihonkai-Chubu earthquakes. The U.S. and Japanese case history studies are being coordinated by Professors M. Hamada of Tokai University and T.D. O'Rourke of Cornell University.

The products of the research will include: 1) case history volumes with assessments of the most important geologic features, siting criteria, and structural features which have influenced previous lifeline performance in response to soil displacements, 2) US-Japan workshops and associated publications covering case history data, analytical modeling, and recommendations for improved practices, and 3) a technical summary and recommendations for improved modeling, siting, design, and construction of buried structures.

U.S. institutions involved in the collaborative research include the University of Arizona, Brigham Young University, City University of New York, Cornell University, EQE, Inc., Lamont-Doherty Geological Observatory, Princeton University, Rensselaer Polytechnic Institute, Southern California Gas Company, State University of New York, United States Geological Survey, University of Tulsa, and Weidlinger Associates, Inc. Japanese institutions involved in the research include Association for Construction Technology for Concrete Piles, Central Research Institute of Electric Power Industry, Chubu Electric Power Co., Inc., JDC Corporation, Kajima Corporation, Kansai Electric Power Inc., Kiso-Jiban Consultants Co., Ltd., Kumagai Gumi Co., Ltd., Kyushu Institute of

Technology, Niigata University, Nippon Telegraph & Telephone Corp., NKK Corporation, Okumura Corporation, Port & Harbor Research Institute-Ministry of Transportation, Public Works Research Institute-Ministry of Construction, Sato Kogyo Co., Ltd., Shimizu Corporation, Shizuoka Prefectural Government, Taisei Corporation, Takenaka Technical Research Laboratory, Tobishima Corporation, Tohoku Electric Power Co., Inc., Tokai University, Tokyo Electric Power Company, Tokyo Electric Power Services Co., Ltd., Tokyo Gas Co., Ltd., University of Tokyo, Waseda University, and Yamaguchi University.

Major instruments for collaboration and cooperative exchange are program workshops. To date, there have been two workshops. The first was held in Tokyo and Niigata, Japan on November 16-19, 1988. The proceedings of this workshop were published by ADEP, and are available from NCEER. The second workshop was held in Buffalo and Ithaca, NY on September 26-29, 1989. This volume contains the proceedings of the second workshop. A third workshop is planned for December, 1990.

Cooperative research between U.S. and Japanese earthquake engineers has resulted in significant new findings about the ways in which large ground deformations are caused by soil liquefaction, their influence on lifelines, and the most effective means of modeling and protecting both soils and structures in the event of a future earthquake. New developments presented and discussed at the workshops include the use of aerial photographs before and after major earthquakes to map ground displacements by photogrammetric techniques, the effects of large ground movements on water supply pipelines and fire following earthquakes, lateral movement effects and damage to pile foundations, and the most suitable modeling methods for large ground deformation and buried lifeline response.

It is hoped that the spirit of cooperation fostered by these workshops and research program will contribute to a strong and enduring relationship among Japanese and U.S. engineers. It is believed that the research accomplishments of this collaborative activity will encourage additional joint projects and lead to improved understanding and mastery in the field of earthquake engineering.

M. Hamada  
Professor, Tokai University

T.D. O'Rourke  
Professor, Cornell University

## ACKNOWLEDGMENTS

The organizers of the workshop thank the National Center for Earthquake Engineering Research (NCEER) and the Association for the Development of Earthquake Prediction (ADEP) for sponsoring the research program and workshop activities. In particular, thanks are extended to K. Kubo, Professor Emeritus of Tokyo University, and M. Shinozuka, Sollenberger Professor of Civil Engineering of Princeton University, who provided oversight and support for the workshop. Our sincere gratitude also is extended to Professor George Lee and Dr. Ian Buckle, Acting and Deputy Director of NCEER, respectively. We also remember the encouragement and enthusiasm of Dr. Robert L. Ketter, the late Director of NCEER.

We thank the National Science Foundation (NSF) for its support. In particular, we thank Dr. Robert Hanson and Dr. S.C. Liu of NSF for their interest and encouragement.

We are pleased that I.M. Idriss, Professor of the University of California at Davis, and K. Ishihara, Professor of Tokyo University, were able to give special invited lectures at the workshop. Professor Ishihara lectured on "Liquefaction-Induced Flow Failure of Slopes and Embankments", and Professor Idriss lectured on "Risk Assessment Incorporating Large Ground Displacements Due to Earthquakes".

We extend our sincere thanks to the members of NCEER and Cornell University, who helped organize the workshop and assisted during the technical gatherings to facilitate the exchange of information and execution of the program. In particular, we thank Andrea Dargush of NCEER and Laurie Mayes of Cornell for their dedication and excellent service in developing a successful workshop. Special recognition is extended to NCEER staff: Don Goralski, Iku Ishihara, Ane Marie Hengstler, Karen Johnson, Laurie McGin, and Anthony Rotundo whose help and excellent support were indispensable for a successful event.

M. Hamada  
Professor, Tokai University

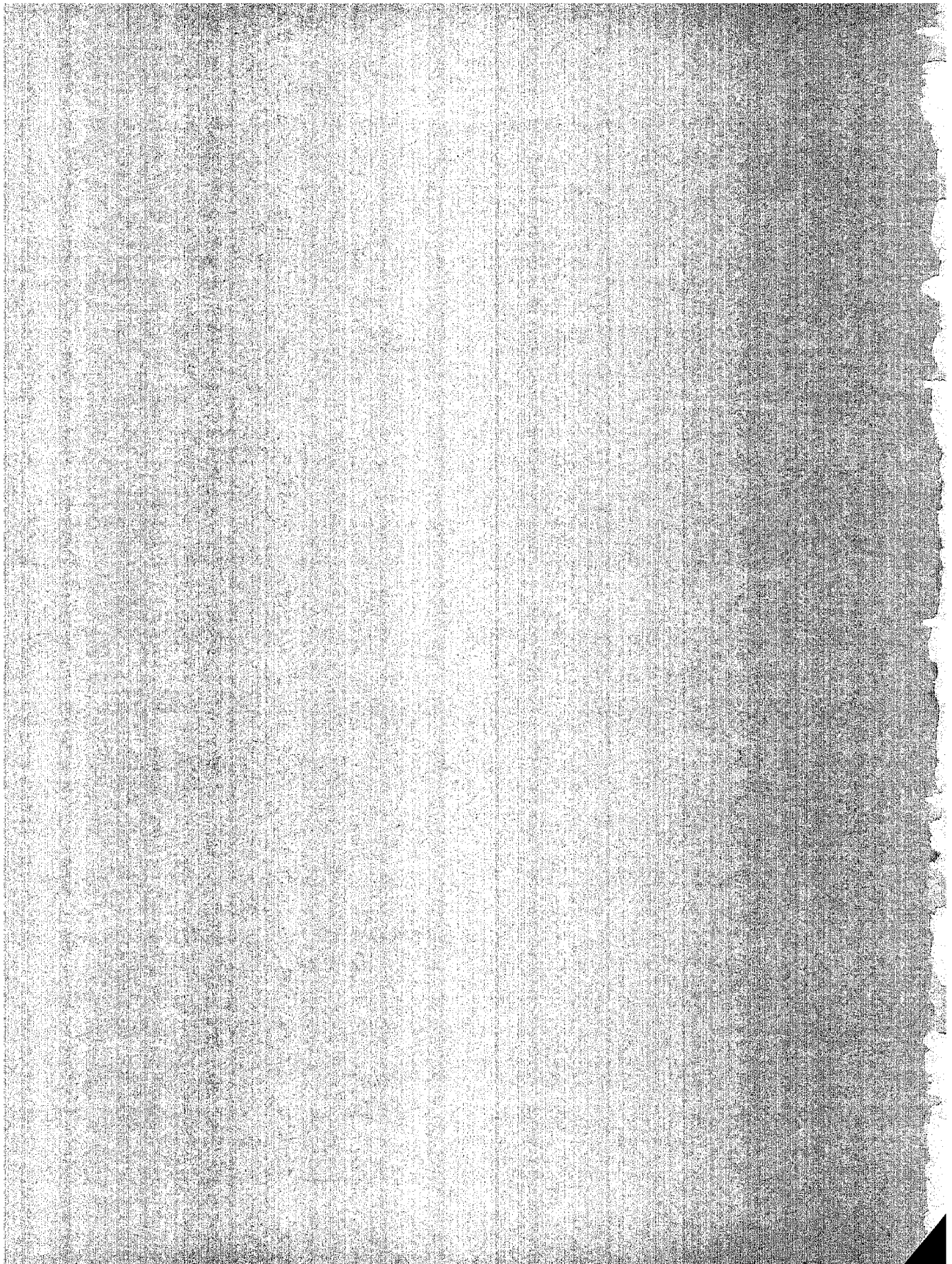
T.D. O'Rourke  
Professor, Cornell University

Conference Organizers



# ORGANIZATION

The Organization of Research Works Related to Large  
Scale Projects in Japan





THE CURRENT STATUS OF RESEARCH WORKS  
RELATED TO LARGE GROUND DISPLACEMENT IN JAPAN

Keizaburo Kubo  
Professor Emeritus,  
University of Tokyo, Japan.  
Director, Association for the Development  
of the Earthquake Prediction.

## INTRODUCTION

It has been one year and nine months since the launch of Japan-U.S. Cooperative Research and Collaboration on Liquefaction, Large Ground Deformation and Their Effects on Lifeline Facilities. It is the strenuous efforts made by more than seventy researchers from nearly forty institutions that has thus far advanced the status of research designated to this collaborative project. The entire team is divided into three Working Groups: WG I on study on permanent ground deformation induced by liquefaction, WG II focusing on mechanism of fracture of in-ground structures induced by permanent ground deformation including numerical analysis model studies, and WG III on development of preventive measures against permanent ground deformation induced by liquefaction by consolidating research results of WG I and II. The First Joint Workshop held in Tokyo, November last year served as an opportunity to confirm and review the progress made by both Japanese and U.S. teams during the first year and to construct the guidelines for the achievement of the objectives.

With respect to the research resumed by the Japanese team following the First Workshop, it has been clarified through interviews conducted at the locale that more often than not liquefaction phenomena of sandy ground characterized as sand boilings or subsidence, inclination and floating of structures take place together with permanent ground deformation triggered by landslides. In addition, it has been discovered pre- and post-earthquake air photos are available for the research of other earthquakes than the 1964 Niigata or the 1983 Nihonkai-Chubu, which contributes substantially to the study of permanent ground deformation. By WG I members, experiments have been conducted on horizontal ground movement triggered by liquefaction of sandy layer and so has the research on numerical analysis to explicate the mechanism and the magnitude of permanent ground displacement.

Ground liquefaction observed at various locations during the Niigata and the Nihonkai-Chubu earthquakes left the researchers with sufficient data to work on liquefaction and subsequent permanent ground displacement. Accordingly our WG II has been engaged with the analytical research on fracture of in-ground structure caused by these two earthquakes (buried pipes of gas, water, electricity, etc.) versus fracture of foundation piles of superstructures.

On the other hand, WG III has concentrated on the research of prevention of liquefaction in the sandy layer and damage reduction measures induced by horizontal movement of ground and/or structures due to the occurrence of an earthquake. At the same time, this group is to review existing engineering techniques against liquefaction and is also to present updated recommendation on preventive measures against permanent ground displacement.

## RESEARCH ON EARTHQUAKE DAMAGE AND PREDICTION OF PERMANENT GROUND DISPLACEMENT

Attempts have been made by participating researchers to re-examine the existing data and apply new analytical approaches to the 1964 Niigata and the 1983 Nihonkai-Chubu earthquakes. Research subjects have come to include the 1923 Kanto and the 1948 Fukui earthquakes, and a series of interviewing the witnesses have presented new information on the cause of permanent ground displacement induced. In the past it was presumed that the gravity force was the major cause of permanent displacement of liquefied ground. Newly collected data disclosed, however, that permanent ground displacement does occur at locations where the gradient of surface ground or the lower boundary of liquefied layer is relatively small. This new fact finding has offered another aspect of research and study.

Small-scale model experiments have been conducted at several institutions. At the same time, analytical models and theories on the occurrence of permanent ground displacement have been presented and comparative review of those models and theories has been attempted.

## RESEARCH ON EARTHQUAKE-DAMAGE TO FOUNDATION PILES AND IN-GROUND LINEAR STRUCTURES

Ever since it was presented that permanent displacement of liquefied ground can cause serious damage to in-ground structures as foundation piles or gas pipes, extensive research and studies have been carried out on its cause and the mechanism of fracture. These are recognized as most significant efforts in reducing earthquake-induced damage and in developing preventive measures.

Various numerical models have been presented to analyze the fracture of foundation piles of N Building (caused during the 1964 Niigata earthquake) and computation has been completed on each model. Although the definitive model is yet to be established, substantial progress has been made on reviewing the accuracy of numerical models, which is expected to reach a new comprehensive finding.

In addition, foundation piles of four-story A Building were excavated to conduct an investigation on the fracture, and quantitative analysis was applied to obtain further data.

Any breakage in lifeline facilities can directly affect civil life by causing a great deal of confusion. As has been clarified by the survey conducted after the Niigata earthquake, the damage ratio of such facilities is much higher in areas with liquefied ground when compared to other areas. Under the circumstances, it is indispensable to examine the damage to lifeline facility structures focusing on permanent displacement of liquefied ground in order to properly and safely maintain lifeline systems required for the daily life of today. Toward this end

consolidation of detailed data on damage to facilities including gas, water, sewage and electricity was initiated during the first period of this collaborative project. In this year numerical models were established and analytical study was launched.

Along with studies on lifeline structures, investigative research on port and harbor facilities and bridges with foundation piles have been carried out with full involvement of experts on each structure.

#### COUNTERMEASURES AGAINST LIQUEFACTION AND PREVENTIVE MEASURES AGAINST PERMANENT DISPLACEMENT

WG III, the group to pursue this objective started the research about one year behind two other groups as it had been planned that their work would be based on the results of WG I and II. With research work of other two groups still under way, the time allowed for WG III is rather limited for any conclusive suggestion to be prepared by this group. Nevertheless the research theme of this group is most closely related to practical aspects of engineering and has the direct and crucial impact. In other words if effective counter- and preventive measures against permanent displacement are established, damage to RC piles will be reduced substantially and so will the damage to lifeline facilities in general, which ensures further safety in daily living environment.

When effective measures to prevent ground liquefaction are obtained, the occurrence of permanent ground displacement due to liquefaction will become less and any damage induced by permanent ground displacement can be prevented. In case of N Building, however, which had been surrounded by in-ground walls, damage to the building itself was very little with only a small amount of permanent displacement in spite of the fact that the topographical features had made the ground quite vulnerable to liquefaction. This group focuses on this building as the research subject and is seeking to find any preventive measure to reduce permanent displacement of sandy ground although no definite measures have so far been established.

#### SUMMARY AND CONCLUSIONS

This collaborative project between Japan and the U.S. was officially inaugurated in November, 1988. Through this joint effort more data are expected to be obtained for further research on ground liquefaction and permanent ground displacement and concerned researchers of both countries are given opportunities to share individual research result of one another. Data and results of numerical studies by the Japanese team can be evaluated comparing to those of the U.S. From the very start this project is designed to contribute to earthquake engineering of today and not to be limited only to participating researchers and engineers between these two countries.

This project consists of research on permanent ground displacement, study on the mechanism of damage caused to in-ground structures, and development of damage preventive measures, all of which are to reinforce one another. It is intended to establish reliable prediction methodology on permanent ground displacement and to look into the behavior of in-ground structures under the predicted displacement. And as a final goal it is to offer new proposals and preventive measures.

Besides the development in preventive measures. What should not be forgotten in pursuing this project are probability of damage occurrence to in-ground structures induced by permanent ground displacement and the damage to be determined stochastically and statistically. This challenging ultimate objective can only be achieved by close cooperation among experts of Japan and the U.S.

Before closing I would like to take this opportunity to express my sincere appreciation to each and every one of researchers who have devoted their time and efforts to the implementation of this collaborative project, without which this challenging project could not have become a reality. I also would like to extend my gratitude to chairmen of three Working Groups, Prof. M. Hamada, Dr. K. Kawashima and Prof. T. Katayama for their excellent chairmanship. I will be much looking forward to all the further progresses to be achieved in the near future through the close cooperation and working together between Japanese team and the U.S. team.



# STUDIES OF LIQUEFACTION AND GROUND DEFORMATION

Liquefaction-Induced Ground Displacement During the 1948  
Ryukyu Earthquake

*M. Hamada, K. Wakamatsu, and S. Yasuda*

Effects of Ground Failure on Water Supply and Fire Following  
San Francisco, The 1906 San Francisco Earthquake

*W. A. Wilson and T. D. O'Rourke*

Liquefaction-Induced Ground Displacement During the 1923  
Kanto Earthquake

*K. Wakamatsu, M. Hamada, S. Yasuda, and I. Morimoto*

Case Study of Large Ground Deformation During the 1971 San  
Francisco Earthquake

*W. A. Wilson, B. L. Roth, and M. Hamada*

Liquefaction-Induced Permanent Ground Displacements in Niigata

*M. Hamada, M. Hamada, K. Wakamatsu, and I. Morimoto*

Large Scale Field Experiments by the U.S. Geological

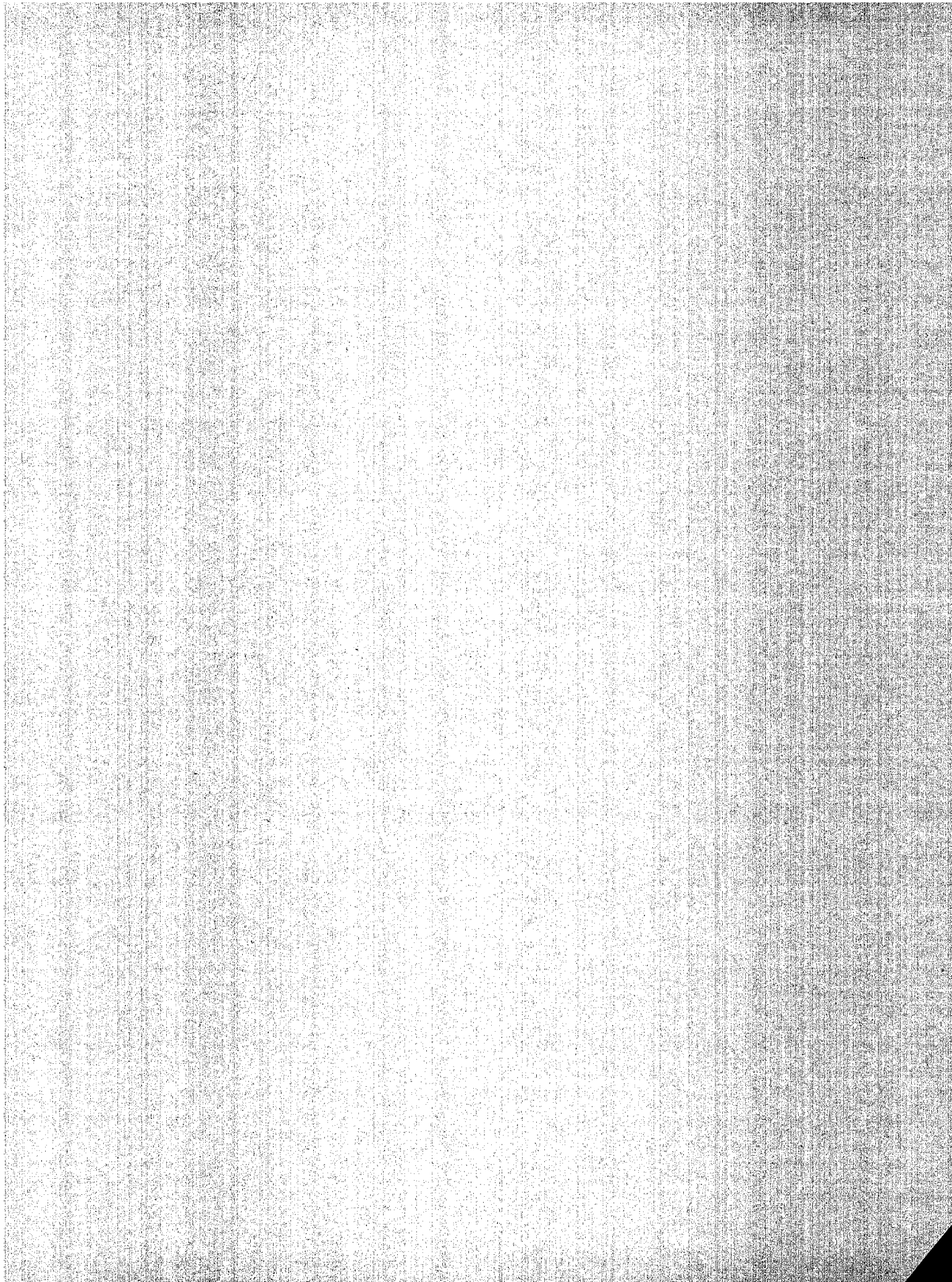
*Survey, W. G. Bennett, and T. L. Youd*

Liquefaction and Ground Failure in Ferland, Quebec triggered  
by the Saguenay Earthquake

*J. M. Houtre, P. Lavoie, L. Seeber, and K. Jacob*

Large Scale Deformations induced by the 1985 Earthquake in  
Santiago, Chile

*J. J. Rocas and J. A. Rodriguez*





LIQUEFACTION-INDUCED GROUND DISPLACEMENT  
DURING THE 1948 FUKUI EARTHQUAKE

M. Hamada<sup>1)</sup>, K. Wakamatsu<sup>2)</sup> and S. Yasuda<sup>3)</sup>

1) Professor of Marine Science and Technology  
Tokai University, Shimizu, Japan

2) Research Associate  
Science and Eng. Research Lab.  
Waseda University, Tokyo, Japan

3) Assistant Professor of Civil engineering  
Kyushu Institute of Technology  
Kitakyushu, Japan

ABSTRACT

The Fukui earthquake with a magnitude of 7.1 occurred in 1948 and caused extensive damage at various locations of the Fukui Plain including Fukui city. This earthquake triggered liquefaction of sandy soil in the alluvial plane along the Kuzuryu River and brought damage to foundations of bridges, embankments and residential housings. The authors took measurements of permanent ground displacements induced by liquefaction by comparing air photos taken before and after the earthquake, and investigated the correlation between such displacements and geological and topographical conditions. Furthermore, by interviewing local residents who had witnessed the earthquake, substantial amount of data were obtained on the occurrence of ground failures including ground fissures, sand boiling settlements and subsidences, which are fundamental to clarifying the mechanism of generation of liquefaction-induced ground displacement.

## INTRODUCTION

Permanent ground displacements induced by the 1964 Niigata and the 1983 Nihonkai-Chubu earthquakes were surveyed and measured by using pre- and post-earthquake air photos <sup>1),2)</sup>. These measurement results indicated that maximum displacements in Noshiro city and Niigata city had been more than 5m and 10m respectively. By soil condition survey in both cities it was clarified that most areas had been situated on sandy dunes and/or natural levees.

It has been reported that ground liquefaction had often been induced by earthquakes occurred in Japan. For this Japan-U.S. cooperative research program Japanese team has conducted case studies on the 1923 Kanto and the 1948 Fukui earthquakes with emphasis on liquefaction-induced ground displacement. This paper is to present the findings obtained from the case study on the 1948 Fukui earthquake.

The 1948 Fukui earthquake hit Fukui City area severely with a magnitude of 7.1 since its hypocenter had been located at a very shallow point underneath the soft alluvial plain. By this earthquake liquefaction was induced in areas along the Kuzuryu River.

The author measured liquefaction-induced ground displacements caused by this Fukui earthquake using air photos taken before and after its occurrence. In areas where large ground displacement had been observed, surveys on the soil conditions were conducted so that causes of ground displacement would be clarified. Furthermore, an interview survey was applied to witnesses of the earthquake for the purpose of obtaining data on ground failures occurred such as fissures, settlement and heaving.

## LIQUEFACTION-INDUCED GROUND DISPLACEMENT

Pre-earthquake air photos used for ground displacement measuring were taken in 1946 at a reduction scale of 1/12,000. On the other hand, post-earthquake air photos were taken one month after its occurrence at a reduction scale of 1/5,400. Both pre- and post-earthquake air photos were taken by the General Head quarters, Far East Command which occupied Japan at that time. (Photo-1)

As shown in Figure-1 ground displacement was measured in Morita-cho area located on the right bank of the Kuzuryu River in the central region of the Fukui Plain. Morita-cho stands on the old river channel and a natural levee where liquefaction was the most clearly observed. The accuracy of the measurement was estimated as 0.87m in horizontal direction.

Shown in Figures-2 and -3 are permanent ground displacements in horizontal direction in the western and eastern parts of Morita-cho. Within Morita-cho, as seen from the Figures, Yoshino Creek runs through in addition to the major stream of the Kuzuryu River, which used to be a stream of the Kuzuryu River. Between the Kuzuryu River and Yoshino Creek is a natural levee with a slight elevation (Figure-2).

According to the measurement results obtained from the western part, ground displacement had occurred toward the south direction in the north of Yoshino Creek, and in the south of the Creek, they had occurred toward the north. In other words, ground displacements in the area along Yoshino Creek were caused toward the Creek. The same was proved to have occurred in the eastern part as shown in Figure-3. The maximum ground displacement in horizontal direction reached more than 3.5m in the area along the Yoshino Creek.

There stand a slightly elevated natural levee between the Kuzuryu River and Yoshino Creek as was stated earlier (Points A, B, C in Figure-2 and D in Figure-3). With these points as each center permanent ground displacements had occurred in almost radial direction. The maximum displacement at these points measured up to nearly 4.0m.

In the areas where permanent ground displacements originated, for example, around points B and C, many fissures were found on the ground surface. On the contrary, sand boilings were observed in the area along Yoshino Creek where permanent ground displacement terminated. Measured result of ground displacement in vertical direction indicated that the ground subsided in areas where ground displacement had originated, and that the ground heaved up along the banks of Yoshino Creek where ground displacement had terminated.

#### TOPOGRAPHICAL AND GEOLOGICAL CONDITIONS

Investigations on soil conditions were conducted in Morita-cho area where permanent ground displacements were observed by gathering existing boring data and conducting Swedish cone penetration tests.

Soil conditions along Line A-A' of Figure-2 are given in Figure-4. Horizontal ground displacements toward right are shown by the white circles and those toward left are shown with the black circles. Ground displacements are indicated to have occurred toward Yoshino Creek as have been mentioned already.

As seen from the Figures, ground surface in the south side of the Yoshino Creek is slightly tilted toward the Creek while ground surface in the north of the Creek is mostly flat. According to boring data of the area, subsurface ground layer up to 10m deep consisted of clay, sandy clay and sand. Beneath this layer are sandy gravel and silty sand whose N-values are high. It is definite that sandy layer situated shallower than 10m was liquefied and it is probable that sandy gravel deeper than 10m was also liquefied considering from the intensity of liquefaction observed in the area.

Figure-4 indicates a distribution of N-values of Standard Penetration Test along Line A-A' converted from rotation numbers of Swedish Penetration Test. Lines with N-values of 10, 15 and 20 were inclined toward the north from the south. If the lower boundary of liquefied layers was to run almost in parallel with these lines, permanent ground displacement on the south side of Yoshino Creek can be considered to have

occurred toward the direction of the inclination of lower boundary of liquefied layers, which would correspond to cases reported in the Niigata and the Nihonkai-Chubu earthquakes. However, permanent ground displacement on the north side of the Creek was against the direction of the inclination, which makes this case different from those of other earthquakes.

It is probable that sandy gravel layer became liquefied at 10m and deeper. Taking these into consideration it is necessary to further examine the correlation between the inclination of the liquefied layer and the direction of permanent ground displacement.

#### RESEARCH ON GROUND FAILURES BY INTERVIEWING WITNESSES

A research was conducted by interviewing local residents who had experienced the 1948 earthquake to collect data on ground failures induced by the earthquake. Comments obtained from the witnesses are fully given in "Research Report on Liquefaction and It's Caused Damage to Inground Structures" edited by the Japanese team which was published in April, 1989 in Japanese. Witnessing remarks thus gathered can be summarized as follows.

- 1) Ground Fissures: Most fissures were caused in parallel with the flow of Yoshino Creek. The maximum width of fissures was nearly 3m and in one case a horse fell into a fissure. The width of fissures continued to be expanded even after earthquake ground motions stopped. One of the witnesses stated that a ground fissure of about 1m wide immediately after the earthquake had grown to be almost 2 - 3m within two to three hours time.
- 2) Sand and Water Boilings: Lots of sand and water boiling were observed in rice or vegetable fields along Yoshino Creek. According to one witness, the height of one of sand and water boilings was taller than that of an adult man. Comments made on the continuation of sand and water boilings vary a lot. While one witness stated they had continued only during the ground vibration, some other one commented that they had continued on for several hours, or even a few days after the earthquake occurrence.
- 3) Yoshino Creek: Both banks of Yoshino Creek had moved toward the center of the Creek, eventually narrowing the width of the Creek. Also due to the rising of the river bed, the Creek overflowed. Because of these phenomena it became necessary to excavate the river bed after the earthquake.
- 4) Road Made to Curve/Enlargement of Real Estate: Many roads along Yoshino Creek which had used to run straight became curved because of the earthquake, one example of which is shown in Photo-1. The road in the photo marked with a-a' used to run almost straight before the earthquake but became clearly curved in the photo taken after the earthquake. Witnessing remarks were also made that in the area along Yoshino Creek

several disputes over real estate were triggered due to enlargement and/or reduction of one's real estate and shifting of boundary lines with neighbors, both of which were induced by the earthquake.

#### CONCLUSION

The author and his co-researchers had reported that ground displacements occurred during the 1964 Niigata and the 1983 Nihonkai-Chubu earthquakes reached a maximum of 10m<sup>1),2)</sup>. Most of the ground both in Niigata and Noshiro city consisted of saturated sand. The sandy layers have been considered to have intensified liquefaction and led to large ground displacement as the result.

The ground of the Fukui Plain was proved to consist not only of sand but clay and silt layers as well unlike those of Niigata and Noshiro cities. It was clarified by this research permanent ground displacement as large as 3m had been caused in the ground including clay and silty layers in addition to sandy soil. This finding indicated that large ground displacement could possibly be induced in the Kanto and Osaka Plains, in the middle of which are major metropolitan areas, once ground liquefaction would occur. In improving earthquake preparedness and countermeasures, ground displacements induced by liquefaction should never be left behind but would have to be studied very closely.

#### ACKNOWLEDGEMENTS

This research was conducted by the Japanese team of Japan-U.S. Cooperative Research and Collaboration. Each member of the team made tremendous contribution for the successful implementation of this research, which deserves full recognition by all means. The authors would like to extend their gratitude to Mr. I. Yasuda of Hasshu Inc. for his skillful assistance, without which necessary data gathering would have proposed a great difficulty.

#### REFERENCES

- 1) Hamada, M., Yasuda, S., Isoyama, R. and Emoto, K., "Study on Liquefaction Induced Permanent Ground Displacement", Association for the Development of Earthquake Prediction, Tokyo, 1986.
- 2) Hamada, M., Yasuda, S. and Wakamatsu, K., "Case Studies on Liquefaction-Induced Permanent Ground Displacement", Proceedings of First Japan-U.S. Workshop on Liquefaction, Large Ground Deformation and Their Effects on Lifeline Facilities, Tokyo, 1988.

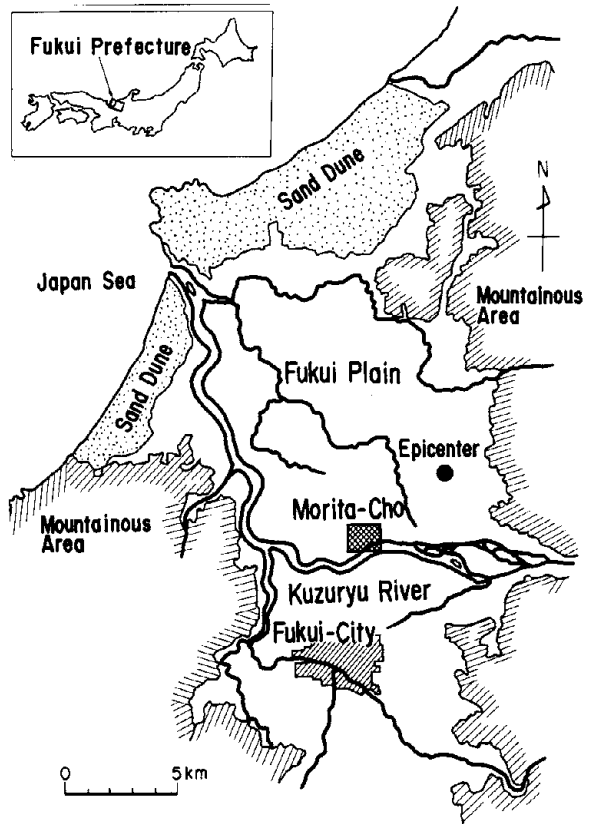
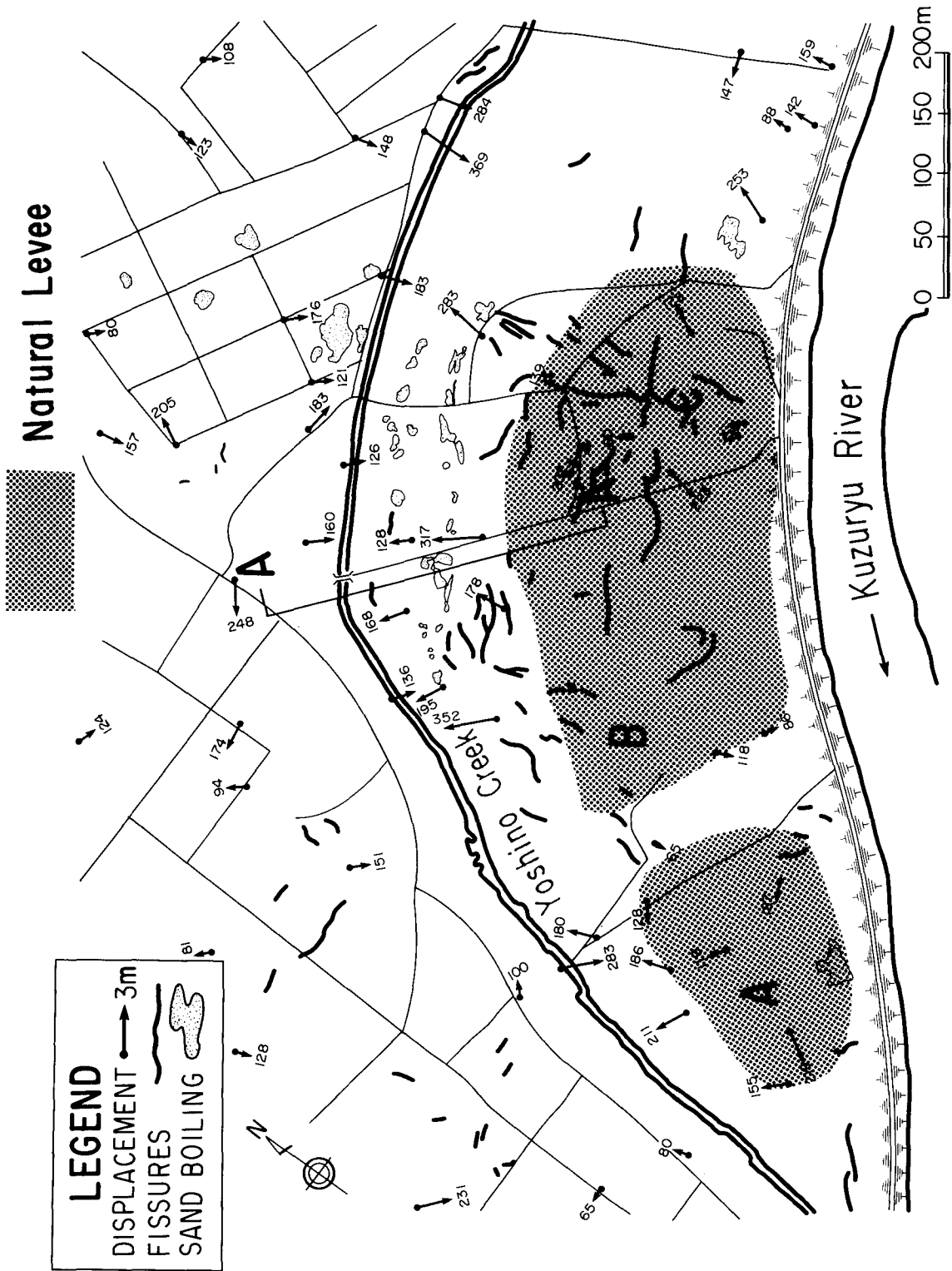


Figure-1. Fukui Plain Attacked by the Earthquake



Photo-1. Aerial Photos for Measurement of Permanent Ground Displacement (post-earthquake)







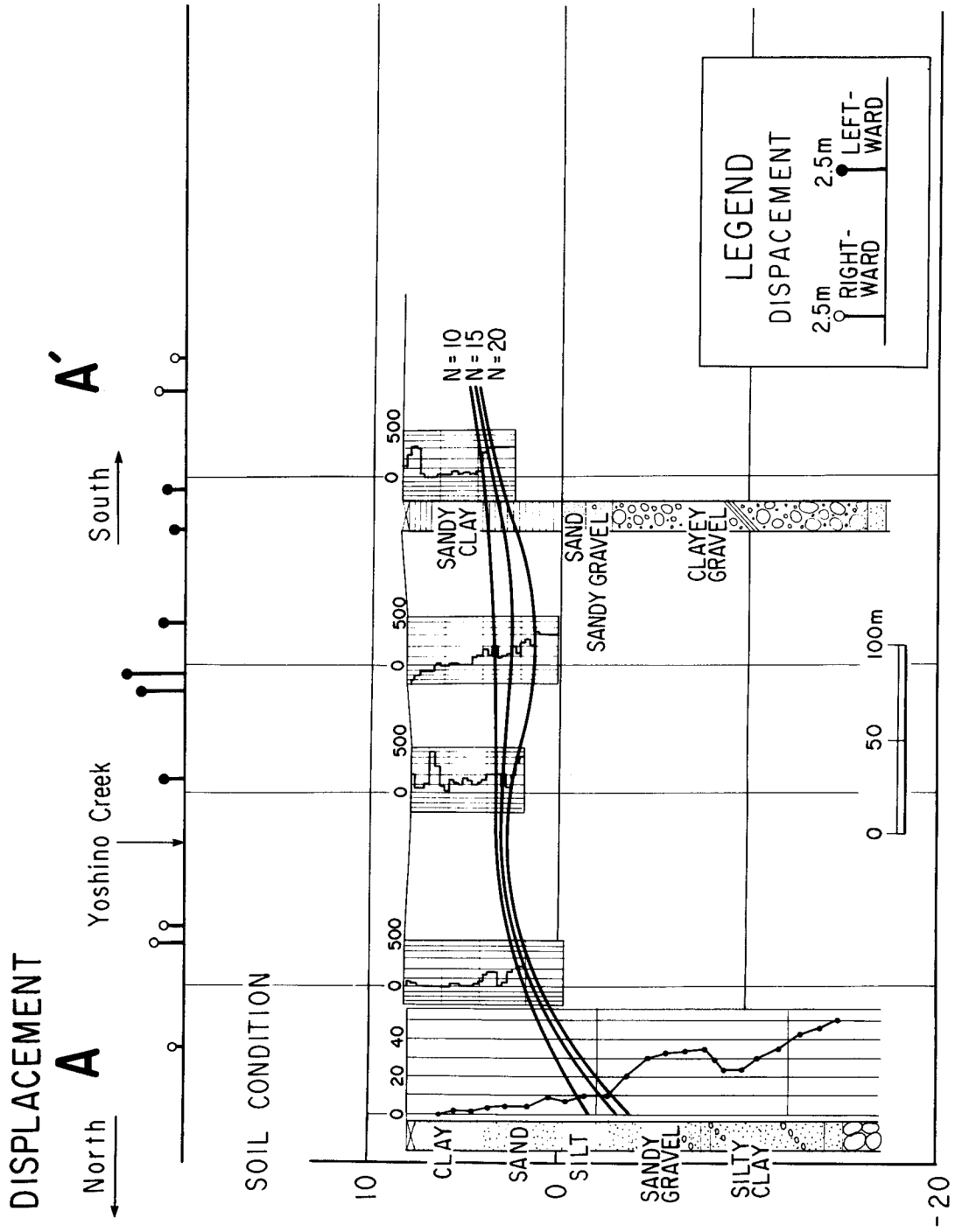
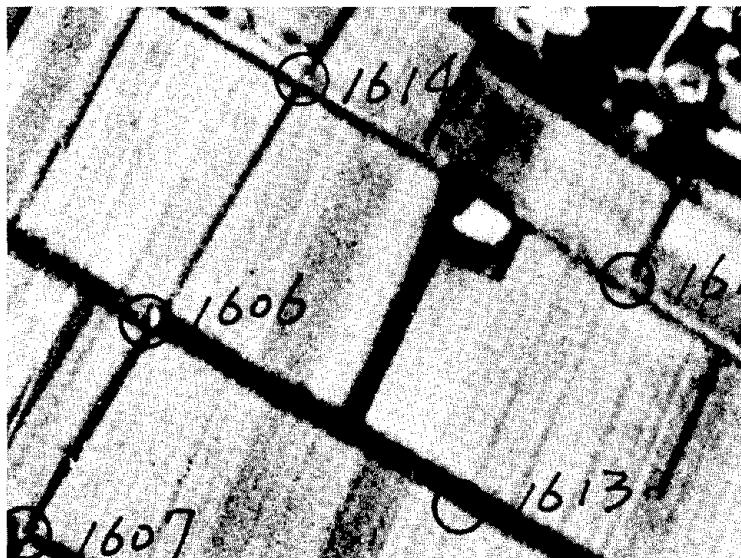


Figure-4. Soil Conditions along Line A-A'



(a) Before the Earthquake



(b) After the Earthquake

Figure-5. Road Curved by the Earthquake

**EFFECTS OF GROUND FAILURE ON WATER SUPPLY AND FIRE FOLLOWING EARTHQUAKE:  
THE 1906 SAN FRANCISCO EARTHQUAKE**

Prepared by  
C. Scawthorn, S.E.  
Vice President, EQE, Inc.  
San Francisco, CA 94105

T. D. O'Rourke  
Professor of Civil & Environmental Engineering  
Cornell University, Ithaca, NY 14853

**ABSTRACT**

Data on water supply pipe breaks and damage are combined with information on ignitions and spread of fires following the 1906 San Francisco earthquake, to study the effect of loss of water pressure and supply on fire department suppression activities and effectiveness. When water was available, such as at the large fire at 20th and Mission streets, containment and suppression was possible although requiring large commitments of fire service resources. Analyses of the 1906 pipeline system, pipeline breaks, and zones of soil liquefaction show that water from the College Hill and University Mound reservoirs was cut off, leaving only 6% of the aggregate reservoir supply for use in the Central Business District (CBD), resulting in a sporadic water supply. Whether water was available in sufficient quantity and pressure, and coincident with sufficient fire service appliances, is unclear. That is, did the conflagration result from insufficient water, or insufficient fire service assets?

To address this question, data on chronological spread of fire fronts have been compared with available information on water supply pipe breaks and damage, as well as information on fire department company activities, to investigate whether large advancing fire fronts could be contained when water supply was relatively unimpaired. The conclusion is that even with a fully functional water supply, the fire department would probably not have been able to contain all fires during the critical first day, and that the conflagration would still have resulted in great damage. The situation in San Francisco today is improved in the water supply aspect, by the Auxiliary and Portable Water Supply Systems, but is still serious, due to the relatively small number of personnel and apparatus available to the fire department and the vulnerability of the pipeline system to earthquake-induced ground movements.

## INTRODUCTION

In both Japan and the United States, fire has been the single most destructive seismic agent of damage in the twentieth century. The fires following the San Francisco 1906 and Tokyo 1923 earthquakes rank as the two largest peacetime urban fires in man's history, and were both terribly destructive. While not widely perceived today by the public or even many professionals in the earthquake or fire service fields, **fire following earthquake is recognized by professionals specializing in this field as continuing to pose a very substantial threat in both countries.**

Although fire following the 1906 earthquake was the overwhelming cause of the damage San Francisco and Santa Rosa, and has continued as a significant cause of damage since, it has received relatively little attention in the U.S. This is perhaps due to several factors:

- (a) Earthquakes historically have been the professional concern of seismologists and structural engineers, who as a class of professionals are largely uninformed of fire,
- (b) Fire protection engineers and fire service personnel have similarly ignored earthquakes, seeing their goal as the mitigation of chronic fire losses by code implementation and other techniques, rather than as earthquake response,
- (c) Major conflagrations were a common occurrence in the US prior to WW2, so that the 1906 experience was seen as more of a conflagration than an earthquake phenomena. The subsequent decline in US urban conflagrations, due to improved fire and building codes, and to improved fire service response due primarily to radios, has only increased this sense of "it can't happen here".

Less apparent but perhaps even more important factors contributing to the lack of attention paid to post-earthquake fire has been:

- (d) The lack of a major urban US earthquake since 1906. It is little appreciated that it takes a great earthquake, striking a large urban region, to create the conditions of dozens or hundreds of ignitions overwhelming the fire service, to create a conflagration. San Francisco 1906 and Tokyo 1923 fulfilled this condition. Earthquakes since 1906 (1933 Long Beach, 1964 Alaska, 1971 San Fernando, 1987 Whittier in the United States; 1968 Tokachi-oki, 1978 Miyagiken-oki, 1984 Nihonkai-chubu in Japan) have not fulfilled this condition.
- (e) The lack of an analytical framework within which to model the many factors involved in post-earthquake fire, and to quantify these factors and the outcome: many small fires, or conflagration?

Until recently, perhaps the only group at all concerned with post-earthquake fire has been the insurance industry, who due to 1906 are quite aware of the potential for catastrophic loss due to this phenomena. Steinbrugge<sup>1</sup> presents probably the best summary of knowledge deriving from this field. The first author, based on work by Hamada<sup>2</sup>, Horiuchi<sup>3</sup>, Kawagoe, Kobayashi<sup>4</sup> and others in Japan, developed a probabilistic post-earthquake fire ignition and spreading model<sup>5</sup>, which has subsequently been applied at two levels: (1) Jurisdictional: a detailed modeling, with ignitions, fire loading, engine location and other parameters modeled gridwise at about the 10 hectare level of resolution. Due to the sizable data collection and computational effort involved, this model has only been applied to one US jurisdiction, the City of San Francisco<sup>6</sup>, and (2) Regional: a coarser model based on approximations derived from the Jurisdictional model. Applied to the San Francisco and Los Angeles regions<sup>7</sup>, this model has permitted for the first time quantified estimates of the aggregate losses due to fire following earthquake. This work relies in part on empirical data and relations derived from the 1906 and 1923 events.

Because these data and relations have been derived from primary sources, many of them relatively obscure, this paper presents and reviews some of this data for the 1906 event, on (a) fire initiation and spread, and (2) water supply performance, in order to examine the interaction of these two factors. The primary question examined is whether the failure of the water supply was the primary factor leading to the large conflagrations in San Francisco in 1906. That is, would the fire department have been able to suppress the fires given its normal water supply?

In order to address this question, we first review the water supply system within the City of San Francisco in 1906, and the damage resulting from the earthquake, then briefly discuss the San Francisco Fire Department in 1906, and next discuss the earthquake generated fires and their spread. We then conclude with a qualitative evaluation of the interaction of these three aspects.

## WATER SUPPLY

### San Francisco Water Supply System in 1906

In 1906 water to San Francisco was supplied from two series of reservoirs. South of San Francisco, water was impounded by earth and concrete dams to form the San Andreas, Crystal Springs, and Pilarcitos Reservoirs. Transmission pipelines conveyed water from these reservoirs to a second series of smaller reservoirs within the city limits. Water then was distributed throughout the city by means of trunk and distribution pipelines. The San Francisco reservoir and pipeline network at the time of the 1906 earthquake has been described by Schussler<sup>8</sup> and more recently by O'Rourke, et al<sup>9</sup>. Reference is made to these works in presenting the overall configuration and operation of the system in this paper.

Figure 1 presents a plan view of the 1906 San Francisco water supply adapted from maps prepared by Schussler. At the time of the earthquake, there was a combined volume of 88.7 billion liters in the San Andreas, Crystal Springs, and Pilarcitos Reservoirs. These reservoirs supplied nearly all water for the City of San Francisco in 1906, whereas today they represent approximately one-half of the local storage capacity in the San Francisco Bay Area. Transmission pipelines conveying water from the southern reservoirs were built mainly of wrought iron.

Within the city limits, there were approximately 711 km of distribution piping at the time of the earthquake, of which roughly 18.5 and 66.5 km were wrought and cast iron trunk lines, respectively. These lines were larger than or equal to 400 mm in diameter. The bulk of the system had been constructed during the years of 1870 to 1906.

### Earthquake Performance of Pipeline System

Superimposed on Figure 1 are the approximate locations of transmission pipeline damage caused by the earthquake. Flow from all transmission pipelines stopped shortly after the earthquake. Because telephone service was out, emergency control information had to be obtained by dispatching personnel into the field where maintenance crews reported on the damage.

Right lateral strike-slip movement along the San Andreas fault ruptured a 750 mm diameter wrought iron pipeline conveying water from the Pilarcitos to Lake Honda Reservoir. Over 29 breaks were reported north of the San Andreas Reservoir, where the pipeline was constructed parallel to the San Andreas fault. Fault movement near the San Andreas Reservoir was measured as 3.6 to 5.6 m<sup>10</sup>. Pipeline ruptures were caused by tensile and compressive deformation of the line. Over three months were required to reconstruct the pipeline.

Within 16 hours after the earthquake, repairs were made to that part of the Pilarcitos Conduit which was located within the city limits. Water then was pumped from Lake Merced through the Pilarcitos line into Lake Honda at a rate of approximately 25 million liters per day. Dynamic distortion of bridges was responsible for rupturing a 925 mm diameter wrought iron pipeline conveying water from the San Andreas to College Hill

Reservoir, and for rupturing at three swamp crossings an 1100 mm diameter wrought iron pipeline conveying water from the Crystal Springs to University Mound Reservoir. The wooden trestle bridges all were damaged by strong ground shaking, with no damage or misalignment observed in their timber pile foundations. Approximately three days were required to repair the 925 mm diameter pipe, and over a month was required to restore the 1100 mm diameter Crystal Springs Pipeline.

Figure 2 is a map of the 1906 water supply within the San Francisco City limits. Table 1 summarizes the city reservoirs, capacities, and elevations above mean sea level. There were nine reservoirs and storage tanks, for a total capacity of 354 million liters. Approximately 92% of this total, or 325 million liters, were contained in the Lake Honda, College Hill, and University Mound Reservoirs. These reservoirs and the pipelines linking them with various parts of the city were the backbone of fire protection.

All trunk lines, 400 mm or larger in diameter, are plotted in Figure 2. These pipelines were plotted on the basis of a careful review and transcription of the oldest extant (1912) pipeline maps in San Francisco, which were provided by the San Francisco Water Distribution Department, and correlated with reservoir and pressure district maps published by Schussler. Trunk lines are shown connected to the Lake Honda, College Hill, University Mound, Francisco Street, and Clay Street Reservoirs; all other reservoirs were connected to piping 300 mm or less in diameter. As listed in Table 1, the University Mound and Francisco Street Reservoirs are at approximately the same elevation. The Francisco Street Reservoir was filled by water from the University Mound Reservoir, which then was pumped to Presidio Heights. Accordingly, the supply for Presidio Heights and Francisco Street depended on the pipelines from University Mound.

Superimposed on the figure are the zones of lateral spreading caused by soil liquefaction, as delineated by Youd and Hoose<sup>11</sup>. Breaks in the pipeline trunk system crossing these zones are plotted from records provided by Schussler and Manson<sup>12</sup>. It can be seen that multiple ruptures of the pipeline trunk systems from the College Hill and University Mound Reservoirs occurred in the zones of large ground deformation, thereby cutting off supply of over 56% of the total stored water to the Mission and downtown districts of San Francisco.

Two pipelines, 400 and 500 mm in diameter, were broken by liquefaction-induced lateral spreading and settlement across Valencia Street north of the College Hill Reservoir. These broken pipes emptied the reservoir of 53 million liters, thereby depriving fire fighters of water for the burning Mission District of San Francisco. As indicated in previous studies<sup>13</sup>, this local deformation ranks as one of the most devastating events of the 1906 earthquake.

Figure 3 shows a map of the San Francisco water supply and area burned during the fire. All trunk lines of the College Hill and University Mound Reservoirs downstream of the pipeline ruptures are removed from this figure to show the impact and lack of hydraulic conductivity caused by severing these conduits.

With the College Hill and University Mound Reservoirs cut off, only the Clay Street Tank and the Lombard and Francisco Street Reservoirs were within the zone of most intense fire, and therefore capable of providing water directly to fight the blaze. The combined capacity of these reservoirs was only 21 million liters, or 6% of the system capacity. The usefulness of such limited supply was further diminished by breaks in service connections, caused by burning and collapsing buildings. Schussler identifies service line breaks as a major source of lost pressure and water. There were roughly 23,200 breaks in service lines, between 15 and 100 mm in diameter. Fallen rubble and collapsed structures often prevented firemen from closing valves on distribution mains to diminish water and pressure losses in areas of broken mains and services.

As is evident in Figure 3, the Lake Honda Reservoir was able to provide a continuous supply of water to the western portion of the city. The fire eventually was stopped along a line roughly parallel to Van Ness Avenue, where water still was available from the Lake Honda Reservoir. Moreover, the southern and southeastern extent of the fire is bounded by areas south and southeast of the trunk system ruptures. It is likely that these unburnt areas had water from the University Mound Reservoir.

Figure 4 presents a bar graph showing the reservoir storage in San Francisco as a function of time after the earthquake. The amounts of water corresponding to day 0 represent the quantities available roughly two hours after the earthquake struck. After four days, less than one tenth of the initial capacity of the College Hill, University Mound, and Lake Honda Reservoirs still was available. Two factors were critically important in preserving flow. Sixteen hours after the earthquake, water was pumped from Lake Merced into the Pilarcitos Conduit to supply Lake Honda. This action provided an additional 25 million liters/day, thereby maintaining capacity in Lake Honda for distribution to the western parts of the city. After repairs of the San Andreas Conduit over three days, approximately 30 million liters/day were conveyed to the College Hill Reservoir for distribution in the South Mission area of the city. By the fourth day, approximately 55 million liters of water were flowing into the city, in addition to the 25 million liters still available in the reservoirs.

## SAN FRANCISCO FIRE DEPARTMENT

### Fire Department in 1906

The San Francisco Fire Department in 1905 protected approximately 400,000 persons occupying an urbanized area of approximately 21 square miles. The department consisted of a total of 585 full paid fire force personnel (resident within the city and on duty at all times), commanded by Chief Dennis T. Sullivan and deployed in 57 companies (38 engine, 1 hose, 10 ladder, 1 hose tower, and 7 chemical)<sup>14</sup>. The distribution of these companies was well conceived, being centered about the congested high value district (i.e., the Central Business District or CBD, known in San Francisco as the Financial District), with 24 engine, 8 ladder, 1 water tower and 7 chemical companies within 2 miles of the center of the CBD. All but two of the 38 steam engine companies dated from 1890 or later, and were rated at an average of 680 gallons per minute (gpm), although the eight engines tested in 1905 averaged only about 70% of their rated capacity, and the "*ability of the men handling the engines was in general below a proper standard*". The rated pumping capacity of the 38 first line and 15 relief and reserve engines totaled 35,100 gpm. In summary, the department was rated by the National Board of Fire Underwriters (NBFU) as efficient, well organized and in general adequate. The NBFU however concluded in 1905 that

*"...In fact, San Francisco has violated all underwriting traditions and precedent by not burning up. That it has not done so is largely due to the vigilance of the fire department, which cannot be relied upon indefinitely to stave off the inevitable."*

### Earthquake Performance of the Fire Department

Within moments after the earthquake on April 18, 1906, Chief Dennis T. Sullivan was seriously injured due to the damage to the fire station where he was sleeping, and afterwards died. Ten fire stations sustained major damage<sup>15</sup>, although no engines were seriously disabled by the earthquake and all went into service<sup>16</sup>. Street passage was in general not a problem, and a number of fires were quickly suppressed, although many more could not be responded to. That is,

*"fires in all parts of the city, some caused directly by earthquake, some indirectly, prevented an early mobilization of fire engines and apparatus in the valuable business district, where other original fires had started and were gaining headway"*.

The NBFU Conflagration Report concluded

*"the lack of regular means of communication and the absence of water in the burning district made anything like systematic action impossible; but it is quite likely that during the early hours of the fire the result would not have been otherwise, even had not of these abnormal conditions existed"*.

That is, the NBFU concluded that even under normal conditions the multiple simultaneous fires would have probably overwhelmed a much larger department, such as New York's, which had three times the apparatus<sup>14</sup>. Nevertheless, Bowlen concluded that by 1 PM (i.e., about 8 hours after the earthquake)

*"the fire department, except that it was without its leader, was in fairly good shape, that is the men and horses were in good trim for fighting, the apparatus was in shape and could be worked where there was water. There is not one report of an engine or man going out of commission during the early hours of the fire, and the department was hard at work all the time, even though there was little to show for its effort"<sup>17</sup>.*

## EARTHQUAKE GENERATED FIRES AND SPREAD

### Initial Ignitions

The actual number of ignitions following the earthquake at 5:12 AM has been variously reported at "about 50" (NBFU, Bowlen), but the precise number, location, cause etc has never been detailed, to the author's knowledge. The first author, through reading of various sources (Bowlen Outline, the Argonaut series<sup>18</sup>, Fire Officers Reports<sup>19</sup>, has identified 52 fires and/or explosions, Table 2. These ignitions are detailed in Figure 5 in general and in Figure 6 (detail of CBD). In both these figures, the Arabic numerals indicate the observed seismic intensity, on the Modified Mercalli Scale.

### Spread

The conflagration following the 1906 earthquake was a complex fire, actually consisting of several separate major fires which grew together until there was one large burnt area, comprising the northeast quadrant of the city and destroying over 28,000 buildings. The progress of these fires has generally been divided into four "periods" (NBFU, Bowlen Outline), although actual times for these periods differ between sources. Generally, the periods comprise the following times (i) from the earthquake until mid or late in Day 1, when most of the south of Market section had been destroyed, but the higher value north of Market section still remained largely intact, (ii) the night of Day 1 and the early hours of Day 2, when the north of Market section was invaded by the fire, progressing from the west, (iii) continued progress of the fire to the north, and a bit to the south, during the remainder of Day 2, and (iv) during Day 3, the last day, when the fire progressed almost entirely to the north, around Telegraph Hill, and burnt down to the Bay.

Based on the same sources as indicated above for initial ignitions, the first author has traced the progress of the initial ignitions during the first 24 hours following the earthquake. Figures 7a and 7b indicates fires extinguished, and spread of the initial ignitions, for this period. Of note for the initial ignitions is the number of fires that were extinguished by the fire department. Examination of Table 2 indicates 20 of the 52 fires were extinguished, although some not without considerable effort. The Lippmann fire at Mission and 22nd Streets (No. 14 in Table 2) for example threatened the major high density residential area known as the Mission District. Four companies fought this fire until late in Day 1, saving the Mission District but being prevented from moving on to other fires. Similarly, fire No. 15, in an area known as the Western Addition, and fires No. 16 and 17 (which quickly merged), nearby 15, required five and four companies respectively. As Bowlen noted in his Outline "...With eight engines on two fires, how could fifty be cared for?"

## EVALUATION

Figure 3 shows a strong correlation between burnt sections of the city and those sections cut off from the College Hill and University Mound Reservoirs by ground failures. Of especial note is the rapid spread of the ignitions south of Market, where water supply was entirely interrupted due to the large ground deformations along Valencia Street and in the immediate south of Market areas. This rapid spread was due to three causes: (i) lack of water for available fire department engines, (ii) highly combustible high density wood frame



construction, and (iii) insufficient fire department engines, which were drawn to concentrate at major fires threatening whole districts, such as at fire Nos. 14-17, where water was available, even if in limited quantities.

The spatial relationship between unburnt districts and availability of water implies that pipeline system integrity played a key role in limiting the spread of fire, and that areas suffering from ruptured pipelines fared poorly. This inference must be made with caution however, since the development of the fire south of Market, by midafternoon, had resulted in a burning perimeter or flamefront on the order of 25,000 feet (7,500 m). Effective defense along this flamefront would require on the order of one to two hundred handheld lines, or virtually the entire steam engine force of the fire department. Even if effective, this (i) ignores branding (i.e., fire spread by burning debris, flying over defense lines and causing fires behind the fireline) and (ii) does not consider whether the water supply system, if intact, could have hydraulically furnished the required water (25,000 to 50,000 gpm). Even if this defense had held, the firefighters, fully occupied south of Market, may have been outflanked by fire No. 39 (the "Ham and Eggs" fire) which did indeed sweep down from the west during the second period, outflanking the defending line along Market.

### CONCLUDING REMARKS

The supply of water for emergency purposes in San Francisco critically depends on the reservoir and piping system within the city limits. Loss of the Pilarcitos, San Andreas, and Crystal Springs Conduits provides a graphic example of the vulnerable nature of transmission pipeline supply, and emphasizes the extreme importance of the local reservoir system. Lake Merced, with approximately 7 billion liters of water, was an important source of backup supply in 1906, and is likely to be a critical resource during a future earthquake. Water delivery from Lake Merced depends on pump operation, so that the electricity required to power the pumps must be safeguarded or alternative generator supply provided.

System redundancy played a critical role in water delivery after the 1906 earthquake. The ability to disengage the Pilarcitos conduit from the ruptured transmission system south of the city and connect it with Lake Merced was of vital significance. Water to Lake Honda was provided in continuous supply to the western districts of San Francisco where the fire was stopped. The lack of redundancy across zones of large ground deformation in the Mission district meant that pipeline failures resulted in the loss of over 56% of the city supply. Only 6% of the total reservoir capacity was directly accessible at the time of the earthquake to fight the fires in downtown San Francisco.

While failure of the water supply in 1906 undoubtedly handicapped the fire department, the question remains whether the department could have suppressed over fifty simultaneous fires, given sufficient water. It appears it would have been a close race, with the probable destruction of thousands of buildings, although perhaps not quite as complete destruction as did occur.

It is of interest to note that the present (1989) fire department in San Francisco protects a resident population of approximately 700,000 (and a daytime population of over 1 million) occupying an urbanized area of approximately 48 square miles. Today's department totals approximately 1,350 personnel, of which approximately 350 constitute a fire force at any given time (i.e., others are off duty and often resident miles outside the city limits). Note that there are less immediately available personnel today than there were in 1906 (if an earthquake were to occur near a shift change however, somewhat more personnel would be available today, relative to 1906). The department has 41 first line engine companies with a total rated pumping capacity of approximately 50,000 gpm.

This case study not only clarifies the state of damage to the 1906 water supply and its relationship with liquefaction-induced ground failure, but also illustrates (i) precisely where the zones of maximum vulnerability are in the present day system, and (ii) how a functional water supply is not sufficient by itself - a functional fire department of sufficient delivery capability is also required. The main trunk lines from the current University Mound and College Hill Reservoirs, representing a total capacity of well over half a billion liters, cross zones of potentially liquefiable soils at the old Mission Creek and Mission Bay areas of San Francisco. Although the

city has constructed an Auxiliary Water Supply System (AWSS) for fire fighting purposes, its limited storage capacity of 43 million liters will be strained severely after an earthquake without the supplemental supply from University Mound and College Hill. The AWSS' Pump Stations 1 and 2 are therefore obviously required, to draw water from the Bay. Lastly, the Portable Water Supply System (PWSS) presently under development by the San Francisco Fire Department is critically required, in order to convey water to those major portions of the City outside the northeast quadrant protected by the AWSS.

## REFERENCES

1. Steinbrugge, K.V. (1982) Earthquakes, Volcanoes and Tsunamis, Skandia-America Group, N.Y.
2. Hamada, M. (1951) On Fire Spreading Velocity in Disasters, Sagami Shobo, Tokyo (in Japanese).
3. Horiuchi, S. (n.d.) Research on Estimation of Fire Disasters in Earthquakes, Disaster Prevention Section, Comprehensive Planning Bureau, Osaka Municipal Government (in Japanese).
4. Kobayashi, M. (1979) A Systems Approach to Urban Disaster Planning, Ph.D. Dissertation, Kyoto University, Kyoto, Japan (in Japanese).
5. Scawthorn, C., Yamada, Y. and Iemura, H. (1981) A Model for Urban Post-earthquake Fire Hazard, DISASTERS, The International Journal of Disaster Studies and Practice, Foxcombe Publ., London, v. 5, n. 2.
6. Scawthorn, C. (1984) Simulation Modeling of Fire Following Earthquake, Proceedings, 3rd U.S. National Conference on Earthquake Engineering, Charleston, SC, Earthquake Engineering Research Institute, El Cerrito, CA.
7. Scawthorn, C. (1987) Fire Following Earthquake, Estimates of the Conflagration Risk to Insured Property in Greater Los Angeles and San Francisco, All-Industry Research and Advisory Council, Oak Brook, IL.
8. Schussler, H., The Water Supply of San Francisco, California, Spring Valley Water Company, (1906).
9. O'Rourke, T. D., Meyerson, W. D., Grigoriu, M. D., and Khater, M. M., Ground Failure Effects on Pipeline System Performance, 9th World Conference on Earthquake Engineering, 7, 79-84, (1989).
10. Lawson, et al., The California Earthquake of April 18, 1906, Carnegie Institution of Washington, (1908).
11. Youd, T. L. and Hoose, S. N., Historic Ground Failures in Northern California Associated with Earthquakes, Prof. Paper 993, USGS, (1978).
12. Manson, M., Report on an Auxiliary Water Supply System for Fire Protection for San Francisco, California, Board of Public Works, San Francisco, CA, (1908).
13. O'Rourke, T. D. and Lane, P. A., A Case Study of Seismic Hazards and Pipeline System Response for San Francisco, 3rd U.S. National Conference on Earthquake Engineering, 3, 2167-2178, (1986).
14. Committee of Twenty, Report of National Board of Fire Underwriters by its Committee of Twenty on the City of San Francisco, Cal., Henry Evans, Chmn., July 1905.
15. Prof. Stephen Tobriner, U. Calif. at Berkeley, Personal Communication, based on various data including Bowlen Outline.
16. Reed, S. Albert, The San Francisco Conflagration of April, 1906, Special Report to National Board of Fire Underwriters Committee of Twenty, May 1906.
17. Bowlen, Fred J., Batt. Chf., S.F.F.D., Outline of the History of the San Francisco Fire, Original Manuscript held in the California Historical Society Library, San Francisco, n.d.

18. The Argonaut, The Great Fire of 1906, May 1, 1926 and weekly thereafter until August 20, 1927, San Francisco.
19. Bowlen, Fred J., Batt. Chf., S.F.F.D., Reports of Fire Officers of the San Francisco Fire Department on the Fire of 1906, Manuscript in the Bancroft Library, U. Calif. at Berkeley, n.d.

**TABLE 1**  
**SUMMARY OF RESERVOIRS AND WATER CAPACITY AT TIME OF EARTHQUAKE**

<u>Reservoir</u>	<u>Capacity (million liters)</u>	<u>Elevation (m)</u>
University Mound	140.0	50.3
Francisco Street	11.4	41.1
College Hill	53.0	77.7
Lake Honda	124.9	111.3
Lombard Street	9.5	93.0
Potrero Heights	3.0	96.0
Presidio Heights	2.6	122.0
Clay Street Tank	0.9	114.3
Clarendon Heights	1.9	182.9

**TABLE 2**  
**ORIGINAL IGNITIONS FOLLOWING 1906 EARTHQUAKE**

No.	Location	Responding Company/Comments
1	211 Clay (100' W of Davis)	E12
2	119-123 Clay St	
3	15 Fremont	
4	Drumm and Jackson Sts (401 Drumm?)	
5	Dupont (Grant)@Pacific & Bdwy	T2 extinguished
6	NW crnr William & O'Farrell	E2; exting w/ sand (Capt. Brown)
7	6th & Howard (130-134 6th St)	E6 retreated E fr 6th bet Folsom & Clementina
8	Montgomery bet Bush & Pine	no fire indicated; gas pressurized
9	307-11 Davis nr Clay	E12 extinguished
10	blk bet Calif, Mkt & Davis	very rapid spread, frame bldg; E1
11	Sansome North of Pine	in basement, very rapid spread, frame bldg
12	Calif & Battery, NW corner	
13	219 Front nr Sacramento	E1 respndd, no water
14	Mission & 22nd St	extinguished after 5 hrs; E13,18,24,37,T7,E25
15	GG ave & Buchanan (NW crnr)	extinguished after 5 hrs; E15,23,27,30,34;
16	Fulton & Octavia (NW crnr)	extinguished after 5 hrs; E14,21,34; Chem4;
17	Hayes & Laguna	extinguished after 5 hrs; E14,21,34,Chem4,T6;
18	Ashbury & Waller	E30, extinguished
19	Masonic & Waller	E30, extinguished
20	Ashbury Hgts	E30 (Argonaut reports E30 exting 3 fires Ashbury Hgts)
21	Homestead Dist (FIRES?)	E32; district is S of Mission dist, nr county line
22	Homestead Dist (FIRES?)	E32; district is S of Mission dist, nr county line
23	Pacific @ Leavenworth (NW crnr)	E31; exting w/ sand (NB: not same as E2)
24	17th & Clement	E36; exting by bucket brigade
25	3rd & Clement	E26; exting small fire rear of store
26	Oak nr Stanyon	E22; exting?
27	2625 1/2 Harrison(22nd & 23rd Sts)	E25, T9; exting
28	"Butchertown" (Hunters Pt?)	E11
29	"Butchertown" (Hunters Pt?)	E11
30	Polk bet Bush & Pine (1312 Polk)	E3, T4
31	Bay & Powell	E28; stack collapse on kiln; exting in 2 hrs
32	Bay & Kearny	E20, no water; redirect to foot of Washington St fire
33	Stuart(E)@Mission & Howard	E1,9,38
34	Fremont (E)@Mission & Howard	little water
35	Howard E of 3rd St	spilled coals; E4 (fire stn next dr), little water;
36	282 Natoma (E of 4th St)	
37	Bet 5th & 6th Sts, Mkt to Harrison	No. FIRES & locations unknown; T3 arrives at 0800
38	Bet 5th & 6th Sts, Mkt to Harrison	No. FIRES & locations unknown; T3 arrives at 0800
39	395? Hayes (S) 75' E of Gough	"Ham & Eggs fire"; E14,24,34; see NBFU Fig 14; no water
40	Davis bet Pacific & Bdwy	exting by Chem Co
41	Front bet Vallejo & Bdwy	exting by Chem Co
42	Davis & Vallejo (crnr)	exting by Chem Co
43	East St bet Bdwy & Vallejo	exting by Chem Co
44	Golden Gate Ave nr Divisadero	E30 (poor water, fire confined to 1/4 blk; 12 hses lost)
45	Bush & Kearny	"noticed in neighborhood"
46	Market & Kearny	no water
47	Geary & Stockton (239-241 Geary)	E2, exting, SAR
48	Howard & 12th (NW crnr)	E22, no water, attempted to draft fr sewer unsuccessfully
49	Sutter & Polk (1215 Sutter)	T4, exting
50	Minna & 5th	soon merged with Jessie & 3rd fire
51	Jessie nr 3rd	soon merged with Minna & 5th fire
52	Market & Beale	E1, but "a dozen powerful streams" reqd.

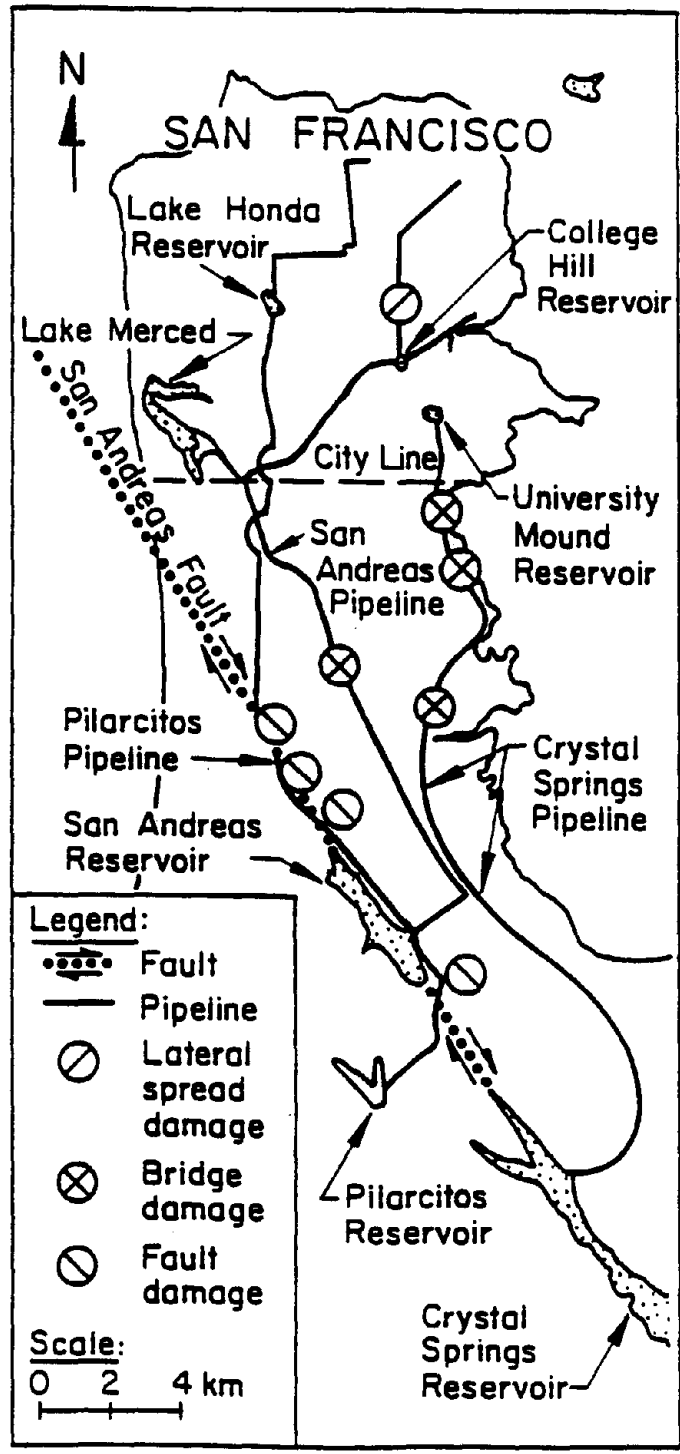


Figure 1: 1906 San Francisco Water Supply (adapted from Schussler)

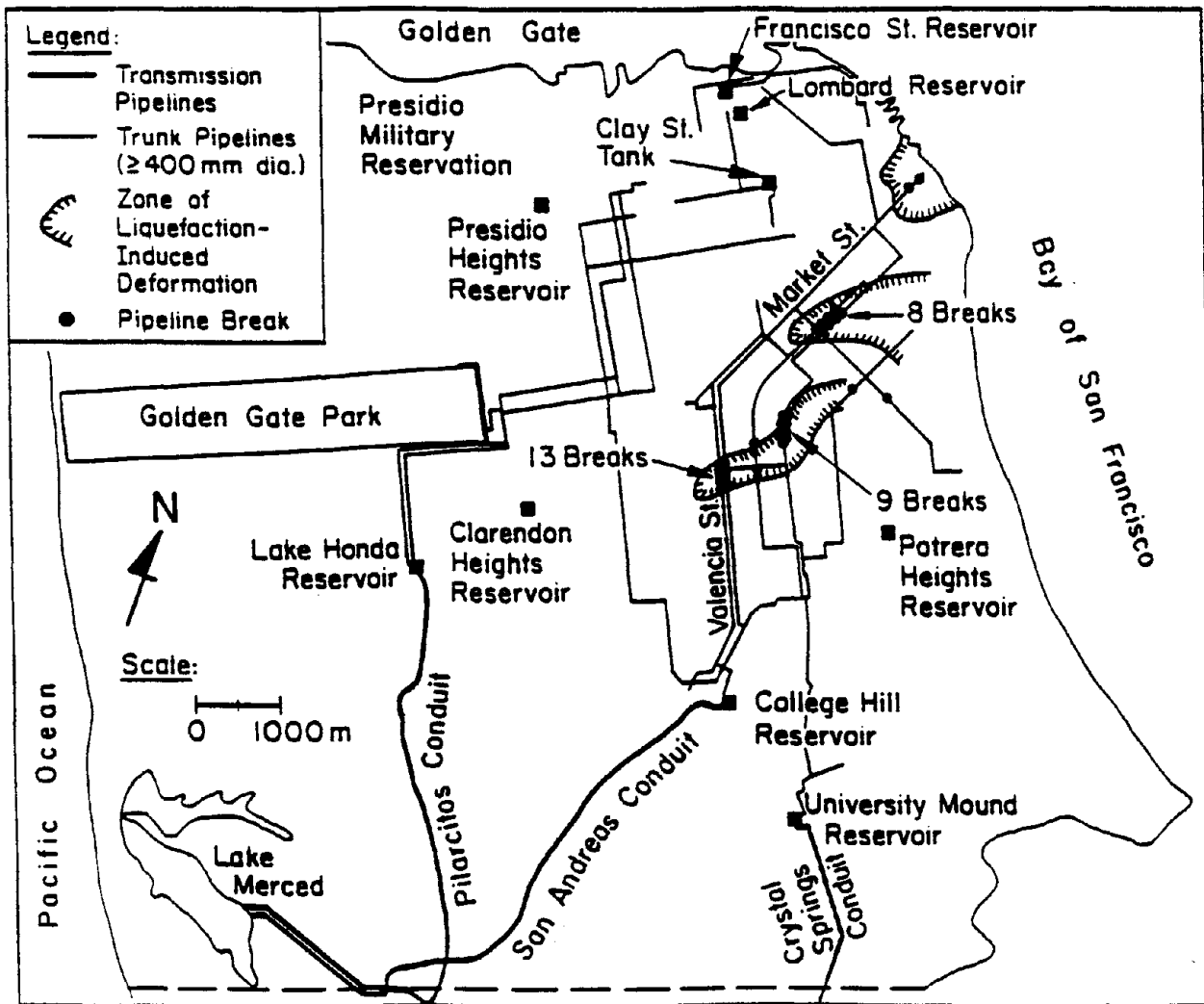


Figure 2: 1906 Water Supply Within San Francisco City Limits



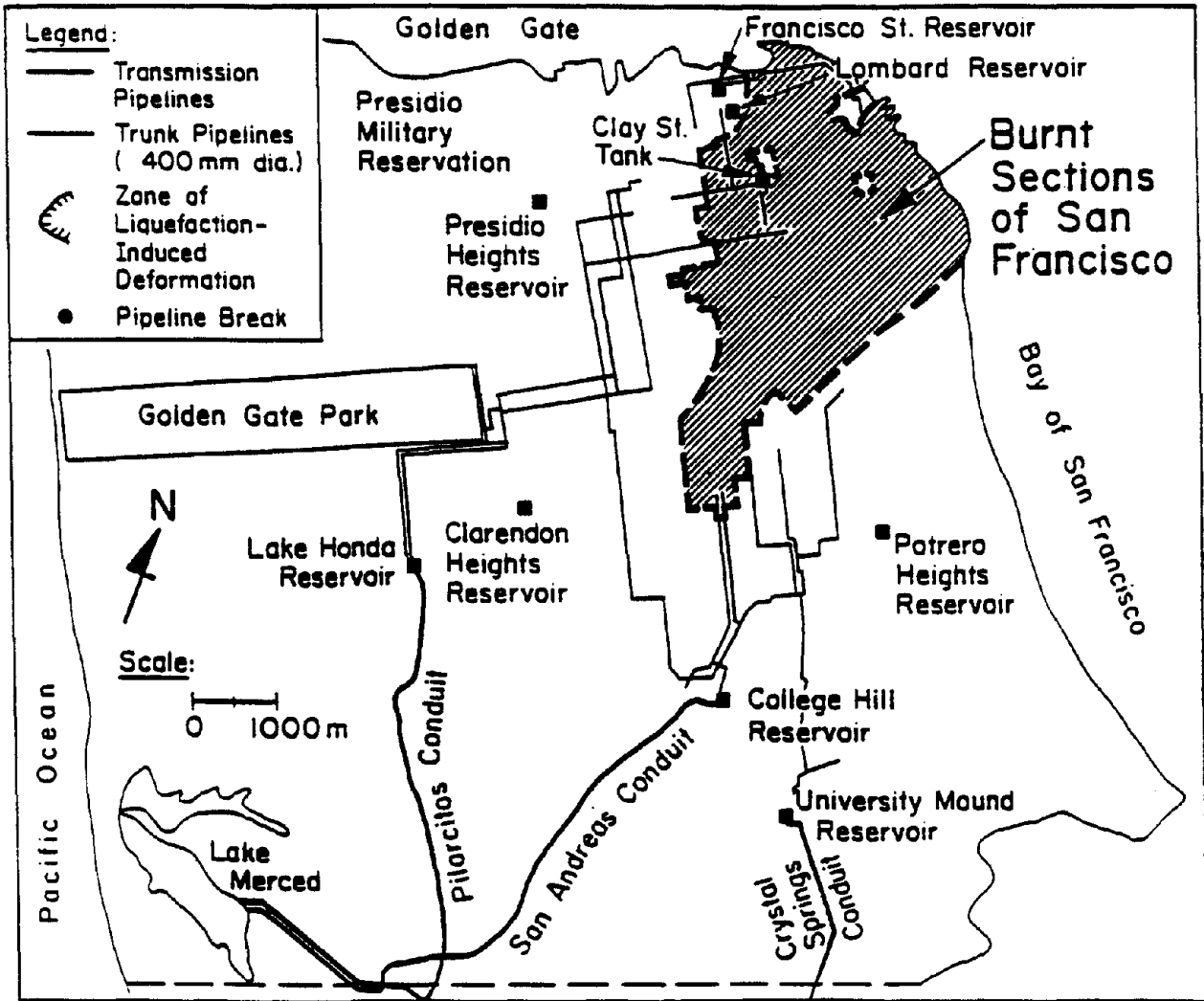


Figure 3: San Francisco Water Supply and Area Burned During the Fire

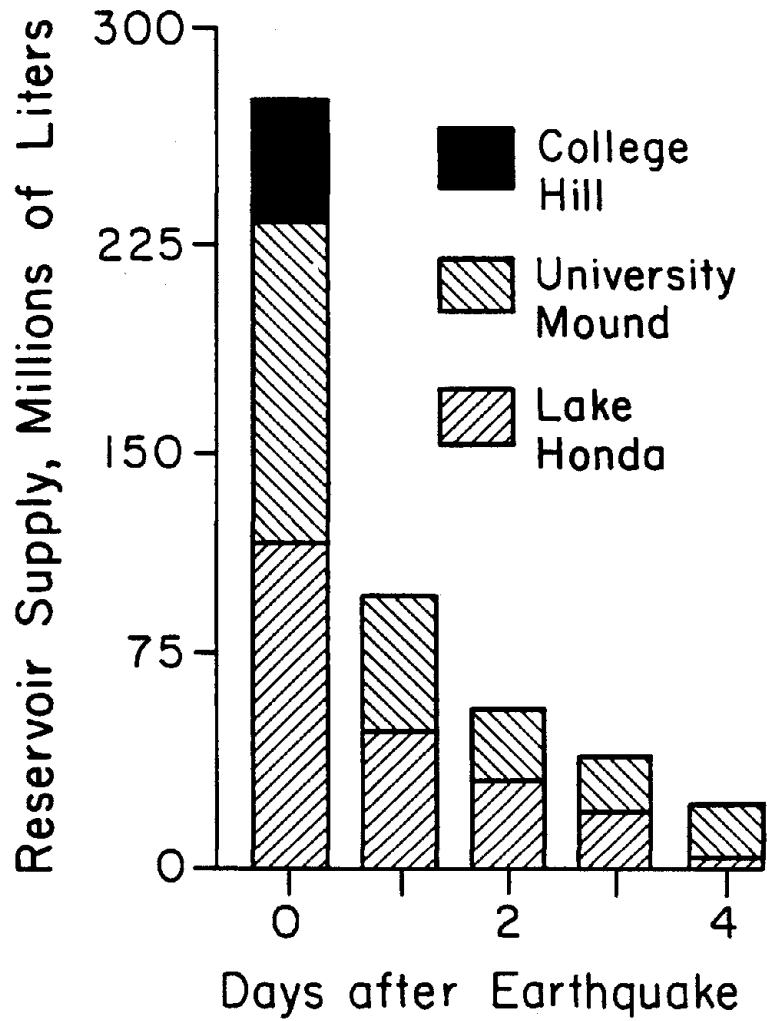


Figure 4: Reservoir Storage in San Francisco, As a Function of Time After the Earthquake

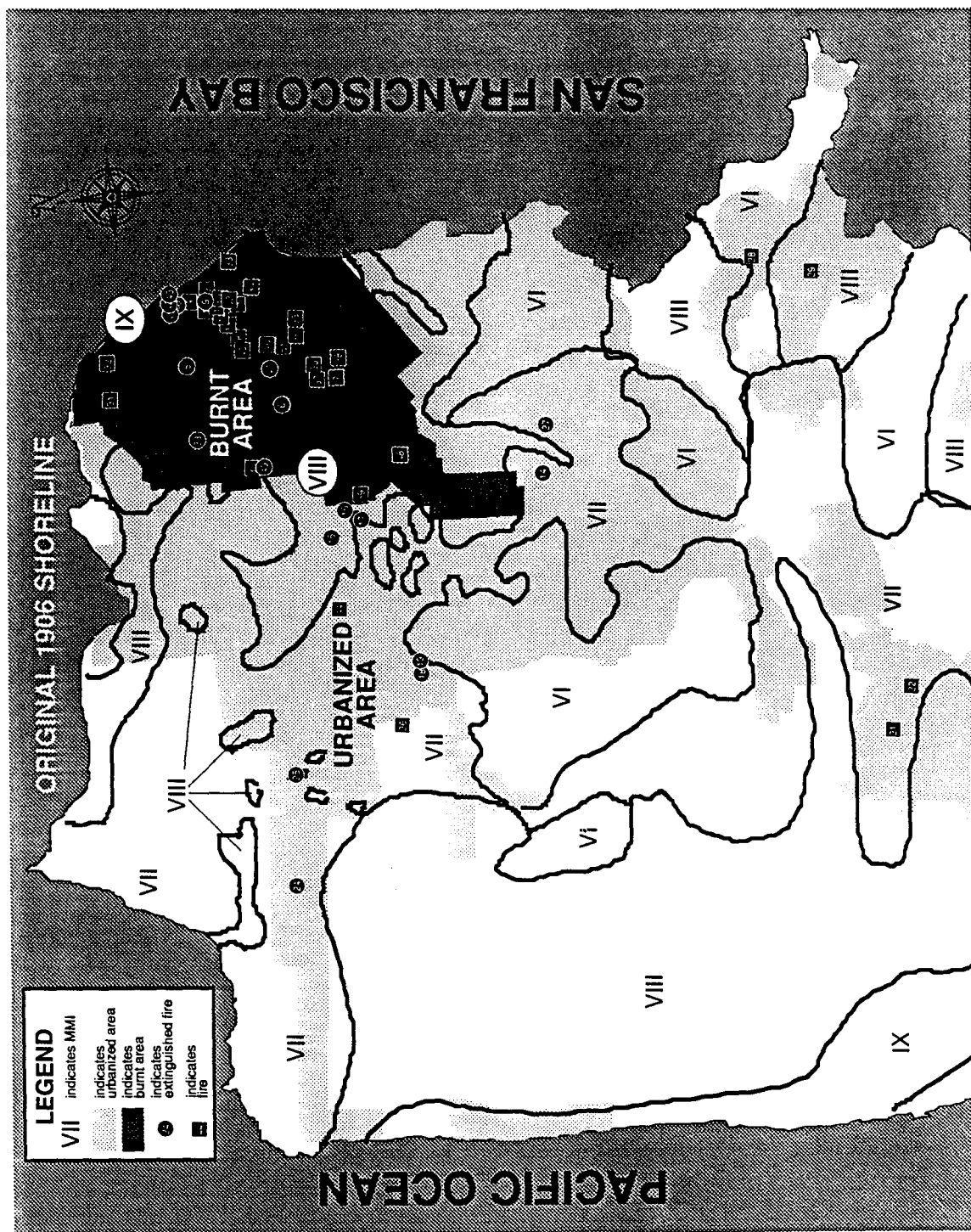


Figure 5: Pattern of Ignitions Following the 1906 San Francisco Earthquake

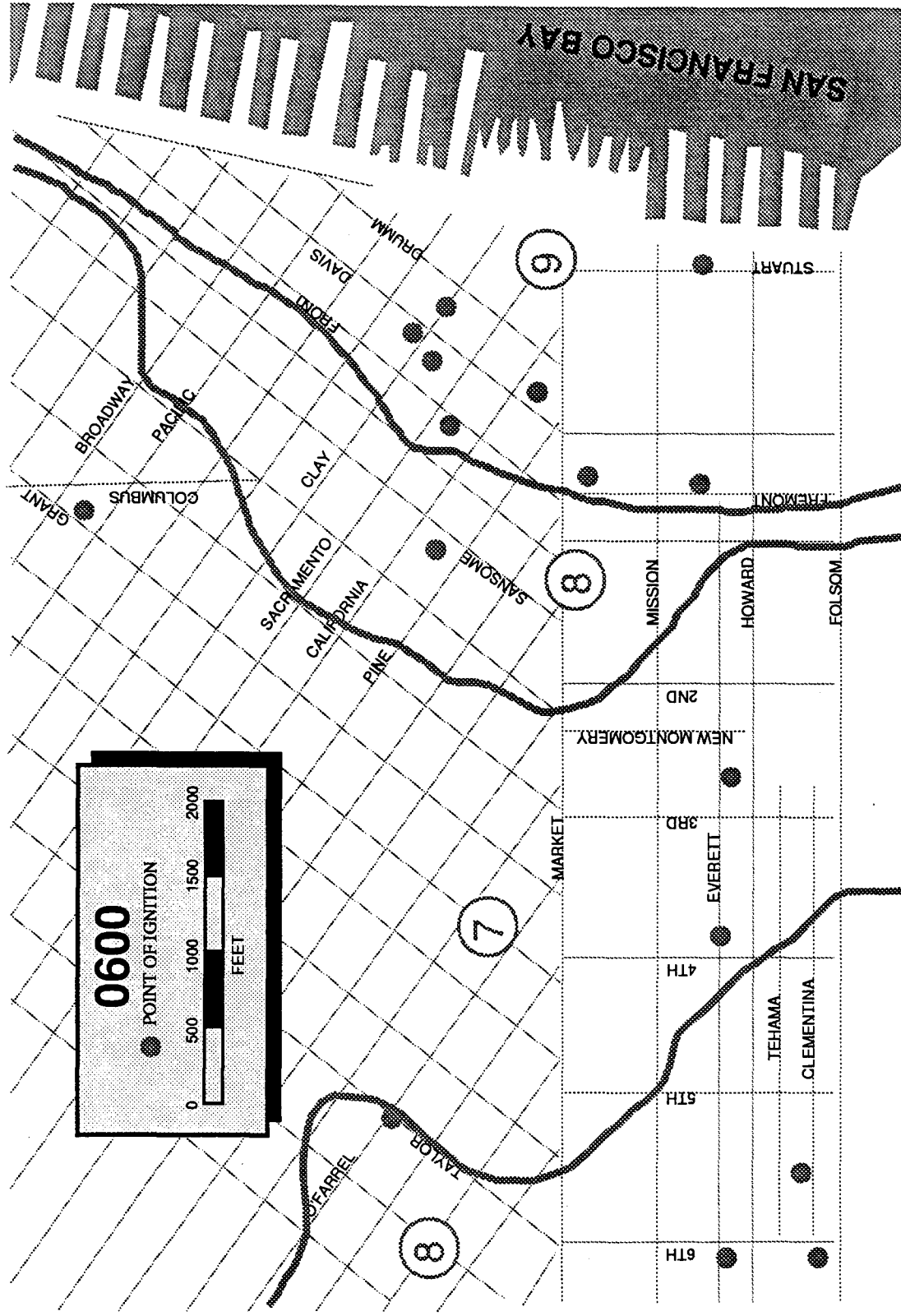
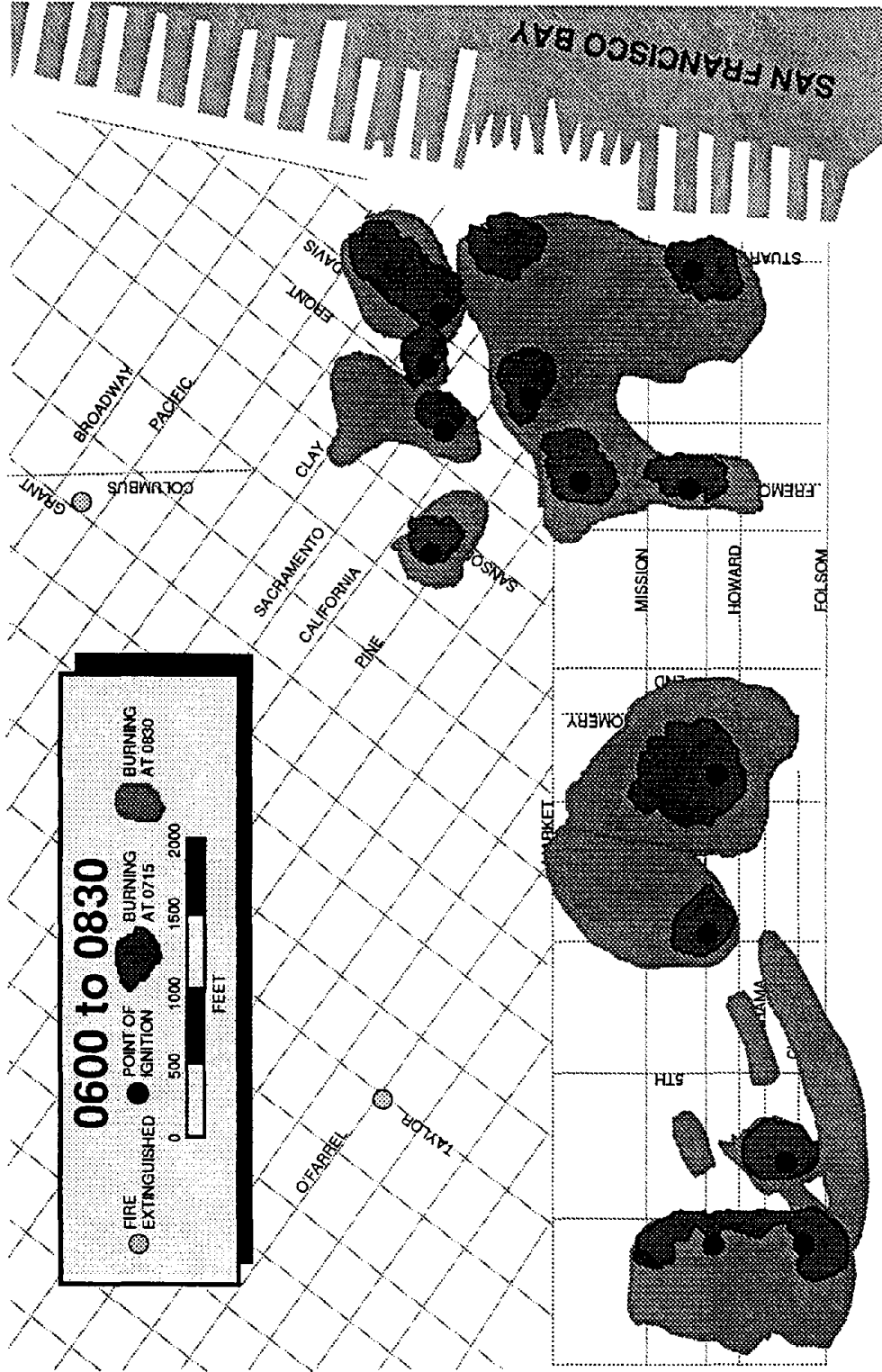


Figure 6: Detail of Ignitions in CBD, Following the 1906 San Francisco Earthquake

0600.DRW 30033-02



6-830 DRW 3/033-02

Figure 7a: Fires Extinguished and Spread of Initial Ignitions, for Period 1

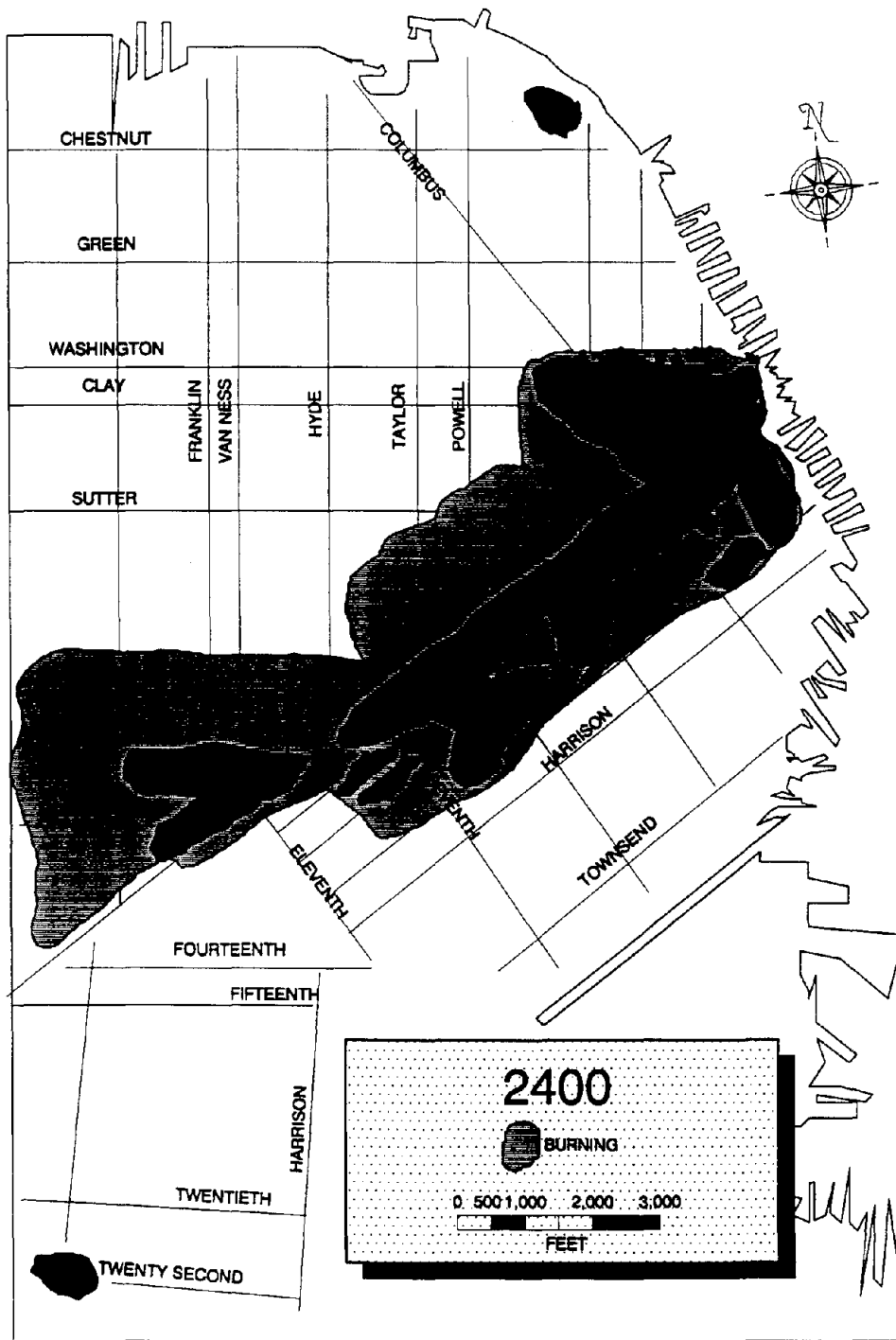


Figure 7b: Fires Extinguished and Spread of Initial Ignitions, for Period 1 (cont.)

# LIQUEFACTION INDUCED GROUND DISPLACEMENT DURING THE 1923 KANTO EARTHQUAKE

K. Wakamatsu<sup>1)</sup>, M. Hamada<sup>2)</sup>, S. Yasuda<sup>3)</sup>, and I. Morimoto<sup>4)</sup>

1) Research Associate, Science and Eng. Research Lab. , Waseda University, Tokyo, Japan

2) Professor, School of Marine Science and Technology, Tokai Univ. , Shimizu, Japan

3) Associate Professor, Faculty of Civil Eng. , Kyushu Institute of Technology, Kitakyushu, Japan

4) Chief Engineer, Kiso-Jiban Consultants Co., Ltd., Tokyo, Japan

## ABSTRACT

Three case histories of liquefaction-induced ground displacement generated by the 1923 Kanto earthquake are reviewed. By re-examining published damage reports and interviewing local residents, sites of liquefaction-induced ground failure and displacement were identified and their types and character were clarified. Geomorphological and geotechnical conditions of the each site were examined and liquefied layers were evaluated by existing data, aerial photographs taken in 1947 and subsurface investigation including borings, SPT tests and Swedish Sounding. The 1923 Kanto earthquake generated horizontal ground displacement at least in three area in Tokyo and its vicinity. The displacement occurred originating from the natural levee or former channel bar toward a small river. The inclination of surface ground of displacement sites was so small as below 1%. Recent borehole data from three sites revealed that saturated layers of fine to sandy gravel of channel deposits underlie each site at shallow depth. These deposits were estimated to have liquefied according to the visual classification and laboratory grain size analyses of the samples, and to the calculation results based on the Japanese Highway Bridge Code.

## INTRODUCTION

Recent investigations have disclosed that liquefaction had generated large-scale ground displacement after the occurrence of several Japanese and the United States earthquakes including the 1906 San Francisco earthquake, the 1964 Niigata earthquake, the 1971 San Fernando earthquake, the 1983 Nihonkai-Chubu earthquake, and other moderate U.S. earthquakes (Ref.1-4). However, more case studies are required to determine the mechanism of ground displacement and to develop widely accepted criteria for assessing ground displacement. The purpose of this study is to: (1) Identify sites of liquefaction-induced ground displacement generated during the 1923 Kanto earthquake in Tokyo Metropolitan area, Japan; (2) further clarify the types and character of ground displacement associated with liquefaction; and (3) provide a data base for geomorphological and geotechnical studies on liquefaction-induced ground displacement.

### OUTLINES OF THE 1923 KANTO EARTHQUAKE

The time of occurrence at the origin was 58 minutes and 32 seconds past 11 A.M., September 1, 1923. The epicenter was originally allocated at 139.5°E and 35.1°N and the magnitude was assessed at 7.9. The Earthquake resulted from a slippage of transform fault between two crustal blocks bounded by the Sagami Trough. The source area was estimated as shown on Fig.1 by Ando (Ref.5). Damage was severest in Kanagawa and Tokyo Prefectures, though it also extended to other parts than the Tokyo Metropolitan area such as Shizuoka Prefecture and as far as Yamanashi and Nagano Prefectures. The number of death in Kanagawa and Tokyo Prefectures totaled about 97,000 including about 60,000 in Tokyo City. The total number of dead and missing reached about 143,000 and approximately 104,000 people were listed as injured. About 128,000 structures were demolished, the other 126,000 were heavily damaged and as many as 447,000 structures were lost in fires. Fires were responsible for the majority of house losses in Tokyo, while about 50 percent of houses lost in Kanagawa Prefecture might be attributed to fires.

### METHOD

Unfortunately, no aerial photographs were found enabling us to measure permanent ground displacements generated by the 1923 Kanto earthquake. Although photos taken in very limited areas immediately after the shock were inserted in the damage reports, they were hardly clear for us to interpret ground displacement or deformations. Possibility of investigation comparing geographic maps before and after the earthquake was also denied because reduction scale of the maps in those days had been highly difficult to measure or to identify several meters of permanent displacements. Eventually decision has been made to interview the witnesses to survey the areas where permanent ground displacements occurred or might have occurred. Prior to the interview, published damage reports, books and/or journals were carefully re-examined and nine sites where liquefaction effects were particularly pronounced were selected for interview surveys.



At the same time, in order to review and to find out geomorphological and geotechnical conditions, topographical maps, geographical maps and existing boring data were gathered and aerial photographs taken in 1947 were interpreted. Several borings, SPT-tests, and Swedish Soundings were also conducted to confirm subsurface conditions and to evaluate liquefied layer.

### Liquefaction sites and detailed investigation sites

Fig.1 shows location where sand and/or water boilings were recorded in the literature on the 1923 earthquake. Sand and/or water boilings extended over a wide area, and occurred as far away as 150km from the epicenter. Interview was conducted at Sites 1 - 9 of the Figure and a total of more than 70 witnesses provided useful information on ground failures by the 1923 earthquake. Their statement revealed and confirmed that liquefaction by the 1923 event caused various type of ground failure including sand boils, ground cracks, settlement, slope failure of embankments, and ground displacement. Among them, the most common and most damaging failure was ground cracks occasionally accompanied vertical and horizontal displacement. In addition, in the following three areas, occurrence of horizontal ground displacement as large as several meters was verified.

#### Nakajima Area, Chigasaki City, Kanagawa Pref. (Site 1)

##### Types of ground failure and displacement

Nakajima area, Chigasaki City lies on the left bank in the lower reaches of the Sagami River (formerly called as Banyu River) (Fig.2). Although this city was located within the source area of the Kanto earthquake as shown in Fig.1, the damage reports issued shortly after the event gave only fragmentary information on the direct effects of the ground failures. The interview survey conducted some 60 years after the earthquake found and confirmed 110 cases of liquefaction effects in the lower reaches of the Sagami (Banyu) River (Ref. 6). According to the survey, among the area of the lower reaches of Sagami River, Nakajima area was most distinctly affected by liquefaction due to the earthquake, and following noteworthy comments were given by the residents of Nakajima; Lots of large ground cracks formed, and all the housings in the neighborhood became flooded by the gurgling ground water, and it took two days to dewater, Almost all 80 housing wells became filled with sand boil deposits, etc. (Ref. 6).

Fortunately, a slanted aerial photograph shooting cracks of this Nakajima area was found in the official damage report of the Kanto earthquake, as shown in Fig.3 (Ref. 7). Based on this photo interpretation and field inspection, outline of ground cracks were drawn on a geographical map as shown in Fig.4. The witnesses reported that the Okawa River, so-called by the residents, used to be a river less than 10m wide and more than 5m deep, paralleling the Sagami River. Ground cracks and scarps formed along this Okawa River, and both river width and depth were reduced to less than half after the earthquake. Currently the width is about 2.5m and the stream is completely dry. The area of fields around the cracks increased or decreased after the event. One prominent example is plowed fields of one witness: before

the earthquake, it used to be a total of 2,336m<sup>2</sup>, and after the earthquake it measured up to 2,501m<sup>2</sup>, which showed an increase by 165m<sup>2</sup>. These accounts indicate that the minimum of several meters of permanent displacement was induced in this area toward the direction of the Okawa River due to the 1923 Kanto Earthquake.

#### Geomorphological and geotechnical conditions

Nakajima area, as indicated in Fig.2 is located on the former channel bar and former branch stream of the Sagami River, namely, it belongs to deltaic fan geomorphologically. The ground cracks and sand boils were observed on both of the former channel bar and former stream channel, and the largest crack formed on their boundaries. The permanent ground displacements occurred originating from the former channel bar passing through the former stream channel and terminated at the Okawa River.

A geotechnical profile along the line A-A' of Fig.4 are shown in Fig.5. The ground surface is slightly sloped toward the Okawa River with a gradient of about 0.5% and is covered with agricultural clay fill. Loose fine sand lies beneath the fill, and moderately dense sandy gravel underlies the fine sand. Both these gravel and sand are channel bar and channel deposits. Only at bore hole B-1 and S-4 where ground cracks occurred, a clay lens containing sand existed over the fine sand layer. The grain size distribution curves for samples taken from the sand layer and gravel layers are plotted on Fig.6. Based on the past experiences, they plot outside the bound for most liquefiable soils. However the only tenable explanation for the ground failure in this area is liquefaction within layers of the fine sand and the sandy gravel based on the following description of the residents; "A lot of water gushed", "the sand boil deposits composed of coarse sand with occasional pebbles". In the case of the Nakajima site, bad drainage of agricultural clay fill and clay lens beneath the fill are likely to have accelerated the liquefaction of the underlying the sand layer and gravel layer. In order to estimate liquified layer, calculation was made using the procedure outlined in the Japanese Highway Bridge Code, under a peak ground surface acceleration of 300gal, which value was also roughly adopted from the above code. According to the calculation results the whole of the fine sand layer under the water table and the part of the gravelly coarse sand layer was estimated to have liquified as indicated by shadowed portion on Fig.5. The analytical results reconfirmed observed phenomena.

#### **Furu-Sumida River Area, Tokyo (Site 4)**

##### Types of ground failure and displacement

This area lies in the northeastern part of Tokyo, and was located about 80 Km north-east of the epicenter (Fig.1). In this area, a small stream called the Furu-Sumida River meanders from the northeast to the southwest and drains into the Sumida River (Fig.7). The width of the stream was about 3m at the time of the earthquake but was estimated more than 50m in the several hundred years ago, because until 1621, this river had been main stream of the Tone River which has the largest drainage area in Japan. The remnant stream channel was outlined by levees and rice field of old maps and 1947 aerial photographs.

Earthquake-induced ground failure in this area were documented in a geological report of a survey conducted shortly after the event (Ref.8). We have used this report to identify sites where ground cracks and sand boils occurred in 1923 and had interviews with residents of the area. Geological Survey of Japan (Ref.8) and residents reported that drastic sand boilings occurred at each point along the Furu-Sumida River shown on Fig.7. Among the points, the most striking effects of the liquefaction developed at several locations in Nishi-Kameari. At site D and E on Fig.7, violent eruptions occurred not only by the 1923 Kanto earthquake but also by the 1855 Ansei-Edo earthquake. At site E and F on Fig.7, extensive cracks formed from the east to the west and from the south to the north direction, erupting a large quantity of blue sand and water flooded the areas. The bottom of the Furu-Sumida River rose up to the ground level or higher from site E to site G on Fig.7.

Nearby Takagi Shrine (site E on Fig.7), the following comments were given by the witnesses; numerous cracks as wide as about 50cm occurred shown in Fig.8, erupting blue sands together with pieces of pumice and sand boil deposits reached 15cm in thickness. The neighborhood became flooded by the ground water as deep as 1m and more, and it took several days to dewater. Wooden houses near the river collapsed, sunk or tilted. Ground of the neighborhood moved toward the direction of the Furu-Sumida River (toward west and north) and the stream which had about 3m width before the earthquake was closed and banked up more than 1m above ground level after the earthquake.

These description indicates that the minimum of several meters of horizontal permanent displacements was generated in the vicinity of Nishi-Kameari toward the direction of the Furu-Sumida River due to liquefaction by the 1923 Kanto earthquake. In addition, in the Furu-Sumida River area, ground failures, including sand boils and cracks, had occurred in times of the 1855 or the 1894 earthquakes, and statements of residents confirmed that some of the sand boilings had occurred at same points as previous earthquake.

#### Geomorphological and geotechnical conditions

The Furu-Sumida River area is located on natural levee and former river channel and delta (Fig.7). A numerous cracks and sand boils occurred on the gentle slope of the natural levee and the largest crack formed on the top of the levee parallel with the river. The sand boils also occurred on the rice field of the former channel along the Furu-Sumida River, but no surface evidence of liquefaction was reported on the delta. The permanent ground displacements occurred originating from the natural levee toward the Furu-Sumida River.

Fig.9 shows a geotechnical section along the line B-B' of Fig.8. The ground surface is gently sloped toward the Furu-Sumida River. The current inclination of the ground is about 0.7% but may have been a little steeper at the time of the 1923 event, because the present ground was graded by leveling. Holocene sediment of this section is as thick as about 30m. Loose fine sand layer, about 10m thick, containing silt lenses lies near the

ground surface. Upper several meters of this layer is levee deposit and lower part is channel deposit. Moderately dense medium sand of beach bar origin is partially accumulated at B-2 and B-3. From the description of the witnesses on color of the sand boil deposits, the ground displacement at this site is attributable to the liquefaction within the fine sand layer of channel deposit and possibly within medium sand layer. Assuming that the peak ground acceleration generated by the Kanto earthquake was 250gal, and applying the procedure outlined in the Japanese Highway Bridge Code, the loose fine sand layer became completely liquefied as indicated by shadowed portion on Fig.9.

### **Kawakubo Area, Kasukabe City, Saitama Pref. (Site 5)**

#### Types of ground failure and displacement

Geological Survey of Japan (Ref.8) reported detailed account of numerous ground cracks formed along the Furu-Tone River and the Moto-Ara River. Kawakubo area in Kasukabe City is one of the areas with prominent sand boilings. This area lies on the right bank of the Furu-Tone River which had been main stream of the Tone River until 1621 same as the Furu-Sumida River, and was located about 100 km northeast of the epicenter.

According to Geological Survey of Japan (Ref.8), numerous cracks developed on housing lots and fields along the Furu-Tone River, as shown on Fig.10 and vented large quantity of blue sand with occasional pieces of pumice as big as eggs or black clay containing rotten wood pieces. Especially in Kawakubo, the houses were flooded up to or above the floor boards, the boiling sands as much as 10cm deposited over the vicinity, and a nearby stream was choked with boiled sand. A road running in front of Mr. Ishikawa's house cracked and became curved with a maximum of 1.5m toward the direction of the river for a distance of 70m after the earthquake as shown in Fig.11. We have relocated the Mr. Ishikawa's home by speaking with the residents of the area. A grandson of Mr. Ishikawa and the residents provided additional information about the ground failure and displacement during the event, and helped to identify the locations described in the damage report. The witnesses stated that the ground cracks reached a maximum of approximately 300m long, 2m wide with vertical gap of 1-2m; that many housings have partially collapsed with their foundations fractured and split apart by the ground cracks; that Mr.Ishikawa's premises and neighboring ground dilated toward the direction of the river; and that the area along the Furu-Tone River subsided.

#### Geomorphological and Geotechnical conditions

The Furu-Tone River has developed typical fluvial geomorphological features including old river channel, natural levee, and back marsh as seen in Fig.10. The ground cracks formed parallel with the river on the natural levee and the old river channel, but no surface evidence were reported on the back marsh. The sites, where the road became curved as shown in Fig.11, and where many houses partially collapsed with their foundation torn apart by the ground cracks, and also where housing lots dilated toward the river, are all located within the former river channel.

Fig.13 is a geotechnical profile along the line C-C' of Fig.10. The ground surface is gently sloped toward the Furu-Tone River with a gradient of about 0.7% and a small scarp as high as 1.5m formed along the boundaries of the natural levee and former river channel. Holocene deposits of this area is as thick as about 30m. A 0.9m to 2.8m layer of fill caps this site. The fill is composed of clay, silt and sand containing fine gravel, peat or debris and probably placed after the 1923 event. Beneath the fill, a fine to medium sand layer about 5m thick overlies the very soft marine silt. The depositional environment of this sand is natural levee and river channel. The grain size distribution curves for samples taken from the sand layer in bore hole B-1 and B-2 are plotted on Fig.14. Except for a little higher fines content of the sample from the bore hole B-1, the distributions plot within the bound for the most liquefiable soils. The only ternable explanation for the ground failure and displacement in this area is liquefaction within the fine to medium sands. In order to estimate the liquefied layer, calculation was made assuming that the peak acceleration of the ground surface was 200gal and using the procedures outlined in the Japanese Highway Bridge Code. According to the calculation results, sand layer, within the area of former and present channel, became liquefied as shown by the shadowed part on Fig.13. The analytical results reconfirmed the observed phenomena.

## CONCLUSION

1. Liquefaction induced ground failures developed at many locations in Tokyo and the neighboring districts during the 1923 Kanto earthquake. The most distant location is approximately 150km from the epicenter.
2. The most common and most damaging ground failures caused by liquefaction were ground crack occasionally accompanied vertical and horizontal displacement.
3. Three area confirmed that large horizontal ground displacement had been induced by the earthquake. The magnitude of the permanent displacement was estimated as large as several meters.
4. The ground displacement occurred from the natural levee or former channel bar toward a stream, which was only several meters wide at the time of the earthquake but had been much wider a few centuries before the earthquake.
5. The ground slope of displacement sites was small, being less than 1%.
6. Recent borehole data from three 1923 ground displacement sites show that saturated layers of fine sand to sandy gravel (with average standard penetration resistances of 5 to 30), which are river channel deposits, underlie each site at shallow depth. These deposits were estimated to have liquefied according to the visual classification and laboratory grain size analyses of the samples, and to the calculation results based on the Japanese Highway Bridge Code.

7. At several locations sand boiling recurred at same place during previous large earthquakes.
8. To date, we couldn't find evidences of ground displacement in artificially filled up land along coast. Further reconnaissance is scheduled to be conducted along the coast.

### ACKNOWLEDGEMENTS

This research was conducted by the Japanese team of Japan-U.S. Cooperative Research and Collaboration. The authors would like to thank each member of the team for their assistance and helpful discussions. The authors would also like to express their gratitude to Mr. I. Yasuda of Hasshu Inc. for his skillful interpretation of the old photographs shooting ground cracks of Nakajima area.

### REFERENCES

- 1) Youd, T.L. and Hoose, S.N., *Liquefaction during 1906 San Francisco Earthquake*, Journal of the Geotechnical Engineering Division, ASCE, Vol.102, No. GT5, pp.425-439, 1976
- 2) Youd, T.L., *Landslides in the Vicinity of the Van Norman Lakes*, U.S. Department of Commerce, The San Fernando, California Earthquake of Feb. 19, 1971, Geological Survey Professional Paper 733, 1971
- 3) Hamada, H., Yasuda, S., Isoyama, R. and Emoto, K., *Study on Liquefaction Induced Permanent Ground Displacement*, Association for the Development of Earthquake Prediction, 1986
- 4) Youd, T.L. and Bartlett, S.F., *US Case Histories of Liquefaction-induced Ground Displacement*, Proc. of First Japan-U.S. Workshop, pp.22-31, 1988
- 5) Ando, M., *Seismo-Tectonics of the Kanto Earthquake*, Journal of Physics of the Earth, Vol.22, pp.263-277
- 6) Kotoda, K., Wakamatsu, K. and Watanabe, K., *Ground Damage in the Lower Reaches of the Sagami River due to the Great Kanto Earthquake of 1923*, Proc. 7th Japan Earthquake Engineering Symposium, pp.43-48, 1986 (in Japanese with English abstract)
- 7) Kokumin Kyoiku Fukyukai (Association for the Development of National Education), *Kanto Daishinsai Shasincho (A Photo Album of the Great Kanto Earthquake)*, 1923 (in Japanese)
- 8) Geological Survey of Japan, *Report on the Kanto Earthquake*, Vol.1 (204pp.), Vol.2 (185pp.), 1925 (in Japanese)

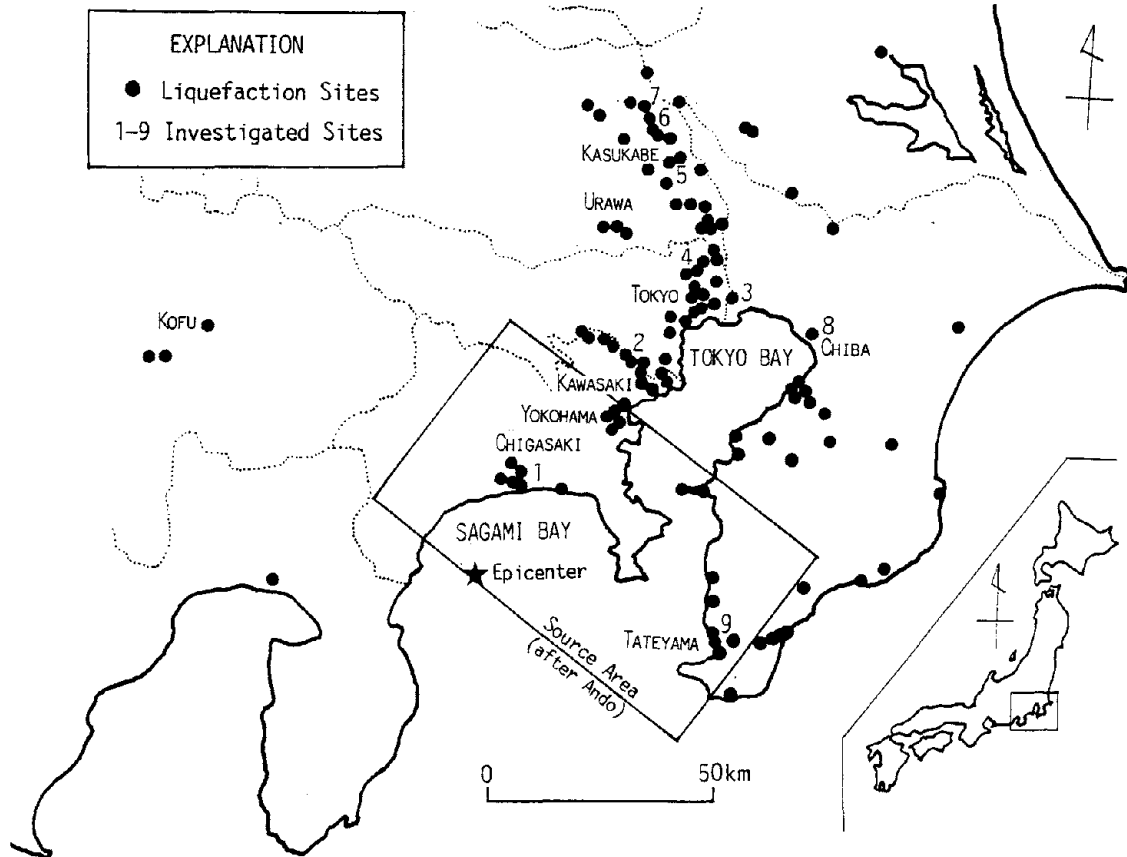


Fig.1 Regional map showing liquefaction sites during 1923 Kanto Earthquake

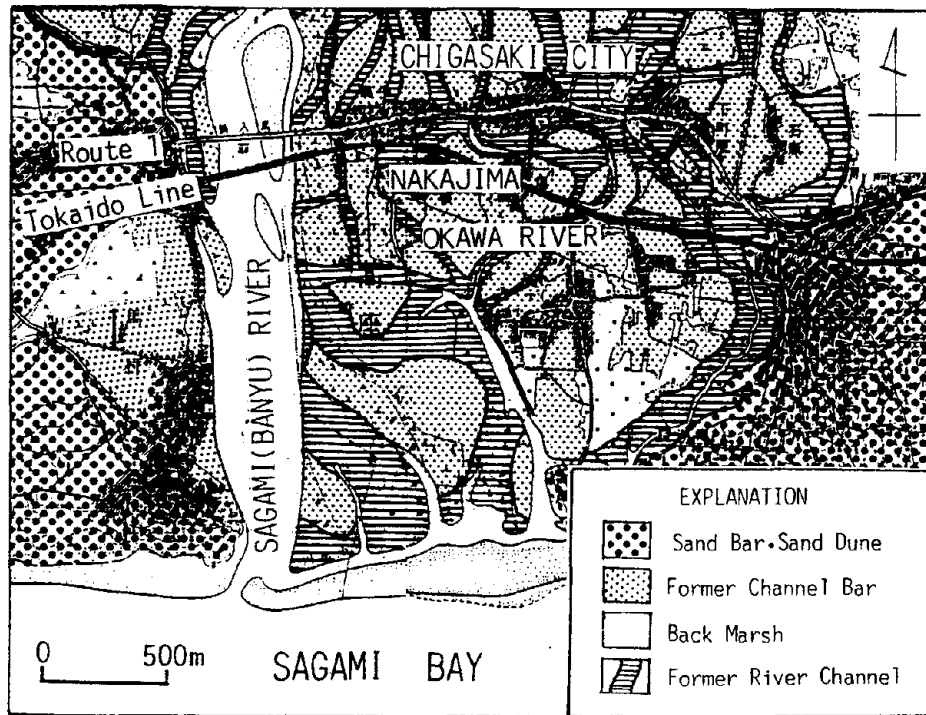


Fig.2 Map of lower reaches of the Sagami River showing geographic and geomorphological features and location of Nakajima area



Fig.3 Aerial photo of Nakajima Area taken shortly after the earthquake showing ground cracks (Association for the Development of National Education, 1923)

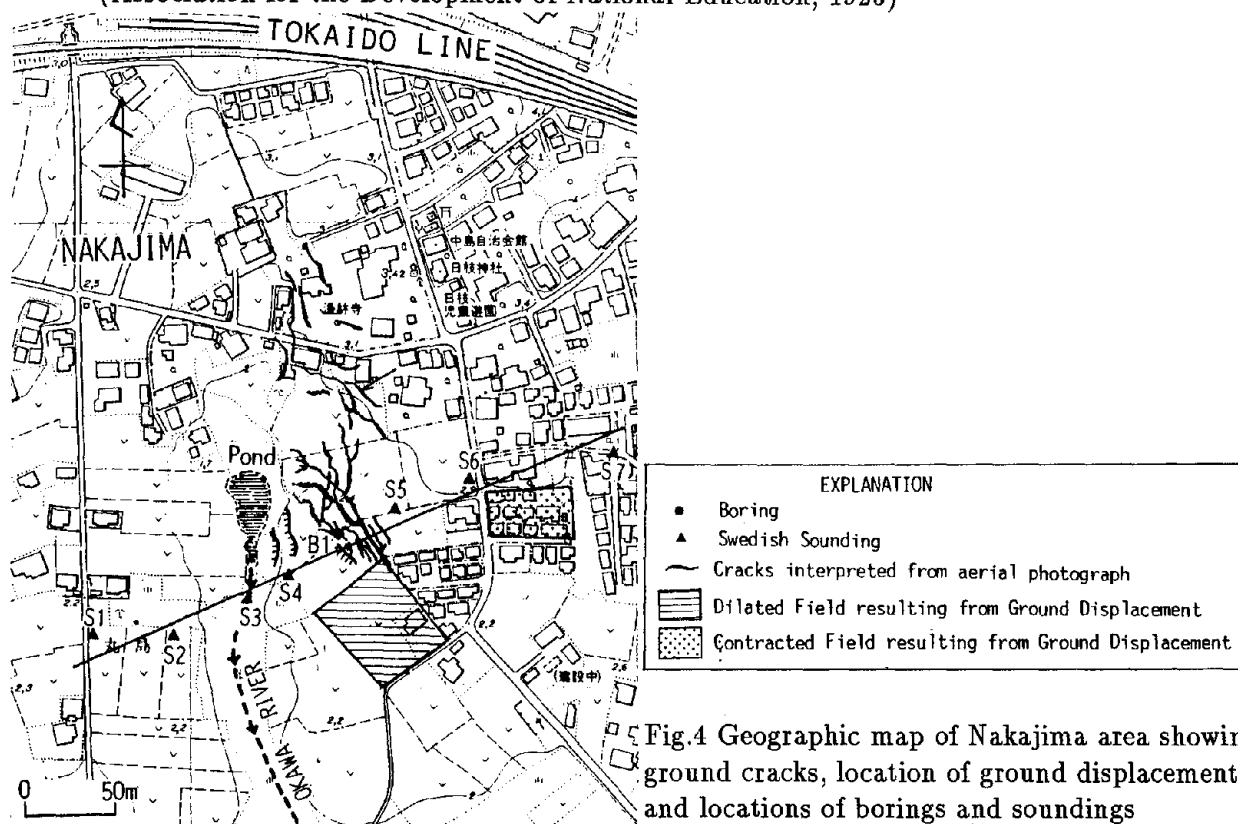


Fig.4 Geographic map of Nakajima area showing ground cracks, location of ground displacement and locations of borings and soundings



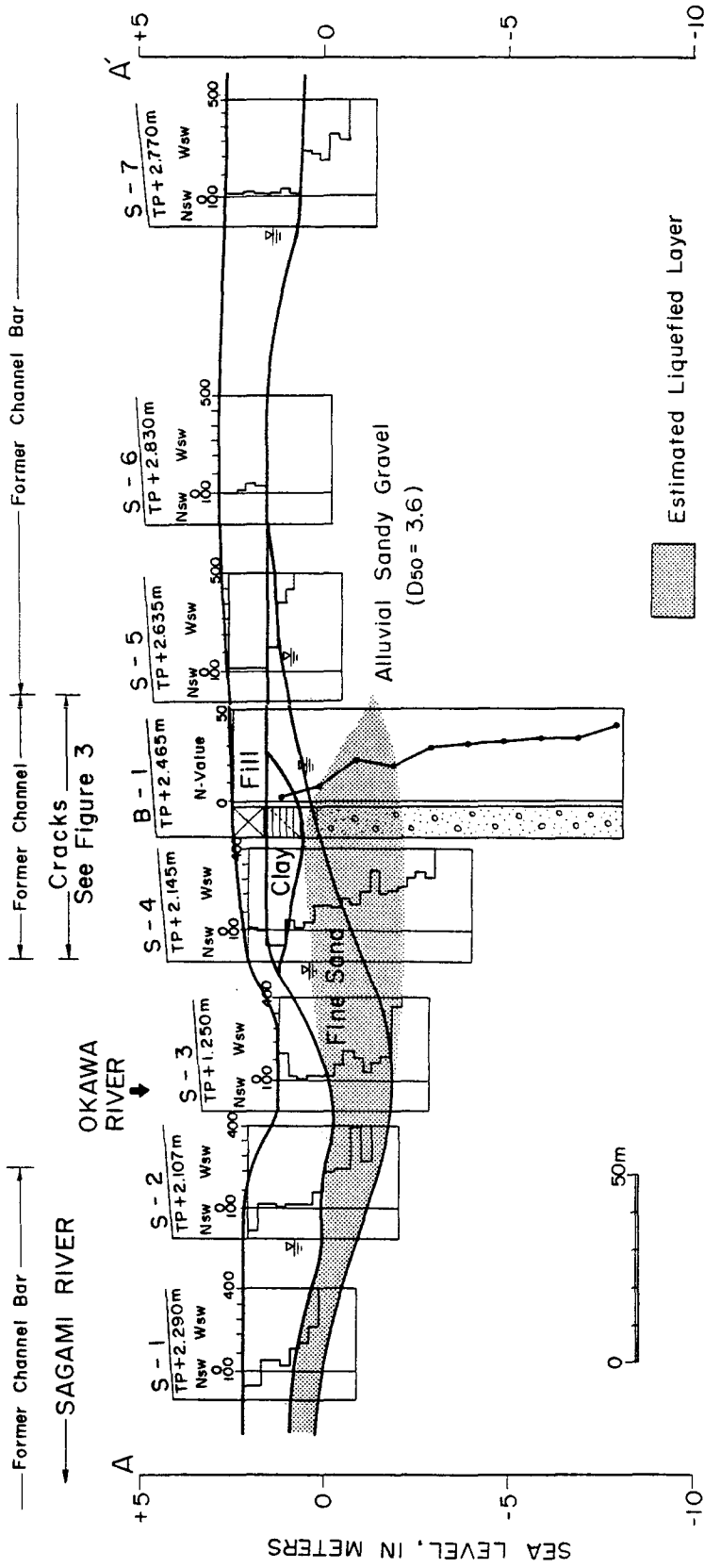


Fig. 5 Cross section of sediment at Nakajima showing geotechnical features and estimated liquefied layer

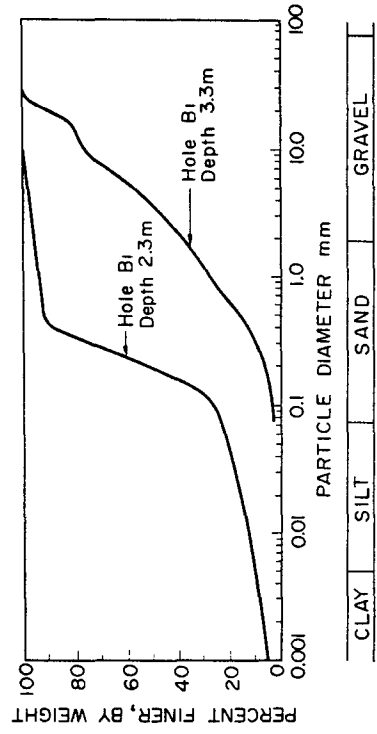


Fig. 6 Grain size distribution curves from fine sand layer and sandy gravel layer at Nakajima

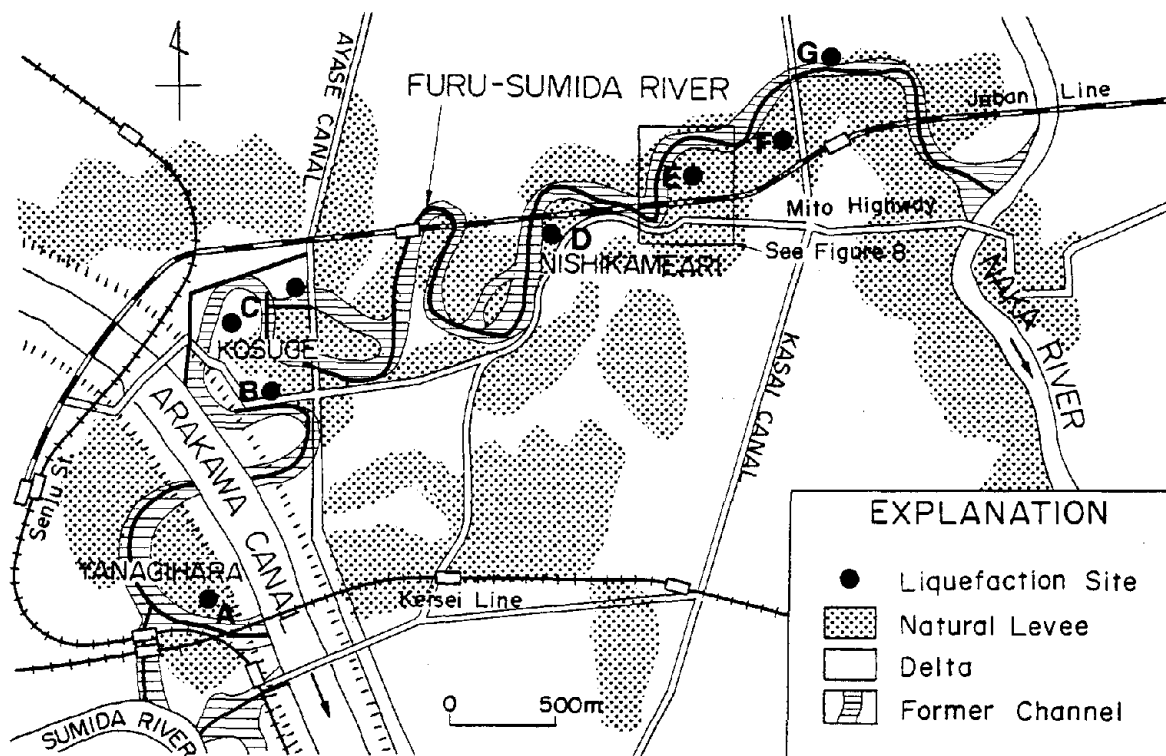


Fig.7 Map of Furu-Sumida River area, showing geographic and geomorphological features and locations of surfacial effects of liquefaction

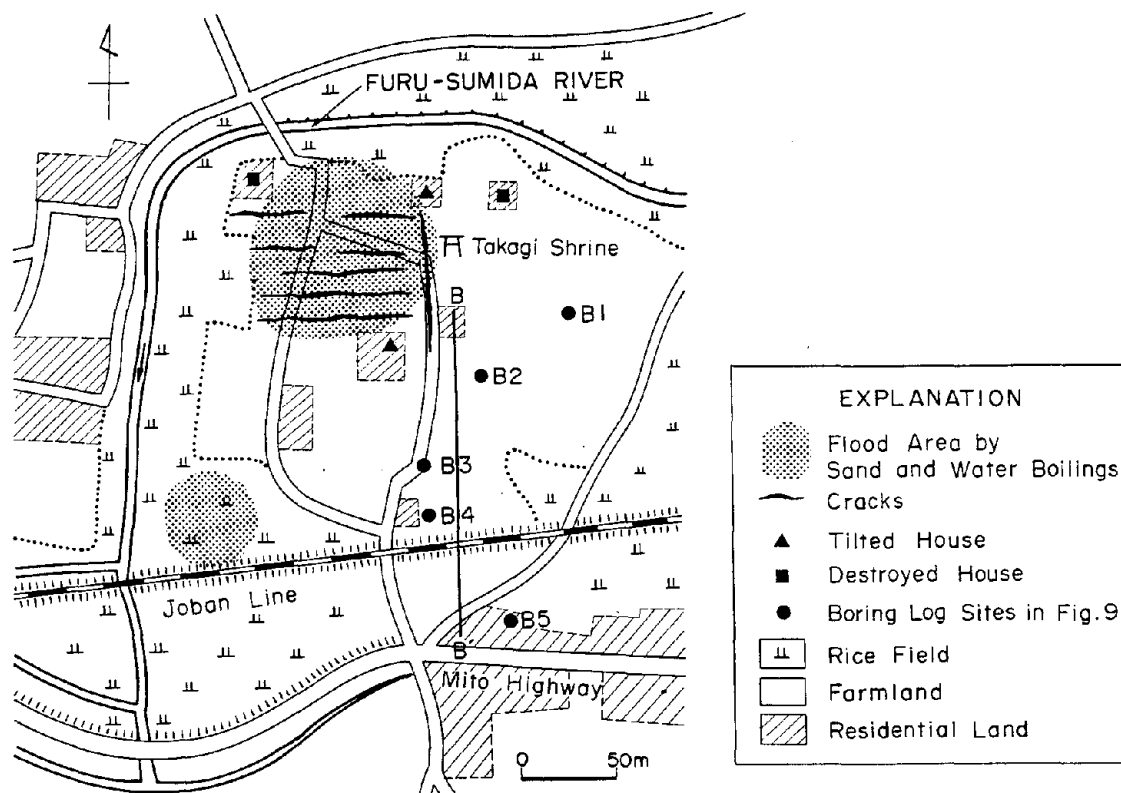


Fig.8 Map of Nishikameari, Tokyo showing geographic feature, locations of effects associated with liquefaction, and boring log sites

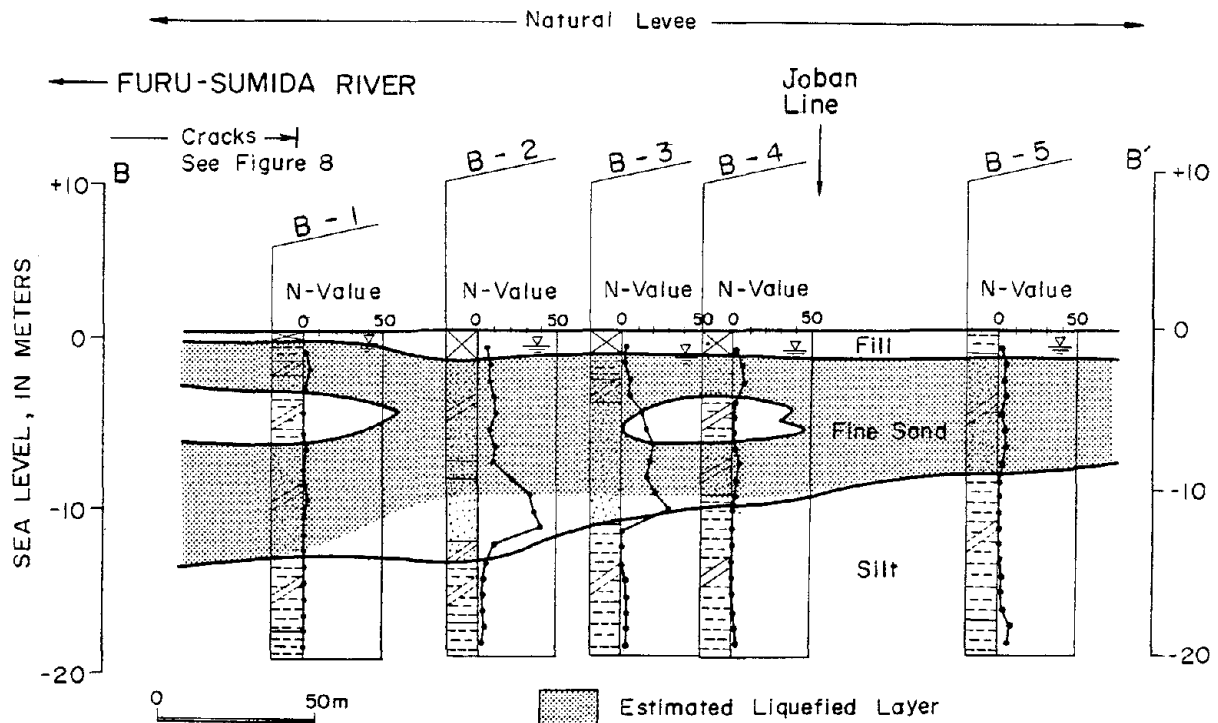


Fig.9 Cross section of sediment at Nishi-Kameari showing geotechnical features and estimated liquefied layer

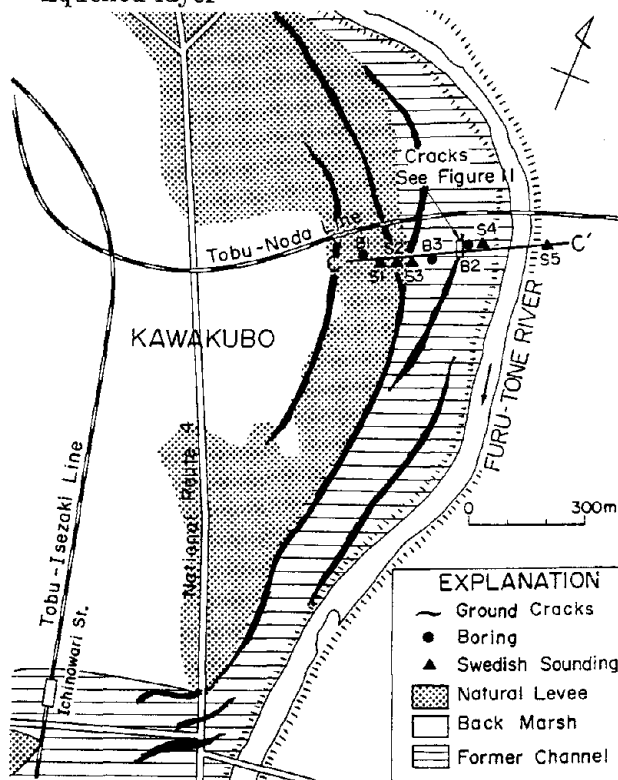


Fig.10 Map of Kawakubo area, Kasukabe City, showing geographic and geomorphological features, locations of surfacial effects of liquefaction and locations of borings and soundings

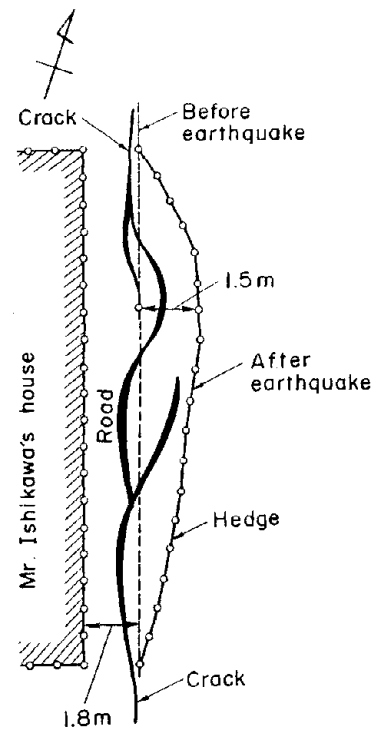


Fig.11 Ground cracks and displacements as large as 1.5m at Kawakubo (Geological Survey of Japan, 1925)

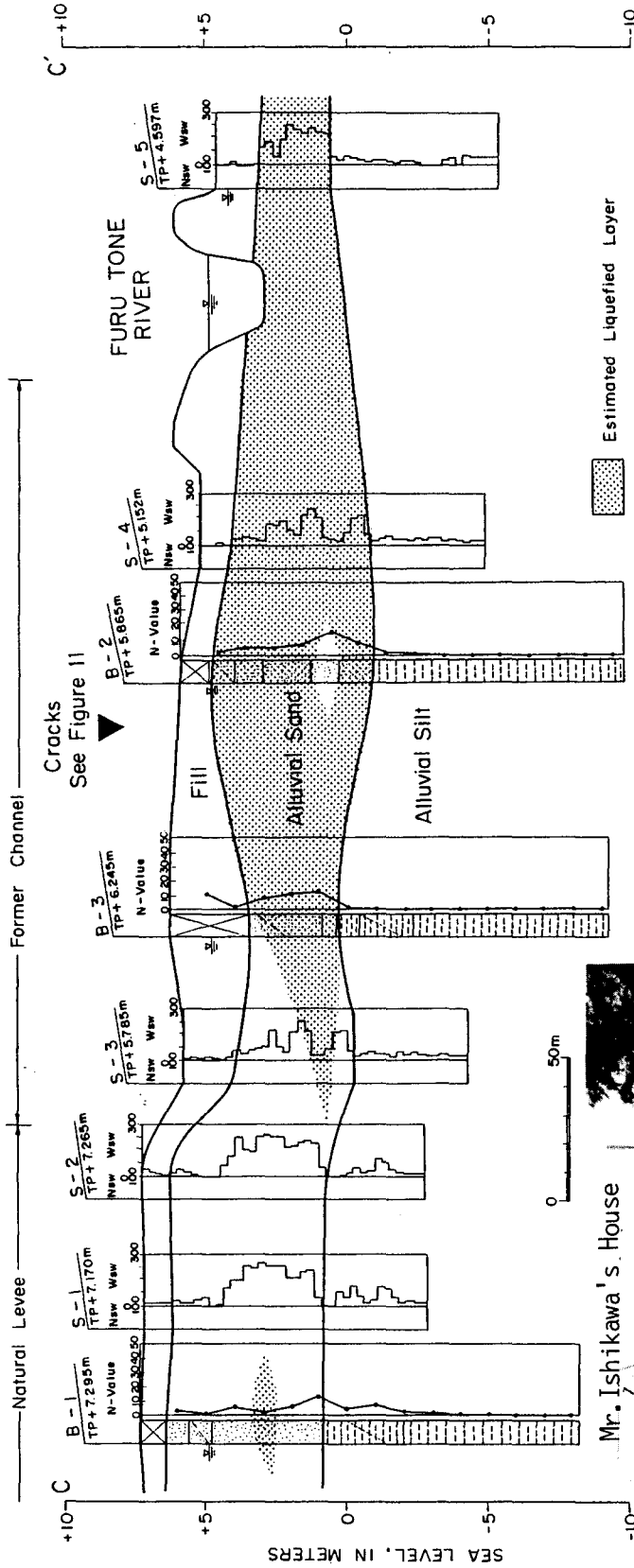


Fig.13 Cross section of sediment at Kawakubo showing geotechnical features and estimated liquefied layer

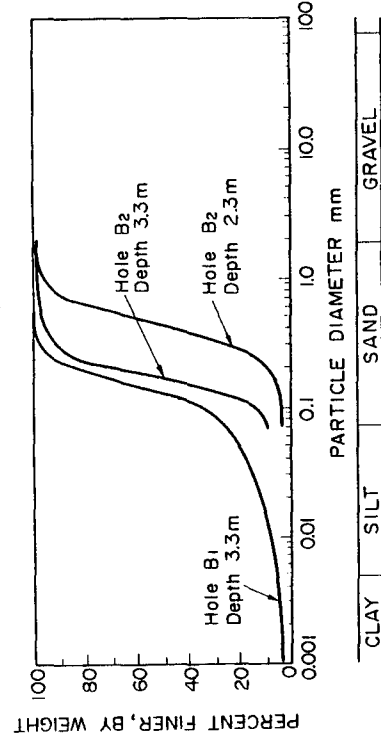


Fig.14 Grain size distribution curves from sand layer at Kawakubo

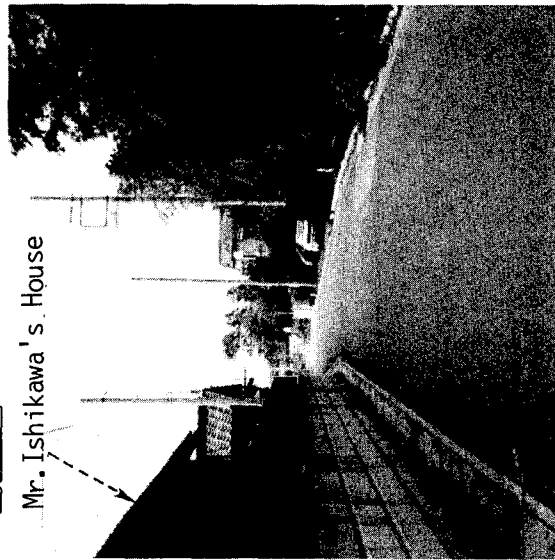


Fig.12 Present view of the site of Fig.11 showing horizontal displacement in road

## A CASE STUDY OF LARGE GROUND DEFORMATION DURING THE 1971 SAN FERNANDO EARTHQUAKE

T.D. O'Rourke  
Professor of Civil Engineering  
Cornell University

B.L. Roth  
Graduate Research Assistant  
Cornell University

M. Hamada  
Professor of Engineering  
Tokai University

## ABSTRACT

During the 1971 San Fernando earthquake, large ground deformations occurred at the Joseph Jensen Filtration Plant along the west side of the Upper Van Norman Reservoir. Numerous soil borings were performed near the Jensen Plant for the Metropolitan Water District of Southern California, making this one of the most densely probed locations of earthquake-induced ground movement. Recent analyses of aerial photographs taken before and after the earthquake have provided a comprehensive view of lateral and vertical movements at the site. In addition, a careful study of damage and displacements in subsurface structures at the Jensen Plant has disclosed detailed patterns of displacement and their effects on lifeline facilities.

This paper summarizes the ground movement patterns and related subsurface conditions at the time of the 1971 earthquake. The movements and borehole data are used to propose mechanisms of displacement and their relation to soil liquefaction. Ground movement effects on buried pipelines are discussed.

## INTRODUCTION

The 1971 San Fernando earthquake was an event of considerable engineering and seismological significance for at least three reasons. To start, the earthquake generated an unprecedented amount of data on strong ground and building motion. More strong motion records of engineering interest were acquired during this one earthquake than during the previous 39-year history of the U.S. cooperative network recording program<sup>1</sup>. From a geotechnical perspective, liquefaction-induced ground movements and slope failures caused substantial structural damage and left the lower San Fernando Dam precariously close to catastrophic failure<sup>2</sup>.

Perhaps the most distinctive feature of the earthquake was its influence on lifeline systems. Nearly 900,000 customers in the combined jurisdictions of the Los Angeles Division of Water and Power and Southern California Edison Company were affected by electrical power outages<sup>3,4</sup>. Telephone equipment in the General Telephone Company Sylmar central office was destroyed, disrupting the use of nearly 10,000 phones<sup>5</sup>. The damage was especially severe for buried conduits, including water supply, gas, liquid fuel, and wastewater pipelines.

This case history focuses on large ground deformations and related lifeline damage near the Upper Van Norman Reservoir. Descriptions are given of site conditions, subsurface soils and groundwater, and ground deformations. Information is presented on damaged pipelines, conduits, and foundations, and relationships are examined between large ground deformations and pipeline response.

## LOCATIONS OF LARGE GROUND DEFORMATION

A regional view of the areas affected by permanent ground deformations in relationship to the earthquake epicenter is shown in Figure 1. Although most surface effects were within the area of the figure, there were some instances of landsliding and ground movements located north and east of the epicenter. Traces of tectonic movement along the San Fernando fault are shown in Figure 1. The greatest length of surface fault breakage occurred at the base of the San Gabriel Mountains, east of the City of San Fernando.

Figure 2 shows two areas of large ground deformation which are the principal zones of interest in this case history. The locations are the area surrounding the Upper Van Norman Reservoir and the area along the Mission Wells and Sylmar segments of the San Fernando fault.

Considerable ground deformation caused by liquefaction was observed near the Upper Van Norman Reservoir. On the west side of the lake, cracks extended from the Van Gough School to the west edge of the Van Norman Lake. The most extensive ground cracks on the northeast side of the lake extended from the Juvenile Hall, through the Converter Station, to the east shore of the lake. Ground cracks caused by soil liquefaction also were seen around the tail race pond and near the San Fernando Powerhouse.

The area immediately west of the Upper Van Norman Reservoir is the location of the Joseph Jensen Filtration Plant, which is owned and operated by the

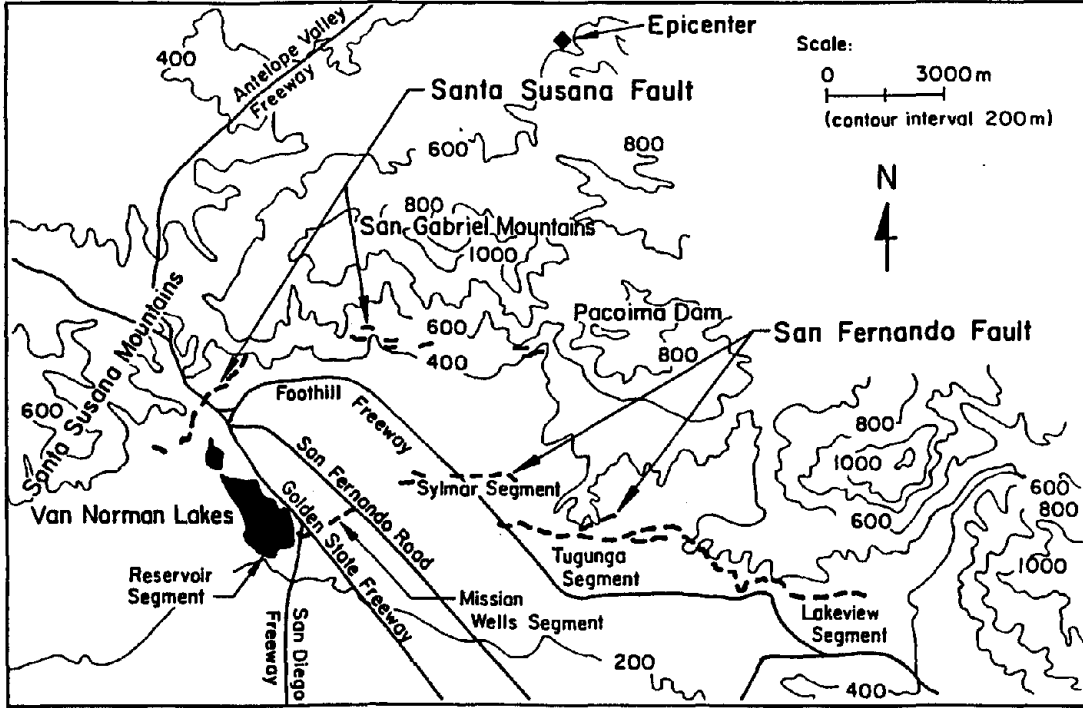


Figure 1. Region of Most Severe Earthquake Damage

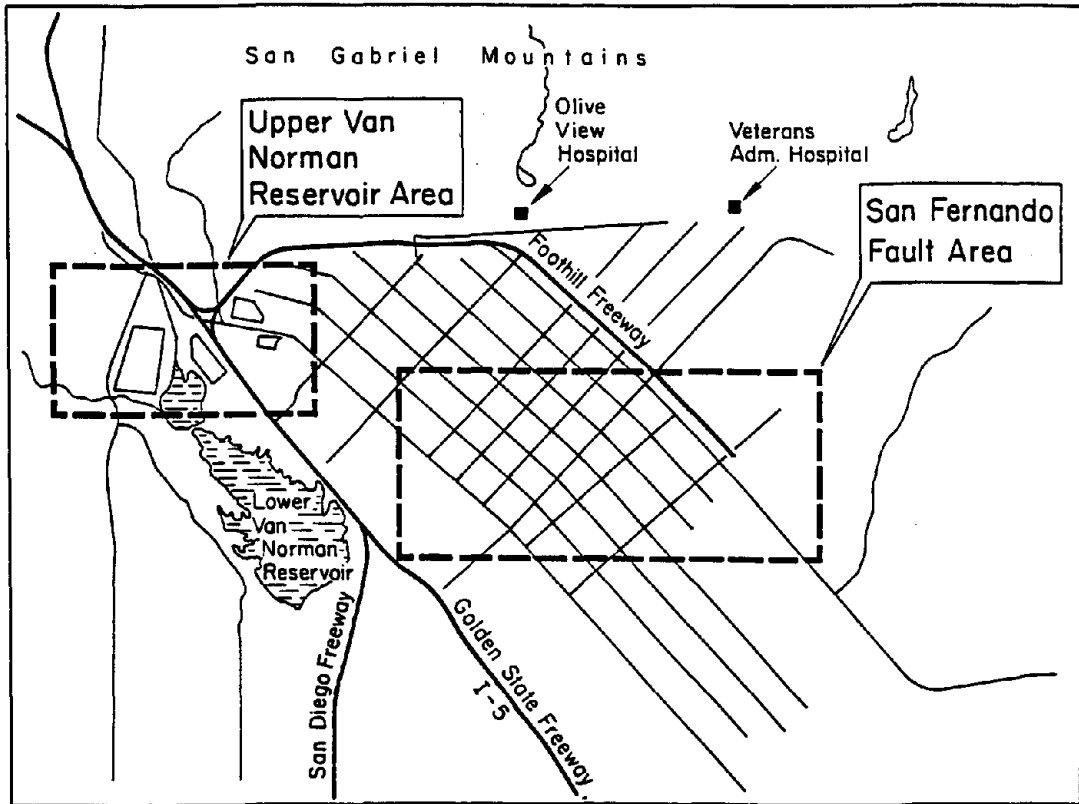


Figure 2. Areas of Large Ground Deformation

Metropolitan Water District of Southern California (MWD). At the time of the earthquake, the plant was under construction, with approximately 85% of the facilities complete<sup>6</sup>. As a result of the earthquake and associated ground deformations, substantial damage was sustained by the plant. The preconstruction exploration, post-earthquake investigations, and subsequent site improvement and new facilities studies represent a formidable body of technical papers and professional reports, making the Jensen Filtration Plant site one of the most intensely investigated and documented sites of earthquake-induced large ground deformation.

#### SURFICIAL GROUND MOVEMENTS

Figure 3 shows ground cracks and fissures, sand boils, and locations of soil heave along pressure ridges, as mapped and reported by Converse Davis and Associates<sup>7</sup>, Woodward-Lundgren<sup>8</sup>, and Youd<sup>9</sup>. Stereo pair air photo interpretation, in combination with a careful study of oblique aerial and ground level photographs, was used to supplement the information summarized on existing maps. Most of the large ground deformations and cracks were east of the north-south plant axis. Cracks to 240 mm wide were mapped, with a maximum vertical displacement of 490 mm. A pressure ridge about 330 m long, 1.5 m wide, and 0.3 to 0.6 m high developed at the base of the slope<sup>9,10</sup>. Several sand boils were seen at the base of the fill slope and in the southeast part of the site.

Figure 4 is a composite view of three vertical aerial photographs, taken after the earthquake, of the Jensen Filtration Plant and surrounding areas. Selected facilities and ground deformations are labeled in the figure.

#### CUMULATIVE LATERAL AND VERTICAL MOVEMENTS

There are three groups of structures at the Jensen Plant which provide records of cumulative lateral and vertical movement in the east-west direction. They include the 1) Finished Water Reservoir (FWR) and Overflow Conduit, 2) Filters, Settling and Mixing Basins, Main Control Building (MCB), and Influent Conduit, and 3) the Balboa Inlet Tunnel. As part of this study, site survey information, photos, field notes, and post-earthquake measurements of these structures were used to develop cumulative displacement plots, as shown in Figure 5.

Settlements and horizontal movements are plotted as dashed and solid lines, respectively. Much of the cumulative displacement was evaluated from measured joint separations and offsets along the Overflow Conduit, the portion of the Influent Conduit oriented east-west beneath the MCB, and the Balboa Inlet Tunnel. Lateral and vertical ground movements were transmitted directly to these buried structures, which responded much like linear extensometers by showing relative displacements at joints. The resulting cumulative displacement plots in Figure 5 indicate how movements were distributed across the facilities and provide indirect evidence for the distribution of permanent ground deformation.



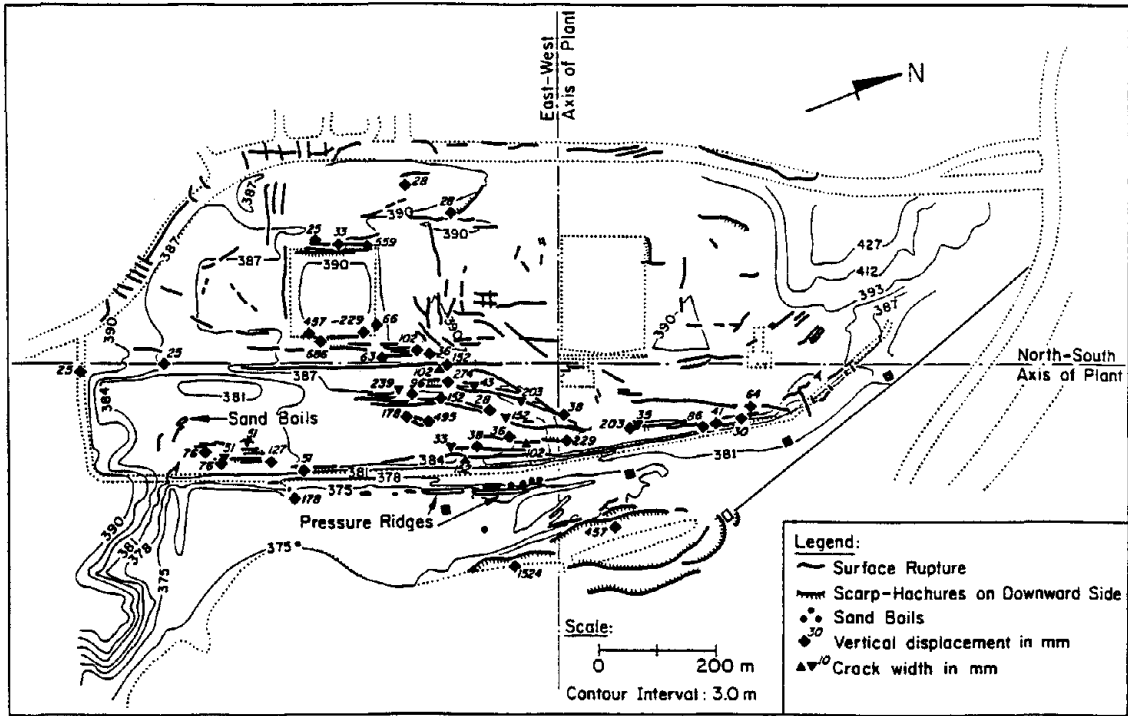


Figure 3. Map of Surficial Ground Cracks, Sand Boils, and Pressure Ridges near Jensen Filtration Plant

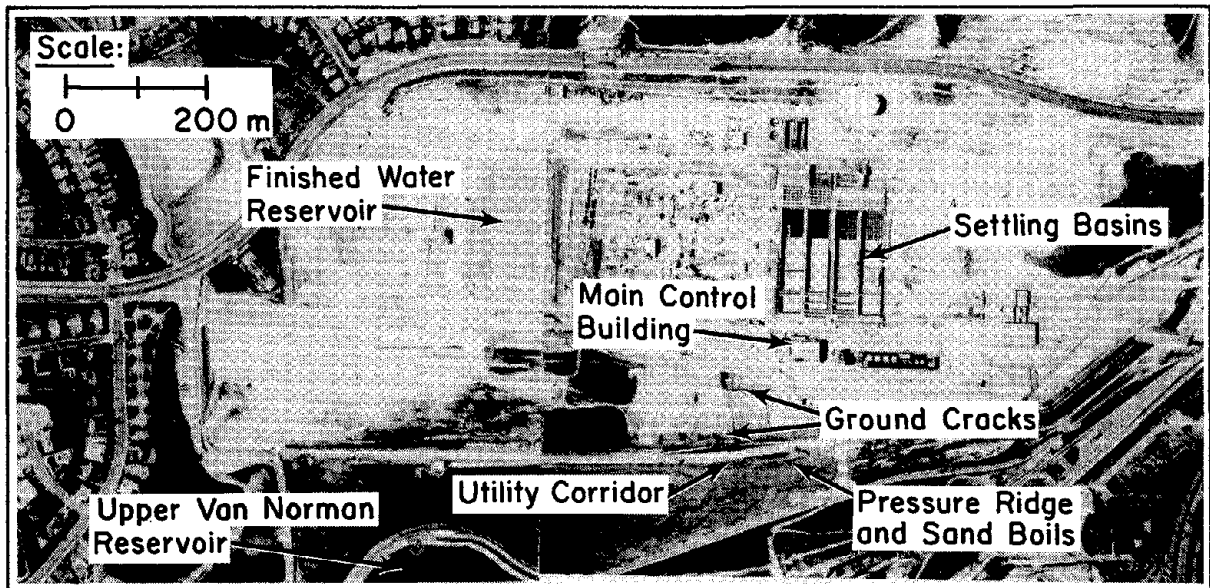


Figure 4. Aerial View of Jensen Filtration Plant

## AIR PHOTO AND OPTICAL SURVEY MEASUREMENTS

Photogrammetric analyses were performed by Japanese researchers on air photos taken before and after the earthquake. The results of these analyses are shown in Figure 6 as vectors of horizontal movement and measurements of settlement and heave. Optical survey measurements performed by MWD also are shown at various locations. For example, lateral offsets surveyed along the north-south plant axis and settlements at several key structures are included in the figure.

The air photo analyses show lateral movements along the Utility Corridor, typically 2 to 3 m, in an easterly direction toward the reservoir. At the eastern terminus of the Outlet Conduit, air photo measurements show lateral movements of 1.3 to 2.2 m, which agrees reasonably well with the total cumulative movement shown at this location in Figure 5.

As an additional check on accuracy, measurements of the alignment along the eastern edge of the Utility Corridor were made from high quality vertical air photos and compared with LADWP records of the as-built alignment. The comparison showed an eastward displacement of the alignment of approximately  $2 \text{ m} \pm 1 \text{ m}$ .

## SUBSURFACE CONDITIONS

Published accounts of the soils and groundwater conditions at the Jensen Filtration Plant<sup>10,11</sup> disclose three types of deposits: artificial fill, alluvium, and weathered to intact sandstone of the Saugus Formation. The eastern portion of the site was filled with materials described as mixtures of silty sands, sandy silts, and sands with gravel and occasional zones of silt and clayey silt<sup>10</sup>. The thickness of the fill varies from zero on the west side of the site to 17 m on the east.

As part of this study, 130 boring logs and 62 CPT soundings were reviewed, representing over 2500 m of probing performed for site preparation, post-earthquake investigations, and site expansion evaluations.

Figure 7 shows a plan view of selected borehole and CPT soundings used to delineate subsurface conditions. The borings and soundings are identified in the legend according to the various engineering studies for which they were performed. Figures 8 through 10 show soil profiles along transverse cross-sections as interpreted from the borehole and cone penetration data. The SPT and CPT values registered in the figures were acquired from tests performed according to ASTM D1586 and D3441<sup>12</sup>, respectively.

Water tables are shown on the soil profiles for two different times. Groundwater levels measured during post-earthquake investigations are shown as open triangles. In general, they varied from approximately El 370 to 375. Preconstruction water tables are shown in the soil profiles as solid triangles, and are indicative of a slightly higher level. Dewatering is the most likely reason for the relatively low levels during construction<sup>11</sup>. In general, it appears that the water table at the time of the earthquake was approximately at the contact between the fill and alluvium under those portions of the site east of the north-south plant axis.

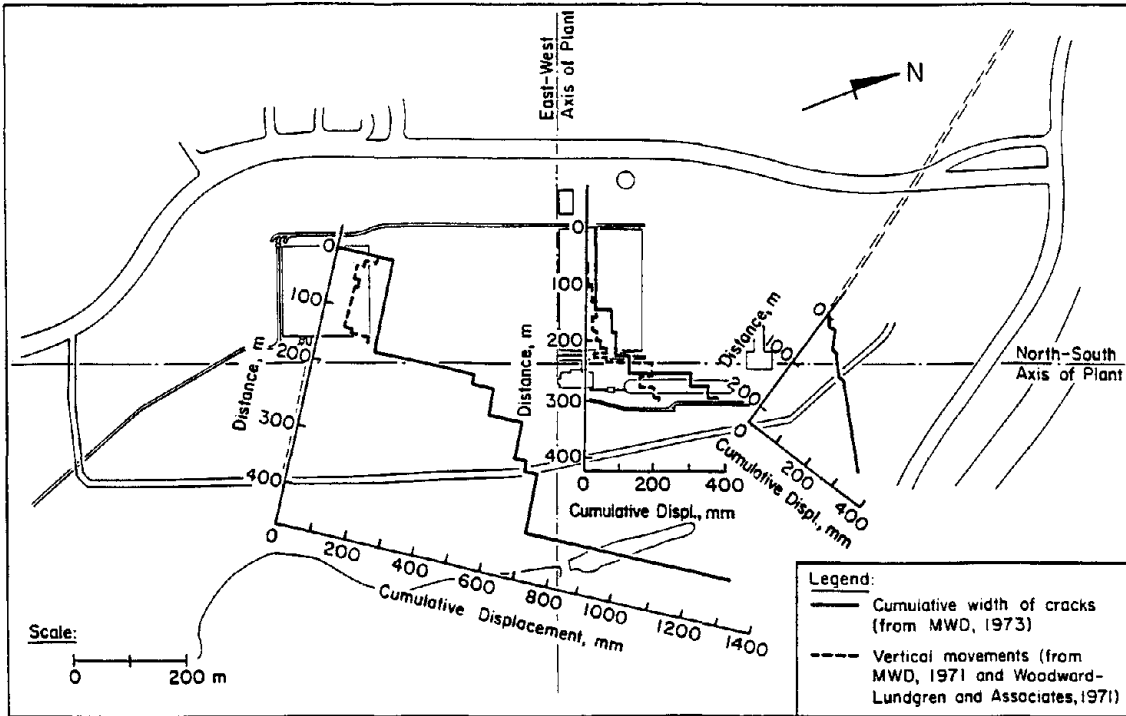


Figure 5. Cumulative Displacements Across the Jensen Plant

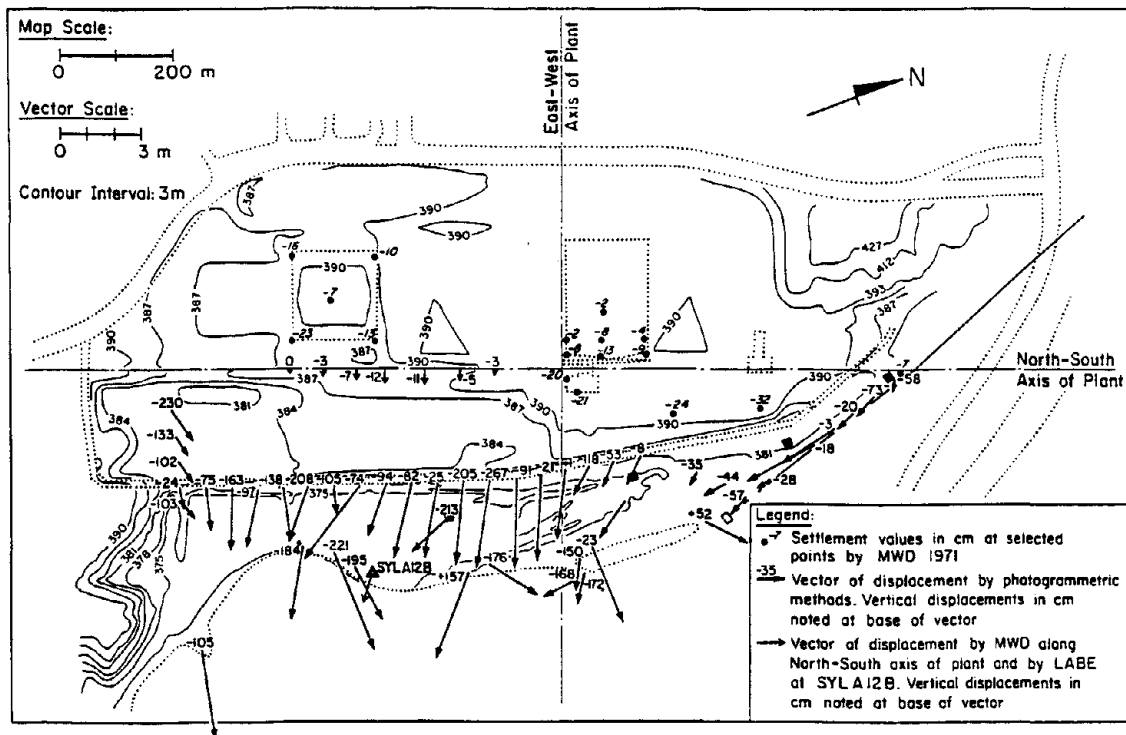


Figure 6. Displacements Determined from Air Photo Analyses and Optical Surveys, Jensen Plant

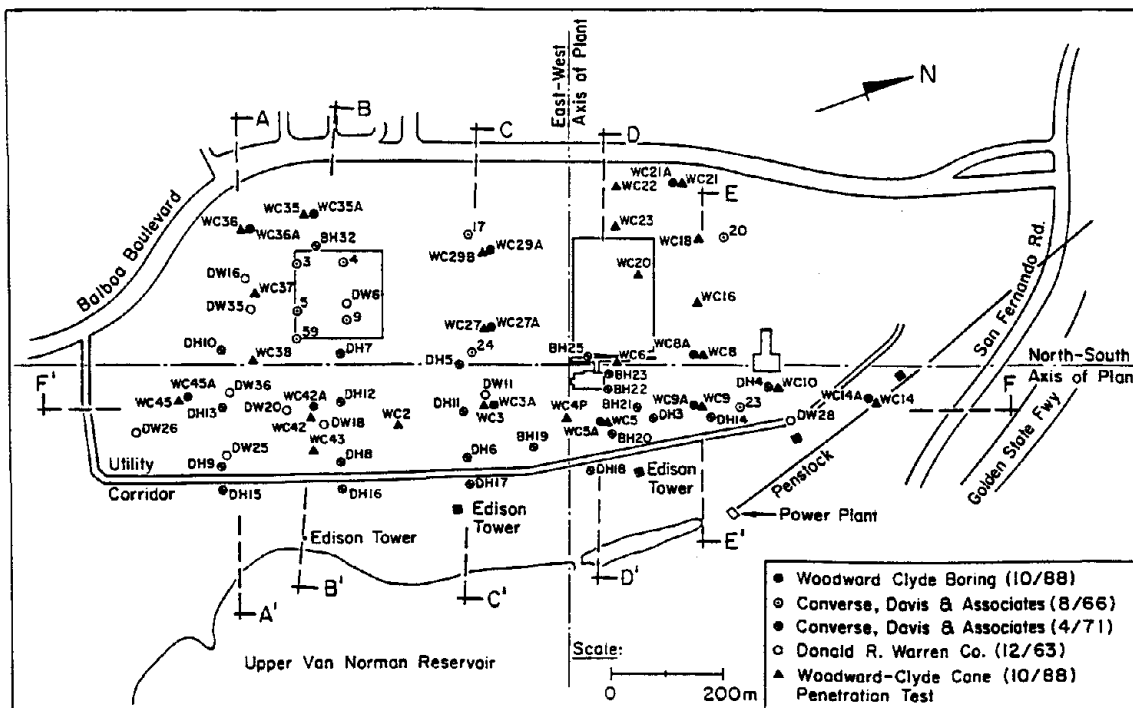


Figure 7. Locations of Soil Borings and Soundings at the Jensen Plant

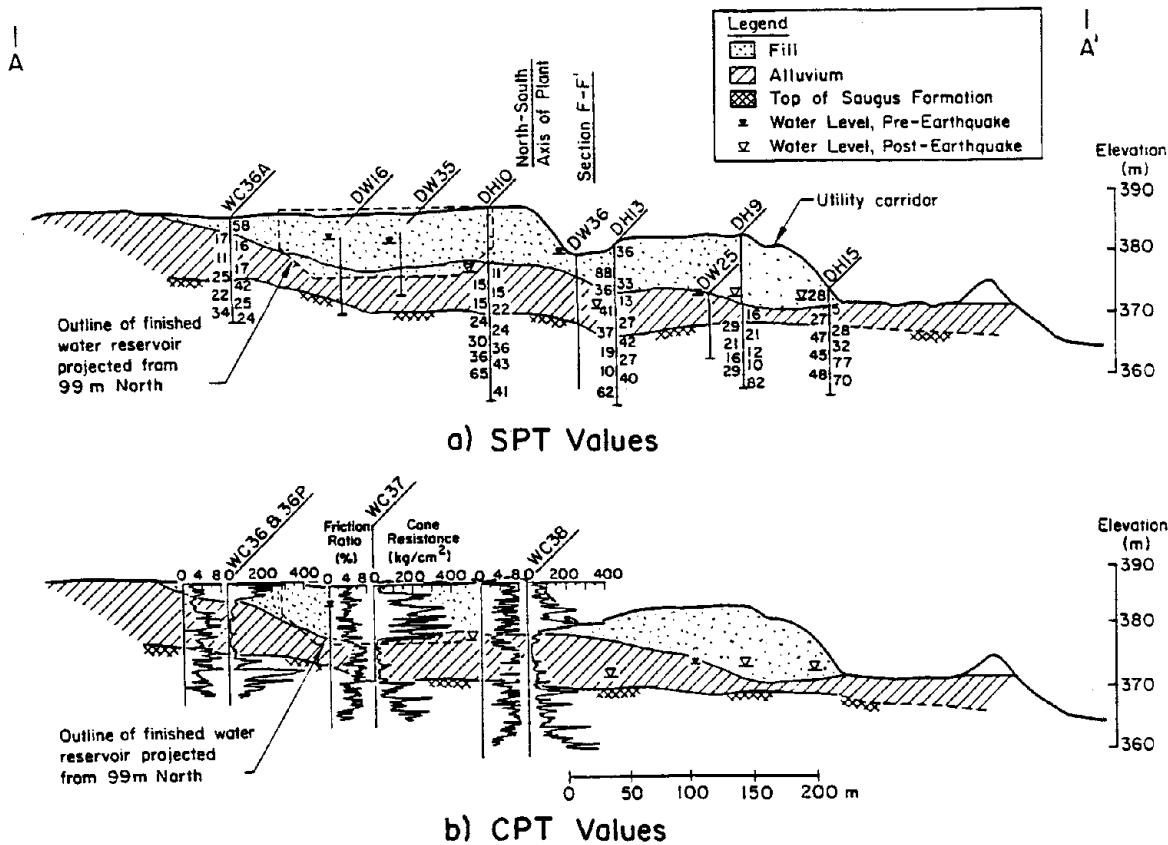


Figure 8. Soil Profile at Cross-Section A-A', Jensen Plant

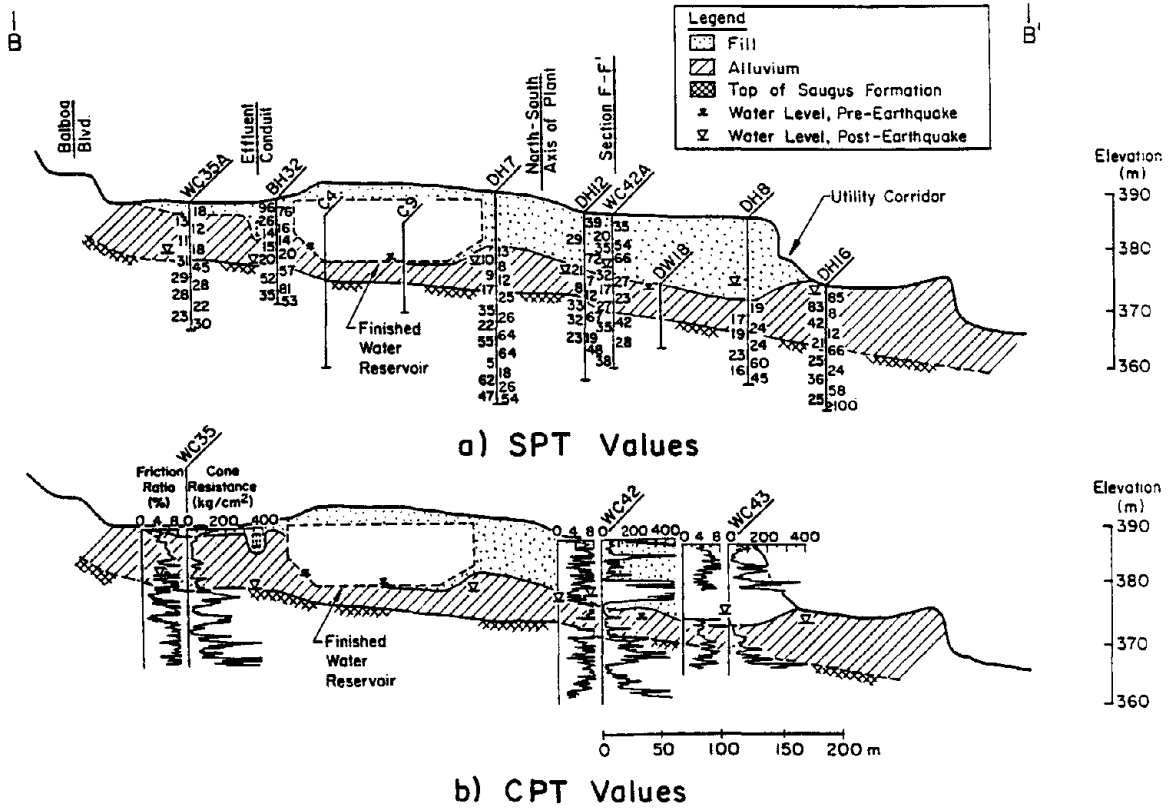


Figure 9. Soil Profile at Cross-Section B-B', Jensen Plant

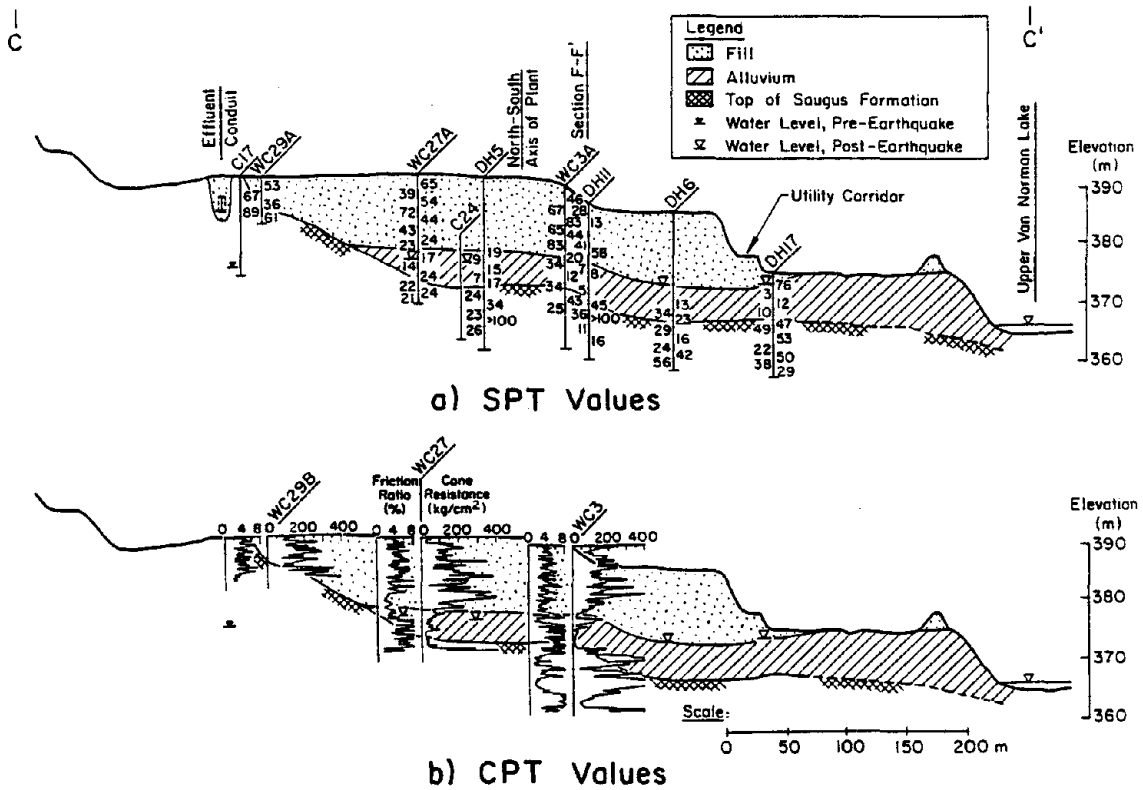


Figure 10. Soil Profile at Cross-Section C-C', Jensen Plant

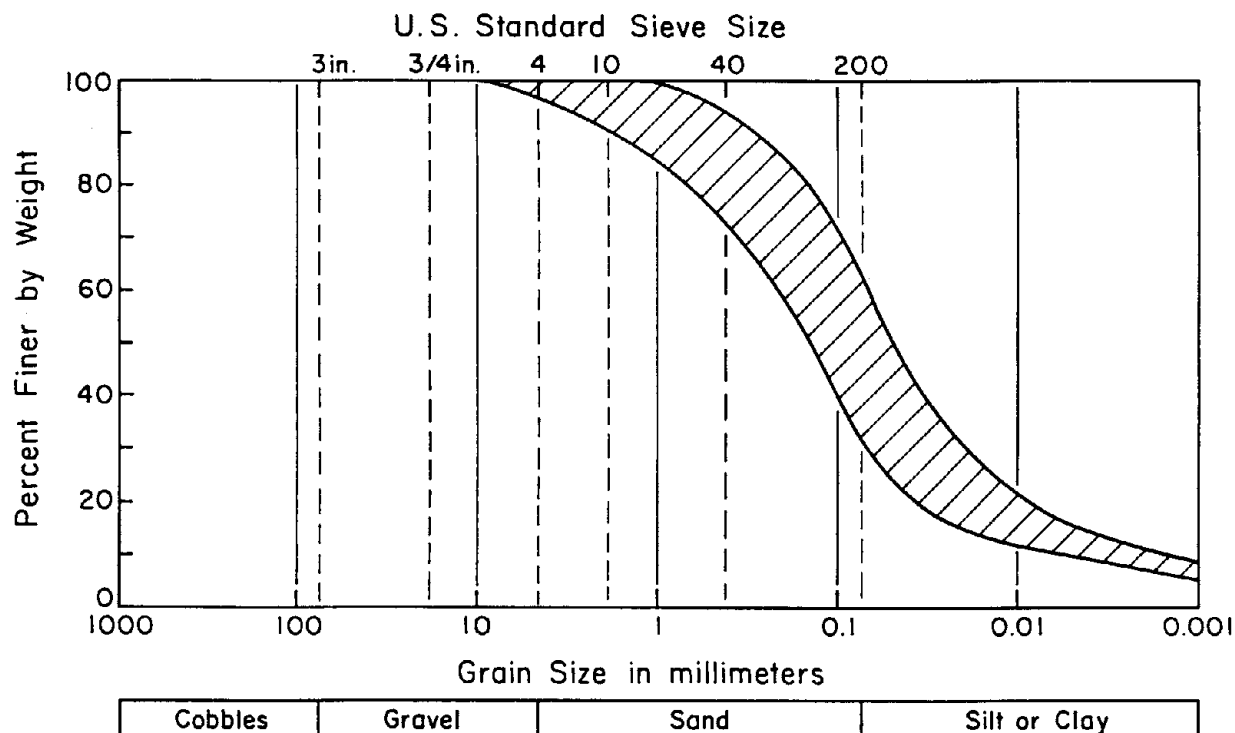


Figure 11. Typical Grain Size Distribution Curves for Alluvial Soils at Jensen Plant

The alluvium, as indicated by the low SPT and CPT measurements, was in a relatively loose saturated state, and therefore subject to liquefaction. Soil liquefaction has been proposed by several investigators<sup>9,10</sup> as the principal cause of large ground deformations at the Jensen Plant. The alluvium contains a substantial amount of fine grained material, generally consisting of 30 to 60% by weight of fines<sup>10</sup>. Typical grain size distribution plots are shown in Figure 11. The alluvium increases in thickness north to south across the site, which correlates closely with the trends of increasing ground deformation. As shown in Figure 10, the alluvium is locally thick near the central part of the plant, about 100 m south of the MCB. This was the location of the largest and most severe ground deformation, as evidenced by the ground cracks and measured displacements shown in Figures 3 and 6, respectively.

A three-dimensional perspective of the zone of loose alluvium at the Jensen Plant can be gained by examining Figures 12 and 13. Figures 12 and 13 show the depth to the bottom and thickness of the loose, saturated alluvium, respectively. Vectors of displacement, mapped by photo-grammetric techniques, also are shown in the figures.

The bottom of the loose alluvium was established on the basis of the boring log descriptions, SPT and CPT data. The base of the loose alluvial soils usually coincided with the top of the Saugus Formation. However, in some cases, a meter or so of the upper surface of the Saugus Formation was highly weathered and thus was considered to behave as loose soil. The highly weathered Saugus Formation

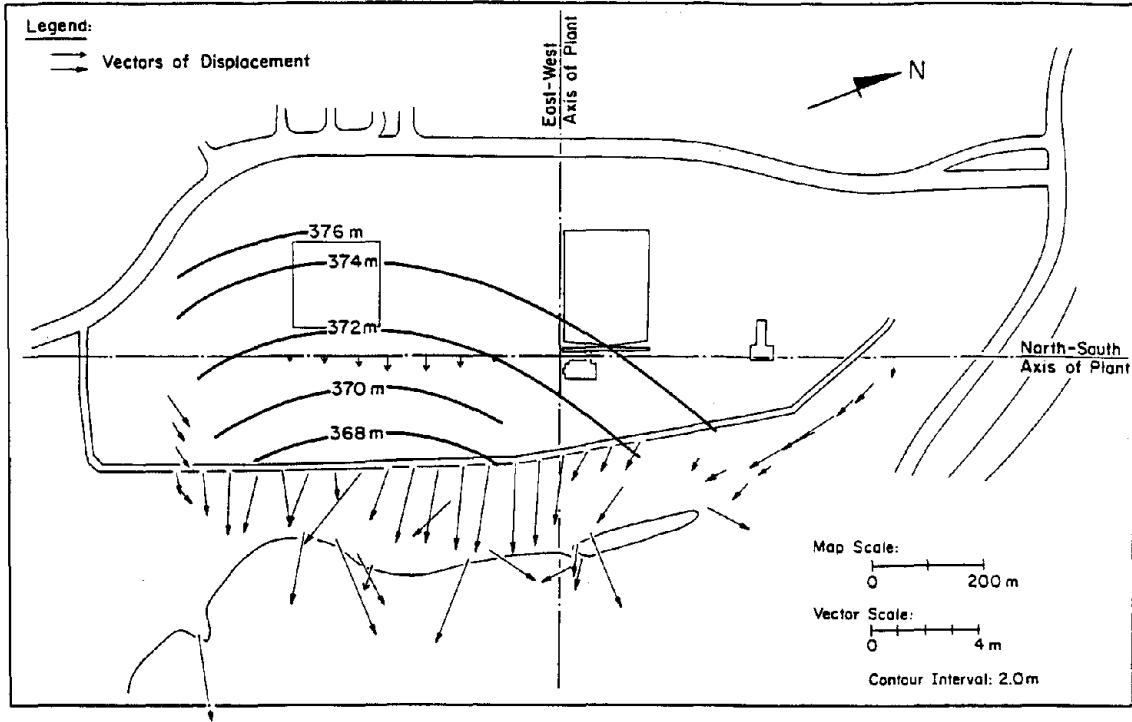


Figure 12. Contours of Equal Elevation for the Base of Loose Saturated Alluvium at the Jensen Plant

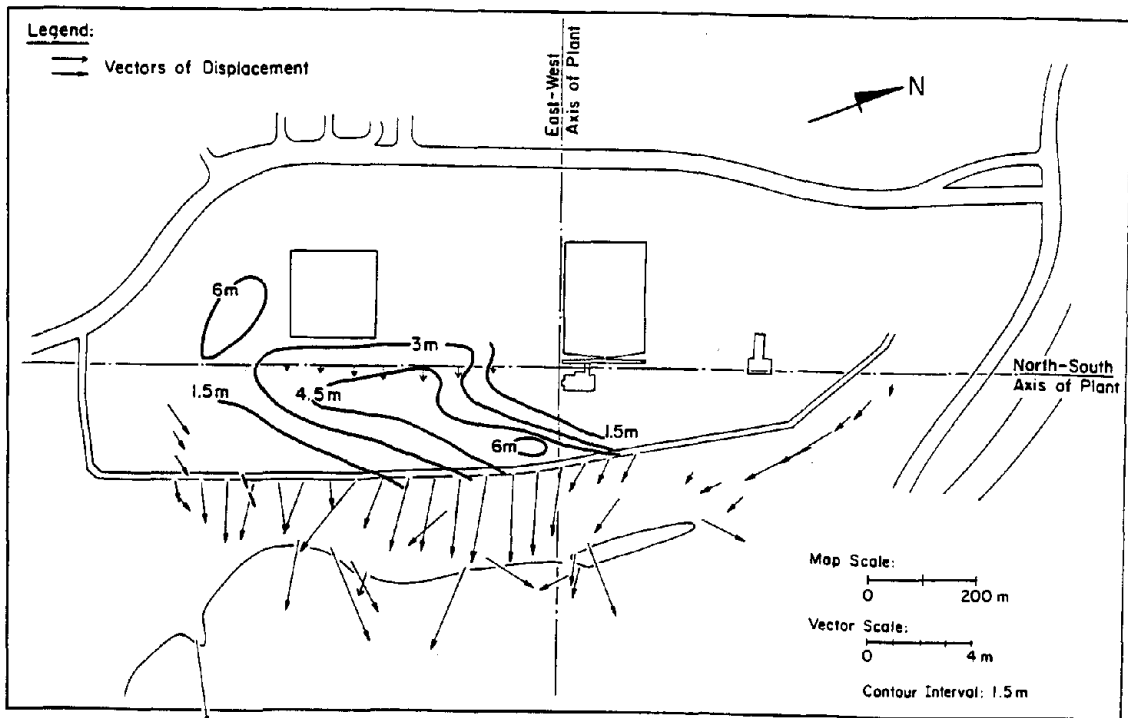


Figure 13. Contours of Equal Thickness of Loose Saturated Alluvium at the Jensen Plant

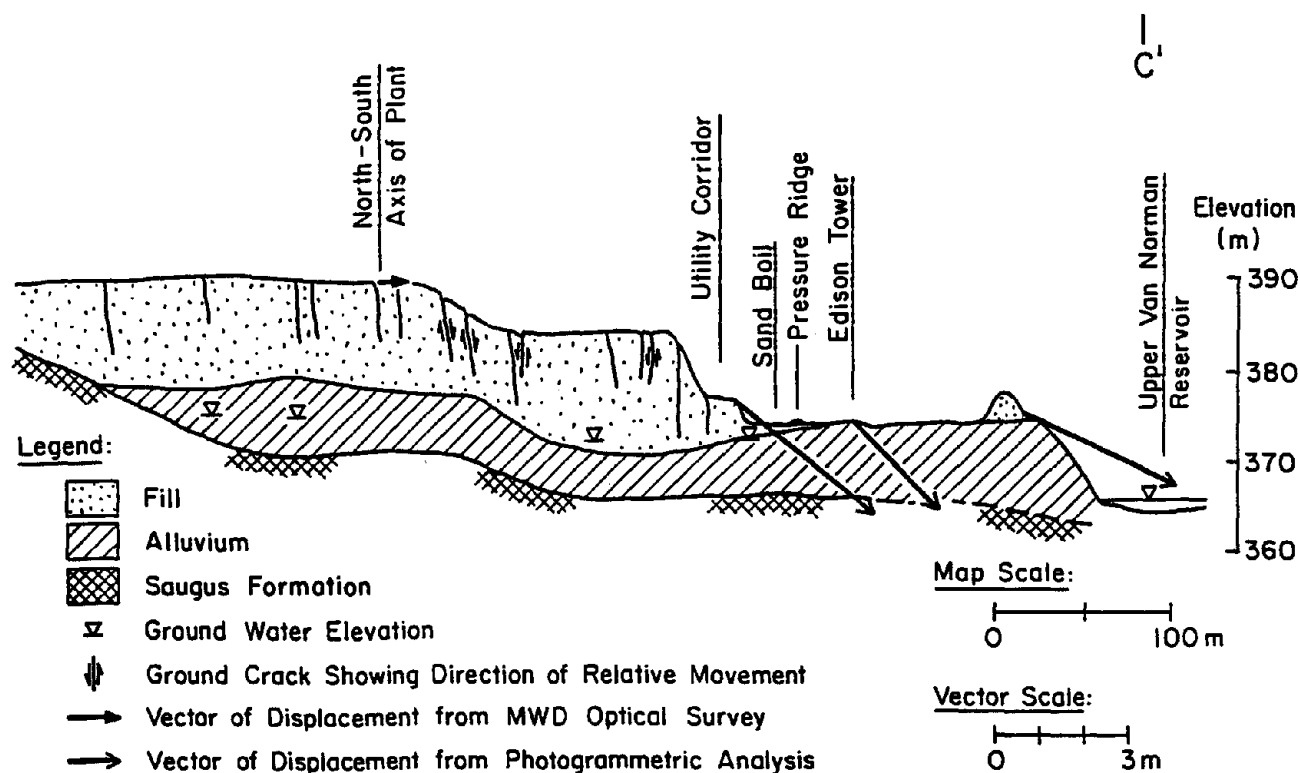


Figure 14. Cross-Section of Large Ground Deformation at Jensen Plant

was most prevalent near the intersection of the north-south and east-west plant axes. The corrected SPT values are as low as 7 within the upper 1 m of the Saugus Formation at this location. The contours in Figure 12 show the elevation above sea level of the base of the loose alluvium. It is apparent that this basal surface slopes downward toward the Upper Van Norman Reservoir at an angle of about 1.0 to 2.0°. Moreover, the contours show a concave pattern with greatest depth and slope near the central part of the site, where the most severe ground deformations were mapped.

Figure 13 shows contours of constant thickness for the zone of loose, saturated alluvium. The thickness of this zone was determined from borehole records, SPT and CPT data, and water level measurements, and corresponds roughly with the thickness of alluvium below the water table. The greatest thickness of loose, liquefiable alluvium is located under the zone of largest permanent ground deformation.

#### CHARACTERISTICS OF LARGE GROUND DEFORMATION

Figure 14 shows a detailed view of the deformational features of the lateral spread at the Jensen Plant. This cross-section is at Section C-C' through the zone of largest ground deformation. The open-headed vectors in the figure represent the horizontal and vertical components of displacement as determined by photogrammetric analyses. The solid-headed vector represents the horizontal



and vertical component of displacement as determined by optical surveys conducted by MWD<sup>9</sup>. Figure 12 also shows the ground cracks projected below the ground surface and an exaggerated scale profile of the sand boils and the pressure ridge.

The landslide has been described by Converse, Davis, and Associates<sup>7</sup> as liquefaction of the loose alluvium, followed by eastward movement of the east face of the fill slope and subsequent graben formation in the areas west of the fill slope. The vectors of movement east of the utility corridor are approximately the same magnitude, implying that this section moved as a discrete unit. The thickest deposits of loose saturated alluvium are located beneath this block, as shown by the contours presented in Figure 13. Moreover, this location of thick alluvium corresponds with the debris deposits shown in historic photographs, as well as former stream channels.

As the eastern part of the soil deposits moved toward the Upper Van Norman Reservoir, tensile stresses developed in the fill which were relieved by cracks, joint openings in conduits, and grabens. Further west, in the zone where the Influent Conduit, MCB, and the west edge of the FWR are located, shaking and loss of lateral support led to settlement and eastward lateral movement. The zone of ground deformation was, thereby, effectively extended into other areas of the fill by the relief of horizontal restraint at the margins of the lateral spread. This mechanism, where loss of lateral support and continued slumping occur beyond the zone of permanent lateral spreading, has been described as marginal slumping by O'Rourke and Lane<sup>13</sup>.

#### PIPELINE DAMAGE AT UPPER VAN NORMAN RESERVOIR

Figure 15 shows a plan view developed by O'Rourke and Tawfik<sup>14</sup> of the area west of the Upper Van Norman Reservoir on which are superimposed ground ruptures associated with liquefaction-induced slope failures in this locality. The locations of pipeline damage were determined from repair records provided through the courtesy of the LADWP and the Getty Oil Company. The information in the repair records was supplemented by discussion with utility personnel. Table 1 summarizes information about the pipelines that includes dimensions, installation date, composition, joint type, coating, depth of soil cover, and nominal operating pressure at the time of the earthquake. The outside diameter (O.D.) and wall thickness for each pipe are listed. Each pipeline is numbered for purposes of referencing the pipeline as shown in the figure with information summarized in the table. In general, the pipelines were buried in medium to dense sand and silty sand above the water table. Transmission pipelines for natural gas, liquid fuel, and water were involved, representing different dimensions, joint design, operating pressures, welding practices, and age. Pipelines operated by the Los Angeles Department of Water and Power and the Southern California Gas Company are prefaced by DWP and SCG, respectively.

Most pipelines in the utility corridor were not damaged, including the three lines operated by the Southern California Gas Company and one operated by the Mobil Oil Corporation (see Figure 13 and Table 1). Some gas pipelines were cut and rewelded after the earthquake, principally to relieve residual stresses and make adjustments for deformations caused by the ground movements. Pipeline 8,

Table 1. Information Summary for Pipelines Affected by Ground Movements

Number	Pipeline	Dimensions	Installation Date	Composition	Joints	Coating	Depth of Cover	Operating Pressure
1	DWP Granada Trunk Line	1260mm O.D.; 6.4mm wall thickness	1967	Steel, ASTM A-283 Grade C	Arc welded slip joints on 9m centers	Cement, 25.4mm thick	1.0m	0.7-1.4MPa
6a, 6b	SCG Lines 3000 & 3003	760mm O.D.; 9.5mm wall thickness	1966	Steel, X-52 Grade	Arc welded girth joints on 12m centers	Asphalt, fiber-glass, asbestos felt	1.0-1.2m	1.4-3.2MPa
7	SCG Line 120	560mm O.D.; 7.2mm wall thickness	1966	Steel, X-52 Grade	Arc welded girth joints on 12m centers	Asphalt, fiberglass and asbestos felt	1.0-1.2m	1.4MPa
8	Getty Oil Company Line	170mm O.D.; 7.2 mm wall thickness	1966	Steel, API Grade B	Arc welded girth joints on 12m centers	Coal tar enamel & fiberglass	1.0-1.2m	0.7-1.0MPa
9	Mobil Oil Corporation Line	400mm O.D.; 7.9mm wall thickness	1966 1969	Steel, X-52 Grade	Arc welded girth joints on 12m centers	Coal tar enamel & fiberglass	1.0-1.2m	No internal pressure at time of earthquake
10	DWP Plant Connection	1524mm O.D.; 9.5mm wall thickness	1970	Steel, ASTM A-283 Grade C	Arc welded slip joints on 9m centers	0.6m thick reinforced concrete encasement	2.0m	No internal pressure at time of earthquake

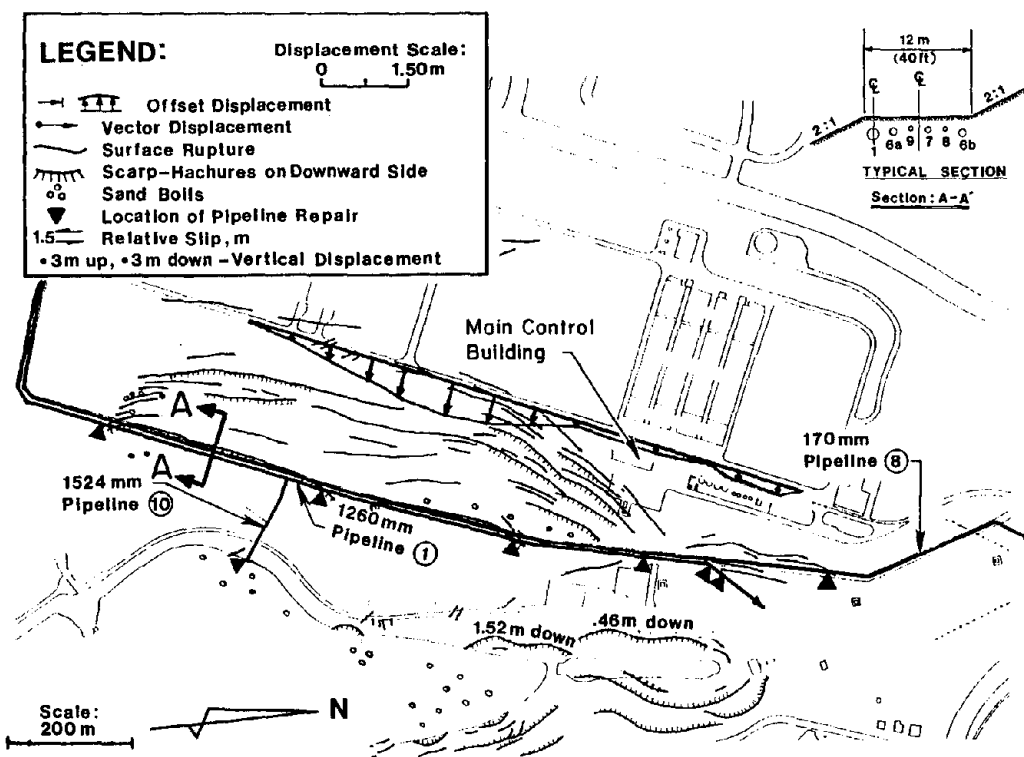


Figure 15. Locations of Pipeline Repair, West Side of Upper Van Norman Reservoir

operated by the Getty Oil Company, failed in tension across a weld at the northern boundary of the landslide area.

The most prominent damage was sustained by Pipeline 1. Damage to this pipeline, known as the Granada Trunk Line, occurred in three principal ways, including deformations at a bend, welded slip joints, and mechanical couplings. The most severe damage occurred where the pipeline branches to the northeast and leaves the utility corridor. The combined bend at this location involves a change in both horizontal direction and vertical elevation as the pipeline angles down the 1V:2H slope of the utility corridor embankment. Severe bending deformation occurred near this location, with approximately 0.5 m of transverse displacement over an axial distance of 3 to 4 m. Immediately to the northeast, a mechanical coupling had been installed with a special harness to allow up to 50 mm of axial displacement. The coupling was severely battered and compressed. Its harness was deformed substantially. Damage to another mechanical coupling was observed at the southernmost boundary of the landslide area. South of the combined bend, there were several locations of severe compressive wrinkling at welded slip joints. The Subcommittee on Water and Sewerage<sup>6</sup> reports that there were eight slip joints damaged. Only three locations of repair between the combined bend and the damaged mechanical joint at the southern boundary of movement could be confirmed by reference to repair records, and these are shown in the figure. Discussions with utility engineers indicate that most of the damaged slip joints were located within 300 m south of the combined bend.

Pipeline 10 was damaged at its eastern end. This pipeline transports water from the Overflow Conduit of the filtration plant to the Upper Van Norman reservoir. The Overflow Conduit was affected by ground movements in two areas, including a 0.6-m opening about 150 m west of its connection with Line 10 and a 0.3-m opening near its western connection with the Finished Water Reservoir. Pipeline 10 was damaged at two mechanical couplings that joined the pipeline to a discharge structure at the west side of the reservoir. The couplings were severely battered and compressed.

#### CONCLUSIONS

The 1971 San Fernando earthquake provides the opportunity to relate large ground deformation, various soil conditions, and the response of buried pipelines of different size, composition, and age. Of particular interest is the area west of the Upper Van Norman Reservoir, where liquefaction-induced soil movements subjected six different pipelines to virtually the same pattern of ground displacement. Both the construction of the lines and distribution of ground movements are well defined. A reliable record of pipeline performance has been developed in which the locations and specific characteristics of damage are described. Moreover, the record of response involves both failed pipelines and those which were able to sustain large differential movement. The information in this case history is sufficiently detailed to characterize the soil properties, deformation patterns, and pipeline characteristics such that analytical models can be tested against the observations, and the field data used as a basis for verifying or modifying analytical methods.

The case history includes several implications for earthquake resistance pipeline design. The pipelines which failed near the Upper Van Norman Reservoir either

were constructed with welded slip joints or made of steel with relatively low yield stress. Compressive failures of slip joints in the Granada Trunk Line underscore the vulnerability of these joints to compressive ground strains and bending, which can induce pipe wall wrinkling on the compressive side of the longitudinally flexed pipe.

Steels with relatively low yield stress, particularly those manufactured over 20 to 30 years ago, may be characterized by a relatively flat slope when tensile stress is plotted with respect to strain in the post-yield range of axial deformation. O'Rourke, et al.<sup>15</sup> have shown that the post-yield slope is critically important for the level of maximum strain in the steel when a buried pipeline is subjected to tensile ground movements. In contrast, the steeper post-yield slopes of high stress steels, such as the X-52 steel used for construction of the SCG and Mobil pipelines on the west side of the Upper Van Norman Reservoir, would be able to accommodate ground movement with significantly lower levels of local strain. These pipelines were able to sustain the large ground deformations.

#### ACKNOWLEDGMENTS

The research on which this paper was based was sponsored by the National Center for Earthquake Engineering Research in Buffalo, NY under Project Number 883014. The authors wish to thank the Metropolitan Water District of Southern California for sharing information concerning the 1971 San Fernando earthquake.

#### REFERENCES

1. Cloud, W. K. and D. E. Hudson, "Strong Motion Data from the San Fernando, California Earthquake of 9 February, 1971," San Fernando, California Earthquake of 9 February, 1971, Bulletin 196, California Division of Mines and Geology, Sacramento, CA, 1975, pp. 273-302.
2. Cortwright, C., "Effects of the San Fernando Earthquake on the Van Norman Reservoir Complex," San Fernando, California Earthquake of 9 February, 1971, Bulletin 196, California Division of Mines and Geology, Sacramento, CA, 1975, pp. 395-406.
3. Wong, P. J., "Earthquake Effects on Power System Facilities of the City of Los Angeles," San Fernando, California Earthquake of February 9, 1971, Vol. 2, U.S. Department of Commerce, N.O.A.A., Washington, D.C., 1973, pp. 9-25.
4. Southern California Edison Company, "Earthquake Damage to Southern California Edison Power Facilities," San Fernando, California Earthquake of February 9, 1971, Vol. 2, U.S. Department of Commerce, N.O.A.A., Washington, D.C., 1973, pp. 27-38.

5. Steinbrugge, K. V., E. E. Schaader, H. C. Bigglestone, and C. A. Weers, San Fernando Earthquake, February 9, 1971, Pacific Fire Rating Bureau, 1971, 93 p.
6. Subcommittee on Water and Sewerage Systems, "Earthquake Damage to Water and Sewerage Facilities," San Fernando, California Earthquake of February 9, 1971, Vol. 2, U.S. Department of Commerce, N.O.A.A., Washington, D.C., 1973, pp. 75-193.
7. Converse, Davis, and Associates, "Interim Report: Soil and Geologic Investigation, San Fernando Earthquake, Joseph Jensen Filtration Plant Near Sylmar, California," Unpublished Report Prepared for the Metropolitan Water District of Southern California, Pasadena, CA, April 30, 1971.
8. Woodward-Lundgren and Associates, "Evaluation of the Effects of the February 9, 1971 San Fernando Earthquake on the Balboa Water Treatment Plant," Unpublished Report Prepared for Gibson, Dunn, and Crutcher, Oakland, CA, Dec. 1971.
9. Youd, T. L., "Ground Movements in Van Norman Lake Vicinity During San Fernando Earthquake," San Fernando, California Earthquake of February 9, 1971, Vol. 3, U.S. Department of Commerce, N.O.A.A., Washington, D.C., 1973, pp. 197-206.
10. Dixon, S. J and J. W. Burke, "Liquefaction Case History," Journal of the Soil Mechanics and Foundations Division, ASCE, Vol. 99, No. SM11, Nov. 1973, pp. 921-938.
11. Smith, S. J., Jr., "Repair of Earthquake Damaged Underground Reservoir," Journal of the Construction Division, ASCE, Vol. 100, No. C03, Sept. 1974, pp. 449-468.
12. American Society for Testing and Materials, "Soil and Rock: Building Stones; Geotextiles," Annual Book of ASTM Standards, Vol. 4.08, Section 4, ASTM, Philadelphia, PA, 1989.
13. O'Rourke, T.D. and P.A. Lane, "Liquefaction Hazards and Their Effects on Buried Pipelines," Technical Report NCEER-89-0007, National Center for Earthquake Engineering Research, Buffalo, NY, Feb. 1989.
14. O'Rourke, T. D. and M. S. Tawfik, "Effects of Lateral Spreading on Buried Pipelines During the 1971 San Fernando Earthquake," Earthquake Behavior and Safety of Oil and Gas Storage Facilities, Buried Pipelines, and Equipment, PVP-Vol. 77, ASME, New York, NY, 1983, pp. 124-132.
15. O'Rourke, T.D., W.D. Meyersohn, M.D. Grigoriu, and M.M. Khater, "Ground Failure Effects on Pipeline System Performance," Proceedings, 9th World Conference on Earthquake Engineering, Vol. IV, Tokyo, Japan, 1988, pp. 79-84.

LIQUEFACTION INDUCED PERMANENT GROUND  
DISPLACEMENTS IN NIIGATA CITY

*Susumu Yasuda*<sup>1)</sup> *Masanori Hamada*<sup>2)</sup>

*Kazue Wakamatsu*<sup>3)</sup> *and Iwao Morimoto*<sup>4)</sup>

- 1) Kyushu Institute of Technology, Kitakyushu, Japan
- 2) School of Marine Science and Technology, Tokai Univ., Shimizu, Japan
- 3) Science and Eng. Research Lab., Waseda University, Tokyo, Japan
- 4) Kiso-jiban Consultants Co., Ltd., Tokyo, Japan

ABSTRACT

Permanent ground displacements resulting from the 1964 Niigata Earthquake were studied. In addition to the primary studies, presented during the First Japan-U.S. Workshop, other studies have been continued. Around Niigata Port, very large displacements, up to 10 m, were observed near the Shinano River. The testimony of inhabitants of several areas affected clarified the process of occurrence of the ground displacements. Detailed investigation in the Ohgata Area suggested the existence of a very loose sand layer around the Ohgata Elementary School.

## INTRODUCTION

During the 1964 Niigata Earthquake, violent liquefaction occurred in Niigata City and caused extremely large permanent displacements in some areas. The authors measured the permanent ground displacements by pre-and post-earthquake aerial surveys, and studied on the soil conditions at three areas: (1) area along the Shinano River, (2) Ohgata area, and (3) Shitayama area. The results of these studies were presented at the First Japan-U.S.Workshop, in 1988.

After the workshop, permanent ground displacements at other areas in Niigata City were measured. Damage due to ground displacements was described by inhabitants of the areas. Moreover, detailed studies on the Ohgata area were conducted. The results of these studies are presented in this paper.

### PERMANENT GROUND DISPLACEMENTS AROUND NIIGATA PORT

In the first stage, in 1986, permanent ground displacements in an area along the Shinano River were measured. After that, permanent displacements were measured in almost all areas where liquefaction occurred, as shown in Fig.1.

As the permanent ground displacements in three areas were discussed at the First Japan-U.S.Workshop, the displacements in an area around Niigata Port are discussed here. Niigata Port is located at the mouth of the Shinano River. Fig.2 shows the measured horizontal permanent ground displacements around Niigata Port. Large displacements occurred at Umibe Town and Irifune Town, which are located at a pointed end of the left bank of the Shinano River. The directions of the vectors of the displacements are almost perpendicular to the river, and the maximum displacements reached about 10 m.

Directions of the vectors of the displacements at the right bank of the Shinano River were complicated. The directions at the D-quay, the C-quay, Shinmei Town and the South-quay were south, north, south and west, respectively. Most displacements at these districts were 3 to 4 m. At Bandai Island and the North-quay, displacements of about 2 to 5 m were induced perpendicular to surrounding quay walls.

### DAMAGE DESCRIBED BY INHABITANTS

To obtain first-hand information about the process of ground displacement, and damage due to the displacement, local inhabitants were interviewed. The investigated sites are shown as hatched zones in Fig.1. The more interesting observations are recounted below.

At Kawagishi-cho, wooden houses "c" and "b", shown in Fig.3, were tilted and sank gradually almost five minutes after the earthquake. A crack about 4 m in width ran under house "c", parallel to the Shinano River. The distance between house "c" and house "d", which did not tilt, expanded eight meters.

At Hakusan Elementary School, near Showa Bridge, large horizontal shaking, like the rolling of a ship, occurred after the vertical shock. The ground pitched violently, almost 1 m in amplitude at the height of the wave. Big cracks opened on the surface of the ground, and sand and water was ejected, as shown in Fig.4. A swimming pool was split and its water flowed out.

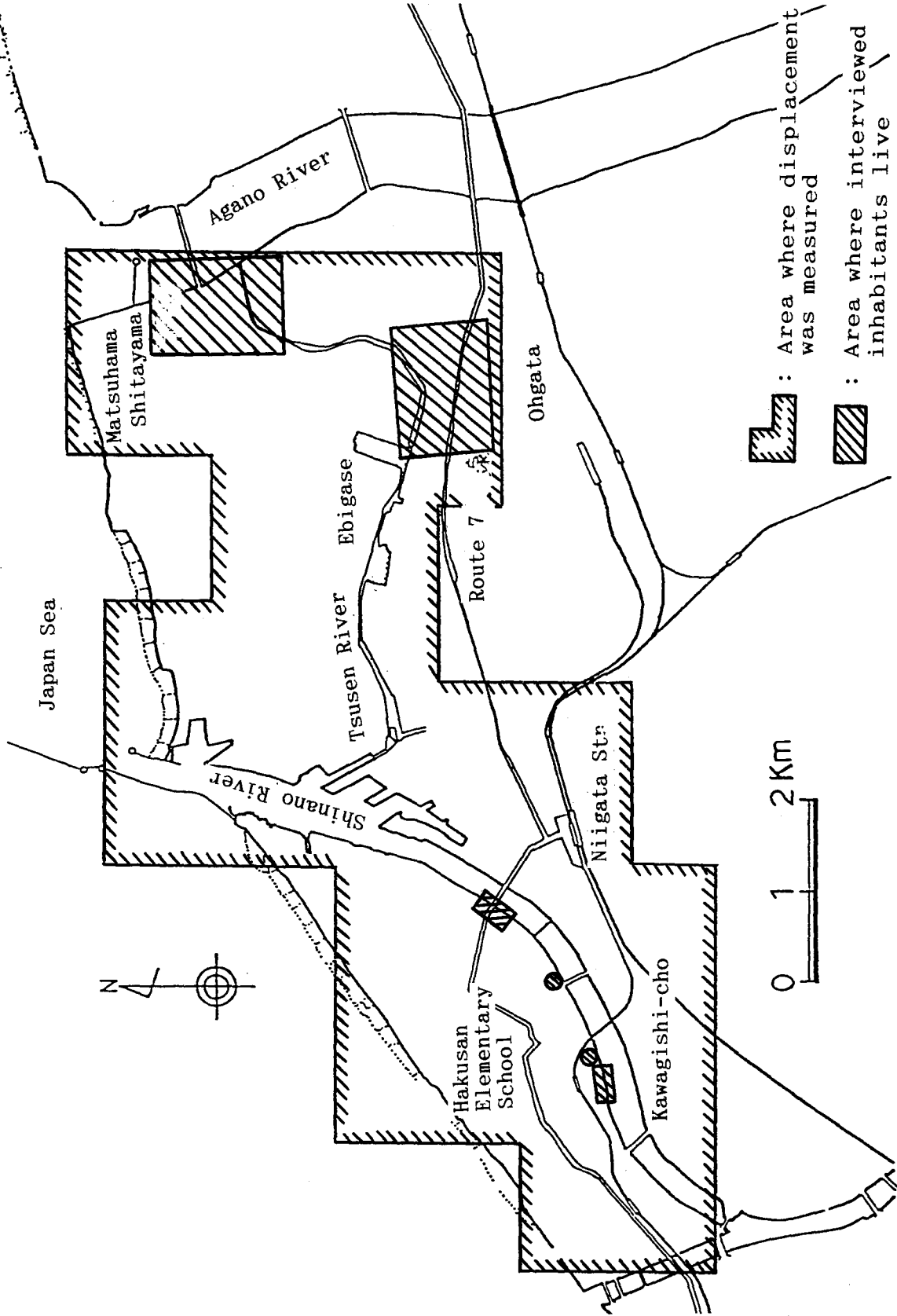


Fig.1 Measured area of permanent ground displacement in Niigata City



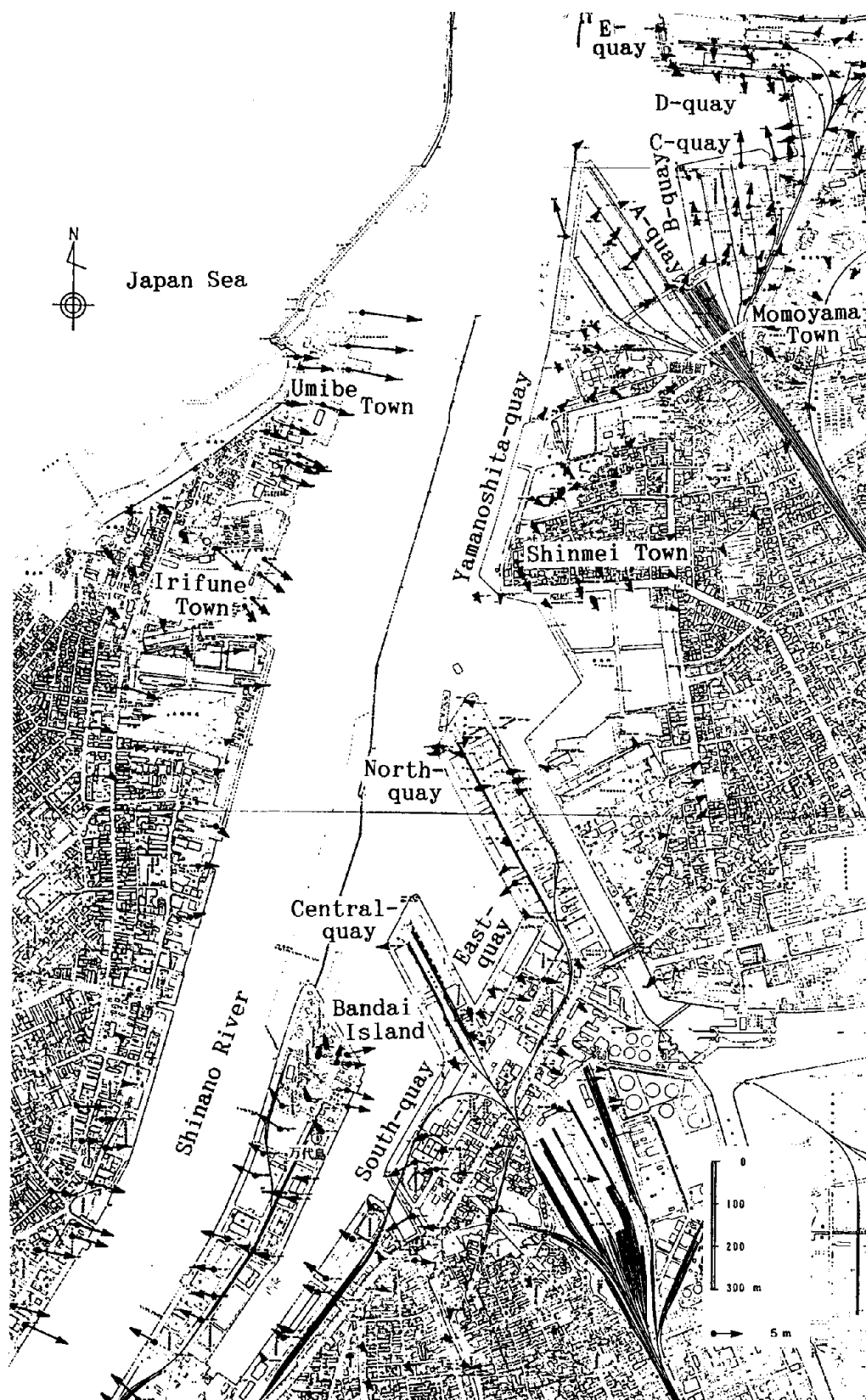


Fig.2 Permanent horizontal ground displacements around Niigata Port

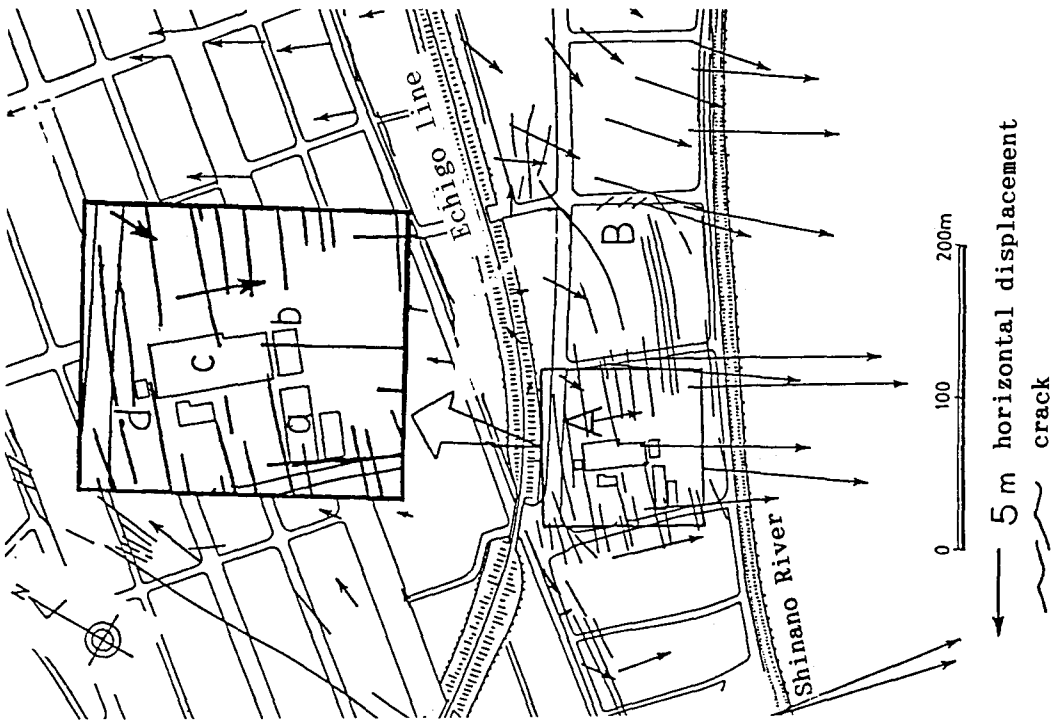


Fig.3 Damaged houses due to displacement at Kawagishi-cho

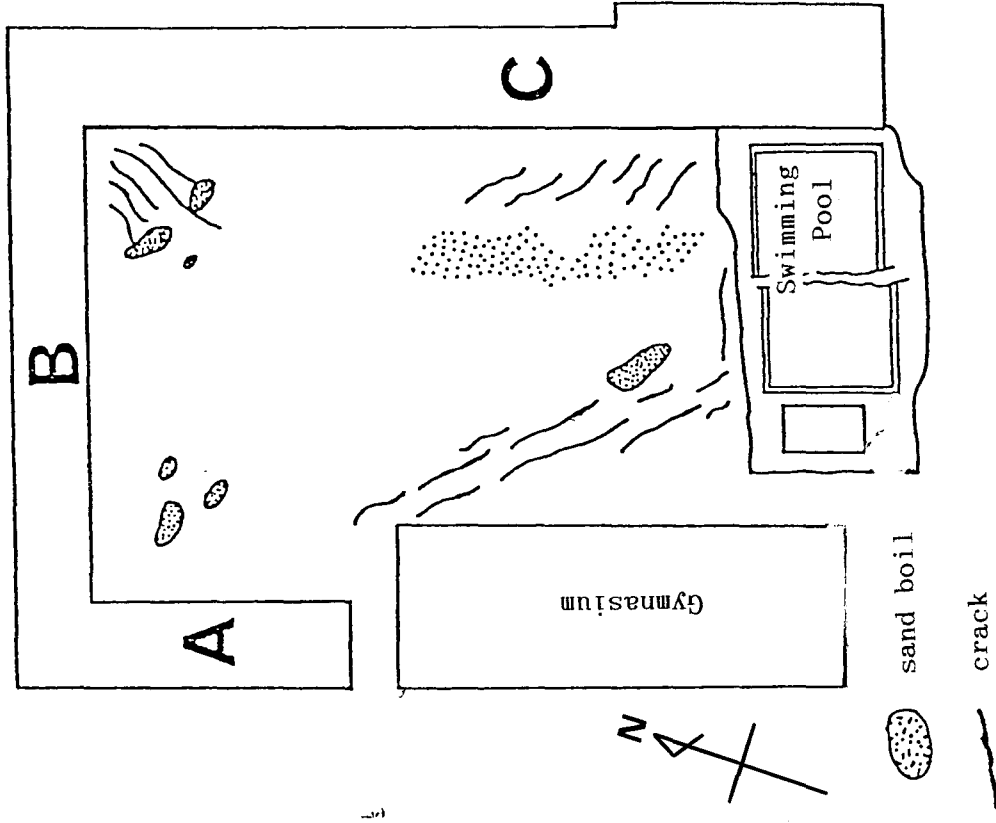


Fig.4 Cracks and sand volcanoes induced at Hakusan Elementary School

Many cracks were induced at Ohgata Elementary School, as shown in Fig.5. Schoolhouses were damaged by the cracks. At schoolhouses "b" and "e", floors were torn due to the cracks and passageways waded to and fro. A passage connecting schoolhouses "c" and "d" was torn up to 2m. One witness said schoolhouse "d" had moved northeast with its foundation ground.

#### DETAILED STUDIES IN THE OHGATA AREA

Extremely large permanent displacements, up to 10 m, were induced in the Ohgata Area, though the ground surface was almost flat (Hamada et al. 1988). To ascertain the mechanism of such large displacement, several detailed studies were conducted.

Ground levels at many points before the earthquake were measured using the pre-earthquake aerophotographs, and are indicated as contour lines with 25 cm pitch, as shown in Fig.6. The ground surface was almost flat, but a very small highland, of 1.5 m in height, was developed at the south side of the Tsusen River. It can be seen that large permanent ground displacements were concentrated at almost the wedge of the highland. In geomorphological aspect, the highland coincides with a natural levee of the Tsusen River, as shown in Fig.7.

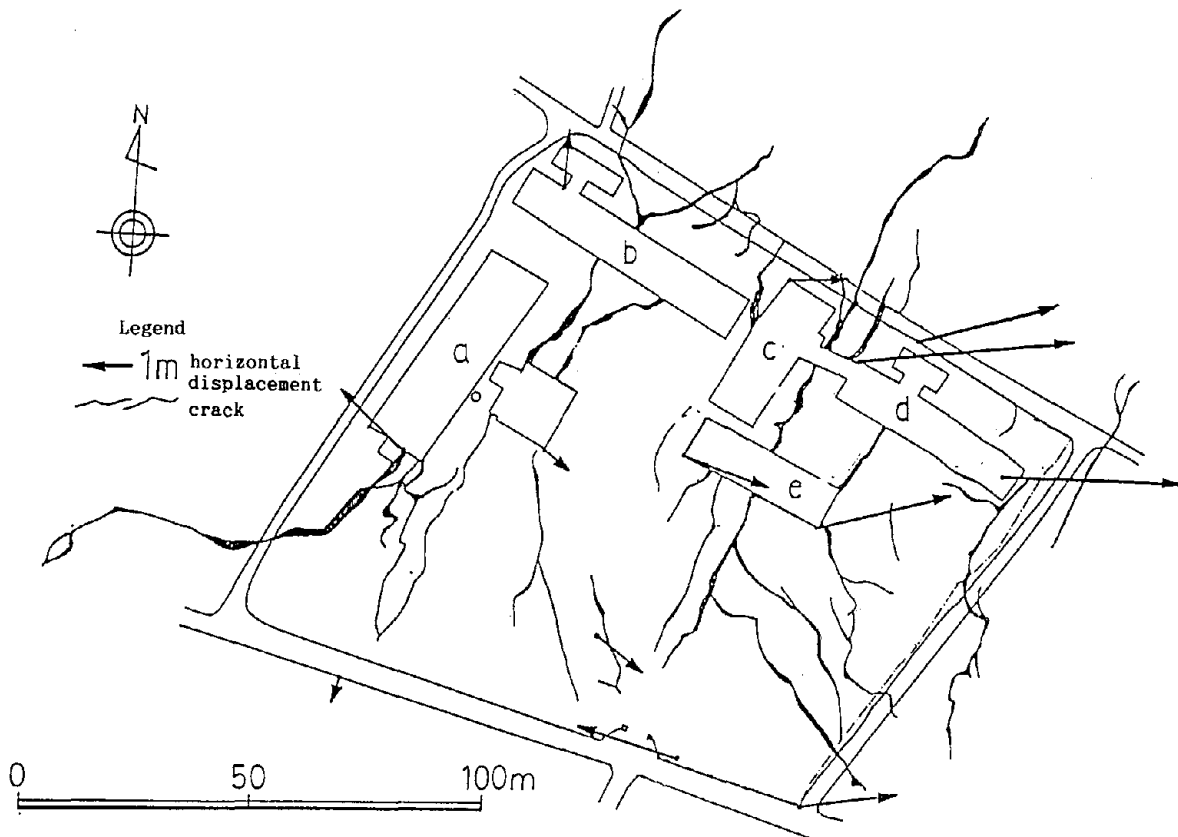


Fig.5 Sites of damaged schoolhouses at Ohgata Elementary School



Fig.6 Permanent horizontal displacement , and contour lines in Ohgata Area

Borings, standard penetration tests, Swedish soundings, dynamic cone tests and measurements of the ground water table were carried out at many sites. Fig.8 shows the results of these tests conducted at four sites along the B-B' line in Fig.6. As shown in this figure, loose sand layers are deposited from the ground surface to a depth of several meters at all sites. Especially, the upper soil layer up to 4 to 5 m in depth at site 1 and site 2 is very loose. Fig.9 shows the grain-size distribution curves of the loose sands at four depths at each site in Fig.8. All sands are very clean and the diameters of the sands at site 1 are smaller than those at site 3 and site 4.

Based on the results of the soil investigations, soil layer profiles along many section lines were estimated. Liquefied soil layers for each section were evaluated by the method proposed by Iwasaki et al.(1978). Fig.10 shows an estimated profile along the B-B' line in Fig.6. In this section, the estimated liquefied layer slopes gently toward the Tsusen River and has a thickness of about 4 m. The ground surface has also slopes gently, the average gradient of the slope being only 0.5 %.

Fig.11 shows the detailed soil layer profile of the surface layer along B-B' line judged from the dynamic cone tests. It can be seen that the surface layer up to a depth of about 2 m, within the natural levee, is extremely

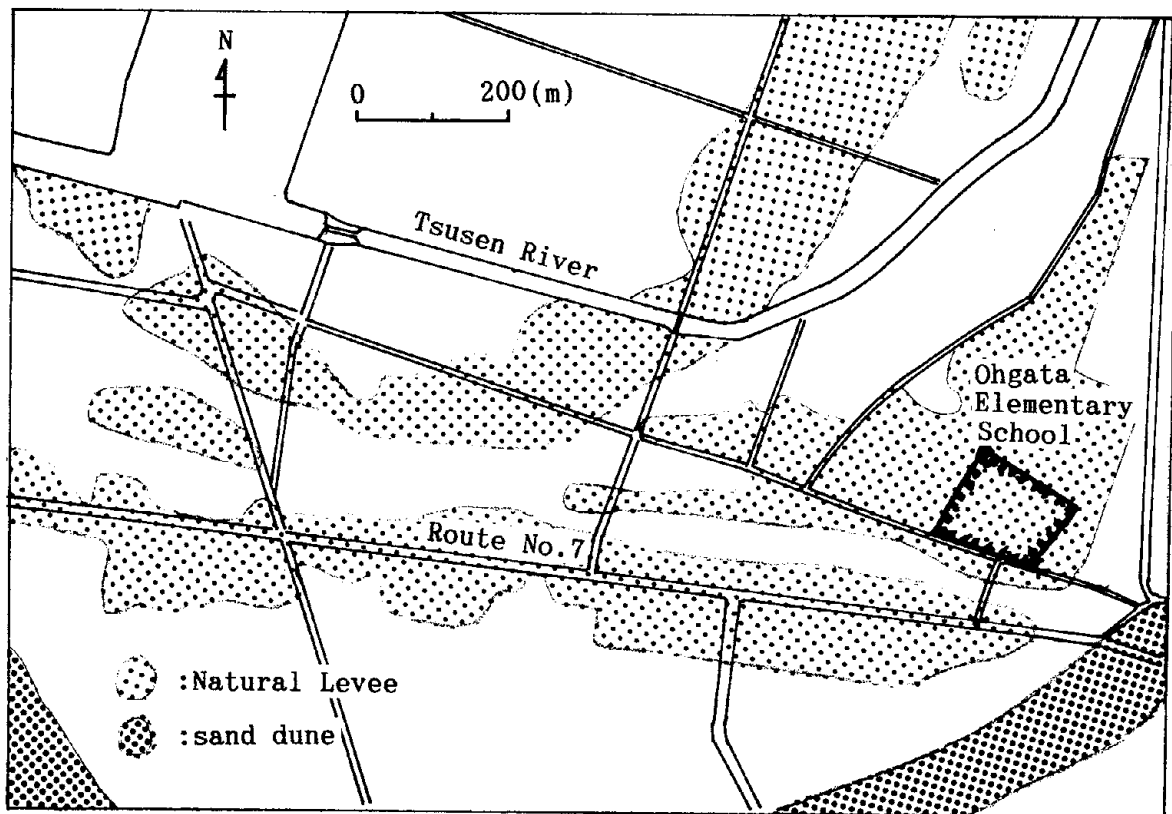


Fig.7 Geomorphological map of Ohgata Area

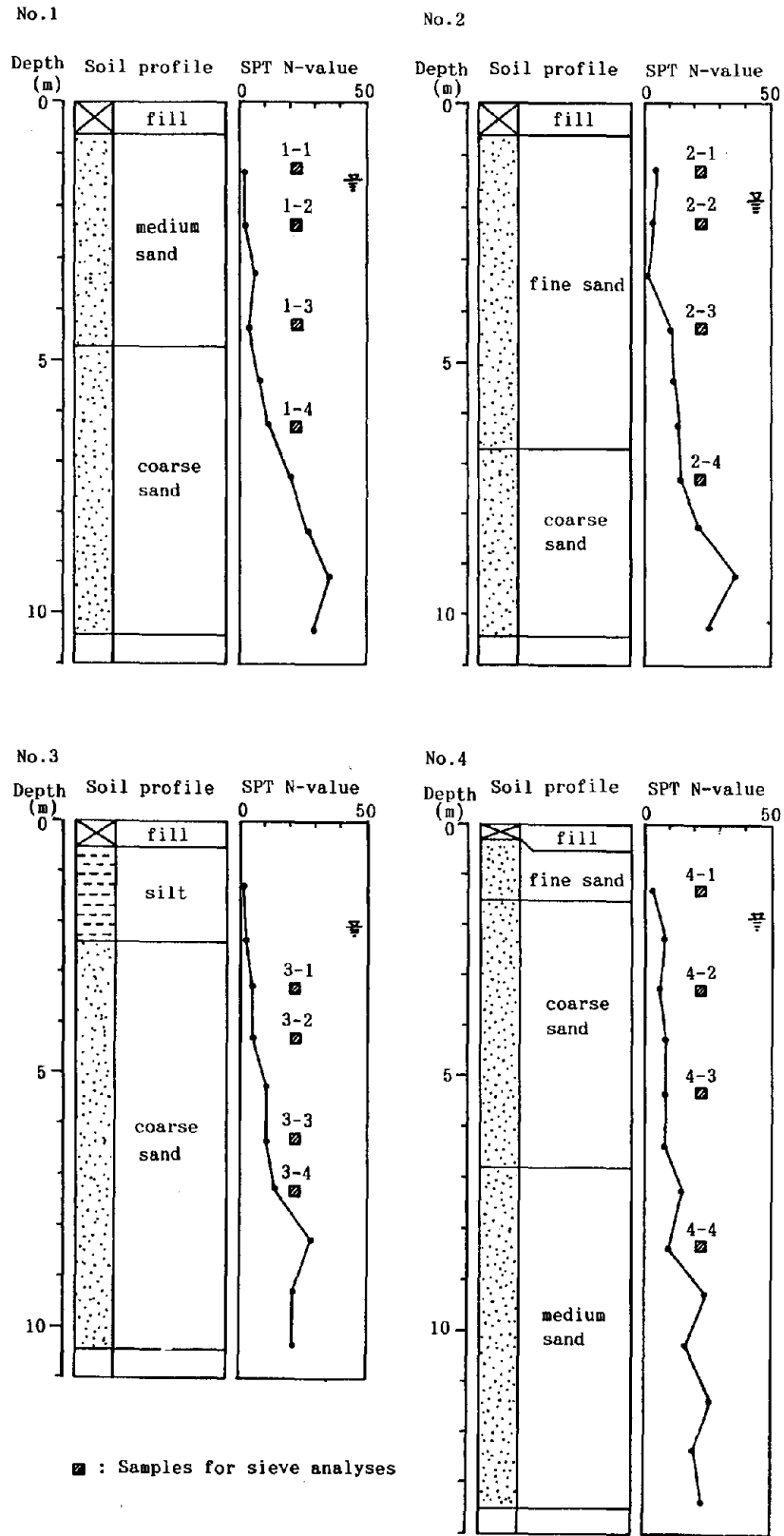


Fig.8 Soil profiles at four sites along B-B' line

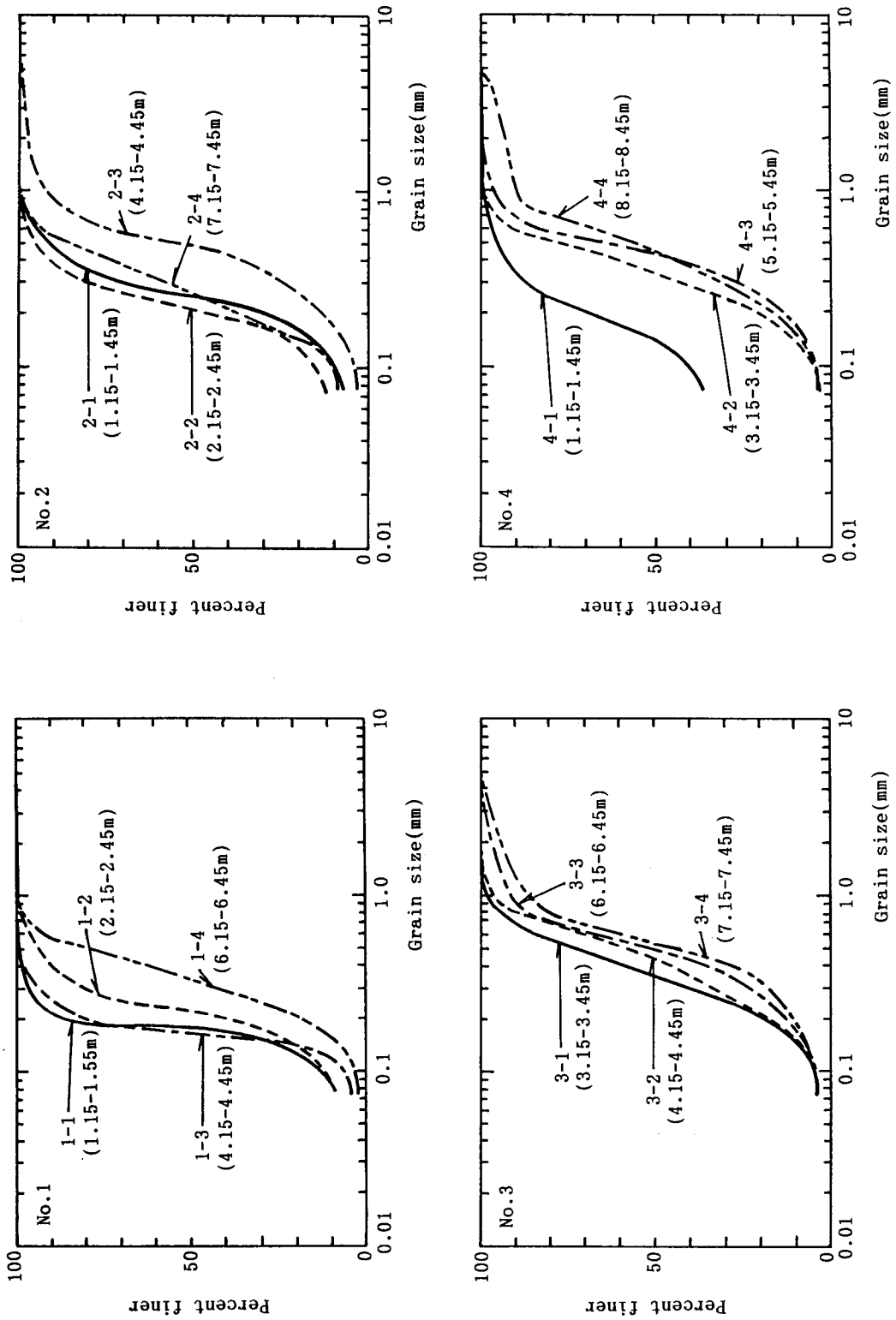


Fig.9 Grain-size distribution curves of loose sands

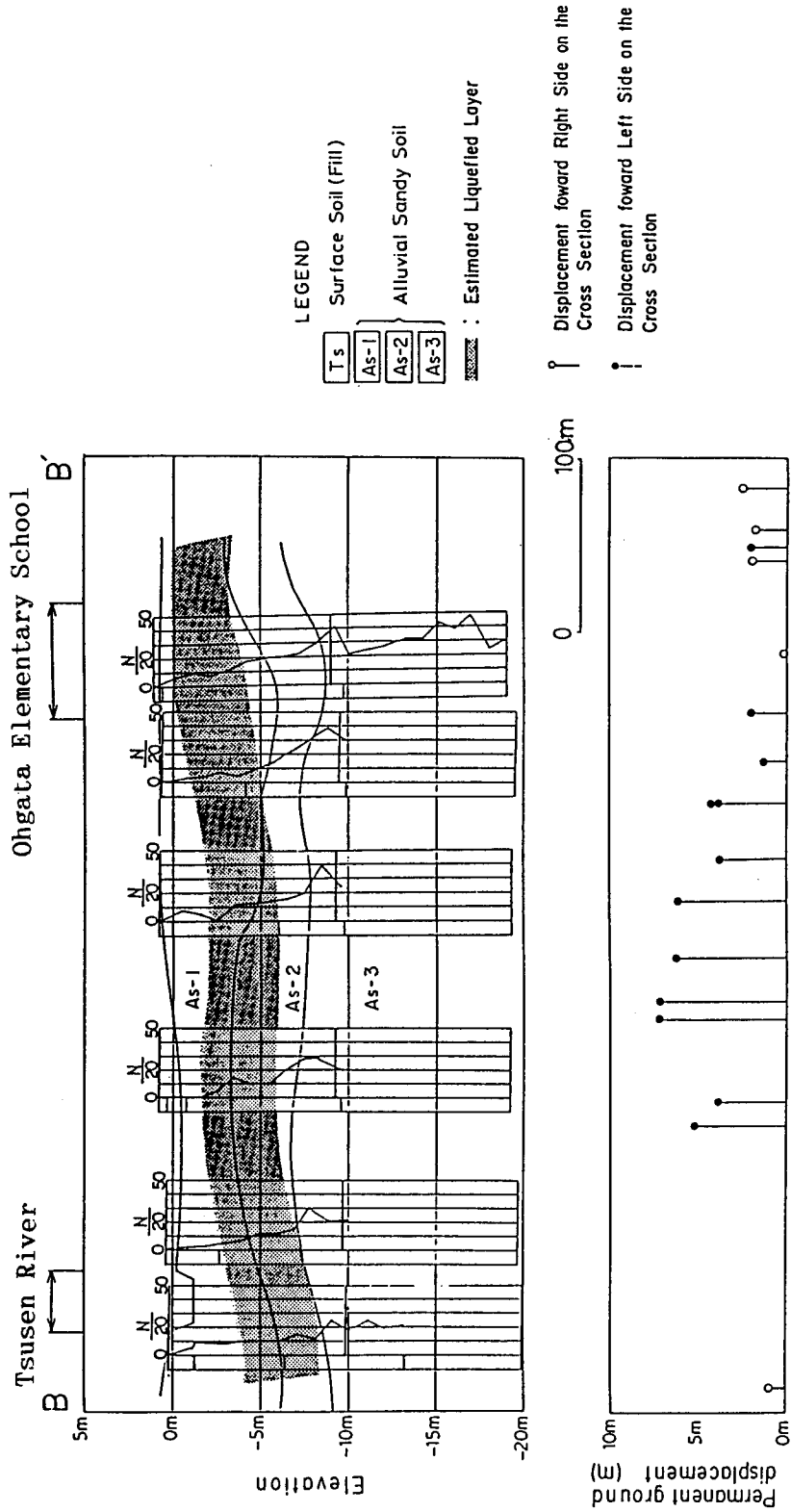


Fig.10 Estimated soil profile and liquefied layer along B-B' line



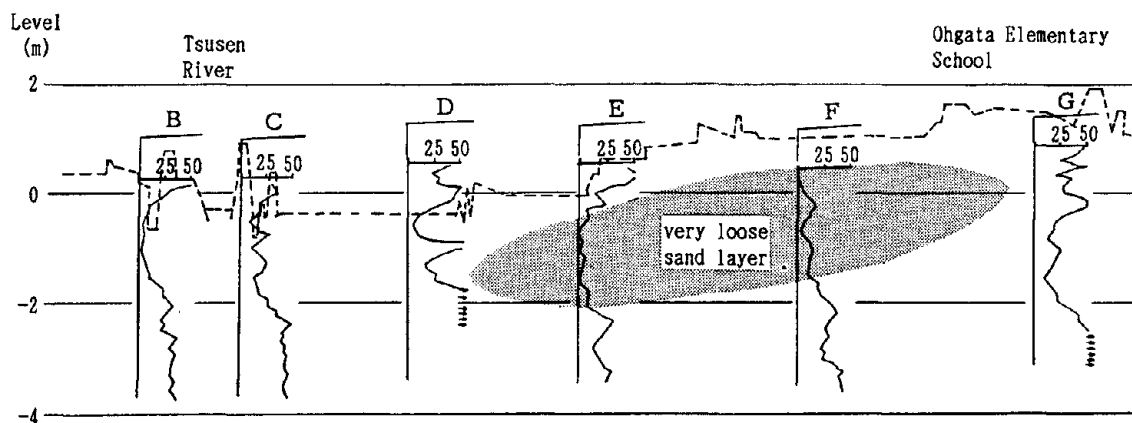


Fig.11 Detailed soil layer profile of the surface layer along B-B' line

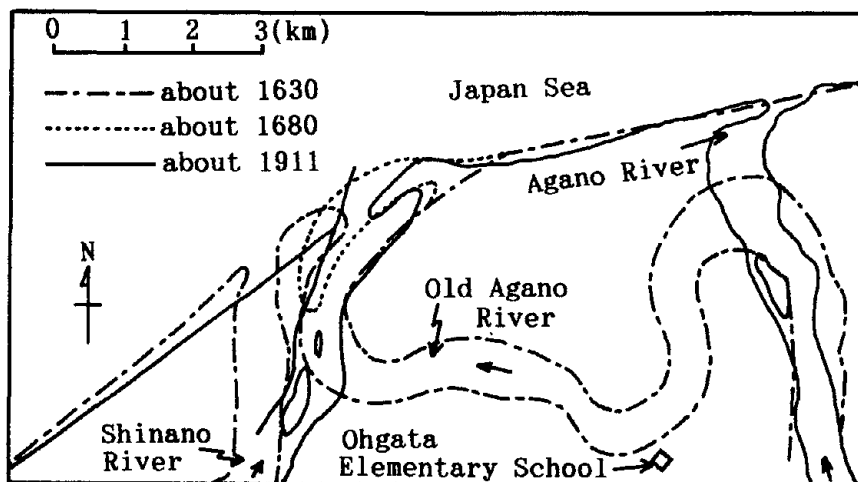


Fig.12 Change of the flow of the Agano River

loose. It may be estimated that this very loose layer contributed to a high incidence of large permanent ground displacements. This very loose sand layer may have been formed for the following reasons:

Formerly, the Agano River, a big river, flowed through the present Tsusen River towards the mouth of the Shinano River, as shown in Fig.12. In the 18th century, the course of the Agano River was changed to empty into the Japan Sea directly, and the volume of water flowing in the Tsusen River decreased. Therefore, the old Tsusen River was probably wider than the present river. The water might have frequently flooded the site of the Ohgata Elementary School. After decreasing the water level, aeolian very loose sand became deposited in the dried area, which might nearly coincide with the area of the natural levee.

#### CONCLUDING REMARKS

Permanent ground displacements caused by the 1964 Niigata Earthquake were studied. Large displacements were induced along the Shinano River, around the Niigata Station, Ohgata district etc. Soil conditions at these sites have been fairly clarified. However, study on the mechanism of the occurrence of the displacement must be continued.

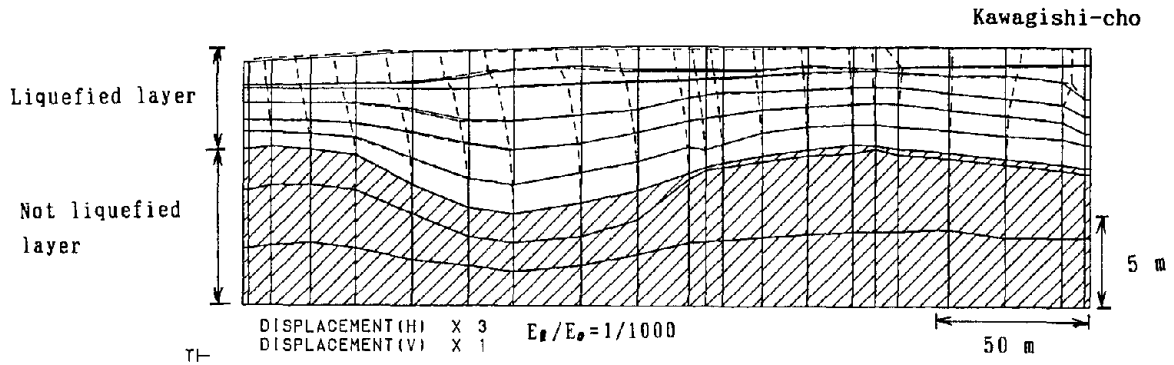
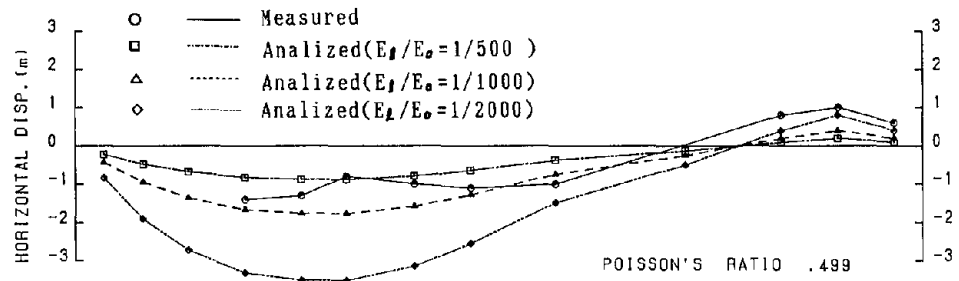
#### APPENDIX

Among the authors, Yasuda et al.(1989) proposed a simplified procedure for the analysis of the permanent ground displacement. In this procedure, the finite element methods are applied twice. In the first stage, distribution of stresses in the ground is calculated by the finite element method using the elastic modulus before the earthquake. Then, holding the stresses constant, the finite element method is conducted again using the decreased modulus due to the earthquake. The difference in deformation measured by the two analyses is supposed to equal the permanent ground displacement.

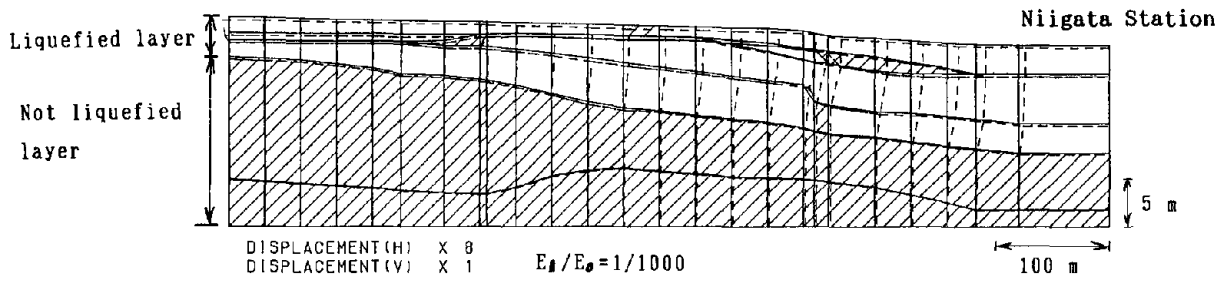
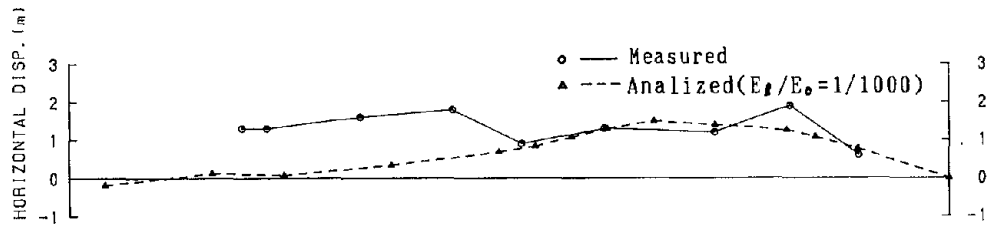
By using this procedure, permanent ground displacements at Kawagishi-cho, around Niigata Station and around the Ohgata Elementary School were estimated. In these analyses, the decreasing ratio of the elastic modulus was assumed as 1/1000. Fig.13 compares the analyzed displacements and the measured ones. The displacements coincide fairly well in the cases of Kawagishi-cho and Niigata Station. However, a larger decreasing ratio might be needed in the case of Ohgata Elementary School.

#### REFERENCES

- 1) M.Hamada, S.Yasuda and K.Wakamatsu: Case Study on Liquefaction-incuced Ground Failures during Earthquakes in Japan, Proc.of the First Japan-U.S. Workshop on Liquefaction, Large Ground Deformation and Their Effects on Lifeline Facilities, pp.3-21, 1988.
- 2) T.Iwasaki, F.Tatsuoka, K.Tokida and S.Yasuda: A Practical Method for Assessing Soil Liquefaction Potential Based on Case Studies at Various Sites in Japan, Proceedings, 5th Japan Symposium on Earthquake Engineering, pp.641-648, 1978.(in Japanese)
- 3) S.Yasuda, H.Kiku and H.Marui: An Analysis of Countermeasures against Permanent Ground Displacement due to Liquefaction, Proc. of the 24th Japan National Conf. on S.M.F.E., JSSMFE, pp.1041-1042, 1989.(in Japanese)

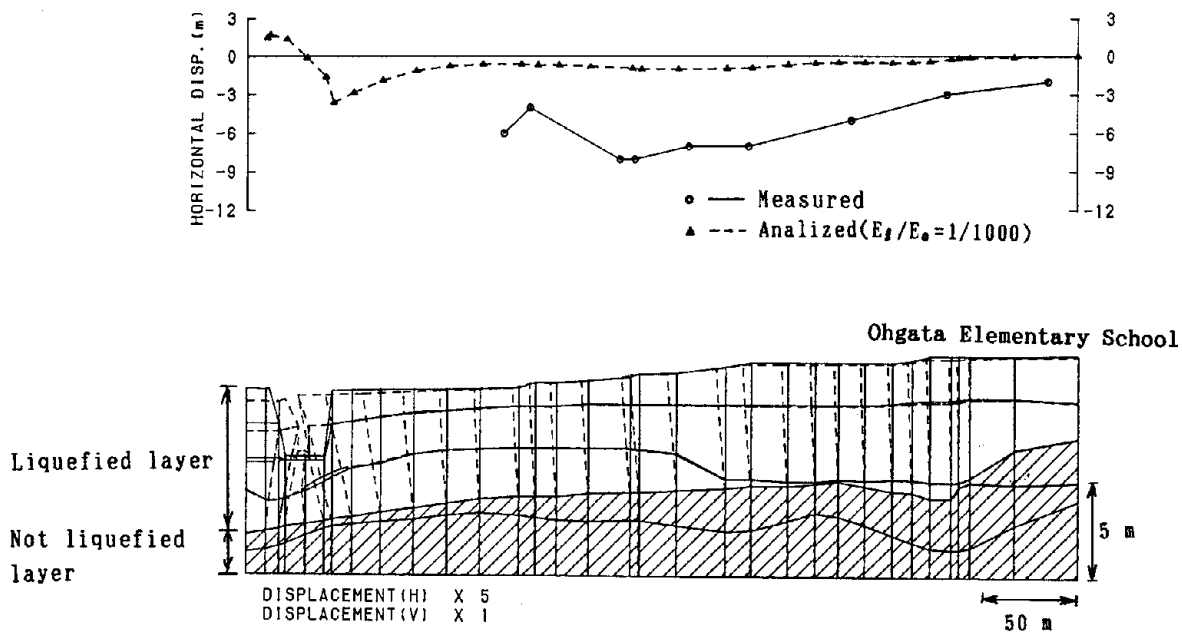


(a) Kawagishi-cho



(b) Niigata Station

Fig.13 (1) Comparison calculated displacements with measured displacements



(c) Ohgata Elementary School

Fig.13 (2) Comparison calculated displacements with measured displacements

**LATERAL SPREADING FIELD EXPERIMENTS  
BY THE U.S. GEOLOGICAL SURVEY**

Thomas L. Holzer<sup>1</sup>, Michael J. Bennett<sup>1</sup>, and T. Leslie Youd<sup>2</sup>

<sup>1</sup>Geologist  
U.S. Geological Survey

<sup>2</sup>Professor of Civil Engineering  
Brigham Young University

**ABSTRACT**

The U.S. Geological Survey maintains two strong ground-motion arrays in California--Parkfield and Wildlife--that are specially instrumented to record simultaneously accelerations and pore pressures in liquefiable sands. Local bench-mark networks and inclinometer casings at both arrays permit detection of permanent surface and subsurface displacements. The Wildlife array was triggered in 1987 by an earthquake large enough to cause liquefaction and lateral spreading and produced a rich data set on liquefaction phenomena. Although experience with these two arrays demonstrates their feasibility, a long-term commitment is required to ensure site characterization data and instrument specifications are available long after instrument installation. Further evaluation of transducer installation and retrievability is also needed.

## INTRODUCTION

Liquefaction of saturated cohesionless soils is commonly a significant cause of damage during earthquakes. In some earthquakes, such as Alaska 1964, it has been the principal cause of losses. In the last two decades, major laboratory investigations, theoretical studies, and post-earthquake field investigations have greatly improved our understanding of liquefaction. Nevertheless, few direct observations of natural soils undergoing liquefaction have been made. *In situ* monitoring of the response of natural soils to earthquake loading can provide both new insight into liquefaction phenomena and an opportunity for field testing the reliability of site response models used by the engineering profession.

This report describes two sites in California that were instrumented to monitor liquefaction under field conditions. The sites are maintained as part of the National Strong Motion Instrumentation Network that is operated by the U.S. Geological Survey (USGS). Both sites have downhole instrumentation that includes triaxial accelerometers and pore-pressure transducers to monitor dynamic soil response and inclinometers and bench marks to detect permanent subsurface and surface displacements. These instrumented sites are herein referred to as liquefaction arrays. The primary purposes of the arrays are to monitor the build up of pore pressure in saturated sand while it is undergoing earthquake loading and to record how the character of strong motion changes as seismic waves propagate vertically through the sand to the land surface. Resurveys of bench marks and inclinometer casings, however, may provide insight into lateral spreading.

The arrays, Parkfield and Wildlife, are located in central and southern California, respectively, near seismically active segments of the 950-km-long San Andreas fault system (Fig. 1). Other operational liquefaction arrays known to the authors are in Japan (Ishihara and others, 1981), China and Taiwan (C.K. Shen, oral comm., 1987). Several reasons account for the rarity of these specially instrumented arrays. First, recurrence intervals for moderate to large earthquakes typically are several decades, even in the most seismically active areas. Thus, a commitment to long-term maintenance is required to ensure that an array successfully functions. Second, the drilling for exploration and instrument

installation and the instrumentation itself are costly. Third, the long-term reliability of pore-pressure transducers is not demonstrated. For these reasons, liquefaction arrays in general are most suitable when short-term seismic activity is anticipated.

Selection of the general locations of the USGS liquefaction arrays was dictated by the frequency of at least moderate-sized earthquakes on the San Andreas fault system (Lindh, 1983). Location of the Parkfield array was based on the work of Bakun and Lindh (1985). They predicted that a moderate earthquake, about magnitude 6, will occur between 1983 and 1993, at a 95 percent confidence level, near Parkfield and will rupture a 25-km-long segment of the San Andreas fault. Their prediction was based on the inference that a characteristic moderate earthquake causes the Parkfield segment of the San Andreas fault to rupture with an approximate recurrence interval of 22 years. The last characteristic earthquake was in 1966. Selection of the Wildlife array site was based on the very high historical incidence of earthquakes in the Imperial Valley in which the array is located. The earthquake history compiled by Johnson and Hill (1982) indicates that earthquakes with magnitudes ranging from about 6 to 7 occur with an average recurrence interval of 12 years. Following the methodology of Lindh (1983), we estimated in 1987 that there was a 91 percent chance of a moderate earthquake in the Imperial Valley in the next 10 years. With these two arrays in place, we estimated that there was a 99 percent probability of monitoring at least one moderate earthquake capable of causing liquefaction in the next 10 years. Liquefaction at the Wildlife array during the 1987 Superstition Hills earthquake justified our optimism (Holzer and others, 1989b).

## **PARKFIELD LIQUEFACTION ARRAY**

### **Background**

The Parkfield liquefaction array was established in the summer of 1986 primarily for two purposes--to monitor the build up of pore pressure in sands undergoing earthquake loading and to provide data to test the accuracy of models designed to

predict ground response. Although the array is on approximately level ground, it includes instrumentation to measure permanent deformation. The array was established through a joint agreement between the USGS and the Electric Power Research Institute (EPRI). Most of EPRI's operational responsibilities were executed through a contract to Brigham Young University.

The array is located about 15 km southeast of Parkfield, California, in Cholame Valley, a narrow rift valley within the San Andreas fault zone (Fig. 1). Cholame Valley near the array is a 2-km wide, flat, featureless plain that is drained by Cholame Creek. The land surface at the array, which is on the east bank of Cholame Creek, slopes toward the creek with a gradient of 0.4 percent (Fig. 2). Cholame Creek, in the reach adjacent to the array, is a braided intermittent stream that is depositing most of its bedload. The modestly incised creek recharges the shallow ground-water system during the winter and spring periods of stream flow. The seasonal recharge keeps the water table at the array from falling below a depth of about 2.5 m from the land surface.

Field evidence is suggestive of liquefaction at the array location during previous earthquakes. Brown and others (1967) reported that unverified waterspouts near the future location of the array were observed by local residents during the 1966 Parkfield earthquake. In addition, W.H. Bakun (written comm., 1986) reported that water seeps and earth fissures after the 1966 earthquake were mapped near the array location by employees of the landowner. The best documented evidence for earthquake-induced liquefaction in Cholame Valley consists of sand boils found following the 1966 earthquake (Brown and others, 1967). The closest sand boil to the array mapped during the post-earthquake reconnaissance was 3.5 km to the southeast.

## **Geology**

The following is a brief summary of the geologic and geotechnical setting of the array that was previously described by Holzer and others (1986) and Youd and others (1988). Four stratigraphic units in the upper 30 m were identified (Fig. 3). Typical stratigraphic conditions from top to bottom as shown in the boring in



Figure 3 are: unit A, a 2.1-m-thick sand; unit B, a 3.0-m-thick clayey silt; unit C, a 6.4-m-thick sand; unit D, a predominantly clayey silt of unknown thickness. Unconfirmed reports by water-well drillers of "blue clay" indicate that unit D may be as much as 240 m thick. Two sandy subunits, D1 and D2, 1.4 and 1.2 m thick, respectively, are intercalated in the upper part of unit D. Units A and C and subunits D1 and D2 probably are fluvial. Units B and D may be lacustrine.

Unit C, the unit in which most of the pore-pressure transducers were installed, may be subdivided into 3 subunits on the basis of texture and density. The upper subunit, C1, which extends from 5.1 to 5.7 m, is a dark-grayish brown, moderately sorted, loose, medium-grained sand. The middle subunit, C2, which extends from 5.7 to 7.7 m, is a dark-grayish brown, poorly sorted, medium dense, medium-grained sand. The lower subunit, C3, which extends from 7.7 to 11.5 m, is a dark brown, poorly sorted, medium dense, gravelly sand. Gravel clasts up to 40 mm in diameter occur near the bottom of C3. Contacts of the subunits within units C are gradational but the top and bottom of unit C are sharp.

### Liquefaction Resistance

The upper part of unit C was considered the most susceptible to liquefaction of all of the units. Liquefaction resistances of unit C and subunits D1 and D2 were evaluated by the procedures of Seed and others (1985), which is based on the standard penetration test (SPT), and of Ishihara (1985), which is based on the cone penetration test (CPT). Typical SPT blow counts are shown in Figure 3. Evaluations by Holzer and others (1986, 1988) included corrections for fines content and for gravel. A peak horizontal ground acceleration of 0.4 g was assumed in the analysis.

Liquefaction resistance was estimated in terms of the cyclic stress ratio--the average horizontal shear stress generated by the earthquake divided by the static vertical effective stress. The cyclic stress ratios required to cause liquefaction were compared to the induced cyclic stress ratios predicted for the Parkfield earthquake (Fig. 3). The liquefaction resistances shown in Figure 3 include corrections for fines only. For the complete analysis the reader is referred to

Holzer and others (1986). The evaluation suggests that C1, the upper part of C2, and D1 will liquefy during the earthquake. The base of C3 is marginally resistant to liquefaction.

The clayey silt units, B and D, are too fine grained and plastic to liquefy. The resistance of unit A was not analyzed because only the lower 0.3 m is permanently below the water table.

## **Instrumentation**

A total of 24 pore-pressure transducers were installed in three steps at the array (see piezometers in Fig. 2). Eight pore-pressure transducers were installed in subunit C1, six in subunit C2, four in subunit C3, and three each in subunits D1 and D2. There were two reasons for the large number. First, redundant measurements in each layer were desired to increase the confidence in the records of pore-pressure build up. Second, the first eight transducers that were installed failed. Leakage of water between the electrical cable, which had a polyethylene sheath, and the potting compound is suspected.

Pore-pressure transducers include Data Instruments model AB and AK, bonded strain gage, absolute transducers, Druck model PDCR 10/D integrated silicon strain gage bridge transducers, and Sinco model 964 bonded strain gage transducers. Data Instruments and some of the Druck transducers were mounted in 2.5-cm diameter nylon housings that permitted them to be pushed into position from the end of a borehole. The Sinco transducers came premounted in a steel push-in housing. The remaining Druck transducers were installed by lowering them out the bottom of a hollow-stem auger. Following insertion, the drilled holes were backfilled with bentonite-cement grout, thus permanently burying the transducers. The functional status of the transducers is tested by comparison of transducer outputs with pore pressures computed from water-level measurements in a standpipe piezometer screened in unit C.

Downhole accelerometers, Kinometrics model FBA-13DH, were set at depths of 2.7, 4.3, 11.7, and 30 m by wedging them into the bottoms of separate but adja-

cent PVC casings. A special wedging system that permits retrieval of the accelerometers was designed and built (Youd and others, 1989). The accelerometers at 4.3 and 11.7 m bracket unit C and will permit estimates of shear strain across the unit during an earthquake.

A network of eight surface bench marks (Fig. 2) was established at the array to permit detection of both vertical and horizontal permanent surface displacements. Vertical surveys were done with a precise geodetic level and Invar survey rod; horizontal surveys were done with an electronic distance meter. Both shallow seated compaction of unit C and vertical crustal deformation can be detected by referencing the network to two specially set deep bench marks, X and Y (Fig. 2), at the array. The bench-mark rod of each deep mark is protected by a plastic casing that is set in unit D that isolates the bench-mark rod from vertical deformation in units above unit D. The eight bench marks in the network were driven into the top of unit B. Thus, vertical settlements caused by compaction of unit C can be measured. The deep bench marks are also tied to the regional vertical control network. In addition to the bench marks, an 11.5-m-deep inclinometer casing was installed at the array (Fig. 2) to detect permanent horizontal displacements within the subsurface.

## WILDLIFE LIQUEFACTION ARRAY

### Background

The Wildlife liquefaction array was established in the fall of 1982 primarily to monitor pore pressure in sand undergoing earthquake loading. The array is located in southern California at a site about 36 km north of El Centro (Fig. 1). It is in the Imperial Valley which is one of the most seismically active areas in the United States. The array is located on the floodplain of the Alamo River, about 20 m west of the river channel (Fig. 4). Although the array is on level ground, the river is incised to a depth of about 3.7 m which creates an opportunity for lateral spreading. The geologic and geotechnical settings of the array were described by Bennett and others (1984) and Youd and Wieczorek (1984).

## Geology

The stratigraphy and sediment properties at the array are shown in Figures 4 and 5. The site is capped by a 2.3-m-thick fine-grained floodplain deposit, unit A. The unit consists of alternating layers of silt with varying amounts of clay and sand. Most of the unit has a sufficiently high clay content that it is not susceptible to liquefaction. The water table, which is at a depth of about 2 m, fluctuates within unit A.

Unit B1, a loose, moderately sorted sandy silt, which underlies unit A, is about 1 m thick and appears to be highly susceptible to liquefaction on the basis of its geotechnical properties. The grain-size distributions of ejecta from sand boils which formed at the Wildlife site during the 1981 M5.9 Westmorland earthquake are similar to those of sediment in unit B1 which indicates unit B1 liquefied during the 1981 earthquake (Bennett, 1988).

Unit B1 grades downward into a coarser deposit consisting of well-sorted silty fine sand to very fine sand. This unit, B2, is about 3.5 m thick. The deposit is moderately dense.

Unit C, a 5-m-thick unit of silty clay and clayey silt, underlies unit B2. Unit C in turn is underlain by thick layers of silt with interbeds of clayey silt and poorly sorted sandy silt. Units C and the underlying layers are too dense and fine grained to be susceptible to liquefaction.

## Liquefaction Resistance

Unit B is the unit most susceptible to liquefaction. Its liquefaction resistance is shown in Figure 5. The analysis is based on the Seed simplified procedure (Seed and others, 1985) using a M6.6 earthquake with a peak horizontal acceleration of 0.21 g. Blow counts used for the analysis were from SPT's reported by Bennett and others (1984). The seismic loading is that which was observed during the Superstition Hills earthquake on November 24, 1987, which caused liquefaction

(Holzer and others, 1989b). Comparison of liquefaction resistance to induced stress ratio indicates that the top and bottom of the silty sand is susceptible to liquefaction under moderate seismic loading.

Although the upper silt layer is predominantly fine-grained and not amendable to analysis by the simplified procedure, approximately 20 percent of layer A is liquefiable according to Seed and others (1981). Their criteria include a natural water content greater than 90 percent of the liquid limit, a liquid limit less than 35 percent, and a clay fraction ( $< 5 \mu$ ) that is less than 15 percent.

### **Instrumentation**

The Wildlife liquefaction array consists of 6 Data Instruments model AB pore-pressure transducers and two 3-component accelerometers (Fig. 4). Instrumentation is similar to that at the Parkfield array. Pore-pressure transducers were placed in borings with a horizontal spacing of 4.6 m around the circumference of a 9.2-m diameter circle that is centered on the single triaxial downhole accelerometer.

Pore-pressure transducers were emplaced by pushing them about 30 cm into the sediment at the bottom of a drilled bore hole. The drill holes were then filled with a bentonite-cement grout to provide a seal. Two transducers were set in unit B1 at depth of 2.8 and 3.0 m; three transducers were set in unit B2 at depths of 4.0, 5.0, and 6.3 m; and one transducer was set near the top of unit D at a depth of 12.1 m in a silt layer.

The downhole accelerometer is wedged into the bottom of PVC casing at a depth of 7.5 m. The surface accelerometer is mounted on a concrete pad supporting a fiberglass instrument house erected at the site.

The bench-mark network at Wildlife is not as sophisticated as the network at Parkfield. It consists of 6 wooden stakes at cone penetration test sites (Fig. 5). Only horizontal positions of bench marks relative to each other were originally determined. An inclinometer casing (Fig. 4) permits measurement of permanent horizontal displacements in the subsurface.

## RESULTS FROM WILDLIFE ARRAY -- NOVEMBER 24, 1987

Although both liquefaction arrays have been triggered by earthquakes, excess pore pressures have been generated only at Wildlife. Wildlife was triggered on November 24, 1987, by the Superstition Hills earthquake which caused lateral spreading and sand boils to erupt water and sediment (Fig. 6). The dynamics of the records are discussed by Holzer and others (1989b) and the discussion here is limited to the lateral spreading.

Extensive ground cracking accompanied liquefaction (Fig. 6). Although most of the cracking appears to have been caused by local slumping along the west bank of the Alamo River toward the river, ejection of sand from some of these cracks confirms that they were associated with liquefaction. Cumulative opening across ground cracks at the array was 126 mm. The top of the inclinometer casing was deflected approximately 180 mm in a N15°E direction relative to its base beneath the liquefied layer (Fig. 6), indicating that the upper layer slid obliquely into the Alamo River. The oblique slip is confirmed by displacements computed from resurveys of the bench marks (Youd and Bartlett, 1988) and the long crack, orthogonal to the slip direction, that passes through the instrumentation area (Fig. 6). Subsurface horizontal shear strain, estimated from the curvature of the casing, was greatest, approximately 4 percent, in the upper part of unit B.

The dynamics of the lateral spreading measured in the inclinometer casing may be expressed in the records of strong motion and pore pressure (Fig. 7). Distinct negative accelerations in the north-south (360°) surface accelerometer at 31.2, 37.5, 40.7, 53.7, and 77.5 seconds, correspond to transitory drops in pore pressure at 2.9 m, the depth of the shallowest transducer, P5. We suspect that these drops of pore pressure were caused by episodic lateral spreading because there are no incoming acceleration pulses on the parallel component in the downhole accelerometer, and the north-south accelerometer is almost parallel to the N15°E slip direction recorded by the inclinometer casing.

## OPERATIONAL LESSONS LEARNED

The records of the 1987 Superstition Hills earthquake at the Wildlife liquefaction array provide an important data set for testing and validating models of liquefaction and lateral spreading and justify the efforts required to establish these field experiments. Two major operational lessons have been learned, however. The long wait that is possible before significant results are obtained mandates that site characterization data and equipment specifications be either carefully organized and stored by an institution or placed in the public domain. This information tends to be slowly misplaced or lost over time with changes of technical personnel. Only by formal storage or publication of this information can chances of its loss be minimized. Additional evaluation of pore-pressure transducers also is needed. Analysis of the Wildlife records by Holzer and others (1989a) indicated that emplacement of the transducer may have compromised the pore-pressure records by disturbing the soil around the transducer and decreasing the response time of the transducer to conditions in the undisturbed soil. Further testing of this hypothesis is needed. A technique for installing retrievable pore-pressure transducers also needs to be developed to facilitate their replacement when they fail.

## ACKNOWLEDGMENTS

Many individuals have contributed to the completion of these arrays. People who have made major contributions include Donald Anderson, Paul G. Carter, Albert T.F. Chen, Garrett O. Jackson, Jerry L. King, John Sarmiento, Sam Shaler, J. Carl Stepp and Y.K. Tang. Financial support by the Electric Power Research Institute for the Parkfield array is gratefully acknowledged. We thank A. Gerald Brady and Gerald F. Wiczorek for thoughtful reviews.

## REFERENCES CITED

- Bakun, W.H., and Lindh, A.G., 1985, The Parkfield, California, earthquake prediction experiment: *Science*, v. 229, p. 619-624.
- Bennett, M.J., 1988, Sand boils and their source beds--November 24, 1987, Superstition Hills earthquake, Imperial Valley, California: *Association of Engineering Geologists, 31st annual meeting, Abstracts with Program*, p. 38.
- Bennett, M.J., McLaughlin, P.V., Sarmiento, J., Youd, T.L., 1984, Geotechnical investigation of liquefaction sites, Imperial Valley, California: *U.S. Geological Survey Open-File Report 84-252*, 103 p.
- Brown, R.D., Jr., Vedder, J.G., Wallace, R.E., Roth, E.F., Yerkes, R.F., Castle, R.O., Waananen, A.O., Page, R.W., and Eaton, J.P., 1967, The Parkfield-Cholame, California, earthquakes of June-August 1966--Surface geologic effects, water-resources aspects, and preliminary seismic data: *U.S. Geological Professional Paper 579*, 66 p.
- Holzer, T.L., Bennett, M.J., Youd, T.L., and Chen, A.T.F., 1986, Field investigation to identify a site for monitoring liquefaction, Cholame Valley, California: *U.S. Geological Survey Open-File Report 86-346*, 34 p.
- Holzer, T.L., Bennett, M.J., Youd, T.L., and Chen, A.T.F., 1988, Parkfield, California, liquefaction prediction: *Bulletin of the Seismological Society of America*, v. 78, no. 1, p. 385-389.
- Holzer, T.L., Youd, T.L., and Bennett, M.J., 1989a, *In situ* measurement of pore pressure build up during liquefaction: *U.S.-Japan panel on wind and seismic effects*, 20th, Gaithersburg, MD, 1988, Proceedings, p. 118-130.
- Holzer, T.L., Youd, T.L., and Hanks, T.C., 1989b, Dynamics of liquefaction during the 1987 Superstition Hills, California, earthquake: *Science*, v. 244, p. 56-59.
- Ishihara, K., 1985, Stability of natural deposits during earthquakes: *Proceeding, 11th International Conference on Soil Mechanics and Foundation Engineering*, San Francisco, CA, v. 1, p. 321-376.
- Ishihara, K., Shimizu, K., and Yamada, Y., 1981, Pore water pressures measured in sand deposits during an earthquake: *Journal of the Japanese Society of*



- Soil Mechanics and Foundation Engineering*, v. 21, no. 4, p. 85-100.
- Johnson, C.E., and Hill, D.P., 1982, Seismicity of the Imperial Valley, in The Imperial Valley, California, Earthquake of October 15, 1979: *U.S. Geological Survey Professional Paper 1254*, p. 15-24.
- Lindh, A.G., 1983, Preliminary assessment of long-term probabilities for large earthquakes along selected fault segments of the San Andreas Fault system in California: *U.S. Geological Survey Open-File Report 83-63*, 15 p.
- Seed, H.B., Idriss, I.M., and Arango, I., 1981, Evaluation of liquefaction potential using field performance data: *ASCE Journal of the Geotechnical Engineering Division*, v. 109, no. 3, p. 458-482.
- Seed, H.B., Tokimatsu, K., Harder, L.F., and Chung, R.M., 1985, Influence of SPT procedures in soil liquefaction resistance evaluations: *ASCE Journal of the Geotechnical Engineering Division*, v. 111, no. 12, p. 1425-1445.
- Youd, T.L., and Bartlett, S.F., 1988, U.S. case histories of liquefaction-induced ground displacement: *US-Japan workshop on liquefaction and ground deformation*, 1st, Tokyo, 1988, Proceedings, p. 22-31.
- Youd, T.L., Carter, P.G., and Jackson, G.O. 1988, Instrumentation of a ground motion-liquefaction site, Cholame Valley, California: *Final Report to Electric Power Research Institute, Project no. RP 2225-11*, 80 p.
- Youd, T.L., Tang, Y.K., Stepp, J.C., Holzer, T.L., and Jackson, G.O., 1989, A wedging system for downhole accelerometers: *Earthquake Spectra*, v. 5, no. 4 (in press).
- Youd, T.L., and Wieczorek, G.F., 1984, Liquefaction during the 1981 and previous earthquakes near Westmorland, California: *U.S. Geological Survey Open-File Report 84-680*, 36 p.

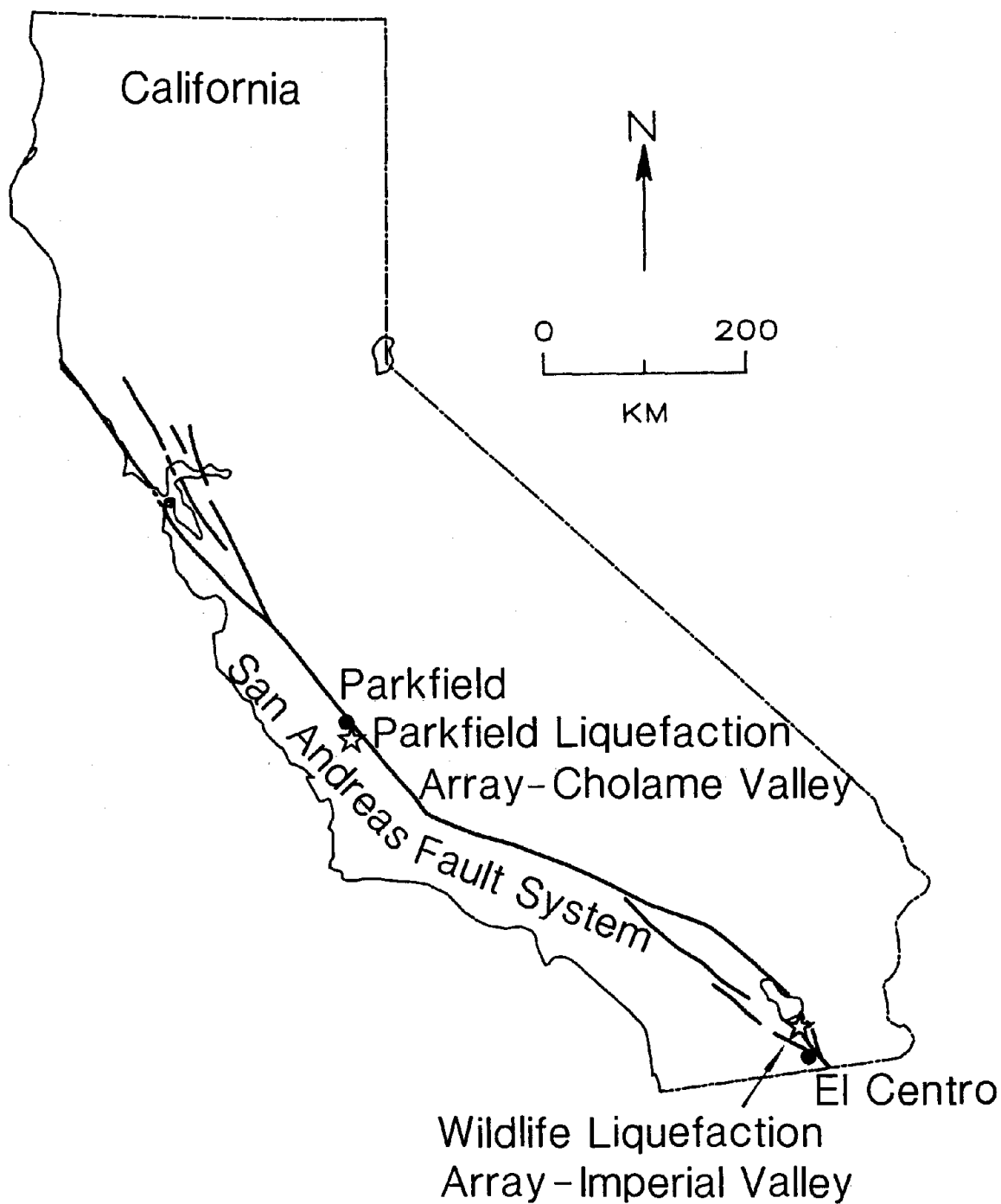
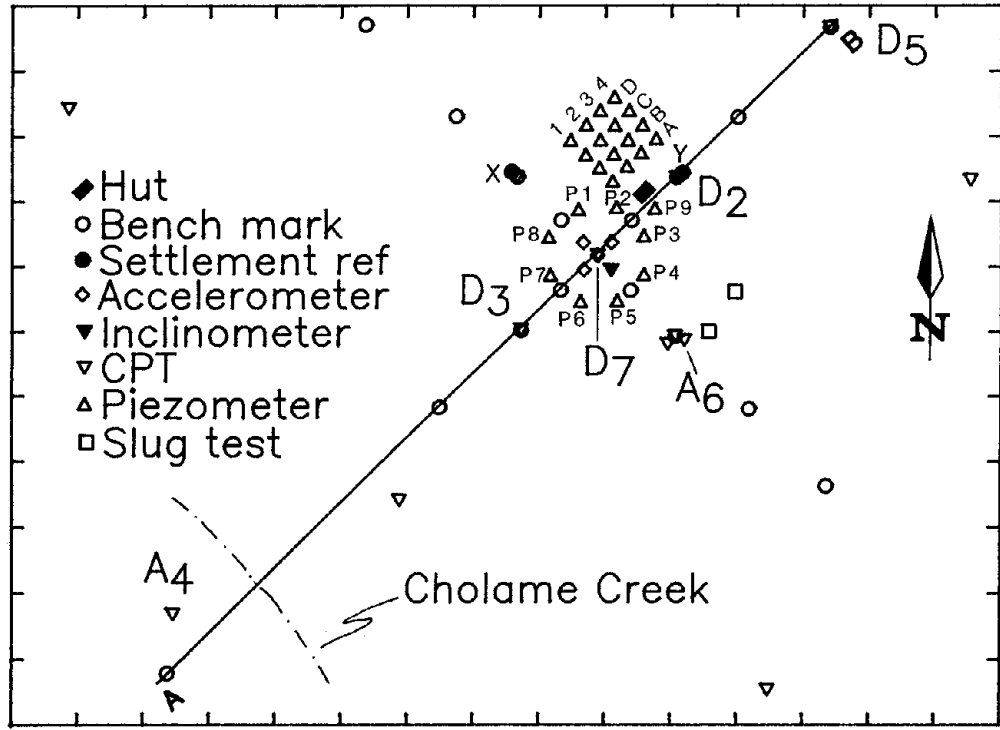


**Figure 1. Map of California with locations of Parkfield and Wildlife liquefaction arrays.**





(A) Map

(B) Cross section

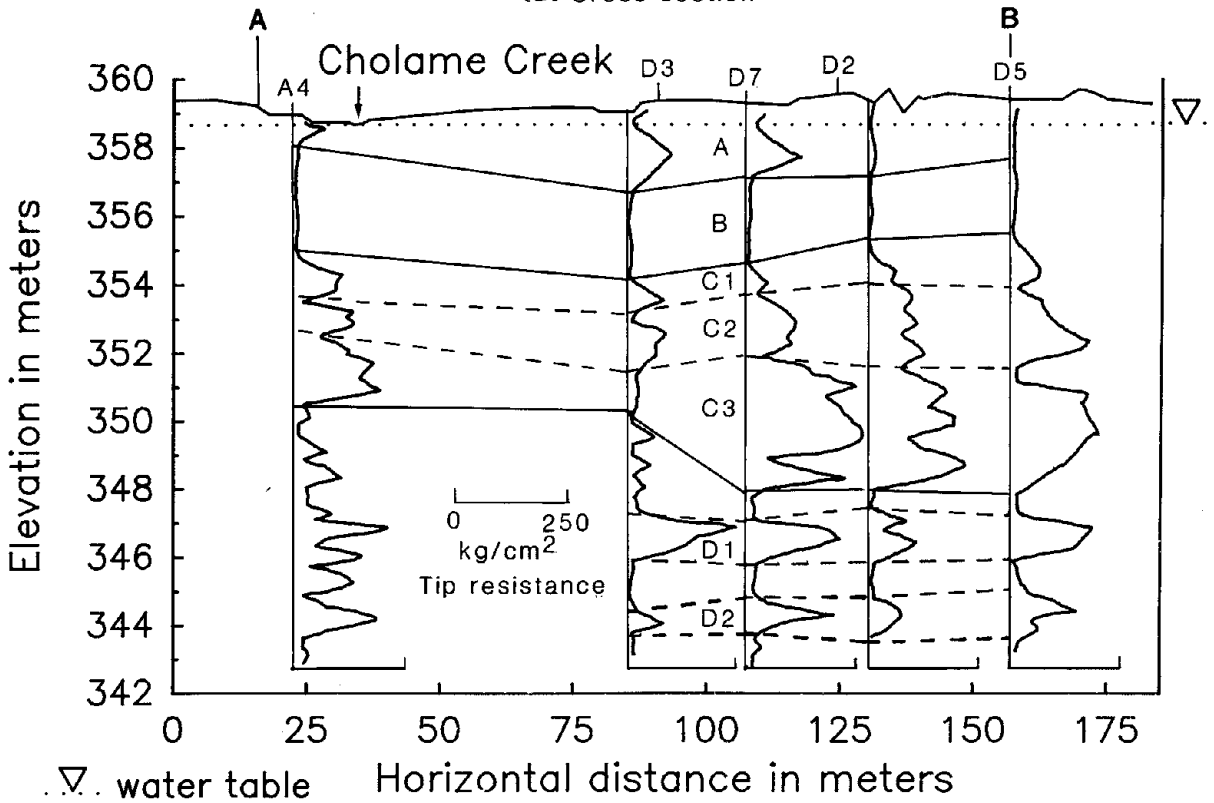
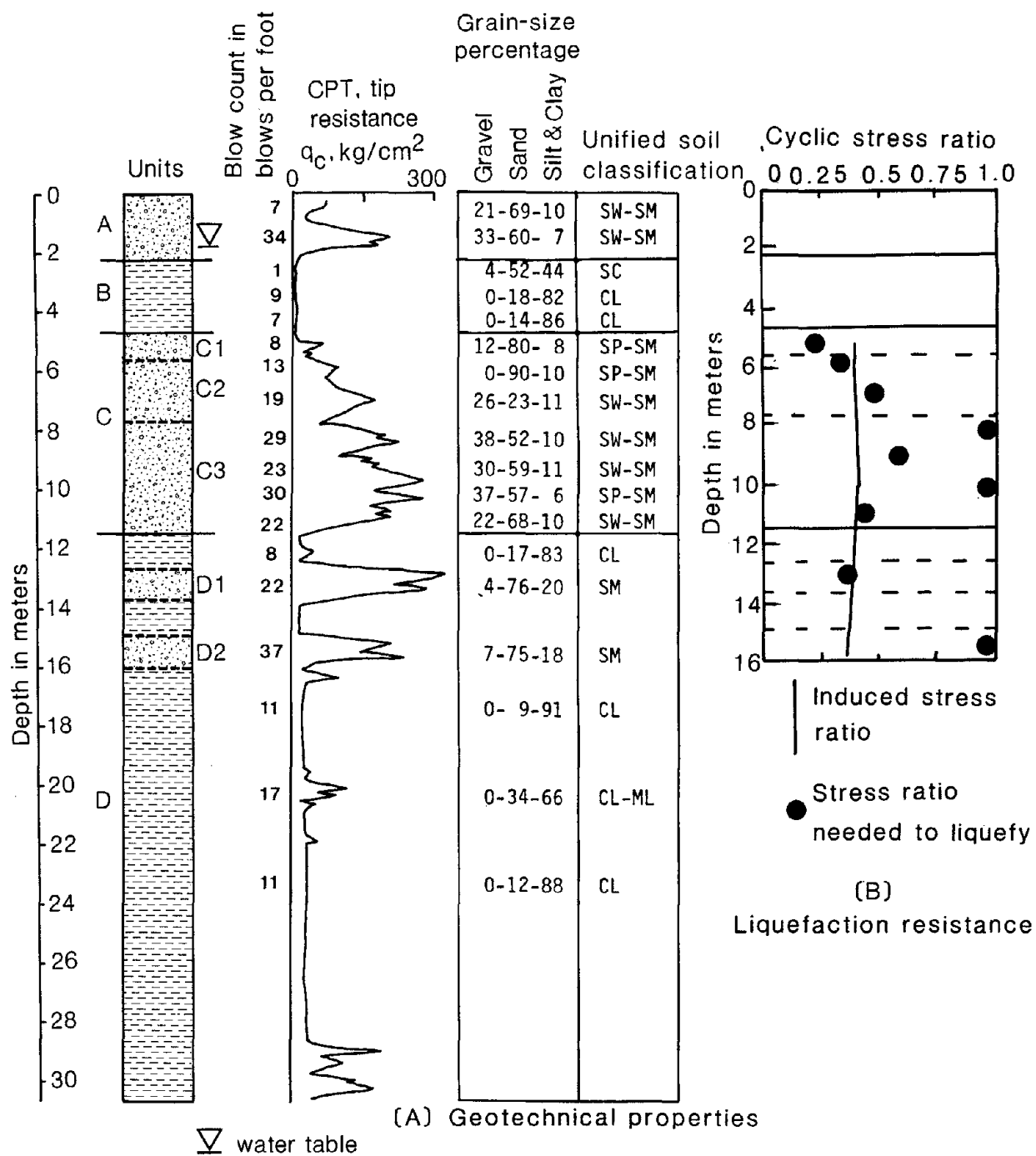
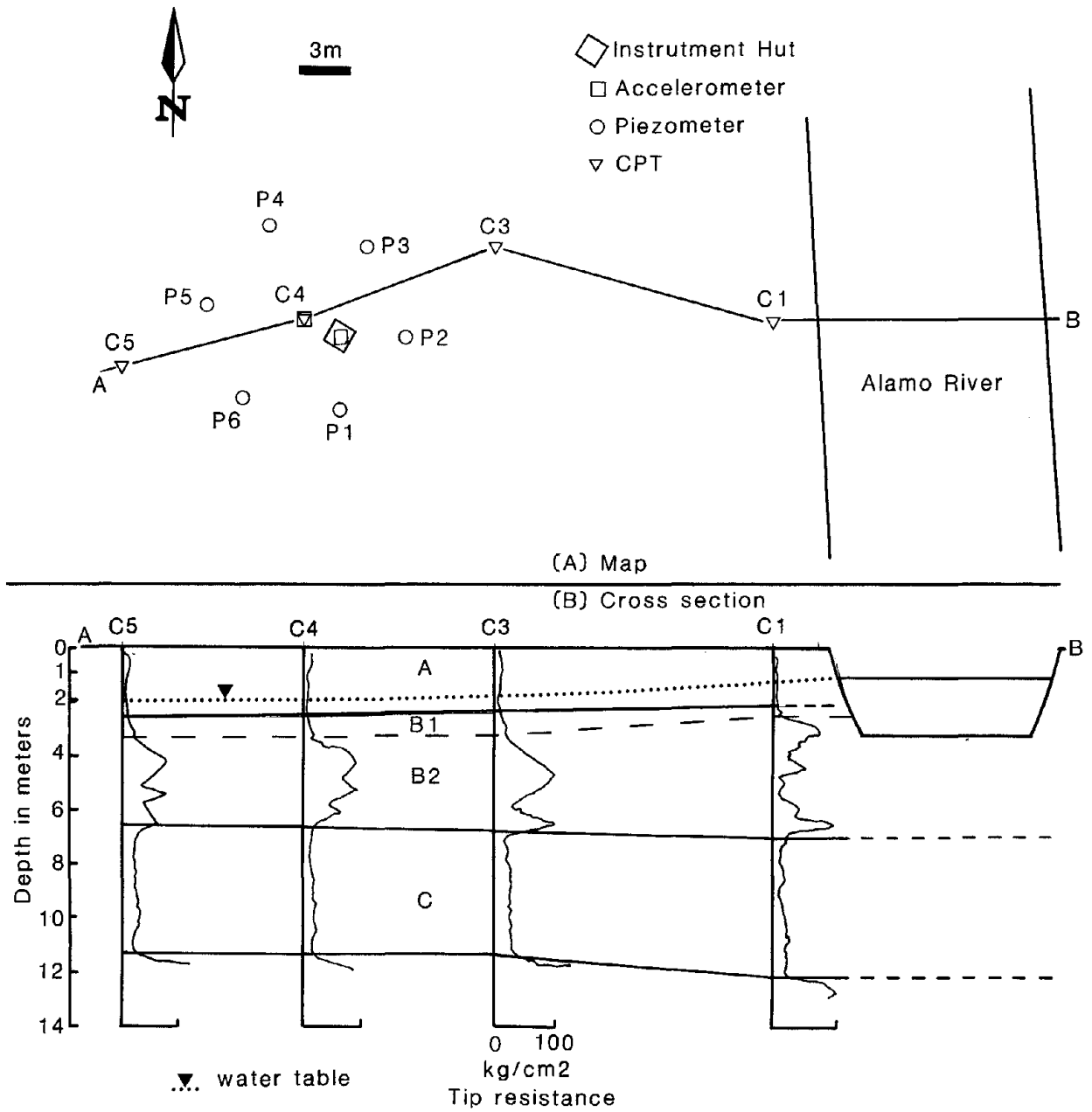


Figure 2. Parkfield liquefaction array.

A. Map of instrumentation. B. Cross section based on CPT's.



**Figure 3. Parkfield liquefaction array.**  
**A. Geotechnical properties (Sand and silt sizes range from 0.074 to 2.0 and 0.005 to 0.074 mm, respectively). B. Liquefaction resistance and induced stress ratio for predicted Parkfield earth.**



**Figure 4. Wildlife liquefaction array.**  
**A. Map of instrumentation. B. Cross section based on CPT's.**

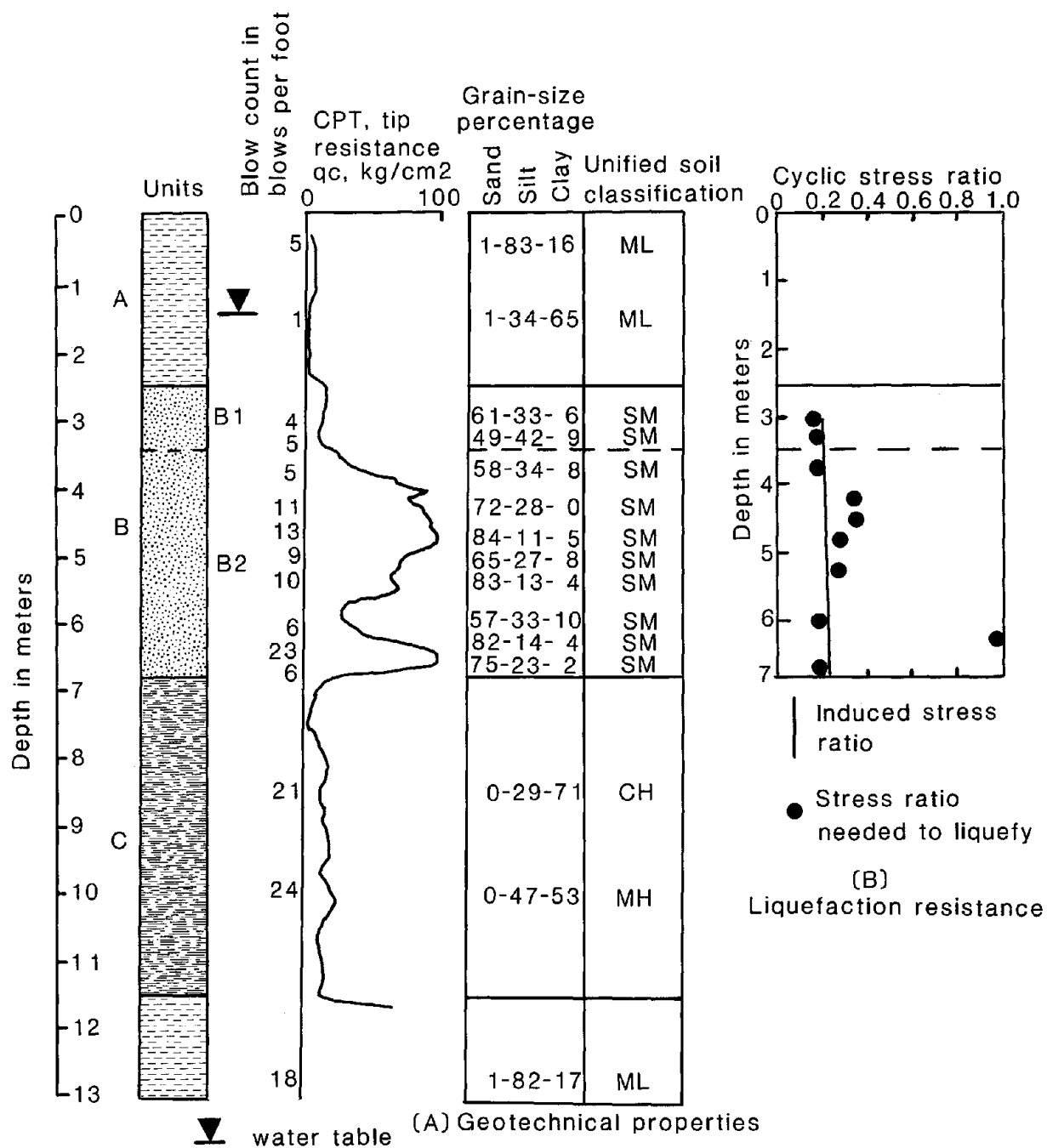


**Figure 5. Wildlife liquefaction array.**  
**A. Geotechnical properties. B. Liquefaction resistances and induced stress ratios for 1987 M6.6 Superstition Hills earthquake.**

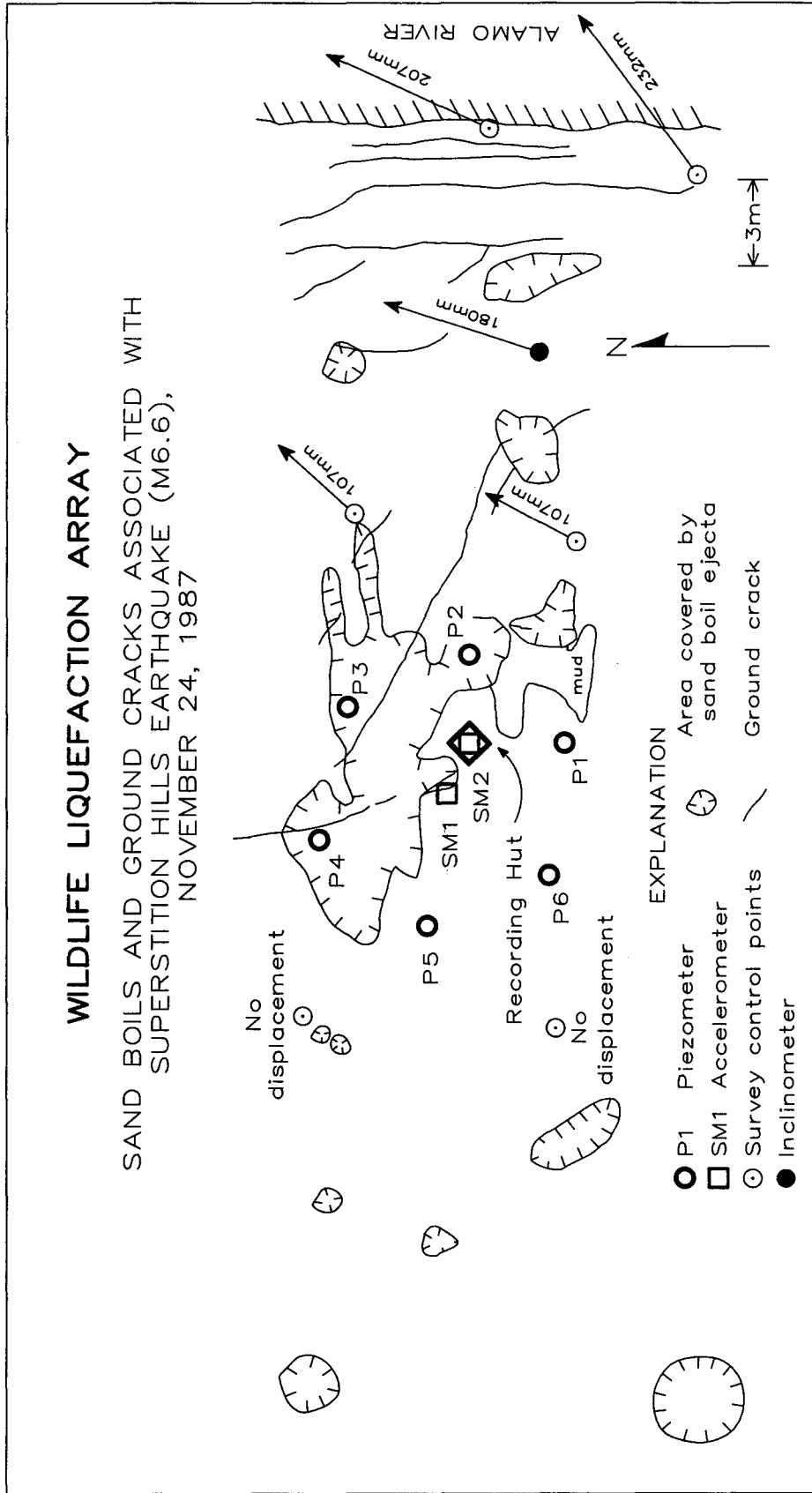


**Figure 6. Map of sand boils, lateral spreading cracks, and ground displacements caused by the Superstition Hills earthquake (Holzer and others, 1989a; Youd and Bartlett, 1988).**

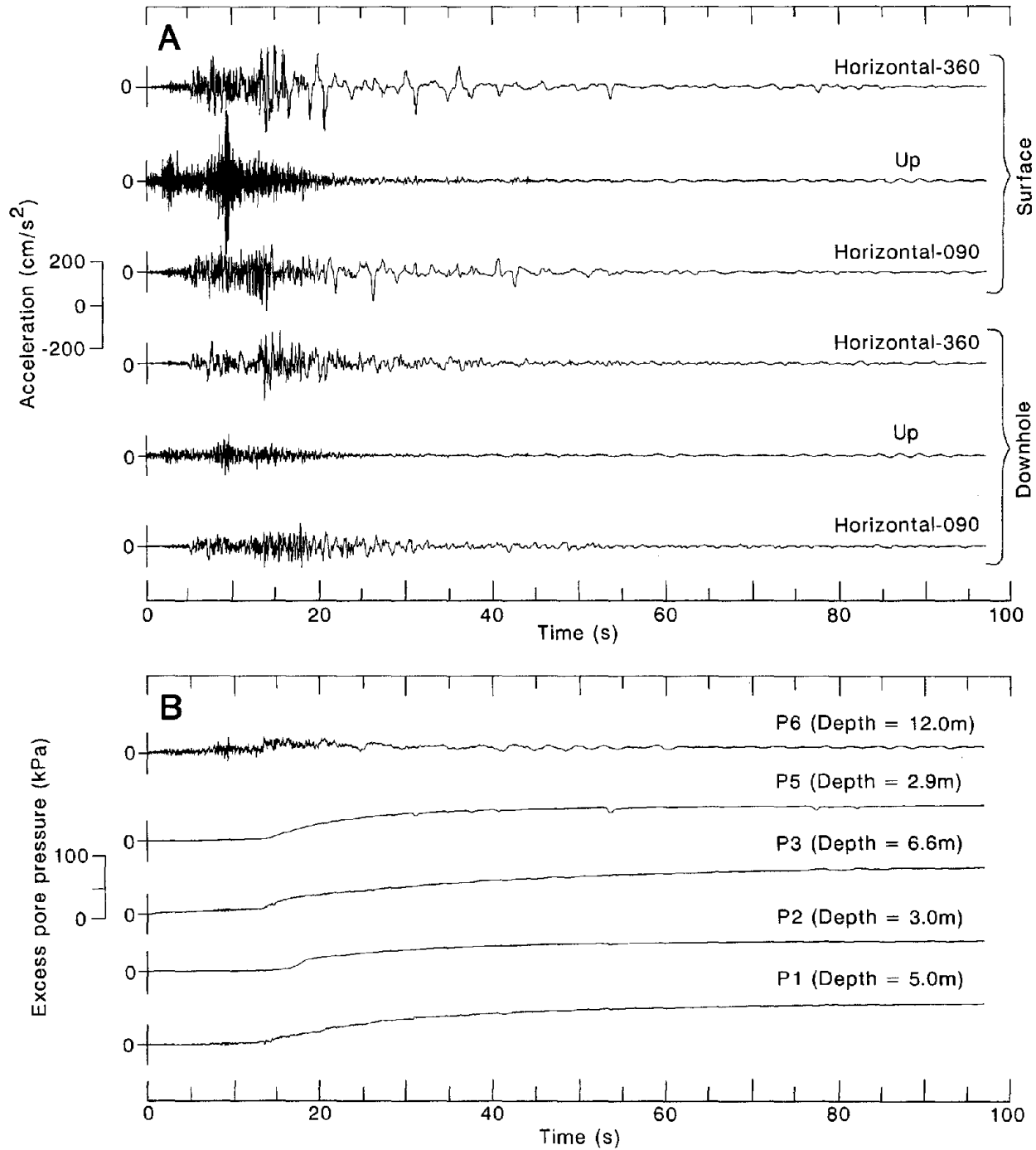


**Figure 7. Superstition Hills earthquake records at the Wildlife liquefaction array (Holzer and others, 1989b).**  
**A. Accelerations recorded by surface and downhole accelerometers.**  
**B. Excess pore pressures recorded by piezometers.**



**LIQUEFACTION AND GROUND FAILURE IN FERLAND, QUEBEC  
TRIGGERED BY  
THE 1988 SAGUENAY EARTHQUAKE**

Martitia Tuttle, Tim Law\*, Leonardo Seeber and Klaus Jacob

Lamont-Doherty Geological Observatory  
Palisades, New York 10964

\*National Research Council of Canada  
Ottawa, Ontario K1A 0R6

**ABSTRACT**

Geological and geotechnical investigations are currently under way for two sites in Ferland, Quebec where sand boils, ground fissures and liquefaction-related damages to homes were documented immediately following the M=5.9 Saguenay earthquake of November 25, 1988. Both sites are about 26 km from the epicenter. To date, the geological investigation of the sites suggests that (1) liquefaction and ground failure have occurred in this area in the past, (2) lateral spreading was the principal mode of ground failure in 1988 and in the past, (3) 1988 and earlier displacements due to lateral spreading were on the order of centimeters, and that (4) topography played an important role in the localization and characterization of ground failure. The geotechnical investigation suggests that (1) liquefaction at these sites is predictable using Seed's method, and that (2) the material that liquefied during the Saguenay earthquake is a gray, silty sand or sandy silt that is about 0.3 m thick and occurs at a depth ranging from 2.5 to 4.5 m below the surface. These preliminary results suggest that the potential for liquefaction and related damages in the Saguenay region may be higher than previously recognized.

## INTRODUCTION

The  $M=5.9$  Saguenay earthquake was located in the Laurentide Mountains at 48.121 N latitude, 71.186 W longitude and at 29 km depth by the Geological Survey of Canada, in a region believed to be relatively aseismic (Basham et al., 1979) (Fig. 1). A peak ground acceleration of 0.13 g was recorded on a hard-rock site about 43 km north of the epicenter. Liquefaction was documented at 5 sites in the Ferland-Boileau area about 25 to 30 km from the epicenter (Tuttle et al., 1989), a much greater distance than has been reported for liquefaction triggered by  $M\sim 6$  earthquakes in the western United States (Youd and Perkins, 1987).

This is the first earthquake in eastern North America for which both liquefaction was documented and ground motion recorded. This provides the opportunity to study the liquefaction potential and the ground failure hazard of glacial sediments typical of large areas of eastern North America, both in Canada and the United States. For this purpose, two sites have been selected in Ferland for exploratory field investigations. Earthquake effects documented at these liquefaction sites and preliminary results of geological and geotechnical investigations are summarized below. Also, other types of ground failure that were triggered by the Saguenay earthquake are mentioned briefly.

## LIQUEFACTION AND GROUND FAILURE IN FERLAND

### Documentation of liquefaction and ground failure effects

During a ground failure survey conducted during a two-week period following the Saguenay earthquake, sand boils, ground fissures and liquefaction-related damages to homes were observed in Ferland. Many of the ground effects were identified by questioning local residents who had observed sand boils and fissures before they were covered by snow that fell the day after the earthquake. Most people's observations were made close to their homes. For these reasons, the survey was incomplete and strongly biased towards populated areas.

At Site 1, located 25.6 km northeast of the 1988 epicenter, a sand boil (A), 0.5 to 1 m in diameter and 7.5 cm thick, formed 6 m from a house (Fig. 2). In addition, large quantities of gray sand were observed in the bed of a creek that traverses the site. Within 3 m of the house, a small fissure, 1 cm wide, at least 0.6 m long, and trending  $N33^\circ E$  was observed. Along the same trend and only 0.6 m away, a pre-existing crack in the sidewalk widened by upward buckling. Damage to the cinder-block house was greatest in the basement apartment where almost every wall was cracked. Displacements on these cracks indicated that the outside walls had moved down relative to the inside walls by about 1 cm (Fig. 3). The western wall, closest to the fissure and sand boil, was bulging inward, into the basement. Near the center of the basement, wooden floorboards buckled up by about 1 cm. On the east side of the house, the floor was separated from the baseboard by about 1 cm and sand and water entered the basement through this crack during the earthquake. Water and sand also backed up the drain into the bathtub and shot out of the toilet. The tenant had removed gray, fine sand, 22 cm thick, from the bathtub. Few cracks were visible in the walls of the upstairs apartment. However, the floor in the upstairs kitchen had a noticeable bulge that the resident claimed was caused by the earthquake. On the exterior of the house, every cinder-block wall was cracked and the chimney was tilted.

During a visit to the site in June 1989, a large sand boil (B), 4.5 to 10 m in diameter and 22 cm thick, was observed in the creek bed 46 m from the house. Several smaller sand boils, about 10 cm in diameter, were still visible along the banks of the creek. The water well which had been filled in by gray, fine sand during the earthquake went dry in July 1989. During the topographic survey of the area in August 1989, another sand boil (C) 30 cm in diameter was discovered south of Rue Paquet. The basement floor of a nearby house suffered damage during the earthquake including an apparent elevation of the center portion of the basement floor and cracking of the concrete foundation. In addition, the water well for this house also had filled with sand during the earthquake.

The formation of sand boils, the intrusion of water and sand into the house, and the sanding in of wells indicate that a subsurface layer of very fine, gray sand of liquefied over an area of at least 60 m<sup>2</sup> during the earthquake. The relative shear between the exterior and interior walls of the house suggests foundering of the footing in the liquefied material. Buoyant forces of liquefied sand or sediments displaced by the foundering of footings may have pushed up the unattached basement floor. The formation of the fissure west of the house, the bulging of the western wall, and the buckling of both the basement and upper-story floors suggest a small amount of lateral movement towards the east.

At Site 2, located 26.3 km from the 1988 epicenter, two sand boils and three fissures formed within 30 m of another house that was damaged during the earthquake (Fig. 4). One sand boil (E), which was about 3 m in diameter, formed 7.6 m from a creek that defines the eastern boundary of the site. The other sand boil (F), which was about 1 m in diameter, formed 3 m from the western edge of an artificial pond. The three fissures were roughly parallel and exhibited separations of about 8 mm. Sand and water also entered the basement of this house during the earthquake. Water as deep as 10 cm briefly covered the basement floor before draining away. A 20 to 30 cm thick layer of gray, fine sand was deposited on the basement floor and injected up between the studs along the western, northern and southern walls. In the walls of the first floor, there were a few cracks exhibiting small displacements indicating that the exterior walls had moved down relative to the interior walls by about 1 cm. The foundation of the northwestern corner of the house had separated from the garage floor also by 1 cm. According to the home owner, the excavation for the foundation had been in coarse sand and gravel. Gray, fine sand similar to that which had entered the basement during the earthquake had been observed in the northwest corner of the excavation.

The formation of two sand boils and the intrusion of large quantities of sand and water into the basement indicate that subsurface material liquefied during the earthquake. The shear between the interior and exterior walls of the house suggests that the footings foundered in the liquefied material that may underlie much of the foundation. The formation of fissures and the separation of the house foundation from the garage floor suggest a small amount of lateral movement towards the creek. A distance of 71.93 m between property markers near the edge of Route #381 and the western edge of the creek, Bras Hamel, had been measured with a tape some time before the earthquake. This distance which spans the three fissures was remeasured after the earthquake and was found to be about 1.8 cm longer. Although compelling, this measurement may be irrelevant due to possible errors in the technique used.

### **Geological investigation of liquefaction sites**

Two sand boils at Site 1 and one sand boil at Site 2, excavated in August 1989, are characterized by aprons deposited on the ground surface and by dikes, sills and conduits emplaced within glacial sediments and modern soils. In addition to these 1988 liquefaction

features, other structures were revealed in the excavations that are suggestive of two earlier liquefaction events.

At Site 1, sand boil A, located close to the damaged house, was about 1 m in diameter, 7 cm thick and composed of very fine, sandy silt (Fig. 2). In the excavation of the boil, a well-developed system of subsurface dikes and faults was exposed (Fig. 5). These dikes could be followed along a northeast trending, linear zone just below the modern soil for a distance of 4 m. The main dike was subvertical and was well defined below 1 m. Above this depth, the dike split into a family of thin and discontinuous dikes. Several subsidiary dikes branched upward from the main dike, occurring along faults exhibiting centimeters of displacement. Where dikes encountered pebbles or stones, sand had accumulated below the obstacles. Dikes injected along normal faults terminated at the contact between silty, very fine sand below and medium sand above. Sedimentation within the dikes varied with depth. Below 1.5 m, the dikes exhibited vertical grading and were finer-grained near their edges; above this depth, dikes exhibited horizontal grading. Two normal faults and one thrust fault offset a 27 yr-old layer of fill by 1.5 to 3 cm. The trend of the dikes and normal faults were roughly parallel to the topographic contour. Displacements up to 11 cm of depositional contacts were greater than the displacements of the fill. This suggests that these faults were older than the fill, were reactivated during the 1988 event, and experienced at least one pre-1988 displacement.

Sand boil B at Site 1 was about 10 m in diameter and upto 22 cm in thickness. It was the largest boil observed at either site and was comprised of at least 4 coalesced aprons. The fans of the aprons were composed of laminated and graded, gray, fine sand and silty, very fine sand. The vents of the aprons were characterized by steep truncation of the subhorizontal laminae of the fans and by normally graded, fine to coarse sand. Clasts of soil occurred locally within both the fan and vent deposits. The sand boil was fed from below via 4 conduits through the organic-rich surface horizon and at least 1 steeply-dipping dike through a subsurface layer of medium-grained sand. The conduits ranged from 5 to 15 cm in width and were widest near the surface. The dike was about 30 cm in width and dipped 70° to the northeast. The trend of the dike is subparallel to the creek bed in which the sand boil formed. Sills upto 10 cm wide were emplaced below the organic-rich surface horizon.

At Site 2, sand boil E which is located within 8 m of the creek, Bras Hamel, was about 3 m in diameter and composed of very fine to coarse sand. Like sand boil B, the fan deposit was comprised of laminated and normally graded, gray, fine sand and silty, very fine sand. The vent deposit truncated the subhorizontal laminae of the fan and was composed of normally graded, fine to coarse sand. The boil was fed from below by a dike dipping 40° to the northeast that could be traced below boulders to a depth of 1 m. Sand had accumulated below these boulders as well as smaller stones that were in the pathway of the dike. The trend of this dike as observed near the surface is perpendicular to the topographic contour. This is opposite to observations at Site 1 where dikes were oriented roughly parallel to the local topographic contour. In this case, the large boulders may have played a large role in the near surface emplacement of the dike.

Based on observations at both sites, dikes appear to be the primary pathway for liquefied sand as it moves towards the ground surface from its source. Textural and structural characteristics of 1988 dikes suggest that the pore pressure of escaping liquefied sand is significantly affected by the permeability of host sediments. Therefore, the permeability of near-surface sediments may play an important role in determining the types of structures formed during liquefaction events. If the permeability of the near-surface sediments is high, then the pore pressure of the liquefied sand is reduced and structures either terminate or are only weakly developed. If the permeability of the host sediments is low, which is the case for thick soil or organic-rich layers, then sills and conduits may form as secondary pathways. Furthermore, boulders or

other impermeable objects can obstruct the movement of liquefied sand resulting in accumulations of sand below these obstacles and possible deflection of the course of the dikes.

The occurrence of several 1988 sand boils near slope breaks suggest that topography may influence the localization of ground failure. Furthermore, the orientation of the sand dikes and related faults parallel to the topographic contour suggests that lateral spreading resulting from liquefaction is the principal mode of ground failure. The relationship of normal faults to a well developed system of 1988 sand dikes supports this hypothesis. The thrust fault exposed in the excavation of sand boil A is perpendicular to and cross-cuts normal faults suggesting that its formation post-dates the other structures and is due to forceful injection or diapirism. Hypothetically, once a subsurface layer has liquefied, overlying material could begin to move downslope or towards a free-face. Tension fractures would form in the upslope portion of the slide block. Downslope or lateral movement of surficial materials would create an unstable boundary condition along the tension fractures leading to normal faulting of adjacent sediments into the fracture. Liquefied sand would forcefully fill the fractures, possibly driving fracture propagation towards the surface and causing reverse faulting in near-surface sediments.

In addition to 1988 structures, two generations of older structures that are likely to be related to past liquefaction events were observed in the excavations. The younger generation is characterized by weathered dikes and sills similar to 1988 structures in texture and morphology. The older generation is strikingly different from the more recent dikes and sills in size and morphology. The older structures exhibit a high degree of weathering, primarily iron-staining and -cementation and are cross-cut by younger generation as well as 1988 dikes and sills.

In the excavation of boil A, several weathered dikes and sills were exposed which are suggestive of an earlier liquefaction event. Some of the weathered dikes are associated with the normal and reverse faults mentioned above and appear to have been intruded by 1988 dikes, including the main dike. In addition, a much larger structure was exposed that was comprised of a weathered, 10 cm wide sand dike at depth and an iron-stained and -cemented, 2 m wide sand crater near the surface. Organic material lined the base of the crater and clasts of host sediment were contained within the crater. Reverse faults with up to 20 cm of displacement occurred within 0.5 m of the crater and rooted into the associated sand dike. Although different from 1988 liquefaction structures, this feature exhibits many of the characteristics of sand-blows in Charleston, South Carolina (Obermeier et al., 1986) suggesting that it is also related to liquefaction. The relationship of the reverse faults to the sand dike is not clear. However, the reverse faults do not cut the dike and therefore may pre-date it. The reverse faults may have controlled the emplacement of the dike. The iron-stained sand crater and the proposed feeder dike are cut by 1988 as well as the older weathered sand dikes.

Weathered dikes and sills were also observed at Site 2 in the excavation of sand boil E. The weathered dikes cross-cut a charcoal layer which may be related to a fire that burned much of the region in 1870. Furthermore, they cross-cut older deformation structures including sand lenses located below boulders and 30 cm wide dikes and diapirs. Overlying organic-rich sediment and soil are deformed by these older structures. A post-depositional bearing-strength failure due to liquefaction is one plausible mechanism for the formation of these structures. The degree of iron-staining of the sand in these structures is similar to that of the sand filling the crater at the other site, suggesting that the oldest deformation event at both sites may be contemporaneous.

Evidence for an earlier liquefaction event similar to the 1988 event suggests that the Ferland area has been subjected to moderate ground shaking in the recent past. If the charcoal layer that is cut by weathered dikes does date back to the 1870 fire, then these structures would post-date

the fire. Perhaps these structures were induced by the large 1925 earthquake. There are older structures that are suggestive of an even earlier liquefaction event. The size and nature of the structures suggest that pore pressures were much higher during this event and that the earthquake may have been either larger than the 1988 earthquake or closer to Ferland.

### **Geotechnical investigation of liquefaction sites**

Ten soil profiles at six sites in the Ferland-Boileau area have been determined using a GMF 50-kN piezocone penetrometer. This penetrometer is fitted with a 60° tapered, 10 cm<sup>2</sup> area cone to measure tip resistance and sleeve friction. Pore pressure generated during the penetration test was measured through a 4 mm thick cylindrical filter attached immediately behind the conical tip. The measured tip resistance, sleeve friction and pore pressure were used to identify soil types based on existing charts by Jones and Rust (1982) and Searle (1979). At each site, soil samples from the ground surface to the liquefied layer were taken by means of 15.2 mm diameter flight augers.

The liquefied layers have been identified in two ways. The first is based on the method of Seed et al. (1983) for use with the standard penetration resistance, *N*, which is then converted to cone tip resistance as proposed by Robertson et al. (1983) (Fig. 7). No information on the peak horizontal acceleration was available for these sites, which are closer to the epicenter than any sites where ground motion was recorded. After consideration of the substantial depth of the hypocenter and possible soil amplification at the sites, a peak horizontal acceleration at the ground surface of 0.25 *g* was assumed where *g* is the gravitational acceleration. The second method is a comparison of the color, texture and grain size distribution of the vented material at the sites and of the soil samples taken at depth (Fig. 8). The two methods identified the same liquefied layer.

A soil profile for Site 1 near sand boil A is shown in Figure 7. The top 1.5 m is composed of top soil and fill comprised of gravelly sand and clayey silt. The fill is underlain by a 7.5 m thick silty sand deposit. This deposit exhibits very loose to medium dense compactness. The liquefied layer is about 0.3 m thick and is found in this deposit between 4.4 to 4.7 m depth. The silty sand deposit is underlain by a 3 m thick silty clay deposit. Below the silty clay deposit, a hard gravelly layer was encountered at 11 m.

Except for variations in deposit thicknesses, the soil profiles at other sites are similar to the profile at Site 1. At the other sites, the liquefied layer appears to be of similar material but occurs at different depths, ranging from 2.5 to 4.5 m. At Site 2 in Ferland and two sites in Boileau, layers of black to dark brown organic silt, 1 to 3 m thick, were found near the surface.

The grain size distributions have been determined for the vented sand in the boils at three sites in Ferland, including Site 1 (Fig. 8). The material is a gray, silty sand or gray, sandy silt with a mean grain size, *D*<sub>50</sub>, varying from 0.04 to 0.1 mm. The clay content is less than 5%. The grain size distributions of the liquefied layer sampled at depth are very similar to those of the material collected at the surface.

## OTHER TYPES OF GROUND FAILURE

Several earthquake-induced landslides were also documented during the initial survey, including a failure of a  $10^\circ$  slope in St. Thecle about 180 km southwest of the epicenter (Tuttle et al., 1989). The slide is about 88 m across from one side of the scarp to the other, extends 150 m from the main scarp across the valley and has the morphology of a slump-flow failure (Fig. 9). The creek at the bottom of the slope was buried by about 10 m of slide debris which covered the entire span of the valley. Minimum horizontal and vertical displacement of 52 and 12 m, respectively, can be measured from the main scarp to the pile of debris at its base. A geotechnical investigation currently under way has not yet resolved whether the failure occurred within marine clay or at the contact of the clay and the underlying sandy till (Lefebvre, personal communication, 1989).

Rock slides triggered by the 1988 event were prevalent in the high relief areas of the Laurentide Mountains. The largest slide observed was south of Lac Ha! Ha! about 25 km from the epicenter. The slide was about 100 m in height and 50 m in width and composed of blocks with dimensions as large as 10 m. The vertical displacement was at least 80 m. At the base of this and other rock slides, there was clear evidence of past slides including large blocks exhibiting weathered surfaces and previously damaged trees. The prevalence of 1988 slides and the presence of pre-1988 liquefaction features observed in the excavations in Ferland suggest that many of the older rock slides may also be earthquake-induced.

## CONCLUSIONS

Sand boils, ground fissures and liquefaction-related damages to homes and to water wells were documented in Ferland, Quebec following the  $M=5.9$  Saguenay earthquake. Several sand boils were excavated and physical and sedimentological characteristics described. Sand boils ranged in size from 10 cm to 10 m in diameter and up to 22 cm in thickness. They were comprised of fan and vent deposits ranging in grain-size from very fine, sandy silt to coarse sand. The largest sand boil was composed of at least 4 coalesced aprons. Below the surface, sand boils were fed by sand conduits, dikes and sills. The conduits were typically 5 to 15 cm in diameter and the dikes and sills ranged from 1 to 30 cm in width. Sills occurred below soil or organic-rich horizons and sand conduits occur within these horizons. Sills and conduits are best developed where the soil is at least 0.3 m thick. Dikes were better developed at depths greater than 1 m. In addition to these structures, lenses of sand accumulated below stones, boulders or other obstacles which had been in the pathway of the escaping sand.

In every excavation, there were weathered dikes and sills similar in size, texture and morphology to 1988 structures. These structures are likely to have formed during a past event of similar intensity. In addition, even older sand dikes, craters, diapirs and lenses have been recognized from cross-cutting relationships and advanced weathering characteristics. These older structures are much larger than the 1988 and weathered dikes and sills and may be indicative of more elevated pore pressures than was achieved during the 1988 event. The physical characteristics and degree of weathering of the pre-1988 structures are consistent between excavations supporting the hypothesis that they formed during two separate events.

The occurrence of several 1988 sand boils near slope breaks suggests that topography may have exerted influence on the localization of ground failure. Furthermore, the orientation of recent and old sand dikes and related faults parallel to the topographic contour suggests that

lateral spreading resulting from liquefaction was the principal mode of ground failure during the recent Saguenay earthquake as well as during past earthquakes.

A comparison of old structures with 1988 liquefaction features suggests that the Ferland area has been subjected to moderate ground shaking in the recent past, perhaps during the 1925 St. Lawrence Valley earthquake, and to more severe shaking in the prehistoric past. In the future, radiocarbon dating of organic-rich samples from the excavations will help to constrain the ages of these structures. If the two generations of older structures are indeed earthquake-induced liquefaction features, then at least three moderate to large events have occurred in the area since the deposition of the sediments about 10,000 years ago. This would suggest as an upper limit a 3,300 year recurrence interval for moderate to large earthquakes in this region. Actual recurrence times could be shorter. A broader-based survey would help to test these preliminary results and to determine the sizes, dates and locations of possible past earthquakes.

Results of the geotechnical investigation indicate that the material in Ferland that liquefied in 1988 ranges from a silty sand to a sandy silt, usually occurs at depths between 2.5 and 4.5 m and is about 0.3 m in thickness. The liquefied layer was identified both by Seed's method using an estimated peak horizontal acceleration of 0.25 g and by comparison of the vented material with auger samples taken at various depths. Peak ground accelerations greater than 0.25 g would probably result in liquefaction of a considerably larger thickness of material.

The November 25, 1988 earthquake triggered various types of ground failures as far as 180 km from the epicenter. Landslides exhibited tens of meters of displacement; whereas, displacements resulting from liquefaction were on the order of centimeters. Liquefaction occurred 26 km from the epicenter or about 39 km from the hypocenter, approximately ten times farther from the Saguenay earthquake epicenter than documented for western U.S. earthquakes of similar magnitude. This phenomenon is not surprising (Youd and Perkins, 1987) and may be due to various factors including soil properties, site amplification due to the impedance contrast between hard, crystalline rock and soft, Quaternary sediments, topography, duration of ground shaking, and frequency content and attenuation characteristics of the ground motion. One striking implication is that liquefaction potential may significantly contribute to seismic hazards in eastern North America.

## ACKNOWLEDGEMENTS

Supported by National Center for Earthquake Engineering Research contracts 88-1303 and 88-1508. Many thanks to John Adams of the Canadian Geological Survey for his encouragement to conduct a post-earthquake ground failure survey in Quebec and to many people of the Saguenay region for their generous assistance, particularly Francoise Lange and Professors Duberger and Roy at l'University du Quebec a Chicoutimi, Roland Veilleux at the Ministere de l'Energie et des Ressources, and Sylvie Gagnon at the Ferland-Boilleau municipal office. Thanks to the many property owners of Ferland especially Josee Simard and Michele Simard for permission to work on their land. Caroline Moseley and Claude Otis provided valuable assistance in the field and Sue Hough and John Beavan faithfully reviewed this manuscript. Lamont-Doherty Geological Observatory Contribution #4549.



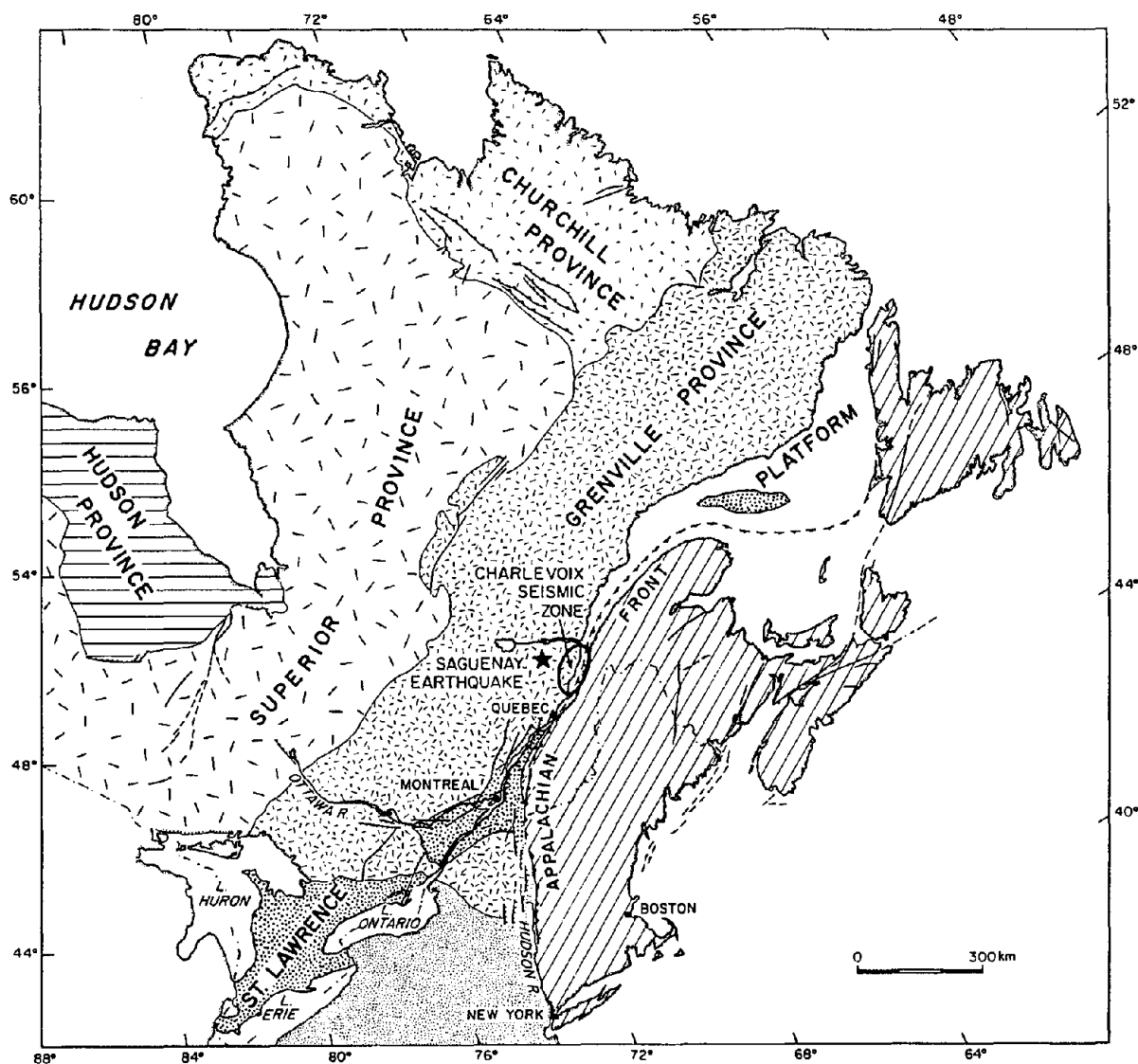


Figure 1. The November 25, 1988 Saguenay earthquake occurred west of the Appalachian Front within the Precambrian Grenville Province. In sharp contrast to the active Charlevoix Seismic zone located about 80 km southeast of the Saguenay earthquake, the Saguenay region was thought to have experienced few historic earthquakes and therefore to be relatively aseismic.

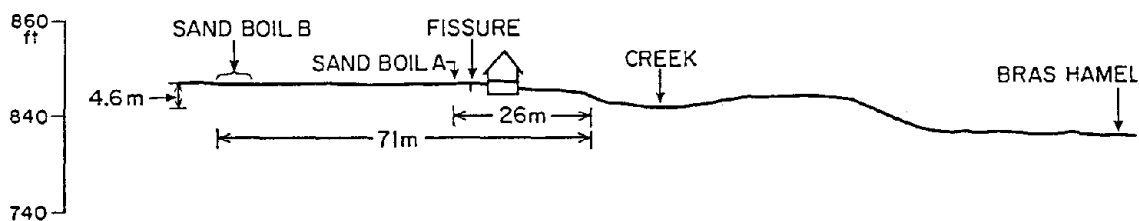
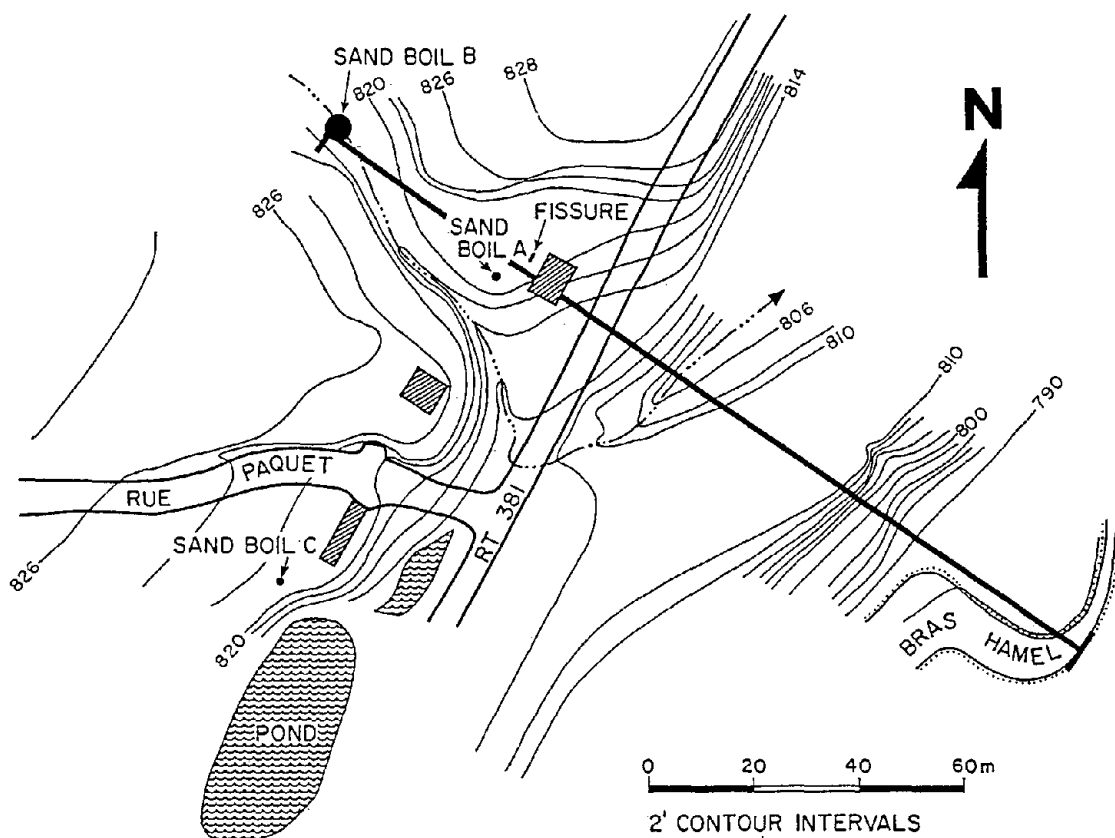


Figure 2. Topographic map and profile of Site 1 in Ferland with locations of sand boils and ground fissures induced by the Saguenay earthquake. The house along the line of section suffered damage due to the earthquake (see Fig. 3).

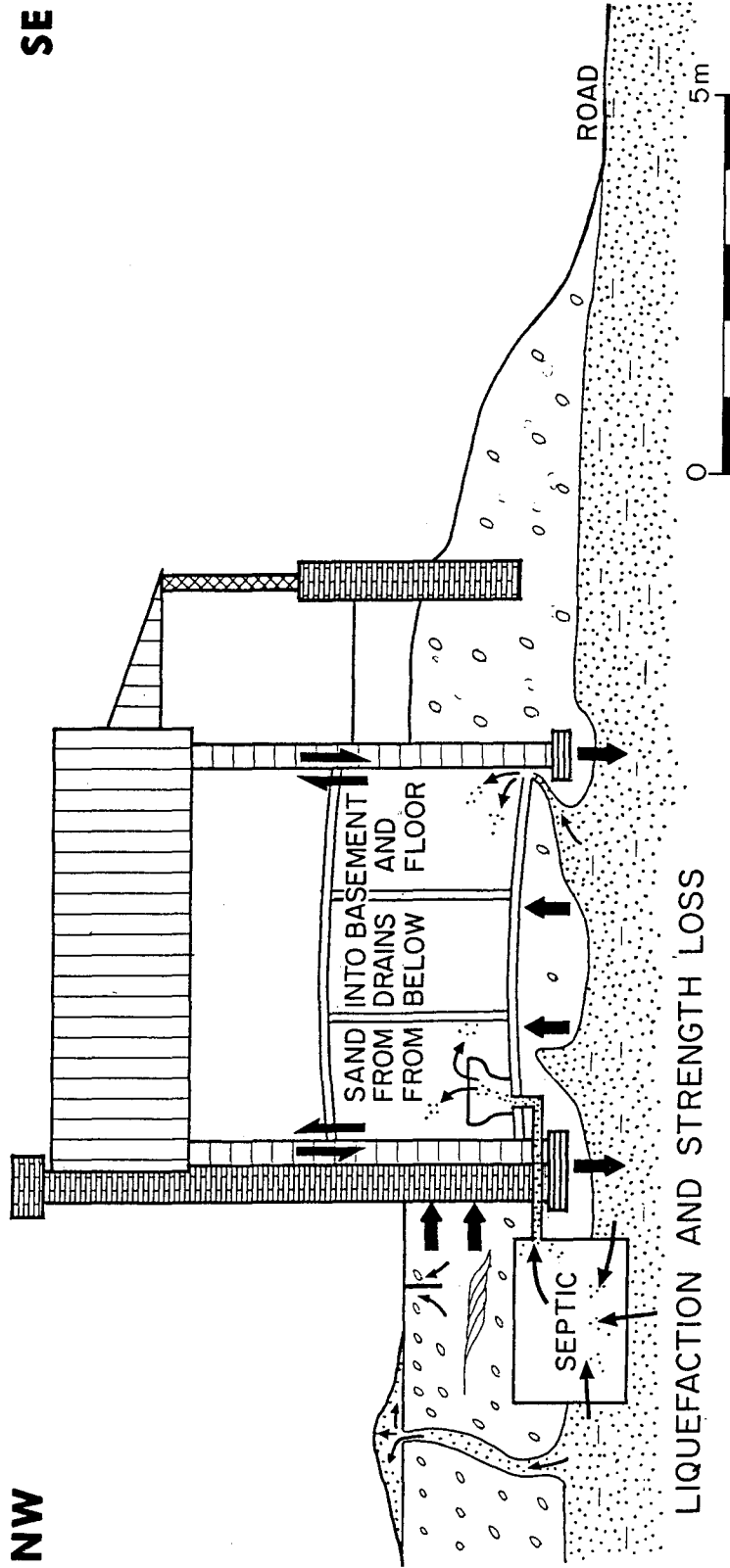


Figure 3. Sketch of damage caused by liquefaction to a house in Ferland. The floors buckled upward and the interior walls were sheared upward relative to the outside bearing walls by about 1 cm. Very fine, gray sand and water entered the cellar via the drains and a 1 cm gap that formed between the floor and the foundation. A ground fissure and sand boil formed a few meters from the house and a nearby stream was choked with vented sand. Liquefaction of a subsurface layer, probably glaciolacustrine in origin, may have caused lateral spreading and foundering of the house footings. In addition, the cement-block walls cracked in many places, substantially weakening the building. Very similar kinds of damage were observed at another cement-block home in Ferland.

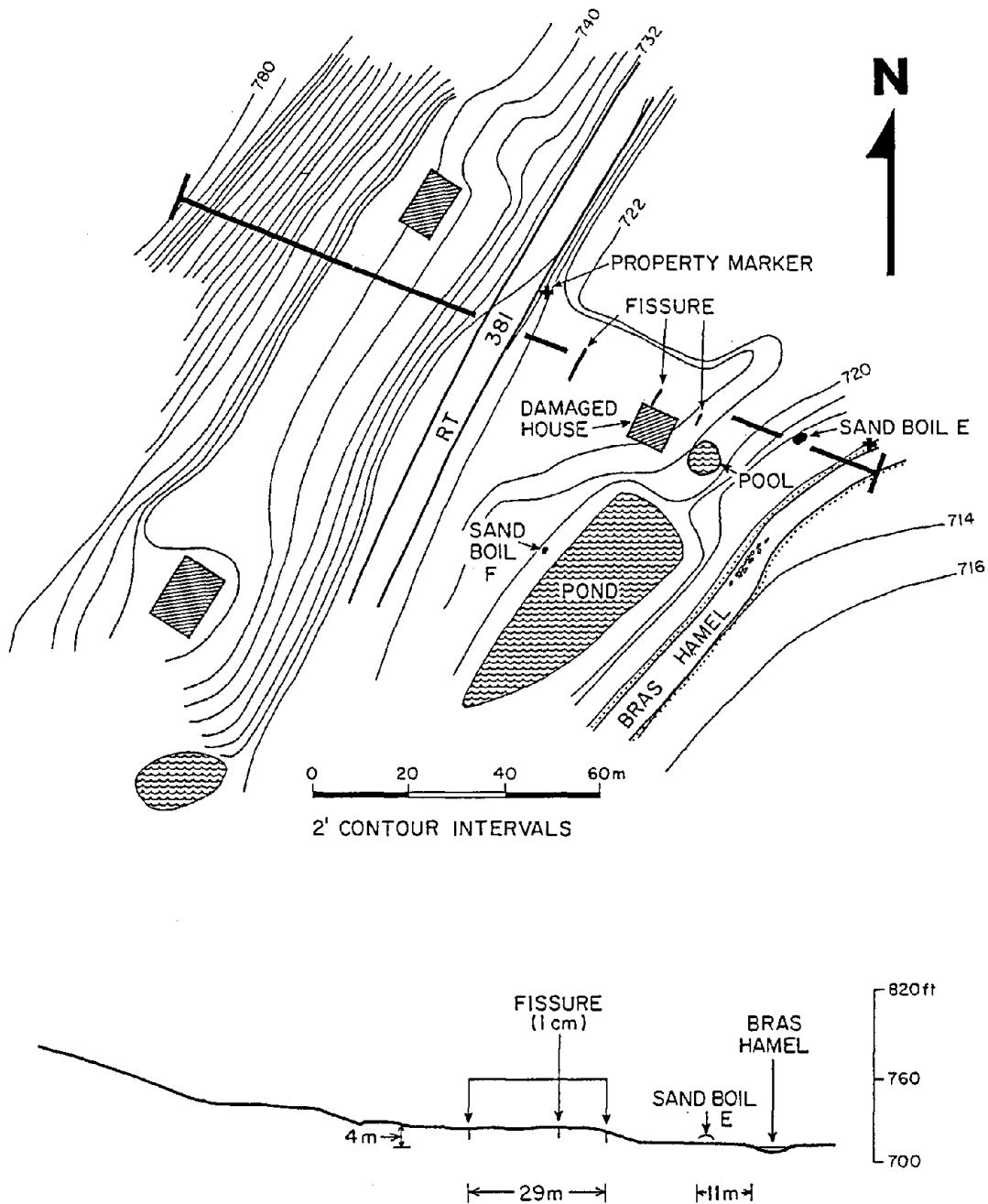


Figure 4. Topographic map and profile of Site 2 in Ferland with locations of sand boils and ground fissures induced by the Saguenay earthquake. The house east of Rt. 381 located along the line of section sustained damages similar to those of the house at Site 1 (Fig. 2 and 3).

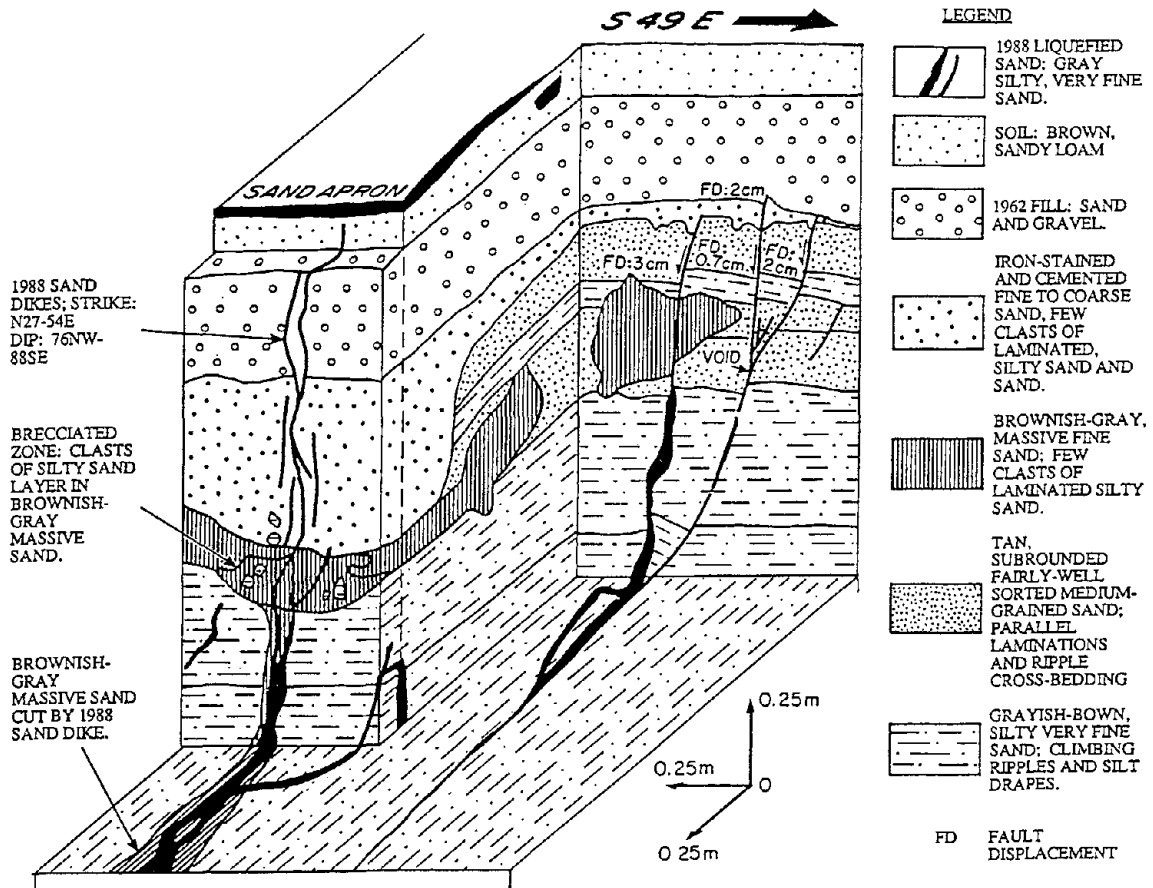


Figure 5. Block diagram of an excavation of the sand boil A at Site 1. Sand liquefied during the 1988 earthquake was intruded along a steeply dipping dike directly below the sand boil and also along several subsidiary dikes that are associated with normal faults. The subsidiary dikes are subparallel to the main dike. The system of 1988 dikes is subparallel to the topographic contour and occurs upslope from a topographic break. The emplacement of the dikes may be linked to the formation of tension cracks in unconsolidated sediments during downslope movement over a liquefied layer. Older liquefaction structures include weathered sand dikes and a crater filled with iron-stained sand.

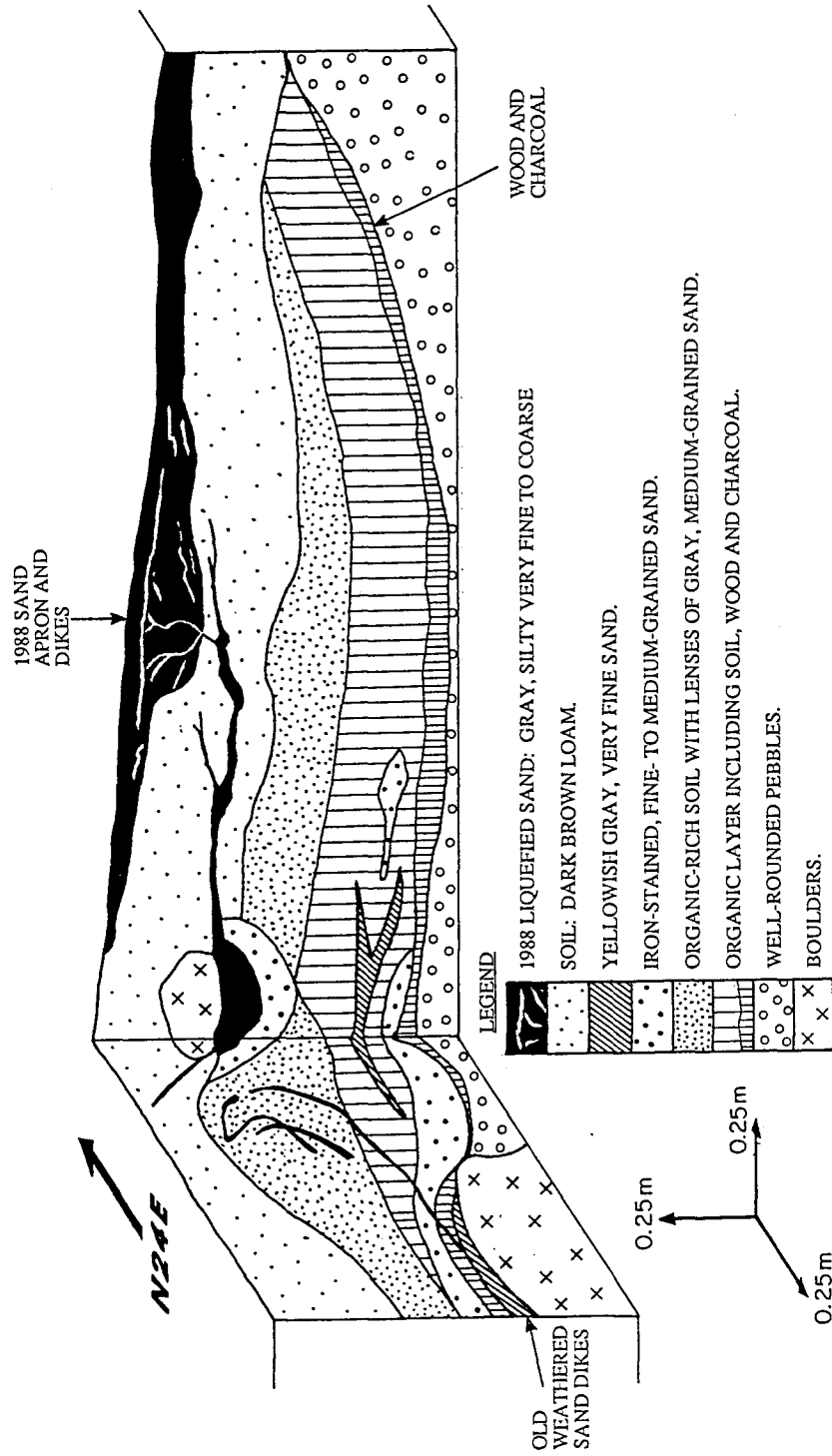


Figure 6. Block diagram of an excavation of sand boil E next to the creek, Bras Hamel, at Site 2 (Fig. 4). Sand liquefied during the 1988 earthquake was intruded along a moderately dipping dike. The dike is roughly perpendicular to the topographic contour and occurs downslope from a topographic break. The formation of the dike may be linked to compression in the toe of a lateral spread or may reflect the influence of boulders on the emplacements of dikes. An older dike cross-cuts a charcoal layer that may date back to an 1870 fire. Other old structures that may be related to liquefaction include dikes, diapirs and lenses of iron-stained sand.

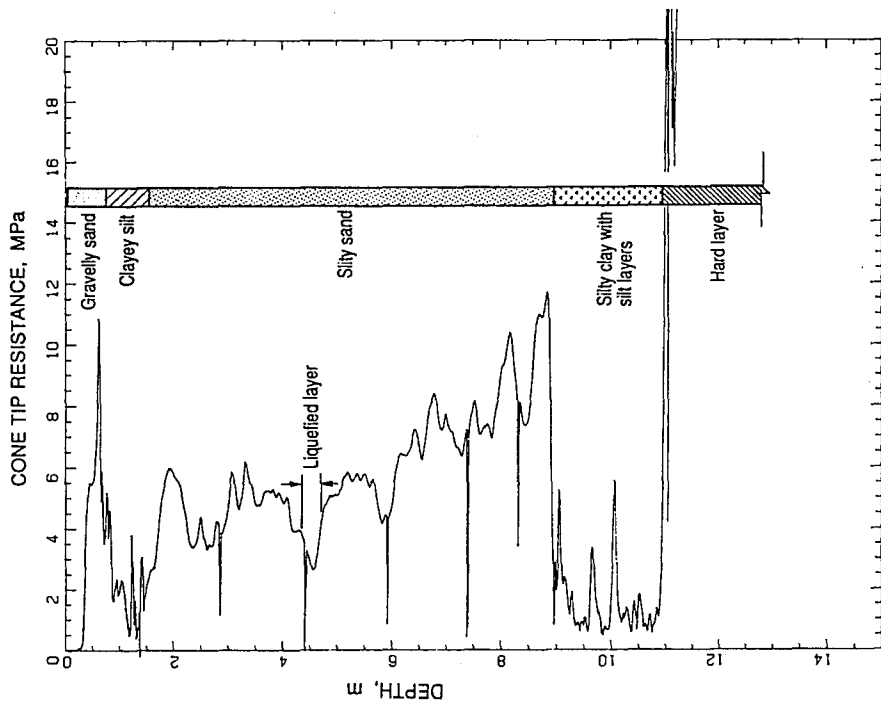


Figure 7. Soil profile determined with piezocone penetrometer at Site 1 adjacent to sand boil A. A liquefiable layer is identified at about 4.4 to 4.7 m depth based on an assumed peak horizontal acceleration of 0.25 g.

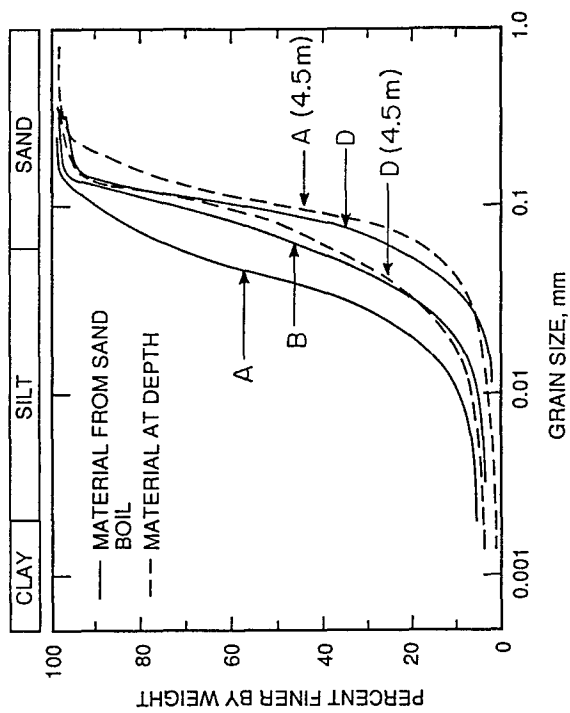


Figure 8. Grain size distribution curves for material sampled from sand boils at the surface and from auger holes drilled adjacent to the sand boils. Sand boils A and B were sampled at Site 1. A sand fissure (D) located southwest of sand boil C along Rue Paquet was also sampled (not shown in Figure 2).

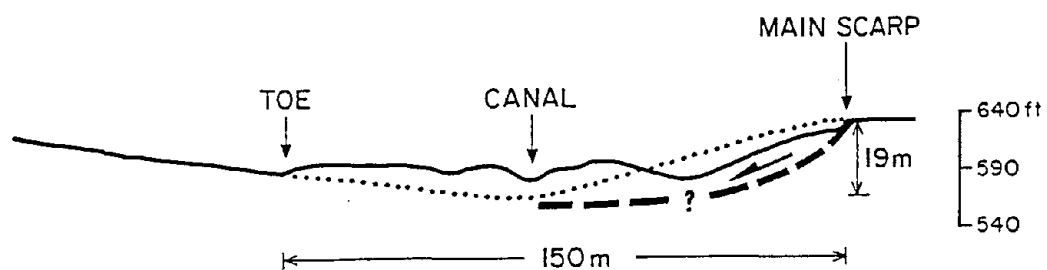
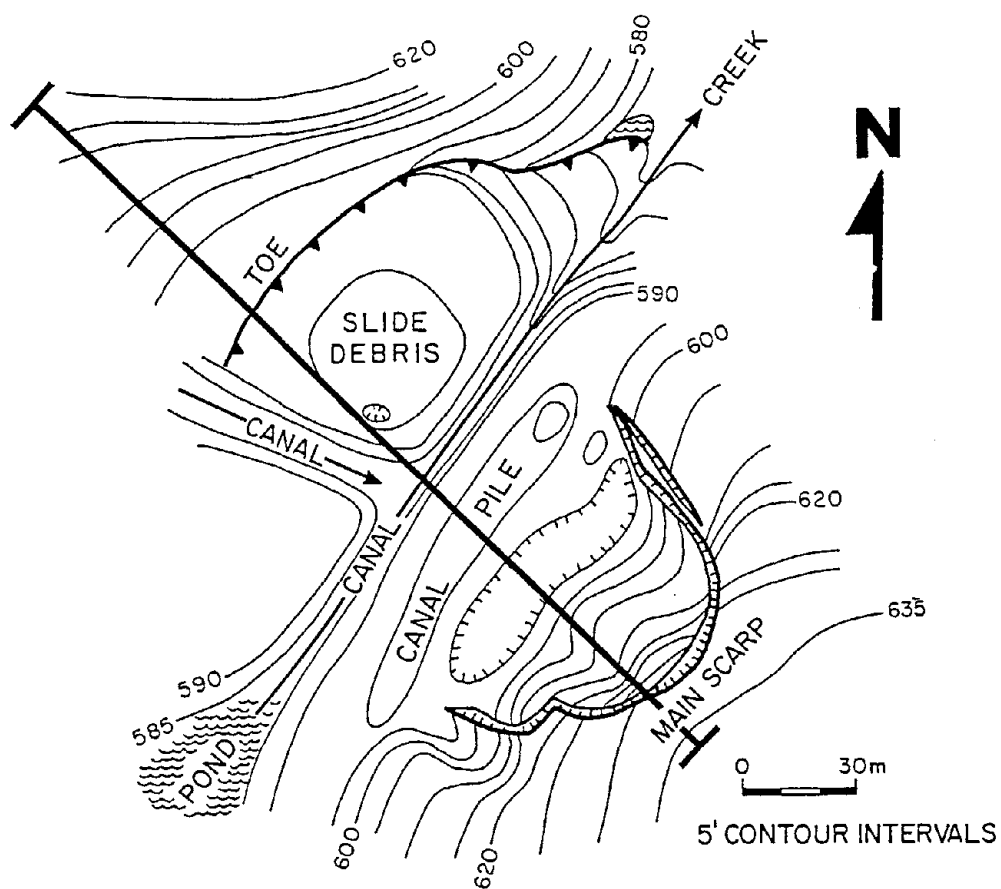


Figure 9. Topographic map and profile of St. Thecle slide induced by the Saguenay earthquake. The slide is about 88 m across and extends 150 m across the valley. Before channelization of the creek, it was buried by about 10 m of slide debris. The mechanism of the failure is currently under investigation (Lefebvre, personal communication, 1989).



# LARGE GROUND DEFORMATIONS INDUCED BY THE 1985 EARTHQUAKE IN PORT FACILITIES IN CHILE

by

Chalm J. Poran<sup>1</sup> and Jorge A. Rodriguez<sup>2</sup>

Submitted to The Second US-Japan Workshop on

*Liquefaction, Large Ground Deformation  
and Their Effects on Lifeline Facilities*

## ABSTRACT

A large earthquake took place on March 3, 1985 in the central region of Chile. The earthquake had a surface wave magnitude of  $M=7.8$  on the Richter scale and the epicenter was located in the Pacific Ocean approximately 40 km from San Antonio. The earthquake's intensity in the port was VIII on the modified Mercalli scale and the damage to port facilities was very extensive. Most spectacular were the liquefaction-related failures of portions of a seawall. Also, heavy settlements occurred in many backfill and yard areas. Based on previous publication by Poran et al. (1989) this paper presents the application of simplified available procedures to evaluate liquefaction potential as well as to estimate settlements of sandy deposits using the SPT N-values and the earthquake parameters, and, in several locations the results show good correlation to actual observations. In addition, shear wave velocity measurements are compared with the SPT results, and, generally, good correlations are obtained.

## INTRODUCTION

The Chilean earthquake of March 3, 1985, became one of the most significant, well recorded, and major earthquakes to date. The main earthquake occurred at 19:47 hours local time. Figure 1 shows the general area affected by the earthquake, which included San Antonio, Valparaiso, the metropolitan region and Santiago, and many surrounding cities. Significant ground motions were recorded for a relatively long duration. Seismological records indicate that the earthquake actually consisted of two main shocks occurring within 11 seconds of each other as shown in Figure 1, with surface wave magnitude of 5.2 and 7.8 respectively.

As reported by Poran et al. (1989) and others, the maximum recorded peak ground

- 
1. Assistant Professor, Dept. Of Civil Engineering, University of North Carolina at Charlotte, Charlotte, NC 28223, USA.
  2. Graduate Student, Dept. of Civil Engineering, University of North Carolina at Charlotte, Charlotte, NC 28223, USA.

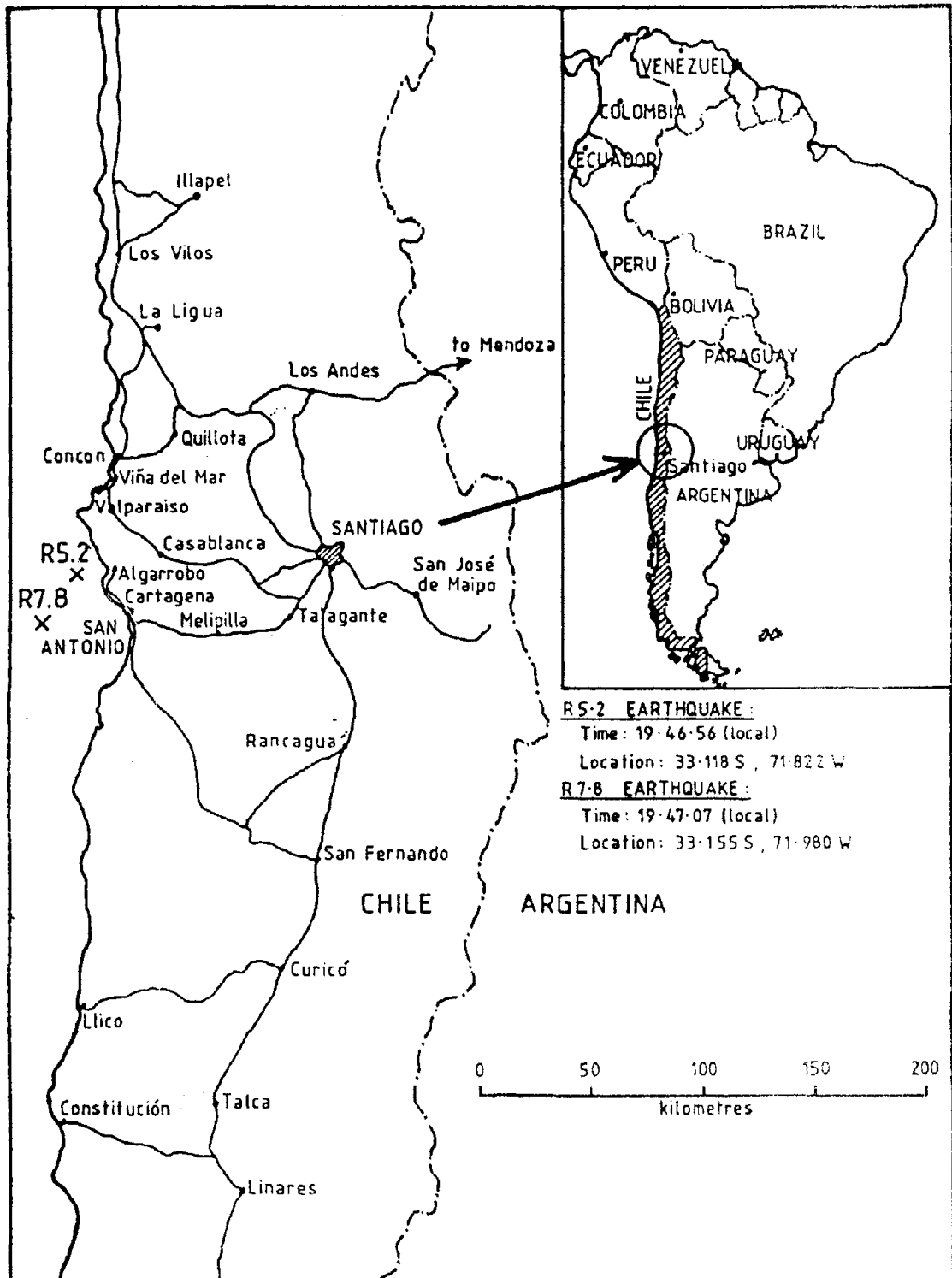


Figure 1. The General Area of the Earthquake.

acceleration (PGA) was 0.67 g for the N10E component at Lilloe. An earthquake intensity of VII on the modified Mercalli scale was generally applicable in the coastal area between the cities of Valparaiso and San Antonio (near the central zone of the energy release). However, in the city and port of San Antonio intensity was rated as VIII.

The geotechnical effects of the earthquake were of great interest to the profession, and are still subject to ongoing research. A Large area was affected by strong ground shaking for a relatively long duration and geotechnical failures were observed in many areas as described Wyllie et al. (1986), Ortigosa (1986), and others. The port of San Antonio, which suffered significant damage during the earthquake, is of particular interest. The liquefaction-related failure of portions of a seawall, substantial seaward movements of anchored sheetpile seawall, and large settlements in the backfill areas of these walls are the focus of this paper and discussed in detail as follows.

## **THE PORT OF SAN ANTONIO**

The port of San Antonio is one of the two major ports that function as a gateway of the Santiago metropolitan area, and therefore the activities of this port significantly affect the Chilean economy. The extensive damage to the port from this earthquake has caused significant problems in cargo handling capacity and port operations. The general port layout is shown in Figure 2, and typical cross sections of sites 1 and 3 are shown in Figures 3 and 4, respectively.

Soil data included in this paper is based on a large number of soil reports summarized by Poran et al. (1989), Ortigosa (1986), and Ortigosa et al. (1986).

Unfortunately no instruments were installed at the port and therefore no ground acceleration records are available. However the ground station located at Lilloe, less than 4 km south of the port, recorded PGA values of 0.426g and 0.669g for the S80E and N10E components, respectively. It is estimated that the base rock depth for both the Lilloe station and the south breakwater at the port is approximately 100 m. Therefore, it was assumed (consistent with the literature) that the ground motion in the port is similar to the motion recorded at Lilloe.

The main damage from the earthquake occurred at sites 1 and 2. The typical cross section of site 2 is generally similar to site 1, as shown in Figure 3, except that the seawall in site 2 collapsed into the sea. The sheetpile wall in site 3 suffered severe seaward tilt and copeline deformations of up to 1 m, and severe settlements were reported at the apron and backyard areas of sites 1, 2 and 3 as subsequently discussed in more detail.

## **LIQUEFACTION ANALYSIS**

The hydraulic fill between the gravity seawall and the rockfill of the breakwater in sites 1 and 2 consists of loose, sandy soils. Similar hydraulic fill is found beyond the anchors of the sheetpile bulkhead in site 3 (Figure 4). In some locations these sands included occasional gravel. The  $D_{50}$  values range between 0.26 mm for the clean sands to 0.12 mm for the silty sands, which generally contain no more than 20% fines of low plasticity silts.

Low SPT N-values were recorded in many borings performed in this sandy fill area before

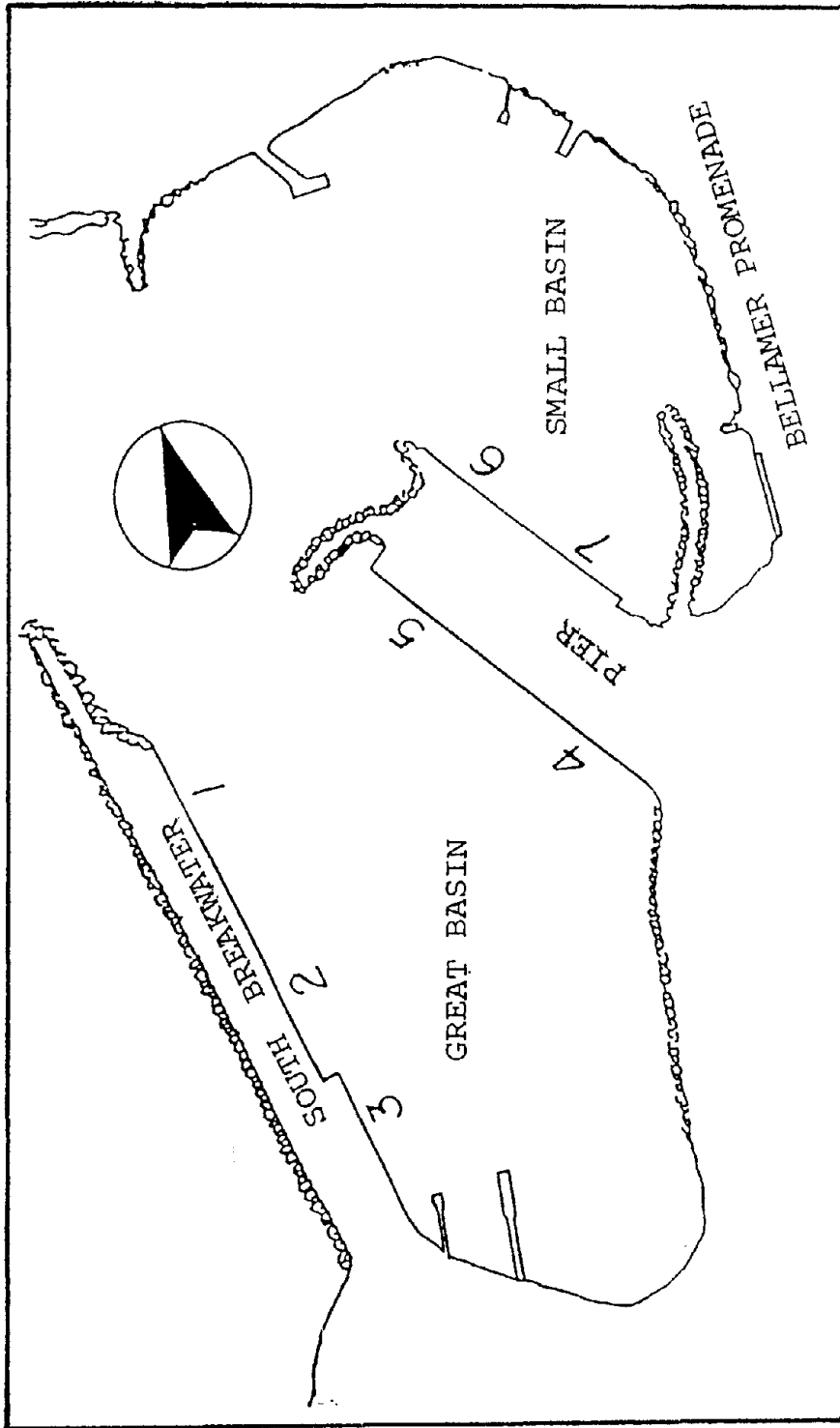


Figure 2. Port of San Antonio and Site Locations.



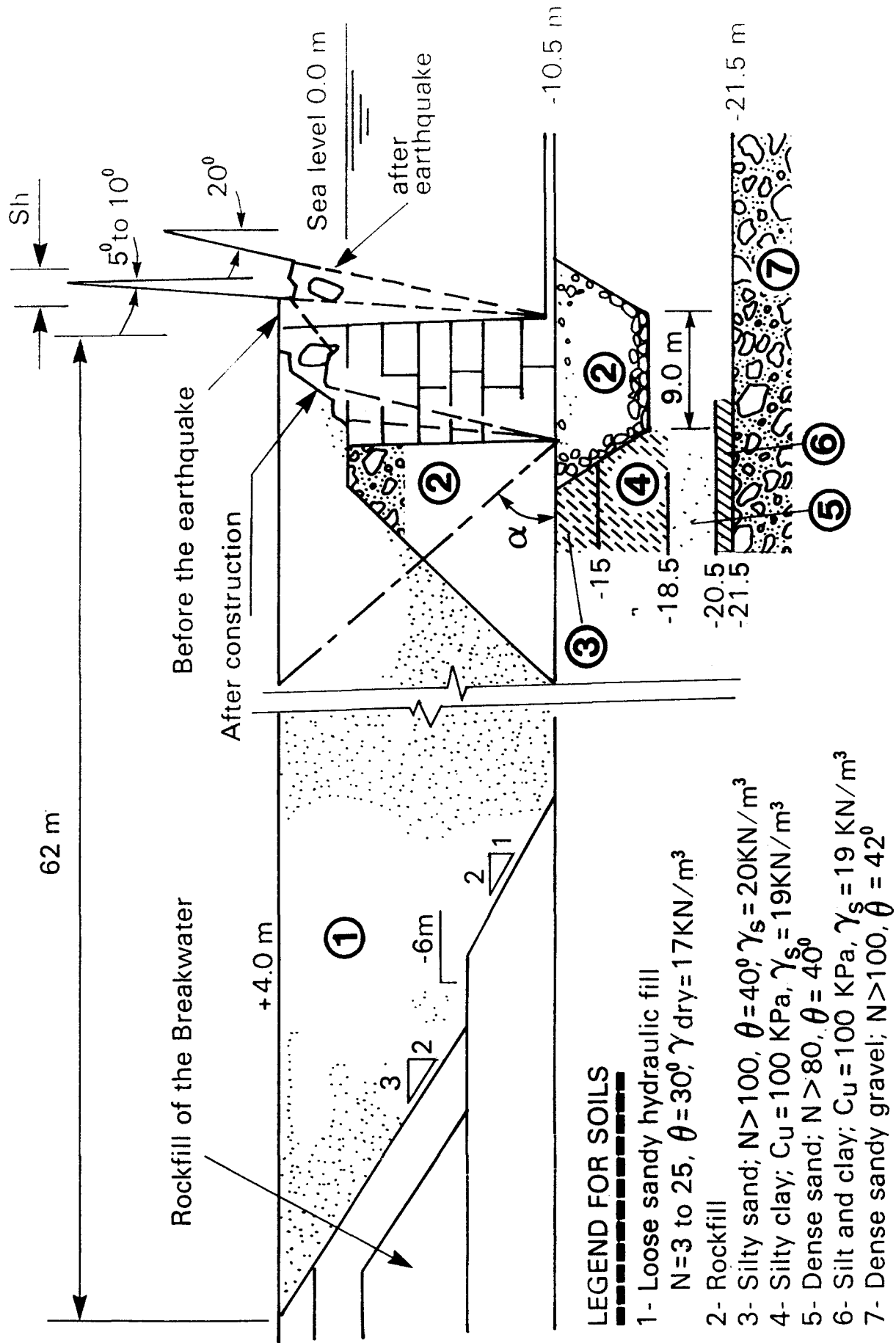


Figure 3. Typical Cross Section of Site 1.

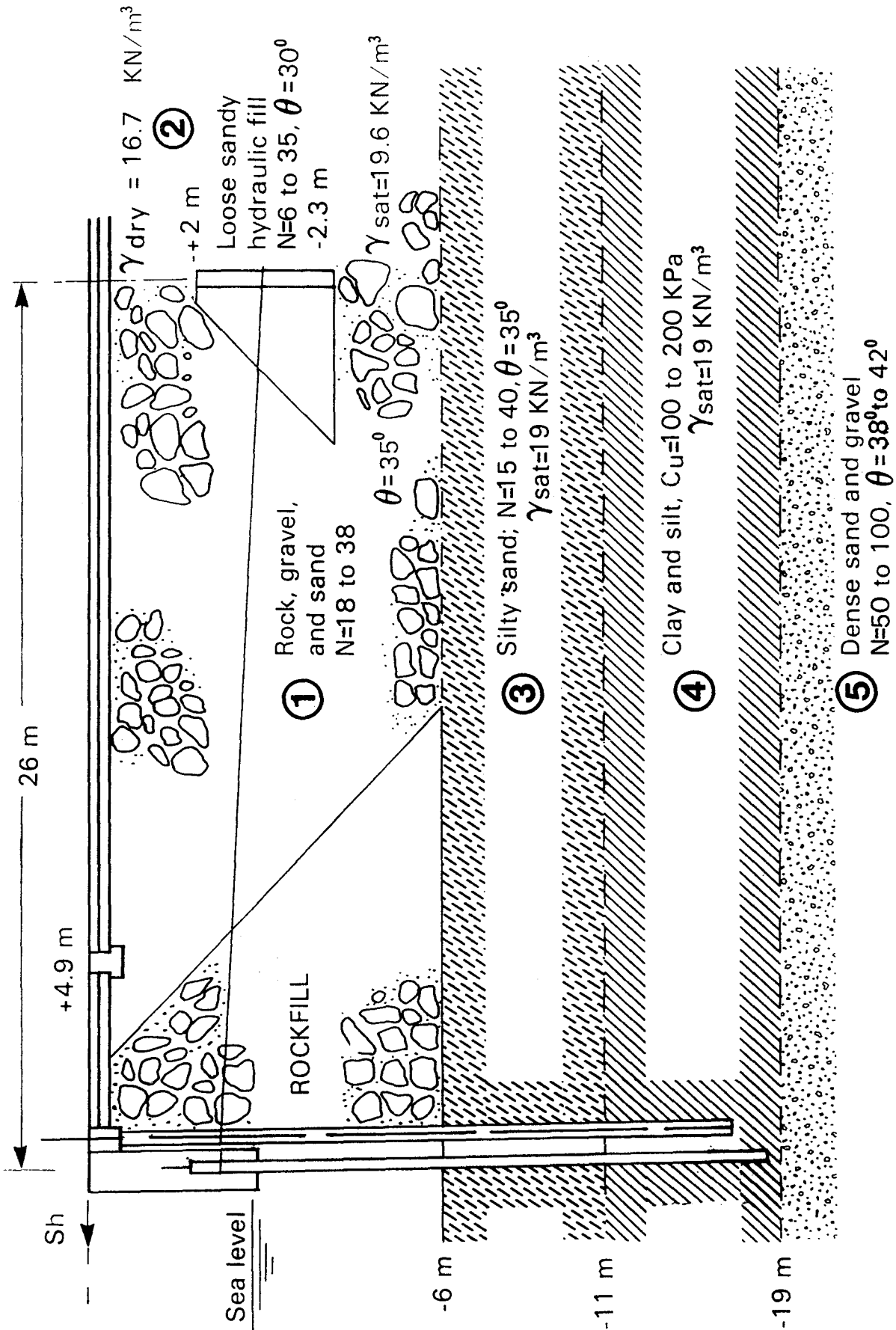


Figure 4. Typical Cross Section of Site 3.

and after the earthquake, indicating low relative densities and high liquefaction potential. The failure of the seawall in sites 1 and 2 indicates increased lateral pressure against the wall which occurred, most probably, due to the liquefaction of the sandy backfill. The loss of strength of the backfill material is the result of high water pressure development due to shear strains induced by the earthquake. A large sand volcano was observed in the backfill debris behind the collapsed wall, as shown in Figure 5. This volcano is typical when a sand layer liquefies below denser surface layers as is the case near the seawall where the top 4 m (above the sea level) consists of relatively well compacted sandy soils with little fines and some content of gravel and rock. The backfill immediately adjacent to the seawall apparently consists of rockfill as indicated in Figure 3. In spite of the fact that only one sand volcano was observed, it is believed that the liquefaction of the sandy hydraulic fill was extensive.

In site 3 the soil between the rockfill immediately adjacent to the sheetpile wall and the anchors consists of sandy gravel and rocks from the surface to approximately 6 m below sea level (Figure 4). It is unlikely that liquefaction occurred in this layer, which is generally well compacted. However, partial liquefaction may have occurred in the underlying silty sand layer, which extends between 6 and 11 m below sea level. Liquefaction may have been more extensive in the hydraulic fill between the anchors and the breakwater. This fill consists of loose, sandy soils similar to sites 1 and 2. Liquefaction of the fill near the anchors may have caused anchor displacements, which contributed to the large seaward deformations of the sheetpile wall.

Liquefaction analysis was conducted based on the procedure outlined by Seed et al. (1983, 1984) and the results are presented in Figure 6. The critical envelope shown in Figure 6 is a convenient method for evaluating liquefaction potential based on SPT  $N$ -values for a large number of borings in leveled ground in which the water table and soil conditions are similar, such as the conditions at sites 1, 2, and 3. The critical envelope was determined by the cyclic stress ratio induced by the earthquake. The overburden pressures were calculated based on a dry unit weight of  $19.6 \text{ KN/m}^3$  and a saturated unit weight of  $19.6 \text{ KN/m}^3$ , which is typical for these loose, silty sands and which corresponds to a relative density of approximately 50%. Based on boring data, an average water table was assumed at 4 m below ground level.

The limits of the critical range were calculated based on induced stress ratios for ground accelerations of 0.67 and 0.43 g for the upper and lower limit curves, respectively, based on earthquake magnitude  $M=7.5$ . These stress ratios were then used to obtain the critical values of  $(N_1)_{60}$ , which is the normalized SPT  $N$ -value corrected for a 60% energy ratio. The upper limit curve (for  $a_{\text{max}}=0.67 \text{ g}$ ) corresponds to  $(N_1)_{60}$  values obtained from the correlation presented by Seed et al. (1983) for sands with  $D_{50}>0.25 \text{ mm}$ , and therefore represents the most severe conditions for these sands. The lower limit curve (for  $a_{\text{max}}=0.43\text{g}$ ) corresponds to the correlation presented by Seed et al. (1984) for silty sands with 15% fines. Generally, SPT in Chile is considered to have an energy ratio of 60% and therefore, the final step to determine the critical range boundaries in terms of recorded SPT  $N$ -value was based on  $C_n$ , which is a correction coefficient proposed by Seed et al. (1983) to normalize  $N$ -values for an overburden pressure of 1 tsf (106 KPa).

As shown in Figure 6, boring data from sites 1 and 2 indicate that liquefaction of the sandy hydraulic fill was probably very extensive during this earthquake. The concrete slabs in the apron and backyard areas at these sites suffered significant settlements as a result of liquefaction. Many of the data points from site 3 fall within the critical range in Figure

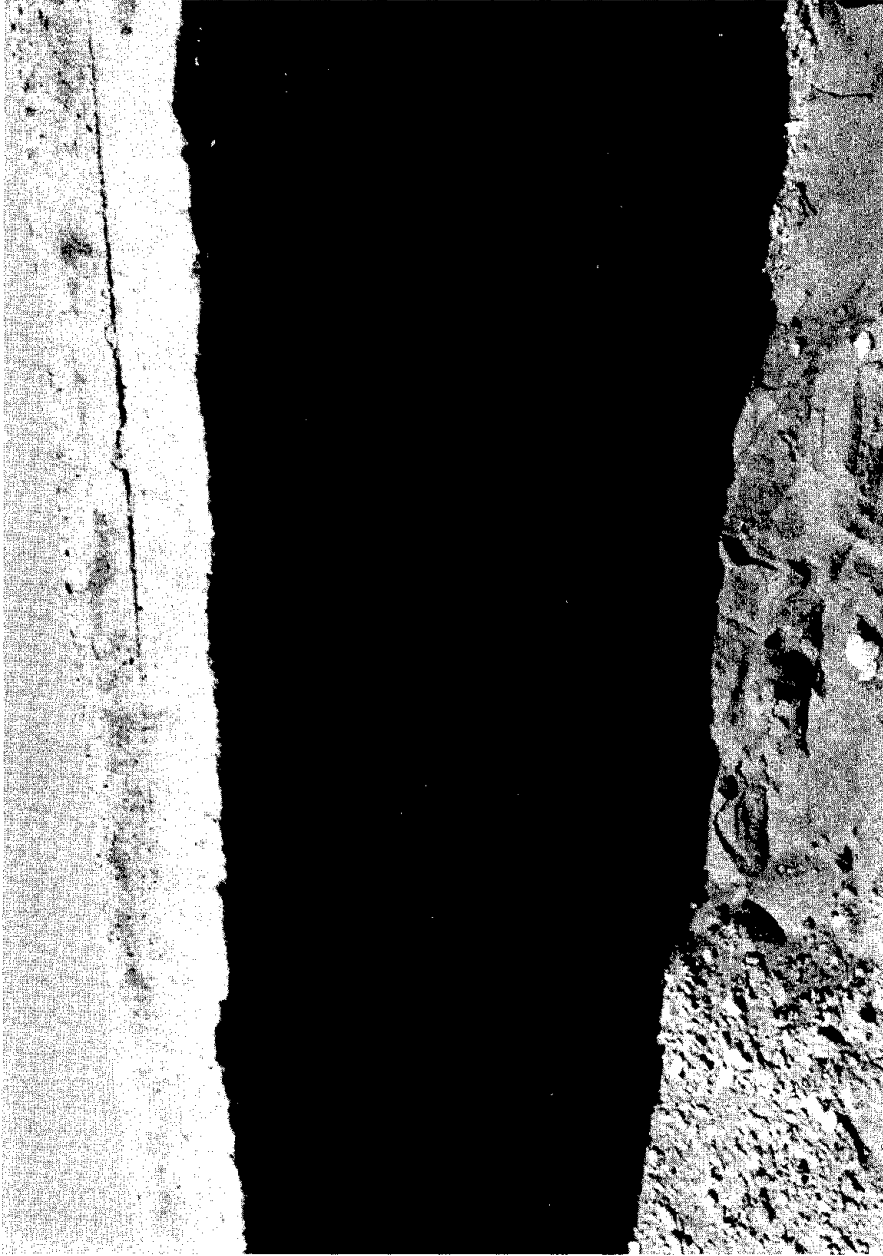
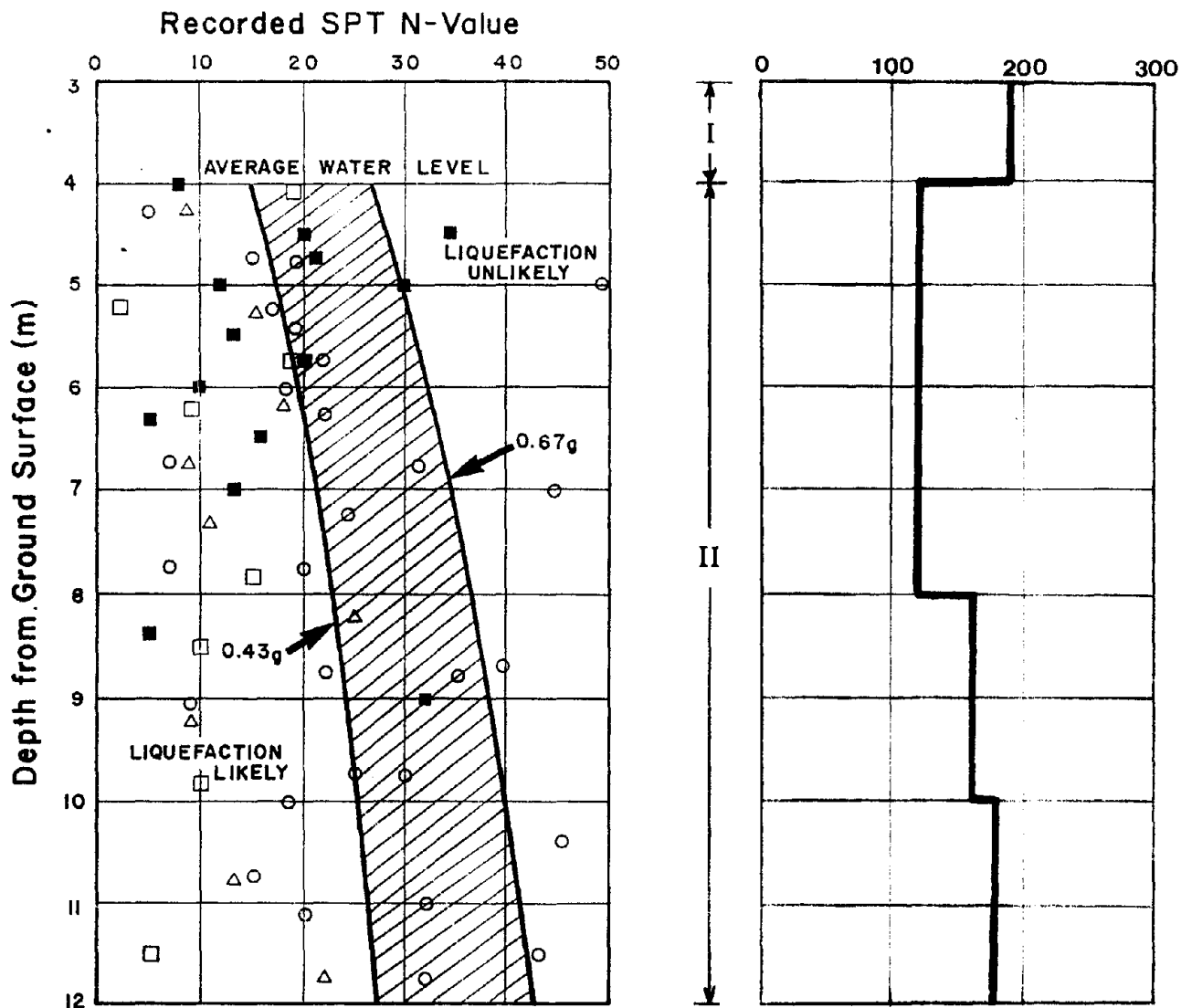


Figure 5. Liquefaction Induced Sand Volcano at Site 1.

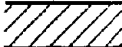




Representative Shear Wave Velocity (m/s)



Legend:

 Critical Range

SPT Results

Before the March 3, 1985 earthquake:

■ Berth 1

After the March 3, 1985 earthquake:

□ Berth 1

△ Berth 2

○ Berth 3

For backfill area of Berths 1 and 2:

- I) Gravely sand with concrete slabs debris.
- II) Silty sand (SM).

Figure 6. Critical Liquefaction Range Based on SPT N-values, and Representative Shear Wave Velocity Profile.

6. It is possible that these sands, which have higher fines content, did not liquefy, especially in the zone between the sheetpile bulkhead and the anchors. Some of these data points, from depths greater than 10 m below ground surface, are probably natural soil deposits that are less likely to liquefy. On the other hand, N values from borings in the hydraulic fill between the anchors and the breakwater (which consists of loose, clean sands) indicate that these sands liquefied during the earthquake.

## SHEAR WAVE VELOCITY MEASUREMENTS

Several downhole shear wave velocity measurements records from the backfill were compared with SPT results. These measurements were taken in areas of sites 1 and 2 in 1986 and 1987 as part of the port rehabilitation study (Poran et al. 1989). The shear wave velocities agree well with the trend shown by the SPT results, and the liquefiable strata is verified by the representative shear wave velocity profile shown in Figure 6.

## EARTHQUAKE - INDUCED GROUND DEFORMATIONS

Ground deformations in apron and yard areas of sites 1, 2 and 3 were severe. Several mechanisms were involved in these deformations: vertical settlements, which were the result of the horizontal soil deformations in the failure zone of the fill adjacent to the failed seawall; earthquake-induced vertical settlements of the dry, sandy deposits in the top 4 m of the fill areas; liquefaction-induced settlements of the saturated sandy deposits; and certain combinations of these mechanisms.

**Settlements Due to Horizontal Deformations:** As shown in Figure 3, the seawall at site 1 failed by severe tilting. Based on the literature, it is reasonable to assume that the wall had an average initial tilt of 7.5 degrees, and as a result of this earthquake the average wall tilt increased to 20 degrees when measured at the copeline. In order to estimate vertical settlement the following assumptions are made: the extent of the soil mass affected by the wall tilt is confined by the wedge shown in Figure 3 where  $\alpha = 45$  degrees (this assumption is consistent with Ortigosa et al. [1986]); and the soil mass in the wedge has no volume change. Based on these simplifications, the maximum vertical settlement equals the horizontal seaward deformation at the copeline  $S_h$ , therefore the calculated vertical settlement is 2.95 m. This result correlates well with the measured settlement of 2.98 m in the fill immediately adjacent to the failed seawall.

Vertical settlement near the sheetpile wall in site 3, shown in Figure 4, was calculated based on similar assumptions. The maximum seaward deformations of the copeline were between 70 to 100 cm where the sheetpile wall had approximately 5 degrees seaward bend. Maximum vertical settlement of 65 cm was measured in the adjacent apron area, which is slightly less than what is calculated based on the previously mentioned assumptions.

The design of site 4 is essentially identical to site 3. However, site 4 suffered very slight damage from the earthquake compared to the several damages to site 3. Boring data from site 4 reveal that the backfill in the apron and yard area consists primarily of rock with some gravel and sand. This rock fill is superior to the fill found in site 3, and therefore the seismic performance of the sheetpile wall in site 4 was much better than in site 3.

**Settlement of Dry Sand Deposits:** Generally, at the top of the fill are the dry soils from underneath the yard pavements to water level consists of relatively well-compacted sand and gravel. However, very low SPT N-values were recorded in several locations at which large settlements were observed. An analysis of the possible settlement of these loose sandy deposits was conducted using the procedure proposed by Tokimatsu et al. (1987). The analysis is based on average properties for a 4 m layer of dry sand with recorded SPT N-value of 3 and dry unit weight of  $16.7 \text{ KN/m}^3$ , and on the cyclic strains induced by an  $M=7.5$  earthquake with  $a_{\text{max}} = 0.67 \text{ g}$ . It should be noted that the calculated values for the dynamic shear modulus at low strain level correlate well with values obtained from PS prospecting performed in these sites. The results indicate that settlement of up to 21 cm may have occurred at the location with loose sandy fill.

**Liquefaction Settlements:** Liquefaction settlements were calculated according to the procedure proposed by Tokimatsu et al. (1987). The calculations for sites 1, 2 and 3 were based on the average SPT N-values for the saturated sandy soils at each location and on the induced shear strains evaluated for a  $M=7.5$  earthquake with  $a_{\text{max}}=0.67\text{g}$ . Liquefaction settlements of 12, 18, and 15 cm were calculated for sites 1, 2, and 3 respectively.

**Total Settlements:** The earthquake-induced settlement at any location is obviously, some combination of the three mechanisms previously discussed. Good correlation is obtained between calculated and observed total settlements at several locations as shown in Table 1.

## CONCLUSION

This paper examines liquefaction and large ground deformations induced by the Chilean earthquake of March 3, 1985 in the port of San Antonio. A simplified available method based on SPT N-values and the cyclic stress ratio induced by the earthquake was used to evaluate liquefaction potential of several sandy deposits, and generally the results show good correlation to the observations. In several locations good correlations were obtained between downhole shear wave velocity measurements and SPT results. This demonstrates the usefulness of such measurement for locating potentially liquefiable sites.

Available simplified methods are also used to estimate settlements of sandy deposits; the cyclic stress ratio and maximum shear strain induced by the earthquake motion in saturated sands and the cyclic strains induced in dry sands, together with the SPT N-values and the earthquake magnitude are the parameters used for these estimates; and, in several locations settlements are also correlated to horizontal deformations of seawalls. Generally, the estimated results show good correlation with settlements observed during the earthquake. These results demonstrate that these simplified methods may be useful to estimate liquefaction potential and earthquake-induced large deformations provided that local site conditions are taken into consideration.

## REFERENCES

- Ortigosa, P. (1986). *Algunos Efectos Geotecnicos, EL SISMO DEL 3 DE MARZO 1985 - CHILE*, Universidad de Chile, pp. 179-196.

TABLE I. COMPARISON OF CALCULATED AND OBSERVED SETTLEMENTS

Site	Vertical Settlements (cm)					Observed Total
	C a l c u l a t e d					
	Due to seawall tilt	Dry sand	Liquefaction	Total		
1	295	0	0	295		298
2	0	21	18	39		50
3	70-100	0	0	70-100		65
	0	21	12	33		30

Ortigosa, P., Retamal, E., Acevedo, P., and Hidalgo, E. (1986). "Aspectos Geotecnicos en los Malecones de los Puertos de Valparaiso y San Antonio," Universidad de Chile, IDIEM.

Poran, C.J., Greenstein, J., and Berger, L. (1989). "Earthquake Induced Settlements in Port Facilities in Chile," Proceedings of the XII International Conference on Soil Mechanics and Foundation Engineering, Vol. 3, A.A. Balkema Publishers, Rotterdam, Netherlands, pp. 1991-1994.

Saragoni R. (1986). **Analisis de los Acelerogramas del Terremoto del 3 de Marzo de 1985, EL SISMO DEL 3 DE MARZO DE 1985 - CHILE**, Universidad de Chile, IDIEM.

Seed, H.B., Tokimatsu, K., Harder, L.L., and Chung, R.M. (1984). **The Influence of SPT Procedures in Soil Liquefaction Resistance Evaluations**, NSF, UCB/EERC-84/15.

Seed, H.B., Idriss I.M., and Arango, I. (1983). "Evaluation of Liquefaction Potential Using Field Performance Data," **Journal of the Geotechnical Engineering Division**, ASCE, Vol. 109, No. 3, March, pp. 458-482.

Tokimatsu, K., and Seed, H.B., (1987). "Evaluation of Settlements in Sands Due to Earthquake shaking," **Journal of the Geotechnical Engineering Division**, ASCE, Vol. 113, No. 8, August, pp. 861-878.

Wyllie, L. A. (1986). "The Chile Earthquake of March 3, 1985," **Earthquake Spectra**, Vol. 2, No. 2, February, pp. 249-291.



# NUMERICAL AND PHYSICAL MODELING OF LIQUEFACTION AND GROUND DEFORMATION

ANALYSIS OF THE EFFECT OF PERMANENT DISPLACEMENT OF GROUND  
ON THE BEHAVIOR OF FOUNDATION

*Y. Yamada, H. Yamada, H. Kubo, and M. Kikuta*

SEISMIC RESPONSE AND ACCELERATION RESPONSE OF WILDLIFE SITE  
DURING THE 1994 NORTHERN CALIFORNIA EARTHQUAKE

*Y. Yamada, A. W. Elgamal, and M. Baziar*

THE EFFECTS OF STRESS AND RESIDUAL DEFORMATION - EFFECTIVE STRESS  
ANALYSIS OF ANCHORED SHEET PILE QUAYWALL

*Y. Yamada and M. Kameoka*

AN ANALYSIS OF EARTHQUAKE DATA OBSERVED AT THE WILDLIFE  
SITE OF THE ARROYO DUCE, IMPERIAL COUNTY, CALIFORNIA

*Y. Yamada and J. K. Prevost*

THE EFFECTS OF LIQUEFACTION

*Y. Yamada and K. Ohtomo*

AN ANALYSIS OF THE EFFECTS OF LIQUEFACTION-INDUCED LARGE  
PERMANENT GROUND DISPLACEMENTS

*Y. Yamada*

AN ANALYSIS OF THE EFFECTS OF LARGE GROUND MOTIONS AND THEIR EFFECTS

ON FOUNDATIONS

*Y. Yamada*

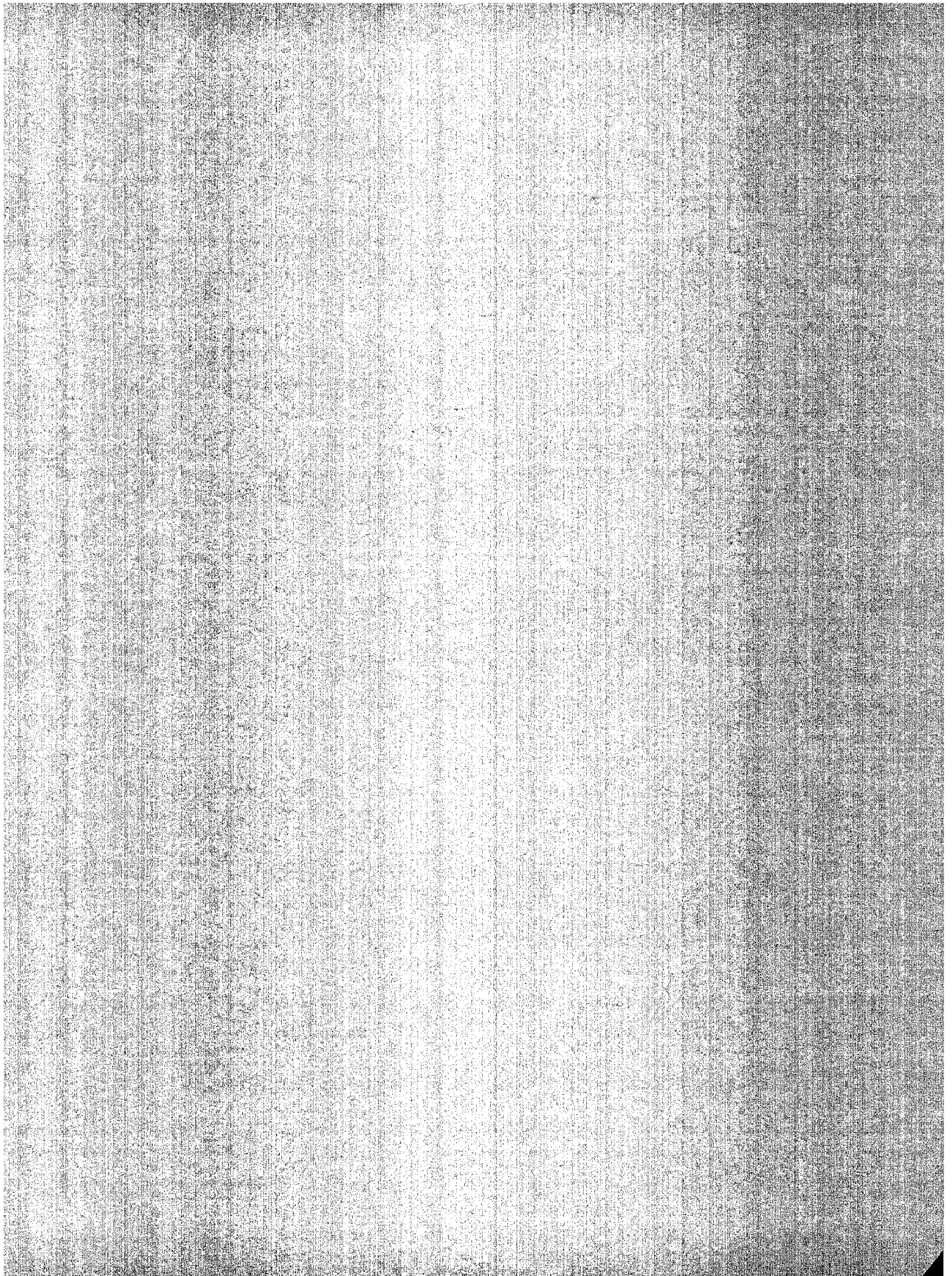
THE EFFECTS OF CLAY LAYERS ON LIQUEFACTION OF SAND DEPOSITS  
BY FINITE ELEMENT MODELS

*Y. Yamada, E. Dobry, and K. Adalier*

THE EFFECTS OF LIQUEFACTION ON THE MECHANICS OF POST-LIQUEFACTION

ON FOUNDATIONS

*Y. Yamada*





ANALYTICAL SOLUTION OF PERMANENT DISPLACEMENT OF GROUND  
CAUSED BY LIQUEFACTION

Ikuo Towhata

Associate Professor of Civil Engineering  
University of Tokyo

Kazuhiko Yamada

Senior Engineer  
Fudo Construction Corp.

Hiroaki Kubo

Graduate Student  
University of Tokyo

and

Masashi Kikuta

Former Student  
Chiba Institute of Technology

ABSTRACT

A series of shaking table tests were carried out on the permanent displacement of a liquefied sandy ground. These tests had the advantage of being able to show the distribution of displacement of subsoil, and thereby gave an important information on the manner of soil behavior in the course of liquefaction. Based on the knowledge thus obtained, an analytical solution was developed of the permanent displacement of ground during liquefaction.

## INTRODUCTION

This text presents a simplified method to predict the permanent displacement of a liquefied ground whose slope is nearly level. The author<sup>1</sup> already proposed another simplified method to predict the permanent displacement of a liquefied gentle slope. Thus, the present text is expected to deal with what the former one could not.

The development of a simplified prediction method requires to have a deep insight into the mechanism of the liquefaction-induced permanent displacement, which is unfortunately not yet fully understood. As was observed in Noshiro City<sup>2</sup>, the permanent displacement in a gentle slope is always oriented in the downward direction of the slope. It suggests, therefore, that the gravity force is somehow involved in the generation of the ground movement. The former method of prediction<sup>1</sup> made use of the gravity as the driving mechanism. However, when it was attempted to analyze the Niigata case where the ground surface is essentially level<sup>2</sup>, the former method was found not to function properly because the gravity force does not have any component in the horizontal direction in which significant ground movement was observed.

Boring log data suggests that the bottom of the liquefied soil layer in Niigata was inclined, although the surface was level<sup>2</sup>. Thus, it may sound reasonable that the liquefied soil flows along the inclined bottom plane. This idea is, however, not agreeable for a level ground, as is supported by the fact that the sea water does not flow away from the coast along the inclined seabed.

In consequence of the recent developments of computers and numerical techniques, it has been felt that any deformation problem of the ground can be solved if the stress-strain relationship of soils is precisely known. This feeling is not agreeable in the case of a liquefied ground. This is because the soil is subject not only to a nonlinear behavior and excess pore water development but to a transformation of its phase from solid to liquid, at the onset of liquefaction, and then back to solid when the excess pore pressure dissipates. This type of phenomenon is beyond the scope of the conventional solid mechanics and requires a highly-advanced technique of numerical analysis. Furthermore, the boiling of sand and water which induces a ground settlement consists of a mixed flow of solid and liquid materials, and cannot be dealt with by Darcy's law which is popular in the current practice of numerical analysis.

This difficult problem can be solved by a simplified analytical method which is going to be described in what

follows. The method is concerned with a nearly level ground. Those displacements caused by the movement of retaining structures are out of its scope.

#### METHODS OF SHAKING TABLE TESTS

Since the mechanism of the permanent displacement was unknown, the study was initiated with shaking table tests. A container of 1.0 m in length and 0.4 m in depth and width was filled with water and sand was dumped into it to form a model ground. The physical properties of the sand are  $G_s = 2.612$ ,  $D_{50} = 0.277$  mm,  $U_c = 2.07$ ,  $e_{max} = 1.04$ , and  $e_{min} = 0.65$ . The relative density of the model ground was around 50%. The fixed end walls of the container were not equipped with a soft material.

The permanent displacement of the ground surface is caused by the permanent deformation of the subsurface soil. Thus, it seems that the understanding of the mechanism of the permanent displacement requires us to study the behavior of the subsoil. This idea was practiced by observing through the transparent side of the container the displacement of targets embedded in the model ground. A suitable target has to be of the same unit weight as the liquefied soil so that they attain the identical displacement. In the present study, the tested sand itself but dyed was employed as the target. The dyed sand was frozen to be short sticks which measured approximately 1 cm in diameter and 10 cm in length. They were then inserted into the model ground during its preparation. Melting under room temperature, the sand sticks became a colored grid of the same unit weight as that of the surrounding sand. The grid was of no stiffness, being able to follow the movement of the model ground.

The model ground was shaken at 3Hz, with the constant acceleration amplitude of 250 gals. The shaking was continued until all the possible deformation of the ground did occur.

#### GROUND DEFORMATION OBSERVED IN TESTS

A discussion is going to be made of the observed test results. Fig. 1 indicates the permanent deformation of a ground with a dry embankment. This embankment rested on a thin layer of coarse sand which prevented the ground water from being absorbed into the dry soil due to the meniscus force. The coarse sand had a particle size of more than 2 mm and the layer thickness was 2 cm. It is seen in Fig. 1 that the liquefaction in the underlying sandy ground resulted in the settlement of the embankment, upward movement of the toe of the

slope, and consequently, the level ground surface. A soil displacement in the lateral direction is also seen. Note that the displacement is negligible at the bottom of the liquefied layer.

Fig. 2 shows the behavior of a liquefied level ground whose bottom is inclined by 150/920. The bottom plane was made of a wooden board with sand particles glued on its surface. The shaking caused liquefaction in top 2/3 of the ground, and the permanent displacement was observed to occur in the downward direction of the bottom slope. The magnitude of the permanent displacement was large near the surface and negligible at the bottom of the liquefied part of the ground.

The ground behavior in Fig. 2 reveals one of the limitations of the present testing method. A convection-like flow of soil was observed near the left end of the soil container during shaking. The liquefied soil came up to the surface and then moved toward the center of the ground, hence indicating in Fig. 2 a direction of movement opposite to that of the overall trend. Since this movement near the end is local and erroneous, it should be ruled out of the study and that in the middle third should be employed in the further study.

The test results in Figs. 1 and 2 temporarily suggests the points described below;

- 1) the liquefied soil behaves as a liquid material; hence the ground surface becomes nearly level after liquefaction,
- 2) a horizontal soil movement is necessary to occur in order to make the inclined ground surface level,
- 3) the magnitude of the permanent displacement of soil in the lateral direction is minimum at the bottom, and increases towards the surface.

The points 1) and 2) indicate the mechanism of the permanent displacement in a gentle slope.

Now the mechanism of the displacement of a level ground is discussed. When the bottom is inclined (Fig. 2), the thickness of the liquefied layer varies in the lateral direction. Hence, a differential settlement tends to occur in the course of dissipation of the excess pore water pressure. At the same time, the liquefied part of the ground behaves as liquid; flowing laterally to make the surface level again. The differential settlement and lateral flow of soil occur simultaneously to induce the permanent displacement of the ground.

The test results in Figs. 3 and 4 seem to support the above idea. In this case, a water-saturated sandy layer rests at the bottom of the ground, and is enveloped in plastic sheets, which keep the soil undrained. Note that the top of this layer is inclined. This sandy ground is then overlain by a dry layer of sand whose surface is level. At the onset of liquefaction in the lower sandy layer, no lateral movement of sand was observed (Fig. 3), although the top of the liquefied layer was inclined. No permanent displacement occurred at this stage, because the total head of the liquefied soil, the potential head plus the pressure head, was uniform, making the hydraulic gradient of the liquefied soil equal to null. A few seconds later, the plastic envelope of the liquefied layer was broken near the right end of the ground (Fig. 4), and a sand boiling started. This created a significant hydraulic gradient in the liquefied layer, and a soil movement developed. The idea of hydraulic gradient seems to be reasonable as the mechanism of the permanent displacement, when the liquefied sand behaves as a liquid material as mentioned before. Even in a level ground, a differential settlement, if any, can create a hydraulic gradient and consequently a permanent soil movement.

#### ANALYTICAL SOLUTION OF PERMANENT DISPLACEMENT

The simultaneous progress of differential settlement and lateral flow is considered to be the mechanism of permanent displacement. Firstly, Fig. 5 illustrates the situation to be analyzed. A liquefied sandy ground whose thickness is  $H_0$  and unit weight is  $\gamma$  rests on a base of inclination  $\theta$ . The surface soil above the ground water level is replaced by a surcharge  $p$ . The lateral boundary condition at  $x = 0$  and  $L$  is specified by zero displacement which has been observed in reality.  $H_0$  and  $p$  vary linearly with  $x$ ;

$$H_0 = H_{10} + \alpha x, \quad \alpha = (H_{20} - H_{10}) / L \quad (1)$$

$$P = P_1 + \mu x, \quad \mu = (P_2 - P_1) / L \quad (2)$$

When the dissipation of excess pore water pressure induces a consolidation and a vertical soil strain of  $v$ , a soil particle which stayed at  $(x_0, y_0)$  in Fig. 5 comes to a new location of  $(x_c, y_c)$ ;

$$\begin{aligned} x_c &= x_0, \\ y_c &= y_0 - v (y_0 - x_0 \tan \theta) \end{aligned} \quad (3)$$

Hence, the total thickness of sandy layer,  $H_c$ , becomes

$$H_c = (1-v) (H_{10} + \alpha x_c) \quad (4)$$

This layer thickness, however, does not achieve the equilibrium of the total head, and the liquefied sand flows laterally at the same time. This flow occurs under the condition of constant volume, and the new coordinates of a soil particle is expressed by

$$(x_c - u, y_c - w)$$

as shown in Fig. 6. Since the volume change of the ground between Figs. 5 and 6 is solely due to consolidation strain,  $v$ ,

$$H_{1e} + H_{2e} = (1-v) (H_{10} + H_{20}) \quad (5)$$

Secondly, the total head in the liquefied ground is studied. When a very small hydraulic gradient of  $\tan\phi$  is allowed to exist after the termination of soil flow, the modified total head defined by Eq. 6 is uniform or independent of  $x_c$ .

$$\begin{aligned} \text{The modified total head} &= \text{The total head} - (x_c - u - L/2) \tan\phi \\ &= (x_c - u) \tan\theta + H_{1e} + [(H_{2e} - H_{1e})/L] (x_c - u) + [(P_1 + \mu(x_c - u))/\gamma] \\ &\quad - (x_c - u - L/2) \tan\phi = \text{constant} \end{aligned} \quad (6)$$

Since Eq. 6 is independent of  $x_c$ , its values at  $x_c = 0$  and  $L$ , where  $u = 0$ , are equal to each other. Thus,

$$H_{1e} - H_{2e} = L (\tan\theta + \mu/\gamma - \tan\phi) \quad (7)$$

Eqs. 5 and 7 are solved for  $H_{1e}$  and  $H_{2e}$ , which are then linearly interpolated to give the thickness of sandy layer,  $H_e$ , after the completion of lateral soil flow;

$$H_e = (1-v) (H_{10} + H_{20}) / 2 - (\tan\theta + \mu/\gamma - \tan\phi) (x_e - L/2) \quad (8)$$

in which  $x_e = x_c - u$  stands for the  $x$  coordinate of a sand particle.

Now the unknown displacement,  $u$ , is going to be derived. In accordance with the experimental finding that  $u$  is negligible at the bottom but takes the maximum value at the top of the liquefied layer, its distribution in the vertical direction is expressed by a sinusoidal function;

$$u = F(x_c) \sin \left\{ \frac{\pi}{2} \frac{y_c - x_c \tan\theta}{(1-v)(H_{10} + \alpha x_c)} \right\} \quad (9)$$

in which "F" is an unknown function of  $x_c$  and is equal to  $u$  at the surface. The lateral boundary conditions for "F" are given by

$$F(0) = F(L) = 0 \quad (10)$$

Fig. 7 shows the configuration of the liquefied ground before and after the lateral soil flow. Since this flow occurs with constant soil volume, the soil volume DIJ which moves across the section DI is equal to the upheave volume of the ground surface, ABEG. After calculating and equating these two soil volumes by using Eqs. 4, 8, and 9,

$$F(x_c) = x_c + \frac{8}{\pi} \frac{(1-v)(H_{10} + \alpha x_c)x_c}{(C_2 - C_3 x_c) - \left\{ (C_2 - C_3 x_c)^2 - \frac{16}{\pi} C_1 (1-v)(H_{10} + \alpha x_c)x_c \right\}^{1/2}} \quad (11)$$

in which

$$c_1 = \alpha(1-v) + \tan\theta + \mu/\gamma - \tan\phi$$

$$c_2 = (1-v)(H_{10} - H_{20}) - L(\tan\theta + \mu/\gamma - \tan\phi) - [4(1-v)/\pi]H_{10}$$

$$c_3 = [4(1-v)/\pi]\alpha$$

Eq. 11 satisfies the lateral boundary condition (Eq. 10).

The vertical displacement of soil,  $w$ , during the constant-volume soil flow is derived by using

$$\frac{\partial u}{\partial x_c} + \frac{\partial w}{\partial y_c} = 0 \quad (12)$$

By substituting Eq. 9 in Eq. 12 and then integrating for  $y_c$ ,

$$w = [2(1-v)/\pi] \{ \alpha F + (H_{10} + \alpha x_c) (dF/dx_c) \} (\cos S - 1) + [F/(H_{10} + \alpha x_c)] (\alpha y_c + H_{10} \tan\theta) \sin S \quad (13)$$

in which

$$S = (\pi/2) (y_c - x_c \tan\theta) / [(1-v)(H_{10} + \alpha x_c)]$$

This solution for  $w$  satisfies the bottom boundary condition of  $w = 0$  at  $y_c = x_c \tan\theta$ . Eq. 13 is added to the consolidation component of vertical displacement,  $w = v(y_c - x_c \tan\theta)$ , as appeared in Eq. 3, and the total vertical displacement, positive downward, is derived.

#### EXAMPLE CALCULATION

This section is started with a set of parametric studies. The control case is like

$$\begin{aligned} L &= 200 \text{ m. } H_{10} = 10 \text{ m, } H_{20} = 5 \text{ m,} \\ &\text{level ground surface (DZ} = 0\text{m),} \\ v &= 0.05, p = 0, \tan\phi = 0.001. \end{aligned}$$

Fig. 8 demonstrates the distribution of the horizontal as well as the vertical displacements at the ground surface. The latter one includes the consolidation component. The distribution of  $u$  is nearly parabolic, with the location of the maximum value slightly biased in the upstream side. In contrast, the largest vertical displacement occurs at the downstream end where the thickness of liquefied layer attains the maximum.

The following parametric studies make use of  $u$  at the middle ( $x_C = 200$  m) of the ground surface. Fig. 9 shows the effects of the length,  $L$ . The greatest  $u$  occurs at some value of  $L$ , beyond which  $u$  starts to decrease. Particularly,  $L$  longer than 250 m is accompanied by a surface slope less than  $\tan\phi$  after the differential settlement, and hence, no lateral flow is worked out of the analysis. This prediction seems to be reasonable.

Figs. 10 and 11 examine the effects of the thickness of the liquefied layer. When  $H_0$  increases with  $H_{10} - H_{20}$  kept equal to 5 m, the permanent displacement decreases (Fig. 10). This is understood by seeing in Fig. 7 that, when the total amount of soil flow,  $IDJ$ , is maintained constant, the greater  $ID$  results in smaller  $IJ$ . In contrast, when  $H_0$  increases with a constant value of the ratio  $H_{20}/H_{10}$ , the differential settlement increases as well, and generates a greater displacement (Fig. 11). A very thin layer induces a differential settlement of less than  $\tan\phi$ , and does not induce any displacement.

Finally, the effects of surface slope is indicated in Fig. 12 in which the calculated displacement is plotted against the elevation difference  $DZ$  over the distance of  $L = 200$  m. Clearly, the surface slope leads to a drastic increase in displacement.

The capability of the proposed method is examined by analyzing a real case. Fig. 13 compares the observed surface displacement in a gentle slope in Niigata City with those calculated by the present method. Although being a slight overestimation, the calculation seems to give a reasonable magnitude of ground displacement.

## CONCLUSIONS

Shaking table tests were conducted on the liquefaction-induced permanent displacement of a sandy ground in order to develop an analytical solution of the soil movement. From the present study, the following conclusions may be drawn.



- (1) The liquefied soil behaves either as a liquid material or as a solid one of very low stiffness. Hence, the surface of the liquefied ground tends to be level after the completion of soil movement.
- (2) The magnitude of the permanent displacement is negligible at the bottom of the liquefied ground, while being maximum at the top. This distribution of soil displacement seems to be modeled by a sinusoidal curve.
- (3) A soil displacement in the horizontal direction is generated even in a level ground, when the differential settlement and the lateral flow occur simultaneously.
- (4) An analytical solution of the permanent displacement of a liquefied ground was derived by using the three points described above. Being analytical, this solution does not require a long computation time at all.

#### REFERENCES

1. Towhata, I. : "Finite Element Model to Predict Permanent Displacement of Ground Induced by Liquefaction", Proc. 2nd Int. Conf. Numer. Meth. Geomech., Ghent, 1986, 689-697.
2. Hamada, M., Yasuda, S., Isoyama, R., and Emoto, K. : "Study on Liquefaction Induced Permanent Ground Displacements", Assoc. Develop. Earthq. Prediction, 1986.

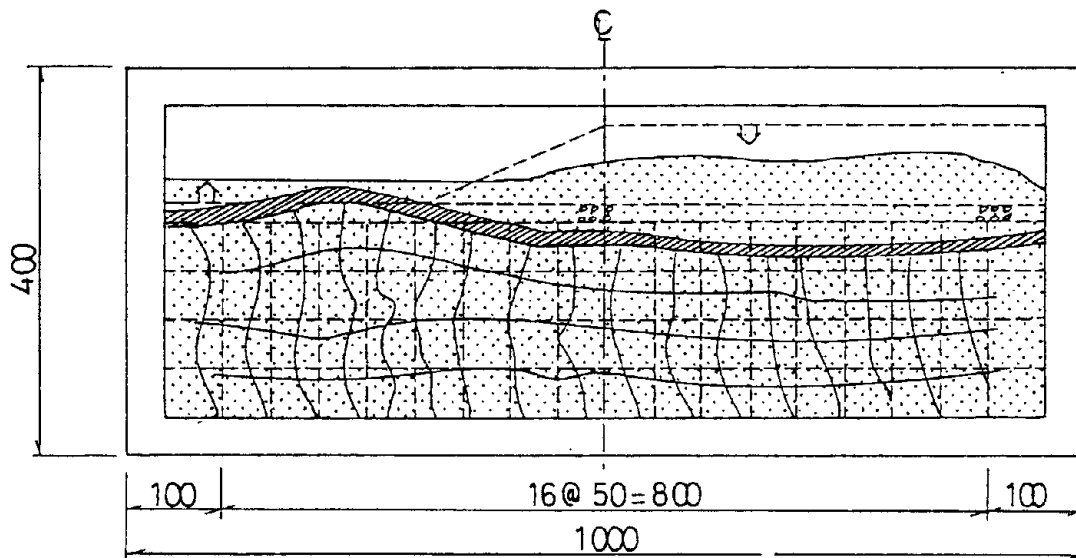


Fig. 1 Deformation of ground with dry embankment.

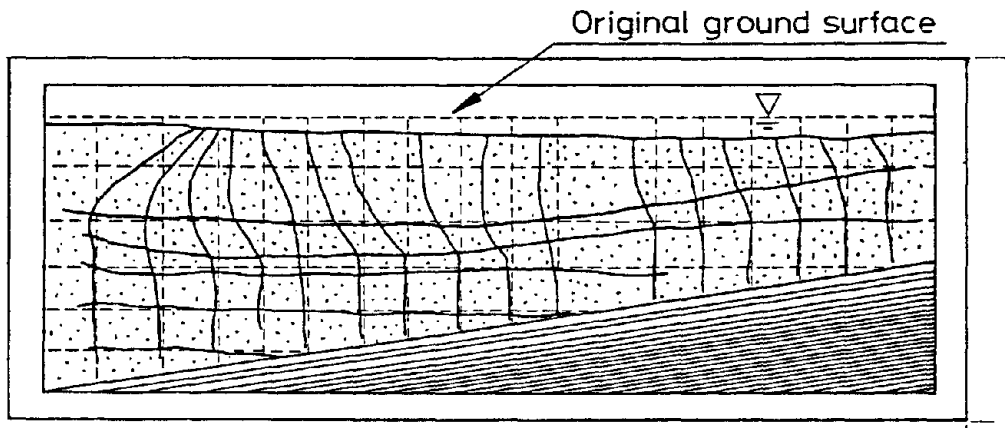


Fig. 2 Deformation of level ground with inclined bottom.

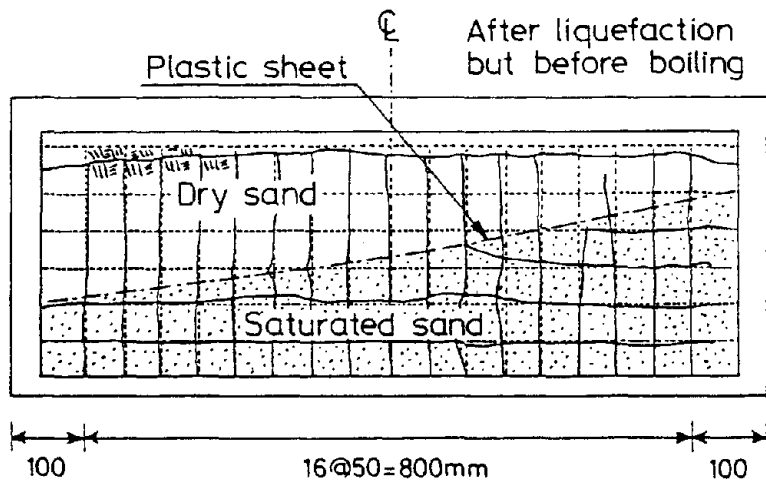


Fig. 3 Liquefied sand layer prior to boiling overlain by dry layer.

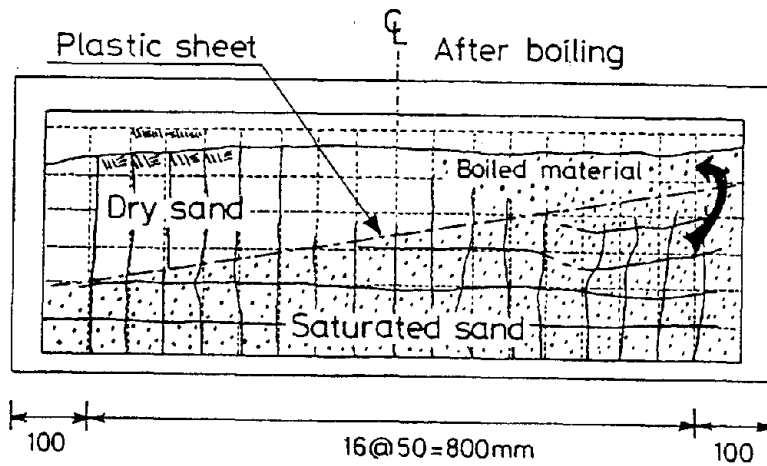


Fig. 4 Deformation of ground in Fig. 3 after boiling.

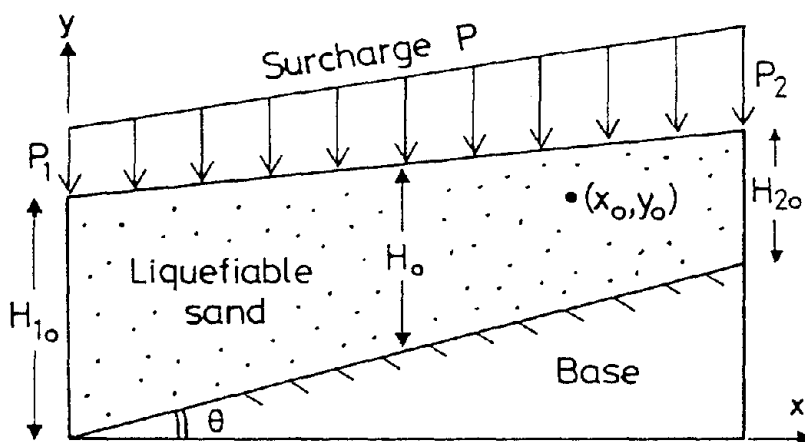


Fig. 5 Model of liquefied ground prior to displacement.

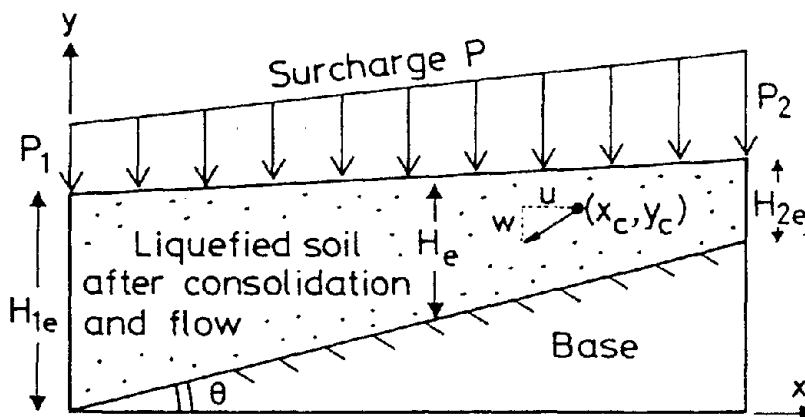


Fig. 6 Configuration of sandy ground after settlement and lateral flow.

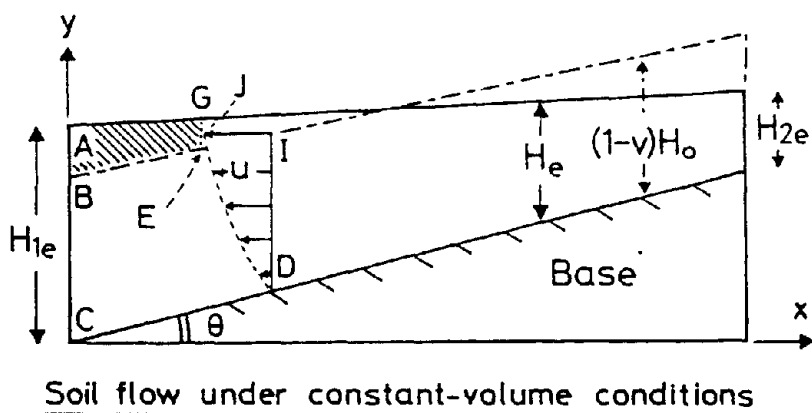


Fig. 7 Soil flow under constant-volume conditions.

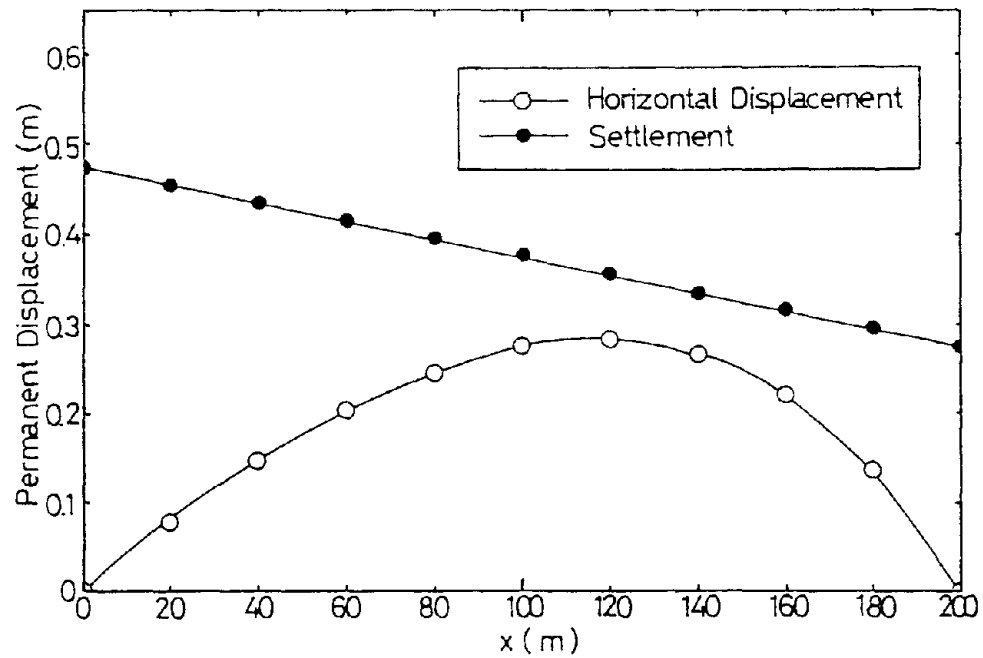


Fig. 8 Distribution of permanent displacement at the ground surface.

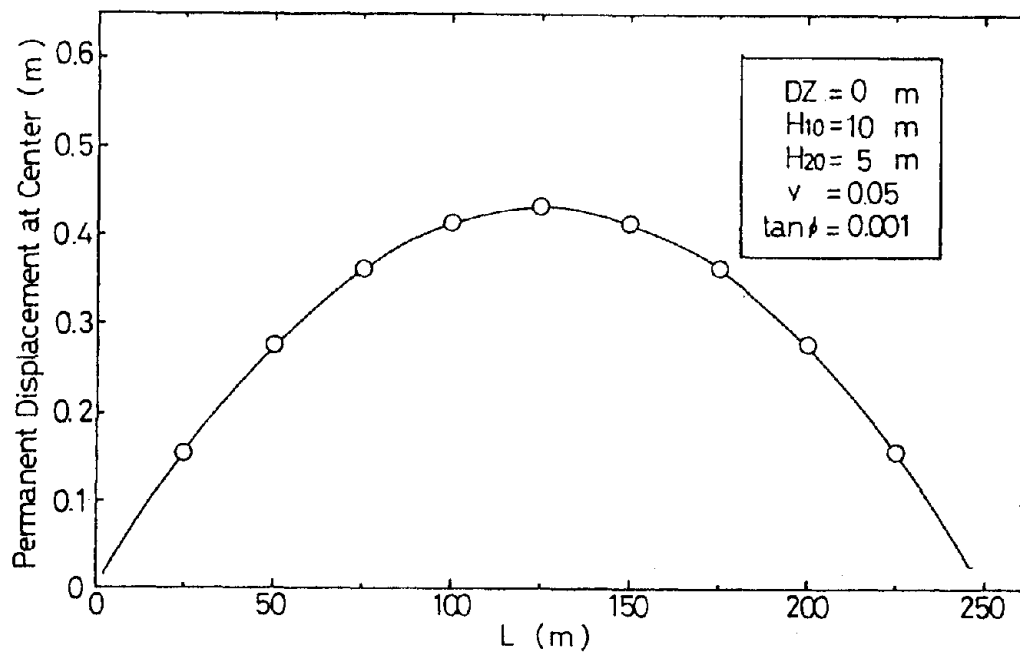


Fig. 9 Variation of permanent displacement with length of ground.

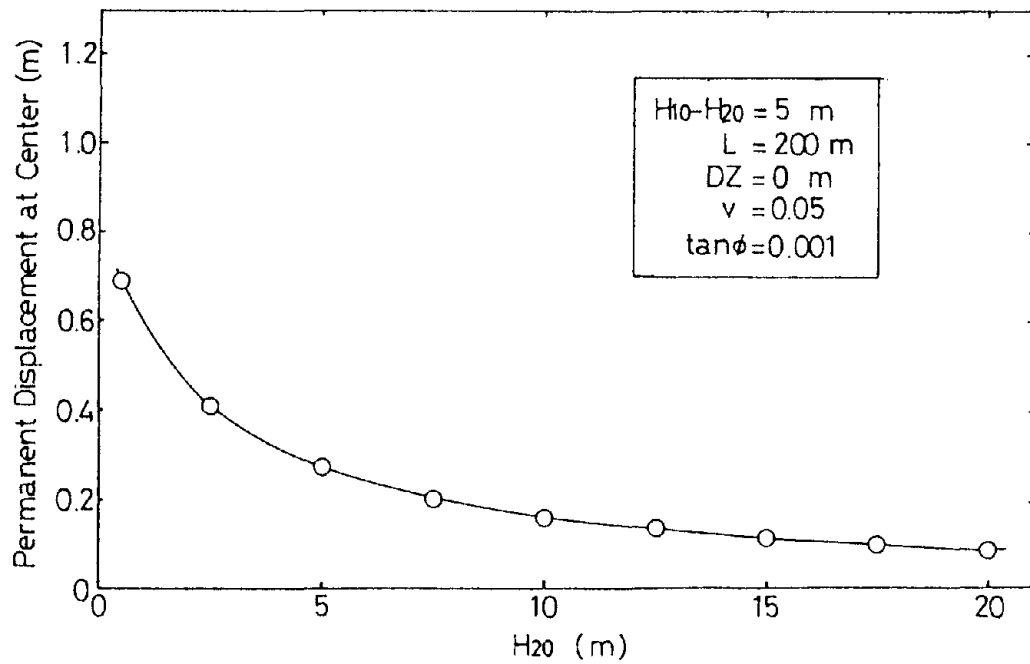


Fig. 10 Effects of thickness of liquefied layer on permanent displacement ( $H_{10} - H_{20} = \text{const.}$ )

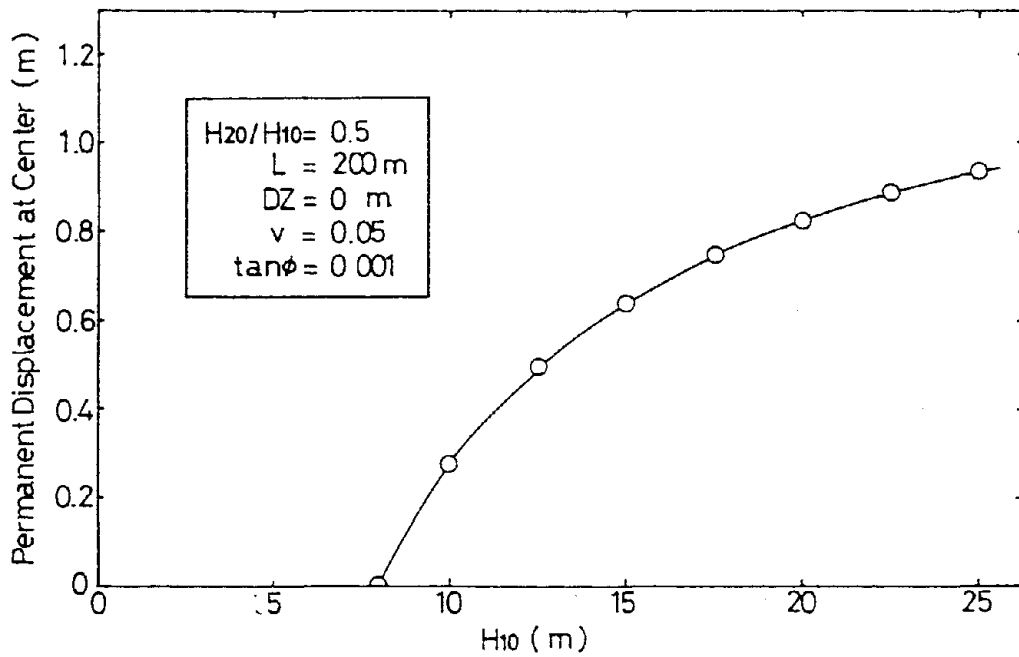


Fig. 11 Effects of thickness of liquefied layer on permanent displacement ( $H_{10} / H_{20} = \text{const.}$ )

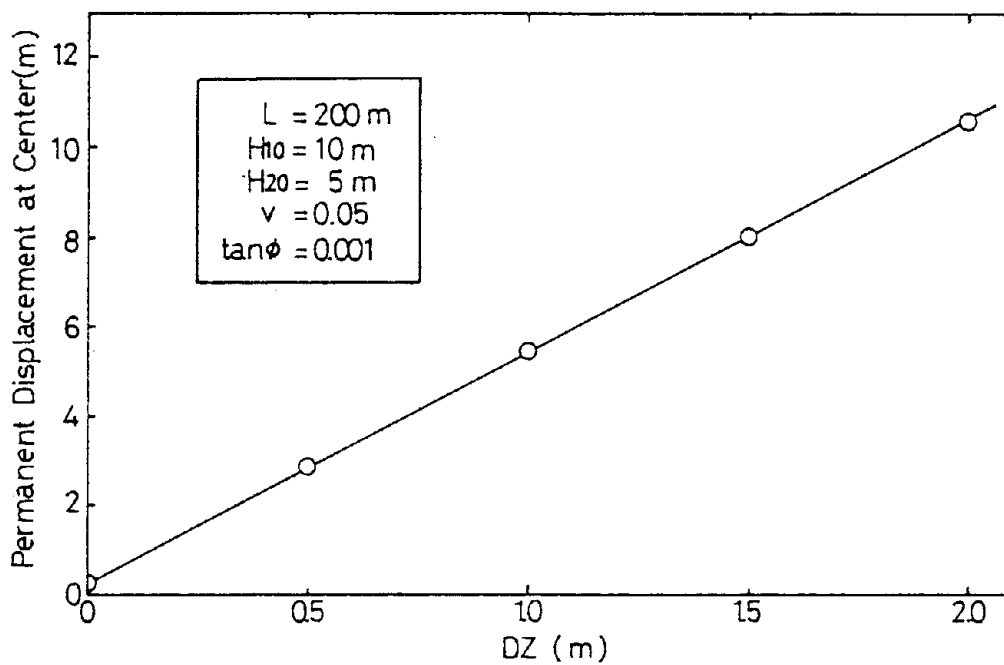


Fig. 12 Effects of surface slope on permanent displacement.

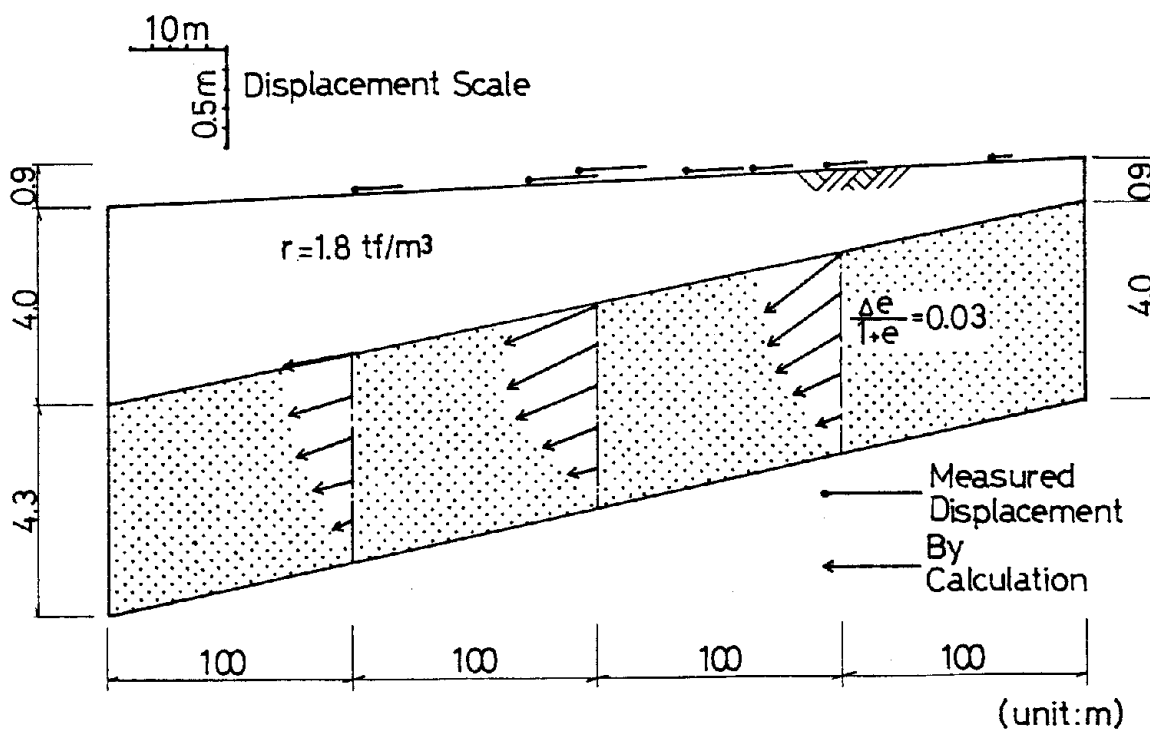


Fig. 13 Comparison of calculated and observed ground displacement in Niigata ground.

**PORE PRESSURE AND ACCELERATION RESPONSE OF WILDLIFE SITE  
DURING THE 1987 EARTHQUAKE**

R. Dobry, A.-W. Elgamal and M. Baziar

Rensselaer Polytechnic Institute, Troy, New York

M. Vucetic

University of California at Los Angeles

**ABSTRACT**

The pore pressure records obtained at the Wildlife Site in Southern California during the November 24, 1987 earthquake are analyzed. A model of the site is used based on prior *in situ* and laboratory measurements including cyclic tests, and an estimate is made of the residual shear strengths of the very loose to loose saturated silt and sandy silt located between about 1.5 and 3.5 m depth (5 to 11.5 feet). Both simplified calculations and site response analyses using program DESRAMOD are performed. The results suggest that the fast buildup in pore pressures observed at the top of the silty sand layer during the strong part of the shaking ( $a_p = 0.21 g$ ), was due to yielding and large straining of the shallow soil when the seismic shear stress reached the residual shear strength of the material.

## INTRODUCTION

During the Superstition Hills, California earthquake of November 24, 1987 ( $M = 6.6$ ) the Wildlife site, adjacent to the Alamo River in the Imperial Valley, liquefied and developed lateral displacements toward the river ranging from 0 to 230 mm. Sand boils and cracking of the ground were observed after the earthquake. Most significantly, the site had been instrumented with both accelerometers and piezometers and, for the first time, excess pore pressure ratios of 100% were measured in the field in a saturated sandy site during an earthquake (Youd and Bartlett 1988, Holzer et al. 1989 a,b). Also, the soil properties of the site had been thoroughly measured prior to the earthquake. Therefore, the 1987 records provide researchers with a unique opportunity of improving our understanding of the mechanics of seismic pore pressure buildup and liquefaction, as well as of the complex relation between pore pressure, water flow, cracking and permanent displacements during lateral spreads.

Interest in this site started after it liquefied in 1981 during the Westmoreland earthquake ( $M = 5.9$ ), when it became clear that there were good chances of its experiencing other earthquakes and liquefying again in a few years. Therefore, USGS decided to instrument the site (Bennett et al. 1984). In addition, a number of in situ and laboratory investigations were conducted by several organizations to document the characteristics of the site and provide the data needed for the analysis of any future recorded event. These included geotechnical exploration, field cone and standard penetration tests, and disturbed and intact piston sampling by USGS (Bennett et al. 1984); field seismic measurements of shear wave velocity by researchers at the U. of Texas (Stokoe and Nazarian 1985, Haag 1985); and extensive static and dynamic laboratory measurements on soil specimens from the site at the U. of Texas (Haag 1985), Woodward—Clyde Consultants (Ladd 1984), and RPI (Vucetic 1986). Equivalent linear and nonlinear site response analyses of both the 1981 earthquake and possible future events were conducted at the U. of Texas and RPI by Biershwale (1984) and Vucetic (1986), respectively. The first and fourth authors of the current paper were involved in those studies done prior to the 1987 earthquake.

This paper summarizes some of the information available on the site, and discusses the 1987 pore pressure and acceleration records vis a vis nonlinear site response analyses. A recent paper by Vucetic and Thilakaratne (1989) also analyzes the 1987 Wildlife records using the same computer code employed herein.

## THE WILDLIFE SITE

Figure 1 presents the cross section of the site with the locations of the two strong motion accelerometers (SM2 at the ground surface and SM1 at the base of the liquefiable silty sand layer) and six piezometers (P1 to P6). The groundwater level is at about 1.5 m depth. The liquefiable layers of interest are the surface silt layer down to 2.5 m depth, and the silty sand between 2.5 and 6.8 m; piezometers P1 to P5 are located in the silty sand. Piezometer P6 is in a dense silt at about 12 m, separated from the liquefiable layer by a thick silty clay, and it recorded very small pore pressures in 1987; thus, this instrument will not be further discussed herein.



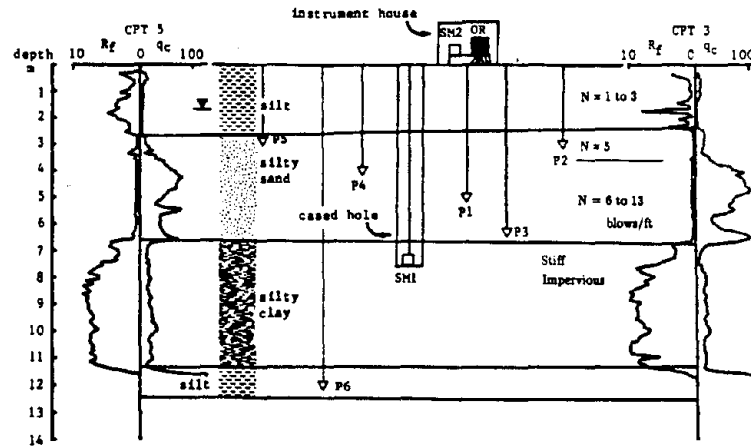


Figure 1. Cross Section of Wildlife Site Including Accelerometers (SM1 and SM2) and Piezometers (P1 to P6).

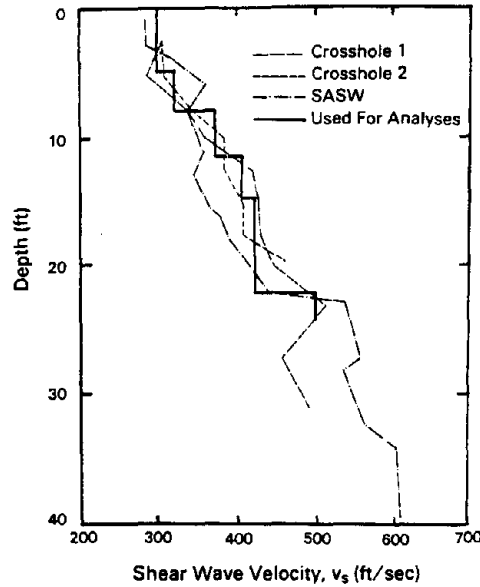


Figure 2. Shear Wave Velocities Measured at Wildlife Site (Stokoe and Nazarian 1985) and Used for the Analyses.

Therefore, three soil layers located between the ground surface and the buried accelerometer SM1 are relevant to this discussion. As described by Bennett et al. (1984), the deposit between 0 and 2.5 m consists of very loose and very soft interbedded micaceous sandy silt, silt, and clayey silt, with a measured Plasticity Index of 7. This is a very soft stratum, with a static cone resistance  $q_c = 6 \text{ Kg/cm}^2$  and with most values of the Standard Penetration Index (SPT),  $N = 1$  to 3 blows/foot.

The silty sand layer between 2.5 and 6.8 m containing the piezometers consists of two subunits. The upper unit between 2.5 to 3.5 m is a very loose to loose ( $N \approx 5$ ) moderately sorted sandy silt with small-scale cross bedding. The lower subunit between 3.5 and 6.8 m is a loose to medium dense ( $N = 6$  to 13) well-sorted silty sand to very fine sand, with the coarsest sediment being at the bottom of the unit.

The deposit below 6.8 m consists of medium to stiff clayey silt, and for all practical purposes it defines an impervious base for the liquefiable silty sand layer above it. Accelerometer SM1 is placed in this material at 7.5 m depth.

Figure 2 includes the three shear wave velocity ( $V_s$ ) profiles obtained at the site from two crosshole tests and one SASW test (SASW = Spectral-Analysis-of-Surface-Waves). SASW is a new, nondestructive method to measure shear wave velocities from Rayleigh wave observations at the ground surface (Stokoe and Nazarian 1985). These measurements are quite consistent, and for the silty sand layer they indicate that  $V_s$  increases from about 350 ft/sec at the top to 450 or 500 ft/sec at the bottom of the stratum.

Laboratory tests on intact and reconstituted samples provided a wealth of information about the properties of the soil at the site with emphasis on the silty sand layer. A representative total unit weight of  $125 \text{ lb/ft}^3$  was estimated for most of the profile; this value may be slightly smaller near the ground surface as the saturation of the soil decreases. Permeability measurements of the silty sand subunit between 3.5 and 6.8 m gave  $k = 2.1 \times 10^{-3} \text{ cm/sec}$  (Ladd 1984), which is consistent with Hazen's correlation between grain size and permeability (Lambe and Whitman 1969). Resonant column, cyclic triaxial and cyclic simple shear tests were used to determine  $G/G_{\max}$  and damping curves versus cyclic strain (Haag 1985, Ladd 1984, Vucetic 1986).

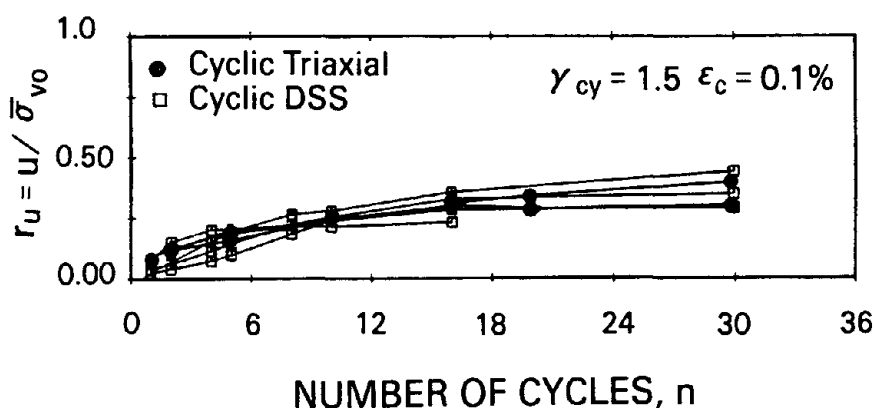


Figure 3. Strain-Controlled Cyclic Triaxial and Cyclic Direct Simple Shear (DSS) Tests on Intact and Reconstituted Specimens of Wildlife Silty Sand (modified from Vucetic 1986).

Several series of strain controlled, constant volume cyclic triaxial and cyclic simple shear tests were conducted on both intact and remolded specimens of silty sand from the site (Ladd 1984, Vucetic 1986). These experiments, aimed at determining the rate at which the pore pressure builds up in the soil with number of cycles of shear strain, provided very consistent results which were independent of type of test, confining pressure and grain size distribution. This is illustrated in Fig. 3, which includes four cyclic simple shear tests and two cyclic triaxial tests on intact and remolded samples from both subunits of the silty sand layer. As a result of all these strain-controlled tests, the following endochronic equation was developed to predict undrained pore pressure buildup throughout the whole silty sand layer after  $n$  cycles of a cyclic shear strain  $\gamma_{cy}$  (Vucetic 1986):

$$r_u = \frac{u}{\sigma_{v0}} = \frac{(1.04) (n) (\Delta\kappa)}{1 + (n) (\Delta\kappa)} \quad (1)$$

$$\begin{aligned} \Delta\kappa &= 2.6 (\gamma_{cy} - 0.02)^{1.7} && \text{for } \gamma_{cy} > 0.02\%, \text{ and} \\ \Delta\kappa &= 0 && \text{for } \gamma_{cy} < 0.02\% \end{aligned}$$

In this expression,  $r_u = u/\bar{\sigma}_{v0}$  is the pore pressure ratio (with  $r_u = 1.0$  indicating initial liquefaction), and  $\Delta\kappa$  is the increase in "intrinsic time"  $\kappa$  induced in the soil by one cycle of strain  $\gamma_{cy}$ , with  $\gamma_{cy}$  in percent (Finn and Bhatia 1980, Dobry 1988). Notice that Eq. 1 includes a threshold strain for the Wildlife silty sand,  $\gamma_t = 0.02\%$  measured in the laboratory tests, such that zero pore pressure buildup is predicted for earthquakes inducing strains smaller than this value in the soil (Dobry et al. 1981, 1982). The expression of  $r_u$  in Eq. 1 can also be used for irregular seismic straining of variable  $\gamma_{cy}$  by simple addition of the corresponding  $\Delta\kappa$  contributed by the different cycles. In first approximation, the increased  $r_u$  due to two-directional cyclic straining such as experienced during an earthquake can be calculated by doubling  $\Delta\kappa$  in the expression above (Vucetic 1986).

### RECORDS OBTAINED DURING THE 11/24/87 EARTHQUAKE

The records and observations for the November 24 earthquake have been described in detail by Holzer et al. (1989 a,b). The day before there had been a smaller earthquake ( $M = 6.2$ ), with a peak ground surface acceleration  $a_p = 0.13$  g, for which the excess pore pressure, if any, was not reported. Aftershocks both on the 23d and the 24th with  $a_p = 0.01$  g and 0.02 g, also failed to produce excess pore pressures. This observed pore pressure behavior at small accelerations, as well as the pore pressure response before the strong part of the main event, are useful to verify the analytical predictions for seismic strains smaller or slightly larger than the threshold strain measured in the laboratory,  $\gamma_t = 0.02\%$ .

Figure 4 includes plots of the strongest (NS) components of the accelerograms recorded at 7.5 m depth and at the ground surface. The figure also includes curves of the measured excess pore pressures for the four piezometers that recorded in the silty sand layer (P5 and P2 at the top of the layer, P3 at the bottom, and P1 at an intermediate

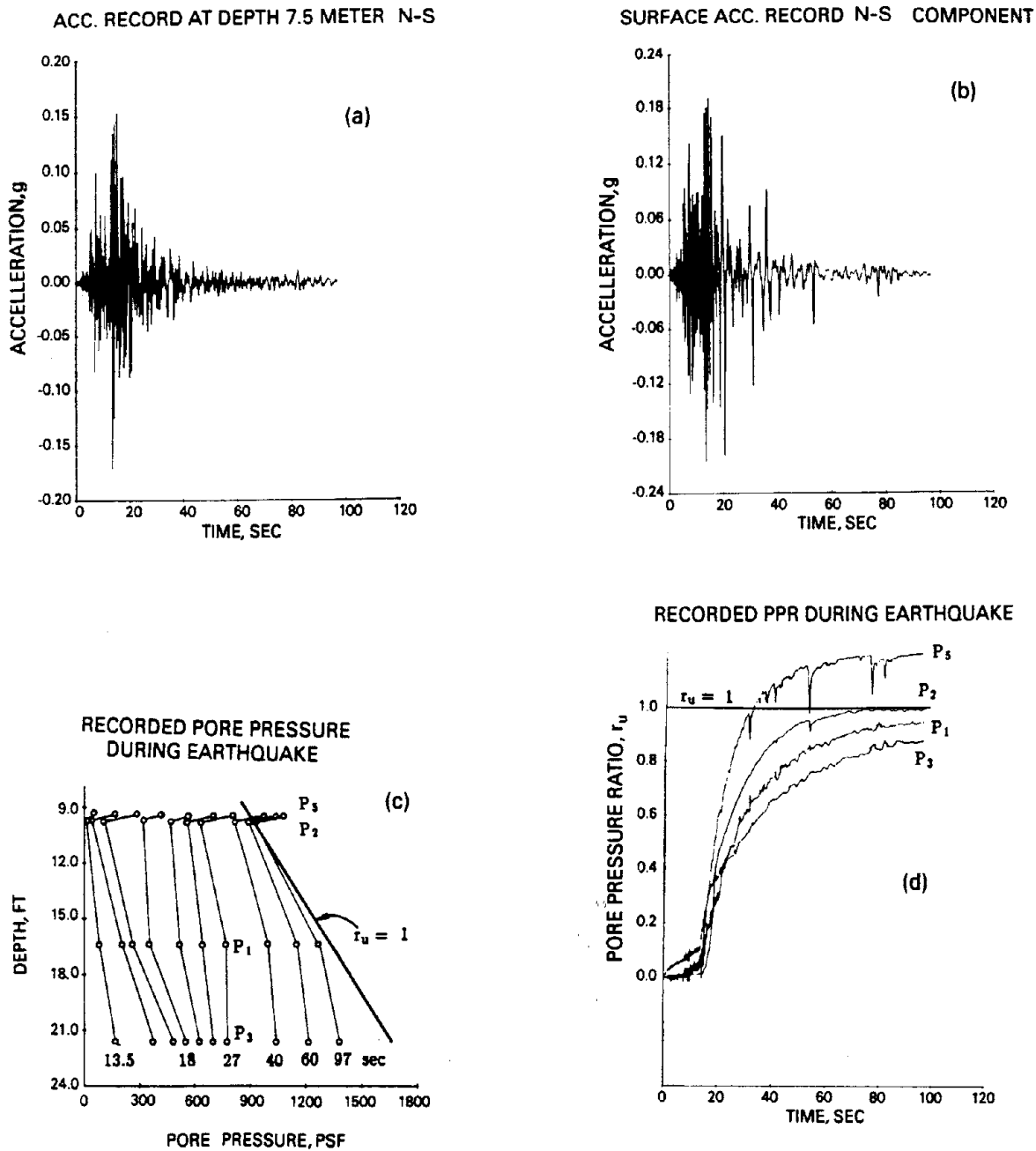


Figure 4. Recorded Accelerations (NS components) and Piezometric Readings at Wildlife Site During the November 24, 1987 Earthquake.

elevation). Most of the layer reached a pore pressure ratio  $r_u \approx 1.0$ , indicating initial liquefaction, with the possible exception of the bottom of the stratum, where  $r_u \approx 0.87$  at the end of the record.

Examination of the records indicates three distinct stages during the shaking:

Stage 1 (0 to 13.6 sec). The maximum acceleration is about 0.13 g at the ground surface (0.10 g at depth) and both accelerograms have a similar high frequency content. The pore pressure buildup is generally small, but it is somewhat greater near the bottom of the layer, with  $r_u = 0.10$  at P3 and  $0.016 \leq r_u \leq 0.06$  in the other piezometers at 13.6 seconds.

Stage 2 (13.6 to about 21 sec). This is the strong part of the shaking, which starts with the strongest acceleration pulse of the record,  $a_p = 0.21$  g at the ground surface (0.17 g at depth), followed by several strong pulses close to 0.2 g. Although not obvious in Fig. 4 due to the scale, the frequency of the surface record decreases compared with the record at depth suggesting stress-strain degradation of the soil. In this strong part there is a fast increase in the pore pressures throughout the layer, with  $r_u > 0.6$  at the top (P2 and P5) and  $r_u \approx 0.4$  at the bottom (P3) at 21 seconds. It is interesting that in this strong stage the rate of pore pressure buildup is faster at the top than at the bottom of the layer, contrary to the behavior in Stage 1.

Stage 3 (21 sec to 97 sec). In both the buried and surface accelerograms the accelerations do not exceed 0.06 g, with the ground surface accelerogram having a very long period. However, the ground surface record exhibits a dozen or so high frequency spikes as high as 0.12 g, predominantly negative, the timings of which coincide with transient pore pressure drops in the shallow piezometers P2 and P5. These acceleration/pore pressure spikes are probably associated with the dynamics of the lateral spreading (Holzer et al. 1989 b), and they demonstrate fast piezometer response during the earthquake. In Stage 3 the pore pressures continue increasing in all piezometers, with  $r_u$  being always greater at the shallower elevations, until  $r_u \approx 1$  in piezometers P2 and P5, and  $r_u = 0.87$  in P3.

## ANALYSIS AND DISCUSSION

The analysis of the pore pressure buildup in the sand layer should be able to predict qualitatively and quantitatively the behavior during Stages 1, 2 and 3. This includes answering the following questions: a) why did the pore pressure build up faster at the bottom of the layer in Stage 1?; b) why did this trend change after 13.6 sec, with the pore pressure building up faster at the top of the layer in Stage 2?; and c) why did the pore pressure continue to increase after 21 sec in Stage 3, despite the very low level of acceleration?

The dynamic soil profile shown in Table 1 and Fig. 2, obtained from the *in situ* and laboratory tests performed at the site, was selected for the analyses. The  $V_s$  and  $G_{max}$  values were extracted from Fig. 2, the hyperbolic stress-strain parameter  $\tau_{max} = G_{max}/1000$  was fitted to the laboratory  $G/G_{max}$  measurements, and so on. The pore pressure model of Eq. 1 was used in all calculations, modified for two-dimensional shaking by using  $\Delta\kappa = (2)(2.6) (\gamma_{cy} - 0.02)^{1.7}$ . This is very similar to the soil profile

TABLE 1  
Dynamic Soil Profile Used for the Analyses

Depth (feet)	Layer	Inst.	Sublayer for Analyses	Total Unit Weight (psf)	$V_s$ (ft/sec)	$G_{max}$ (psf)	$\tau_{max}$ (psf)	$k$ (cm/sec)
0		SM2						
4.92	Silt		1	125	300	$3.49 \times 10^5$	$3.49 \times 10^2$	—
8.20			2	125	320	$3.97 \times 10^5$	$3.97 \times 10^2$	$3.0 \times 10^{-4}$
11.48		P5 P2	3	125	372	$5.37 \times 10^5$	$5.37 \times 10^2$	$3.0 \times 10^{-4}$
14.76	Silty		4	125	406	$6.40 \times 10^5$	$6.40 \times 10^2$	$2.1 \times 10^{-3}$
18.05	Sand	P1	5	125	420	$6.84 \times 10^5$	$6.84 \times 10^2$	$2.1 \times 10^{-3}$
22.31		P3	6	125	420 (460)	$6.84 \times 10^5$ ( $8.20 \times 10^5$ )	$6.84 \times 10^2$ ( $8.20 \times 10^2$ )	$2.1 \times 10^{-3}$
24.61	Clayey Silt		7	125	500	$9.71 \times 10^5$	$9.71 \times 10^2$	$3.1 \times 10^{-5}$

used before and after 1987 by Vucetic (1986, 1989). In sublayer 6,  $V_{s6} = 460$  ft/sec is the "best estimate" obtained from the *in situ* measurements in Fig. 2, while  $V_{s6} = 420$  ft/sec provides a somewhat better prediction of the pore pressure at the end of Stage 1. Therefore,  $V_{s6} = 420$  ft/sec was primarily used in the analyses.

Questions (a) and (b) related to the rates of pore pressure buildup during Stages 1 and 2, can be conveniently discussed with the help of Fig. 5, which plots the predicted pore pressure ratio  $r_u$  throughout the sand layer caused by one cycle of peak ground surface acceleration  $a_p$ , for several values of  $a_p$ . The  $\gamma_p$  curves contained in the figure were calculated from the dynamic soil profile of Table 1. The peak seismic strain  $\gamma_p$  was obtained for each  $a_p$  and depth from  $\gamma_p = \tau_p / [G_{\max}(G/G_{\max})]$ , where  $\tau_p$  is the peak stress and  $\tau_p = (a_p/g) \sigma_v r_d$ ,  $\sigma_v$  = total vertical stress, and  $r_d = 0.8$  to  $1.0$  is a flexibility coefficient for the site obtained from the site response computer runs described later herein (see also Seed and Idriss 1970). The vertical lines of constant  $r_u$  were calculated from Eq. 1,  $n = 1$ , and  $\Delta\kappa = (2)(2.6)(\gamma_p - 0.02)^{1.7}$ , with the factor 2 accounting for the effect of the second acceleration component ( $\Delta\kappa$  and  $\gamma_p$  in percent in this last expression).

For  $a_p \approx 0.02$  g, as in the two aftershocks already mentioned, Fig. 5 predicts strains below the threshold and thus  $r_u = 0$  at all depths. For  $a_p = 0.13$  g, as in Stage 1 of the main event (and also in the earthquake the day before), a small pore pressure of the order of  $r_u \approx 0.02$  or  $0.03$  is predicted in one cycle, with the largest pore pressure occurring at the bottom of the silty sand layer. This predicts the trend actually observed in Stage 1 of the main event.

For a larger acceleration corresponding to the peak in Stage 2,  $a_p = 0.21$  g, Fig. 5 predicts  $r_u = 0.05$  at the top of the silty sand layer in one cycle of acceleration, and  $r_u = 0.15$  at the bottom of the layer. These large  $r_u$  values are consistent with the fast pore pressure buildup recorded by the piezometers in Stage 2, but the prediction of a greater  $r_u$  at the bottom is contrary to the observed behavior

The same conclusions were reached by conducting a site response analysis for the November 24 event with computer code DESRAMOD. Program DESRAMOD (Vucetic 1986, Vucetic and Thilakaratne 1989) is a modified version of program DESRA-2 (Finn et al. 1977, Lee and Finn 1978), where the main modification consists in the use of a pore pressure model such as that of Eq. 1. Other characteristics of DESRAMOD are identical to parent program DESRA-2. It conducts a one-dimensional nonlinear site response analysis using: lumped masses to represent the soil profile; a hyperbolic stress-strain backbone curve for the soil in shear characterized by initial parameters  $G_{\max 0}$  and  $\tau_{\max 0}$  (such as listed in Table 1); and an extended Masing law for cyclic loading. The program provides for stress-strain degradation due to pore pressure buildup by decreasing both  $G_{\max}$  and  $\tau_{\max}$  as follows:  $G_{\max}/G_{\max 0} = (1 - r_u)^{1/2}$  and  $\tau_{\max}/\tau_{\max 0} = (1 - r_u)$ . Migration and dissipation of pore pressures accompanied by reconsolidation, both during and after the shaking, are included in the program.

Figure 6 shows the pore pressure buildup in sublayers 3 and 6 of the silty sand layer calculated with DESRAMOD, with the NS acceleration component recorded by SM1 in 1987 as input, and using the soil parameters of Table 1 and the pore pressure model of Eq. 1 (with a factor of 2 for  $\Delta\kappa$ ). Two runs are included in Fig. 6, corresponding to the

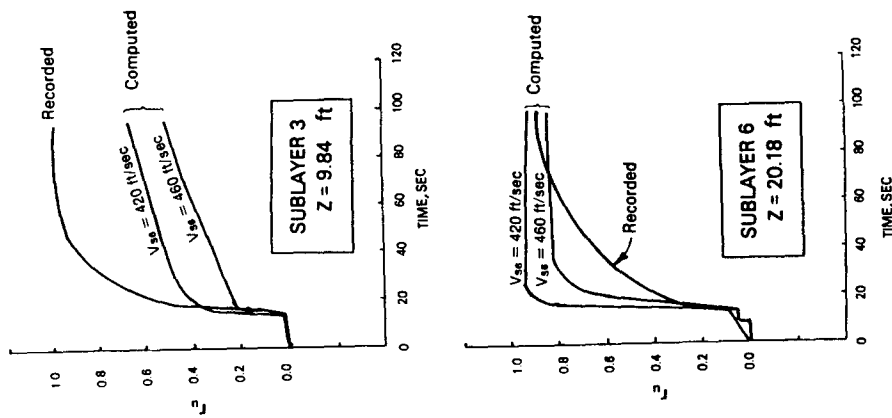


Figure 6. Pore Pressure Ratios Measured in Sublayers 3 (Top) and 6 (Bottom) of the Silty Sand Layer, and Predicted with Program DESRAMOD.

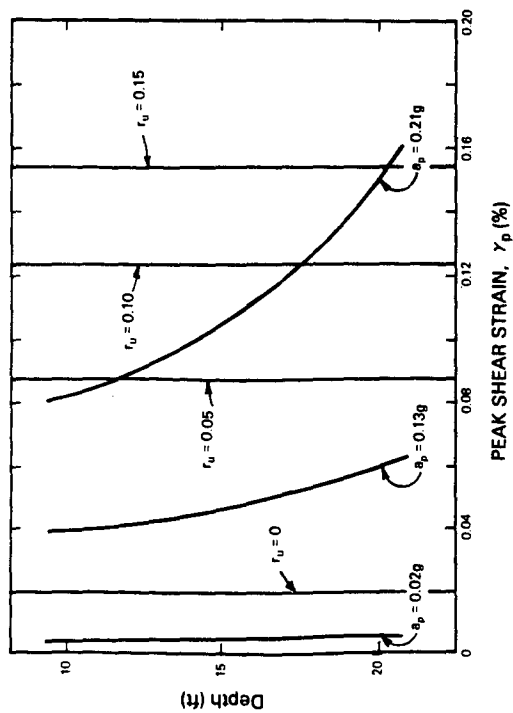


Figure 5. Peak Seismic Shear Strain,  $\gamma_p$ , and Pore Pressure Ratio,  $r_u = u/\sigma_{vo}$ , Caused in the Silty Sand Layer by One Cycle of Ground Surface Peak Acceleration,  $a_p$ .



two initial (nondegraded) values of  $V_{s6}$  for sublayer 6 shown in Table 1. Figure 6 also includes the recorded pore pressure buildup curves from the corresponding piezometers. In Stage 1, up to 13.6 sec, the agreement between computed and recorded pore pressures is quite good, especially when  $V_{s6} = 420$  ft/sec is used. Both predicted and recorded curves indicate a larger  $r_u$  in sublayer 6 than in sublayer 3 at 13.6 seconds. However, between 13.6 and 21 seconds, sublayer 3 at the top of the layer builds up  $r_u$  faster than sublayer 6 at the bottom, while DESRAMOD predicts exactly the opposite behavior. In the DESRAMOD runs, the computed  $a_p$  at the ground surface was 0.24 g versus 0.21 g measured.

Clearly something happened after 13.6 sec when the largest acceleration pulse of  $a_p = 0.21$  g hit the site, which qualitatively changed the pore pressure buildup behavior of the silty sand layer, speeding up the development of pore pressure at the top of the layer more than at the bottom. It is also clear that this change in behavior is not captured by the DESRAMOD runs included in Fig. 6.

The authors suggest that the seismic shear stresses associated with this large acceleration pulse were large enough to mobilize the shear strengths in both the surface silt layer and in the top of the silty sand layer. As noticed before, the soil at the site is very loose to loose down to 3.5 m, with very low  $N$  and  $q_c$  values (see Fig. 1). Therefore, it should be expected that both saturated sublayers 2 and 3 in Table 1 were contractive and had very low shear strengths at the time of the earthquake. This yielding of the soil in sublayers 2 and 3 would suddenly generate large strains and pore pressures shortly after 13.6 sec, just as shown by the record at the top of Fig. 6. Also, it could be anticipated that this yielding of the shallow soil, plus its subsequent stress-strain degradation due to the pore pressure increase, would decrease the seismic shear stresses reaching the bottom of the silty sand layer, thus slowing down the pore pressure buildup there (see also Vucetic and Thilakarathne 1989).

One of the authors (Baziar 1990) recently conducted a series of monotonic compression triaxial (CIU) tests at low confining pressures, on reconstituted sandy silt from the San Fernando Dam. In these tests, the sandy silt was deposited under water in the triaxial mold in five layers, thus allowing for the low density, segregation and layering typical of very loose alluvial deposits and hydraulic fills. Then the layered specimen was isotropically consolidated to a confining pressure,  $\bar{\sigma}_0$ , ranging between 0.2 and 0.9 Kg/cm<sup>2</sup>, and loaded undrained to failure. Figure 7 presents the result of one of the tests, with  $\bar{\sigma}_0 = 0.22$  Kg/cm<sup>2</sup>, and an undrained residual shear strength,  $q_{us} \approx S_{us} \approx S_r = 0.035$  Kg/cm<sup>2</sup>. As it often occurs in sands with a high silt content, the peak and residual strengths are not very different, with failure being plastic rather than brittle. Based on this test series,  $S_r \approx 0.15 \bar{\sigma}_0$  was obtained for a very loose, water-sedimented alluvial or hydraulic fill deposit containing this soil.

Table 2 includes estimates of the residual shear strengths of sublayers 2 and 3 using the results of the tests just described, as well as the correlations between  $N$  and  $S_r$  and  $q_c$  and  $S_r$  reported by Seed (1987) and Ishihara (1989), respectively. The table also presents the peak shear stresses  $\tau_p$  (from the DESRAMOD runs) in the same sublayers, associated with  $a_p = 0.21$  g at the ground surface. While in silt sublayer 2 the  $S_r$  estimates range from about 50 to 110 psf,  $\tau_p = 188$  psf. Similarly, in sandy silt sublayer 3,  $S_r$  ranges from about 100 to 280 psf, while  $\tau_p = 274$  psf. Therefore, this confirms the

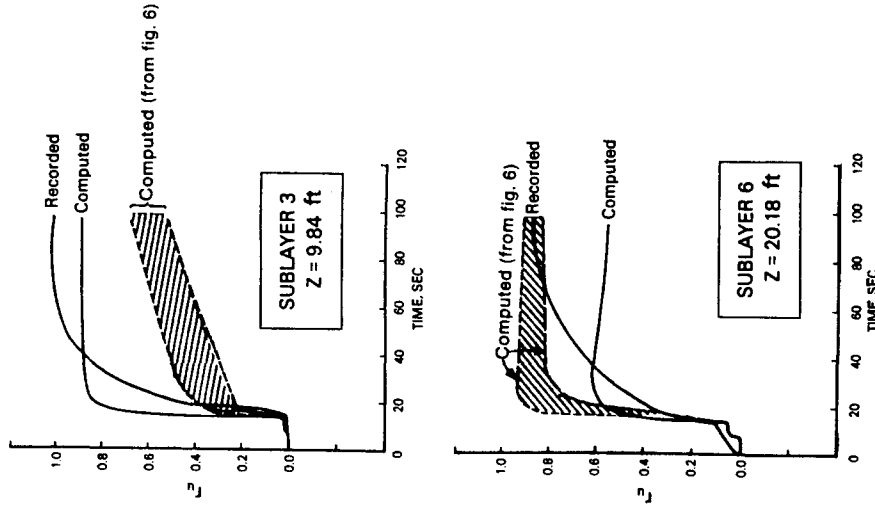


Figure 8. Pore Pressure Ratios Computed in Sublayers 3 (Top) and 6 (Bottom) of the Silty Sand Layer with DESRAMOD, Assuming  $\tau_{max} = 200$  psf for Sublayer 3 after  $t = 13.6$  Seconds.

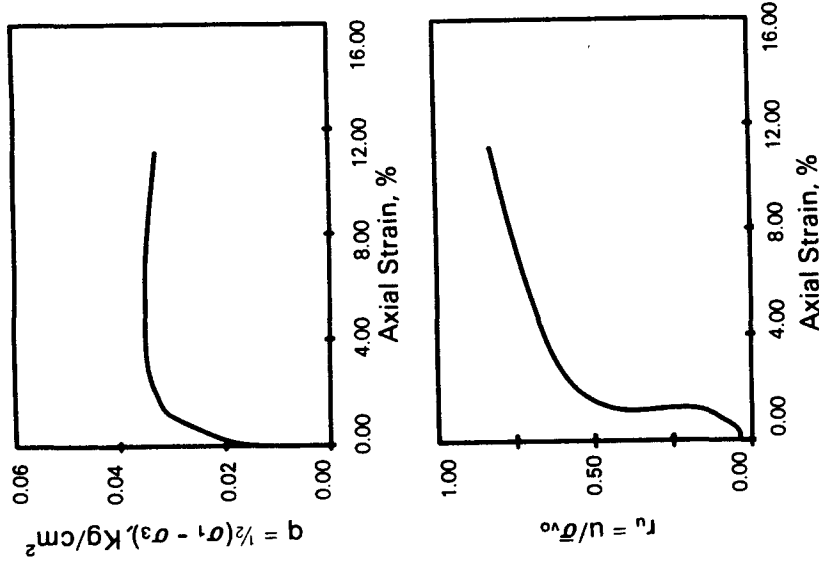


Figure 7. Monotonic Compression Triaxial (CIU) Test on Reconstructed Layered Specimen of San Fernando Dam Sandy Silt. Specimen was Sedimented in Five Layers in Water and Isotropically Consolidated to  $\bar{\sigma}_0 = 0.22$  Kg/cm<sup>2</sup>.

Figure 8.

TABLE 2

Peak Seismic Shear Stresses  $\tau_p$  for  $a_p = 0.21 g$   
and Residual Shear Strengths  $S_r$  in Sublayers 2 and 3

Sublayer	Soil	z (ft)	$\bar{\sigma}_{v0}$ (psf)	N(blow/ft)	$q_c$ (Kg/cm <sup>2</sup> )	Residual Shear Strength $S_r$ (psf)			Peak Seismic Shear Stress, $\tau_p$ (psf)
						From N(*)	From $q_c$ (**)	From CIU Tests (***)	
2	Silt	6.6	718	2	6	0 to 100	80	110	188
3	Sandy Silt	9.8	923	5	21	30 to 250	280	140	274

(\*) From chart relating  $(N_1)_{60}$  and  $S_r$  in sands by Seed (1987)

(\*\*) From correlation between  $q_c$  and  $S_r$  for water-deposited silts and silty sands by Ishihara (1989):  $S_r \approx q_c/150$

(\*\*\*) From undrained monotonic triaxial tests (CIU) on water-deposited, layered, San Fernando Dam sandy silt by Baziar (1990):  $S_r \approx 0.15 \bar{\sigma}_0 \approx 0.15 \bar{\sigma}_{v0}$

hypothesis that during the peak acceleration pulse,  $\tau_p \geq S_r$  in both sublayers and the soil yielded between about 5 and 12 feet in depth.

An additional run of DESRAMOD was conducted to simulate crudely the effect of this yielding of the shallow soil on the dynamic and pore pressure response of the silty sand. As shown in Table 1,  $\tau_{max} = 537$  psf was used for sublayer 3 for the hyperbolic model of the backbone of the soil in shear. This value was essentially unchanged up to 13.6 sec in the DESRAMOD runs of Fig. 6. One of these runs was repeated, in which  $\tau_{max}$  was degraded between 12.6 sec and 13.6 sec down to  $\tau_{max} = 200$  psf, consistent with the residual shear strength for sublayer 3 estimated above.

Figure 8 presents the result of this analysis, which calculated the correct  $a_p = 0.21$  g at the ground surface. Up to 13.6 sec, the pore pressure buildup is about the same as in the previous runs. However, as anticipated, after 13.6 the pore pressure builds up now much more rapidly in sublayer 3 than in sublayer 6, due to the yielding and high strains induced in sublayer 3 by the strong shaking. Also as expected, the calculated pore pressure buildup curve in sublayer 6 is lower than it was in Fig. 6, due to the decrease of seismic shear stresses in the sublayer.

Although somewhat on the high side, the pore pressures predicted by this analysis in Fig. 8 are a reasonable first approximation to the piezometric recordings in Stages 1 and 2, that is until about 21 seconds. An even better agreement should be expected when more refined analyses are performed in which the yielding of the soil, the relation between monotonic straining and pore pressure, and the influence of the second horizontal component, are modelled more precisely.

However, the slow pore pressure development after 21 sec, up to values of  $r_u \approx 0.9$  or 1.0 throughout the sand layer, is not predicted by either of the DESRAMOD analyses presented in Figs. 6 and 8, nor by the runs reported by Vucetic and Thilakaratne (1989). There are at least a couple of possible explanations for the observed behavior: a) after 21 seconds the soil stiffness had degraded much more than assumed in DESRAMOD, so that the small shear stresses induced by the shaking in Stage 3 were able to cause shear strains large enough for the buildup of additional pore pressures, and for liquefaction to continue progressing from the top to the bottom of the layer; or b) there was migration (towards the piezometers) of high pore pressures close to  $r_u = 1.0$  existing at the end of Stage 2 in other parts of the silty sand layer or outside the layer. Hypothesis (b) has been proposed by both Holzer et al. (1989 b) and Vucetic and Thilakaratne (1989). Additional research is needed to clarify this question.

## SUMMARY AND CONCLUSION

From the analysis of the pore pressure response recorded in the silty sand layer at the Wildlife site during the Superstition Hills earthquake, it was possible to divide the shaking in three stages. In Stage 1, corresponding to the initial weak shaking between 0 and 13.6 sec, the pore pressures, while generally small, were larger at the bottom of the layer, and they could be predicted by one-dimensional response analyses using the measured cyclic properties of the soils at the site. In Stage 2, corresponding to the strong shaking part between 13.6 and 21 sec, a very fast pore pressure increase was observed at the top of the layer; this is explained by the seismic shear stresses reaching or exceeding the residual strengths of the very loose to loose sandy silt and silt existing

in the site at shallow depths (sublayers 2 and 3 in Table 1). In Stage 3, after 21 sec, corresponding to very low accelerations in the soil, the pore pressures continued to increase, with liquefaction ( $r_u \approx 1.0$ ) propagating from the top to the bottom of the layer; this behavior has not yet been fully explained and further research is suggested.

### ACKNOWLEDGEMENTS

The study was supported by NCEER under Grant No. 881504.

### REFERENCES

- Baziar, M.H. (1990). "Permanent Deformations due to Seismically Induced Liquefaction," Dissertation to be submitted in partial fulfillment of the requirements for the degree of Doctor of Philosophy, Department of Civil Engineering, Rensselaer Polytechnic Institute, Troy, NY (in preparation).
- Bennett, M.J., McLaughlin, P.V., Sarmiento, J.S., and Youd, T.L. (1984). "Geotechnical Investigation of Liquefaction Sites, Imperial Valley, California," Open File Report No. 84-252, USGS, Menlo Park, California.
- Bierschwale, J.G. (1984). "Analytical Evaluation of Liquefaction Potential of Sands Subjected to the 1981 Westmoreland Earthquake," Research Report, Civil Engineering Department, The University of Texas at Austin, Austin, Texas.
- Dobry, R., Ng, T.-T., Ladd, R.S. and Reese, L.C. (1988). "Modeling of Pore Pressures and Shear Moduli in Calcareous Soils by Strain-Controlled Cyclic Triaxial Testing," *Proceedings of the International Conference on Calcareous Sediments*, R.J. Jewell and M.S. Khorshid, Eds., Perth, Australia.
- Dobry, R., Stokoe, II, R.H., Ladd, R.S. and Youd, T.L. (1981). "In Situ Shear Wave Velocity Measurements to Evaluate Liquefaction Susceptibility," *ASCE National Convention on In Situ Tests to Evaluate Liquefaction Susceptibility*, Preprint Volume 81-544, Session No. 24, St. Louis, Missouri.
- Dobry, R., Ladd, R.S., Yokel, F.Y., Chung, R.M. and Powell, D. (1982). "Prediction of Pore Water Pressure Buildup and Liquefaction of Sands During Earthquakes by the Cyclic Strain Method," National Bureau of Standards Building Science Series, 138, U.S. Dept. of Commerce,
- Finn, W.D.L., Lee, K.W. and Martin, G.R. (1977). "An Effective Stress Model for Liquefaction," *Journal of the Geotechnical Engineering Division*, ASCE, GT6, 517-533.
- Finn, W.D.L., and Bhatia, S. (1980). "Endochronic Theory of Sand Liquefaction," *Proc. Seventh World Conference on Earthquake Engineering*, Istanbul, Turkey, 3, 149-155.
- Haag, E.D. (1985). "Laboratory Investigations of Static and Dynamic Properties of Sandy Soils Subjected to the 1981 Westmoreland Earthquake," Research Report, Civil Engineering Department, University of Texas, Austin, Texas.

Holzer, T.L., Youd, T.L., and Hank, T.C. (1989 a). "Dynamics of Liquefaction During the 1987 Superstition Hills, California Earthquake," *Science*, 244, pp. 1-116.

Holzer, T.L., Youd, T.L. and Bennett, M.J. (1989 b). "In Situ Measurement of Pore Pressure Build-Up During Liquefaction," *Proceedings of the 20th Joint Meeting of the U.S.-Japan Cooperative Program in Natural Resources Panel on Wind and Seismic Effects*, Published by the National Institute of Standards and Technology, Gaithersburg, MD 20899.

Ishihara, K. (1989). Personal Communication.

Ladd, R.S. (1984). "Laboratory Investigation of Sands from Wildlife Site," unpublished.

Lambe, T.W. and Whitman, R.V. (1969). *Soil Mechanics*, John Wiley & Sons, Inc.

Lee, K.W. and Finn, W.D.L. (1978). "DESRA-2, Dynamic Effective Stress Response Analysis of Soil Deposits with Energy Transmitting Boundary Including Assessment of Liquefaction Potential," Faculty of Applied Science, University of British Columbia, Vancouver, Canada.

Seed, H.B. and Idriss, I.M. (1970). "A Simplified Procedure for Evaluating Soil Liquefaction Potential," Report EERC 70-9, University of California, Berkeley.

Seed, H.B. (1987). "Design Problems in Soil Liquefaction," *Journal of Geotechnical Engineering*, ASCE, 113(8), 827-845.

Stokoe, II, K.H. and Nazarian, S. (1985). "Use of Rayleigh Waves in Liquefaction Studies," *Proceedings Measurement and Use of Shear Wave Velocity for Evaluating Dynamic Soil Properties*, GED, ASCE, Denver, Colorado.

Vucetic, M. (1986). "Pore Pressure Buildup and Liquefaction at Level Sand Sites During Earthquakes," Dissertation submitted in partial fulfillment of the requirements for the degree of Doctor of Philosophy, Department of Civil Engineering, Rensselaer Polytechnic Institute, Troy, N.Y.

Vucetic, M. and Thilakaratne, V. (1989). "Liquefaction at the Wildlife Site—Effect of Soil Stiffness on Seismic Response," *Proceedings of 4th International Conference on Soil Dynamics and Earthquake Engineering*, Mexico City, Mexico.

Youd, T.L. and Bartlett, S.F. (1988). "US Case Histories of Liquefaction-Induced Ground Displacement," *First U.S.-Japan Workshop on Liquefaction, Large Ground Deformation and their Effect on Lifeline Facilities*, Tokyo, Japan.

**INITIAL STRESS AND RESIDUAL DEFORMATION  
-EFFECTIVE STRESS ANALYSIS OF ANCHORED SHEET PILE QUAYWALL-**

Susumu IAI and Tomohiro KAMEOKA

Port and Harbour Research Institute  
Ministry of Transport, JAPAN

**ABSTRACT**

A fundamental mechanism in producing deformation of ground and soil structures, when they are subject to liquefaction, is existence of initial stress and its release in accordance with deformation. How the initial stress is released depends on the boundary conditions given to the problem. In this paper, four types of stress release are identified by an effective stress analysis of an anchored sheet pile quaywall. Soil in front of sheet pile, which was initially in nearly passive failure state, shows stress release with cyclic rotation of principal stress axes. Soil behind the sheet pile, which was initially in nearly active failure state, shows stress release with cyclic normal stress difference. Soil between the sheet pile and an anchor, which was initially in  $K_0$  consolidated state, shows cyclic simple shear in horizontal direction with free displacement conditions at the side boundaries. Finally soil in front of the anchor, which was initially sheared in horizontal direction, clearly shows rotation of principal stress axes due to Rayleigh wave generated by the soil-structure interaction.

## INTRODUCTION

When liquefaction occurs, initial shear stress restored in ground and soil structures is released to cause deformation. Even if initial shear stress is very small, deformation occurs because liquefaction is a process in which both shear strength and shear modulus of soil approach zero. Deformation of soil causes redistribution of stress. Redistributed stress, in turn, causes further deformation. How the initial stress is released due to the redistribution of stress depends on the material properties, geometrical configuration and boundary conditions given to the problem.

In order obtain a tangible understanding upon the stress release and associated deformation of ground and soil structures, an effective stress analysis of an anchored sheet pile quaywall is conducted.

## OUTLINE OF THE MODEL

The effective stress model used in this study is composed of two parts; ; a stress-strain relation for shear mechanism and a mechanism for generating excess pore water pressure (Iai[1]).

The stress-strain relation for shear mechanism adopted here is, as shown in Figure 1, the model of a multiple mechanism composed of virtual simple shear mechanisms in arbitrary orientations; each virtual simple shear mechanism is assumed to follow the hyperbolic stress-strain relation with hysteresis given by Masing's rule. This model, originally proposed by Towhata and Ishihara[2], is modified here in order to incorporate the ability to achieve realistic hysteresis loop instead of those given by Masing's rule. The approach for

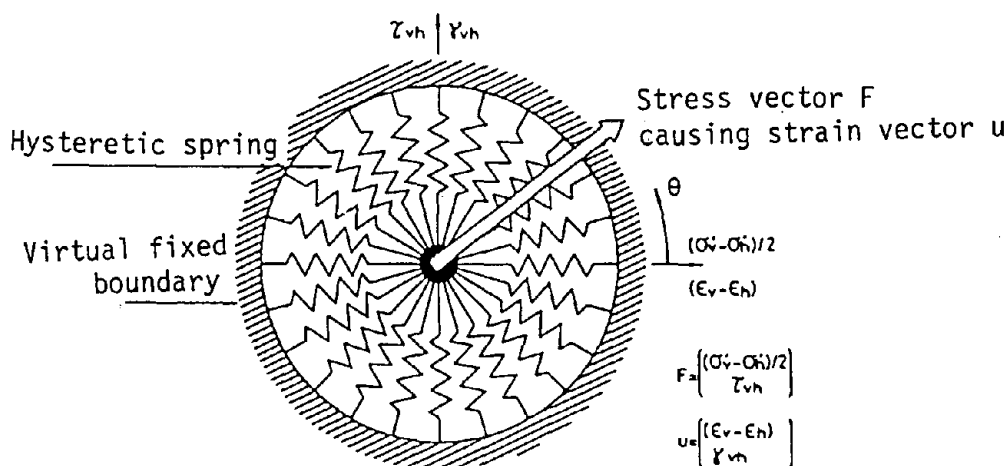


Figure 1 Shear Mechanism Model (After Towhata and Ishihara [1] with a minor change)



modifying the hysteresis loop is similar to that proposed by Ishihara et al [3].

The main features of the model are as follows;

- (1) Behaviors under drained cyclic loading at various cyclic amplitudes are consistent with the laboratory test results.
- (2) Effect of principal axis rotation is taken into account.
- (3) Material anisotropy can readily be incorporated into the model.

The parameters necessary for specifying the hyperbolic relation are friction angle  $\phi_f$  and elastic shear modulus  $G_{mref}$  measured under the confining pressure of  $\sigma_{mref}'$ . These parameters determine the constants of the hyperbolic relation under the initial effective confining pressure of  $\sigma_{mo}'$  as follows;

$$\begin{aligned} \tau_{mo} &= \sigma_{mo}' \sin \phi_f \\ G_{mo} &= G_{mref} \sqrt{\sigma_{mo}' / \sigma_{mref}'} \\ \gamma_{mo} &= \tau_{mo} / G_{mo} \end{aligned} \quad (1)$$

in which

- $\tau_{mo}$  : shear strength
- $G_{mo}$  : elastic shear modulus
- $\gamma_{mo}$  : reference shear strain

Apart from the shear mechanism, excess pore water pressure is generated by the following rule. First of all, a state variable  $S$  is defined as a variable which is equivalent to  $\sigma_m' / \sigma_{mo}'$  under undrained condition with a constant total confining pressure. In the present model, the state variable  $S$  is determined from the shear stress ratio  $r = \tau / \sigma_{mo}'$  and the liquefaction parameter  $S_0$ , to be defined later as a measure of liquefaction, as follows (see Figure 2);

$$\begin{aligned} S &= S_0 && \text{(if } r < r_3) \\ S &= S_2 + \sqrt{(S_0 - S_2)^2 + [(r - r_3) / m_1]^2} && \text{(if } r > r_3) \end{aligned} \quad (2)$$

in which

$$\begin{aligned} \tau &= \sqrt{\tau_{xy}^2 + [(\sigma_y' - \sigma_x') / 2]^2} \\ r_2 &= m_2 S_0 \\ r_3 &= m_3 S_0 \\ S_2 &= S_0 - (r_2 - r_3) / m_1 \\ m_1 &= \sin \phi_f \\ m_2 &= \sin \phi_p \quad (\phi_p \text{ is phase transformation angle}) \\ m_3 &= 0.67 m_2 \end{aligned}$$

Secondly, the liquefaction parameter  $S_0$  appearing in the above equation is given by the normalized plastic shear work  $w$  (i.e.  $w = W_S / W_n$ , in which  $W_S$ : plastic shear work, and  $W_n = (1/2) \tau_{mo} \gamma_{mo}$ ) as follows (see Figure 3);

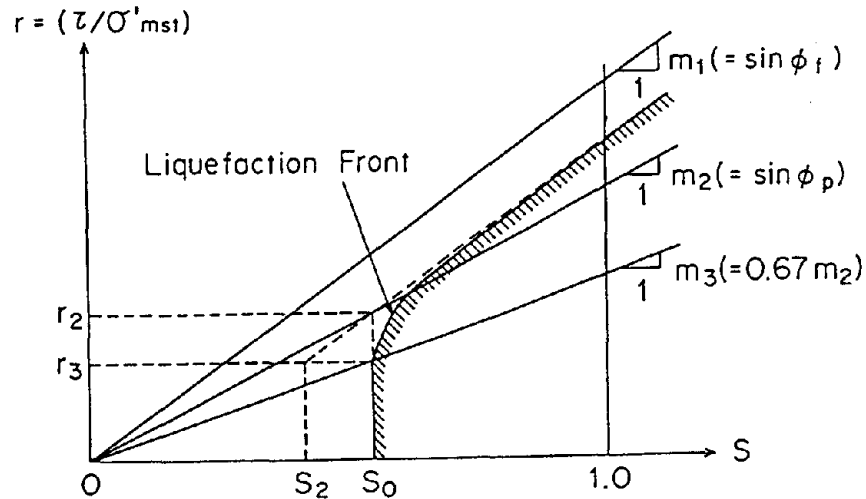


Figure 2 Schematic Figure of Liquefaction Front, State Variable  $S$  and Shear Stress Ratio  $r$

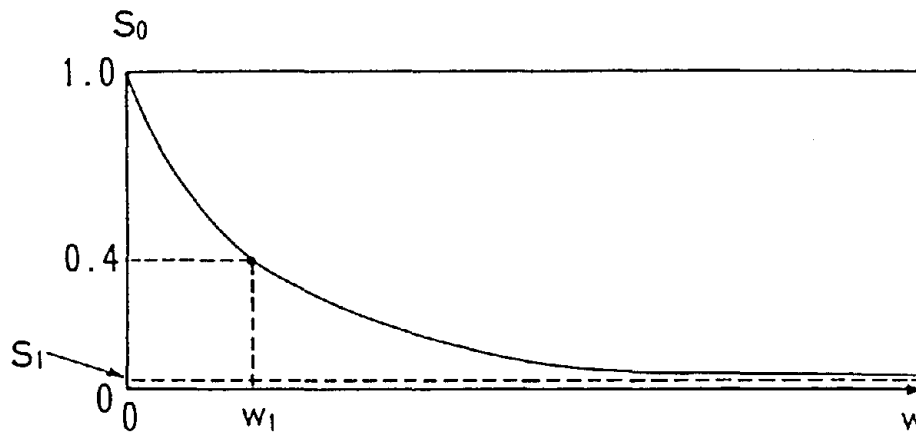


Figure 3 Schematic Figure of Normalized Plastic Shear Work  $w$  and Liquefaction Front Parameter  $S_0$

$$\begin{aligned} S_0 &= 1 - 0.6(w/w_1)P_1 && \text{(if } w < w_1) \\ S_0 &= (0.4 - S_1)(w_1/w)P_2 + S_1 && \text{(if } w > w_1) \end{aligned} \quad (3)$$

The parameters necessary for the above relation are  $S_1$ ,  $w_1$ ,  $p_1$ , and  $p_2$ . These parameters are determined by backfitting to the test results obtained under undrained cyclic loading conditions.

When the effective stress analysis is conducted, the state variable  $S$ , given by Equation (2), is converted into equivalent volumetric strain. Moreover, in accordance with the progress of liquefaction (i.e. variation of the state variable  $S$  and the

liquefaction parameters  $S_0$ ), the constants of the hyperbolic relation, i.e. shear strength  $\tau_m$  and elastic shear modulus  $G_m$ , are given as follows;

$$\text{When } S_0 > 0.4 \quad \tau_m = \tau_{m0} S, \quad G_m = \tau_m / \gamma_{m0} \quad (4)$$

$$\text{When } S_0 < 0.4 \quad \tau_m = \tau_{m0} S + \Delta \tau_m, \quad G_m = \tau_m / \gamma_m \quad (5)$$

in which

$$\begin{aligned} \Delta \tau_m &= \Delta r_m \sigma_{m0}' \\ \Delta r_m &= (m_1 - m_2)(0.4 - S_0) \\ \gamma_m &= \gamma_{m0} / (S_0 / 0.4) \end{aligned}$$

When the initial condition for the dynamic analysis happens to give  $S_0 < 0.4$ , some modifications are applied to the above equation. Moreover, a parameter  $c_1$  is introduced in computing the plastic shear work as a multiplier for the elastic shear work to be subtracted from the total shear work; this makes it possible to simulate the threshold shear stress ratio for generating excess pore water pressure.

Above-mentioned formulation adds the following features to the present model;

- (4) Robustness is incorporated for simulating the cyclic mobility and liquefaction by a scheme for enlarging the shear strain scale with the progress of liquefaction as indicated by Equation (5).
- (5) Liquefaction resistance, i.e. the ratio of cyclic shear stress over initial confining pressure, becomes independent of the initial confining pressure as indicated by the definition of normalized plastic shear work  $w$ .

#### SHEET PILE QUAYWALL AND SOIL CONDITIONS

The sheet pile quaywall to be analyzed by the present effective stress model is with water depth of ten meters as shown in Figure 4. The finite element mesh used for the analysis is also shown in the same figure. The sheet pile is of FSP-VI<sub>L</sub> type and is assumed to have no friction with the soil. The ground water level is assumed to be the same as the sea water level. The ground is assumed to be of uniformly deposited sand of which density is 2.0 t/m<sup>3</sup> and SPT N-value about 8.

The parameters of the sand used for the present analysis are shown in Table 1. By using those parameters, a soil element test (isotropically consolidated at the confining pressure of 73.5 kPa) under undrained cyclic loading conditions is simulated as shown in Figure 5. This result is obtained by applying cyclic stress loading upon one element of the finite

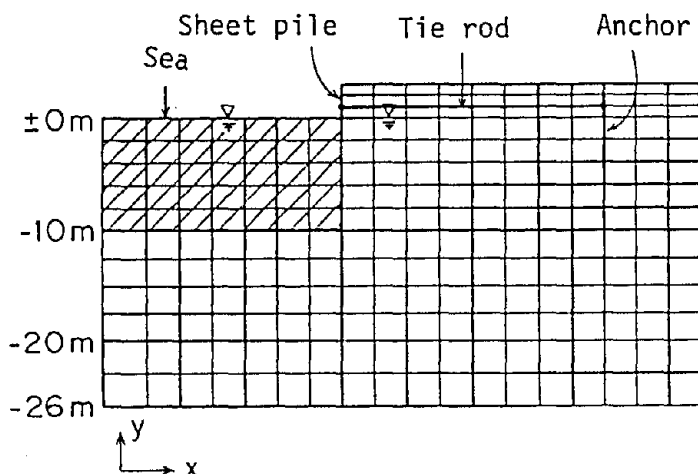


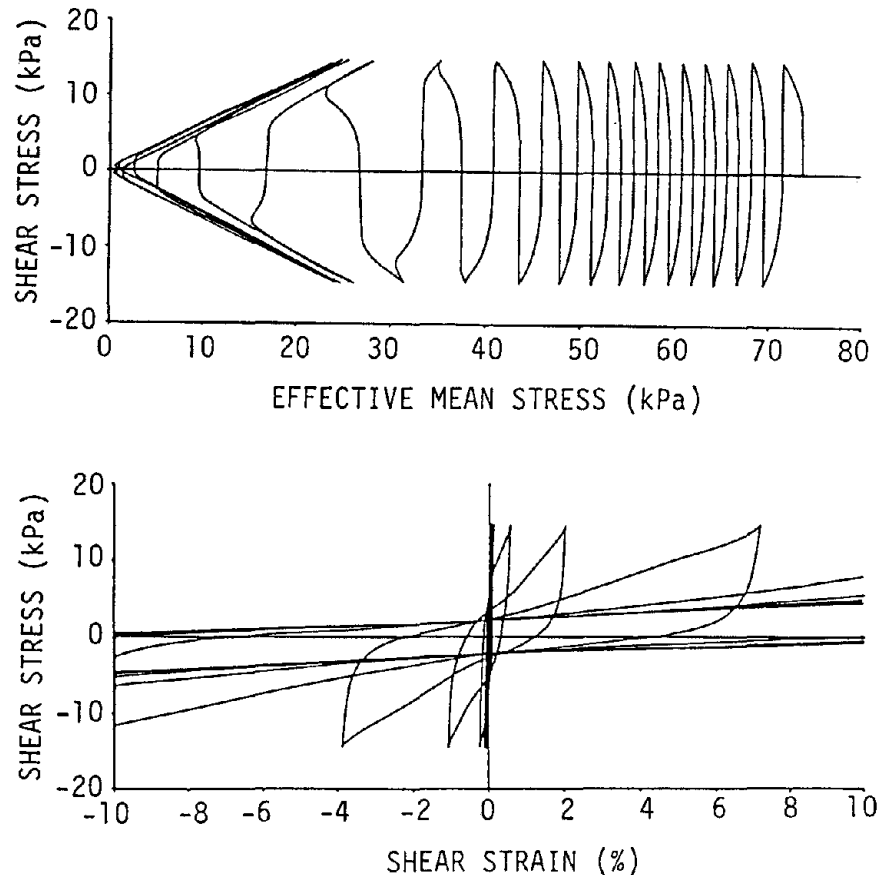
Figure 4 Sheet Pile Quaywall and Element Mesh

Table 1 Parameters of Sand Used for the Simulation

$G_{mref}$	= 65030 kPa
$K_{ref}$ (bulk modulus of soil skeleton)	= 173400 kPa
$\sigma_{mref}'$ (effective confining pressure for $G_{mref}$ and $K_{ref}$ )	= 73.5 kPa
$\phi_f$ (effective friction angle)	= $37^\circ$
$\phi_p$ (phase transformation angle)	= $30^\circ$
$m$ (exponent for pressure dependence of bulk modulus of soil skeleton)	= 0.5
$K_f$ (bulk modulus of water)	= $2 \times 10^6$ kPa
$S_1$	= 0.005
$w_1$	= 7.0
$p_1$	= 0.6
$p_2$	= 1.3
$c_1$	= 1.5

elements. As shown in this figure, typical features of the cyclic mobility and liquefaction are appropriately simulated. The simulation results in the liquefaction when the cyclic shear stress ratio is 0.2 and is applied 14 cycles; i.e. effective mean stress becomes almost equal to zero if the shear stress is zero, and the shear strain peak-to-peak amplitude becomes greater than 5 percent.

The sheet pile is assumed to have, per unit breadth of the beam, the second moment of area of  $8.6 \times 10^{-4} \text{ m}^4$ , cross sectional area of  $0.0306 \text{ m}^2$ , and density of  $7.5 \text{ t/m}^3$ , and is simulated by a linear beam element. The tie rod is simulated by a beam element of which mass is assumed to be zero and is connected with the sheet pile and the anchor sheet pile by



**Figure 5 Numerically Simulated Soil Element Test**

hinges. The sea water is modeled as incompressible fluid and is formulated as an added mass matrix (Zienkiewicz[4]). The side and the bottom boundaries in Figure 4 are simulated by viscous dampers; the free field motions are incorporated at the side boundaries. The constants for the viscous boundaries are shear wave velocities of 150 m/s and 400 m/s at the side and the bottom boundaries, respectively, and P wave velocities of 1500 m/s and density of  $2.0 \text{ t/m}^3$  at both boundaries. By using the model outlined as above, the behavior of the steel sheet pile quaywall, shown in Figure 4, is numerically simulated here under sinusoidal input motion of 200 Gals and 3 Hz for 2.5 seconds. Before the dynamic analysis is conducted, the static analysis with gravity and the effective stress earthquake response analysis of the free fields were conducted.

The dynamic analysis of the quaywall is conducted under undrained condition (Zienkiewicz et al[5]). The numerical integration is done by Wilson- $\theta$  method ( $\theta=1.4$ ) at time step of 0.00833 seconds. Rayleigh damping ( $\alpha=0$  and  $\beta=0.005$ ) which is proportionally decreasing with the degree of liquefaction is used for ensure the stability of the numerical solution process.

### STRESS RELEASE IN SHEET PILE QUAYWALL

The numerical simulation results, after 2.5 seconds of shaking, in deformation of the quaywall as shown in Figure 6; the deformation towards sea is mainly recognized at the soil wedges in front of and behind the sheet pile. The deformation gradually occurs as shaking continues. Time histories of response accelerations, displacements, pore water pressures and bending moment of sheet pile were reported at the first workshop (Iai[6]).

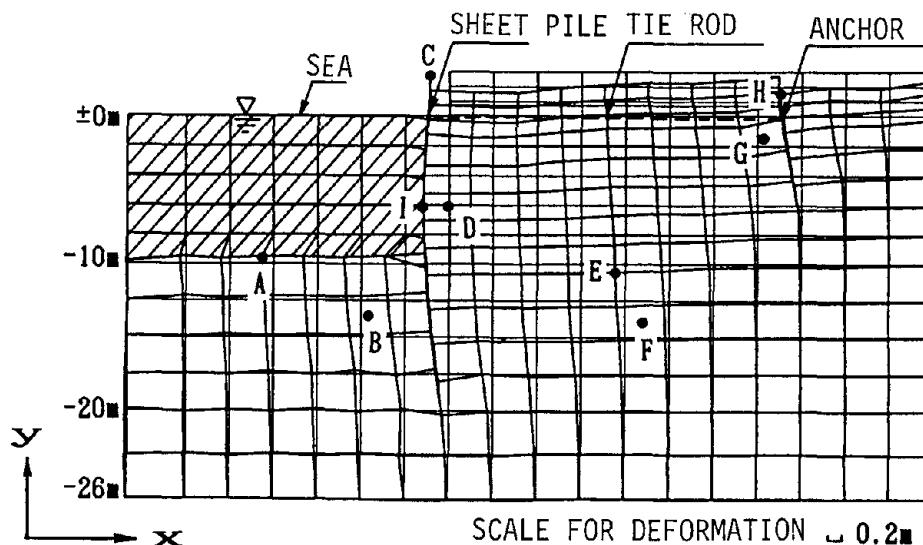


Figure 6 Deformation after Shaking

Response acceleration during shaking ( at time 0.417 seconds), as shown in Figure 7, exhibits rotational motion around the ground surface. This is considered Rayleigh wave generated by soil-structure interaction.

The mechanism of deformation in the sheet pile quaywall is understood by asking how the initial stress is released to produce strain. Four soil elements are selected as representatives for this purpose; soil elements in front of and behind the sheet pile (i.e. elements B and D in Figure 6), a soil element between the sheet pile and the anchor (i.e. element F in Figure 6) and a soil element in front of the anchor (i.e. element G in Figure 6).

In presenting the stress and the strain, the x-y coordinate are taken as shown in Figure 6 and stress components are defined as shown in Figure 8. Definitions for strain components are similarly given. In addition to the effective stress path ( i.e. relation between effective mean stress :  $(\sigma_x' + \sigma_y')/2$  and deviatoric stress :  $\tau = \sqrt{\tau_{xy}^2 + [(\sigma_x' - \sigma_y')/2]^2}$  ), relations

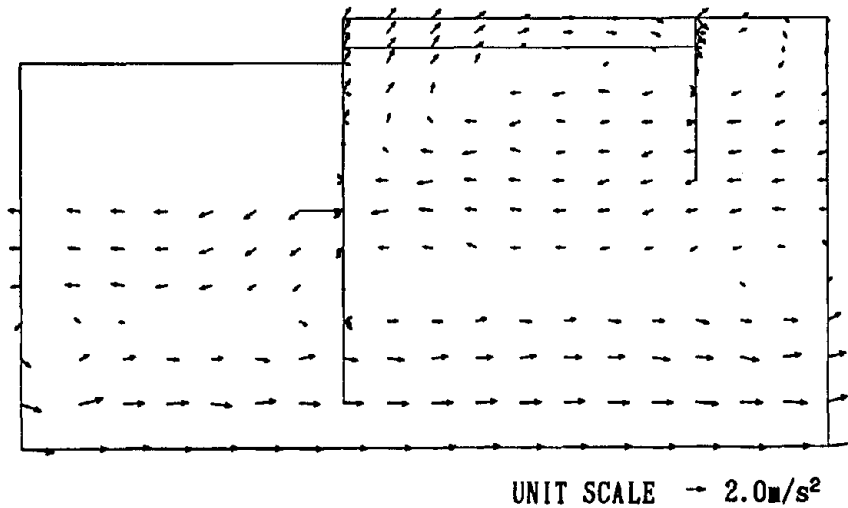


Figure 7 Absolute Acceleration ( at time 0.417 seconds)

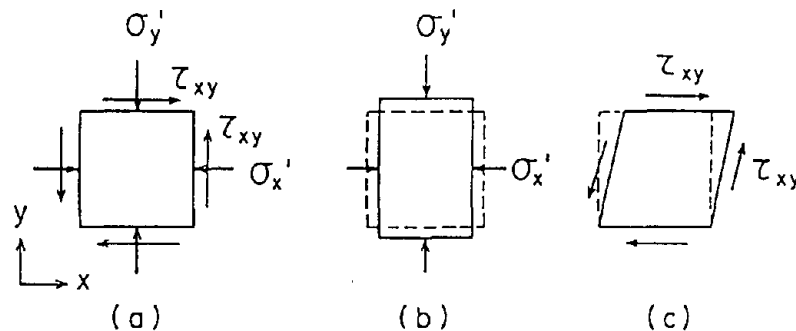


Figure 8 Schematic Figure of Stress Components

between normal stress difference ( $\sigma'_x - \sigma'_y$ ) and shear stress ( $\tau_{xy}$ ) and between normal strain difference ( $\epsilon_x - \epsilon_y$ ) and shear strain ( $\gamma_{xy}$ ) are plotted in order to understand directions in principal axes of stress and strain.

In front of the sheet pile at the soil element B in Figure 6, deviatoric stress  $\tau$  increases just after start of shaking, as shown in the first row in Figure 9, and the effective mean stress increases due to dilatancy of sand but later the effective mean stress gradually decreases with decreasing shear stress. As indicated by positive normal stress difference in the second row in Figure 9, the soil initially undergoes passive earth pressure. The soil is also horizontally sheared as indicated by negative shear stress ( $\tau_{xy}$ ) before shaking due to the deformation of the sheet pile. In contrast to the expectation that the shaking causes cyclic axial loading in the horizontal direction, the shaking causes cyclic fluctuation in

the rotational components. The stress path produces shear strain, as shown in the bottom row in Figure 9, in the principal axes direction similar to that of the initial stress.

Behind the sheet pile quaywall at the soil element D in Figure 6, the effective mean stress fluctuates with the shear stress but in general the effective mean stress tends to decrease as shown in the first row in Figure 10. As indicated by negative normal stress difference in the second row in Figure 10, the soil initially undergoes active earth pressure. The shaking causes cyclic axial loading in the horizontal direction. The main cause for the liquefaction at this soil element is the shear work generated by the normal stress difference and the normal strain difference rather than the shear work generated by the shear stress  $\tau_{xy}$  and the shear strain  $\gamma_{xy}$ , which is small due to the confining effect of the sheet pile as shown in the second row and the bottom row in Figure 10. The increase in the axial strain difference looks like what is caused by the mechanism of "crawling". Direction of principal strain axes is, again, similar to that of initial stress as shown in the bottom row in Figure 10.

In the middle part of the ground between the sheet pile and the anchor at the soil element F in Figure 6, initially  $K_0$  consolidated soil gradually loses mean effective stress as shown in Figure 11. In contrast to the case of horizontally layered ground, initial deviatoric stress is almost kept constant throughout the process of liquefaction. Though cyclic shear stress in the horizontal direction is predominant as in the horizontally layered ground as shown in the second row in Figure 11, the strain generated by the cyclic shear stress is predominant in axial stress difference as shown in the bottom row in Figure 11. This is similar to the behavior of soil in the embankment, in which settlement is associated with bulging in horizontal direction. Direction of principal strain axes is, again, similar to that of initial stress.

Finally, in front of the anchor at the soil element G in Figure 6, the effective mean stress again gradually decreases as shown in the first row in Figure 12. As shown in the second row in Figure 12, initial stress is predominant in horizontal simple shear mode due to deformation of the anchor; axial stress difference is close to zero supposedly due to cancellation of  $K_0$  consolidation effect by passive earth pressure. The shaking remarkably causes rotation in the principal stress axes. This is considered due to the Rayleigh wave generated by the soil-structure interaction as shown in Figure 7. The center of the rotation gradually shifts from the simple shear mode to passive failure mode. This affects the strain, mainly producing axial strain difference as shown in the bottom row in Figure 12.



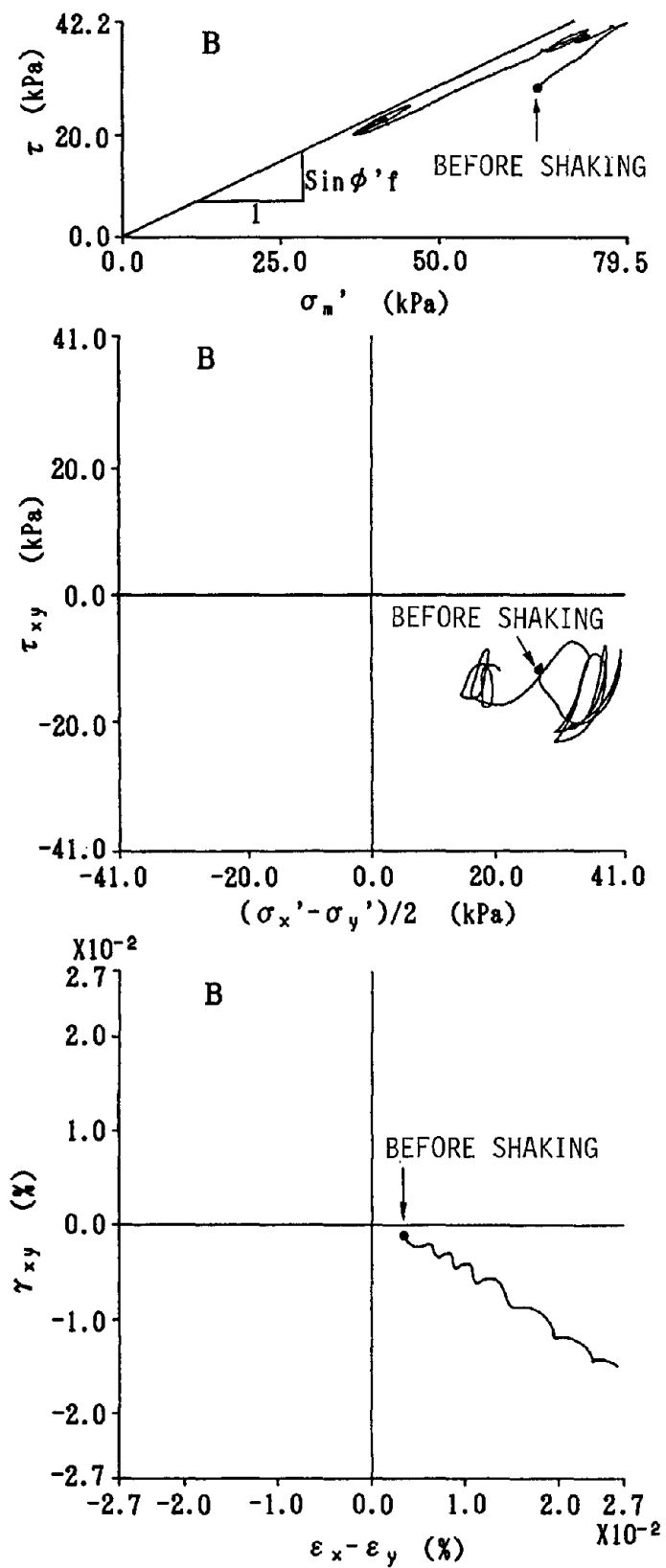


Figure 9 Stress and Strain in Front of Sheet Pile

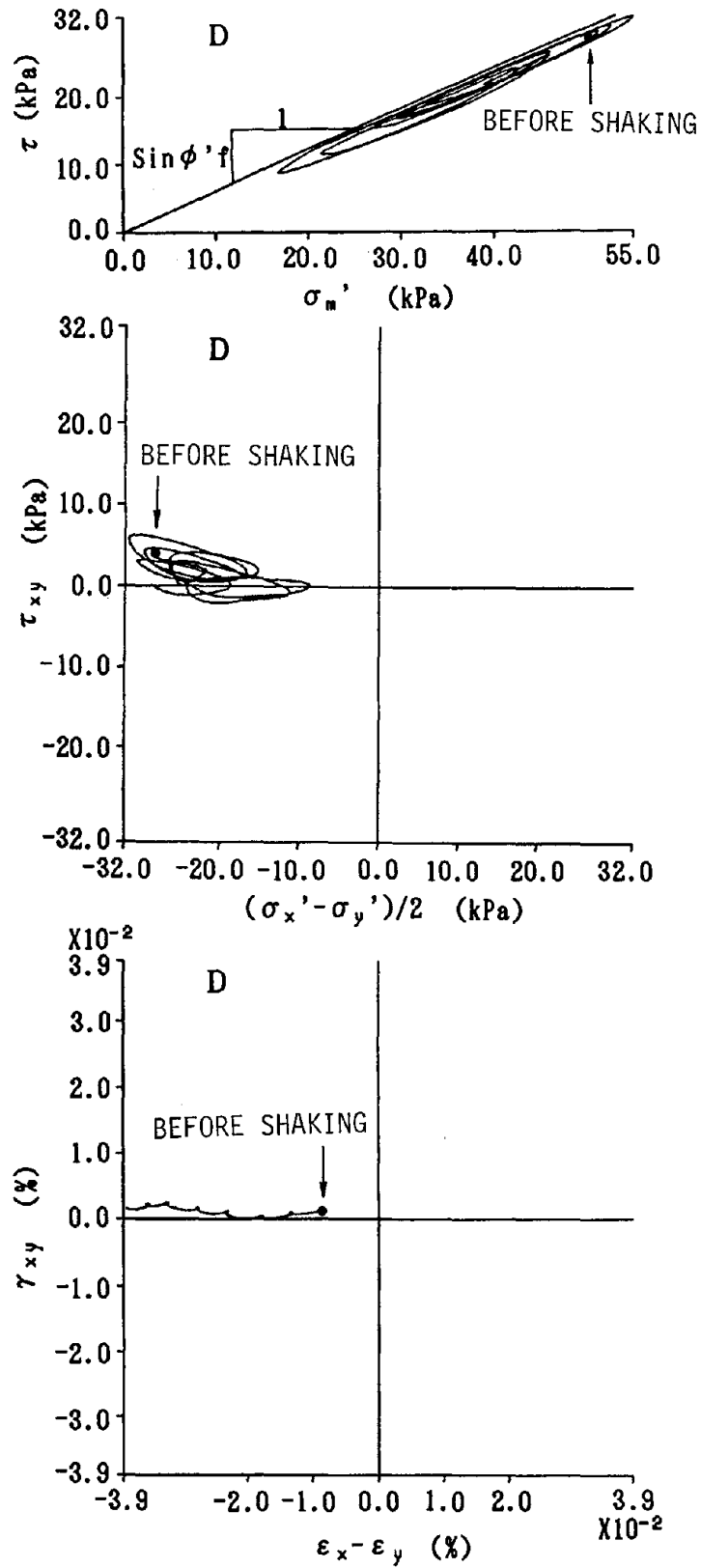


Figure 10 Stress and Strain Behind the Sheet Pile

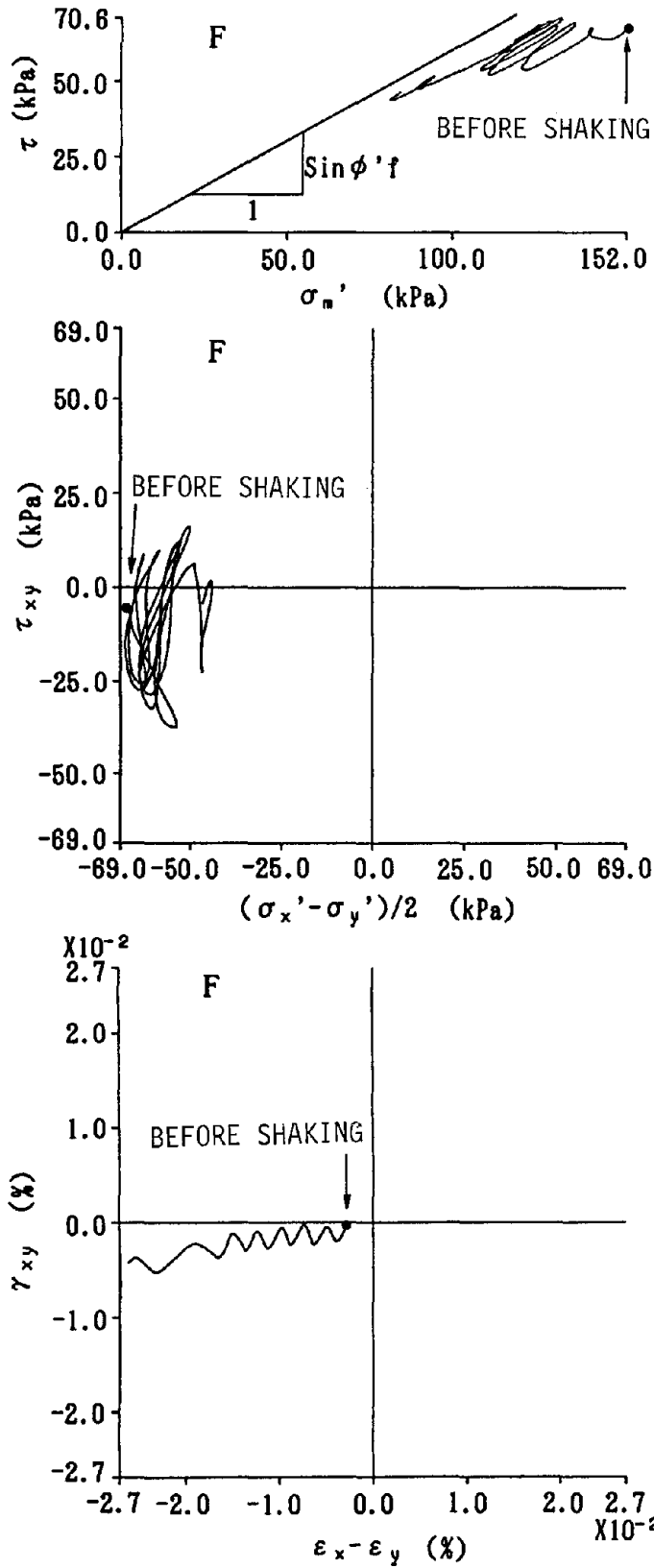


Figure 11 Stress and Strain in the Middle of the Ground

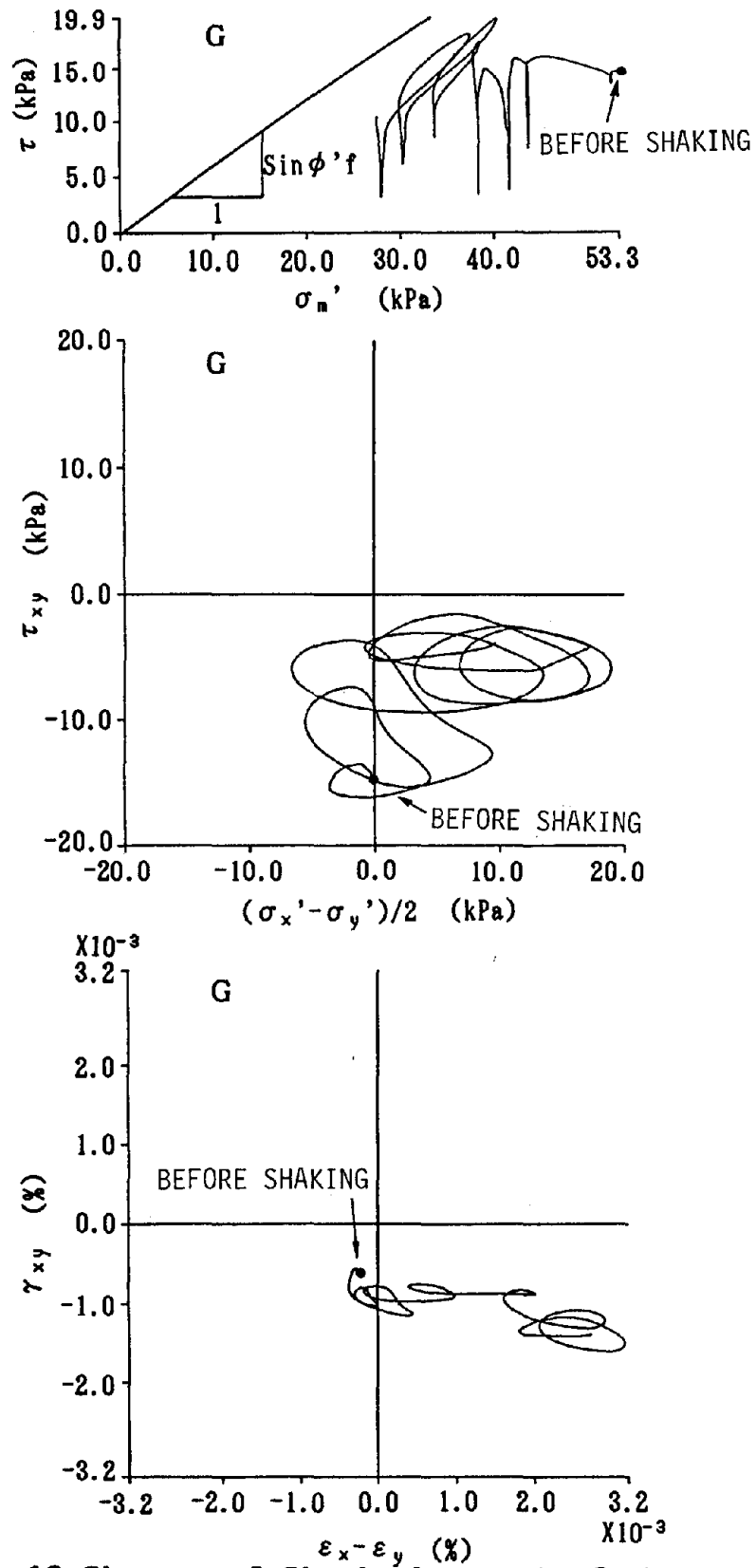


Figure 12 Stress and Strain in Front of the Anchor

## CONCLUSIONS

Effective stress analysis of an anchored sheet pile quaywall suggests that following four types of stress releases are main causes for residual deformation of the quaywall due to shaking and liquefaction.

- (1) Soil in front of sheet pile, which was initially in nearly passive failure state, shows stress release with cyclic rotation of principal stress axes.
- (2) Soil behind the sheet pile, which was initially in nearly active failure state, shows stress release with cyclic normal stress difference.
- (3) Soil between the sheet pile and an anchor, which was initially in  $K_0$  consolidated state, shows cyclic simple shear in horizontal direction with free displacement conditions at the side boundaries.
- (4) Soil in front of the anchor, which was initially sheared in horizontal direction, clearly shows rotation of principal stress axes due to Rayleigh wave generated by the soil-structure interaction.

In accordance with these stress paths,

- (5) strains are gradually produced mainly in the principal axes direction similar to that of initial stress.

## REFERENCES

- 1) Iai, S. (1988) : "A Numerically Robust Model for the Two Dimensional Effective Stress Analysis of Liquefaction," Annual Research Conference of Japanese Society of Civil Engineers, III, pp.418-419 (in Japanese)
- 2) Towhata, I. and Ishihara, K. (1985) : "Modelling Soil Behaviour under Principal Stress Axes Rotation," Proc. 5th International Conference on Numerical Methods in Geomechanics, Nagoya, pp.523-530
- 3) Ishihara, K., Yoshida, N. and Tsujino, S. (1985) : "Modelling of Stress-Strain Relations of Soils in Cyclic Loading," Proc. 5th International Conference on Numerical Methods in Geomechanics, Nagoya, pp.373-380
- 4) Zienkiewicz, O.C. (1977) : "The Finite Element Method," 3rd edition, Chapter 21, McGraw-Hill Book Co.
- 5) Zienkiewicz, O.C. and Bettess, P. (1982) : "Soils and Other Saturated Media under Transient, Dynamic Conditions; General Formulation and the Validity of Various Simplifying Assumptions," Soil Mechanics-Transient and Cyclic Loads, (Pande and Zienkiewicz ed.) John Wiley and Sons, pp.1-16
- 6) Iai, S. (1988) : "Damage to Port and Harbor Facilities by Liquefaction," Proceedings of the First Workshop on Liquefaction, Large Ground Deformation and Their Effects on Lifeline Facilities, Tokyo, pp.185-192

**AN ANALYSIS OF EARTHQUAKE DATA OBSERVED AT THE  
WILDLIFE LIQUEFACTION ARRAY SITE, IMPERIAL COUNTY, CALIFORNIA**

Catherine M. Keane<sup>(1)</sup> and Jean H. Prevost<sup>(2)</sup>

Department of Civil Engineering and Operations Research  
Princeton University  
Princeton, New Jersey 08544

**ABSTRACT**

The Superstition Hills earthquake of November 24, 1987 recorded by the Wildlife Liquefaction Array provides a unique data set to study ground accelerations above and below a liquefiable soil layer. Two analyses of these earthquake records, which include surface and subsurface (depth = 7.5 m) accelerations in the North-South, East-West and vertical directions, and pore-water pressure histories at various depths throughout the semi-infinite cohesionless soil deposit, are presented. Computed and recorded surface accelerations and pore-water pressure histories are compared and discussed in detail.

<sup>(1)</sup> Graduate Student

<sup>(2)</sup> Professor of Civil Engineering and Operations Research

## INTRODUCTION

A special instrumentation array, hereafter referred to as the Wildlife Liquefaction Array, was installed in 1982 on the west side of the Alamo River in Imperial County, California (see Fig. 1), following the Westmorland, California earthquake (MS=6.0) of April 1981 to monitor earthquake-induced pore-water pressures in a cohesionless soil deposit (Youd and Wieczorik, 1984). The array consists of surface and downhole (depth = 7.5 m) accelerometers and six pore-water pressure transducers. Arrangement of the instruments at the site is shown in Fig. 2. Several such arrays exist worldwide (Ishihara, *et al.*, 1982; Harp, *et al.*, 1984), but only the Wildlife Liquefaction Array has been triggered by an earthquake where pore-water pressure build-ups were large enough to reduce the vertical effective stress to essentially zero. Recordings of significant excess pore-water pressure build-up were made during the Superstition Hills (MS=6.6) earthquake of November 24, 1987. The availability of these earthquake records, including surface and downhole accelerations in the North-South, East-West (referred to hereafter as N-S and E-W) and vertical directions, and pore-water pressure histories recorded at various depths throughout the soil deposit (Brady, *et al.*, 1989), provide a unique data set to study ground accelerations above and below a liquefiable layer of silty sand.

## EARTHQUAKE CHARACTERISTICS

The earthquake in Imperial County, CA, of November 24, 1987 triggered the Wildlife Liquefaction Array four times, but only two of these events had accelerations greater than 0.05g (Holzer, *et al.*, 1988). Details of these two events are contained in Table 1. The locations of the two epicenters are shown in Fig. 1. The first event (Elmore Ranch) was the MS=6.2 shock at 01:54 Gmt on November 24, 1987. Recordings for this event continued for 68 sec after the instrumentation array was triggered. No pore-water pressure increases were recorded during this shock. The second event (Superstition Hills) was the MS=6.6 shock at 13:15 Gmt on November 24, 1987. The peak value of acceleration recorded by the surface accelerometer for this event (Brady, *et al.*, 1989) exceeded 20% g as shown in Table 1. Pore-water pressure increases accompanied by reduction of the vertical effective stress were recorded for this event by five of the six installed piezometers. One piezometer, p4 (depth = 4 m), failed to operate correctly. Pore-water pressure increased for 97 sec after recordings began, although most increases occurred during the first 40 sec of the event.

## SITE CHARACTERISTICS

To the depth of 7.5 m where the downhole accelerometer is located, the Wildlife Liquefaction Array site is broken down into five geological soil strata. A geotechnical investigation of the site is contained in Bennett, *et al.*, (1984), and a cross-section of the array site is shown in Fig. 3 which includes shear-wave velocity values (from Bierschwale (1984)). Table 2 contains material parameters for each layer. Note that permeability data for the soil strata at the Wildlife Site are presently unavailable and have therefore been estimated using charts found in Terzaghi and Peck (1967). The five different soil layers are identified as follows:

- Layer 1 at depths 0.0 m to 1.2 m : very loose silt
- Layer 2 at depths 1.2 m to 2.5 m : very loose silt
- Layer 3 at depths 2.5 m to 3.5 m : very loose to loose sandy silt
- Layer 4 at depths 3.5 m to 6.8 m : loose to medium dense silty sand
- Layer 5 at depths 6.8 m to 7.5 m : medium to stiff clayey silt

Note that the water table is at a depth of 1.2 m. The top-most layer (layer 1), extending from the ground surface down to the water table at depth 1.2 m, consists of a very loose silty deposit

with an average in-situ shear-wave velocity of 99 m/sec and a dry density of 1600 kg/m<sup>3</sup>. Layer 2 extends from the water table at a depth of 1.2 m down to 2.5 m is similar to layer 1 with an average in-situ shear-wave velocity of 99 m/sec and a saturated density of 1940 kg/m<sup>3</sup>. The permeability of this layer is taken as  $1 \times 10^{-5}$  m/sec. Layer 3 extends from 2.5 m to 3.5 m and has an average in-situ shear-wave velocity of 116 m/sec and a saturated density of 1970 kg/m<sup>3</sup>. The average void ratio for this layer is given as 0.74, and the permeability is taken as  $1 \times 10^{-5}$  m/sec. Extending from 3.5 m to 6.8 m, layer 4 has an average in-situ shear-wave velocity of 116 m/sec. The saturated density and permeability of this layer are 1970 kg/m<sup>3</sup> and  $1 \times 10^{-4}$  m/sec, respectively. The average void ratio for this layer is also given as 0.74. Both layers 3 and 4 had experienced liquefaction by the end of the second event (MS=6.6) (Holzer, *et al.*, 1988). The bottom-most layer (layer 5) extends from 6.8 m to 7.5 m and has an average in-situ shear-wave velocity of 130 m/sec and a saturated density of 2000 kg/m<sup>3</sup>. Permeability of the layer is taken as  $1 \times 10^{-6}$  m/sec. Underlying the site is a very stiff silty clay. The stiffness of this base is believed to well simulate bed rock conditions.

## ANALYSIS

The finite element mesh used to represent the semi-infinite soil deposit consists of 29 one-dimensional elements (30 nodes). Nodal spacing varies for each geologic layer with the largest spacing of 0.3 m used for layer 5 (the bottom-most layer) and the smallest spacing of 0.175 m used for layer 1 (the top-most layer). Layers below the water table are assumed fully saturated, whereas layers above the water table are assumed dry.

Two approaches are used to study the response of the soil column to base excitation. In the first analysis, 3 dimensional kinematics are used, and six degrees of freedom are assigned to each node at or below the water table; three for the solid phase and three for the fluid phase (for the N-S motion, vertical motion, and E-W motion, respectively). Nodes above the water table are assigned three degrees of freedom for the solid phase only. Using this approach, all downhole acceleration components, N-S, vertical, and E-W, are input at the same time, each acceleration component assigned to a different degree of freedom and the response obtained in one set of computations.

In the second analysis, 2 dimensional kinematics are used, and each node at or below the water table is assigned four degrees of freedom; two for the solid phase and two for the fluid phase (for horizontal motion and vertical motion). Nodes above the water table are assigned two degrees of freedom for the solid phase only. Downhole accelerations in each horizontal direction, N-S and E-W, are input individually along with the vertical component of downhole acceleration, and two separate computations are performed, referred to as 2D Analysis A and 2D Analysis B hereafter.

For each set of computations, acceleration at the top of the soil column (node 30) and vertical effective stress variation with depth are obtained throughout the loading, as well as pore-water pressure time histories at specific depths.

An effective-stress elastic-plastic model developed by Prevost (1985) is used to model the nonlinear and hysteretic stress-strain behavior of the cohesionless soil deposit. To this end, the model makes use of multiple conical yield surfaces.

Implementation of the earthquake loading (Prevost, 1988) proceeded using a time step of 0.02 sec and modified Newton-Raphson iterations were performed to insure proper convergence at each time step.

Attention is focused on the Superstition Hills event (MS=6.6) hereafter since a study of liquefaction is of interest. Only the first 40 sec of the recorded N-S, vertical, and E-W, Figs. 5a, 5b, and 5c, downhole acceleration components are selected as input for the analysis since most of the pore-water pressure increases had occurred within that time duration. Note that the input downhole motion in the N-S direction is stronger than in the E-W direction.



### 3D Kinematical Analysis

Input motions for this computation are shown in Figs. 5a, 5b, and 5c. The computed surface acceleration components in the N-S, vertical, and E-W directions are shown in Figs. 6a, 6b, and 6c, respectively. For the acceleration records, only the strong motion portion (initial 20 sec) is of primary importance since by then, at least partial liquefaction had occurred, resulting in somewhat chaotic later responses at the surface (see Fig. 4). For the strong shaking duration, the computed surface accelerations in the N-S, Fig. 6a, and E-W, Fig. 6c, directions show good agreement with their recorded counterparts shown in Figs. 4a and 4c in terms of magnitude, frequency, and duration of strong shaking. Although the magnitude of the computed vertical surface acceleration component (Fig. 6b) is low compared to the recorded component (Fig. 4b), there is good agreement in the high frequency components.

Computed and recorded pore-water pressure time histories at the locations of the three pore-water pressure transducers (3 m, 5 m, and 6.6 m) are shown in Figs. 7a, 7b, and 7c, respectively. Good agreement is found between computed and recorded pore-water pressure time histories. For example, all plots display the same starting time of pore-water pressure increase, similar rate of pore-water pressure increase once it has begun, similar times at which the rates of pore-water pressure increase begin to slow down, and good agreement in the final value of excess pore-water pressures.

### 2D Kinematical Analysis

For 2D Analysis A, recorded surface ground motion for the N-S component of ground shaking (Fig. 5a) is shown in Fig. 4a; whereas recorded surface ground motion for the vertical component of ground shaking (Fig. 5b) is shown in Fig. 4b. The magnitude, with the exception of one peak, frequency, and duration of strong shaking of the computed N-S acceleration (Fig. 8a) is in good agreement with that of the recorded surface acceleration (Fig. 4a) for the initial 20 sec. The computed vertical surface acceleration (Fig. 8b) agrees well with the recorded surface acceleration (Fig. 4b) in terms of frequency components, but not as well in terms of magnitude.

Input for 2D Analysis B consists of vertical and E-W downhole acceleration components (Figs. 5b and 5c, respectively). Recorded vertical and E-W surface acceleration components are shown in Figs. 4b and 4c, respectively. The magnitude of the computed E-W surface acceleration, Fig. 9a, agrees well with Fig. 4c, although the computed acceleration has more low frequency components below 20 sec. Again, there is good agreement in frequency between the computed (Fig. 9b) and recorded (Fig. 4c) vertical components, but not in terms of magnitude.

Computed and recorded plots of the pore-water pressure time histories at depths of 3 m, 5 m, and 6.6 m as a result 2D Analysis A and 2D Analysis B are shown in Figs. 10a, 10b, and 10c, respectively. It seems that the pore-water pressure increases are largely the result of the N-S acceleration component, which is not unexpected since it is a stronger signal than the E-W motion. The recorded and computed pore-water pressure time histories have the same similarities as in the 3D Analysis: agreement in the starting time of pore-water pressure increase, the same rate of pore-water pressure increase once it has begun, and agreement in the time at which the rates of pore-water pressure begin to slow down.

### Discussion

Better agreement between computed and recorded motions from the 3D Analysis is an expected result since the computed surface acceleration in one direction is the result of all components of

downhole acceleration, and not just the result of the downhole acceleration in the same direction. However, it is also clear that in this case the 3D Analysis only provides marginally better improvements than the 2D Analysis. This point is further emphasized by the vertical effective stress variations with depth as a result of the 3D Analysis, 2D Analysis A, and 2D Analysis B (Figs. 11a, 11b, and 11c, respectively). The stress variation with depth is displayed every 2 sec; the solid line on each plot represents the initial stress condition. Soil strata and location of recording devices are also shown. Note that only three pore-water pressure transducers are located within the soil deposit of interest. It is of interest to note the strong likeness between the results of the 3D Analysis (Fig. 11a) and 2D Analysis A (Fig. 11b). Clearly, the N-S component dominates the response.

## CONCLUSIONS

The earthquake records obtained at the Wildlife Liquefaction Array site, Imperial County, California provide a unique data set to study a liquefiable cohesionless soil deposit. The records for the Superstition Hills earthquake (MS=6.6) of November 24, 1987 have been used to compute the response of the soil deposit using a nonlinear one-dimensional finite-element analysis of the semi-infinite soil deposit. Comparisons of computed versus recorded surface accelerations and pore-water pressure variations have been discussed in detail. Also, the results of the 3-dimensional kinematical analysis and the 2-dimensional kinematical analysis are compared and discussed.

## ACKNOWLEDGEMENTS

This research was supported in part by the National Science Foundation under Grant ECE 85-12311 and sub-contract NCEER # under the auspices of the National Center for Earthquake Engineering Research, and by Kajima Corporation (Japan) as part of a collaborative research program in Earthquake Engineering with Princeton University. These supports are gratefully acknowledged.

## REFERENCES

1. Bennett, M. J., McLaughlin, P. V., Sarmiento, J. S., and Youd, T. L., 1984, "Geotechnical investigation of liquefaction sites, Imperial Valley, California," *U. S. Geological Survey Open-File Report 84-252*, 103 p.
2. Bierschwale, J. G., 1984, "Analytical evaluation of liquefaction potential of sands subjected to the 1981 Westmorland earthquake," *University of Texas Geotechnical Engineering Report GR-84-15*, 231 p.
3. Brady, A. G., Mork, P. N., Seekins, L. C., and Switzer, J. C., 1989, "Processed strong-motion records from the Imperial Wildlife Liquefaction Array, Imperial County, California, recorded during the Superstition Hills Earthquakes, November 24, 1987," *U. S. Geological Survey Open-File Report 89-87*, 115 p.
4. Harp, E. L., Sarmiento, J., and Cranswick, E., 1984, "Seismic induced pore-water pressure records from the Mammoth Lakes, California, earthquake sequence of 25 to 27 May 1980," *Seismological Society of America Bulletin*, Vol. 74, No. 4, pp. 1381-1393.
5. Holzer, T. L., Youd, T. L., and Bennett, M. J., 1988, "In situ measurement of pore pressure build-up during liquefaction," Presented at 20th Joint Meeting of United States-Japan Panel on Wind and Seismic Effects, Gaithersburg, MD.
6. Ishihara, K., Shimizu, K., and Yamada, Y., 1981, "Pore water pressure measured in sand deposits during an earthquake," *Soils and Foundations*, Vol. 21, No. 4, pp. 85-100.

7. Prevost, J. H., 1985, "A simple plasticity theory for cohesionless frictional soils," *Int. J. Soil Dyn. Earth. Eng.*, Vol. 4, No. 1, pp. 9-17.
8. Prevost, J. H., 1988, "DYNA1D: a computer program for nonlinear seismic site response analysis," Report No. NCEER-88-xxx, Dept. of Civil Engineering and Operations Research, Princeton University.
9. Terzaghi, K., and Peck, R. B., 1967, *Soil Mechanics in Engineering Practice* (2nd ed., John Wiley and Sons, New York).
10. Youd, T. L., and Wieczorek, G. F., 1984, "Liquefaction during the 1981 and previous earthquakes near Westmorland, California," *U. S. Geological Survey Open-File Report 84-680*, 36 p.

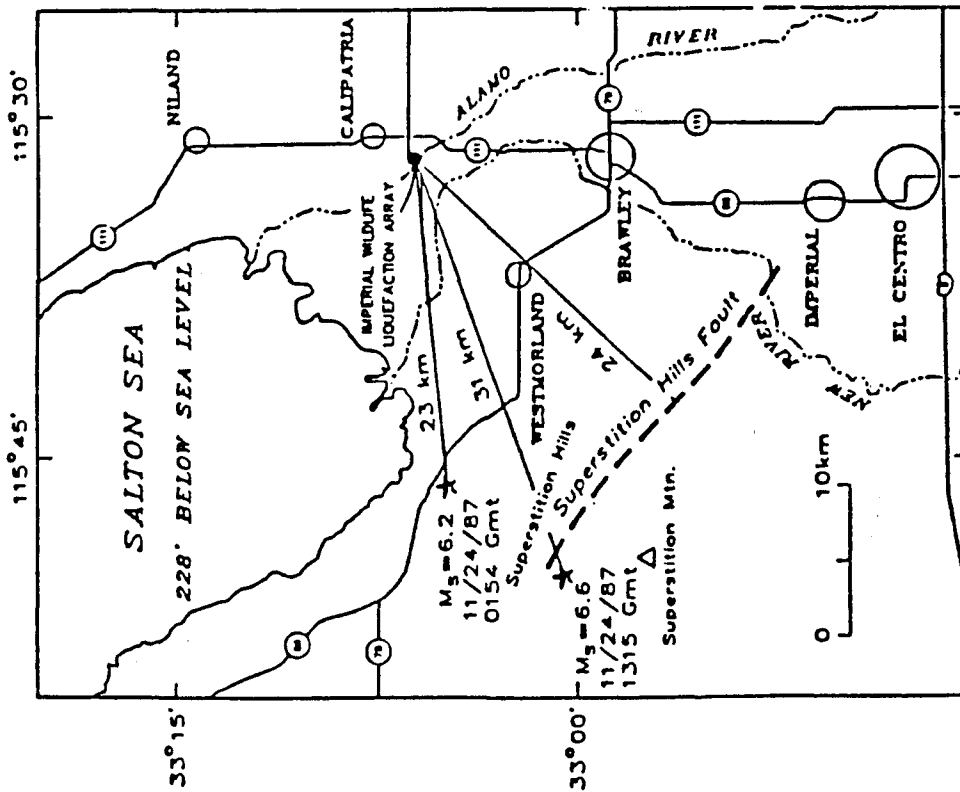


Table 1 : Details of Events 1 and 2 on Nov. 24, 1987 at Wildlife Site

Event	1	2
MS	6.2	6.6
M <sub>L</sub>	5.8	6.1
Epicenter	33.080 North lat.	33.010 North lat.
Coordinates	115.775 West long.	115.840 West long.
Epicentral Distance	23 km	31 km
Peak horizontal surface acceleration	0.13 g	0.21 g
Pore pressure increases	did not occur	occurred

Figure 1 : Location of Wildlife Site and Epicenters for Event 1 (MS = 6.2) and Event 2 (MS=6.6)

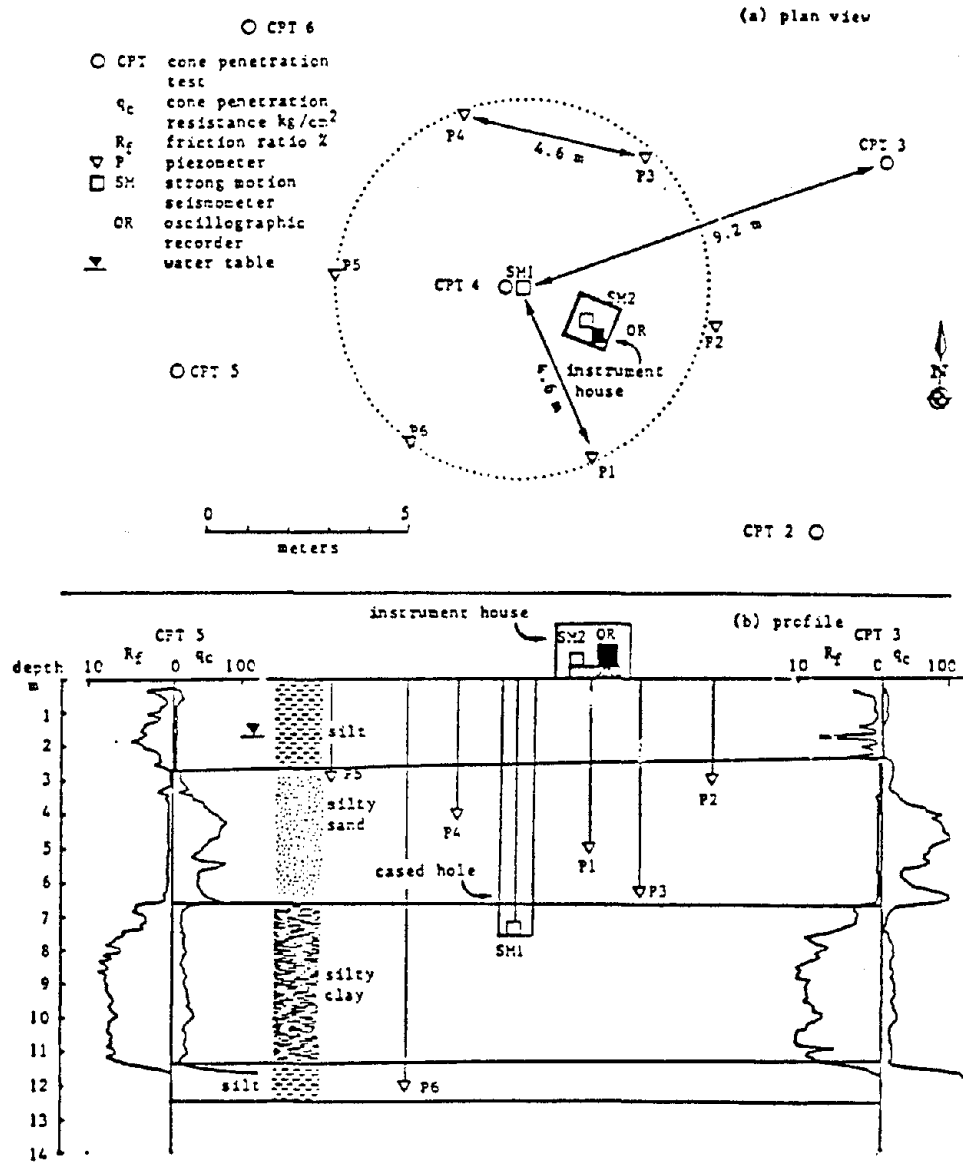


Figure 2 : Arrangement of Instrumentation at Wildlife Site

Table 2 : Material Parameters for Layered Soil Deposit at Wildlife Site

Layer	1	2	3	4	5
Depth (m)	0.0 to 1.2	1.2 to 2.5	2.5 to 3.5	3.5 to 6.8	6.8 to 7.5
Shear Wave Velocity <sup>(1)</sup> (m/s)	99.0	99.0	116.0	116.0	130.0
Total Density <sup>(2)</sup> (kg/m <sup>3</sup> )	1600.0	1940.0	1970.0	1970.0	2000.0
Shear Modulus (solid) (N/m <sup>2</sup> )	1.57x10 <sup>7</sup>	1.47x10 <sup>7</sup>	2.08x10 <sup>7</sup>	2.08x10 <sup>7</sup>	2.70x10 <sup>7</sup>
Poisson's Ratio	0.25	0.25	0.30	0.30	0.30
Bulk Modulus (solid) (N/m <sup>2</sup> )	2.61x10 <sup>7</sup>	2.44x10 <sup>7</sup>	4.50x10 <sup>7</sup>	4.50x10 <sup>7</sup>	5.83x10 <sup>7</sup>
Void Ratio <sup>(3)</sup>	0.6799	0.7955	0.7400	0.7400	0.6878
Porosity	0.4047	0.4431	0.4253	0.4253	0.4075
Reference Mean Normal Stress (N/m <sup>2</sup> )	1.15x10 <sup>4</sup>	2.95x10 <sup>4</sup>	4.10x10 <sup>4</sup>	6.10x10 <sup>4</sup>	8.00x10 <sup>4</sup>
Friction Angle <sup>(3)</sup>	21.3°	20.0°	22.0°	22.0°	35.0°
Dilation Angle	21.3°	20.0°	19.0°	18.0°	5.0°
Coefficient of Permeability (m/sec)	—	1.0x10 <sup>-5</sup>	1.0x10 <sup>-5</sup>	1.0x10 <sup>-4</sup>	1.0x10 <sup>-6</sup>

(1) From Bleschwaile (1984).

(2) From Holzer, et al., (1988).

(3) From Bennett, et al., (1984).

Other parameter values assumed or computed for analysis purposes.

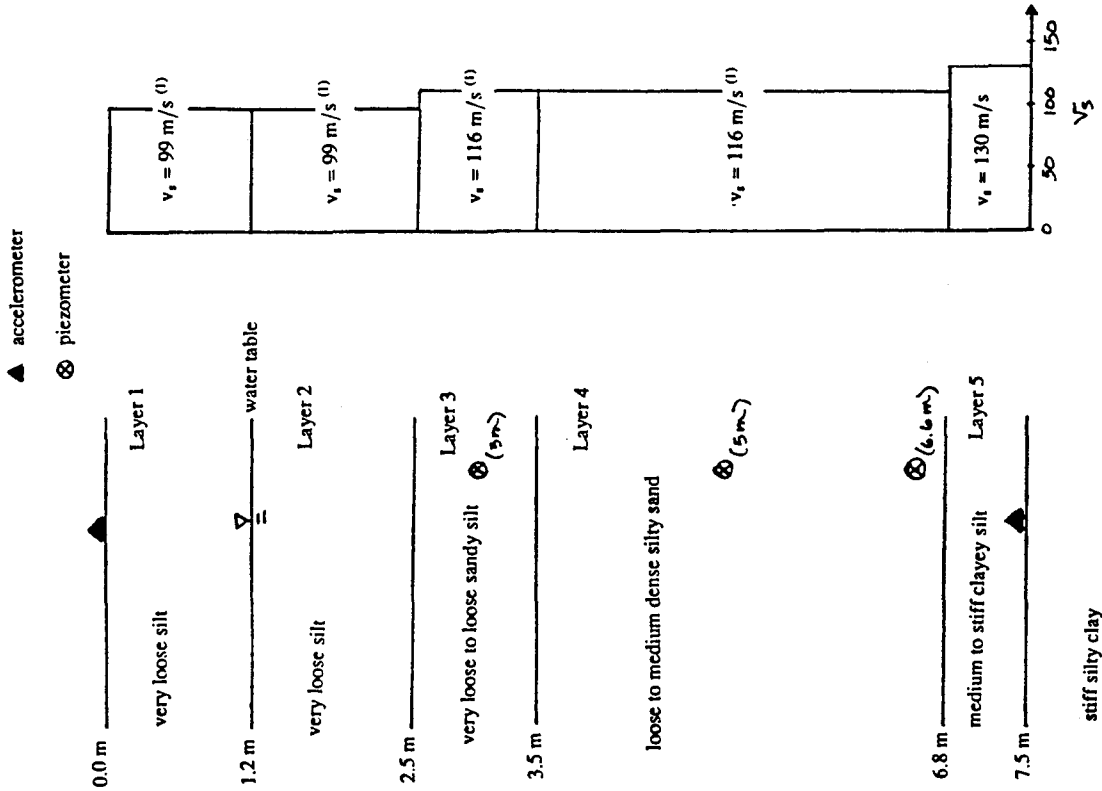
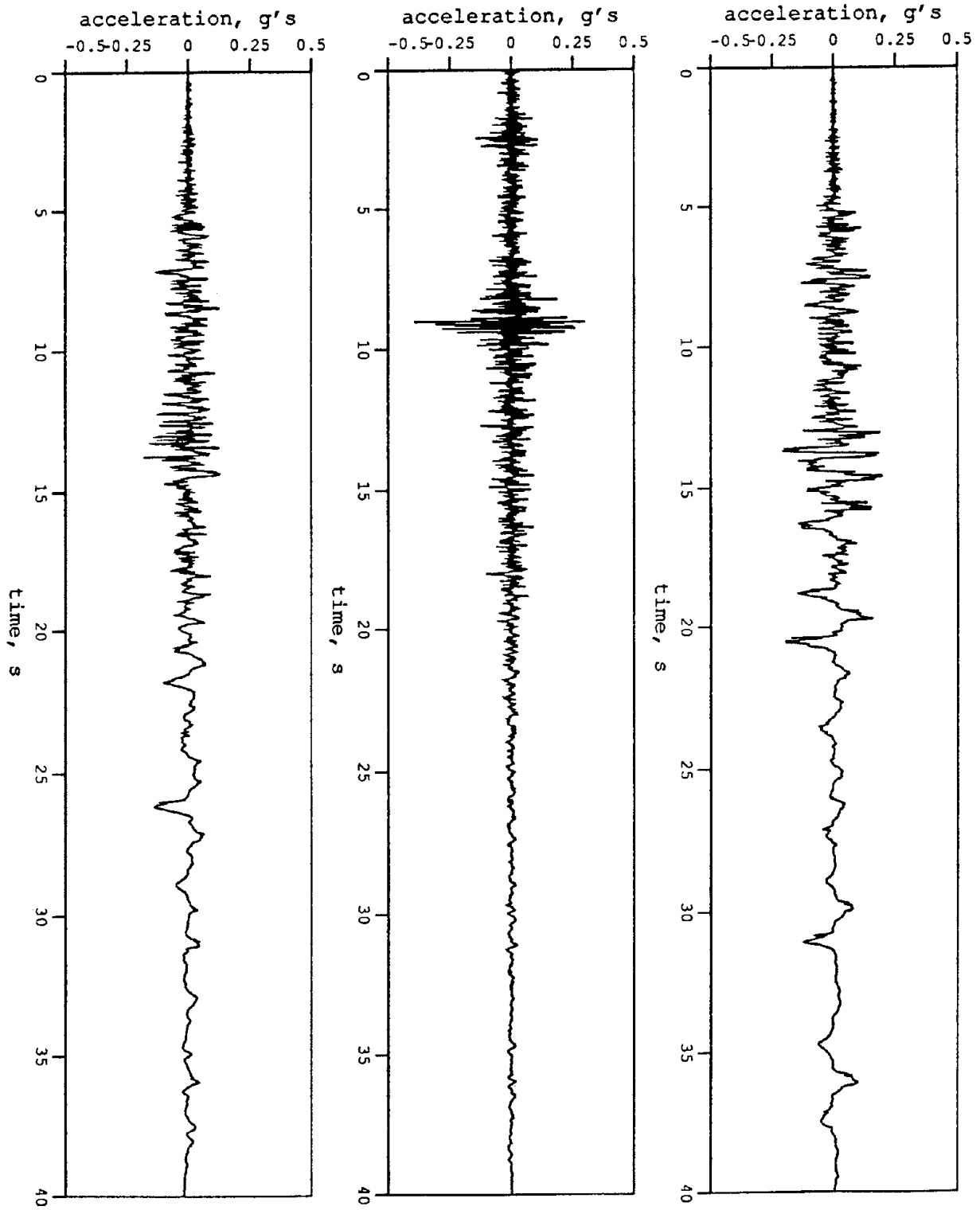
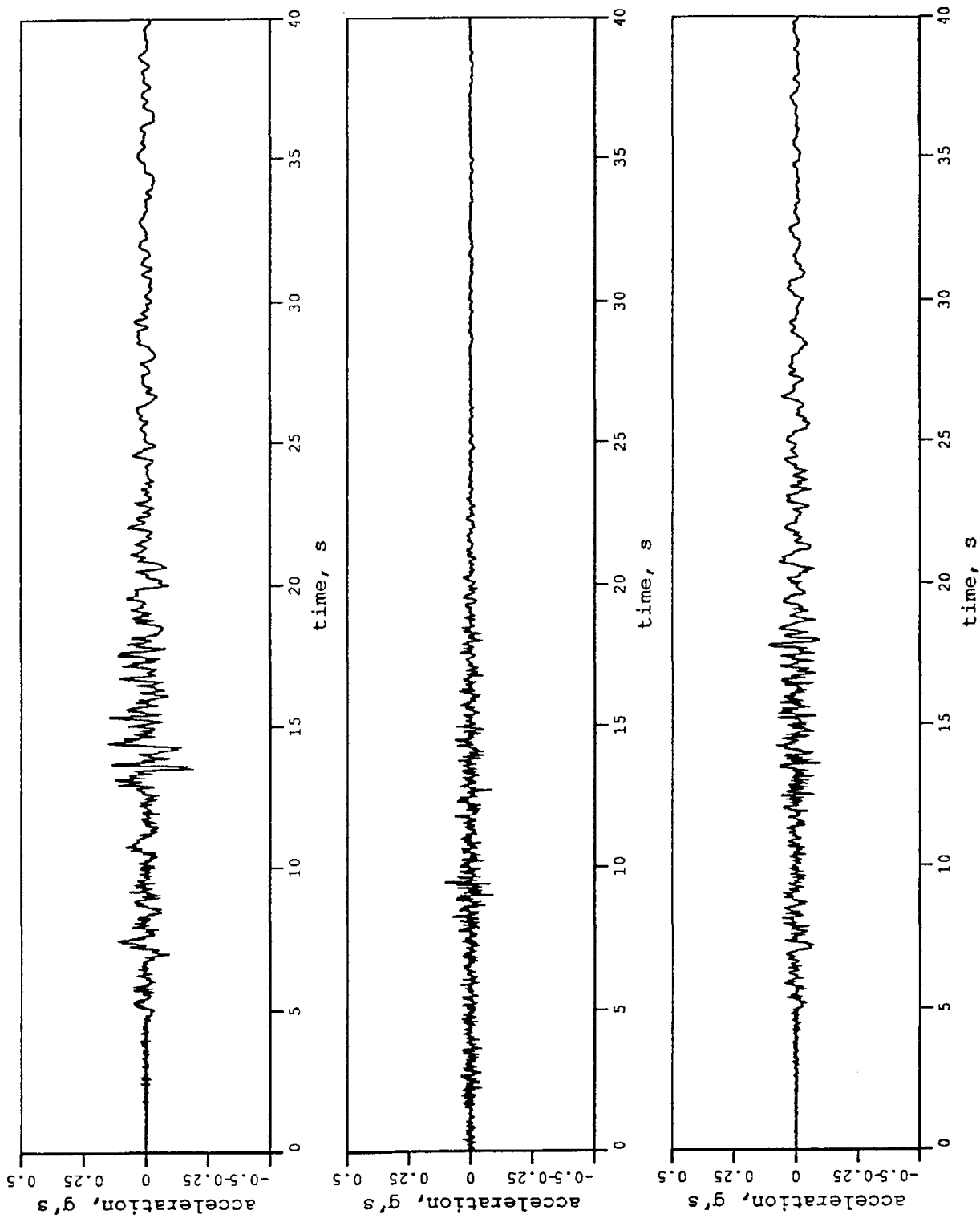


Figure 3 : Profile View of Layered Soil Deposit at Wildlife Site

Figure 4 : Recorded Surface Acceleration  
(a) N-S (b) Vertical (c) E-W





**Figure 5 : Recorded Downhole Acceleration**  
**(a) N-S (b) Vertical (c) E-W**



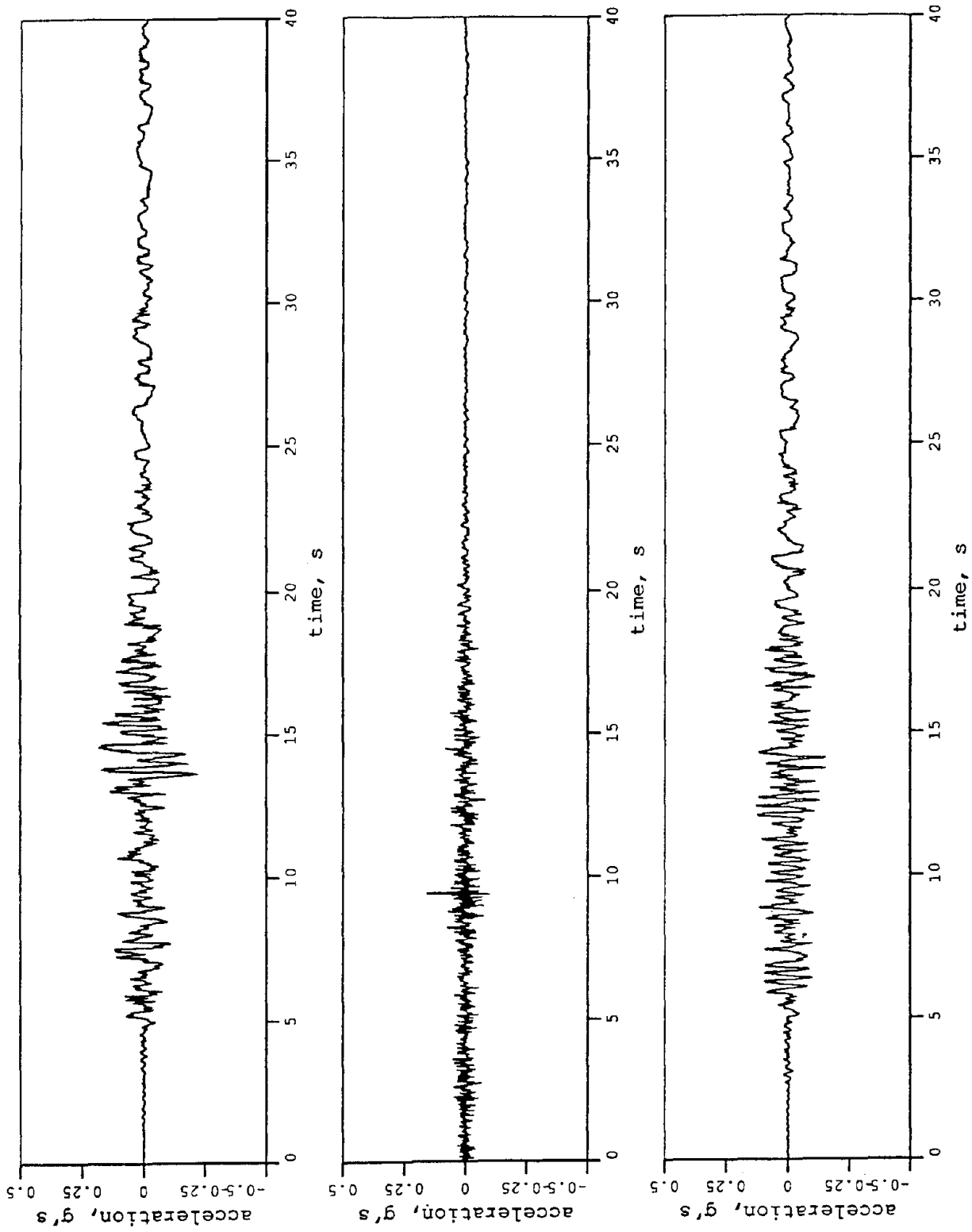


**Figure 6 : 3D Analysis – Computed Surface Acceleration**  
**(a) N-S (b) Vertical (c) E-W**

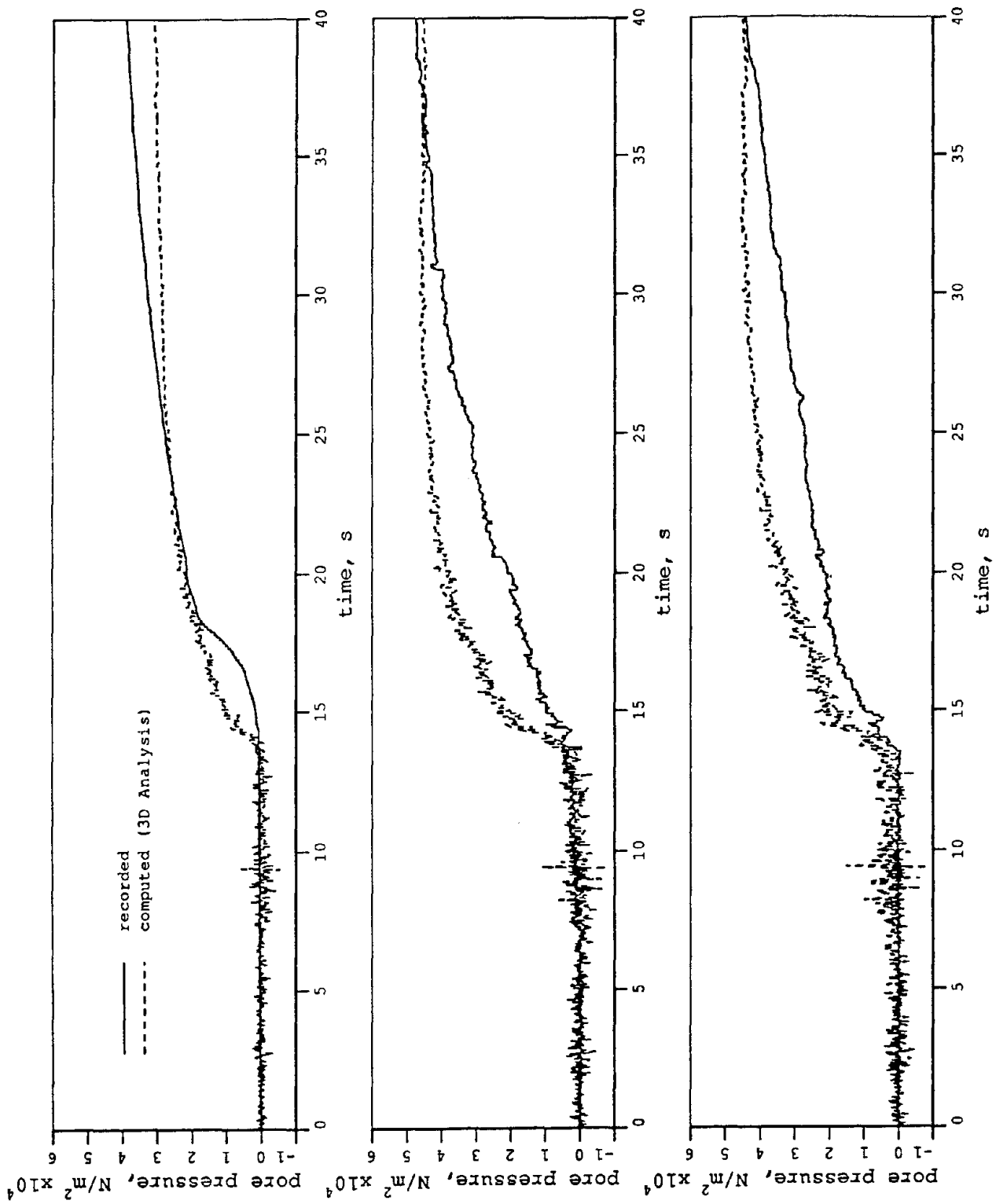
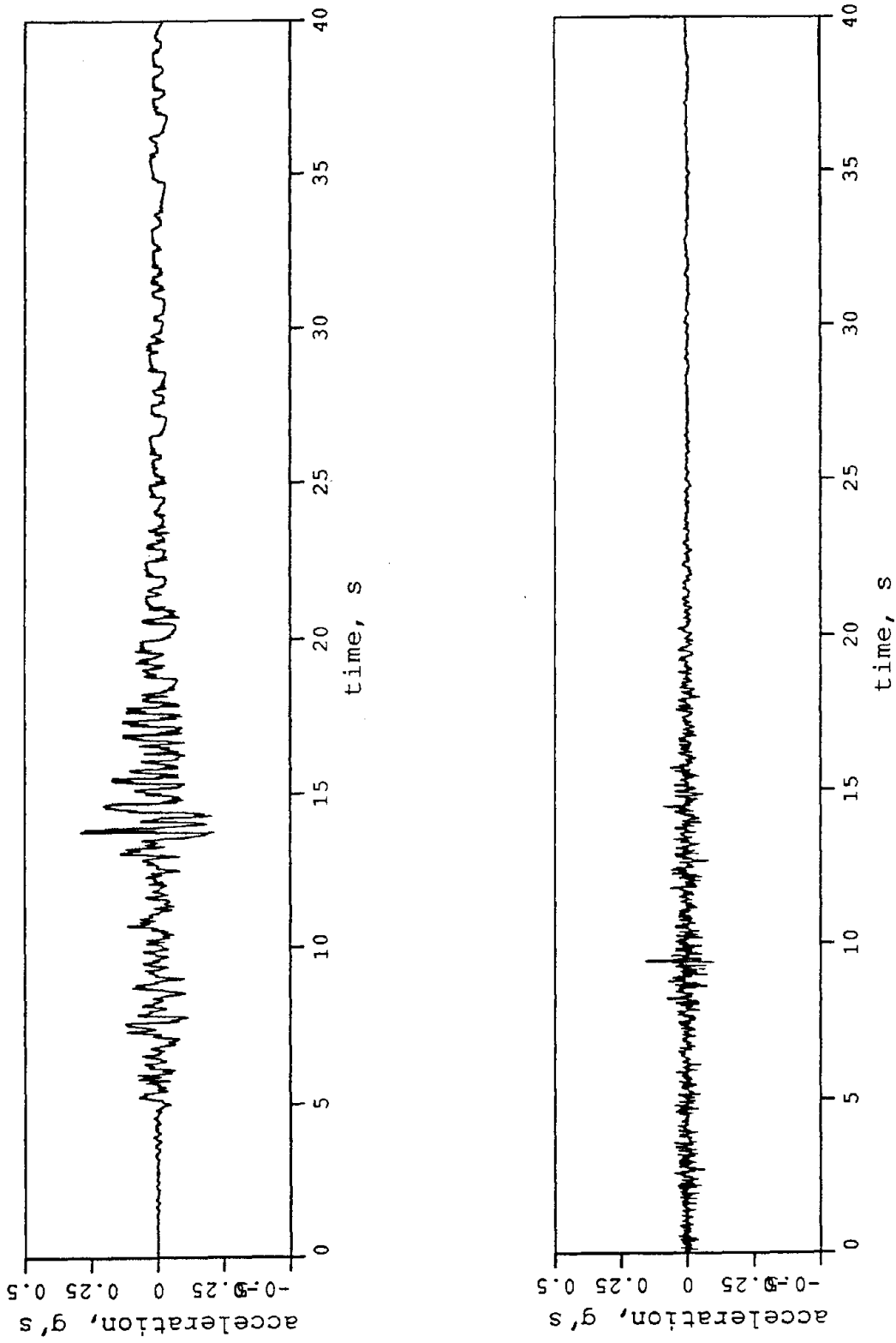


Figure 7 : 3D Analysis – Pore-Water Pressure Time Histories  
 (a) Depth=3m (b) Depth=5m (c) Depth=6.6m



**Figure 8 : 2D Analysis A – Computed Surface Acceleration**  
**(a) N-S (b) Vertical**

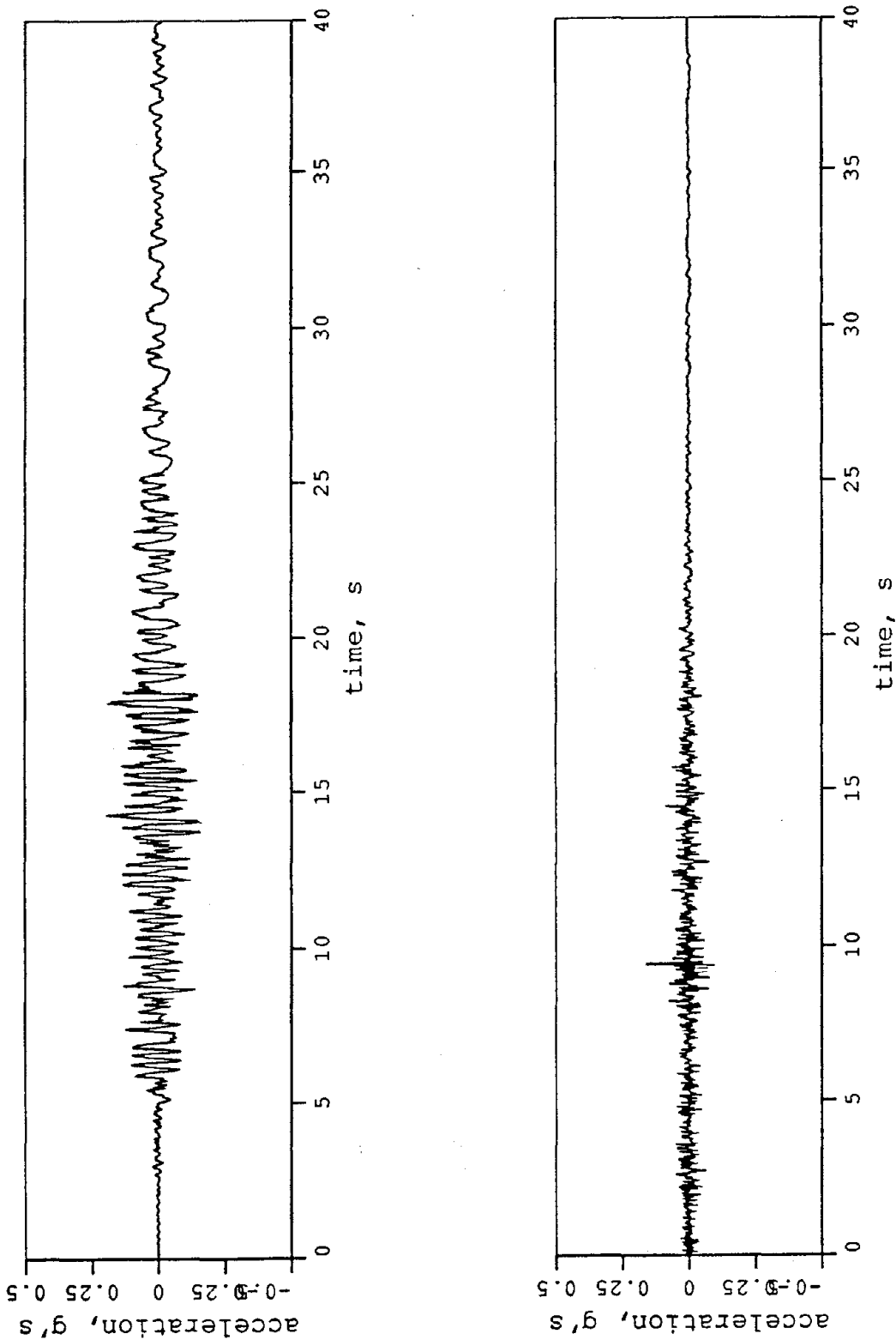
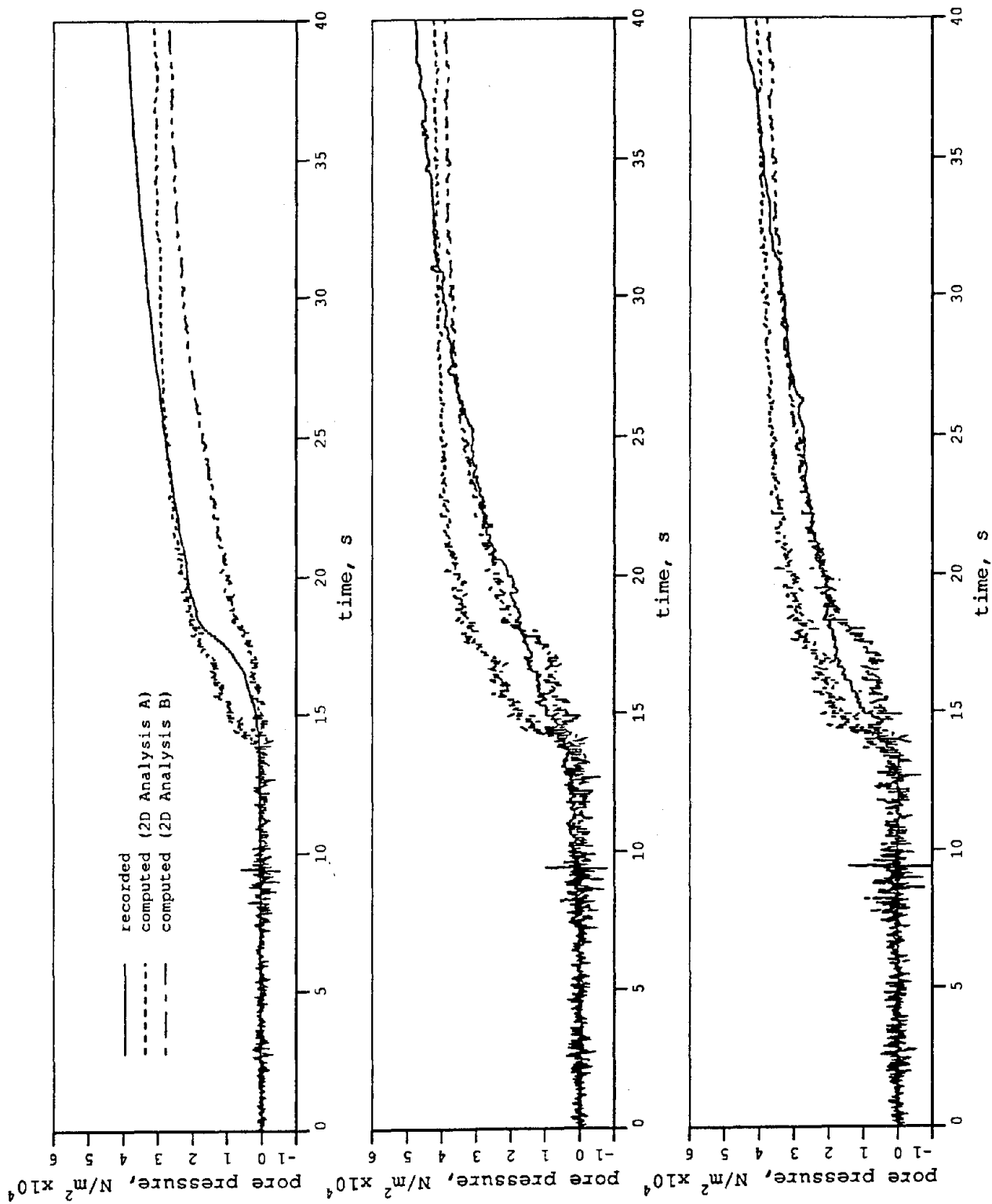
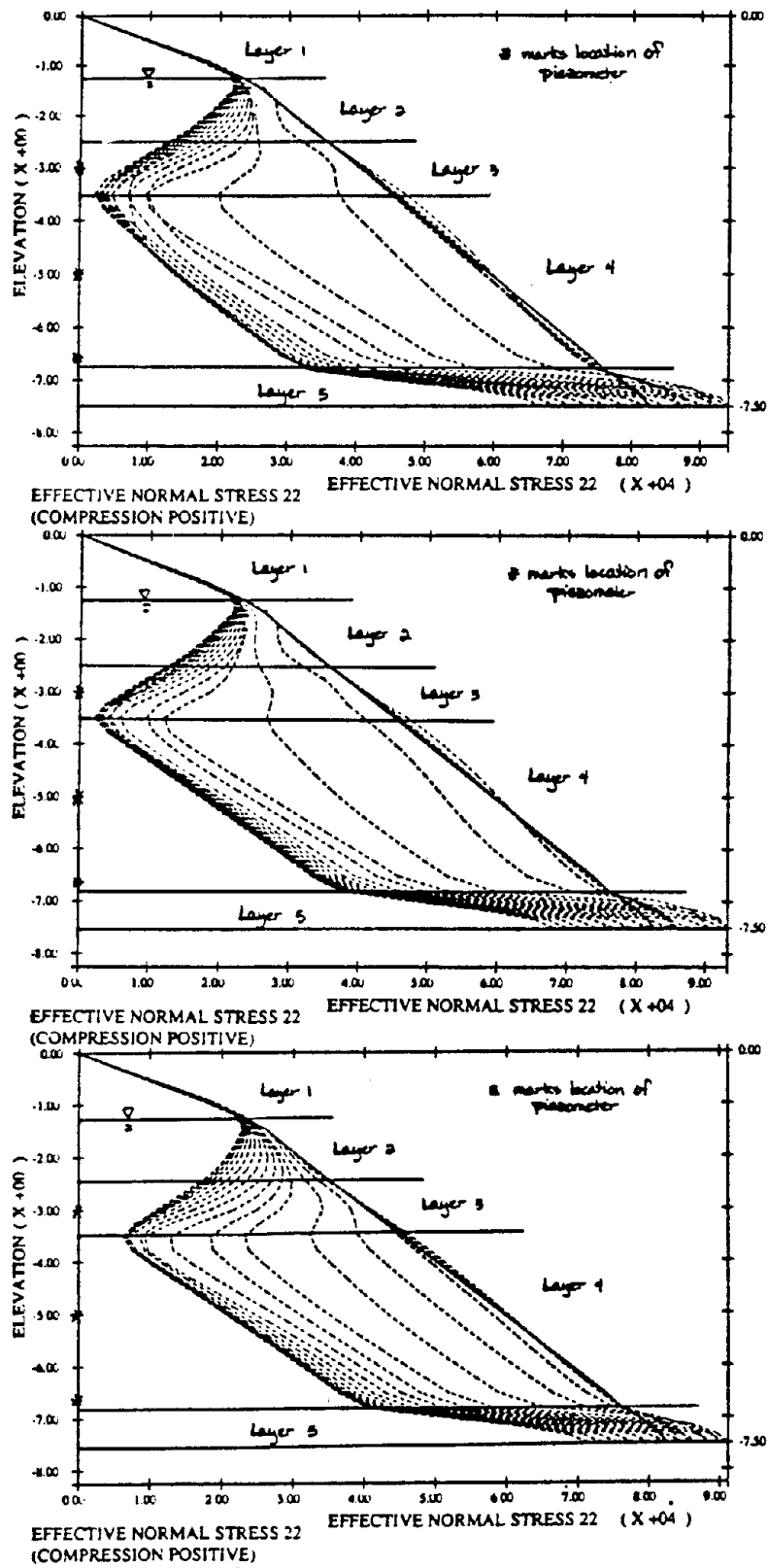


Figure 9 : 2D Analysis B -Computed Surface Acceleration  
(a) E-W (b) Vertical



**Figure 10 : 2D Analysis – Pore-Water Pressure Time Histories**  
 (a) Depth=3m (b) Depth=5m (c) Depth=6.6m



**Figure 11 : Vertical Effective Stress vs. Depth**  
 (a) 3D Analysis (b) 2D Analysis A (c) 2D Analysis B

## SPATIAL SEVERITY OF LIQUEFACTION

Masanobu SHINOZUKA<sup>1</sup> and Keizo OHTOMO<sup>2</sup>

- 1 Sollenberger Professor of Civil Engineering, Princeton University, Princeton, USA
- 2 Visiting Fellow, Department of Civil Engineering and Operations Research, Princeton University; on leave from the Central Research Institute of Electric Power Industry, Abiko, Japan

### Abstract

The primary objective of this paper is to validate the fragility curves for liquefaction potential developed in an earlier paper on the basis of "Liquefaction Potential Index  $P_L$ " with the aid of a more rigorous finite element analysis. The finite element analysis is performed utilizing the code DYN41D which evaluates, among other things, the excess pore pressure along the soil column at any time during the earthquake. The ratio  $u/\sigma'_v$  of this excess pore pressure  $u$  to the effective overburden pressure  $\sigma'_v$  is then integrated through the soil column. The integration assumes a maximum value  $Q$  usually at the end of the earthquake ground motion. For a particular soil profile at a site in Memphis, Tennessee, strong correlations between  $P_L$  and  $Q$  are observed under two specific earthquake acceleration histories applied at the bottom of the soil column. With the aid of these correlations, fragility curves are also developed on the basis of  $Q$  values. In view of the result that indicates fair to good agreements between  $P_L$ -based and  $Q$ -based fragility curves, the use of  $P_L$  in engineering practice appears to be reasonable for the type of soil profile considered in this paper.

### Introduction

In view of the unpredictability of an earthquake, the uncertainty of soil properties, and the errors in laboratory testing and in modeling of soil behavior, a systematic probabilistic and/or statistical treatment for the evaluation of liquefaction potential is necessary. Such a treatment in this field has been discussed by several researchers. Youd and Perkins (Refs. 1 and 2) and Yegian and Whitman (Ref. 3) developed a methodology for mapping the potential for liquefaction-induced ground failure on the basis of observed data. Halder and Tang (Ref. 4) applied linearization and second moment analysis in order to probabilistically characterize the liquefaction phenomena with the aid of the procedure proposed by Seed and Idriss (Ref. 5). A more elaborate approach was developed by Fardis and Veneziano (Ref. 6) to include the effects of pore water pressure dissipation, soil stiffness reduction, and spatial variation of soil properties within a soil column. Chameau and Clough (Ref. 7) have used probabilistic versions of pore water pressure generation models combined with a stochastic description of the earthquake motion. There is no doubt that these efforts contributed toward a better understanding of probabilistic nature of liquefaction potential. However, a further study appears to be needed to develop a measure of liquefaction that reflects its spatial extent along the depth, if not in the two or three dimensional space. Such a measure is undoubtedly quite useful in estimating the degree of

damage sustained by underground structures and eventually developing countermeasures to minimize liquefaction-induced damage.

In this connection and also in relation to the vulnerability and ensuing reliability analysis of the underground crude oil pipelines traversing the New Madrid seismic zone mostly covered by alluvial layers and crossing rivers and creeks underneath in the Mississippi River basin, the authors earlier developed (Ref. 8) an engineering method for constructing fragility curves for liquefaction potential on the basis of the liquefaction resistance factor  $F_L$  (Ref. 5) and liquefaction potential index  $P_L$  (Ref. 9). In constructing the fragility curves, the degree of liquefaction severity was classified into the state of little, minor, moderate, and major severity depending on the  $P_L$  values as shown in Table 1. It is noted, however, that Table 1 was originally developed for identifying the probability of liquefaction at a site depending on the value of  $P_L$  as shown in the first and second columns. The third column was introduced in Ref. 8 to indicate the spatial extent of liquefaction in terms of  $P_L$  values by providing the original definition with an alternative interpretation. Since, however, the  $P_L$  values are developed primarily with the aid of past experience and professional judgement, the fragility curves based on the  $P_L$  values need as much validation as can be provided. Figure 1 is taken from Ref. 9 as an example in which the  $P_L$  value could have correctly predicted the liquefaction risk under the celebrated 1964 Niigata earthquake. In fact, Fig. 1 illustrates two soil profiles at two boring locations along the Showa Ohashi bridge in Niigata, Japan. The  $P_L$  value for the profile on the left is 22.7 and the surface layer liquefied at this site over an estimated depth of 10 m. On the other hand, the profile on the right has a  $P_L$  value equal to 4.6 and no liquefaction was observed at this site.

It is then the purpose of this study to provide such a validation taking advantage of the results of a more rigorous finite element analysis with the aid of computer code DYNA1D (Ref. 10) developed, among other purposes, for excess pore water pressure evaluation .

### Computer Code DYNA1D

In order to accomplish this purpose, the present study takes advantage of an existing computer code DYNA1D which is capable of evaluating the seismic response of dry, partially or completely saturated deposits, taking into consideration the transient flow of pore water through soil strata. The code also implements a plasticity model consisting of constitutive equations, yield function, flow rule, and hardening rule that are applicable to cohesive as well as cohesionless soils. Multisurface  $J_2$  theory is used to account for observed shear non-linear hysteretic behavior and stress-induced anisotropic effects and conical yield surfaces for dependency of shear dilatancy on the effective stress ratio.

A soil profile consisting of late holocene fluvial deposits at a site in Memphis, Tennessee is considered for the finite element analysis as well as for the development of fragility curves. This site exhibits typical soil conditions, as shown in Table 2, representative of a swamp composed of extremely weak soil deposit from the ground surface to about 10 m in depth, with ground water level at -4.5 m.

The calibration of elaborate constitutive soil models used in DYNA1D, especially those using multiple yield levels (Refs. 11 and 12), requires that shear stress-strain curves be obtained from triaxial or simple shear soil tests. However, such laboratory test data on the soil type as shown in Table 2 are not available, but only the SPT- $N$  values are available. Under these circumstances, necessary maximum shear modulus  $G_0$ , maximum shear stress



$\tau_{max}$  and maximum shear strain  $\gamma_{max}$  are determined taking advantage of some empirical relationships (Ref. 13 and 14). Also, the permeability coefficient,  $k$ , is assumed to be  $1.0 \times 10^{-5}$  (m/s) throughout the soil column.

Two input ground motions are considered in the analysis; the one is the Pacoima dam record with a 12.0 sec. duration (1971 San Fernand earthquake,  $M = 6.6$ ) and the other is the El Centro record with a 20.0 sec. duration (1940 Imperial Valley earthquake,  $M = 6.6$ ). Figure 2 shows acceleration histories of these earthquakes with the peak ground acceleration (PGA) values linearly scaled to 0.20  $g$  for both histories. These acceleration histories, properly scaled, will be used as input acting at the base of the soil column assumed to be located at -18 m.

### Development of $P_L$ -Based Fragility Curves

As reported in the earlier study (Ref. 8), only those  $N$  values observed in standard penetration tests (SPT's) are assumed to have an uncertain variability. For simplicity as well as due to lack of more detailed data, it is assumed that the variability can be characterized by a normal distribution function with mean value  $\bar{N}_i$  equal to the measured  $N_i$  value at the  $i$ -th layer and coefficient of variation  $\gamma = 0.20$ . A sample SPT  $N$  value at the  $i$ -th layer can then be written as

$$N_i^s = (1 + \gamma \times RN) \times \bar{N}_i \quad (1)$$

where  $RN$  = an independent realization of the standardized normal random variable. When  $N_i^s$  are considered as realizations of a stochastic field  $N(z)$  at discretized locations, Eq. 1 suggests that  $N_i^s$  are taken from a Gaussian white noise field. More realistically, a non-white field should be considered for  $N(z)$ . However, a preliminary Monte Carlo simulation study performed in which  $N(z)$  is assumed to be colored indicates that this has little effect either on the location or on the shape of fragility curves.

In the present study, the analysis is carried out in Monte Carlo simulation for each of the sample soil columns represented by a set of  $N_i^s$  values ( $i=1,2,\dots,n$ ). First, each sample column is subjected to fifteen (15) ground acceleration histories of the Pacoima type obtained by linearly scaling the acceleration history shown in Fig. 2 so that PGA becomes 0.02, 0.03, 0.04, 0.05, 0.07, 0.08, 0.09, 0.10, 0.11, 0.12, 0.13, 0.15, 0.17, 0.20, and 0.25 $g$ .

Under each acceleration history, the liquefaction resistance factor  $F_{L,i}$  is calculated from  $N_i^s$  at layer  $i$  with the aid of the procedure proposed by Seed and Idriss (Ref. 5), Seed et al (Ref. 15), and Seed and Tokimatsu (Ref. 16). The liquefaction potential index  $P_L$  is then evaluated for this simulated soil column. In this connection, it is noted that the value of the coefficient CM in the Seed-Idriss procedure to account for the number of representative shear stress cycles at 65% of the maximum shear stress,  $\tau_{max}$ , is estimated from the Pacoima record to be 5 or 6 and therefore  $CM=1.32$ ; this value of CM corresponds to an earthquake with a magnitude  $M_S$  between 5.6 and 6.5 according to the same procedure.

Considering twenty (20) such sample soil columns (sample size = 20) and repeating the evaluation of  $P_L$  twenty times for each acceleration history with one of the fifteen (15) PGA values, twenty values of  $P_L$  are obtained in which  $N_1$  of them with  $P_L = 0$ ,  $N_2$  with  $0 < P_L \leq 5$ ,  $N_3$  with  $5 < P_L \leq 15$  and  $N_4$  with  $15 < P_L$  where  $N_1 + N_2 + N_3 + N_4 = 20$ .

Then  $N_2/20$ ,  $N_3/20$  and  $N_4/20$  provide Monte Carlo estimates of the probabilities for the states of minor, moderate and major liquefaction severity, respectively, at that PGA value. Establishing such probability estimates at fifteen (15) PGA values and constructing a curve interpolating these fifteen estimates for each state of liquefaction severity, a set of three fragility curves are obtained respectively for the state of minor, moderate and major liquefaction severity as shown in Fig. 3a (solid curves).

Similarly fragility curves under the El Centro type for the same site are obtained as shown in Fig. 3b (solid curves). In this case, however, the representative cycles at 65% of the maximum shear stress,  $\tau_{max}$ , is estimated from the El Centro record to be 10 and hence  $CM = 1.13$ ; this value of  $CM$  corresponds to a magnitude  $M_s$  between 6.5 and 7.0.

### Evaluation of Q Values

The code DYNA1D is applied to each sample soil column in order to evaluate the excess pore water pressure  $u$  along the column under each ground acceleration history of the Pacoima type (see Fig. 4a). The ratio of the excess pore water pressure  $u$  to the initial effective overburden pressure  $\sigma'_v$  is computed at each layer and integrated through the soil column. The integral assumes a maximum value  $Q$  usually at the end of earthquake ground motion;

$$Q = \int_{-18}^0 \frac{u(t_D, z)}{\sigma'_v(z)} dz \quad (2)$$

where  $t_D=12$  sec is the duration of the Pacoima dam record and  $z$  is the vertical axis positive in the downward direction. Similar evaluation of  $Q$  is possible for the El Centro record (see Fig.4b) in which case, however,  $t_D = 20$  sec.

When the DYNA1D code is used twenty times for the sample of twenty (20) soil columns under each of the fifteen acceleration histories with respective PGA values, twenty values of  $Q$  and hence twenty pairs of  $Q$  and  $P_L$  values are obtained at each PGA values. When these pairs obtained at each of fifteen PGA values are all combined, a total of three hundred (300) pairs of  $P_L$  and  $Q$  values will result and can be plotted as shown in Fig. 5a.

Similarly, three hundred pairs of  $P_L$  and  $Q$  values are obtained for the El Centro earthquake as plotted in Fig. 5b.

### Correlation between $P_L$ and $Q$

Linear regression analysis is performed on the  $P_L$  and  $Q$  pairs plotted in Fig.5. From Fig. 5a (the Pacoima type),  $Q$  is related to  $P_L$  in the form

$$Q = 0.007 + 0.008P_L \quad (3)$$

with correlation coefficient  $\rho = 0.93$ . On the other hand, from Fig. 5b (the El Centro Type)

$$Q = 0.148 + 0.007P_L \quad (4)$$

with correlation coefficient  $\rho = 0.81$ . Eqs. 3 and 4 are plotted as straightlines in Figs. 5a and 5b, respectively.

Judging from the values of correlation coefficients as well as inspection of Figs. 5a and 5b,  $P_L$  and  $Q$  have a relatively strong positive correlation in both cases of the Pacoima and El Centro type earthquakes. This observation implies that the fragility curves developed on the basis of  $P_L$  values may be considered reasonable under the specific earthquake types used for the analysis.

In order to further confirm this observation, the state of liquefaction severity given in terms of  $P_L$  is reclassified in terms of  $Q$  with the aid of Eqs. 3 and 4 for the Pacoima and El Centro type, respectively. The results are indicated in the third columns of Tables 3 and 4 for the Pacoima and El Centro type, respectively.

Following exactly the same procedure as when the fragility curves are constructed based on twenty  $P_L$  values for each of the fifteen earthquake histories, the fragility curves based on  $Q$  values can also be developed for both types of earthquakes. They are plotted in Fig. 3a for the Pacoima type and in Fig. 3b for the El Centro type, both by dashed curves.

Figure 3a shows that, under the Pacoima type earthquakes, the  $P_L$ -based and  $Q$ -based fragility curves are in good agreement both for moderate and major liquefaction severity, while the  $Q$ -based fragility curve provides a substantially more conservative result than the  $P_L$ -based curve. Figure 3b shows, however, that all the  $Q$ -based fragility curves exhibit conservative results, more so as the liquefaction severity further intensifies from the state of minor to that of moderate and to that of major severity.

### Conclusion and Discussion

The liquefaction potential index  $P_L$  as used in Japan and elsewhere is examined in the light of the more recent analytical result obtained from the finite element analysis code DYNA1D. In the present study, the result of the DYNA1D analysis is summarized in terms of  $Q$  which is the integration of the ratio of the excess pore pressure to the effective overburden pressure along the soil column. The correlation between  $P_L$  and  $Q$  appears to be strong for the particular soil profile under Pacoima and El Centro type earthquakes. On the other hand, when the  $P_L$ -based fragility curves are compiled with those based on the  $Q$ -values, the former tend to exhibit unconservative results. However, in view of the large number of sources of uncertainty that exist throughout the process of analytical modeling and parameter estimation, the agreement between the  $P_L$ -based and  $Q$ -based fragility curves may be deemed fair to good, and hence the use of  $P_L$  in engineering practice may be considered reasonable, provided, of course, the  $Q$ -value indeed reflects the degree of spatial liquefaction severity.

To further examine the validity of these observations, future study should focus on;

- a) Additional earthquake acceleration records with differing types of frequency contents.
- b) Different soil profiles.
- c) More than one random parameter, particularly examination of the effect of variability of permeability coefficient; the present study considered only the value of  $N$  to be random with a relatively small coefficient of variation, thus resulting in rather sharply rising fragility curves.
- d) Two-dimensional finite element analysis.

- e) Measures of liquefaction severity other than  $Q$  as defined and used in the present paper.

### Acknowledgement

This work was carried out under the national Center for earthquake Engineering Research contract number NCEER-88-3007. In performing this work, K. Ohtomo was supported by Princeton University and the Central Research Institute of Electric Power Industry, Abiko, Chiba, Japan.

### References

1. Youd, T. L., and Perkins, D. M., "Mapping Liquefaction-Induced Ground Failure Potential", *Journal of the Geotechnical Engineering Division, ASCE*, Vol. 104, No. 4, pp.433-466, 1978.
2. Youd, T. L., and Perkins, D. M., "Mapping of Liquefaction Severity Index", *Journal of the Geotechnical Engineering Division, ASCE*, Vol. 113, No. 11, pp.1374-1392, 1987.
3. Yegian, M. K., and Whitman, R. V., "Risk Analysis for Ground Failure by Liquefaction", *Journal of the Geotechnical Engineering Division, ASCE*, Vol. 104, No. 7, pp.921-938, 1978.
4. Halder, A., and Tang, W. H., "Probabilistic Evaluation of Liquefaction Potential", *Journal of the Geotechnical Engineering Division, ASCE*, Vol. 105, No. 2, pp.165-182, 1979.
5. Seed, H. B., and Idriss, I. M., "Simplified Procedure for Evaluating Soil Liquefaction Potential", *Journal of the Soil Mechanics and Foundation Division, ASCE*, Vol. 97, No. SM9, pp.1249-1273, 1971.
6. Fardis, M. N., and Veneziano, D., "Probabilistic Analysis of Deposit Liquefaction", *Journal of the Geotechnical Engineering Division, ASCE*, Vol. 108, No. 3, pp.395-417, 1982.
7. Chameau, J. L., and Clough, G. W., "Probabilistic Pore Pressure Analysis for Seismic Loading", *Journal of the Geotechnical Engineering Division, ASCE*, Vol. 109, No. 4, pp.507-524, 1983.
8. Shinozuka, M., Kishimoto, S., and Ohtomo, K., "Fragility Curves for Liquefaction", *Proc. of the 1st US-Japan Cooperative Workshop on Liquefaction, Large Ground Deformation and Their Effects on Lifeline Facilities, Tokyo, 1988.*
9. Iwasaki, T., Tatsuoka, F., Tokida, K., and Yasuda, S., "A Practical Method for Assessing Soil Liquefaction Potential Based on Case Studies at Various Sites in Japan", *Proc. of 2nd International Conference on Microzonation, San Francisco, Vol. 2, pp.885-896, 1978.*
10. Prevost, J. H., "DYNA1D : A Computer Program for Nonlinear Seismic Site Response Analysis", *Technical Documentation, Princeton University, 1988.*

11. Mroz, Z., "On the Description of Anisotropic Work Hardening", *J. Mech. Phys. Solids*, Vol. 15, pp.163-175, 1967.
12. Prevost, J. H., "Numerical Modeling of Monotonic and Cyclic Undrained Clay Behavior", *International Journal for Numerical and Analytical Methods in Geomechanics*, Vol. 1, No. 2, pp.195-216, 1977.
13. Imai, T., and Yoshimura, M., "Elastic Wave Velocity and Dynamic Characteristics of the Soft Ground", *Soils and Foundation*, Vol. 18, No. 1, pp.17-22, 1970 (in Japanese).
14. Shibata, T., and Soelarno, D. S., "Stress-Strain Characteristics of Sandy Soil Subjected to Cyclic Loading", *Proc. of JSCE*, No. 239, 1975 (in Japanese).
15. Seed, H. B., Idriss, I. M., and Arango, I., "Evaluation of Liquefaction Potential Using Field Performance Data", *Journal of the Geotechnical Engineering, ASCE*, Vol. 109, No. 3, pp.458-482, 1983.
16. Seed, H. B., and Tokimatsu, K., "Influence of SPT Procedure in Soil Liquefaction Resistance Evaluations", *Journal of the Geotechnical Engineering, ASCE*, Vol. 111, No. 12, pp.1425-1445, 1985.

Table 1 Liquefaction Potential Index  $P_L$ 

	Liquefaction Risk	Liquefaction Severity
$P_L = 0$	very low	little
$0 < P_L \leq 5$	low	minor
$5 < P_L \leq 15$	high	moderate
$15 < P_L$	very high	major

Table 2 Soil Properties

Depth $Z$ (m)	Layer No.	N Value	Unit Weight $\gamma$ ( $t/m^3$ )	Effective Overburden Pressure $\sigma'_v$ ( $t/m^2$ )	Shear Modulus $G_0$ ( $t/m^2$ )	Maximum Shear Stress $\tau_{max}$ ( $t/m^2$ )	Maximum Shear Strain $\gamma_{max}$	Permiability Coefficient $k$ ( $m/s$ )
1.5	1	2	1.5	1.13	1700	0.6	$2 \times 10^{-2}$	—
3.0	2	2	1.6	3.45	1700	1.0	$3 \times 10^{-2}$	—
4.5	3	2	1.7	5.85	1700	1.3	$4 \times 10^{-2}$	—
6.0	4	4	1.8	7.58	3000	2.6	$5 \times 10^{-2}$	$10^{-5}$
7.5	5	6	1.9	8.70	4000	3.8	$5 \times 10^{-2}$	$10^{-5}$
9.0	6	7	1.9	9.98	4500	4.6	$5 \times 10^{-2}$	$10^{-5}$
10.5	7	7	2.0	11.33	4500	4.9	$6 \times 10^{-2}$	$10^{-5}$
12.0	8	18	2.0	12.75	9500	10.8	$6 \times 10^{-2}$	$10^{-5}$
13.5	9	20	2.0	14.25	10300	12.4	$6 \times 10^{-2}$	$10^{-5}$
15.0	10	50	2.0	15.75	21100	26.5	$7 \times 10^{-2}$	$10^{-5}$
16.5	11	50	2.0	17.25	21100	27.8	$7 \times 10^{-2}$	$10^{-5}$
18.0	12	32	2.0	18.75	14900	20.4	$7 \times 10^{-2}$	$10^{-5}$
G.W.L = -4.5 m								

Table 3 States of Liquefaction Severity (Pacoima)

Liquefaction Severity	$P_L$	$Q$
little	$P_L = 0$	$Q \leq 0.007$
minor	$0 < P_L \leq 5$	$0.007 < Q \leq 0.046$
moderate	$5 < P_L \leq 15$	$0.046 < Q \leq 0.126$
major	$15 < P_L$	$0.126 < Q$

Table 4 States of Liquefaction Severity (El Centro)

Liquefaction Severity	$P_L$	$Q$
little	$P_L = 0$	$Q \leq 0.148$
minor	$0 < P_L \leq 5$	$0.148 < Q \leq 0.184$
moderate	$5 < P_L \leq 15$	$0.184 < Q \leq 0.285$
major	$15 < P_L$	$0.285 < Q$

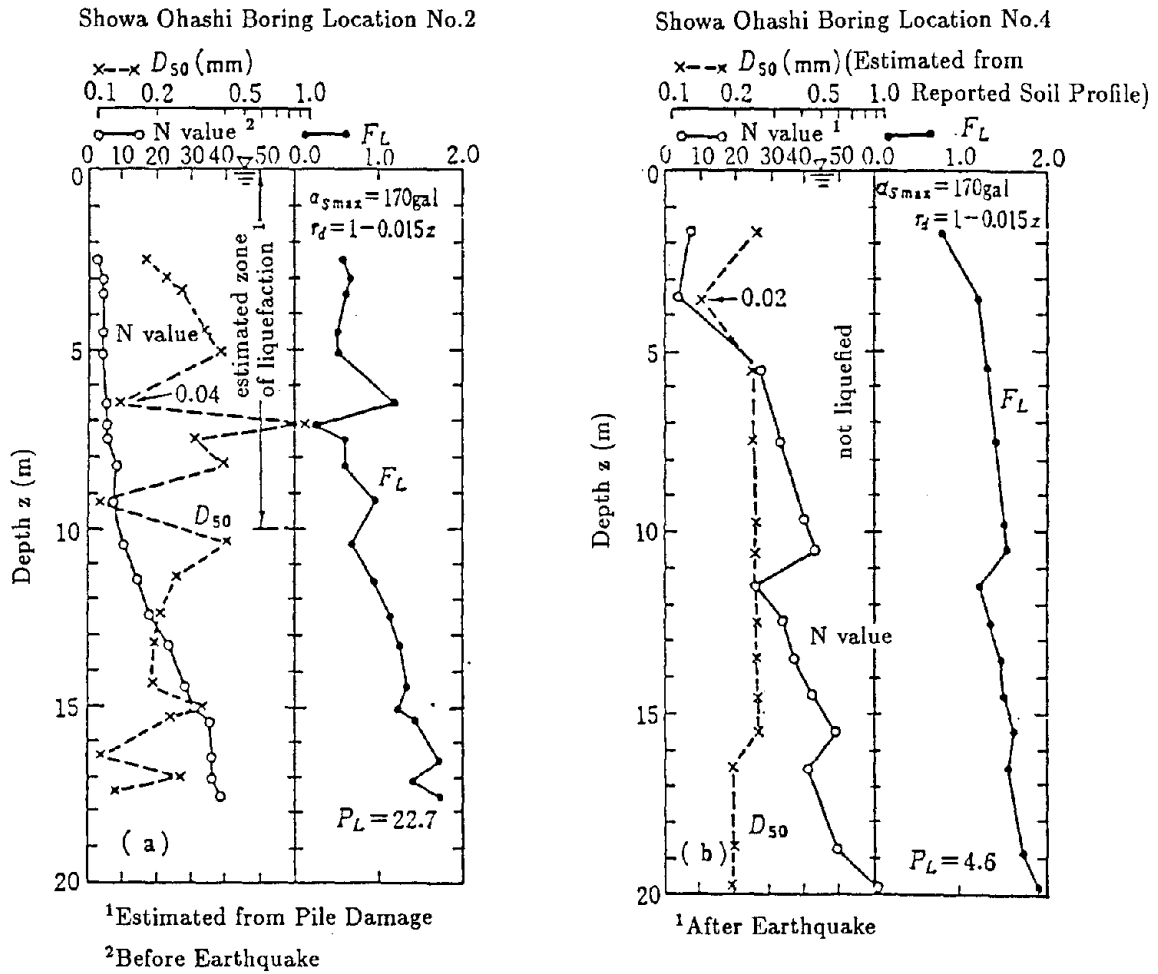


Fig. 1 Soil Profiles and  $P_L$  values (Ref. 9)



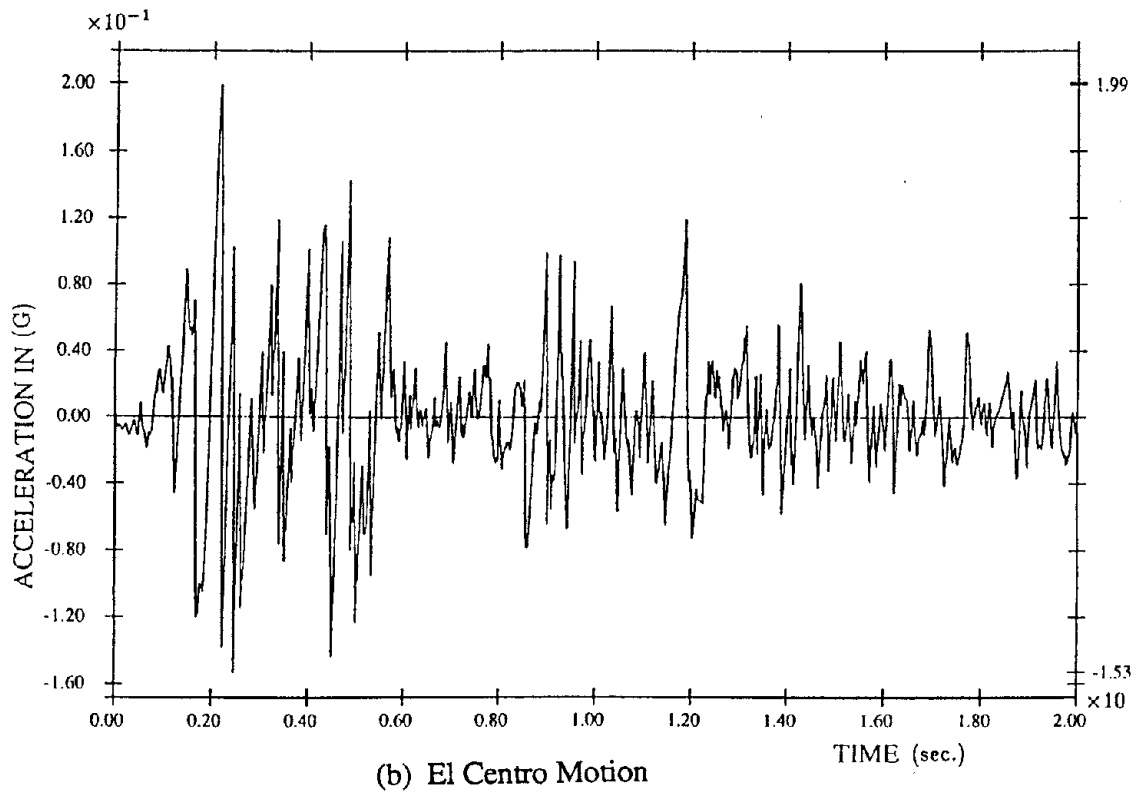
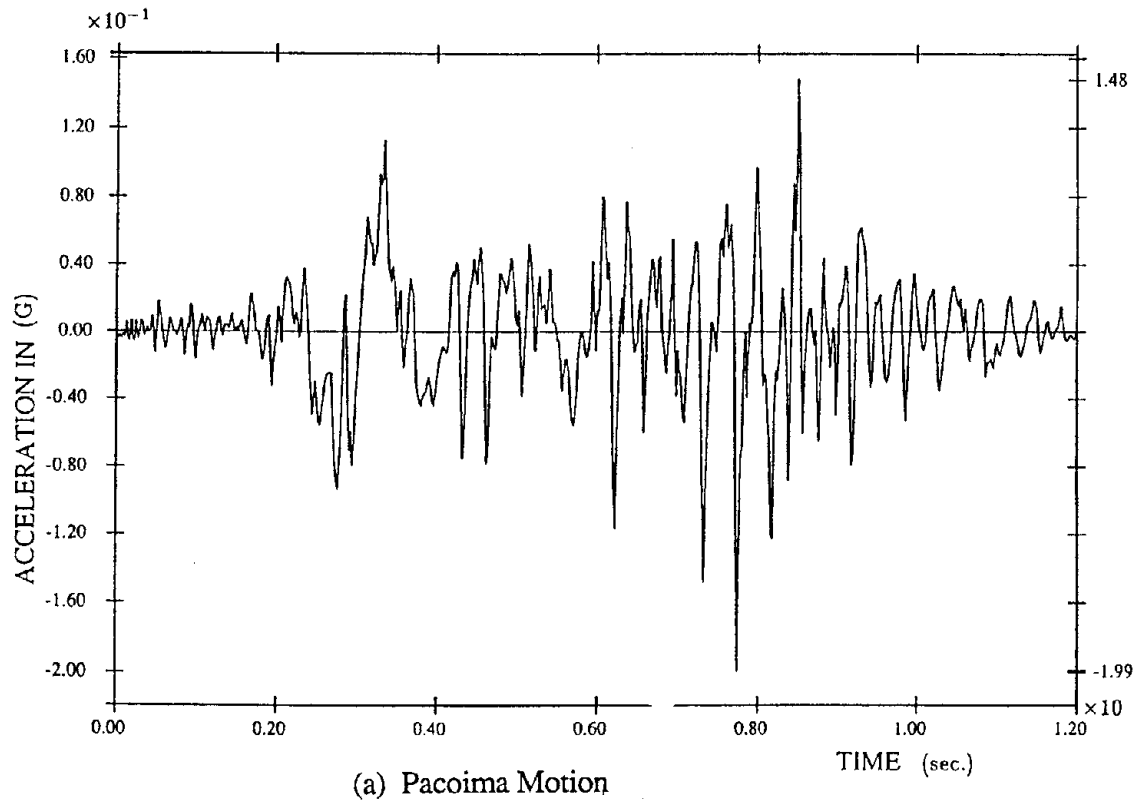
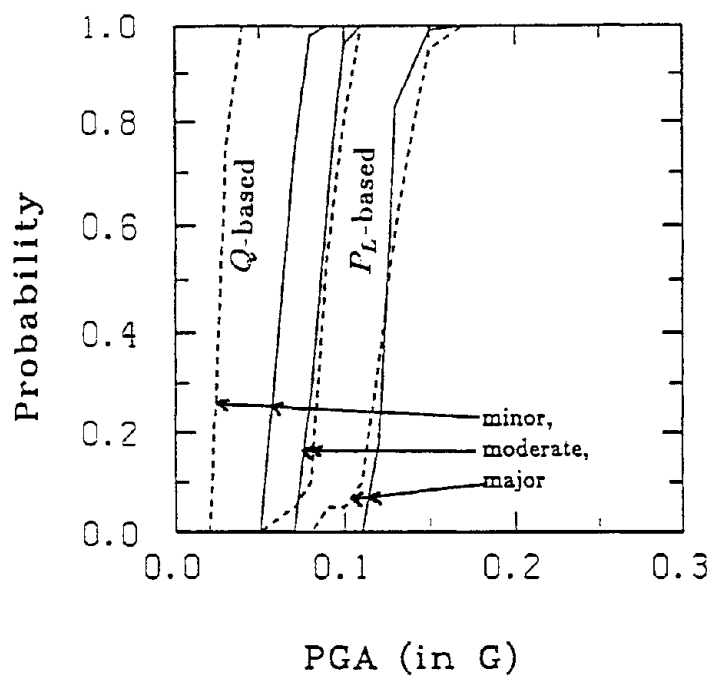


Fig. 2 Input Ground Motions

(a) Pacoima Motion



(b) El Centro Motion

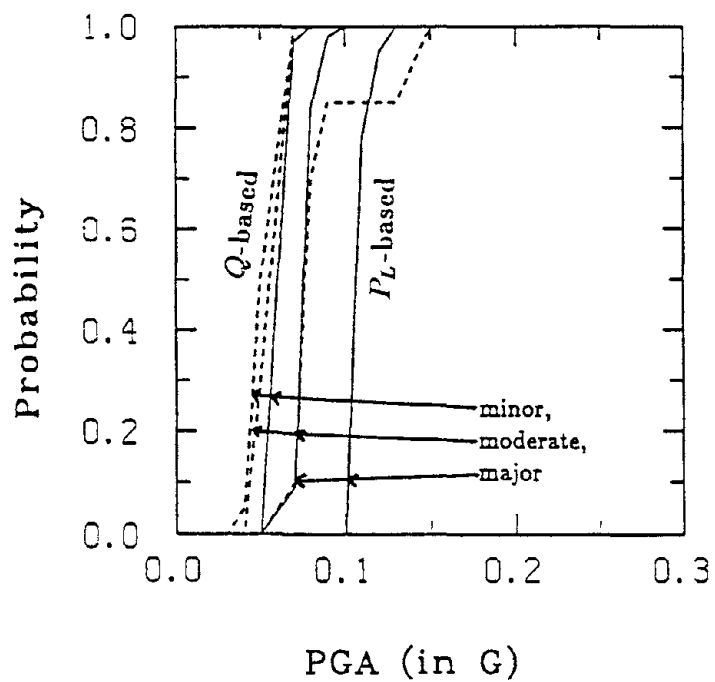
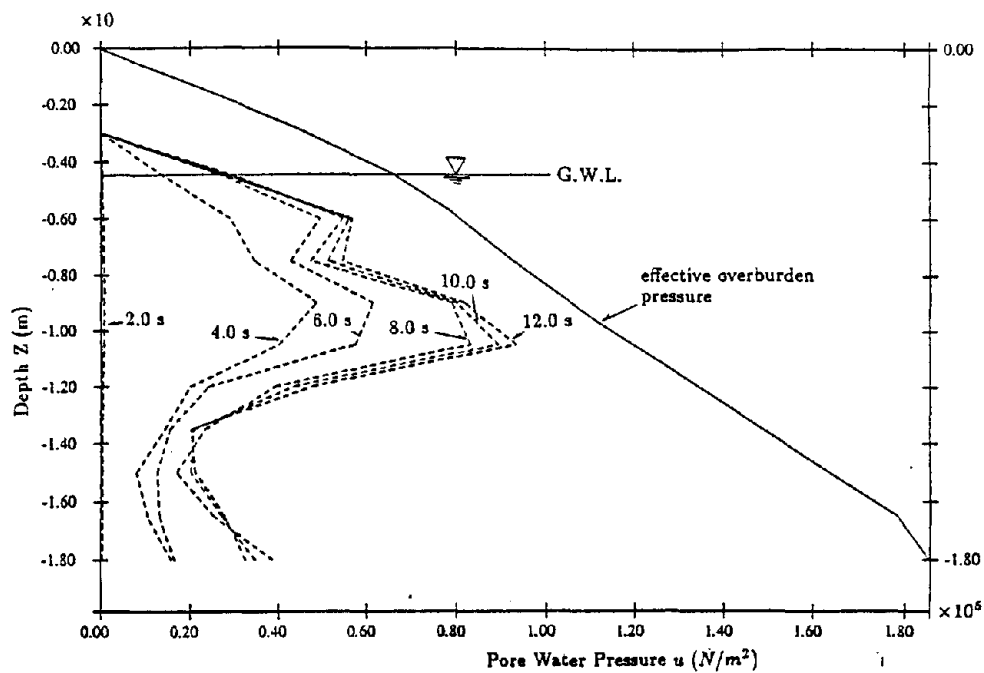
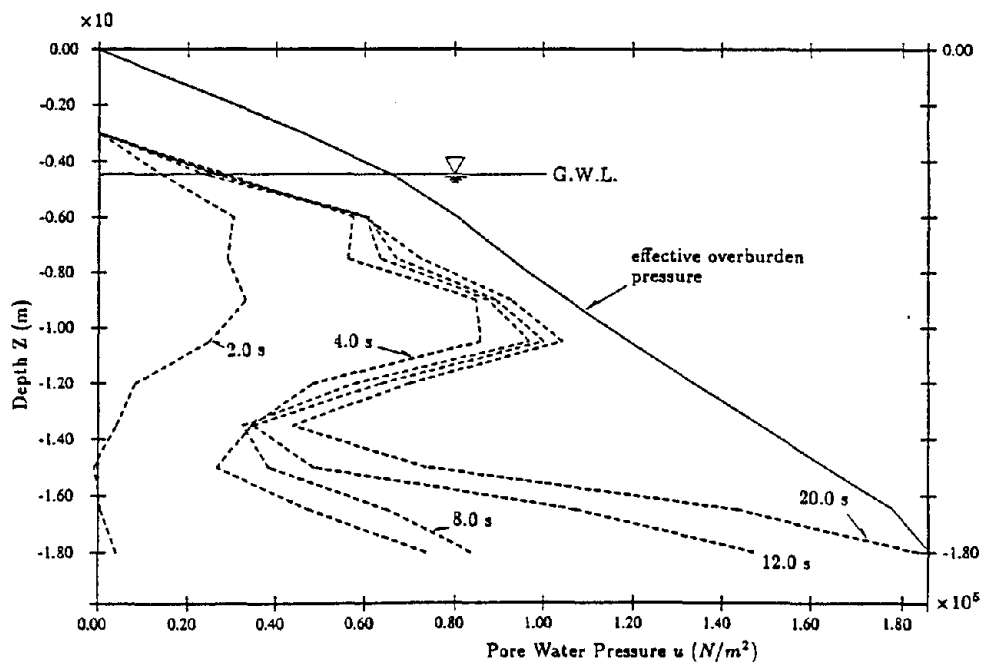


Fig. 3 Fragility Curves

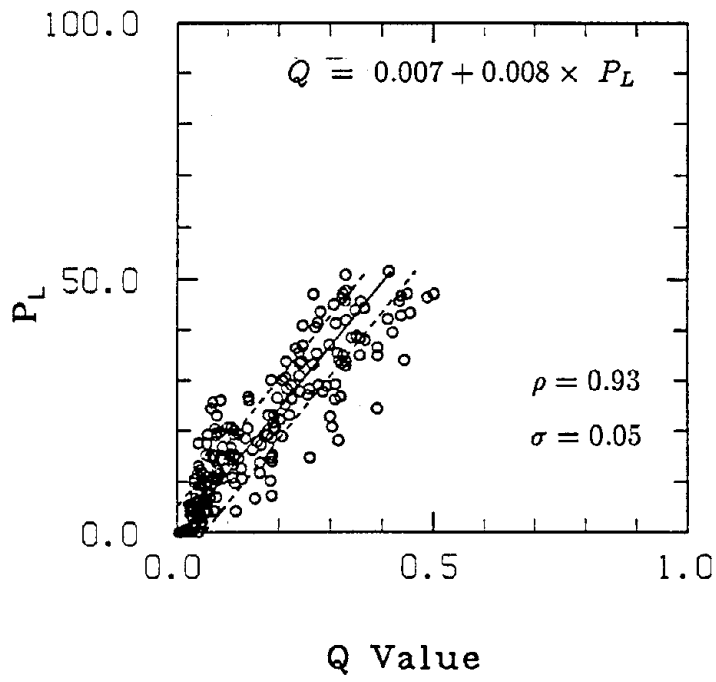


(a) Pacoima Motion with PGA = 0.20g

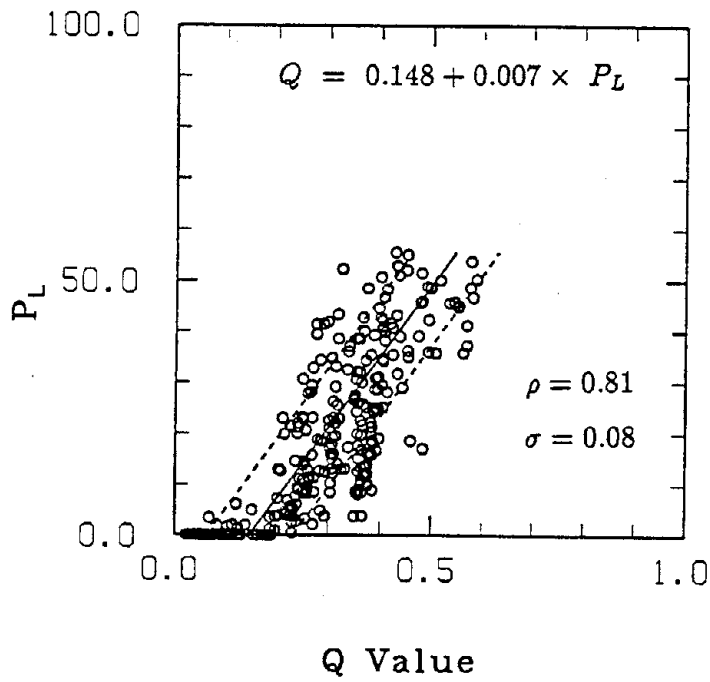


(b) El Centro Motion with PGA = 0.20g

Fig. 4 Vertical Distributions of Excess Pore Water Pressure



(a) Pacoima



(b) El Centro

Fig. 5 Correlation between  $P_L$  and Q values

**FINITE DISPLACEMENT ANALYSIS  
ON LIQUEFACTION-INDUCED LARGE PERMANENT GROUND DISPLACEMENTS**

Nozomu YOSHIDA

Engineering Research Center  
Sato Kogyo Co., Ltd.

**ABSTRACT**

A method to calculate liquefaction-induced large permanent ground displacements is proposed. The analysis is based on the updated Lagrange concept to analyze large displacements. Considering the result of the site investigation that liquefaction-induced large ground displacements seem to depend on the geological and topographical conditions and not to depend on the earthquake motion, the effect of the earthquake motion is removed in the analysis. Undrained behavior and proportional decrease of the effective confining pressure are assumed for this purpose. One point Gauss integration and anti-hourglass matrix are employed to calculate stiffness matrix under no volume change condition which comes from the undrained assumption. Main conclusions obtained through the parametric study are as follows:

- a) Large ground displacement occurs when effective confining pressure becomes nearly zero even if ground surface is nearly horizontal.
- b) The direction and the magnitude of the displacements are predominantly controlled by the slope angle of the ground surface. They are also affected by the slope angle of the lower boundary of the liquefied layer, but not so large compared with the effect of the ground surface.

## INTRODUCTION

Many research studies have been carried out to clarify the mechanism of liquefaction and to predict the occurrence of liquefaction after two big earthquakes occurred in 1964 (Niigata and Alaska) at which severe damages occurred due to liquefaction. If liquefaction takes place, bearing capacity of the ground is lost, which directly result in the damage of structures. Therefore many researches have focused for predicting the occurrence of liquefaction and countermeasures against them. As a fruit of these studies, the mechanism of liquefaction was made clear and it became possible to predict the occurrence of liquefaction with a high accuracy.

Hamada et al<sup>1)2)</sup> showed another aspect of the damage due to liquefaction. They compared the aerial photographs taken before and after the earthquake and showed that large ground displacements may take place when liquefaction occurs. For example, permanent ground displacement of order of several meters took place at many places in Niigata City at the 1964 Niigata Earthquake. It is important to predict these liquefaction-induced large ground displacements because wide area of ground, sometimes several hundreds meters of width, moves in the same way even if the ground surface is flat in engineering sense. Several research studies have been carried out to clarify the mechanism of them<sup>3)4)</sup>, but do not seem to succeed completely.

In the case of a level ground, the direction and the magnitude of the displacements are predominantly controlled by the direction and magnitude of the earthquake motion. From the site investigation, however, the directions of the permanent displacements seem to depend mainly on the geological and topographical conditions even if the ground surface is nearly horizontal. In other wards, earthquake load works to trigger liquefaction, but hardly control the magnitude and direction of large ground displacements. It may be reasonable because shear wave, which causes horizontal displacements, hardly propagate through the liquefied layer when liquefied layer behaves like liquid.

In this paper a new method is proposed to predict permanent ground displacements removing the effect of the earthquake motion.

## METHOD OF ANALYSIS

The following assumptions are used in the present analysis to remove the effect of the earthquake motion.

- 1) Undrained condition holds.
- 2) The decrease of the effective confining pressure,  $d\sigma'_m$ , is expressed using the loading parameter  $\lambda$  as

$$d\sigma'_m = \lambda k \sigma'_{m0} \quad (1)$$

where  $\sigma'_{m0}$  denotes initial effective confining pressure and  $k$  denotes the ratio of the maximum decrease of effective confining pressure to  $\sigma'_{m0}$ . Maximum porewater pressure generation at each element can be controlled by changing the value of  $k$  in each element. The value of  $\lambda$  increases from 0 to 1. When  $k = 1$ ,  $\lambda$  denotes the ratio of the decrease of the effective

confining pressure to  $\sigma'_{m0}$ .

Basic relationships for a porous saturated material used in the analysis are as follows:

(1) Constitutive equation of soil skeleton

$$\{d\sigma'\} = [D](\{d\epsilon\} - \{d\epsilon_d\}) \quad (2)$$

where  $\{d\sigma'\}$  denotes effective stress increment vector,  $[D]$  denotes tangent modulus matrix,  $\{d\epsilon\}$  denotes (engineering) strain increment, and  $\{d\epsilon_d\}$  denotes components of volumetric strain increment,  $d\epsilon_{vd}$ , due to dilatancy. Tangent modulus matrix  $[D]$  in Eq. 2 is computed by using incremental elastic relation on the elastic volume change behavior and hyperbolic equation on the shear deformation.

(2) Mass balance equation under undrained condition

$$\{m\}^T \{d\epsilon\} - n dp / K_w = 0 \quad (3)$$

where  $\{m\}^T = \{1 \ 1 \ 1 \ 0 \ 0 \ 0\}$ ,  $n$  denotes porosity,  $dp$  denotes excess porewater pressure increment, and  $K_w$  denotes bulk modulus of water.

(3) Definition of effective stresses

$$\{d\sigma\} = \{d\sigma'\} + \{m\}dp \quad (4)$$

where  $\{d\sigma\}$  denotes total stress increment.

Stress-strain relationship under the undrained condition is obtained by eliminating excess porewater pressure and effective stresses from Eqs. 2-4 as

$$\{d\sigma\} = [D](\{d\epsilon\} - \{m_d\}d\epsilon_{vd}) + \{m\}\{m\}^T \{d\epsilon\} K_w / n \quad (5)$$

where  $\{m_d\} = \{d\epsilon_d\}/d\epsilon_{vd}$  is a vector which determine the distribution of volumetric strain into each normal component. Zienkiewicz et al<sup>5)</sup> assumed that volumetric strain takes place homogeneously, hence  $\{m_d\} = \{m\}/3$ . However, it is obvious that  $\{m_d\}$  depends on the boundary conditions especially when lateral displacement are constrained. In the present analysis, therefore,  $\{m_d\}$  is calculated as the ratio of the normal strains obtained by the analysis done preceding the nonlinear incremental analysis in which excess porewater pressure is assumed to develop in only the referent element.

Finite element formulation using Eq. 5 is obtained by the ordinary method, which leads

$$[K]\{du\} = \{E_d\}d\epsilon_{vd} \quad (6)$$

where  $\{du\}$  denotes nodal displacement and

$$[K] = \int_v [B]^T ([D] + \{m\}\{m\}^T K_w / n) [B] dv \quad (7)$$

$$\{E_d\} = \int_v [B]^T [D] \{m_d\} dv \quad (8)$$

in which [B] denotes strain-displacement matrix.

In this analysis, apparent Poisson's ratio becomes nearly 0.5 because bulk modulus of water is usually much larger than shear modulus and because shear modulus becomes very small at large strains, in which case much error may occur to compute Eq. 7 if ordinary Gauss integration is used. So as to avoid these problems, one point Gauss integration is used to compute Eq. 7.

The use of the one point Gauss integration, however, may cause another problem, hourglass mode deformation. It is because the stiffness matrix is singular with respect to the hourglass patterns and is non-singular only with respect to the constant strain modes. Anti-hourglass matrix is employed in addition to the stiffness matrix in Eq. 7 to constraint hourglass mode deformation.

Flanagan et al<sup>6)</sup> showed that for the 2-dimensional quadrilateral element a shape function  $\{\gamma\}$  defined as

$$\{\gamma\} = \{h\} - (\{h\}^T \{x\} \{b_x\} + \{h\}^T \{y\} \{b_y\}) / A \quad (9)$$

is perpendicular to both rigid body motion and constant strain modes. Here  $\{h\}^T = \{1 \ -1 \ 1 \ -1\}$  is hourglass base vector,  $\{x\}$  and  $\{y\}$  are nodal coordinate vectors whose components are represented as  $x_i$  and  $y_i$ , A denotes cross sectional area, and

$$\begin{aligned} \{b_x\}^T &= \{y_{24} \ y_{31} \ y_{42} \ y_{13}\} \\ \{b_y\}^T &= \{x_{42} \ x_{13} \ x_{24} \ x_{31}\} \end{aligned} \quad (10)$$

$$x_{ij} = x_i - x_j \quad y_{ij} = y_i - y_j$$

By the use of the above shape function, the relationship between the nodal force increment corresponding the hourglass deformation,  $\{df_H\}$ , and nodal displacement increment  $\{du\} = \{du_x \ du_y\}^T$  is expressed as

$$\{df_H\} = \begin{bmatrix} \{\gamma\} c_x \{\gamma\}^T & 0 \\ 0 & \{\gamma\} c_y \{\gamma\}^T \end{bmatrix} \begin{Bmatrix} du_x \\ du_y \end{Bmatrix} \quad (11)$$

Anti-hourglass matrix is the coefficient matrix of the right hand side of Eq. 11 and is added to the stiffness matrix in Eq. 7. The coefficients  $c_x$  and  $c_y$  can take arbitrary value. For the rectangular element they are frequently determined so as to coincide with the bending rigidity<sup>7)</sup>. In the case of quadrilateral element the computation of exact bending rigidity is difficult, so here approximate value is used;  $c_x$  and  $c_y$  are calculated as

$$c_x = ER/12, \quad c_y = E/(12R) \quad (12)$$

$$R = \sqrt{(\{b_x\}^T \{b_x\} / \{b_y\}^T \{b_y\})}$$



$$E = 4G(4B+G)/(3K+4G) \text{ for plane strain condition}$$

where B and G are tangent bulk modulus and tangent shear modulus, respectively. In the case of the rectangular element computed anti-hourglass matrix is equivalent with the bending rigidity.

The value of the volumetric strain increment,  $d\epsilon_{vd}$ , is to be specified through the loading condition. However, it cannot be obtained explicitly from the loading parameter  $\lambda$  because total strain changes when excess porewater pressure generates. In the present analysis,  $d\epsilon_{vd}$  is approximately estimated by dividing the specified change of effective confining pressure by the bulk modulus. Therefore the resulting stress states at each incremental analysis do not exactly coincide with the stress state given by Eq. 1, but the difference can be made small by using small increment.

If the effective confining pressure reduces to almost zero, shear modulus also becomes nearly zero. Vertical displacement will become infinitely large under these conditions if small deformation theory is used. It is necessary to satisfy the equilibrium condition after deformation to get reasonable order of displacements. Updated Lagrange concepts or moving coordinate concept is employed in the present analysis. Additional matrices such as geometrical matrix are required in Eq. 6 based on the updated Lagrange formulation. These terms are considered in the iterative procedure to satisfy the equilibrium condition after deformation. The procedure in each incremental analysis is as follows:

- 1) Compute displacement increment by solving Eq. 6.
- 2) Change nodal coordinate and compute unbalanced nodal force, i.e., the difference between the nodal load due to its own weight and nodal force equivalent to total stress based on the deformed shape.
- 3) If unbalanced nodal forces are not negligible, then they are applied as load instead of the right hand side term of Eq. 6, and go to 2).

#### PARAMETRIC STUDY AND DISCUSSIONS

Hamada et al showed<sup>2)</sup> three types of the permanent ground displacement shown in Fig. 1. Among them, type C, the case that lower boundary of the liquefied layer inclines and ground surface is nearly flat, seems the most difficult to explain, so this case is selected to be examined as examples.

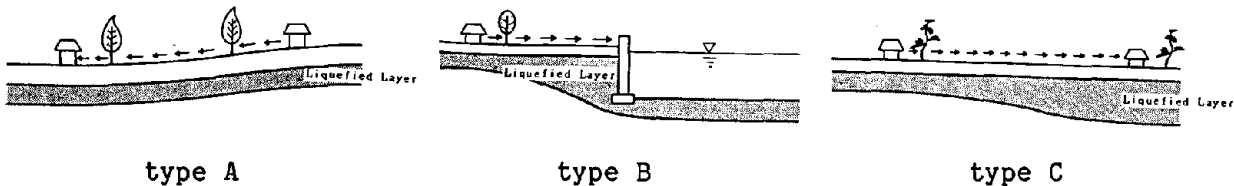


Fig. 1 Types of the permanent ground displacement

A 2-layered ground shown in Fig. 2 is used in the parametric study. The upper layer, shadowed portion in Fig. 2, is supposed to be a liquefied layer ( $k=1$ ), and the lower layer is supposed to be an unliquefied layer ( $k=0$ ). The width of the model is 100 meters and the average thicknesses of the upper and lower layers are 10 m and 3.5 m, respectively. Horizontal displacements are constrained at both end, and both horizontal and vertical displacements are constrained at the bottom of the model. The displacement at the point A in Fig. 2 which locates near the center of the ground surface is used as an index of the magnitude of the ground deformations in the following, hence is simply called the displacement at the center of the ground surface.

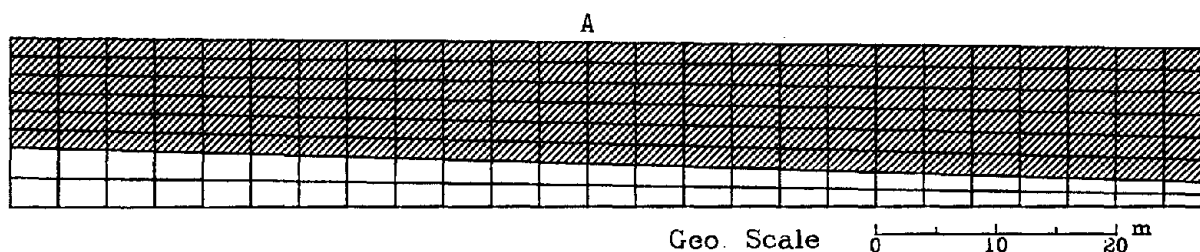


Fig. 2 Model ground and finite element mesh

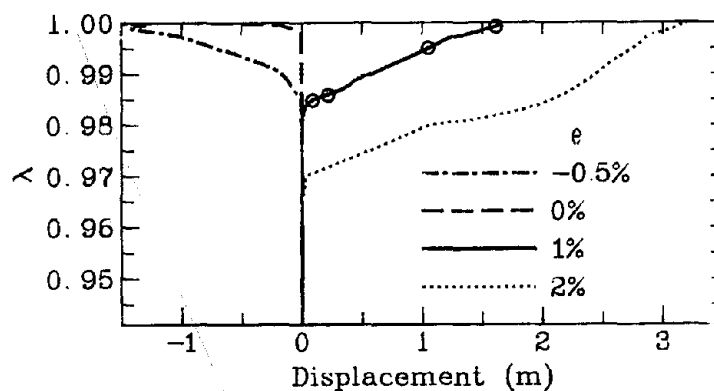


Fig. 3 Effect of the slope angle on the horizontal displacement at the center of the ground surface

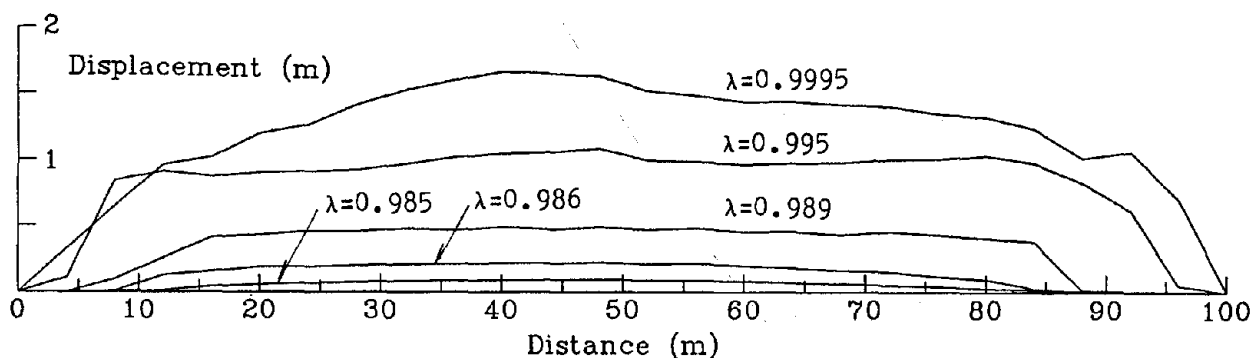


Fig. 4 Horizontal displacement along the ground surface (standard model)

Initial stresses are computed by the self weight analysis. The slope angle of ground surface,  $\theta$ , and the slope angle of the lower boundary of the liquefied layer,  $\phi$ , are taken as parameters keeping the average thickness constant. The value of the slope angles  $\theta$  and  $\phi$  of the standard model ground are 1% and 3%, and one of them are changed in the parametric study hereafter.

First, the behavior of the standard model,  $\theta=1\%$  and  $\phi=3\%$ , is investigated. The change of the horizontal displacement at the center of the ground surface against the decrease of the effective confining pressure is shown in Fig. 3 as solid line. It hardly changed until  $\lambda$  exceeds 0.98 ( $\sigma'_m=0.02\sigma'_{m0}$ ) and then it increases nearly proportional to the decrease of the effective confining pressure. It becomes 1.64m when  $\lambda=0.9995$  and hold until the last step of the analysis,  $\lambda=0.99999$ . Figure 4 shows displacement patterns at a few loading steps which are shown by circles in Fig. 3 (Note that the scales are different in each figure). Figure 5 shows horizontal displacement distribution at the ground surface. The portion where large deformations occurs appears near the center of the ground surface at first and expands toward both end according the the decrease of the effective confining pressure. The ground at the left hand side of the largely deformed area settles and that at the right hand side lifts, hence the ground surface gradually becomes horizontal. Since constraints against lateral deformation are weaker at the center than at the end, center portion yields earlier than the end, which is the reason why large deformation portion appears at the center first. However, yielding of an element does not directly result in the large deformation; the deformation is small if displacement is constrained by the surrounding elements. Therefore appearance of the large deformation portion is delayed from the yielding of the element.

Figure 3 compares horizontal displacements at the center of the ground surface when the slope angle of ground changes. In the case that  $\phi = 2\%$ , 1% larger than the standard model, displacements begin to increase earlier than the standard model and the magnitude is larger than that. Large displacement hardly occurs when  $\theta = 0\%$ , i.e., horizontal ground surface, but at very low effective stresses the ground surface moves toward the opposite direction to the standard model. Figure 6 shows displacement pattern at this state. Only the elements at the ground surface exhibit large deformation in this case. In the case that  $\theta = -0.5\%$ , the displacements begin to increase in an earlier stage than the case of horizontal ground surface and the direction is opposite to the one of the standard model. As shown, the slope angle of the ground surface has significant effect of the direction and the magnitude of the permanent ground displacements. As the slope angle increase, large displacement takes place earlier and the magnitude becomes larger.

Next, parametric study changing the slope angle of the lower boundary of the liquefied layer is performed. Figure 7 shows the relationships between the horizontal displacement at the center of the ground surface and loading parameter. Large ground displacement appears at almost same time regardless the slope angle of the lower boundary of the liquefied layer. The rates of the increase of the horizontal displacements are different depending on the slope angle; the rate is larger as the value of the slope angle of the lower boundary of the liquefied layer decreases. Figure 8 compares displacement patterns of the model grounds with  $\phi=1\%$  and  $-1\%$ . It is recognized that

displacement patterns are different a little to each other, which result in the difference of the rate of the increase of the displacement.

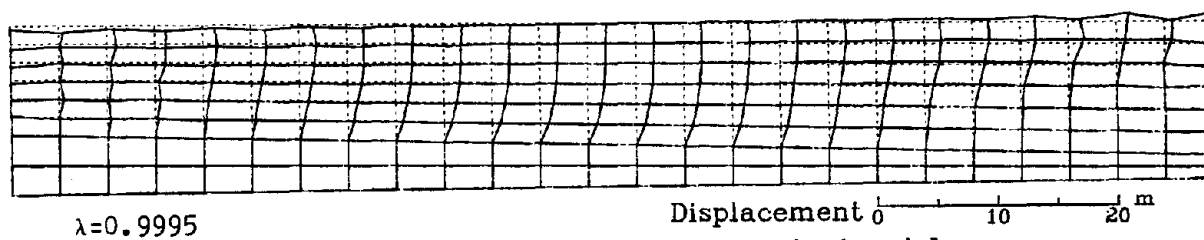
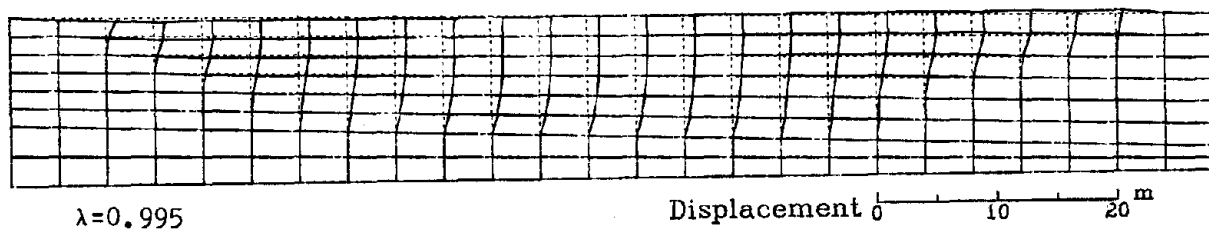
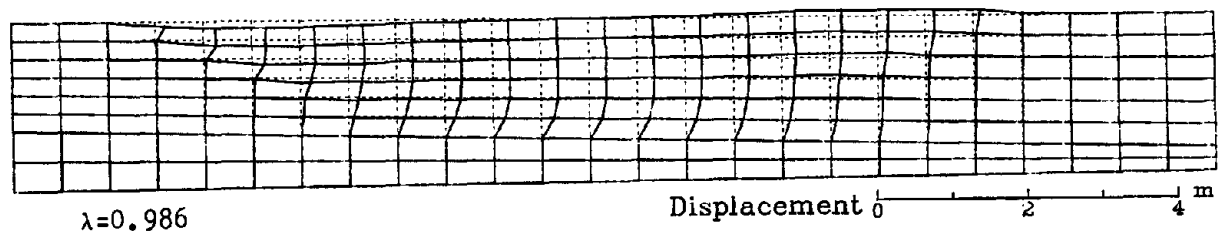
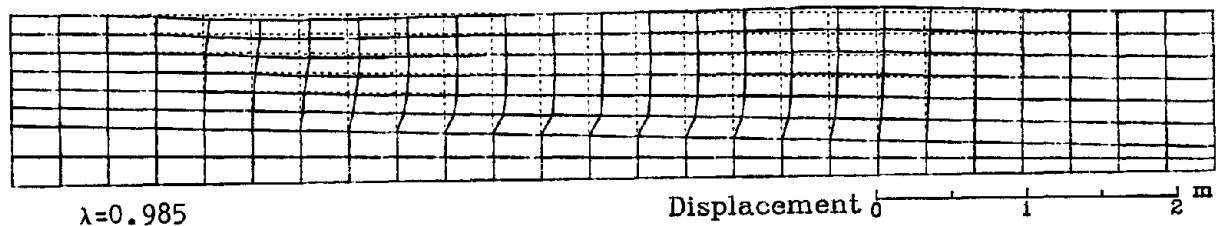


Fig. 5 Deformed shape of the standard model

Geo. Scale 0 10 20 m

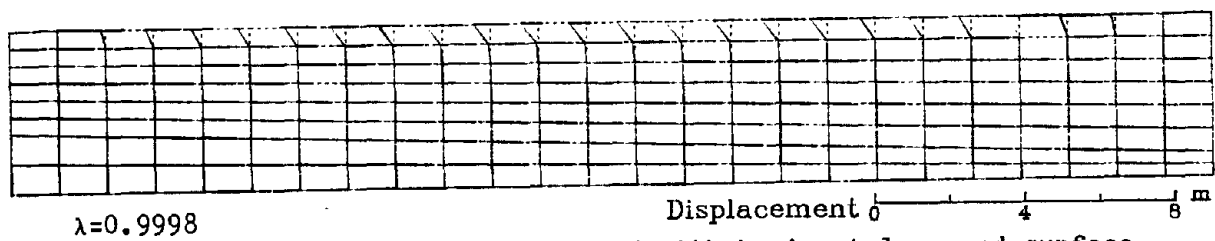


Fig. 6 Deformed shape of the ground with horizontal ground surface

Lastly, standard ground is analyzed using different finite element mesh. Each layers are equally divided to make the finite element meshes used in the previous analyses, but the shape of the elements of above three layers are parallelogram in the new mesh as shown in Fig. 9. Figure 10 compares

horizontal displacement at the center of the ground (anti-hourglass matrix is not used in this case). The behaviors are, in general, similar to each other, but magnitude of the displacement is a little different. This difference is supposed to be the result of the error in finite element calculation; the mesh size may be too large.

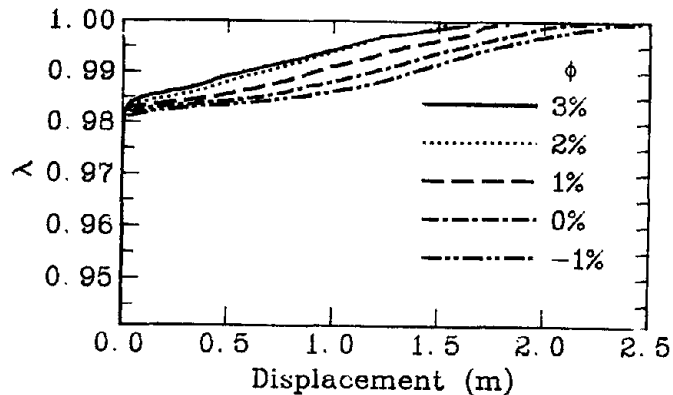


Fig. 7 Effect of the slope of the lower boundary of the liquefied layer on the horizontal displacement at the center of the ground surface

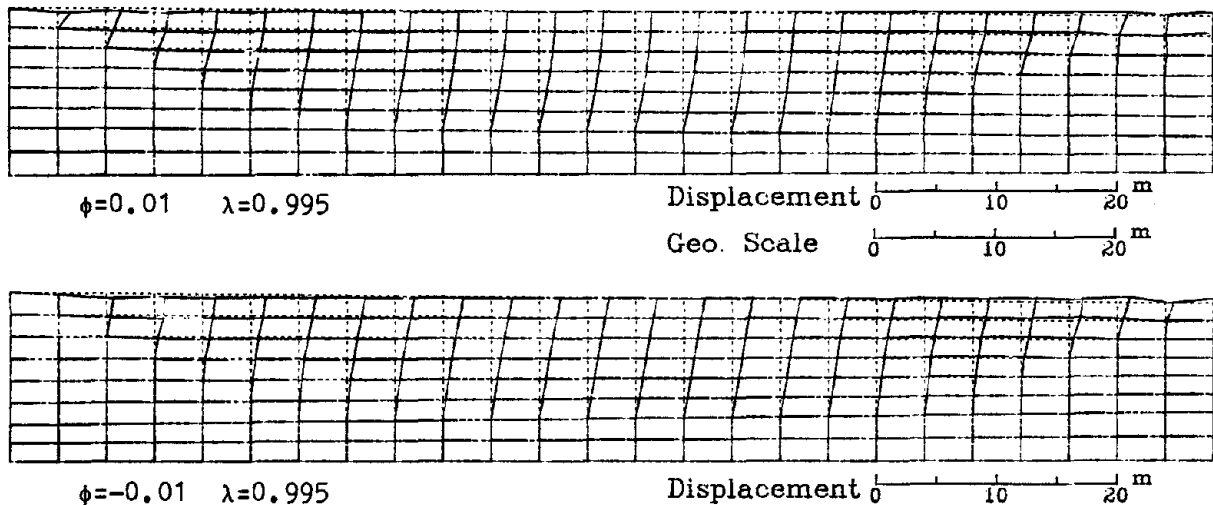


Fig. 8 Deformed shape of the ground ( $\theta=0.01$ )

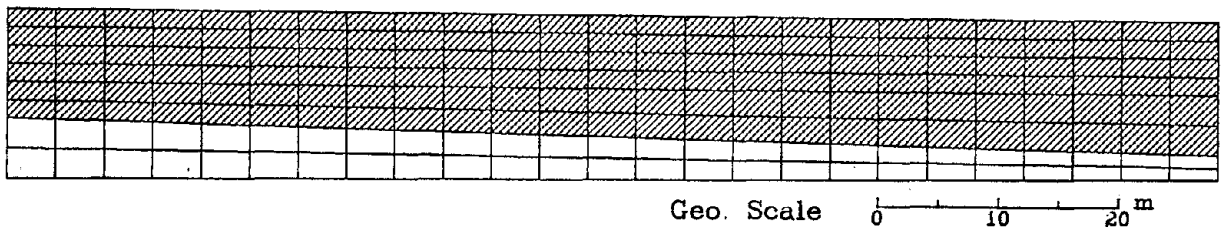


Fig. 9 New finite element mesh for standard model ground

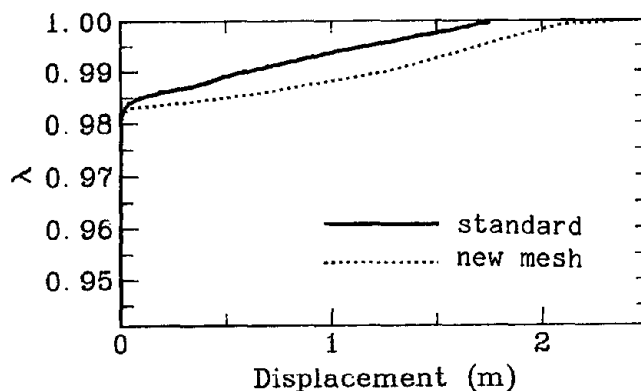


Fig. 10 Effect of mesh division on the permanent displacement

#### CONCLUDING REMARKS

A method to calculate liquefaction induced permanent ground displacement is proposed. General behavior of the ground when effective confining pressure decreases due to liquefaction is explained through the numerical examples. However, The analysis is very sensitive as can be seen, for example, as small disturbances of the displacement patterns at the end of the model in several figures. The difference of the mesh division may cause not a small difference of the displacements at low effective confining pressure. Therefore it may be difficult to predict the exact value of the permanent ground displacement without special case, but reasonable order of the displacement is obtained relatively easily.

Through the parametric study of the 2-layered ground, following conclusions are obtained:

- 1) Large permanent ground displacement occurs even if ground surface is nearly horizontal when liquefaction takes place in wide area.
- 2) Large ground displacements begin to appear at the same time regardless of the slope of the lower boundary of the liquefied layer if the slope angles of the ground surface are the same. As the slope of the ground becomes larger, large displacement portion appears earlier and the magnitude of the displacement becomes larger.
- 3) The slope angle of the lower boundary of the liquefied layer affects the deformation pattern, hence final displacements.

#### REFERENCES

- 1) Hamada, M., Yasuda, S., Isoyama, R. and Emoto, K: Observation of Permanent Ground Displacements Induced by Soil Liquefaction, Proc. JSCE, No.336/III-6, pp.211-220, Dec., 1986 (in Japanese)
- 2) Hamada, M., Yasuda, S., Isoyama, R. and Emoto, K: Study on Liquefaction Induced Permanent Ground Displacements, Report, Association for the Development of Earthquake Prediction, Nov., 1986
- 3) Yoshida, N., Numerical Analysis on Liquefaction Induced Ground Displacement -Summary of the work by the working group in Japan-, Abstract, First Japan-US Workshop on Liquefaction, Large Ground Deformation and Their Effects on Lifeline Facilities, Nov. 1988

- 4) Report on the studies on Ground Deformation and Damage of Underground Structures due to Earthquake, Association for the Development of Earthquake Prediction, 1989 (in Japanese)
- 5) Zienkiewicz, O.C., Leung, K.H., Hinton, E., and Chang, C.T., Liquefaction and Permanent Deformation under Dynamic Conditions—Numerical Solution and Constitutive Relations, Chapter 5, Soil Mechanics and Cyclic Loads, G.N.Pande and O.C.Zienkiewicz ed., John Wiley & Sons, 1982
- 6) Flanagan, D.P. and Belytschko, T., A Uniform Strain Hexahedron and Quadrilateral with Orthogonal Hourglass Control, International Journal for Numerical Methods in Engineering, Vol. 17, pp.679-706, 1981
- 7) Kosloff, D. and Grazier, G.A., Treatment of Hourglass Patterns in Low Order Finite Element Codes, International Journal for Numerical and Analytical Methods in Geomechanics, Vol. 2, pp.57-72, 1978

# CENTRIFUGE MODELING OF LARGE GROUND MOTIONS AND THEIR EFFECTS ON STRUCTURES

R. S. Steedman

Cambridge University Engineering Department,  
Trumpington Street, Cambridge CB2 1PZ, UK

## ABSTRACT

Physical modeling of soil-structure interaction under earthquake loading in a geotechnical centrifuge has advanced to a stage where specific design problems can be addressed. The paper discusses the data of centrifuge model tests showing the onset of softening, large ground motions and liquefaction observed around a long anchored quay wall which led to the failure of the structure. This class of failure, similar to that observed at Akita Port during the Nihonkai-Chubu earthquake of 1983, is explained and the sequence of events described. Analysis of the soil-structure system shows how the high overall stiffness of long structures embedded in the ground deteriorates in the presence of high excess pore pressures and this leads to dynamic effects and failure coincident with, rather than as a result of, liquefaction around the structure. The effects of pore pressure migration are considered and the implications for the physical modeling of field problems subject to earthquake loading are discussed.

## INTRODUCTION

There has been a great deal of attention in recent years focused on the physical modeling of soil-structure interaction and of pore pressure generation and liquefaction phenomena. In part this has arisen from a dissatisfaction with other approaches and with the lack of high quality field data. Improvements in data acquisition techniques, digital signal processing and miniature instrumentation have permitted a rapid and widespread growth in the use of small scale physical models as a tool to study the earthquake response of geotechnical structures.

Centrifuge models in particular have demonstrated repeatedly that the physical model has a vital role not just in the field of research but as a tool for designers and engineers in the field. Geotechnical centrifuges are being installed and commissioned worldwide and there is a growing



trend for the development of such facilities in the commercial sector as well as in Universities and research establishments. The centrifuge is on the point of emerging from the research and academic community into the harsh spotlight of industrial application. Such a transition is now inevitable; many organisations have already recognised the value of direct physical modeling to improve their database, to validate their calculations or to reduce their requirements for expensive field testing. These new developments place heavy demands on the research community who must now reach conclusions on what is and what is not established practice.

## PHYSICAL MODELING

One of the primary difficulties in the construction of models at 1g is to make allowance for the enhanced tendency for an aggregate of interlocking particles to dilate at low stress levels. The strength of the aggregate, expressed as  $\tan \phi'$  where  $\phi'$  is the angle of shearing resistance, is primarily a function of friction and interlocking between the particles. To a first approximation a relatively loose sand body might be used to model a dense sand in the prototype, for example, and adapting an empirical relationship between relative density and  $\tan \phi'$ , Bolton (1986), it is possible to arrive at a relationship between the relative density required in the 1g model and that in the prototype

$$I_{DM}(10 - \ln \frac{p'}{N}) = I_{DP}(10 - \ln p') \quad (1)$$

where  $I_{DM}$ ,  $I_{DP}$  are the relative densities of the model and prototype respectively,  $N$  is the model scale and  $p'$  the mean effective confining pressure in a region of the prototype. Relative density is defined as  $I_D = (V_{max} - V)/(V_{max} - V_{min})$ , where  $V = 1+e$  is the Specific Volume and  $e$  the void ratio.  $V_{max}$  and  $V_{min}$  correspond to the maximum and minimum void ratios achievable in a quick tilt test or by vibratory compaction. Fig. 1 shows this relationship for different values of  $p'$  reproduced from Schofield and Steedman (1988). Consider, for example, a 1g shaking table test of a soil body with a layer of sand in the model at a relative density of  $I_{DM} = 0.6 I_{DP}$ . If the model layer was at a mean effective stress of 2.5 kPa when tested, then its peak strength would be equivalent at scale  $N = 40$  to a dense sand in the prototype under  $p' = 100$  kPa. However, it would clearly be necessary in the 1g model to vary the density of the sand throughout the model to achieve the necessary range of peak strength varying with depth and structural interaction from a footing or retaining wall for example.

Iai (1989), in a comprehensive discussion of the scaling of 1g model tests, shows that it is possible to arrive at internally consistent scales for most of the parameters of interest and it is concluded that provided the soil is limited to small strains and low stress ratios useful predictions of deformations may be made using 1g models.

However, the mobilisation of strength in a cohesionless aggregate is not simply a function of friction and interlocking. At very low stress levels grain crushing is usually assumed to be insignificant but even at moderate stress levels crushing of particle asperities contributes to a highly non-linear relationship for stress-strain relationships as a function of confining pressure. The 1g scaling laws show that for the same soil in model and prototype, strain is predicted to scale as the square root of the difference in mean effective confining pressure - a unique function. If this were the case in practice then a low stress triaxial test could be used as a scale model of a high stress triaxial test and strains would scale accordingly. Even at low stress ratios this is clearly not the case. The use of a 1g model to predict deformation or strain will then be subject to an increasing error as the effective confining pressure in the prototype increases and the actual strains deviate further from the scaled prediction. Specifying the maximum acceptable error could be looked upon as providing an upper limit to the application of the 1g model. The error would vary for different sands depending on its crushing strength and angularity and each sand used in a 1g model would require careful qualification to evaluate the error before useful tests could be carried out.

The 1g model therefore has an application to study field problems under very low prototype effective confining pressures and subject to small strains. The versatility of the shaking table in multi-axis shaking and control under feedback is a valuable asset which should not be neglected. It is likely that the 1g shaking table could be most usefully applied to investigate initial mode shapes and fundamental frequencies for small field structures. This would assist the preparation of centrifuge model tests which would study the development of excess pore pressures, the build-up of strain and the degradation of stiffness and strength.

The data of the centrifuge model tests of saturated soil-structure interaction have shown clearly that the degradation of stiffness through pore pressure build-up and strain-softening leads to a transition from an initially stiff system generally with a high natural frequency to a much more flexible system with a considerably reduced fundamental frequency. If the softened system has a fundamental frequency below the driving frequency of the earthquake or base shaking, then phase shifts and large amplification of response are observed.

The second feature of the centrifuge model test data which is apparent is the important role that pore pressure migration during shaking plays in the response of the system. This is readily understood by considering the 1-dimensional problem of the liquefaction of a level bed or a column of loose sand. The liquefaction of a column of sand requires the downward propagation of a liquefaction 'front' and is followed by the upward propagation of a solidification 'front' as the liquefied soil consolidates from the base upwards, Scott (1986). The advance of the liquefaction front is associated with the rate of settlement of the sand column which is increasing from zero at the base to a maximum at the surface. In a saturated column the maximum rate of

settlement is limited and equal to the settling velocity of hydraulic fill ie. the terminal velocity of the mass of particles, Schofield (1981) Scott (1986). Once the rate of settlement at the surface equals the maximum the grains near the surface become fluidised. As shaking progresses the liquefaction front advances downwards. An upward hydraulic gradient is established. There is clear experimental evidence for such a development of excess pore pressure with depth from centrifuge model tests such as those reported by Heidari and James (1982) and shown in Fig. 2.

A particle with a specific gravity of 2.65 'in suspension' in a fluid of specific gravity 1.0 will accelerate downwards until it reaches its terminal velocity. If it appears stationary in space the fluid must be moving upwards with a velocity equal to the terminal velocity of the particle. In either case there must be a movement of fluid past the particle. It is therefore a necessary condition that seepage is taking place for a zone of liquefied material to exist in equilibrium in an acceleration field.

The speed of a compression wave in water is 1500 m/s which is therefore the velocity at which a pressure wave can propagate from one region of the ground to another. In a typical geotechnical structure distances of less than 30 m may separate regions which are under high stress ratio and supporting structural loads from regions which are, for example, compressing and generating large excess pore pressures. Information about high excess pore pressure in one region may be transmitted to another region practically instantaneously; for this example the distance of 30 m would be covered in only 20 ms. This is then the speed at which a hydraulic gradient may be established and excess pressure from one region supplied to another, perhaps a region which is sustaining structural loads.

#### **THE ONSET OF FAILURE IN A LONG ANCHORED WALL (ZENG X. (1989))**

The significance of such a model for the migration of excess pore pressures during shaking and the subsequent softening and deterioration of structural integrity can best be appreciated by an example. Fig. 3(a) shows a typical cross-section through such an anchored wall and Fig. 3(b) shows a simple mechanical idealisation of the soil-structure system as a cantilever subject to an outward pressure and restrained by a spring (representing the anchor) of a finite stiffness  $K_a$ . The natural frequency of such a system is straightforward to determine using an energy method by assuming a distribution of earth pressure and hence deflection. A fixed restraint has been assumed for simplicity at the base. The passive pressure has been neglected because its effect on the natural frequency is small.

A straightforward expression for the anchor force in terms of the stiffness of the wall and the anchor may be deduced by considering compatibility at the anchor position, Steedman and Zeng (1989a). This gives

$$F_a = \frac{q_0 \left( \frac{H_0^4}{30} - \frac{aH_0^3}{24} + \frac{a^5}{120 H_0} \right)}{\frac{EI}{Ka} + \frac{(H_0 - a)^3}{3}} \quad (2)$$

where  $F_a$  is the force in the anchor,  $q_0$  the maximum outward pressure at  $y = H_0$  and  $EI$  is the bending stiffness of the wall. Solving for  $F_a$  in equation 2 shows a clear dependance on the relative stiffness of the anchor system. For the case of a rigid anchor  $Ka \rightarrow \infty$  and  $EI/Ka \rightarrow 0$ .

In the case of a failed anchor, the stiffness of the anchor might be considered to have greatly reduced, and clearly letting  $Ka \rightarrow 0$  the anchor force  $F_a \rightarrow 0$  reducing the problem to a simple cantilever. These two extremes provide an upper and lower bound on the anchor force and natural frequency of the structure. Assuming the displacement of the wall is given by  $u = \delta(y) \sin \omega t$ , where  $\delta(y)$  is the assumed deflection profile of the wall, then equating maximum kinetic and potential energies leads to an expression for the natural frequency  $f_n$  as a function of the bending stiffness  $EI$ , the mass per unit height  $m$ , the total height of the wall  $H_0$ , the depth to the anchor  $a$  and the stiffness of the anchor system  $Ka$ .

In the case of a rigid anchor system, the depth of the anchor  $a$  is a key factor. Figs. 4 and 5 show the variation of the natural frequency of the anchor wall model, the maximum bending moment in the wall and the tie force for different anchor positions. It is clear that the ideal depth for the anchor is around  $0.4 H_0$  for the anchored wall models in the test programme, which gives the maximum reserve of natural frequency against the possibility of resonance while the bending moment and tie force are not very high.

Typically the depth of the anchor in the centrifuge model tests was  $a = H_0/6$  and for the rigid anchor case

$$\omega_n = \frac{21.70}{H^2} \sqrt{\frac{EI}{m}} \quad (3)$$

Substituting the appropriate values for the model ZENG8 leads to  $f_n = 578$  Hz, Steedman and Zeng (1989a). Depending on the stiffness of the anchor system the natural frequency of the wall will be less than this, reducing to a minimum in the case of a completely failed anchor system with  $f_n = 97$  Hz (a cantilever wall).

The stiffness of the anchored wall may be estimated using dimensional analysis by analogy with the stiffness of a strip footing bearing on an elastic foundation. This can be expressed in terms of the shear modulus of the soil  $G$ . The maximum value for shear modulus (sometimes referred to as the resilient modulus  $G_{\max}$ ) is commonly expressed as a function of the square root of the mean confining pressure  $p'$  following Hardin and Drnevich (1972) and Drnevich (1975). The tangent shear modulus at any instant will determine the current stiffness of the anchor and this may be estimated using a hyperbolic model for the stress-strain equation of the sand. The tangent shear modulus  $G_t$  is then

$$G_t = \frac{d\tau}{d\gamma} = G_{\max} \left(1 - \frac{\tau}{\tau_{\max}}\right)^2 \quad (4)$$

where  $\tau$  is the current shear stress and  $\tau_{\max}$  the shear stress at failure. The initial stress state in front of the wall can be estimated and the effects of a pseudo-static lateral acceleration field imposing a shear stress increment on a horizontal plane, or of a pore pressure increment or both, can be incorporated in a straightforward manner, Steedman and Zeng (1989a). This allows the natural frequency of the soil-wall system to be calculated as a function of excess pore pressure in front of the anchor wall, as shown in Fig. 6.

For low levels of excess pore pressure the natural frequency  $f_n$  is about 4.5 times higher than the base shaking frequency  $f_e$  and there is only a slow reduction in the natural frequency for a further increment of pore pressure. The magnitude of shaking of the wall model should be small and this agrees with experimental results.

Contrast for example the data of model test ZENG8 in Fig. 7 where Earthquake 3 shows small amplitude cycles of bending moment response at mid-height on the wall but Earthquake 7 on the same model shows very large amplitude shaking although the input base shaking has only been moderately increased.

This model was tested at 80g with a retained height of 90mm, a penetration of 30mm and a wall stiffness  $EI = 20.4 \text{ Nm}$ . The soil in model ZENG8 was a fine Leighton-Buzzard 52/100 sand with a nominal particle size of 0.225 mm placed at a void ratio of 0.705 corresponding to a relative density of 65%. The sand was saturated with silicon oil of 80cS viscosity (80 times the viscosity of water) and the phreatic surface was at the top of the wall. The use of silicon oil as a pore fluid is to bring together the time scales governing the generation and the dissipation of pore pressure as both of these phenomena play an important role in the response of the system. The use of silicon oil as a pore fluid has been widely discussed and accepted, see for example Lee and Schofield (1988).

However in Earthquake 7 (Fig. 7), once the pore pressure buildup in front of the wall exceeded about 60% of the initial vertical effective stress, there a clear phase shift in the response of the wall vibration. Strong cyclic bending moments and tie forces were recorded with large outward displacements of the wall. The increase in shaking generated more excess pore pressure in the backfill, and the vibration of the wall is greatly amplified as resonance developed and the anchor wall approached failure. Cyclic bending moments during the earthquake were of the order of 15 times the peak values in previous earthquakes although the level of base shaking was only doubled. The phase of the wall vibration shifted by  $180^\circ$  as these large amplitude vibrations built up. Failure of the wall by gross outward movement was then inevitable because the model walls had a high reserve of plastic moment capacity against local failure in order to correctly scale the prototype bending stiffness - a parameter which has already been shown to be of great significance in the response of the soil-structure system. However, the observation of large increases in peak cyclic bending moments at around mid-height could explain the common observation of the local failure of sheet pile walls in bending such as happened in the Nihonkai-Chubu earthquake of 1983, Tohno and Shamoto (1985).

Liquefaction of the sand backfill was not the direct cause of failure of the retaining wall. Instead the degradation of stiffness of the soil and hence the fall in the natural frequency of the wall accelerated rapidly beyond a critical value of pore pressure generation which in this case was at around 60% of the vertical effective stress. Vibration of the retaining structure was greatly amplified causing larger cyclic strains in the backfill and therefore even higher excess pore pressures leading to the liquefaction of the upper layers of backfill and to failure of the structure.

Model ZENG8 failed with the wall moving seawards and the toe rotating out, Fig. 8, suggesting a loss of passive resistance. This would occur as the greatly increased cyclic moments in the wall exceeded the maximum available passive resistance. The phreatic surface in the model was at the top of the wall.

### THE MODELING OF LIQUEFACTION PHENOMENA

This example of the transition from a stiff soil-structure system to a flexible system exhibiting a dynamic response illustrates well the benefit to be gained from a model study. Based on the analysis of the deterioration of natural frequency with pore pressure generation, Fig. 6, it is clear that upto a certain level of excess pore pressure the system remains essentially stiff and capable of being analysed using pseudo-static calculations (which assume a rigid backfill and infinite shear wave velocity).

Beyond a certain point, however, the system exhibits a dramatic deterioration of stiffness and there is a transition to a dynamic problem which must be analysed using appropriate calculations.

For example Steedman and Zeng (1989b) describe how the Mononobe-Okabe analysis may be extended to allow for a finite wave speed and dynamic amplification. Such a calculation is termed pseudo-dynamic as it incorporates features of the dynamic problem such as the frequency of base shaking and the shear wave velocity but it avoids the rigour of a full dynamic analysis.

There have been many other examples of centrifuge model tests which have shown the significance of degradation of soil stiffness and pore pressure migration. Studies of the earthquake response of a stiff coastal dyke overlying discontinuous dense and loose sand layers showed clearly that large excess pore pressures generated by a compacting loose zone could transmit themselves to adjacent regions of dense material, Habibian (1987) Steedman and Habibian (1987). The distribution of miniature pore pressure transducers within the foundation of such a model enables sketches to be made at discrete time intervals of the development of excess pore pressure, expressed as a percentage of the initial vertical effective stress. Fig. 9 shows a 'snapshot' after roughly two cycles of base shaking of the distribution of excess pore pressure beneath a strong dyke. It is clear that this is not a 1-d problem and that there is an interaction between the distribution of excess pore pressure and the dyke response. In Fig. 9 the dyke is shown at an instant immediately before it becomes isolated from the foundation which then alters the dynamic response of the system. Regions which were carrying a shear load from the dyke were observed to become suddenly flooded and whatever cyclic mobility existed was almost instantaneously lost.

Lee and Schofield (1988) showed how the response of an embankment to base shaking could be interpreted using a 'dilation front' which propagates from the interior of the embankment in an alternating sequence within each cycle of the earthquake. The observation in the centrifuge model tests was of a pore pressure response consistent with a pattern of cyclic mobility with soil elements alternating between very low stress ratios and a fully softened condition and very high stress ratios and a stiff dilative response. This was revealed in the acceleration records by a 'spiky' response as the dilation front passed the transducer on each cycle. Fig. 10 shows this mechanism of dynamic response.

It is clear from each of these examples, each of a different boundary value problem, that in no sense can small elements in a cohesionless foundation be imagined as acting independently of one another. Using a mechanical analogy, feedback which can alter the system response is provided at the speed of a pressure wave in water which means almost instantaneously. Pore pressures can therefore migrate in the form of hydraulic gradients at the same speed. A cohesionless foundation will generate strength if it is sheared but the dynamic response of the system may not lead to the same distribution of shear stress which might be expected from a static calculation.

For example, an anchor wall which is generating a large passive resistance will be unloaded on each cycle of lateral shaking. This permits the pore pressures to rise rapidly, and the soil is alternately fully softened or dilating on each cycle. Clearly large deformations can build up by this mechanism even in a dense sand.

## CONCLUSIONS

1g models were discussed above and shown to have limited application to problems of low-stress and low-strain. In critical regions of the foundations of soil-structure systems however, the dynamic response has been shown to involve soil both in a fully fluidised condition and at a maximum stress ratio, often within the same cycle of base shaking. Problems which involve any significant degree of excess pore pressure rise are therefore impractical to model at 1g.

The centrifuge models described here greatly extend the capability of the modeler to present the whole range of dynamic behavior of soil-structure systems. The objectives of the modeler are to define the transition from small-strain to large-strain behavior, to describe the onset of failure and the modes of failure, and to show the limits within which calculation procedures are valid.

There are a growing number of centrifuge centres around the world which are capable of such model studies. These include Princeton, Colorado, Caltech, UC Davis, MIT, Cambridge University and shortly RPI. In Japan shaking tables have been mounted on geotechnical centrifuges including PWRI, PHRI, Tokyo Institute of Technology, DPRI, Kyoto and Utsunomiya Universities. Many different shaking systems, containment systems and model sizes are available.

The centrifuge model studies of field problems have shown that the influence of pore pressure migration and softening and degradation of soil stiffness has a marked effect on the dynamic response of soil-structure systems. Extrapolation from the response of an isolated element to the response of the system may omit global mechanisms of response for example the influence of high excess pore pressures from a compacting region on an adjacent zone under cyclic load. Correct model tests can provide the analyst and the designer with both a broad view of the structural response and also detailed pictures of the magnitude of bending moments or pore pressures at specific locations.

## ACKNOWLEDGEMENTS

The centrifuge model tests of the behaviour of quay walls subject to base shaking were accomplished with great skill by a research student, X Zeng, working under the supervision of



the author. The data of the response of coastal dykes came from the thesis of another of the author's students, A Habibian. Their contributions have been very significant.

## REFERENCES

- Bolton M D (1986). The strength and dilatancy of sands, *Geotechnique* 36, No. 2, pp175-195.
- Drnevich V P (1975). Constrained and shear moduli for finite elements, *JGE Div., ASCE*, No. GT5, pp459-473.
- Habibian A (1987). Seismic modelling of coastal dykes on layered sand foundations, PhD Thesis, Cambridge University.
- Hardin B O and Drnevich V P (1972). Shear modulus and damping in soils: design equations and curves, *JSMFE Div., ASCE*, No. SM7, pp667-692.
- Heidari M and James R G (1982). Centrifuge modelling of earthquake induced liquefaction in a column of sand, *Proc. Conf. SMEE*, Vol. 1, pp271-281, Southampton University.
- Iai S (1989). Similitude for shaking table tests on soil-structure-fluid model in 1g gravitational field, *Soils and Foundations, Jap.SSMFE*, Vol. 29, No. 1, pp105-118, March.
- Lee F H and Schofield A N (1988). Centrifuge modelling of sand embankments and islands in earthquakes, *Geotechnique* 38, No. 1, pp45-58.
- Steedman R S and Habibian A (1987). Modelling the failure of coastal dykes during earthquakes, *Proc. 9 ECSMFE*, Vol. 2, pp633-636, Dublin.
- Steedman R S and Zeng X (1989a). The seismic response of waterfront retaining walls, Report CUED/D-soils TR228, Cambridge Univ. (to be published ASCE Spec. Conf., Ithaca, 1990).
- Steedman R S and Zeng X (1989b). The influence of phase on the calculation of pseudo-static earth pressure on a retaining wall, Report CUED/D-soils TR222, Cambridge University (to be published *Geotechnique*).
- Schofield A N (1981). Dynamic and earthquake geotechnical centrifuge modelling, *Proc. Int. Conf. Recent Adv. Geotech. Earthquake Eng. Soil Dy.*, Univ. Missouri-Rolla, St Louis, April.
- Schofield A N and Steedman R S (1988). Recent development of dynamic model testing in geotechnical engineering, *Proc. 9 WCEE*, Vol. VIII, pp813-824, Tokyo-Kyoto, 2-9 August.
- Scott R F (1986). Solidification and consolidation of a liquefied sand column, *Soils and Foundations, Jap.SSMFE*, Vol. 26, No. 4, pp23-31, Dec.
- Tohno I and Shamoto Y (1985). Liquefaction damage to the ground during the 1983 Nihonkai-Chubu (Japan Sea) earthquake in Akita Prefecture, Tohoku, Japan, *Proc. Natural Disaster Science*, 7, No. 2, pp67-93.
- Zeng X (1989). Modelling the behaviour of quay walls in earthquakes, PhD Thesis in preparation, Cambridge University.

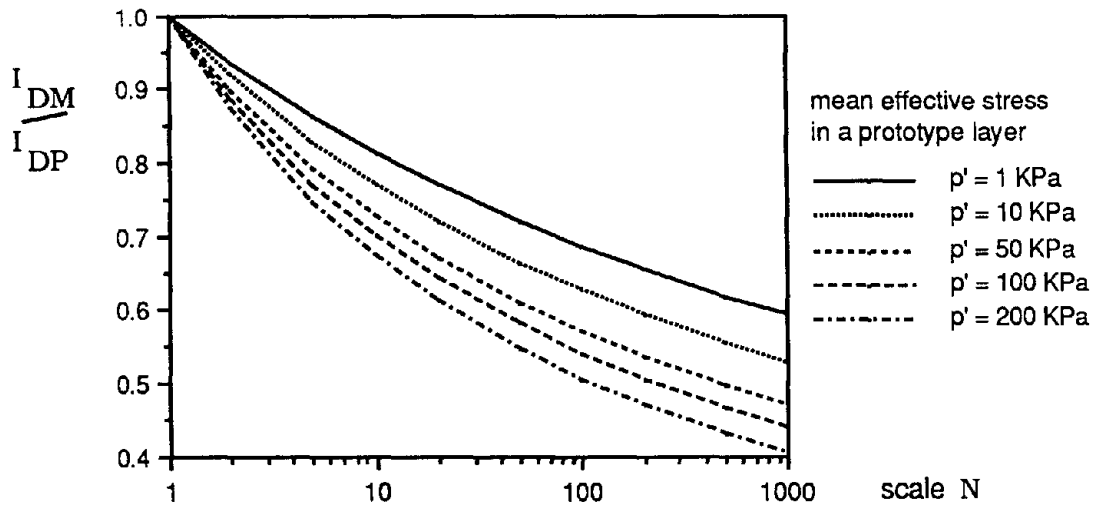


Fig. 1 Relative density as a function of scale and mean effective stress (after Schofield and Steedman)

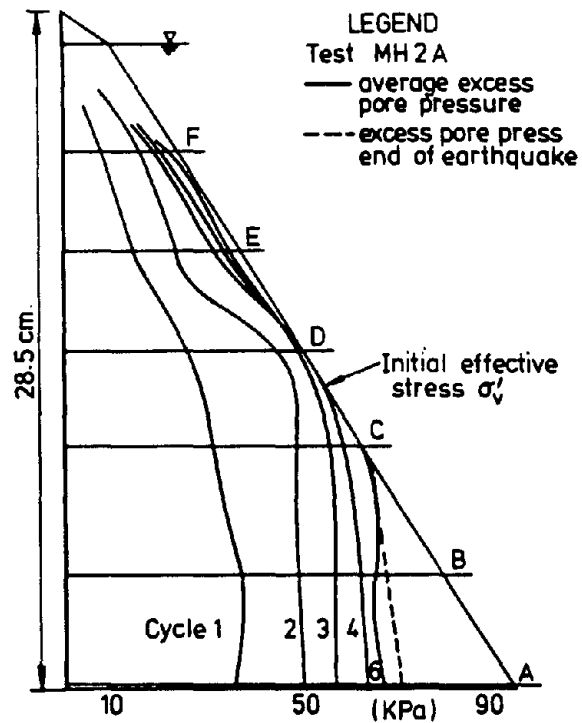


Fig. 2 The generation of excess pore pressure in a column of saturated sand at 35g (after Heidari and James)

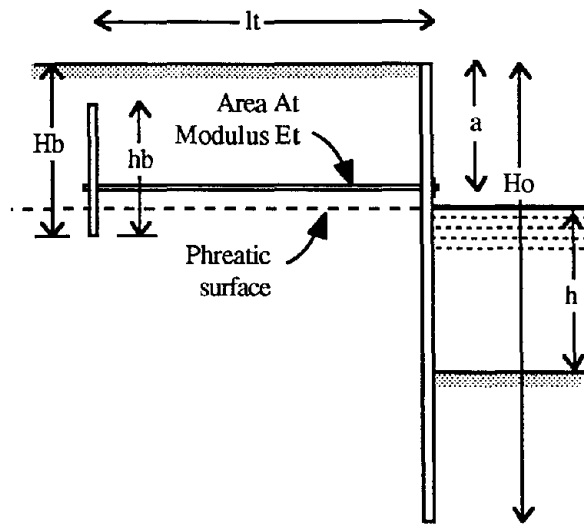


Fig. 3a Cross-section through an anchored quay wall

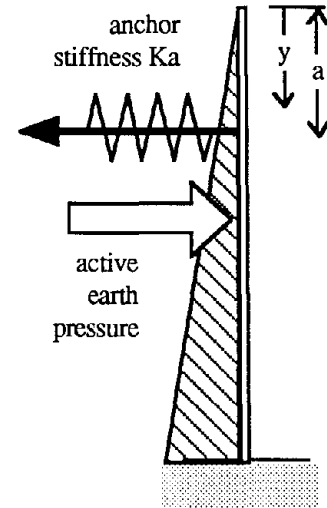


Fig. 3b Idealised loading to calculate natural frequency

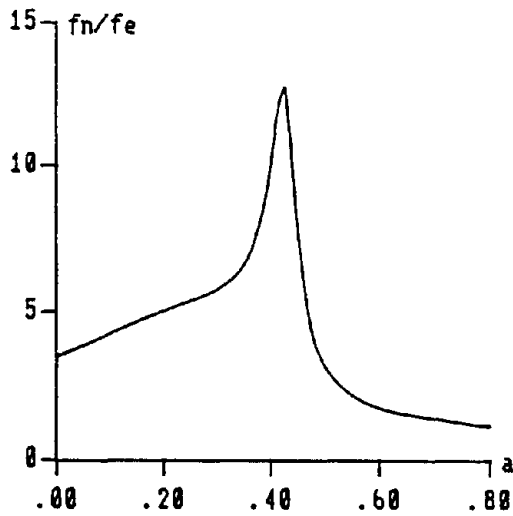


Fig. 4 The variation of natural frequency with depth of anchor

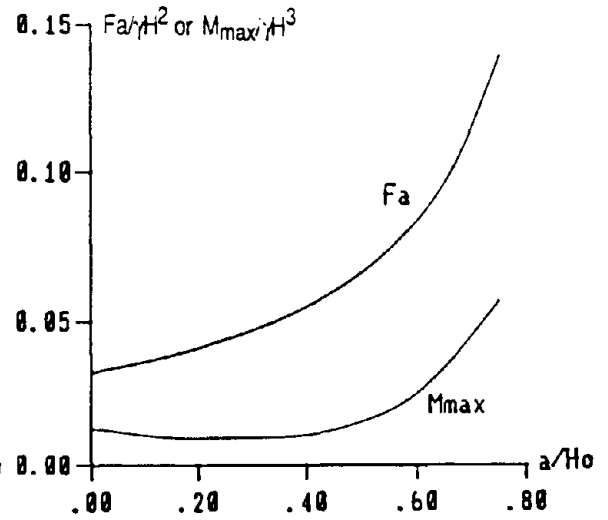


Fig. 5 Anchor force and maximum moment vs depth of anchor

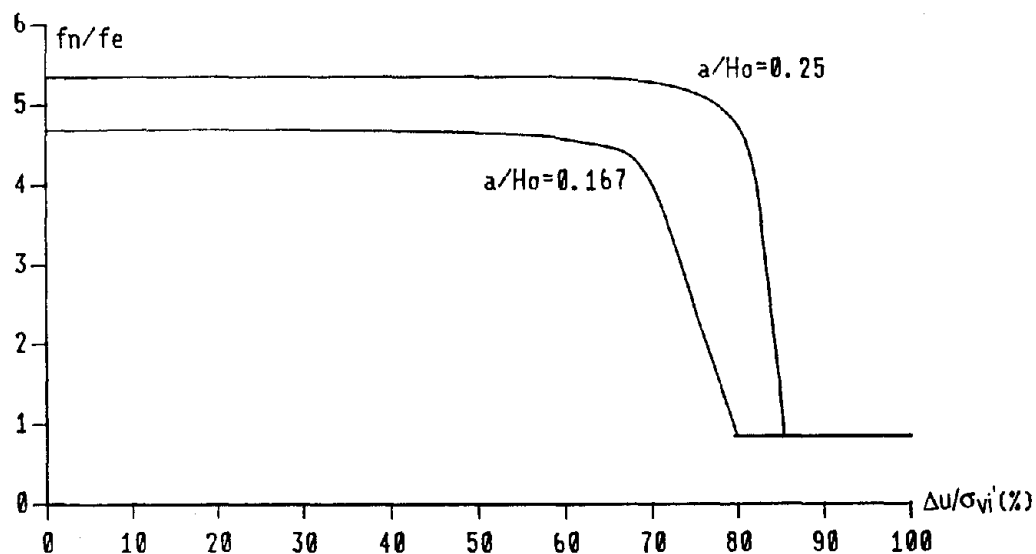
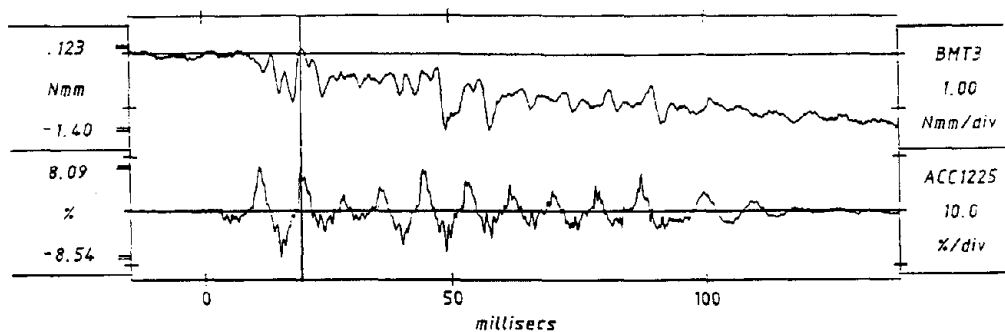


Fig. 6 The deterioration of natural frequency with excess pore pressure expressed as a multiple of the earthquake driving frequency  $f_e$

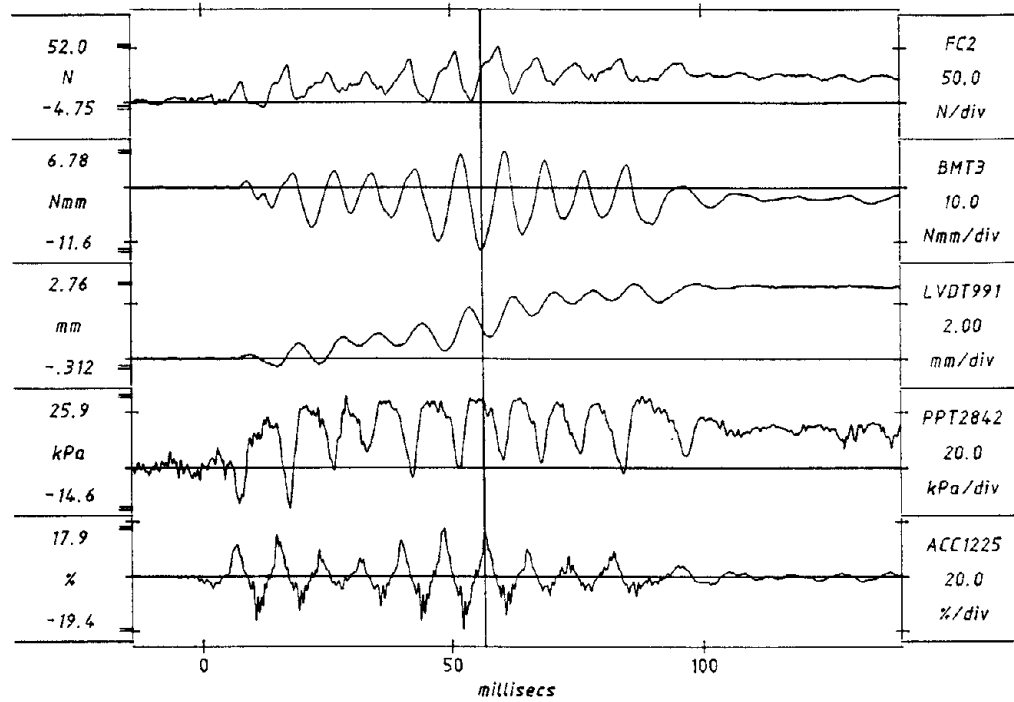


Earthquake 3, Model Test ZENG8 : Bending moment in phase with the base acceleration

Note :

PPT2842 pore pressure in front on anchor	ACC1225 reference accelerometer
BMT3 bending moment at mid-height ( $H_o/2$ )	LVDT991 displacement at wall top
	FC2 force cell on tie rod

Fig. 7 Phase relationship of wall response with small or large excess pore pressures



Earthquake 7, Model Test ZENG8 : Bending moment out of phase with the base acceleration  
 Fig. 7 (contd) Phase relationship of wall response with small or large excess pore pressures

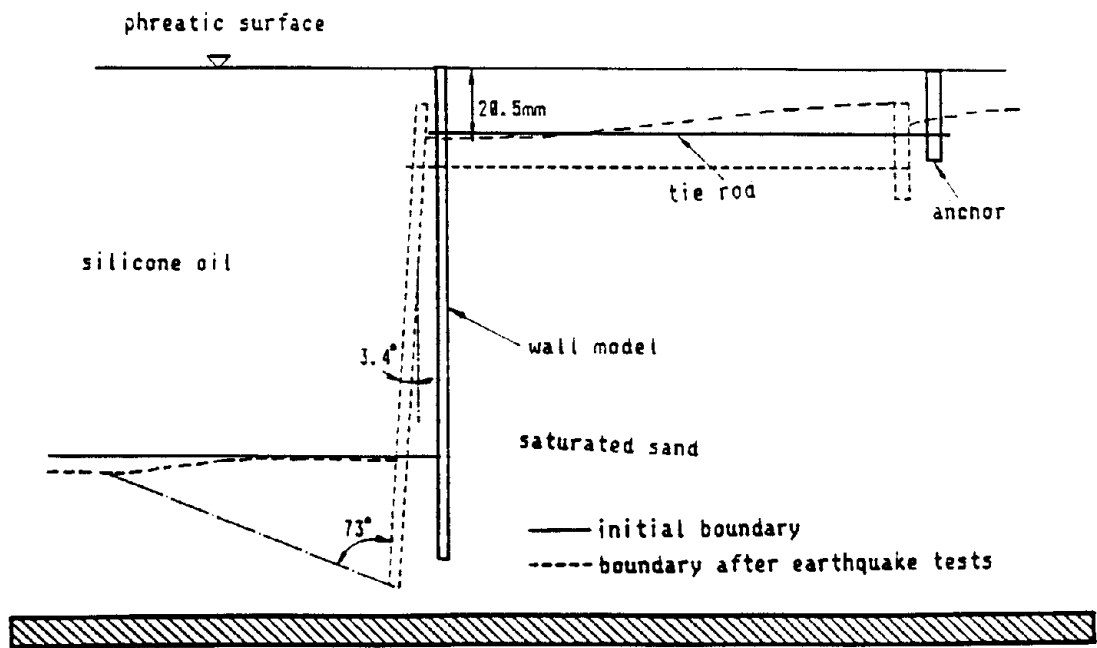


Fig. 8 Toe rotated outwards and anchor pulled out during the failure of model ZENG8

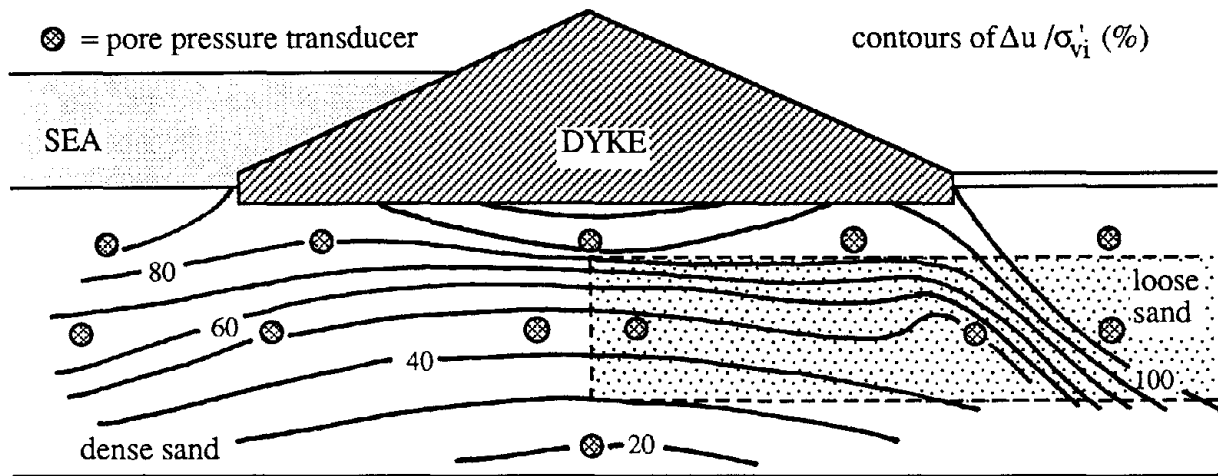


Fig. 9 Contours of excess pore pressure at time instant  $t = 25\text{ms}$ , model AH14 earthquake 2

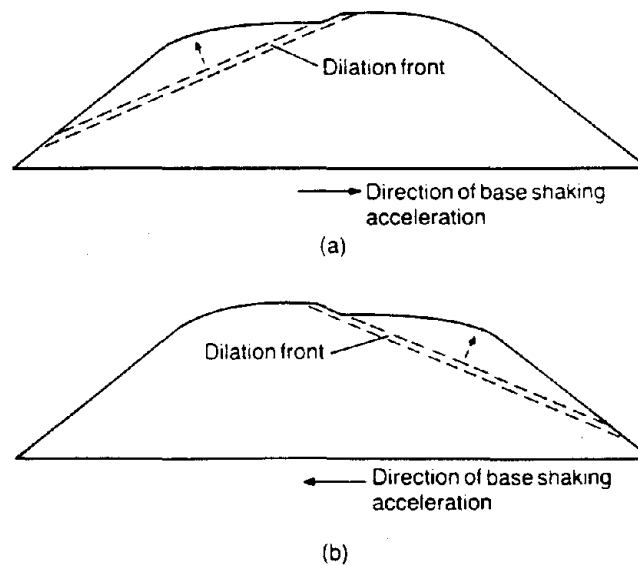


Fig. 10 Propagation of a dilation front in a saturated embankment during 1 cycle of base shaking (after Lee and Schofield)

## STUDY OF EFFECT OF CLAY LAYERS ON LIQUEFACTION OF SAND DEPOSITS USING SMALL-SCALE MODELS

Ahmed-W. Elgamal, Ricardo Dobry, and Korhan Adalier

Rensselaer Polytechnic Institute, Troy, NY 12180, USA.

### ABSTRACT

A series of qualitative small-scale tests are performed with the primary aim of investigating the liquefaction mechanism of a stratified sand-clay soil deposit. It is observed that the presence of layers of varying properties such as permeability and plasticity will significantly alter the mechanisms of pore-pressure buildup, water accumulation and dissipation mechanisms as compared to that of a uniform sand deposit. Possible implications of such mechanisms for earthquake induced ground deformation are discussed. Low permeability strata may slow down the pore pressure buildup in overlying layers, expedite the pore-pressure buildup in underlying layers, facilitate the development of large lateral deformations and lead to delayed sand boil activity.

## INTRODUCTION

Many natural and artificial liquefiable sand deposits contain finer, more impervious silty or clayey layers. Sometimes, the sand itself may contain finer or siltier zones. The effect of such drastic changes in permeability on liquefaction and ensuing ground deformation has not yet been thoroughly investigated, despite a growing consensus as to its importance. For example, the NRC (1985) report on liquefaction postulates – based on small sample laboratory results – mechanism B for flow failure development in a slope resulting from such layering (Fig. 1). Obviously, the same phenomenon can be postulated in a horizontal or mildly sloping site, resulting not in flow failure but in a permanent horizontal displacement of the ground surface. Dobry (1988) suggested that the amount of water accumulated at an impervious interface such as shown in Fig. 1 can play a key role in determining the ensuing consequences of liquefaction.

Small-scale shaking model tests have clarified some aspects of the liquefaction phenomenon in both homogeneous and layered horizontal deposits. These have been performed both in a 1 g (Florin and Ivanov, 1961) and in a centrifuge environment (e.g., Heidari and James, 1982), and have modeled mainly homogeneous deposits. Similar conclusions were drawn from these tests by the different authors: liquefaction progresses from the top down, followed by densification or solidification occurring from the bottom up. Florin and Ivanov (1961) also reported that the presence of a free draining surcharge reduces the possibility of underlying sand liquefaction as well as the duration of the phenomenon if the layer liquefies. Yoshimi (1967) describes the liquefaction of a small sand deposit (about 1 ft. in height) to which an overburden air pressure was imposed by means of a surface rubber membrane. A gradual rise in pore water pressure was observed in the sand during shaking followed by a sudden increase leading to liquefaction of the stratum. After liquefaction and subsequent solidification, an interlayer of water (having a thickness equal to 6% of the original sand height) was observed under the rubber membrane. Scott and Zuckerman (1972) tested a thin sand stratum (3 in. in height) with and without a cohesive silt upper layer (0.125–0.25 in. thick). It was found that the presence of the silt or of a suitably fine grained layer at the surface was conducive to the generation of sand boils. Huishan and Taiping (1984) investigated – using a shake table – the liquefaction of a uniform sand deposit as well as of a stratified deposit of the same sand (1.6 ft. high in both cases). The behavior of the stratified deposit differed from the uniform deposit mainly in the formation of water interlayers along the boundaries of lower coarser and upper finer layers. These interlayers eventually burst in the form of large sand boils.

A series of qualitative (1-g) tests were conducted by the authors and are reported herein to investigate the effect of stratification of soil deposits on liquefaction. The results of these tests are consistent with the above-mentioned earlier studies. In addition, evolution and dissipation of water interlayers entrapped below clay strata is studied. Finally, the implications of the presence of clay or other low permeability/high plasticity interfaces is discussed.

## TEST SET-UP

A transparent rectangular glass box (1 ft. x 2 ft. in cross-section) was employed. Dynamic excitation was imparted by either: a) rolling the box supported on cylindrical tubes on a roughened flat surface, or b) tapping the side of the box using a rubber



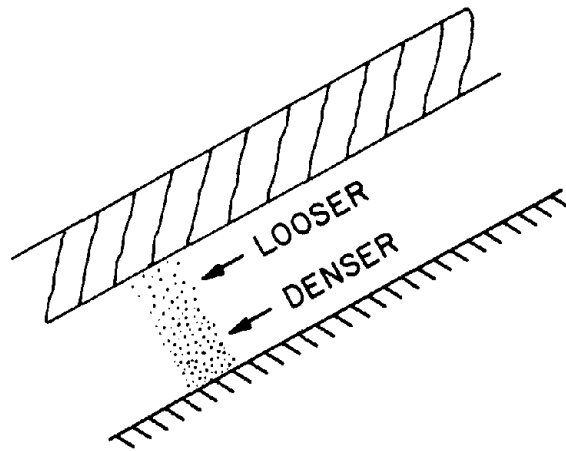


Figure 1. Example of a potential situation for mechanism B failure arising from the rearrangement of the soil into looser and denser zones. Local volume change occurs, but the sand as a whole remains at a constant volume and is "globally" undrained. (From NRC, 1985)

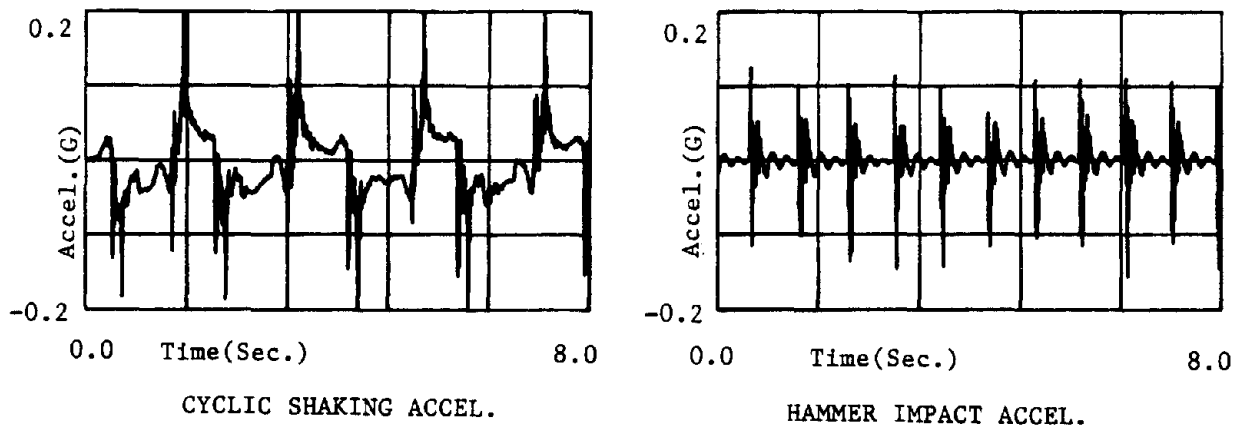


Figure 2. Sample input acceleration.

hammer. Samples of input acceleration are shown in Fig. 2. Standpipe piezometers at different depths were used to monitor excess pore pressure buildup and dissipation. The transparent box allowed visual inspection of water and solid movement along the box boundaries during testing. This movement was recorded on video-tape which was later employed to review each test.

## TESTING PROGRAM

Three experiments are discussed herein and are sketched in Figs. 3, 4 and 6: liquefaction of a uniform silty sand layer (Test No.1); a silty sand layer underlying a silty clay layer with an elevated center island (Test No.2); and a layered clay-clean sand stratum (Test No. 3). A summary of properties of the soils used is included in Table 1.

### Test No.1. Uniform Silty Sand Layer (Fig. 3):

Cyclic motion was applied to the box. A gradual rise in pore pressure led to liquefaction (in this paper the term liquefaction denotes liquid-like response emanating from loss of vertical effective stress). Liquid-like motion oscillations of the soil-water mass during shaking appeared to progress from the top downwards. No sand boils were observed, neither during dynamic loading and liquefaction nor during subsequent densification and consolidation of the stratum which progressed from the bottom upwards. These observations are in agreement with those typically observed (eg., Florin and Ivanov, 1961; Scott and Zuckerman, 1972). A similar pattern has also been observed in more elaborate centrifuge experiments (eg., Lambe, 1981; Heidari and James, 1982; Arulanandan et al., 1983; Hushmand et al., 1988).

### Test No. 2. Silty Sand Layer Underlying A Silty Clay Blanket (Fig. 4):

The upper clay blanket was constructed with an elevated clay island in the center. Cyclic motion was applied to the box. Onset of liquefaction appeared at the sand layer top. The upper clay layer was observed to float from there on and the elevated clay island gradually subsided and totally disappeared. Water lenses were observed to accumulate (Fig. 5) below the clay layer. These water lenses eventually broke through the clay layer forming sand boils (Fig. 5). The observed sand boil action is attributed to the low permeability and high plasticity of the upper clay layer (Fig. 5), similar to earlier observations by Scott and Zuckerman(1972). Little sediment was ejected by the observed sand boils.

### Test No. 3. Interlayered Clay-Loose Sand Stratum (Fig. 6):

Hammer-impact dynamic excitation was employed. Upon initiation of the impacts an increase in pore pressure along with a densification process was observed in the loose sand layers. A water interlayer accumulated gradually and was well developed along the entire lower boundary of each clay layer prior to liquefaction of the sand layers. These interlayers continued to grow with the progress of dynamic excitation and finally reached a thickness of about 0.16 in. each (5% of the corresponding underlying sand layer height). A mechanism of slow progressive upward piping or hydraulic fracture in the lower boundary of each clay layer was then noticeable at few isolated locations. This process, which intensified with time (as flow paths were being formed in the clay layers) eventually led to the eruption of sand boils after about 100 seconds of continued dynamic excitation. In the process, the fully developed water interlayers gradually

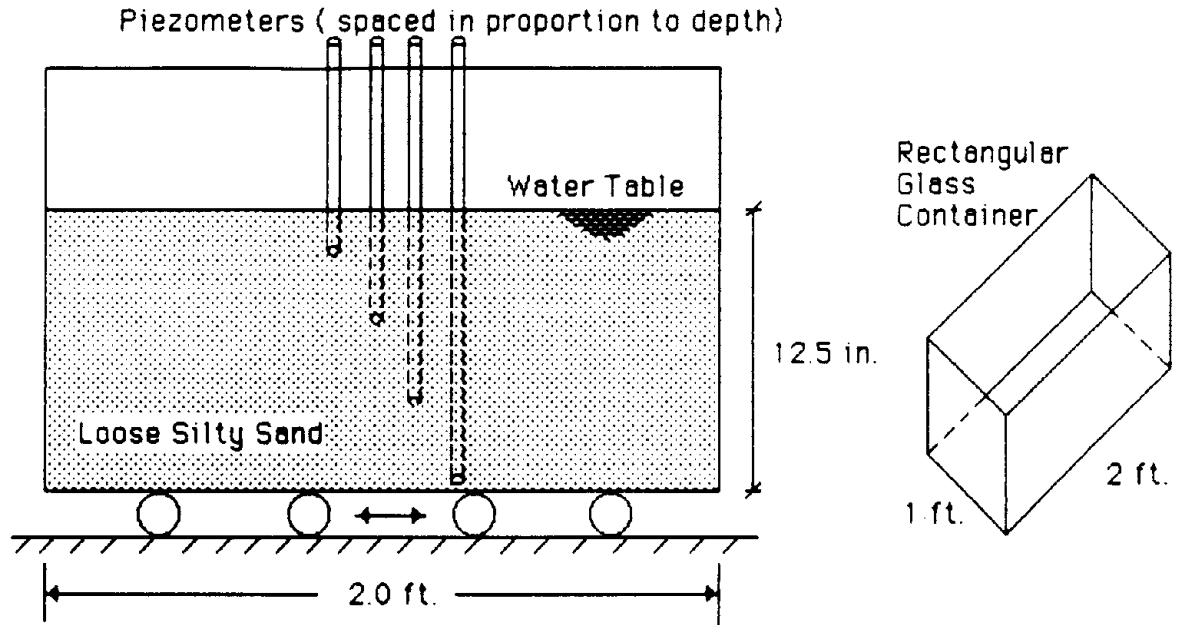


Figure 3. Liquefaction Test Setup of a Homogeneous Loose Silty Sand Layer.

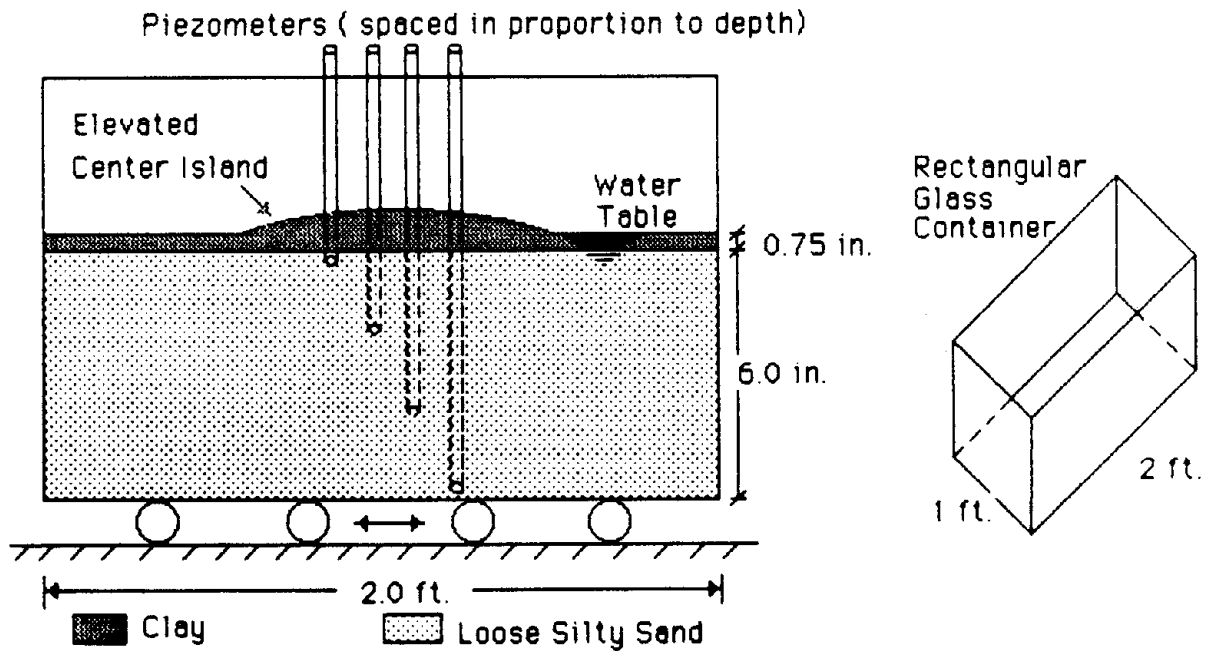


Figure 4. Liquefaction Test Setup of a Loose Silty Sand Layer with an Upper Clay Blanket.

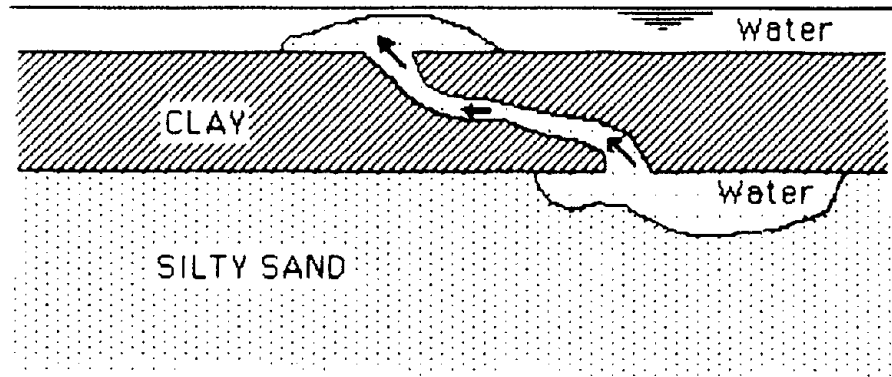


Figure 5. Schematic of Observed Path Followed by Sand Boil(s).

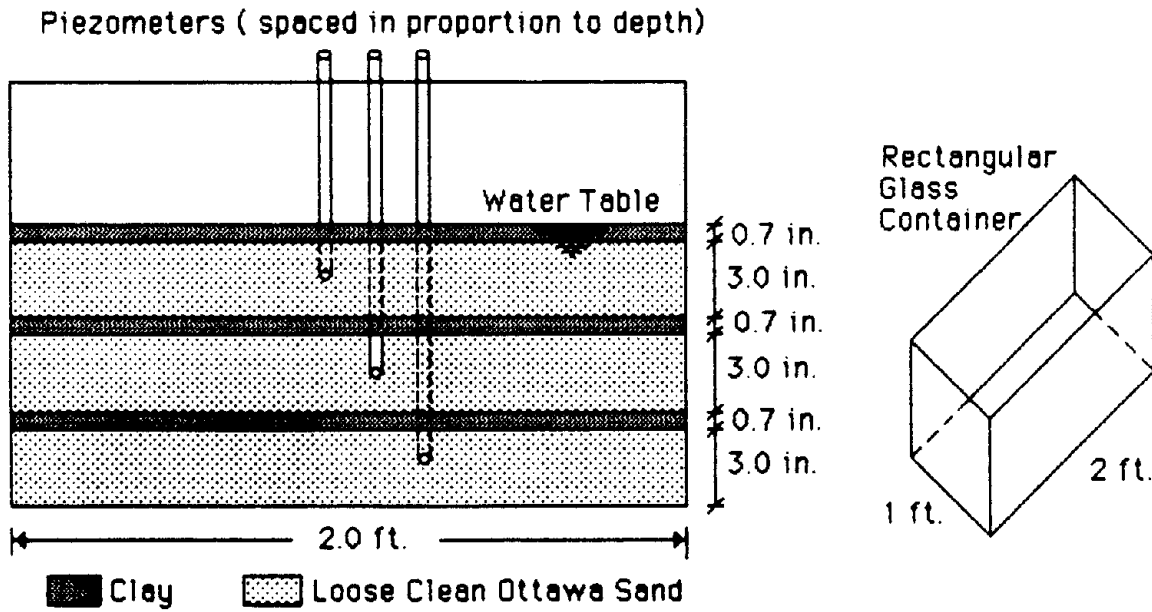


Figure 6. Liquefaction Test Setup of Interlayered Clay - Loose Clean Sand Stratum.

Table 1. Summary Of Main Soil Properties.

Soil Type	$\gamma$ (lb/ft <sup>3</sup> )	k (ft/sec)	e	w <sub>g</sub> , w <sub>p</sub> , P. I. (%)	Soil Placement	Test
Clay	122	$\approx 1 \times 10^{-7}$	—	50.8, 32.7, 18.1	Molding	Test No. 2
					Dumping under water (dry)	Test No. 3
Silty Sand	110	$1.65 \times 10^{-2}$	0.82	—	Dumping under water	Test No. 1 Test No. 2
Ottawa Sand (F-series 125)	119	$2.70 \times 10^{-2}$	0.83	—	Dumping under water	Test No. 3

shrunk in thickness and a mixture of water, clay, and sand was vigorously ejected above the ground surface.

The phenomenon of water interlayers was observed earlier by Scott and Zuckerman (1972), and Huishan and Taiping (1984) in small-scale tests of stratified deposits of varying permeability. Arulanandan et al. (1988), in a centrifuge test of an interlayered sand and clay embankment, observed large lateral deformations which were attributed to the development of a liquid film or a film of very loose sand below the clay layer. Test No. 3 described above demonstrates two additional effects of engineering importance which have not been discussed in previous work: a) the relatively large thickness of accumulated water interlayers which may develop (see also Dobry, 1988); and, b) the long time during which this thickness is sustained following the end of dynamic load. The test also sheds light on the following mechanisms associated with liquefaction of soil deposits with low permeability/high plasticity "impervious" clay interlayers:

1. Under dynamic excitation, a well defined water interlayer may develop below any impervious clay boundary due to densification of the underlying loose granular soil. In principle, these water interlayers may appear even if the granular soil is never liquefied by the cyclic shear stresses and strains induced by the earthquake.
2. As the water interlayer develops (creating an interface of zero effective stress) the underlying granular soil is quickly relieved of its initial effective overburden pressure, and as a consequence it may perhaps become more susceptible to liquefaction than originally deduced on the basis of this confining overburden (eg., see Seed, 1986). This may be important if the stratum is subjected to a second strong motion event before dissipation of the water interlayer created by the first event.
3. A large quantity of liberated water will contribute to a more significant water interlayer in the aftermath of liquefaction of a lower granular layer (Dobry, 1988) overlain by an upper impervious clay boundary. The liquefied layer will solidify and consolidate due to its own weight only (Scott, 1985). Additional consolidation of that layer will occur as the accumulated water interlayer dissipates allowing the overburden pressure to become effective.
4. The shear strength along a water interlayer approaches zero. Such an excessively weak interface may cause large lateral ground deformation (and lateral loading on underground structures) even in mildly sloping terrains. Water interlayers entrapped below "impervious" boundaries may not dissipate for hours or even days after an earthquake shaking event. Lateral deformations in a mildly sloping terrain may thus continue to accumulate long after the end of the shaking. It is noted however that lateral spreading and associated tension cracking will in general create vents for this interlayer water to escape, eventually bringing the process to an end.
5. Formation of water interlayers in the field in soil profiles similar to the one under investigation (Fig. 7) may have a substantial impact on pore pressure increase and subsequent dissipation. In particular, the following mechanisms may occur upon development of a water interlayer:

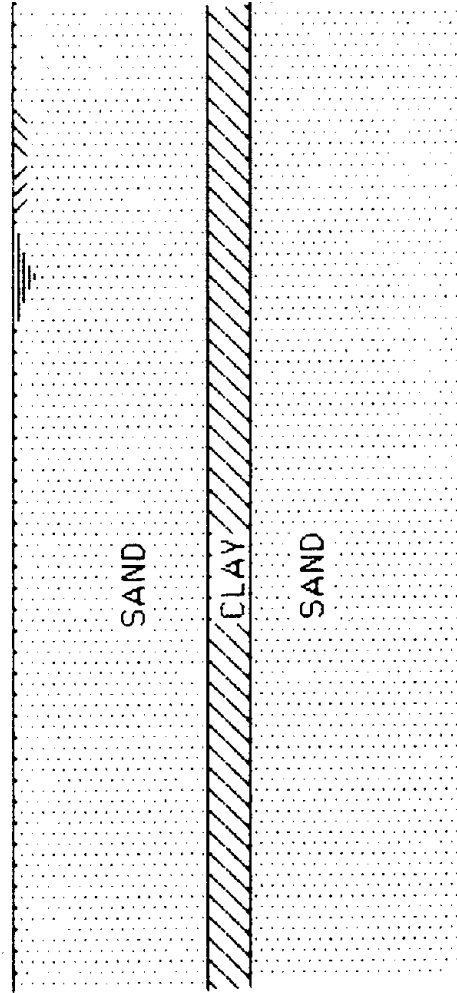


Figure 7. Simple Interlayered Profile.

- 5.1 Slowing down of the pore pressure buildup in the upper layers as a consequence of partial isolation from additional dynamic shaking.
- 5.2 Development of a large hydraulic gradient in a buried "impervious" clay stratum (Fig. 8). Note that this gradient may increase and reach a maximum value after the end of shaking, as the liquefied upper sand layer solidifies and the pore pressures there comes back to a hydrostatic condition, while the top of the lower sand layer is still at zero effective overburden pressure due to the water interlayer (Fig. 8). Hydraulic fracture may consequently intensify at some point after the earthquake. This in turn will increase the possibility of occurrence of delayed sand boils. Such sand boils will eject clay material along with substantial amounts of water and overlying materials (Fig. 9). Note that although this overlying material may have no direct contribution to the sand boil mechanism, it will still appear in the sand boil, at the ground surface. This suggests that the conclusion often made about location of liquefaction from grain size analyses of sand boil material may not be always correct. Youd (1989) suggested that large hydraulic gradients in buried clay layers such as those depicted in Fig. 9, may be responsible for explosive sand ejections and development of craters ("sand blows") rather than mounds ("sand boils"), as observed in the 1886 Charleston and 1977 San Juan, Argentina, earthquakes.

### SUMMARY AND CONCLUSIONS

A series of qualitative small-scale tests was performed with the aim of investigating the liquefaction mechanism of stratified sand-clay deposits. It was observed that well developed water interlayers accumulate at the base of the low permeability/high plasticity clay boundaries. If these water interlayers appear they may have engineering significance even if the seismic shear stresses and strains cause only densification and no liquefaction of the underlying granular soil. Large lateral ground deformations along these water interlayers may develop (see also Arulanandan, et al. 1988) even in mildly sloping terrains. Poor clay permeability may cause such deformations to continue for a long period of time (following the end of earthquake shaking). Significant delayed sand boil action may also occur pending completion of hydraulic fracture which can intensify after the earthquake. These sand boils are apt to eject large quantities of water originally accumulated and trapped below the clay boundaries. Effects such as those described, with varying degrees of severity, have been also observed to occur in other stratified deposits of varying permeability and plasticity (Scott and Zuckerman, 1972; Huishan and Taiping, 1984).

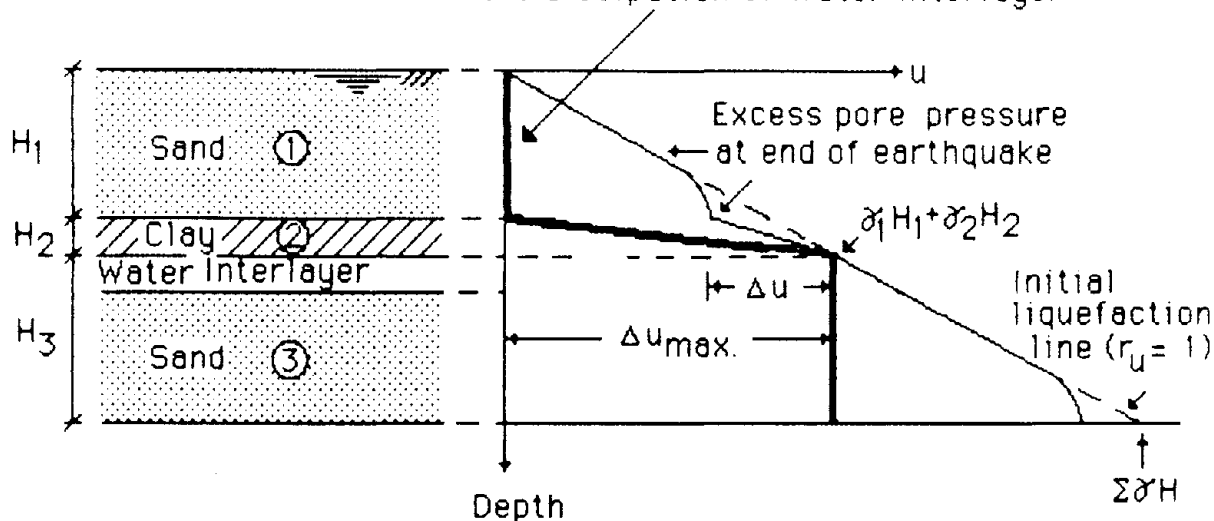
### ACKNOWLEDGEMENTS

This study was supported by NCEER under grant No. 881504. Paul Van Laak participated in soil preparation and test setup.



$\gamma$  = Buoyant unit weight  
 $\gamma_w$  = Unit weight of water  
 $u$  = Excess earthquake-induced pore pressure  
 $\bar{\sigma}_v$  = Vertical effective stress  
 $r_u$  = Pore pressure ratio =  $u/\bar{\sigma}_v$

Excess pore pressure some time after earthquake but before dissipation of water interlayer



Average hydraulic gradient in clay layer =  $\Delta u / (\gamma_w H_2)$

Average maximum hydraulic gradient in clay layer =  $\Delta u_{max} / (\gamma_w H_2)$

$$\Delta u_{max} = \gamma_1 H_1 + \gamma_2 H_2$$

Example: ( $\gamma_1 = \gamma_2 = \gamma_w$ )

$H_1$ (ft.)	$H_2$ (ft.)	Average Max. Hydraulic Gradient In Clay Layer
5	5	2
5	1	6
10	5	3
10	1	11

Figure 8. Development of High Gradients in Clay Layer. Notice That The Average Hydraulic Gradient in the Clay Layer Reaches a Maximum of  $\Delta u_{max} / (\gamma_w H_2)$  Some Time After The Earthquake. Local Gradients At The Lower Boundary Of The Clay Layer Will Be Even Larger Due to Low Clay Permeability.

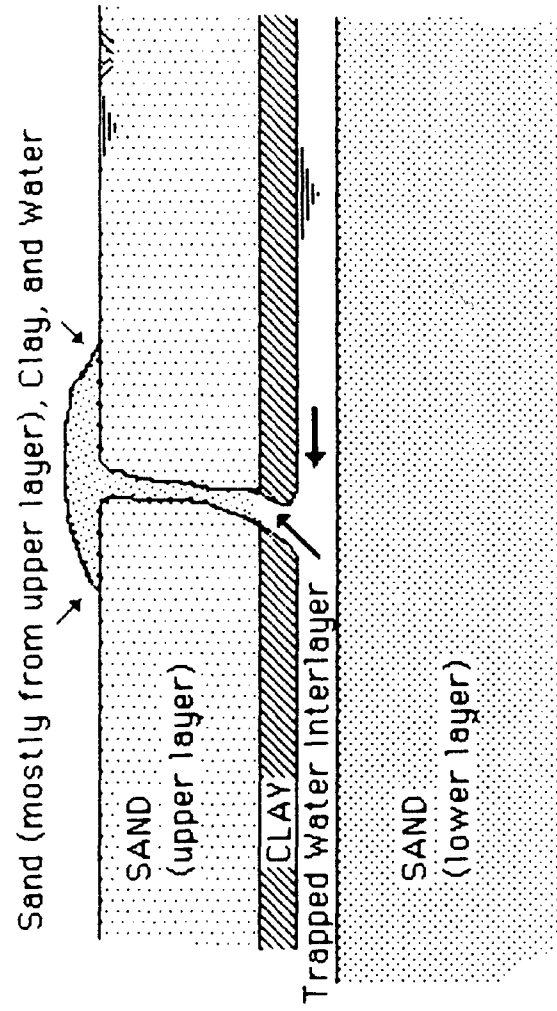


Figure 9. Delayed Sand Boil Following A Hydraulic Fracture Mechanism.

## REFERENCES

- Florin, V. A., and Ivanov, P. L. (1961), "Liquefaction Of Saturated Sandy Soils", *Proc. 5th International Conference on Soil Mech. and Found. Eng.*, Paris, 1, pp. 107–111.
- Yoshimi, Y. (1967), "An Experimental Study Of Liquefaction Of Saturated Sands, *Soils And Foundations*, Vol. VII, No. 2. pp. 20–32.
- Scott, R. F., and Zuckerman, K. A. (1972), "Sandblows and Liquefaction", in *The Great Alaska Earthquake Of 1964—Engineering Publication 1606*, National Academy Of Sciences, Washington, D.C., pp. 179–189.
- Lambe, P.C. (1981). "Dynamic Centrifuge Modelling of a Horizontal Sand Stratum," Sc.D. Thesis, Massachusetts Institute of Technology, Cambridge, MA.
- Heidari, M., and James, R. G. (1982), " Centrifugal Modelling Of Earthquake Induced Liquefaction In A Column Of Sand", *Proc. Conf. On Soil Dynamics And Earthquake Engineering*, Southampton, England, Balkema, Rotterdam, pp. 271–281.
- Huishan, L., and Taiping, Q. (1984), "Liquefaction Potential Of Saturated Sand Deposits Underlying Foundation Of Structure", *Proc. 8th World Conf. on Earthquake Eng.*, San Francisco, California, Vol III, July, pp. 199–206.
- NRC. (1985), "Liquefaction Of Soils During Earthquakes", Report by the Committee On Earthquake Engineering, National Research Council, National Academy Press, 240 pages.
- Seed, H. B. (1986), "Design Problems In Soil Liquefaction", University Of California, Report No. UCB/EERC–86/02, Berkeley, California, Feb.
- Scott, R. F. (1986), "Solidification And Consolidation Of A Liquefied Sand Column", *Soils And Foundations*, Vol 26, No. 4, Dec., pp. 23–31.
- Hushmand, B., Scott, R. F., and Crouse, C. B. (1988), "Centrifuge Liquefaction tests In A Laminar Box", *Geotechnique*, 38, No. 2, pp. 253–262.
- Arulanandan, K., Yogachandran, C., Muraleetharan, K. K., Kutter, B. L., and Chang, G. S., (1988), "Laboratory Flow Slide During Earthquake Simulation", *Centrifuge 88*, Corte, J.–F., ed., Paris, Balkema, Rotterdam, April, pp. 539–544.
- Dobry, R. (1989), "Some Basic Aspects Of Liquefaction During Earthquakes", *Conf. on Earthquake Hazard And The Design Of Constructed Facilities In The Eastern United States*, in *Annals Of The New–York Academy Of Sciences*, Vol. 558, June.
- Youd, T.L. (1989). Personal communication.

**SOME OBSERVATIONS ON THE MECHANICS  
OF POST-LIQUEFACTION DEFORMATIONS**

Geoffrey R. Martin

Vice President of Engineering  
The Earth Technology Corporation, Long Beach, CA

**ABSTRACT**

Large ground deformations, both cyclic and permanent, are a major source of damage to lifeline facilities as a result of major earthquakes and are a feature of ground behavior at sites where liquefaction has occurred. The observations made in this paper pose questions and challenges with respect to our ability to model analytically observed post liquefaction deformation behavior in the field. Two types of post liquefaction deformation behavior are discussed, namely large horizontal shearing deformation, and settlement arising from dissipation of liquefaction induced pore water pressures. Suggestions are made for further research focusing on the development of mechanistically based constitutive relationships for post liquefaction deformation behavior of sand.

## INTRODUCTION

Large ground deformations, both cyclic and permanent, are a major source of damage to lifeline facilities as a result of major earthquakes. Such deformations are a feature of the ground behavior at sites where liquefaction has occurred. They may occur during the earthquake itself at times following initial liquefaction, or continue to occur or be initiated subsequent to the earthquake in situations where the static factor of safety against lateral movement is reduced to values less than 1.

The observations made in this paper are primarily designed to pose questions and challenges with respect to our ability to model analytically observed post-liquefaction deformation behavior in the field. To accomplish analytical predictions with a reasonable degree of confidence, we must understand the mechanics of the physical processes taking place, which in turn provide the basis for sound constitutive relationships.

A typical site profile susceptible to post-liquefaction deformations is shown in Figure 1. This profile is that of the Parkfield liquefaction instrumentation array in the Cholame Valley, California, described by Holzer, et. al., 1989. In general terms, such sites comprise alternating layers of sandy silts, clays and silty sands with sandy silt or silty sand layers ranging in relative density from loose to moderately dense. Large post-liquefaction deformations may be induced by nonlinear ground deformations, spatially varying ground motions, slightly sloping strata or the presence of an unrestrained lateral boundary (e.g., a cut or river bank).

Two types of post-liquefaction deformations will be discussed:

- (1) Horizontal shear deformations arising from the large shearing strains occurring in zones where the earthquake has induced initial liquefaction.
- (2) Settlements arising from volume changes which occur on re-consolidation accompanying dissipation of the large excess pore pressures in liquefied zones.

## POST-LIQUEFACTION HORIZONTAL SHEAR DEFORMATIONS

Whereas the mechanics of pore water pressure build up during earthquake ground shaking in saturated sand deposits is reasonably well understood (Martin et. al., 1975), and related effective stress constitutive models included in earthquake site response programs such as DESRA (Lee and Finn, 1978), our understanding of post liquefaction deformation behavior and our ability to model this behavior is by no means complete. Nonlinear constitutive models describing the shearing behavior of saturated sands in a pre-liquefaction state generally assume hyperbolic stress strain curves which soften as pore pressures increase. Such models which are incorporated in computer programs such as DESRA, are widely used to make

predictions of earthquake response and pore pressure build up in saturated sand deposits. Modified versions of these models may also be used to predict pre-liquefaction deformations arising from nonlinear response of saturated slopes and embankments (e.g., the program TARA, Finn et. al., 1986). However, the constitutive relationships used in these programs may only be reasonably used up to the point of initial liquefaction. As large cyclic shearing strains develop at the point of initial liquefaction, stress-strain behavior becomes significantly influenced by the dilation behavior of the sand and hysteresis loops may show strong strain stiffening as shown in Figure 2. Our ability to model such behavior with mechanistic constitutive relationships expressed in terms of effective stresses is very limited at the present time and more research is needed in this area. The large strain dilation behavior during undrained static shearing of sands is also clearly recognized as shown in Figure 3, and can mobilize large undrained shearing strengths.

The earthquake site response of a saturated soil deposit must be recognized as a coupled problem where shearing stress and associated shearing strain levels in the deposit are a function of both the stiffness characteristics of the soil profile and the input earthquake motions. For saturated sands which exhibit dilation behavior under large post liquefaction strains, significant shearing stresses may continue to be transmitted to the surface following initial liquefaction. Consequently the reliable prediction of post-liquefaction deformations requires that we can model the stress-strain behavior of liquefied soil deposits. Centrifuge tests provide the ideal means for generating experimental data to study this problem.

Figure 4 shows the laminar simple shear box used for centrifuge site response experiments on saturated sands conducted at the California Institute of Technology and described by Hushmand et. al., (1987, 1988). The simulated earthquake response studies were performed in a test container comprising a stack of rectangular sliding rings containing a deposit of fine saturated sand. Liquefaction tests have been performed at a centrifugal acceleration of 50 g on a model subjected to input accelerations with a frequency content and duration corresponding the to 1940 El Centro earthquake scaled to a peak base acceleration of 0.55 g. Recorded accelerations at various depths in a centrifuge test conducted on a saturated medium dense sand are shown in Figure 5. The measured pore pressure response at the third height is compared to computed pore pressure response (using the program DESRA) to the point of initial liquefaction in Figure 6. The DESRA program cannot compute the pore pressure fluctuations arising from the cyclic dilation effects which occur at the larger cyclic strains both approaching and following initial liquefaction. With initial liquefaction occurring after five seconds, it is clear from Figure 5 that input accelerations continue to be transmitted to the surface through the liquefied soil illustrating the influence of residual stiffness arising from the dilation behavior of the sand.

The reliable prediction of post-liquefaction stress strain behavior during earthquakes not only affects our ability to predict horizontal ground

deformations, but also influences the evaluation of residual undrained strength (which may control post-earthquake stability) and the evaluation of post-liquefaction settlement as discussed further below.

### POST-LIQUEFACTION SETTLEMENT

Although large horizontal ground deformations are clearly one of the primary factors inducing damage to lifeline facilities, one shouldn't overlook the potential effects of post-liquefaction settlement arising from excess pore pressure dissipation over a period of time. Field observations of earthquake induced settlements in saturated sand range from a fraction of an inch to 20-inches (Tokimatsu and Seed, 1987). For lifeline facilities transitioning from firm ground to liquefiable soil deposits, ground settlements on the order of several inches may become significant with respect to damage potential.

For problems where earthquake induced shearing strains are limited to those values prior to or just up to the point of initial liquefaction, (where shearing strain amplitudes are say less than 0.5 percent), induced settlements resulting from dissipation of excess pore pressures may be expected to approximately equal the summation of elastic one dimensional vertical rebound strains. This is consistent with the mechanistic understanding of excess pore pressure generation described by Martin et. al., 1975, and schematically shown in Figure 7. Elastic rebound at grain contacts occurs to compensate for volume changes in the grain structure arising from slip at grain contacts, that is, rebound from point B to point C (Figure 7) occurs to maintain a constant volume undrained conditions. During subsequent dissipation of the excess pore pressure, the sand structure may be expected to reconsolidate along the path C to B.

For sand subjected to large undrained cyclic shearing strains, a different reconsolidation path may potentially be followed. Representative one-dimensional loading and unloading characteristics of a silty sand are shown in Figure 8. Volumetric or vertical strains for the elastic rebound and reloading curves for such sands typically range 0.1 to 1 percent depending on initial confining stress, relative density and the percentage of silt in the soil. For larger post-liquefaction shearing strains, however, where significant particle re-orientation arising from dilation effects may be expected to occur at conditions of constant volume (assuming no pore pressure dissipation is occurring during cyclic loading), the soil structure may lose its "memory" of its initial elastic regime, depending on the number of cycles of large shearing strain and the amplitudes of the shearing strain cycles. The reloading path may then tend to move towards a virgin consolidation curve representative of a first loading curve in one-dimensional compression. Referring to Figure 8, for an 18 psi initial vertical stress this could lead to about 1.4 percent strain on reconsolidation as opposed to only about 0.2 percent for the elastic rebound. For a more silty material much higher values of reconsolidation strain could be expected as a result of structural re-orientation.

Laboratory cyclic torsional tests on saturated sands conducted by Tatsuoka et. al., 1984, have demonstrated the influence of cyclic shearing strain amplitude on the post liquefaction settlement occurring on reconsolidation. Representative test results are shown in Figure 9. In general terms, the results show that for cyclic strain amplitudes greater than about 1 percent, reconsolidation settlements increase as the cyclic shearing strain amplitudes increase and as the initial relative density reduces. For the higher cyclic strain amplitudes, the magnitudes of settlement approach values one would expect for a virgin sand. Such test results have been re-interpreted by Tokimatsu and Seed, 1987, as a function of blowcount and cyclic stress ratio as shown in Figure 10, and compared to observed field observations. For looser sands and high cyclic stress ratios capable of producing high post-liquefaction cyclic shearing strains, volumetric strains on reconsolidation are seen to be relatively high. These results again emphasize the need for more reliable constitutive relationships for post-liquefaction behavior enabling more accurate post-liquefaction shearing strain predictions from earthquake site response analyses.

#### EXCESS PORE PRESSURE REDISTRIBUTION OR DISSIPATION

For most practical situations, particularly for those involving fine sands and silts, it may be assumed that there is relatively little pore pressure redistribution or dissipation during earthquake loading, and reconsolidation will be a post earthquake process. However, for coarser sands or stratified cohesionless soils involving layers of significantly different coefficients of consolidation,  $C_v$ , significant redistribution or dissipation may occur both during and following earthquake loading. This is illustrated for example in Figure 11, which shows pore pressure dissipation functions for an initial triangular pore pressure profile. A constant coefficient of volume decrease  $m_v$  is assumed. Dissipation functions vary as the layer thickness and the coefficient of permeability. For example for a one-foot layer, 50 percent dissipation will occur in 1/10 of a second for a fine sand and in 10 seconds for a silt. These dissipation times rapidly increase as the layer thicknesses increase.

During the pore pressure build up phase of an earthquake, it is often reasonable to assume a constant average value of  $m_v$  to evaluate redistribution or dissipation effects. However, where effective stresses are very low corresponding to times near or immediately after the point of initial liquefaction, values of  $m_v$  increase significantly as the unloading/reloading curve in one-dimensional compression tends to be asymptotic to the strain axis. Consequently, it is inappropriate to use an average value of  $m_v$  as often assumed. The high values of  $m_v$  lead to low values of the coefficient consolidation  $C_v$  which in turn lead to relatively slow rates of initial dissipation and redistribution of pore pressures following liquefaction. Further research is needed to better define the variation of coefficient consolidation with low confining stresses during post-liquefaction pore pressure redistribution and dissipation.



It has been observed in past earthquakes that large slope displacements are often initiated sometime after the earthquake ground shaking ceases. This suggests that excess pore water pressure redistribution effects are influencing the residual undrained strength of the sand deposits involved. Seed (1987) has observed through back analyses of post-liquefaction slope or embankment failures, that the residual undrained strengths mobilized are significantly less than those expected based on the initial void ratio of the sand involved in the failures. This has led to the development of a tentative relationship for design purposes between undrained residual strength and standard penetration blowcount, as shown in Figure 12. For the case of a layer of sand located beneath an impervious clay boundary, it has been suggested that pore pressure redistribution effects under conditions of constant volume will tend to increase void ratios in the upper half of the layer and decrease those in the lower half (U.S. National Research Council, 1985). In the extreme, a thin zone of water may accumulate at the upper sand clay interface. These phenomena could possibly account for the apparent low residual strengths reported by Seed.

With respect to the question of the influence of pore pressure redistribution and void ratio changes on residual undrained strength, a centrifuge model test recently conducted at the University of California, Davis (Arulanandan, et. al., 1988) is of interest. A cross section of the embankment studied is shown in Figure 13a. The model embankment which was only about 4 inches high, was subjected to a centrifugal acceleration of 30g. The model hence represented about a 12 foot high prototype. The saturated sand chimney drain and upstream blanket were placed at an initial relative density of about 57 percent. The model was subjected to about 20 cycles of horizontal earthquake loading using an electro hydraulic shaker. The base acceleration time history is shown in Figure 13c and in terms of prototype loading, corresponds to about 20 cycles of loading at 1 hz with a maximum acceleration of about 0.47g. Instrumentation comprised accelerometers on the slope, an LVDT placed on the upstream clay slope to record vertical deformations, and pore pressure transducers embedded in the saturated sand. Recorded acceleration's were essentially constant with height.

Average pore pressure increases representative of those in the sand blanket, are shown in Figure 13b. Pore pressures can be seen to rapidly increase during shaking, leveling off to an initial liquefaction state near the end of shaking. Recorded vertical displacement of the upstream slope indicated that a slope failure was initiated near the end of shaking with movement ceasing at the end of the earthquake as shown in Figure 13d. The clay slope profile before and after the test is shown in Figure 13a. The movement pattern clearly shows a lateral block failure of the upstream slope on the clay-sand interface. Lateral deformations in the sand blanket were very small. Vertical displacements in the upstream sand blanket were also small reflecting an undrained state.

Back analyses (Arulanandan et. al., 1988) of the block slide using the Newmark procedure indicated that the residual strength mobilized along the surface of the sand blanket was of the order of 100 psf. This is significantly less than the

undrained residual shear strength calculated assuming a void ratio corresponding to the initial relative density of 57 percent. A residual undrained shear strength of 100 psf corresponded approximately to the residual strength at the loosest void ratio, suggesting that void ratio redistribution had occurred with sand at the base of the blanket becoming denser and that at the surface, looser.

Clearly the pore pressure redistribution phenomenon is a complex problem and is linked with the question of constitutive relationships for sand during post liquefaction large cyclic shearing strains and the associated changes in sand structure which may occur during these strains. A knowledge and understanding of the compressibility characteristics of sand at low confining pressures, the mechanics of changes in sand structure at constant volume during high shearing strains, and the potential for accumulation of free water at a clay-sand interface are not well understood or able to be quantified at the present time.

### CONCLUSIONS

The analytical prediction of post-liquefaction earthquake induced deformations in the field is clearly a complex and difficult problem. Large deformations may arise from the large shearing strains induced by earthquake loading or from settlements resulting from dissipation of pore pressures in liquefied zones. Our ability to model such behavior using mechanistic constitutive relationships expressed in terms of effective stress, is very limited at the present time. Further basic research is needed to develop an improved mechanistic understanding of observed deformation behavior to underpin the development of constitutive relationships. Such research should focus on:

- o a study of post-liquefaction large shear strain dilation behavior during undrained cyclic simple shear loading
- o studies leading to an improved mechanistic understanding of changes in soil structure which occur during large cyclic shearing deformations
- o a study of the effects of large shearing strains on the compressibility and coefficient of consolidation at low confining stresses
- o a study of void ratio changes which may accompany redistribution of excess pore pressures, particularly where sand-clay interfaces exist.

It is believed that laboratory testing programs complemented by well-designed and instrumented centrifuge experiments on shaking tables are ideally suited for providing a database for both understanding the mechanics of the physical processes taking place during large earthquake induced shearing strains, and the verification post-liquefaction constitutive relationships for use in response analyses.

## REFERENCES

- Arulanandan, K., Seed, H. B., Seed, R. B., Yogachandran, C., and Muraleethan, K. K., (1988), Centrifuge model tests to study the effect of volume change characteristic on the dynamic stability of heterogeneous earth dams, University of California, Davis, Internal Research Report, to be submitted to ASCE for publication.
- Finn, W. D. Liam, Yogendrakumar, M., Yoshida, N., and Yoshida, H., (1986), TARA-3: A Program to Compute the Response of 2-D Embankments and Soil Structure Interaction Systems to Seismic Loadings, Department of Civil Engineering, University of British Columbia.
- Holzer, Thomas L., Bennett, Michael J., and Youd, Leslie, T., (1989), Lateral spreading field experiments by the U.S. Geological Survey, Second U.S. - Japan Workshop on Liquefaction, Large Ground Deformation, and Their Effects on Lifeline Facilities, September.
- Hushmand, B., Crouse, C. B., Martin, G. R., and Scott, R. F., (1987), Site response and liquefaction studies involving the centrifuge: Structures and Stochastic Methods, Developments in Geotechnical Engineering, Editor, A. S. Cakmak, pp. 3-24.
- Hushmand, B., Scott, R. F., and Crouse, C. B., (1988), Centrifuge liquefaction tests in a laminar box, Geotechnique, Vol. 38, No. 2, pp. 253-262.
- Ishihara, K., (1985), Stability of natural deposits during earthquakes, Proceedings, 11th. International Conference on Soil Mechanics and Foundation Engineering, A. A. Balkema Publishers, Rotterdam, Netherlands.
- Lee, M. K. W., and Finn, W. D. L., (1978) DESRA-2 - Dynamic effective stress response analyses of soil deposits with energy transmitting boundary including assessment of liquefaction potential, Soil Mechanics Series, No. 38, Department of Civil Engineering, University of British Columbia, Vancouver B. C.
- Martin, G. R., Finn, W. D. Liam, and Seed, H. B., (1975), Fundamentals of liquefaction under cyclic loading, Journal of the Geotechnical Engineering Division, ASCE, Vol. 101, No. GT5, pp. 325-438.
- Martin, G. R., Lam, I., and Tsai, C. F., (1980), Pore-pressure dissipation during offshore cyclic loading, Proceedings, Journal of the Geotechnical Engineering Division, ASCE, Vol. 106, No. GT9, pp. 981-996, September.
- Seed, H. B., (1987), Design problems in soil liquefaction, Journal of the Geotechnical Engineering, ASCE, Vol. 113, No. GT3, pp. 827-845.

Tatsuoka, F., Sasaki, T., and Yamada, S., (1984), Settlement in saturated sands induced by cyclic undrained simple shear, Proceedings, 8th. World Conference on Earthquake Engineering, San Francisco, pp. 95-102.

Tokimatsu, K., and Seed, H. B., (1987), Evaluation of settlements in sands due to earthquake shaking, Journal of Geotechnical Engineering, Vol. 113, No. 8, pp. 861-878.

U. S. NATIONAL RESEARCH COUNCIL, (1985), Liquefaction of soils during earthquakes, National Academy Press, Washington, D.C.

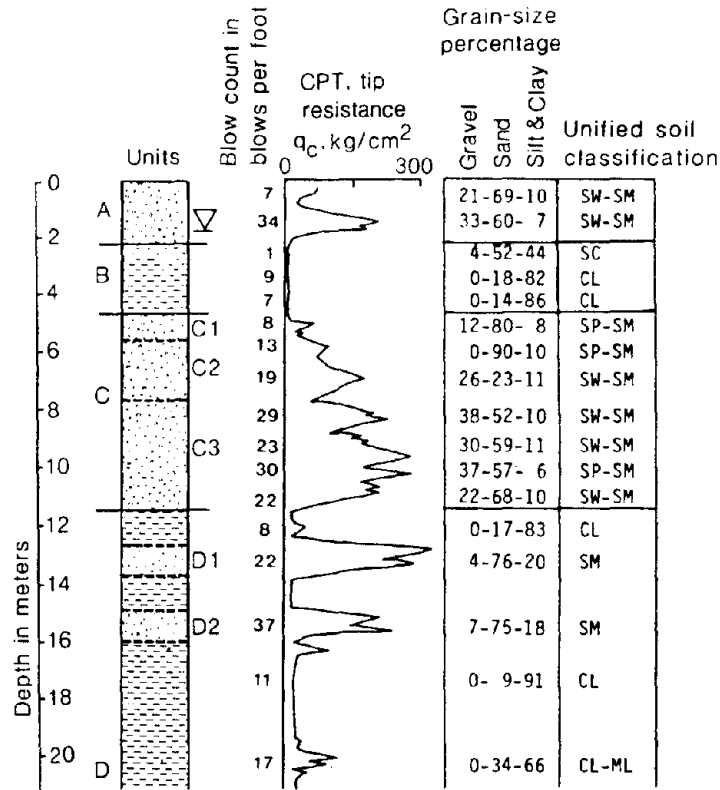


Figure 1. Representative Site Profile Susceptible to Post Liquefaction Deformations

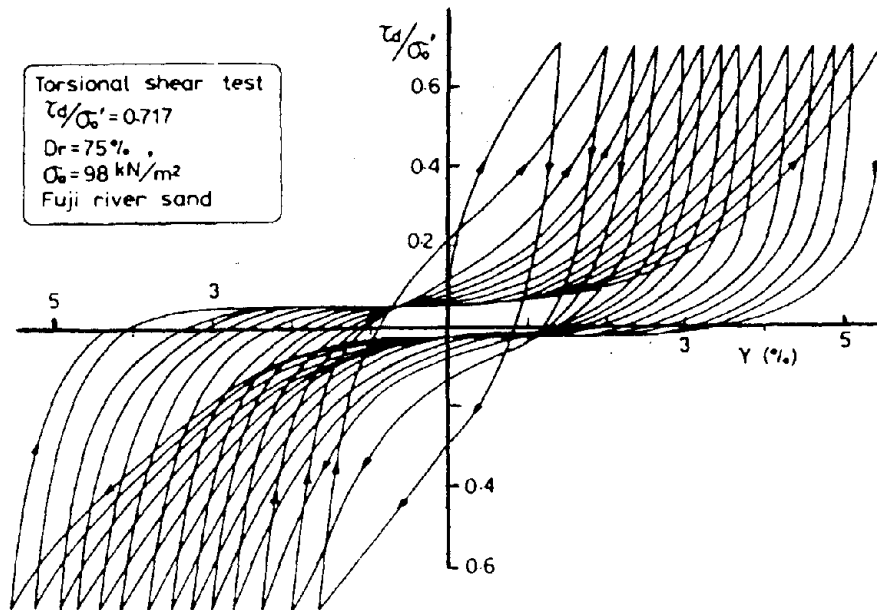


Figure 2. Undrained Cyclic Stress-Strain Curves for a Saturated Sand (After Ishihara, 1985)

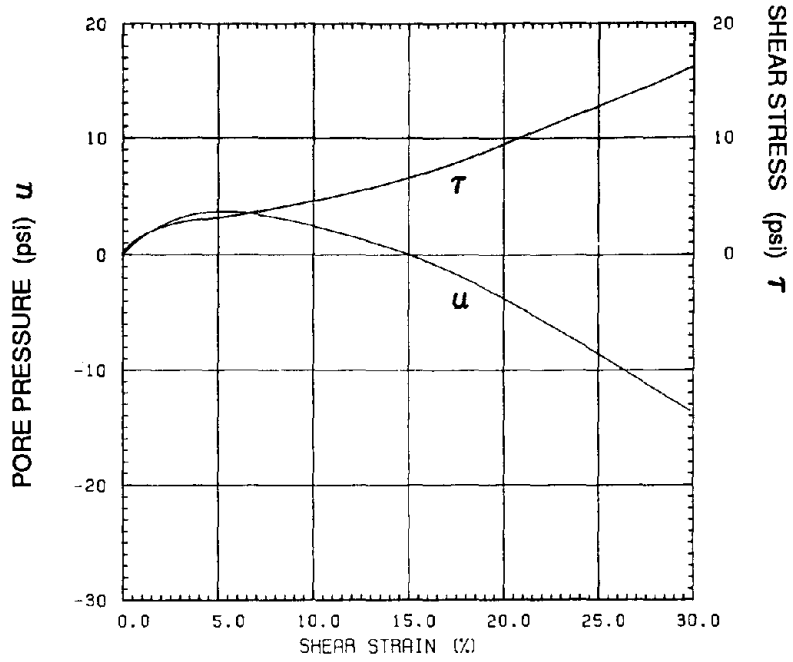


Figure 3. Rapid Monotonic Undrained Simple Shear Test on a Medium Dense Silty Sand

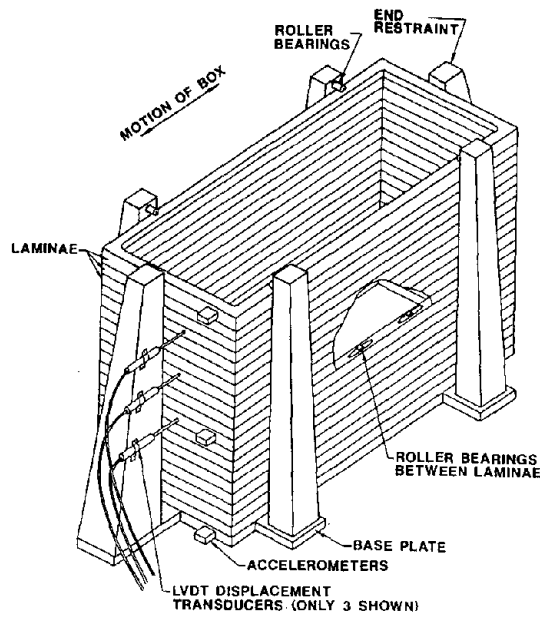


Figure 4. Laminar Simple Shear Box for Centrifuge Experiments (After Hushmand et. al., 1988)

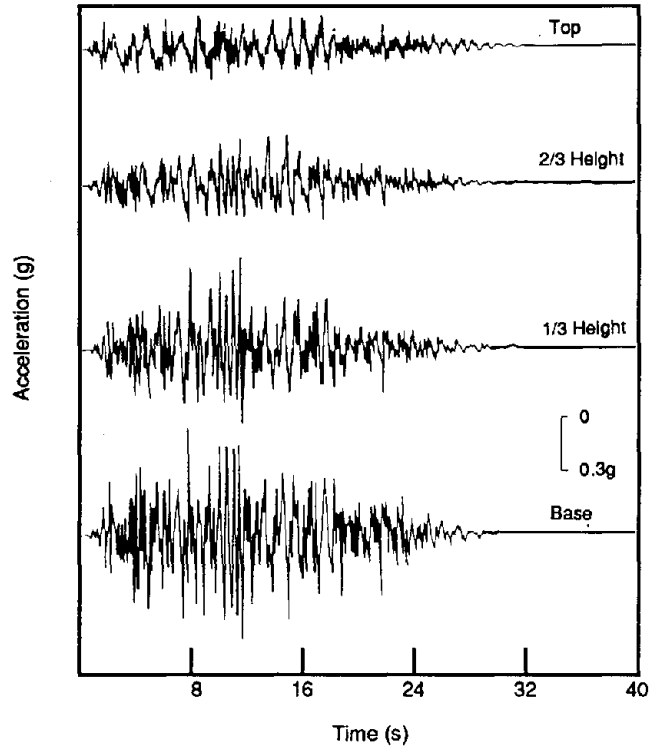


Figure 5. Recorded Accelerations at Various Depths in the Centrifuge (After Hushmand et. al. 1988)

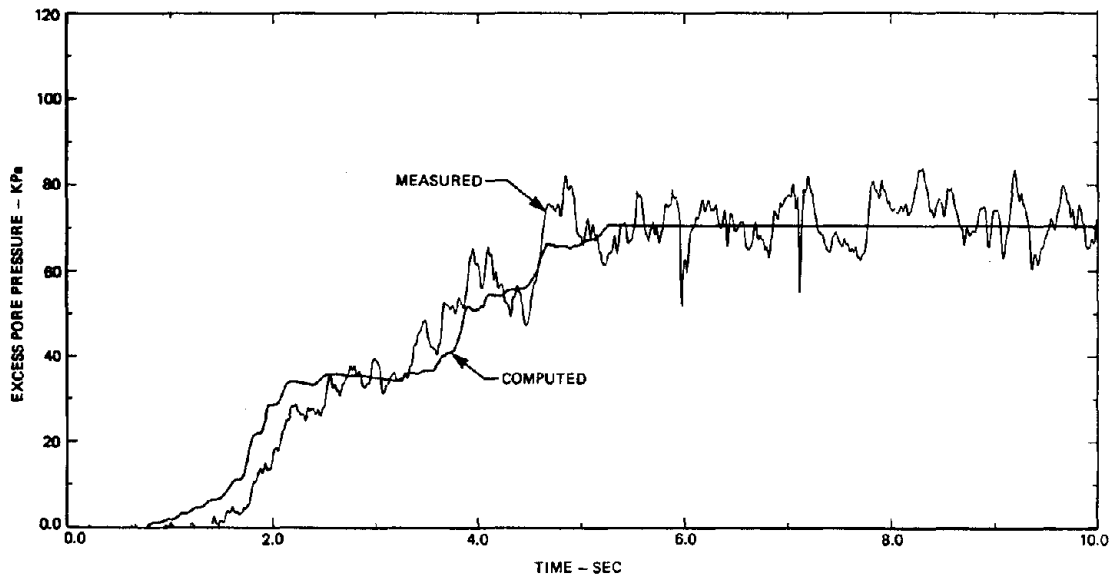


Figure 6. Measured Pore Pressure Response Versus Computed Response using DESRA (After Hushmand et. al., 1988)

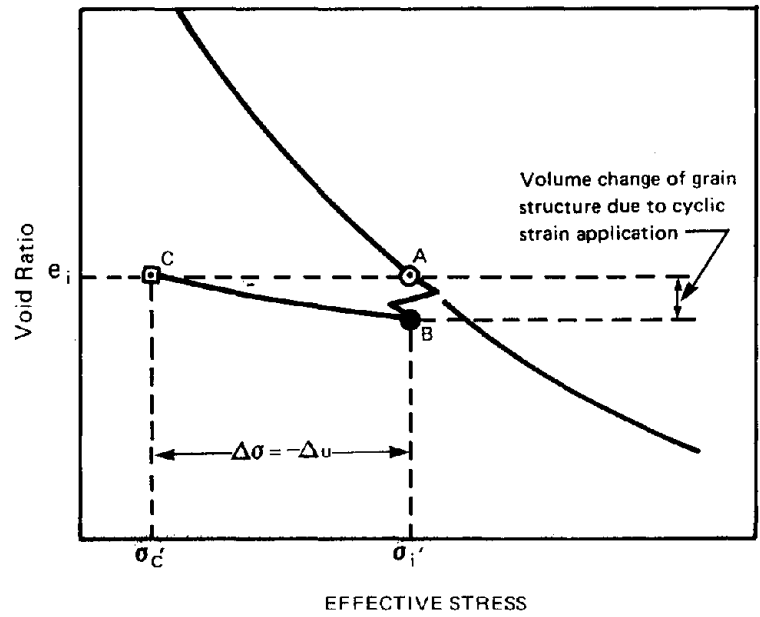


Figure 7. Mechanism of Pore Pressure Generation under Cyclic Loading

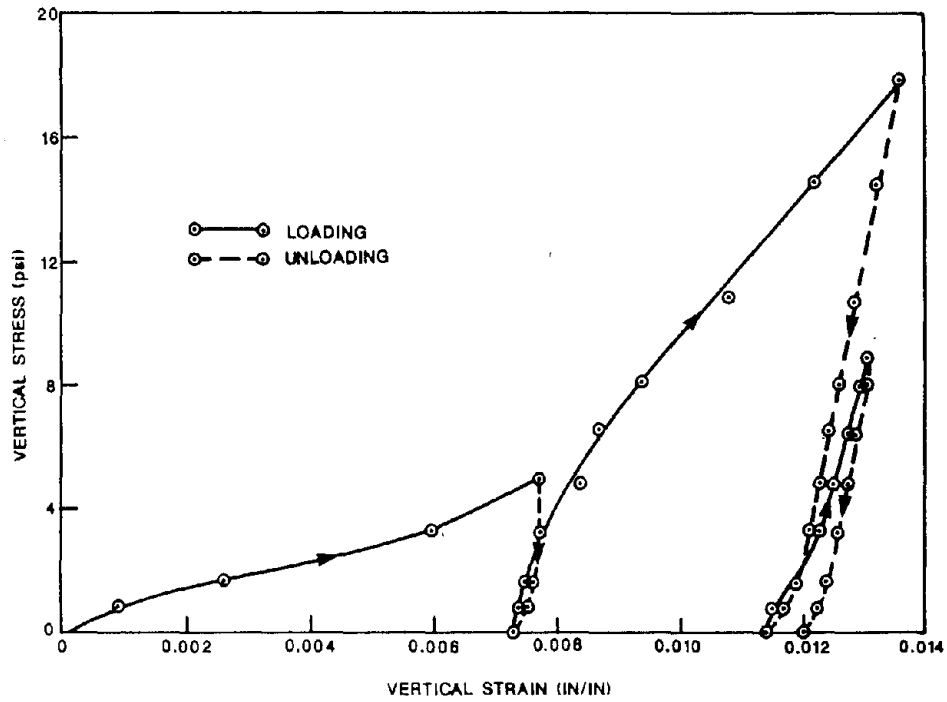


Figure 8. One Dimensional Loading and Unloading Characteristics of a Sand



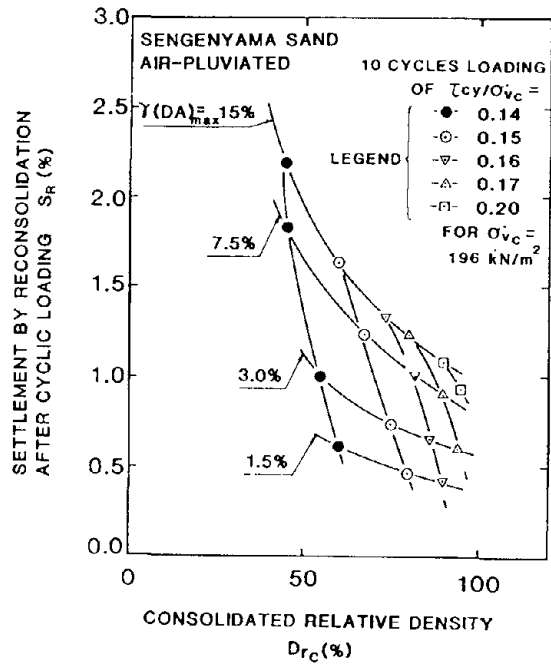


Figure 9. Post Liquefaction Settlement Versus Relative Density for Saturated Sands (After Tatsuoka et. al., 1984)

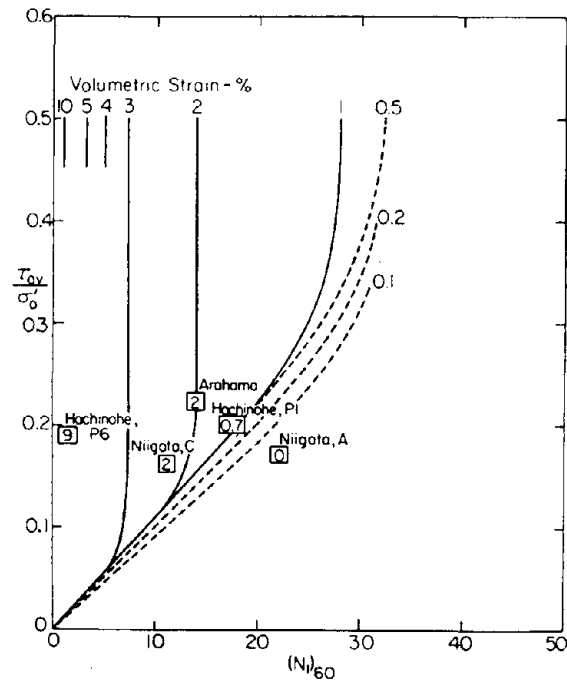
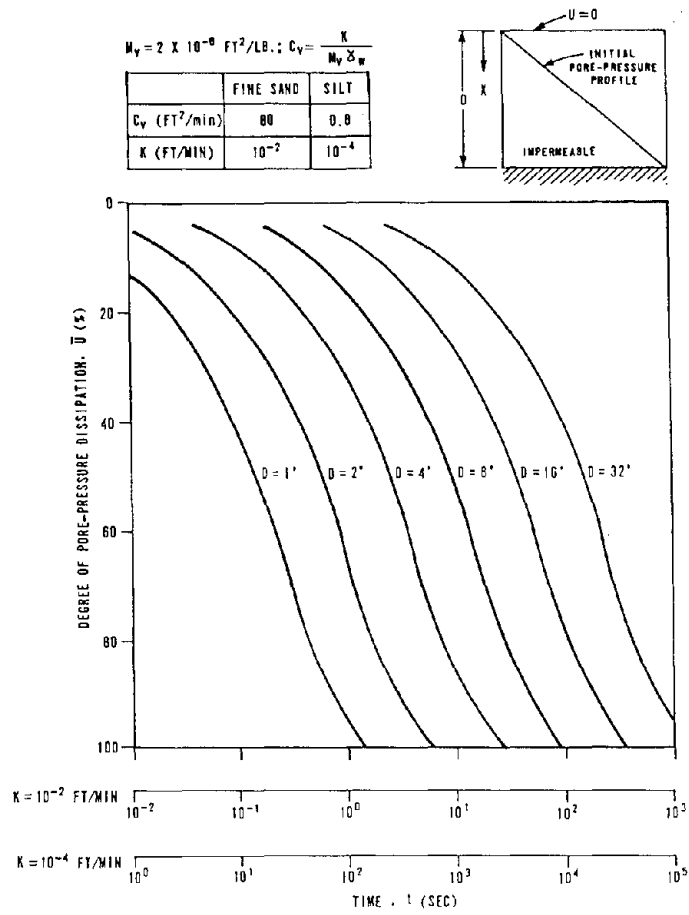
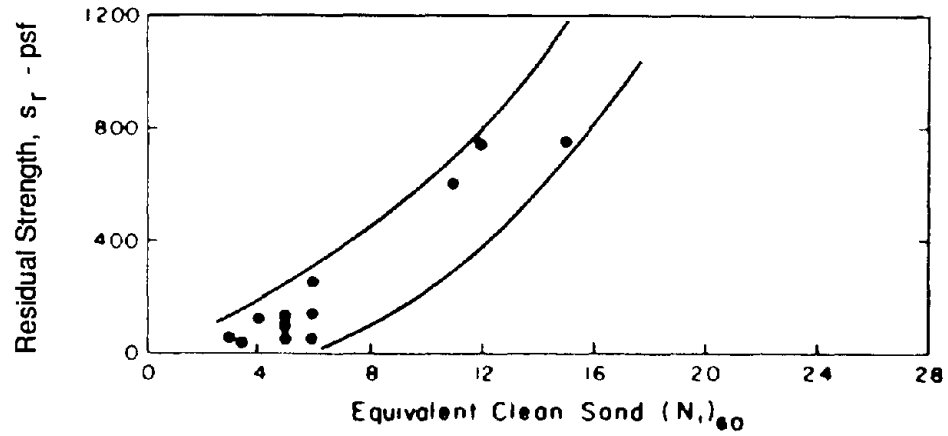


Figure 10. Proposed Chart for Determination of Post-Liquefaction Volumetric Strain of Saturated Sands (After Tokimatsu and Seed, 1987)



**Figure 11. Pore Pressure Dissipation Functions (After Martin et. al., 1980)**



**Figure 12. Tentative Relationship Between Undrained Residual Strength and Standard Penetration Blowcount for Saturated Sands (After Seed, 1987)**

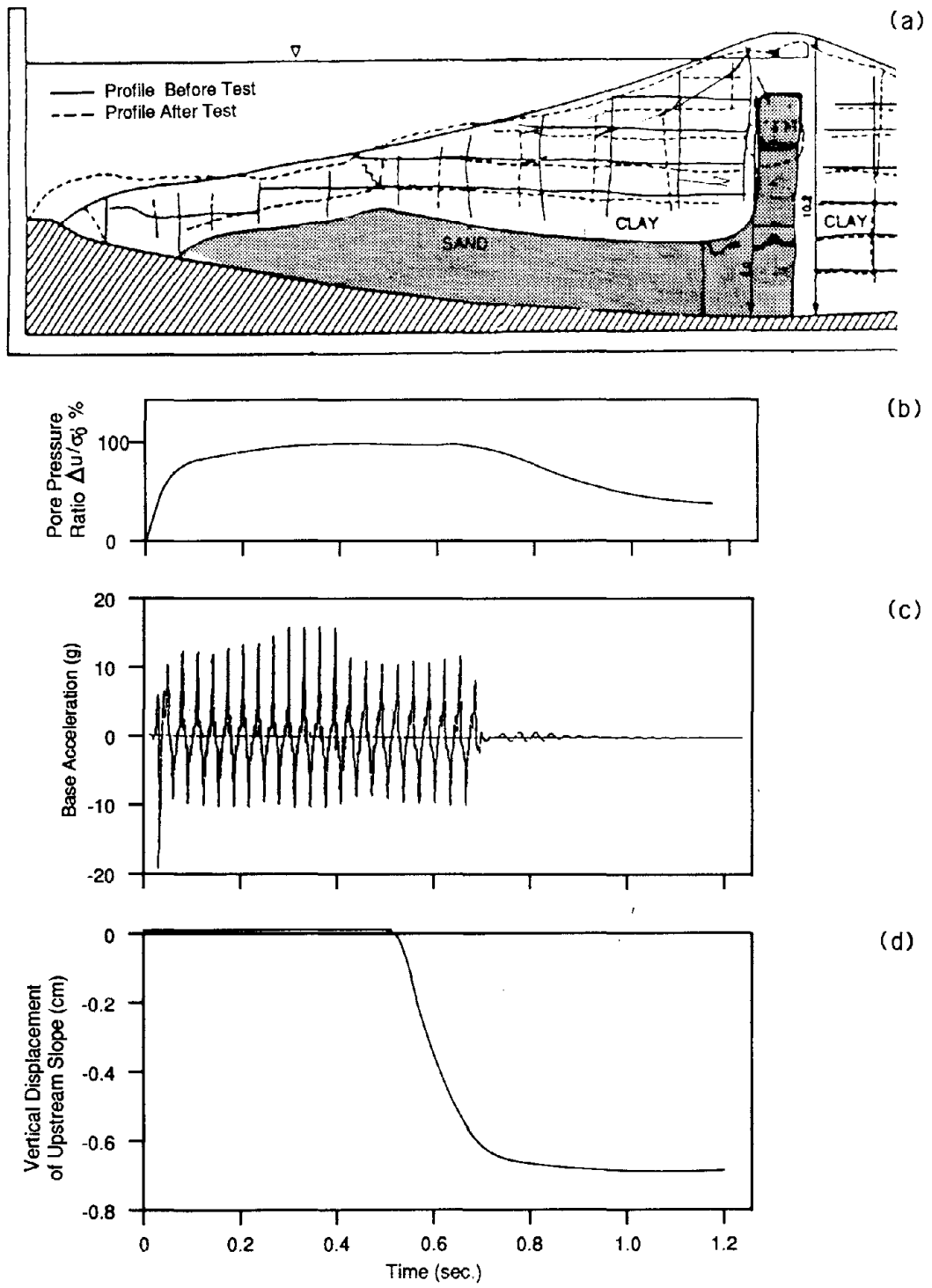


Figure 13. Centrifuge Test Data on a Liquefaction Induced Slope Failure (After Arulanandan, et.al., 1988)



# SOIL-STRUCTURE INTERACTION OF PILE FOUNDATIONS, WATERFRONT WALLS, AND BURIED PIPELINES

Dynamic Response Analysis of Pile Foundation-Structure Systems Taking into Account Nonlinear Behavior of Ground  
*Y. Iwazaki, K. Shimizu*

Dynamic Laboratory Tests of Piles  
*Y. Iwazaki, K. Shimizu, and T. Hirose*

Spreading Effects on Pile Foundations  
*T. O'Rourke, H. E. Stewart, and T. D. O'Rourke*

Seismic Stability of Waterfront Tied-Back Walls  
*S. K. Meekandani, M. Budu, and R. Richards, Jr.*

Dynamic Analysis of Seawall during 1983 Nipponkai-Chubu Earthquake  
*T. Kashi, M. Hatanaka, T. Shiomi, and Y. Tanaka*

Dynamic Analysis Procedures for Permanent Ground Deformation Effects on Buried Pipelines  
*T. O'Rourke*

Laboratory Study on Flexibility of Buried Pipeline Subject to Large Ground Displacement  
*T. Kobayashi, H. Nakane, N. Suzuki, and M. Ishikawa*

Relieving Seismic Stresses Locked in Gas Pipelines  
*T. O'Rourke*

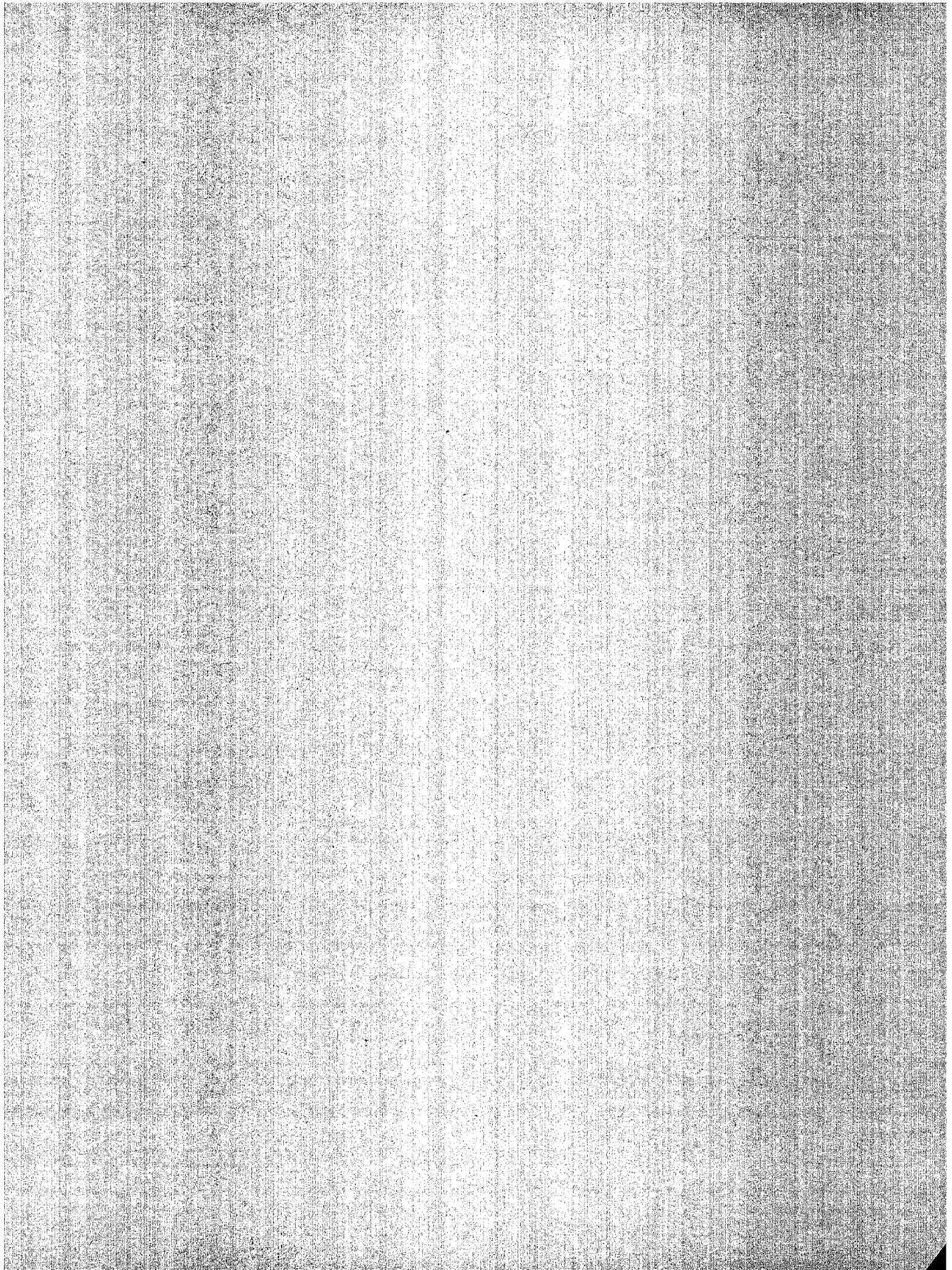
Effects of Large Ground Deformation on Buried Water Pipes of Various Materials  
*T. Kobayashi, M. Satoh, and S. Fukui*

Effects of Liquefaction-Induced Ground Movement on Pipeline  
*T. Kobayashi and M. Kitaura*

Dynamic Model of Buckling of Buried Pipelines  
*T. O'Rourke and J. Lee*

Modeling of Permanent Ground Deformation for Buried Pipelines  
*T. Kobayashi, H. Nakane, and M. Ishikawa*

Dynamic Behavior of Framed Foundation-Ground Systems during Earthquake  
*M. Yoshikawa and M. Arano*



SEISMIC RESPONSE ANALYSIS OF PILE FOUNDATION-STRUCTURE SYSTEMS  
TAKING INTO ACCOUNT NONLINEAR BEHAVIOR OF GROUND

Takashi TAZOH<sup>(1)</sup> and Katsumi SHIMIZU<sup>(2)</sup>

1. Senior Research Engineer  
Institute of Technology of Shimizu Corporation

2. Research Engineer  
Institute of Technology of Shimizu Corporation

ABSTRACT

A method for the analysis of the seismic response of pile foundation-structure systems taking into account the nonlinear behavior of the ground is proposed in this paper. Seismic response of pile foundations affected by nonlinearity of ground is investigated in order to identify the actual response characteristics based on data obtained from shaking table tests of a model. From a comparative study using various levels of input motion, significant differences in the variations of the fundamental natural frequencies and the magnification ratios of the acceleration amplitude, corresponding to inertial and kinematic interactions, are recognized. A method of analysis is proposed in which nonlinearities in the effective motion and the pile-head impedance are evaluated separately. Validity of the method is demonstrated by comparing analytical and test results.

## INTRODUCTION

A strong tendency has arisen in recent years towards the use of pile foundations for many structures on soft soil deposits. There are high expectations of wide application of this type of foundations due to their workability and economical efficiency.

Since soil is a material of strong nonlinear properties, nonlinear seismic response of the ground can be expected from strong seismic motions. High correlation between damage to structures and ground failure has been indicated in many reports of past destructive earthquakes. Therefore, it is very important to evaluate accurately the nonlinear seismic behavior of grounds at construction sites in order to accomplish the aseismicity of structures.

It is widely recognized that the establishment of a reliable earthquake-proof design method for pile foundations taking into consideration the nonlinear behavior of ground, is a matter of great importance at present. However, very few proposals have proved to be efficient enough to be adopted in engineering practice. The purpose of this study is to propose a practical method for the analysis of the seismic response of pile foundation-structure systems including the nonlinear characteristics of the ground.

In the first part of this paper, a seismic response analysis method for grouped piles foundations is proposed. It has been obtained by expanding the analytical method proposed by H. Tajimi<sup>(1)</sup> in order to allow the analysis of grouped piles including a multi-degree-of-freedom model for the superstructure. This method is based on the three dimensional elastic wave propagation theory within the limits of elasticity for all the materials of the system. Validity of this method is verified through a comparison between observed seismic data and analytical results. Effective seismic motion of grouped piles foundations is also presented together with a numerical study.

In the second part, the nonlinearity of the seismic response of soft soil deposits is studied by using strong seismic motion records. At first, an identification study is carried out and it is found that the predominant period and the damping constant increase their values due to the nonlinearity. Next, numerical studies are performed using analytical models and it is concluded that the Modified Ramberg-Osgood model is the most suitable for the seismic response analysis of the ground.



In the last part, seismic response characteristics of pile foundation-structure systems affected by nonlinear behavior of ground are investigated using data obtained from shaking table tests of a model. A special soil container for shear mode vibration is utilized for the experiments. The variations of two main parameters, namely natural frequency and the magnification ratio of the acceleration amplitude, are studied at the peaks corresponding to inertial interaction and kinematic interaction. The frequency transfer function between the pile-tip and the superstructure, obtained from the experimental data, is used for this study and significant differences in the variations of the above mentioned parameters are identified. The results of the described studies are compiled and analyzed and, by using them as a basis, a method for the analysis of the seismic response of pile foundation-structure systems taking into account nonlinear behavior of the ground is developed. Nonlinearities in the effective motion and the pile-head impedance are evaluated separately in this method. Validity of the proposed method is demonstrated by comparing analytical and test results.

#### SEISMIC RESPONSE ANALYSIS METHOD OF PILE FOUNDATION-STRUCTURE SYSTEMS

Tajimi<sup>(1)</sup> proposed a seismic response analysis method for a pile foundation with a rigid superstructure as shown in Fig.1, based on the three-dimensional elastic wave propagation theory. For a single pile, the horizontal displacement,  $u_p(z, \omega)$ , relative to the displacement of the pile tip, when the tip is excited by the horizontal acceleration  $u_g = -u_g \omega^2 e^{i\omega t}$ , is given by;

$$u_p(z, \omega) = V \cdot F^*(z, \omega) + u_g \cdot G^*(z, \omega) \quad (1)$$

where  $z$  is the coordinate taken along the pile with the origin located at the pile tip and the positive direction defined upward,  $\omega$  is the angular frequency of the excitation, and  $V$  is the lateral load applied at the pile head and defined as  $V = -m \{ \ddot{u}_p(H, \omega) + \ddot{u}_g \}$ . In addition,  $F^*(z, \omega)$  is the inverse of the complex stiffness of the pile-soil system to a lateral load acting on the pile head, and  $G^*(z, \omega)$  is the amplitude of the horizontal displacement of the pile caused by the input motion at the base.  $u_g$ ,  $F^*(z, \omega)$  and  $G^*(z, \omega)$  are defined as follows;

$$F^*(z, \omega) = \frac{1}{EI} \left( \frac{2H}{\pi} \right)^4 \frac{2}{H} F(z, \omega) \quad (2)$$

$$G^*(z, \omega) = \left( \frac{\omega}{\omega_g} \right)^2 G(z, \omega) \quad (3)$$

where  $EI$  is the flexural rigidity of the pile,  $H$  is the thickness of the surface layer, and  $\omega_g$  is the natural angular frequency of the surface layer. A detailed explanation of  $F(z, \omega)$  and  $G(z, \omega)$  can be found in reference 1.

Now, let us consider a one-degree-of-freedom model for the superstructure<sup>(2)</sup> as shown in Fig. 2. The lateral load can be defined as follows

$$V = -m_1(\ddot{u}_g + \ddot{u}_0 + \ddot{u}_1) - m_0(\ddot{u}_g + \ddot{u}_0) + P_e \quad (4)$$

where  $m_1$  and  $m_0$  are the masses of the superstructure and the footing, respectively,  $u_1$  and  $u_0$  are the horizontal displacements of the superstructure and the footing, and  $P_e$  is the earth pressure acting on the side of the footing.

Substituting equation (4) into equation (1), and defining

$$u_0 = u_p(H, \omega) \quad (5)$$

and solving simultaneously equation (5) and the following differential equation of motion derived for the superstructure system,

$$m_1 \ddot{u}_1 + c_1 \dot{u}_1 + k_1 u_1 = -m_1(\ddot{u}_g + \ddot{u}_0) \quad (6)$$

$u_1$  and  $u_0$  are defined as functions of  $u_g$ .  $u_1$  and  $u_0$  are explained in detail in reference 2.

The bending strain of the pile,  $\epsilon_p(z, \omega)$ , can be derived by calculating the 2nd derivative of  $u_p$  with respect to  $z$  and is given by

$$\epsilon_p(z, \omega) = -a \left\{ V \frac{\partial^2}{\partial z^2} F^*(z, \omega) + u_g \frac{\partial^2}{\partial z^2} G^*(z, \omega) \right\} \quad (7)$$

Equation (1) was derived for a single pile with radius  $a$  and length  $H$ . By expanding equation (1) to include the entire group of piles, the horizontal displacement of the pile head,  $u_p^G(H, \omega)$ , is written as<sup>(2)</sup>

$$u_p^G(H, \omega) = V \cdot F^{G*}(H, \omega) + u_g \cdot G^{G*}(H, \omega) \quad (8)$$

where  $F^{G*}(H, \omega)$  and  $G^{G*}(H, \omega)$  are

$$F^{G*}(H, \omega) = F^*(H, \omega) / (N \cdot e_N^l(\omega))$$

$$G^{G*}(H, \omega) = e_N^g(\omega) \cdot G^*(H, \omega) \quad (9)$$

$N$  is the number of piles, and  $e_N^l(\omega)$  and  $e_N^g(\omega)$  are the grouped piles effect factors for the cases of a lateral load acting on the pile head and ground shaking, respectively. Fig.3 shows the most general case whose response can be analyzed by this method. In this case the superstructure is represented by a multi-degree-of-freedom model.

#### SEISMIC RESPONSE ANALYSIS OF PILE FOUNDATIONS USING SEISMIC OBSERVATION DATA

The seismic response analysis of the pile foundation of a bridge pier based on the seismic observation data is carried out in order to verify the validity of the above presented method. Fig.4 shows the bridge pier at which the seismic observation was carried out<sup>(2)</sup>. This pier is supported by 64 (8 rows  $\times$  8 columns) steel pipe piles (diameter  $\phi = 600$  mm, length  $l = 22$  m, thickness of vertical piles  $t = 9$  mm, thickness of battered piles  $t = 12$  mm). Seismic observation is performed through the installation of accelerometers and strain meters on the bridge pier and its foundation piles. The details of the seismic observation can be found in reference 2.

Fig.5 shows a comparison between the bending strain of a pile obtained from the analysis and that from the observed records. The maximum values of acceleration recorded at the base and the surface are 114 and 33 Gals, respectively. In spite of the relatively large values of acceleration, studies showed that the ground remained within the limits of the elasticity. Comparison between the analytical results and the observed data shows a good agreement demonstrating the validity of the proposed method within the limits of elastic behavior of the ground.

## EFFECTIVE SEISMIC MOTION OF GROUPED PILES

Dynamic interaction of soil-pile-structure systems can be treated by considering inertial interaction and kinematic interaction separately. Inertial interaction is defined as the interaction due to the inertial force induced by the vibration of the superstructure and kinematic interaction is the one caused by the ground shaking. The total seismic response of soil-pile-structure systems is given by the sum of the responses due to the inertial and kinematic interactions. The seismic motion due to the kinematic interaction is called the effective seismic motion or effective input motion. The effective seismic motion is defined as the seismic response of a massless foundation excited by ground shaking.

The second terms of the right side of equations (1) and (8) correspond to the effective seismic motion of pile foundations. Therefore, from equation (8), the effective seismic motion of a grouped piles foundation can be written as

$$u^{Geff}(H, \omega) = u_g \cdot G^{G*}(H, \omega) = u_g \cdot e^{\eta_N(\omega)} \cdot G^*(H, \omega) \quad (10)$$

In this paper, the coefficient of the effective seismic motion of a grouped piles foundation,  $\eta(\omega)$ , is defined as the ratio of the effective seismic motion to the free-field motion. Acceleration is used as the motion parameter. When the surface layer is a uniform stratum,  $\eta(\omega)$  is evaluated as follows<sup>(3)</sup>

$$\eta(\omega) = \left| \frac{u^{Geff}(H, \omega) + 1}{\left(\frac{\omega}{\omega_g}\right)^2 \sum_{n=1,3,\dots}^{\infty} \frac{4}{n\pi} (-1)^{\frac{n-1}{2}} \frac{1}{\xi_n^2} + 1} \right| \quad (11)$$

where

$$\xi_n^2 = n^2 - (\omega/\omega_g)^2 + i 2h_g n^2 (\omega/\omega_g) \quad (12)$$

In equation (11),  $\eta(\omega) = 1.0$  means that the effective seismic motion has the same value of acceleration as the free-field motion, and  $\eta(\omega) > 1.0$  or  $\eta(\omega) < 1.0$  represents that the acceleration of the effective seismic motion is greater or smaller than that of the free-field motion, respectively.

Fig.6 shows the results of a numerical study of the coefficient of effective seismic motion of a grouped piles foundation,  $\eta(\omega)$ . This study is carried out under the following conditions: number of piles,  $N = 64$  (8 rows  $\times$  8 columns), diameter of the piles,  $\phi = 600$  mm, thickness,  $t = 9$  mm, length,  $l = 20$  m ( $l$  is taken equal to the thickness of the surface layer of the ground,  $H$ ), distance between two adjacent piles,  $d = 2.5\phi (= 1.5$  m), considered predominant periods of the ground,  $T_g = 0.5, 1.0,$  and  $1.5$  seconds. For the grouped piles effect factor due to the ground shaking,  $e^{\xi_N(\omega)}$ , the static value,  $e^{\xi_N(\omega=0)}$ , has been adopted for all the frequencies.

It is seen from Fig.6 that the coefficient  $\eta(\omega)$  is approximately equal to the unity for vibration periods longer than the predominant period of the soil layer,  $T_g$ . This means that the effective seismic motion coincides with the free-field motion in that period range. Furthermore, it can be seen that the effective seismic motion is smaller than the free-field motion for periods shorter than approximately one third of  $T_g$ .

#### STRONG MOTIONS OBSERVED ON SOFT SOIL DEPOSITS

Figs.7 and 8 show strong motions recorded on and inside soft soil deposits<sup>(4)(5)</sup>. The maximum accelerations at the ground surface are 194 and 435 gals, respectively. It is known that for a typical nonlinear seismic response of soft soil deposits, the predominant period grows longer and the magnification of the acceleration amplitude between the ground surface and the base becomes smaller. These phenomena occur as a result of decreasing shear modulus and increasing hysteretic damping of soils caused by the strong seismic excitation.

Tables 1 and 2 summarize the results of the analysis of the records shown in Figs.7 and 8, for which the time-varying predominant period  $T_1$  and damping constant  $h_1$  were evaluated at two-seconds intervals<sup>(6)</sup>. It is found from Table 1 that the predominant period  $T_1$  changes from 0.52 to 0.74 seconds and the damping constant  $h_1$  varies from 0.045 to 0.100. It is clear that the increases in the predominant period and the damping constant are due to the nonlinear response of the ground especially during the interval between 4 and 6 seconds of the records. Similarly, it can be seen from Table 2 that the predominant period of 0.30 seconds corresponding to the elastic seismic response becomes 0.45 seconds, and the damping constant of 0.060 increases to 0.168 in the interval between 3 and 5 seconds.

## NONLINEAR SEISMIC RESPONSE ANALYSIS USING STRONG SEISMIC RECORDS

Modified Hardin-Drnevich and modified Ramberg-Osgood models are generally used in nonlinear seismic response analysis of ground using the step-by-step integration method. Since there are only a few available records of seismic strong motions obtained from array observations, it is still not clear how applicable to the real field these models are.

In Figs.9 and 10, the results obtained from nonlinear seismic response analyses are compared with the observed records at the ground surface shown in Figs.7 and 8. In all cases, the solid lines are the calculated waves and dashed lines are the observed records. Significant differences can be found from the study of Figs.9 and 10, especially for the interval between 3 and 6 seconds of the records. It is concluded that the modified Ramberg-Osgood model provides better results and can be effectively used in nonlinear seismic response analysis<sup>(4)(5)</sup>.

### SEISMIC RESPONSE OF PILE FOUNDATION-STRUCTURE SYSTEMS AFFECTED BY NONLINEAR BEHAVIOR OF GROUND

Soil behaves strongly nonlinear when excited by high levels of seismic motion. It is obvious that the seismic response of pile foundation-structure systems is considerably influenced by the nonlinear behavior of the ground. Since it is important to know the real response characteristics of pile foundations affected by the nonlinear behavior of the ground, studies based on shaking table tests of a model using a special soil container for shear mode vibration are carried out.

Fig.11 shows schematically the test model. Piles are made of aluminium. Diameter of the piles,  $\phi$ , is 30 mm, thickness,  $t$ , is 1 mm, and length,  $l$ , is 900 mm. The pile foundation has 9 piles (distance between piles  $d = 75$  mm) arranged in 3 columns  $\times$  3 rows. The pile-heads and pile-tips are firmly connected to a rigid footing and the base of the container, respectively. An iron board of 33.8 kgf, simulating superstructure, is supported by four plates arranged in such a way to allow only shear deformation. The fundamental natural frequency,  $f_{so}$ , of the superstructure when the ends of the four supports are fixed to a rigid body, is 24.5Hz. Dried sand is used as the material for the ground model. Measurement is performed through the installation of accelerometers in the ground, on the superstructure, and on the footing, strain meters on the piles, and displacement meters on the side of the container.

Fig.12 presents the transfer function between the base (AG-1) and the superstructure (AS-2) calculated by using the accelerations recorded during the tests. The model was excited by sinusoidal input motions and values of maximum acceleration,  $A_{Omax}$ , of 25, 100, and 250 gals were adopted. It can be seen in Fig.12 that two peaks appear clearly for each transfer function curve. The peak towards the left has a corresponding frequency  $f_{g1}$  which was found to have the same value as the fundamental natural frequency of the ground determined by using the transfer function between the base (AG-1) and the ground surface (AG-2). A frequency  $f_{s1}$  corresponds to the peak at the right hand side of the transfer function curves. As expected,  $f_{s1}$  is smaller than  $f_{s0} = 24.5$  Hz. This reduction is the result of the soil-pile-superstructure interaction.

As it was already mentioned, dynamic interaction of soil-pile-structure systems can be treated by considering inertial and kinematic interactions separately. It can be seen that the frequencies  $f_{g1}$  and  $f_{s1}$  are governed by the inertial and kinematic interactions, respectively. Due to the increase of  $A_{Omax}$ ,  $f_{g1}$  and  $f_{s1}$  move toward lower frequencies, that is, 10 Hz, 7 Hz, 5 Hz, and 17 Hz, 14 Hz, 13 Hz, respectively, and the magnification ratios  $\alpha_{g1}$  and  $\alpha_{s1}$ , corresponding to  $f_{g1}$  and  $f_{s1}$ , take also lower values, namely 12.0, 5.3, 3.3 and 17.3, 7.8, 6.7, respectively. These variations are a result of the nonlinear behavior of the ground. However, it is found from the variations of  $f_{g1}$ ,  $f_{s1}$  and  $\alpha_{g1}$ ,  $\alpha_{s1}$  that the decreasing ratios of  $f_{g1}$  and  $\alpha_{g1}$  are not the same as those of  $f_{s1}$  and  $\alpha_{s1}$ . These differences seem to be a very important matter when dealing with seismic response analysis methods for pile foundation-structure systems taking into account the nonlinear behavior of the ground.

The above mentioned phenomenon is the result of the difference in the variation rates of the shear modulus and hysteretic damping corresponding to frequencies  $f_{g1}$  and  $f_{s1}$ . The variations of  $f_{g1}$  and  $\alpha_{g1}$  are produced by the nonlinear behavior of the ground due to the ground shaking (kinematic interaction). The variations of  $f_{s1}$  and  $\alpha_{s1}$  are the result of the nonlinear behavior of the ground surrounding the pile-head due to the inertial force induced by the vibration of the superstructure (inertial interaction).

The differences observed in Fig.12 can be confirmed analytically through the comparison of the numerical results, calculated using equation (8), and the test results. Fig.13 shows the transfer function between the base (AG-1) and the superstructure (AS-2). Solid line and dotted marks represent the analytical and test results, respectively. The analysis was carried out using the values of the equivalent

shear modulus,  $G_{g1}^*$ , and the equivalent damping constant,  $h_{g1}^*$ , of the ground obtained by making the analytical values of frequency  $f_{g1}$  and the corresponding magnification ratio  $\alpha_{g1}$  to coincide with the values of the test. Consequently,  $f_{g1}$  and  $\alpha_{g1}$  agree with the test results, as shown in Fig.13, but remarkable differences are found between the analytical and test results obtained for the frequency  $f_{s1}$  and the corresponding magnification ratio  $\alpha_{s1}$ . From these findings, it is concluded that very significant differences occur between the nonlinear seismic behavior of the ground induced by the inertial interaction and that induced by the kinematic interaction.

### PROPOSED METHOD FOR RESPONSE ANALYSIS OF PILE FOUNDATION-STRUCTURE SYSTEMS CONSIDERING NONLINEAR BEHAVIOR OF GROUND

According to the dynamic sub-structure method, the seismic response of pile foundation-structure systems is obtained by inputting the effective seismic motion of the pile-soil system to the superstructure through the pile-head impedance. The above mentioned difference between the nonlinear seismic responses of the ground caused by the kinematic and the inertial interactions, suggests that the effective seismic motion and the pile-head impedance should be evaluated separately. Different values of equivalent shearing modulus and damping constant of the ground should be adopted for each case.

In this paper, the effective seismic motion and the pile-head impedance, taking into account the nonlinear behavior of the ground, are proposed to be evaluated in the following manner.

- (1) The effective seismic motion is evaluated multiplying the nonlinear seismic motion of the free-field by the coefficient of the effective seismic motion,  $\eta(\omega)$ .
- (2) The pile-head impedance is determined considering nonlinear behavior of the ground surrounding the pile-head and may be evaluated using a nonlinear dynamic analysis method for pile foundations subjected to a lateral load acting on the pile-head, for example the one proposed by T. Nogami et al.<sup>(7)</sup>, or using results from forced vibration tests of real pile foundations, or adopting a prediction equation based on experimental data.



## NUMERICAL ANALYSIS USING THE PROPOSED METHOD

In order to verify the validity of the proposed method, a comparison between the response waves obtained analytically and those obtained from shaking table tests of the model shown in Fig.11, is carried out. By assuming the coefficient of the effective seismic motion,  $\eta(\omega)$ , to be 1.0 for all frequencies, the acceleration data obtained at the ground surface (AG-2) were used as the effective seismic motion in this numerical study. The pile-head impedance was estimated from equation (9), using the equivalent shear modulus,  $G_{s1}^e$ , and damping constant,  $h_{s1}^e l$ , that were obtained making the values of the calculated  $f_{s1}$  and  $\alpha_{s1}$  to coincide with those obtained from tests.

Fig.14 shows the comparison between the analytical and test results of the acceleration response of the superstructure (AS-2) and the footing (AS-1). Except for the maximum values, good agreement between both waves is observed demonstrating the validity of the proposed method.

Fig.15 presents the comparison between the analytical and test results of the bending strain response of the piles. As it was indicated previously, it is also necessary to evaluate the bending strain due to inertial interaction,  $\epsilon_{b^f}(z, \omega)$ , and that due to kinematic interaction,  $\epsilon_{b^g}(z, \omega)$ , separately.  $\epsilon_{b^f}(z, \omega)$  and  $\epsilon_{b^g}(z, \omega)$  can be derived from equation (7) as follows

$$\epsilon_{b^f}(z, \omega) = -a \nu^f_i(z, \omega) (V/N) \frac{\partial^2}{\partial z^2} F^*(z, \omega) \quad (13)$$

$$\epsilon_{b^g}(z, \omega) = -a \nu^g_i(z, \omega) u_g \frac{\partial^2}{\partial z^2} G^*(z, \omega) \quad (14)$$

and the total bending strain of the pile foundation is defined as

$$\epsilon_{b^t}(z, \omega) = \epsilon_{b^f}(z, \omega) + \epsilon_{b^g}(z, \omega) \quad (15)$$

where  $\nu^f_i(z, \omega)$  is the fraction of the lateral load taken by pile  $i$ , and  $\nu^g_i(z, \omega)$  expresses the difference between the deformation of grouped piles and that of a single pile subjected to the same ground shaking. In this numerical study, the equivalent shear modulus  $G_{s1}^e$  and damping constant  $h_{s1}^e$  were used with equation (13), and  $G_{g1}^e$  and  $h_{g1}^e$  were used with equation (14). The values of  $G_{s1}^e$ ,  $h_{s1}^e$ , and  $G_{g1}^e$ ,  $h_{g1}^e$  were obtained separately as follows. The values of  $G_{s1}^e$  and  $h_{s1}^e$  were

determined making the analytical values of  $f_{s1}$  and  $\alpha_{s1}$  to coincide with the test results, the values of  $G_{s1}^e$  and  $h_{s1}^e$  were determined. In the same manner, the analytical values of  $f_{g1}$  and  $\alpha_{g1}$  were given the same values as those obtained from the tests and  $G_{g1}^e$  and  $h_{g1}^e$  could be determined. For  $\nu_{f_1}^f(z, \omega)$  and  $\nu_{g_1}^g(z, \omega)$ , the values of  $\nu_{f_1}^f(z, \omega) = \nu_{f_1}^f(H, 0)$  and  $\nu_{g_1}^g(z, \omega) = \nu_{g_1}^g(H, 0)$  were adopted. As it can be seen from Fig.15, a complete agreement between the analytical results and test data was not obtained. However, the results presented in Fig.15 can be regarded as accurate enough to be used effectively in engineering practice.

## CONCLUSIONS

When studying the effects of the nonlinearity of the ground on the seismic response of pile foundation-structure systems, important differences in the variation rates of shear modulus and hysteretic damping constant corresponding to the kinematic and inertial interactions were clearly recognized from the shaking table tests. A seismic response analysis method for grouped piles foundation-structure systems taking into account nonlinear behavior of the ground was proposed. In this method, the effective seismic motion and the pile-head impedance are evaluated separately. The process to estimate the effective seismic motion and the pile-head impedance is as follows.

(1) The effective seismic motion taking into account the nonlinear behavior of the ground is obtained multiplying the nonlinear seismic motion of the free-field by the coefficient of the effective seismic motion,  $\eta(\omega)$ .

(2) Considering a nonlinear behavior of the part of the ground surrounding the pile-head, the pile-head impedance can be derived applying any of the following methods: using a nonlinear dynamic analysis method for pile foundations with a lateral load acting on the pile-head, using data obtained from forced vibration tests of real pile foundations, or using a prediction equation based on experimental data.

Validity of the proposed method was verified by comparing analytical and test results.

## REFERENCES

- (1) H. Tajimi, "Dynamic Analysis of a structure Embedded in an Elastic Stratum," Fourth World Conference on Earthquake Engineering, July, 1969.
- (2) T. Tazoh, K. Shimizu, and T. Wakahara, "Seismic Observations and Analysis of Grouped Piles," Dynamic Response of Pile Foundation — Experiment, Analysis and Observation, Geotechnical Special Publication No.11, ASCE, April, 1987.
- (3) T. Tazoh, T. Wakahara, K. Shimizu, and M. Matsuzaki, "Effective Motion of Group Pile Foundations," Ninth World Conference on Earthquake Engineering, August, 1988.
- (4) T. Tazoh, S. Nakahi, K. Shimizu, and H. Yokota, "Vibration Characteristics of Dynamic Models of Soil and Their Applicability to the Field," Eighth World Conference on Earthquake Engineering, August, 1984.
- (5) T. Tazoh, M. Sato, K. Shimizu, and A. Hatakeyama, "Nonlinear Seismic Response Analysis of Soil Deposit Using Strong Seismic Records," Ninth World Conference on Earthquake Engineering, August, 1988.
- (6) T. Tazoh, K. Shimizu, M. Sato, T. Hirose, and K. Koyama, "Identification of Time-Varying Predominant Period and Damping Constant in Nonlinear Seismic Response of Soft Soil Deposit," Ninth World Conference on Earthquake Engineering, August, 1988.
- (7) T. Nogami and H.-L. Chen, "Prediction of Dynamic Lateral Response of Nonlinear Single-Pile by Using Winkler Soil Model," Dynamic Response of Pile Foundation — Experiment, Analysis and Observation, Geotechnical Special Publication No.11, ASCE, April, 1987.

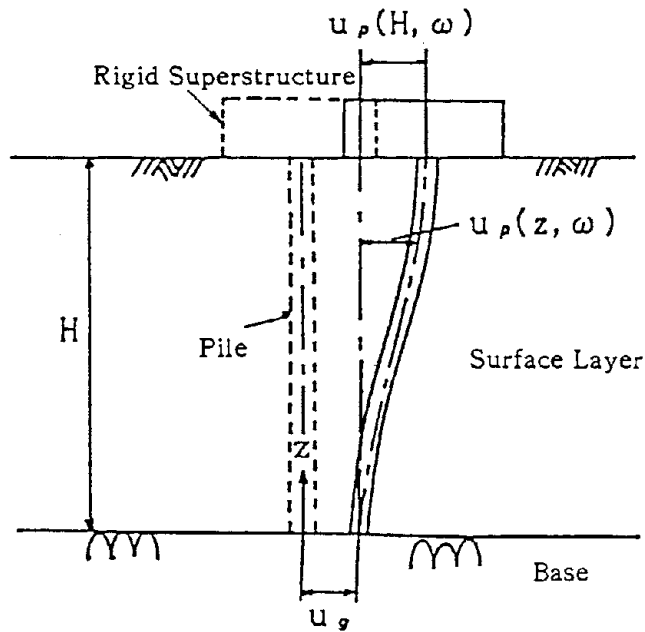


Fig.1 Tajimi Model — Pile foundation with rigid superstructure (Single pile)

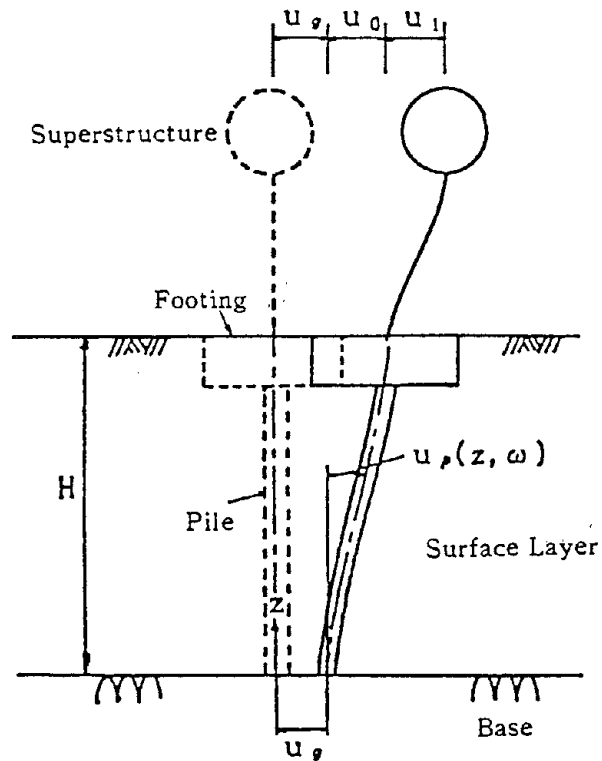


Fig.2 Pile foundation with a one-degree-of-freedom model for the superstructure (Single pile)

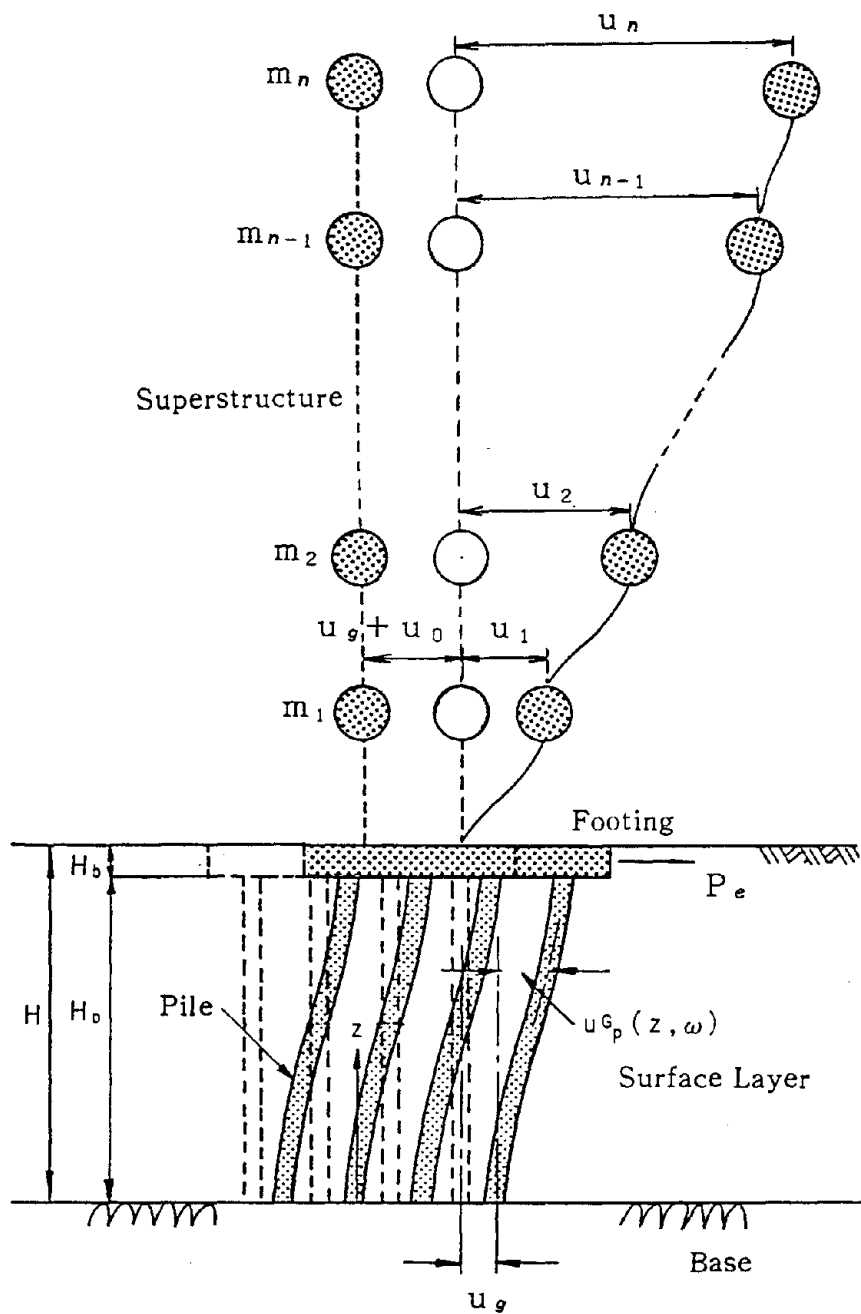


Fig.3 Grouped piles foundation with a multi-degree-of-freedom model for the superstructure

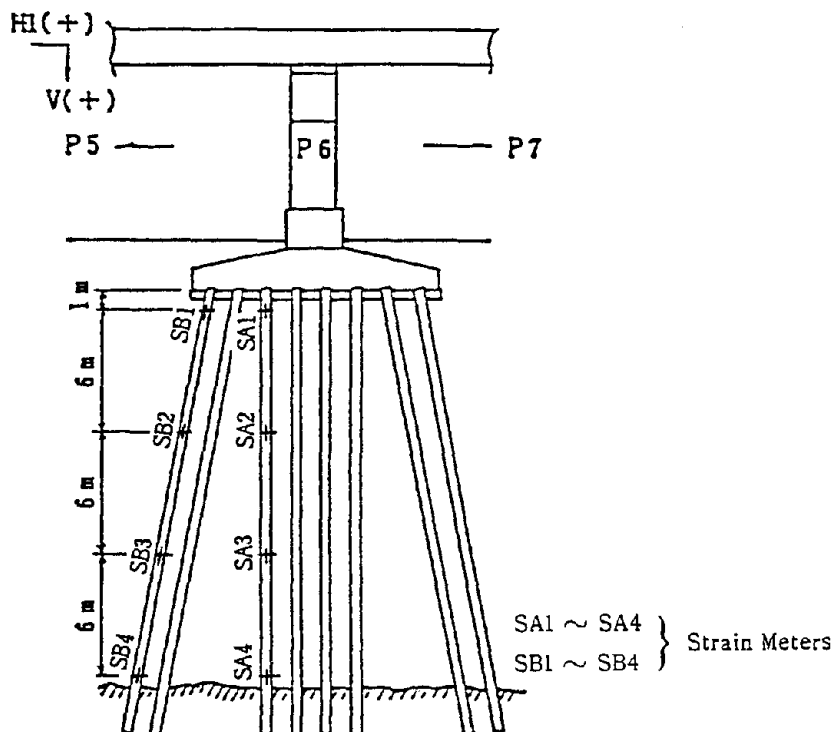


Fig.4 Bridge pier and its pile foundation at which seismic observation was carried out

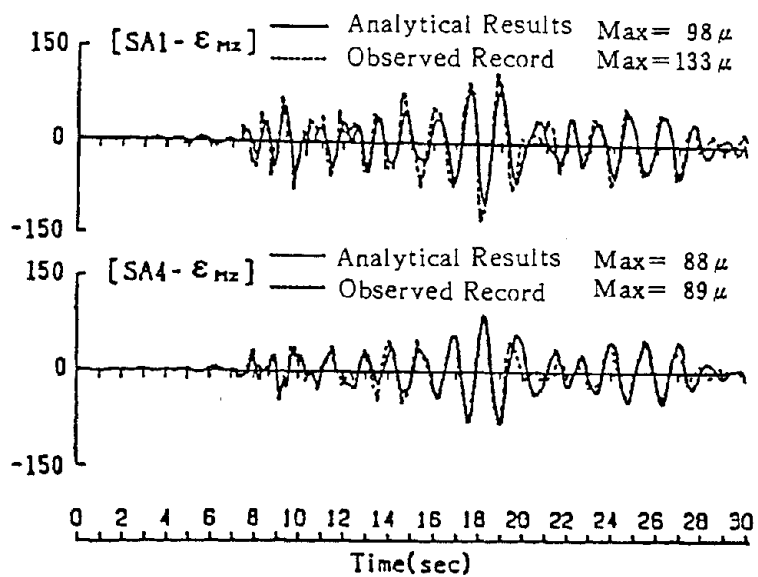


Fig.5 Comparison between bending strains of pile obtained from analytical results and observed data

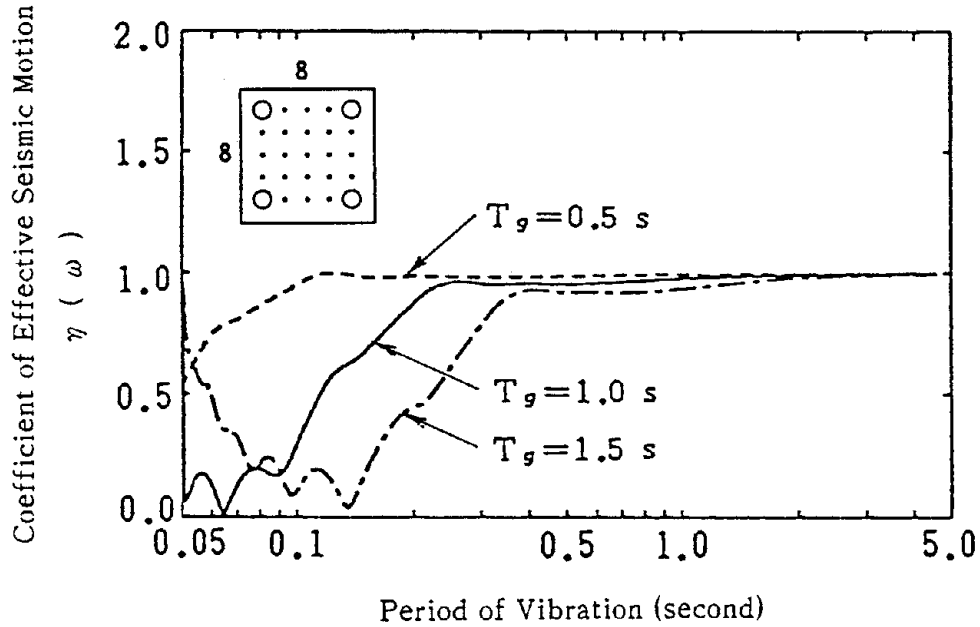


Fig.6 Variation of the coefficient of effective seismic motion  $\eta(\omega)$  with the period of vibration

Table 1 Results of identification studies of strong motion records obtained at ground point A

	Considered Interval of the Record (sec)				
	0 ~ 2 sec	2 ~ 4 sec	4 ~ 6 sec	6 ~ 8 sec	8 ~ 10 sec
Predominant Period (sec)	0.518	0.586	0.738	0.679	0.715
Damping Constant	0.045	0.050	0.100	0.061	0.089

Table 2 Results of identification studies of strong motion records obtained at ground point B

	Considered Interval of the Record (sec)				
	0 ~ 2 sec	2 ~ 4 sec	4 ~ 6 sec	6 ~ 8 sec	8 ~ 10 sec
Predominant Period (sec)	0.302	0.453	0.436	0.421	0.326
Damping Constant	0.060	0.168	0.064	0.020	0.011

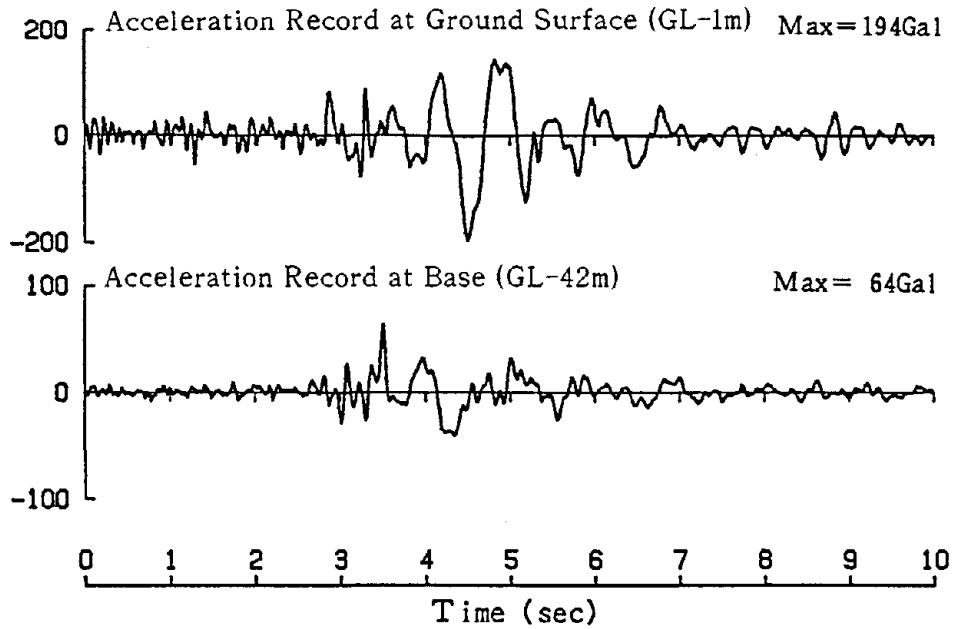


Fig.7 Strong motion records obtained at ground point A

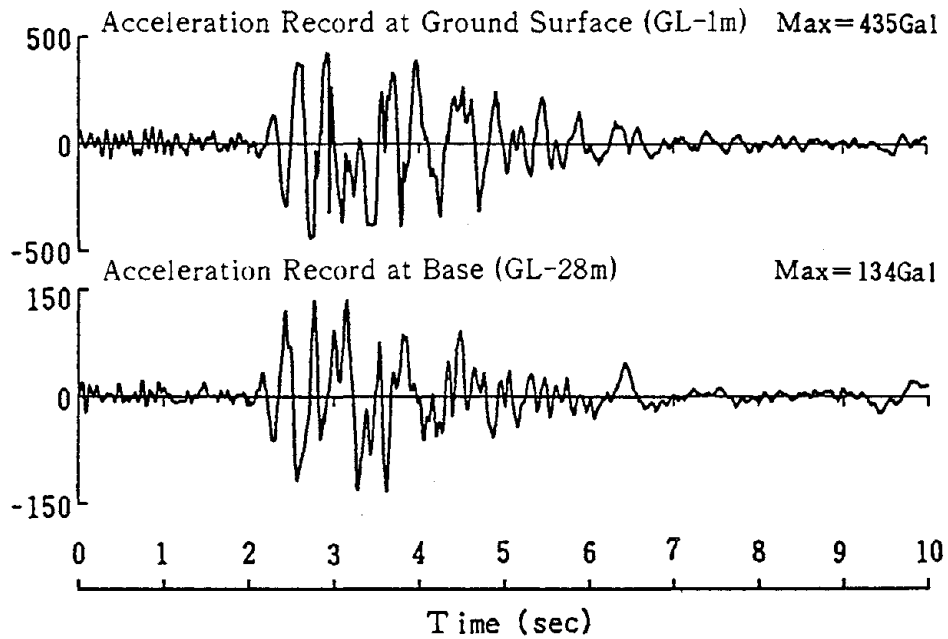


Fig.8 Strong motion records obtained at ground point B



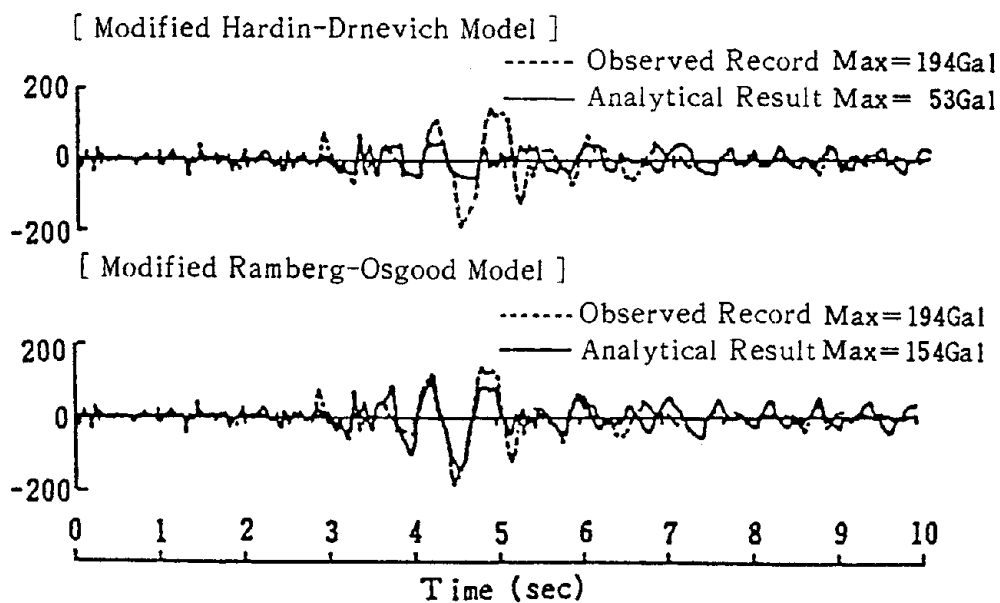


Fig.9 Nonlinear response analysis using strong motion records obtained at ground point A

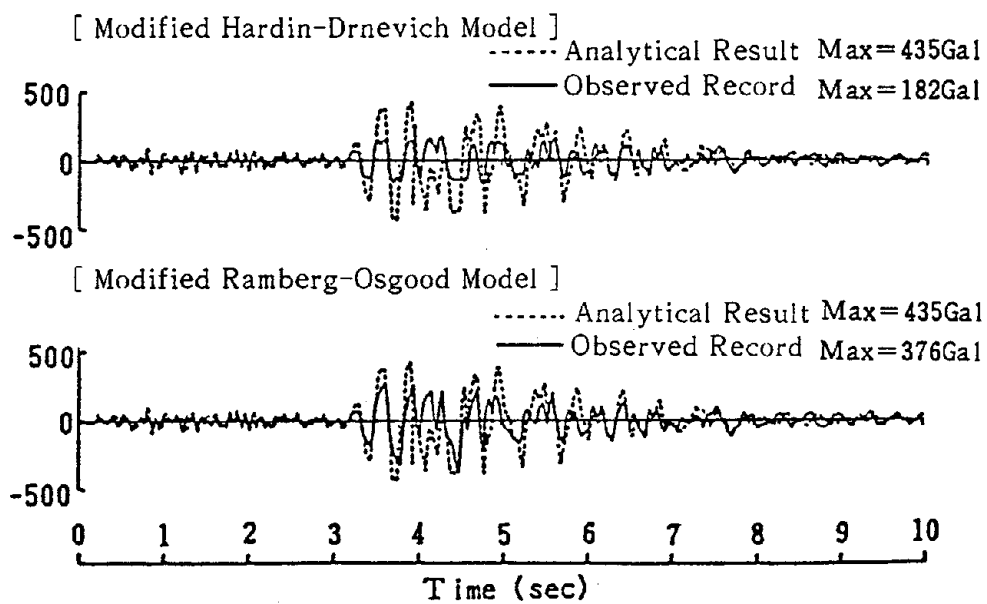
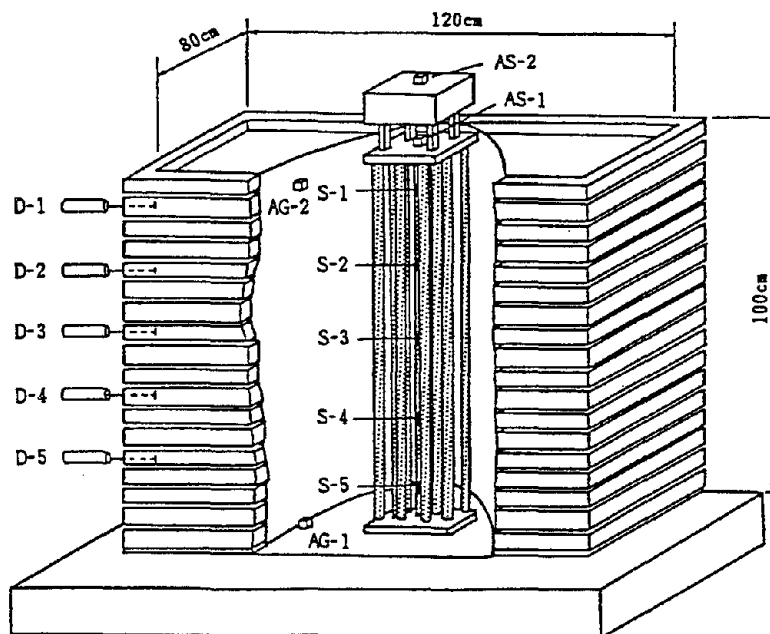


Fig.10 Nonlinear response analysis using strong motion records obtained at ground point B



AG-1,AG-2,AS-1,AS-2 : Accelerometer  
 S-1 ~ S-5 : Strain Meter  
 D-1 ~ D-5 : Displacement Meter

Fig.11 The test model and measurement equipment

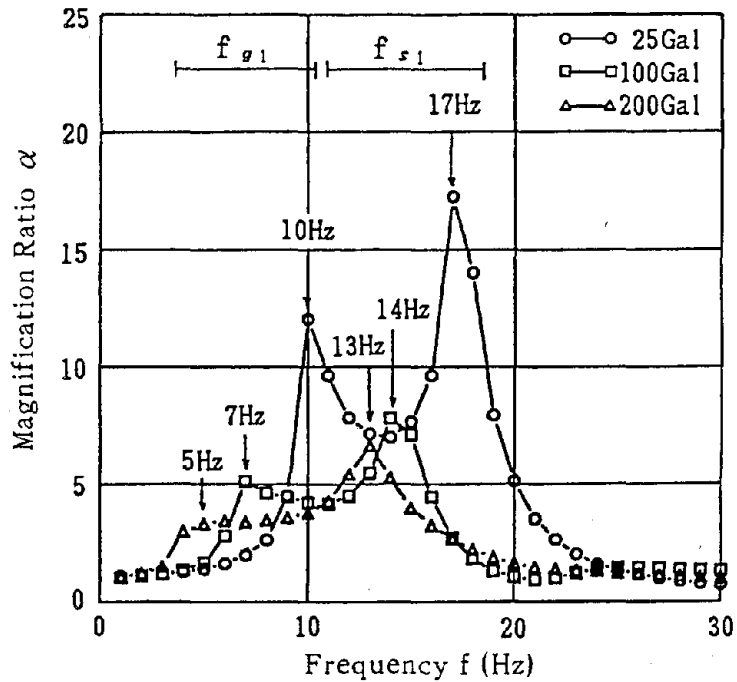


Fig.12 Transfer function between base (AG-1) and superstructure (AS-2) (see Fig.11)

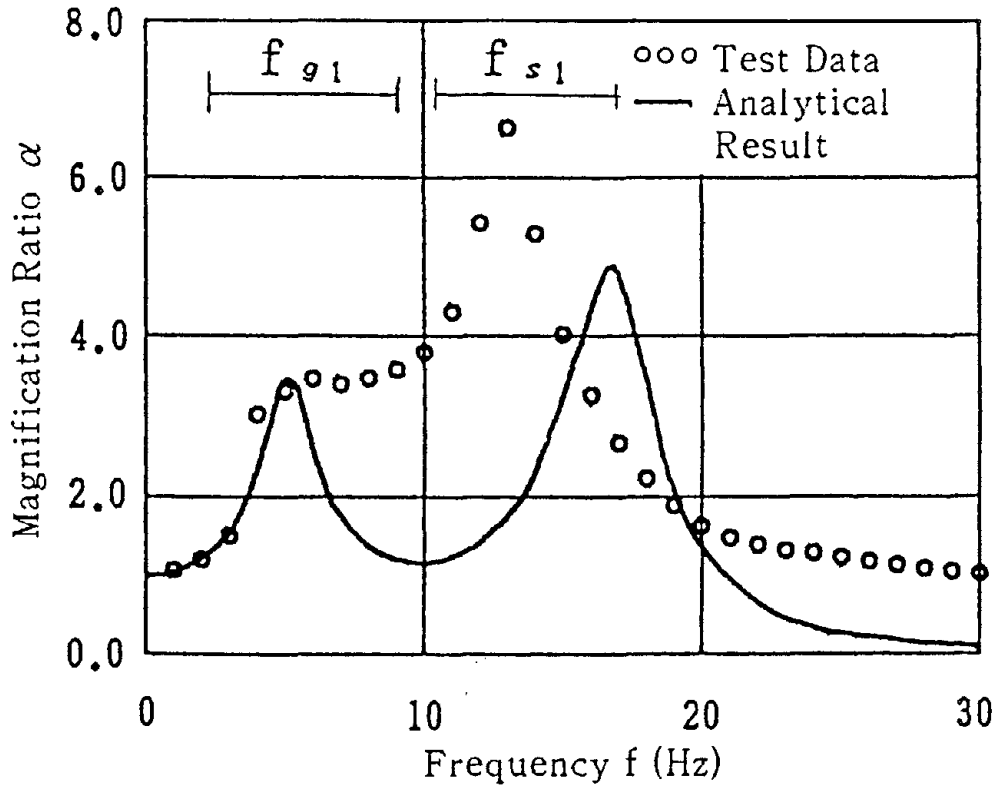


Fig.13 Comparison between analytical and test results obtained for the transfer function between base (AG-1) and superstructure (AS-2)

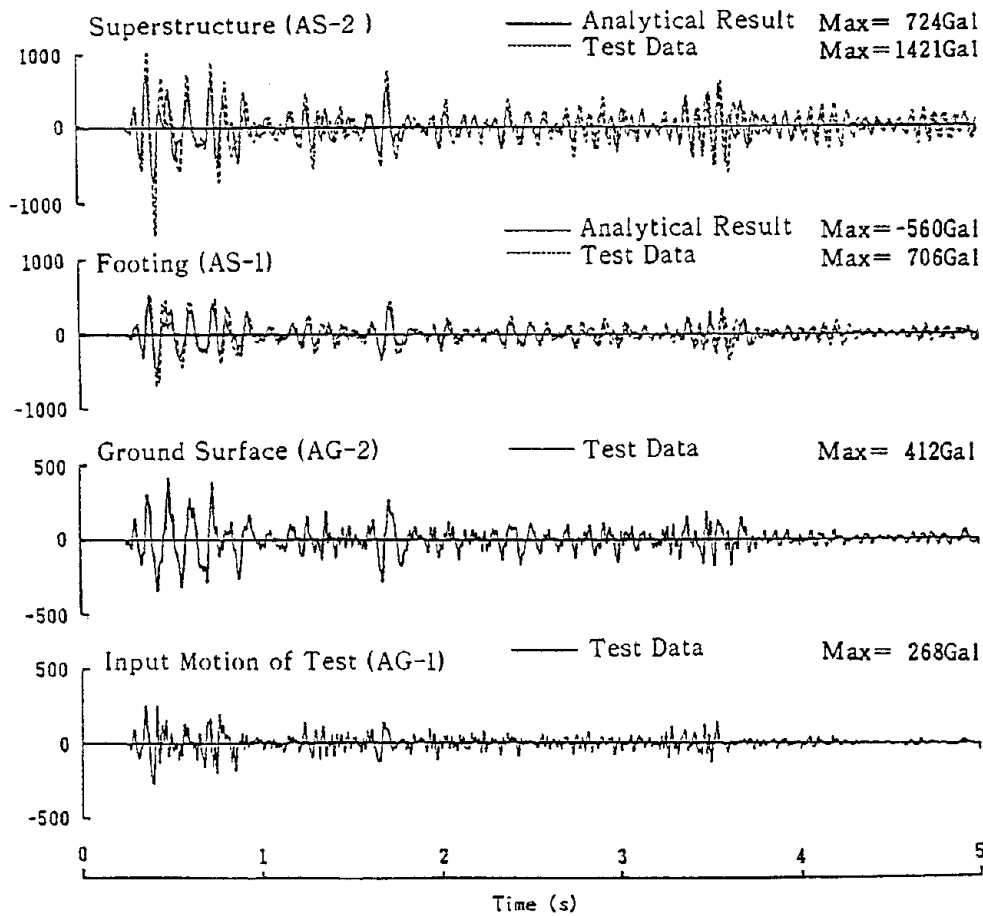


Fig.14 Comparison between analytical and test results of the acceleration at the superstructure (AS-2) and footing (AS-1)

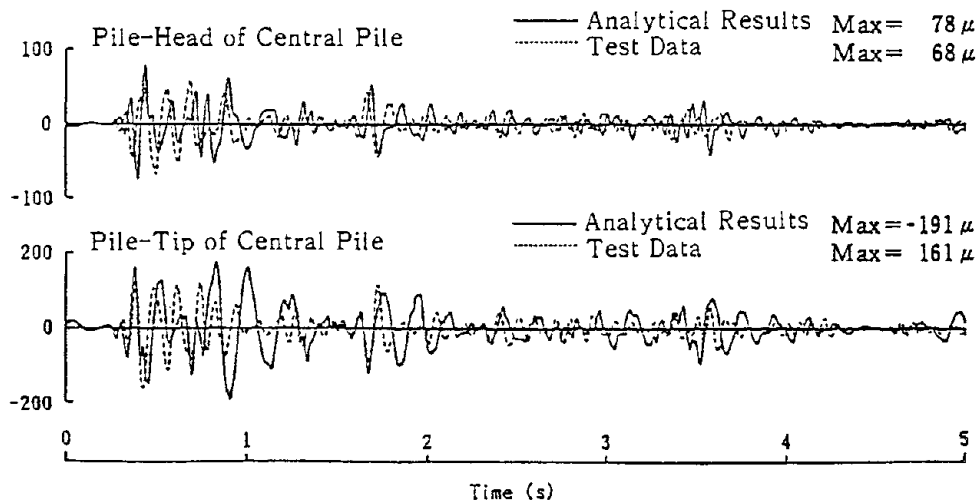


Fig.15 Comparison between analytical and test results of the bending strains of pile-head and pile-tip of central pile

## VIBRATION FAILURE TESTS OF PILES

Takashi TAZOH<sup>(1)</sup>, Katsumi SHIMIZU<sup>(2)</sup>,  
and  
Toshimitsu HIROSE<sup>(2)</sup>

1. Senior Research Engineer  
Institute of Technology of Shimizu Corporation

2. Research Engineer  
Institute of Technology of Shimizu Corporation

### ABSTRACT

Vibration failure modes of piles caused by destructive earthquakes are investigated based on the results of forty-three vibration failure tests. The tests are conducted using piles made of plaster. The testing models of pile foundation are set into sand in a small soil container and are vibrated on a shaking table.

The general resulting situation of each experimental event, may be summarized as follows; (1) any pile in a corner position is sure to be broken, (2) the center pile is comparatively difficult to damage, (3) injuries to the piles occur only at the pile-heads and/or pile-tips.

Progressive vibration failure modes of piles are investigated by continued application of some tests. The results are that a corner-position pile is the first to break, and the piles surrounding the broken pile are the next to experience damage, but no clear pattern is demonstrated in the successive damage.

## INTRODUCTION

Vibration failure modes caused by destructive earthquakes are not only of engineering concern, but also are significant in the argument for stricter requirement for aseismicity of pile foundations. Damage to pile foundations was reported in the 1964 Niigata Earthquake and the 1978 Miyagi-ken-oki Earthquake<sup>(1)-(3)</sup>. Failure phenomena are generally governed by accidental events and there are only few cases in which the damage was investigated over the entire length of piles in detail. Therefore, universal results on the vibration failure modes of piles have not been attained up to this day.

This paper presents the general characteristics of vibration failure modes of piles based on forty-three vibration failure test-cases using a shaking table; with piles made of plaster set into sand in a small soil container(\*).

## VIBRATION FAILURE TESTS

Figure 1 and Photographs 1 and 2 show a testing model of pile foundation and a soil container. The pile foundation has 9 piles (diameter  $\phi = 9\text{mm}$ , length  $l = 100\text{mm}$ , distance between each pile  $d = 22.5\text{mm}$ ) arranged in 3 columns  $\times$  3 rows. Plaster is used as the material of the piles, because it is susceptible to breakage and easy to produce.

The soil container is made of acrylic resin. The inner size of the container is of length 500mm, width 250mm, depth 115mm. The pile-heads are securely connected to a footing of 10mm thick acrylic resin; the tips are secured to the same board as the footing which is fixed to the base of the box. An iron board of 1.5kgf, simulating a superstructure, is set on the footing. Dried Toyoura sand is the material used as the ground model. The predominant frequency of the ground is about 50Hz.

The piles are broken by sinusoidal excitations as acceleration is increased. Two different frequencies of excitation were applied in the testing, 50Hz and 10Hz. Excitation was immediately stopped when the sound of piles breaking was detected. The tests were carried out, without considering the case of ordinary vibration tests (neither methodology nor equipment), because the purpose of the tests was to observe the qualitative characteristics of pile failure only. There were a total of forty-three test-cases performed.

---

(\*) A soil container of this type<sup>(4)</sup> is also called a special soil container for shear mode vibration or a shearing stack box.

## RESULTS AND CONSIDERATION

Strain meters of the guage type were attached to the piles for a few cases in order to study the phenomena of the vibration failure of the piles in detail. The strain meters were set in the direction of the pile axes. Figure 2 shows an example of the strain records obtained from a particular test. The pile's number indicates its position in the arrangement of the foundation shown in Figure 1. The corner piles are numbers 1, 3, 7, 9. In the test shown in Figure 2, piles numbers 6 ~ 9 are broken, but no damage occurred in the other piles (numbers 1 ~ 5).

As shown in the strain record of the number 9 pile-head, when cracks appeared on the pile, strain amplitude suddenly decreased, and vibrations occurred on only one side of the base line. From this moment to the occurrence of failure, a greater load is imposed upon the other piles and the strain becomes large. The reason that the strain records become extremely small when cracks or breaks have occurred on piles is as follows; the occurrence locations of cracks or breaks do not coincide with the installed locations of the strain meters. Cracks or breaks occurred on piles only at the pile-heads or pile-tips, but the strain meters were installed at a location a small distance away from the pile-heads or the pile-tips, therefore the strain at other point on the pile decreased because the strain was concentrated on the injured parts.

In the test shown in Figure 2, it can be understood that the cracks appeared firstly on the pile-head of the number 9 pile, and subsequent cracks and breaks occurred in turn at the pile-head of the number 8 pile, the pile-tip of the number 6 pile, and the pile-head of the number 7 pile. Photographs 3 and 4 show examples of the pile failures.

Table 1 shows the summary of all test results. In this table, Head and Tip represent the break position of the piles, Head and Tip indicate the pile-head and the pile-tip, respectively. As mentioned above, the excitation was immediately stopped when the sound of piles breaking was heard. However, it was difficult to halt all tests uniformly because the progressive failure of piles occurs very rapidly, variation in the timing of stopping the excitation is undeniable. If the test was not stopped, all pile-heads and pile-tips of the pile foundation would have been entirely broken. The cases in which many piles were broken correspond to the cases in which a longer period of time elapsed between detecting the sound of breakage and halting the test.

The opposite cases in which only few piles were broken, correspond to the cases in which the period is shorter.

The general resulting situation of each experimental event, may be summarized as follows:

- (1) any pile in a corner position is sure to be broken.
- (2) the center pile is comparatively difficult to damage.
- (3) injuries occur only at the pile-heads or pile-tips.

Progressive vibration failure modes of piles were investigated by continued application of some tests shown in Table 1. Figure 3 shows the results of progressive vibration failure tests. In Figure 3, symbols ●, ■ and ★ represent the failure of the pile-head, the pile-tip, and the both pile-head and pile-tip, respectively. The results indicate that a pile in a corner position was first to break, and successive breakage occurred in the piles surrounding the broken pile, but no clear pattern was demonstrated in this progression.

### CONCLUSION

A number of tests are required to clarify the general characteristics of the vibration failure modes of piles, so that not very elaborate tests were performed using a small soil container. The results obtained were as follows; (1) the corner piles were most easily broken, (2) the center pile was the least susceptible to damage, and (3) the locations where the piles were injured were limited to the pile-heads and/or pile-tips.

For progressive vibration failure modes of piles, it was found that any one of the piles in a corner position was broken at first, the surrounding piles were next to incur damage, but no clear pattern appeared in this progress.

The results that the corner position piles were easily broken and the center position is less susceptible to damage, can be understood by analysis of the situation. The shear force acting on the corner position piles reached the maximum and that acting on the center position pile became the minimum when a lateral load was applied to the footing. The phenomenon that the middle part of the piles incurred little damage, can be explained by the distribution of the maximum bending moment of the piles. The maximum values occurred at the pile-head or pile-tip, based on the seismic analysis of the pile foundation structures, taking into account both the inertial interaction and kinematic interaction. From the studies<sup>(6)</sup> on the seismic behavior of a pile foundation structure based on seismic observation data, it can be understood that the failures at the pile-head and pile-tip are governed by superstructure inertia and ground shaking, respectively.



## ACKNOWLEDGMENT

We would like to express our sincerest gratitudes to Professor I. Okauchi of Chuo University for his useful advice on the technical aspects of this study. We would also like to thank Mr. Y. Maeda and Mr. T. Miyakawa of Chuo University for help with the experiments.

## REFERENCES

1. H. Mizuno, "Pile Damage During Earthquake in Japan (1923-1983)," Dynamic Response of Pile Foundations - Experiment, Analysis and Observation, Geotechnical Special Publication No.11, ASCE, April, 1987.
  2. Editorial Committee of General Report on the Niigata Earthquake (Editor-in-Chief: H.Kawasumi), "General Report on the Niigata Earthquake of 1964," March, 1968.
  3. Archtectural Institute of Japan, "General Report on the 1978 Miyagiken-Oki Earthquake," February, 1980.
  4. T. Iwatate, "Study on Seismic Stability of Underground Structure," Doctoral Thesis, Tokyo Metropolitan University, March, 1985.
- T. Kokusho, "Liquefaction Analysis Compared with Shake Table Test," Proceedings, Eighth World Conference on Earthquake Engineering, Vol. III, July, 1984.
- T. Matsuda and Y. Goto, "Experiment Technique on Dynamic Properties of Model Ground in Shearing Stack Box (in Japanese)," Proceedings, Seventh Japan Earthquake Engineering Symposium, December, 1986.
5. T. Tazoh, K. Shimizu, and T. Wakahara, "Seismic Observations and Analysis of Grouped Piles," Dynamic Response of Pile Foundations - Experiment, Analysis and Observation, Geotechnical Special Publication No.11, ASCE, April, 1987.

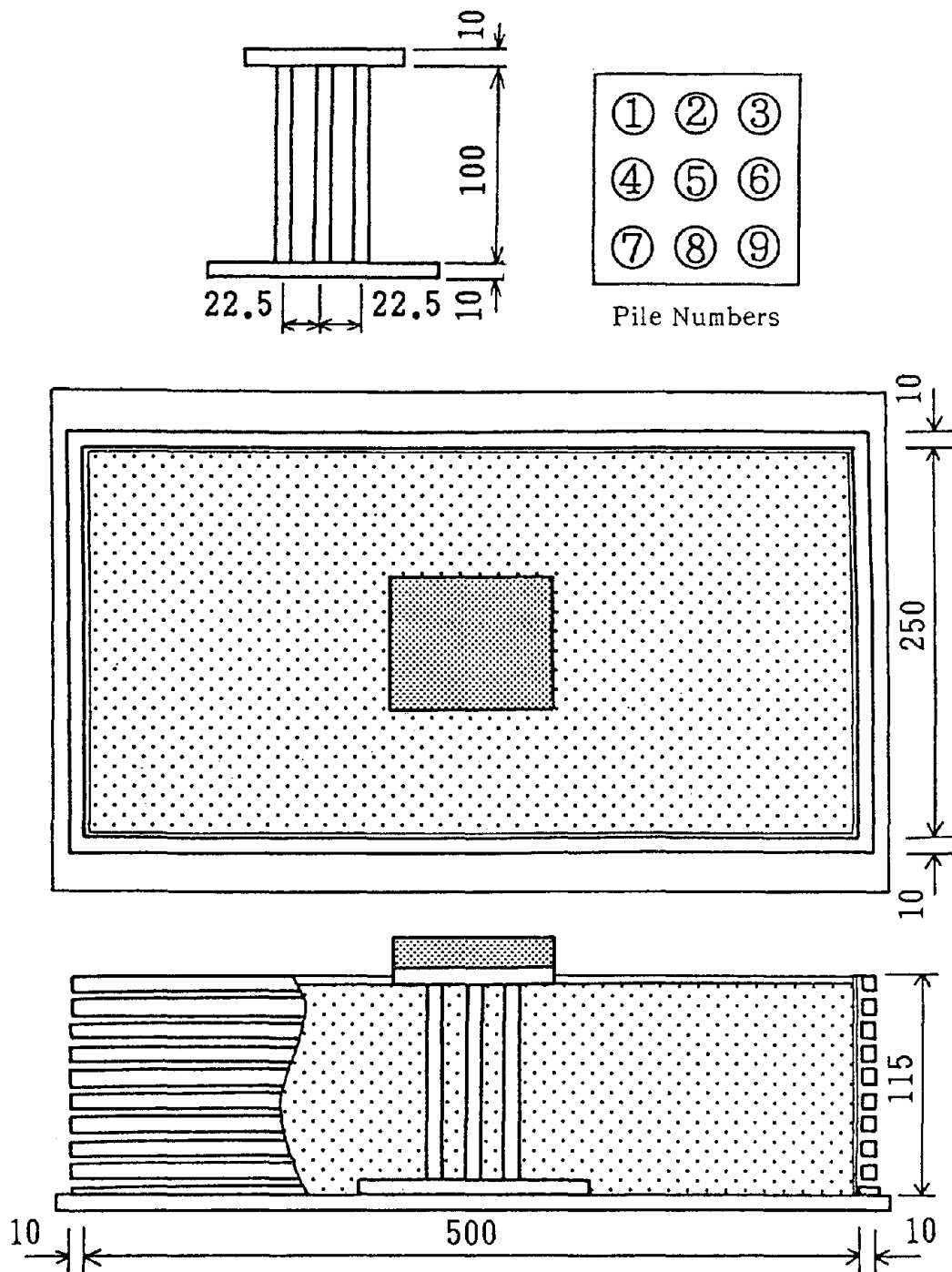


Fig. 1 Testing Model of Pile Foundation and Soil Container

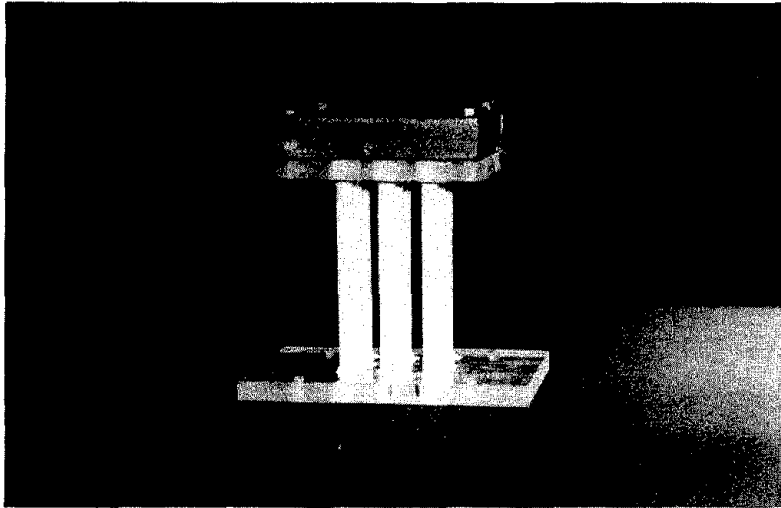


Photo. 1 Testing Model of Pile Foundation

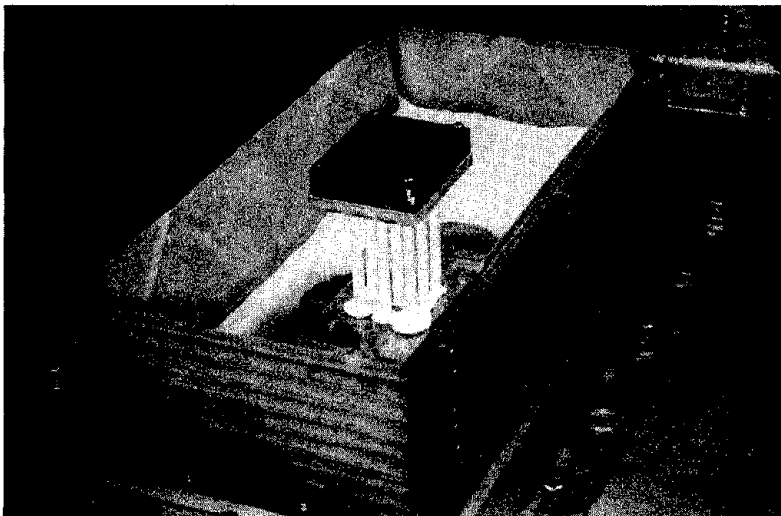
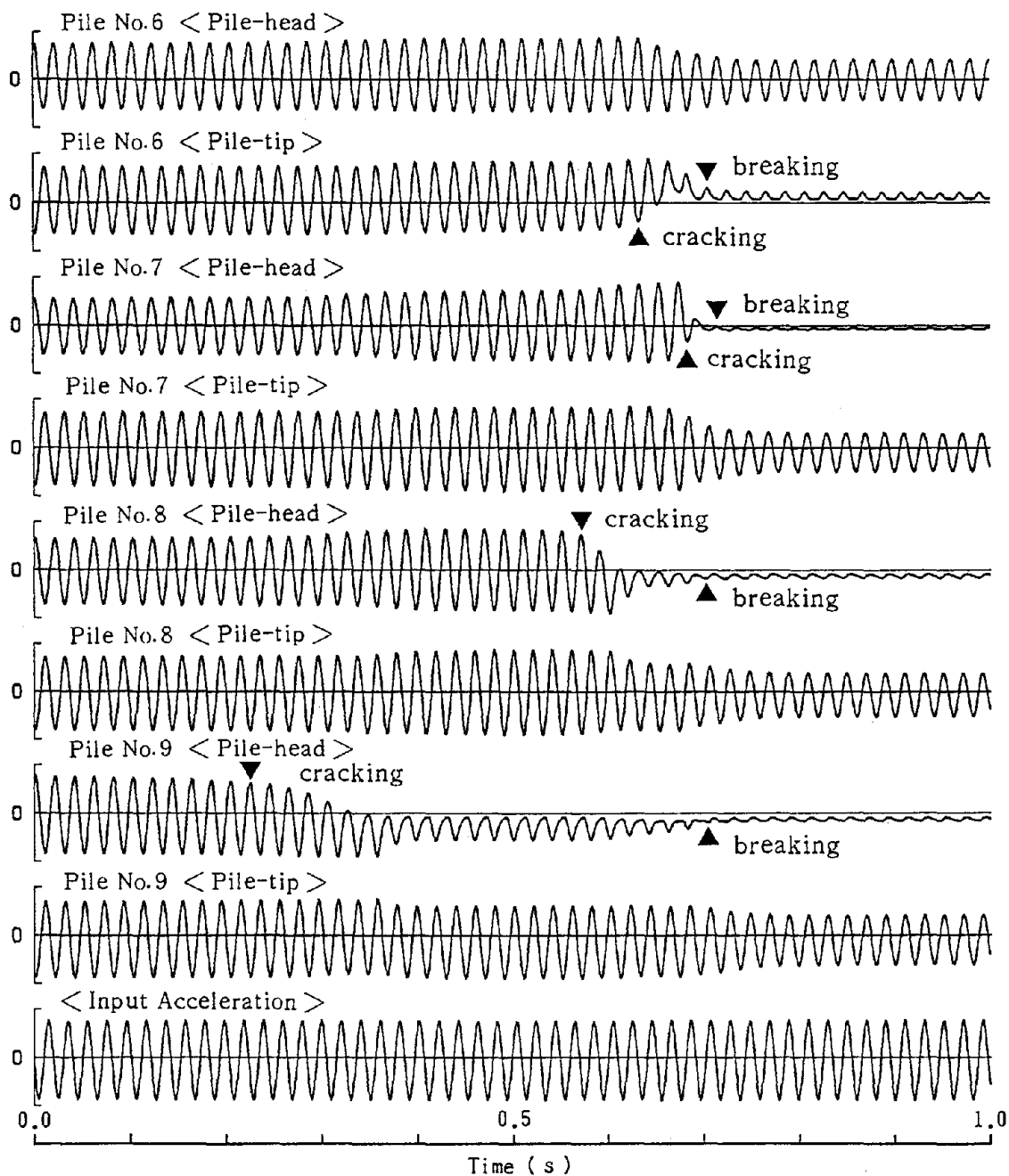


Photo. 2 Situation of Setting Testing Model of Pile Foundation into Soil Container



Notes ; Estimation of the occurrence times of cracking and breaking are accomplished as follows;

cracking; the beginning time is estimated to be when the amplitude of the strain record of the pile starts to decrease.

breaking; the time is estimated to be when the amplitude of the strain record of the pile suddenly drops.

Fig. 2 Example of Strain Records of Piles  
( Records at Pile-Heads and Pile-Tips of Piles Numbers 6~9 )

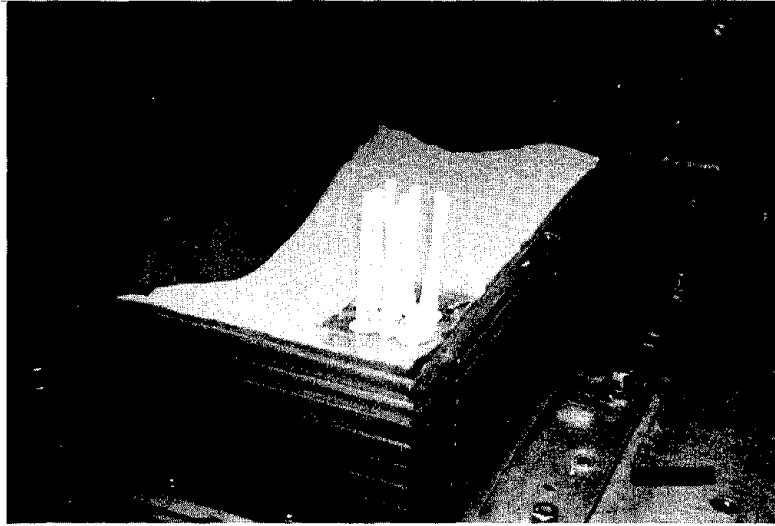


Photo. 3 Situation of Pile Failure

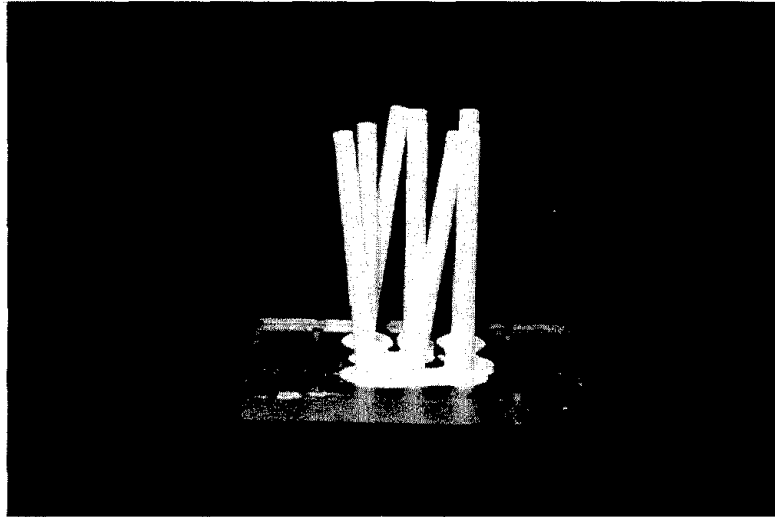


Photo. 4 Situation of Pile Failure

Table 1 Result of Vibration Failure Tests

Test No.	Frequency of Excitation	Pile Number								
		1	2	3	4	5	6	7	8	9
1	50	Head								
2	50							Head		Head
3	50	Head		Head						
4	50			Head						
5	50			Head						Head
6	50	Head								
7	50							Head		
8	50	Head						Head		
9	50	Head								
10	50	Head								
11	50							Head		
12	50	Head								
13	50	Head			Head			Head	Head	
14	50							Head		Head
15	50							Head	Head	Head
16	50	Head			Head			Head		
17	50						Head		Head	Head
18	50						Head		Head	Head
19	50	Tip		Tip				Head		
20	50				Head			Tip		Head
21	50			Head	Head				Head	
22	50						Head	Head	Head	Head
23	50				Head	Head				Head
24	50	Head	Tip						Head	Head
25	50				Head			Head		
26	50		Head	Head	Head		Head	Head	Head	
27	50							Head	Head	
28	50	Tip	Tip							
29	50	Head	Head							
30	10				Tip		Tip			Tip
31	10		Tip	Tip		Tip				Tip
32	10	Tip	Tip	Tip	Tip		Tip	Tip		Tip
33	10			Tip						Tip
34	10			Tip						
35	10			Tip					Tip	Tip
36	10	Tip					Tip			Tip
37	10	Tip								Tip
38	10				Tip					Tip
39	10		Tip	Tip						Tip
40	10	Tip								
41	10						Tip			Tip
42	10	Tip								
43	10		Tip	Tip						Tip
TOTAL		18	8	13	10	2	8	15	10	21

Note 1 ; Pile Numbers 1,3,7,9 are set at corners.

Note 2 ; Head and Tip in Table 1 represent the breakage of the pile at pile-head and pile-tip, respectively.

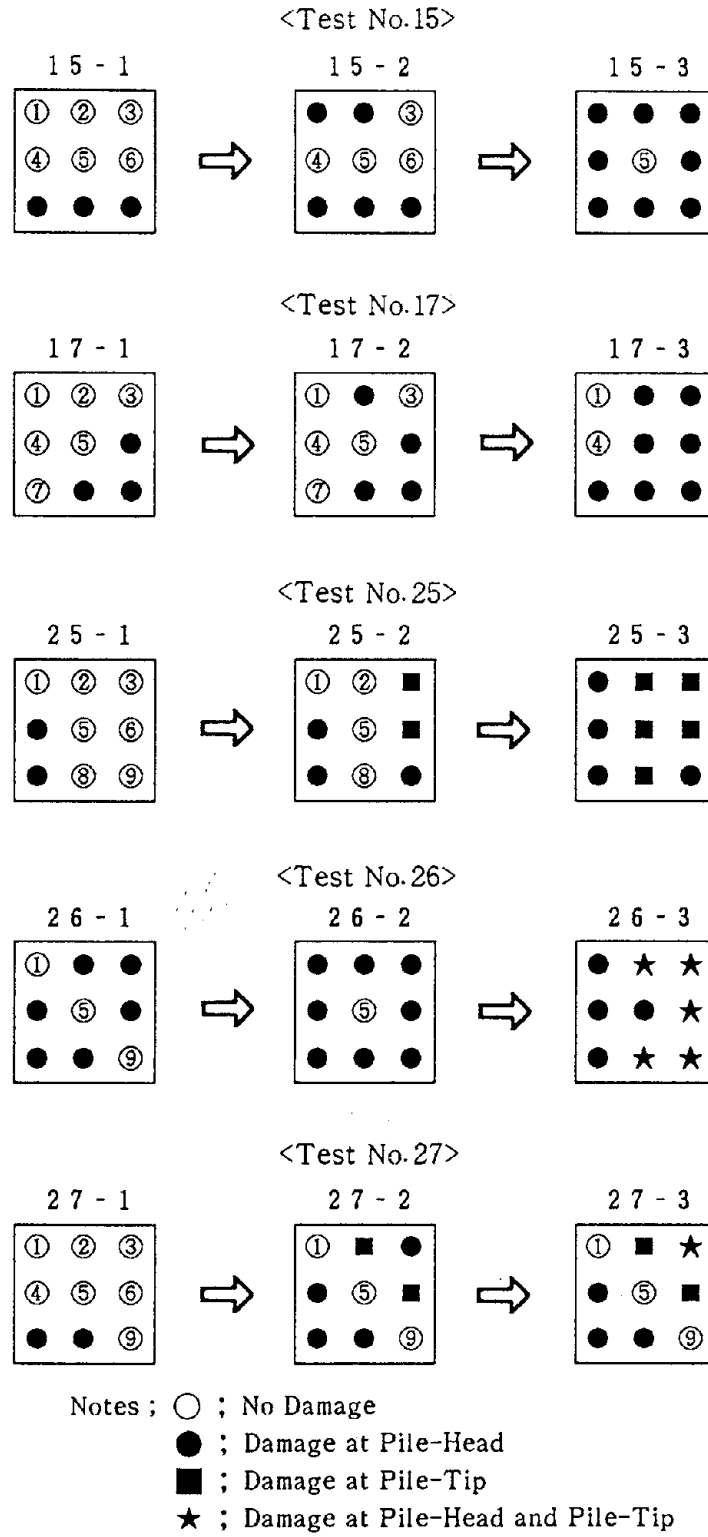


Fig. 3 Progress of Vibration Failure Modes

**LATERAL SPREADING EFFECTS ON PILE FOUNDATIONS**

F. Miura

Associate Professor of Civil Engineering  
Yamaguchi University

H. E. Stewart

Assistant Professor of Civil Engineering  
Cornell University

T. D. O'Rourke

Professor of Civil Engineering  
Cornell University**ABSTRACT**

Liquefaction-induced lateral spreading can cause failure of pile foundations. In this paper, numerical analyses are described which were used to simulate the damage mechanism of broken piles by lateral ground displacement. The finite element method was employed, which took into account the geometrical nonlinearity of the pile and material nonlinearity of the soil. The analyses revealed that the existence of a nonliquefiable layer at the ground surface affected significantly the maximum bending moment of the pile. When a relatively thick nonliquefiable layer exists above a liquefiable layer, neither the material nonlinearity of soil nor loss of soil stiffness within the liquefiable layer significantly affects the maximum bending moment. In this situation, geometric factors are most important, specifically the thickness of intact soil near the ground surface relative to the thickness of the liquefiable layer and the depth of pile embedment in underlying firm material. When the thickness of the liquefiable soils is about three times that of an overlying intact layer, soil stiffness in the liquefiable layer must be chosen carefully because it significantly affects the maximum bending moment.

The results of the parametric studies are summarized in charts using dimensionless parameters. A method for estimating pile foundation response to lateral spreading is recommended on the basis of the results of the parametric studies. First, the maximum bending strain in the pile is selected from the results of linear elastic analyses for assumed fixed end conditions of embedment. Next, the bending strain so estimated is modified by a reduction factor which accounts for the actual conditions of pile fixity in the underlying bearing stratum. Finally, the elastic strains are further modified based on reduction factors derived from nonlinear interaction analyses. The maximum bending moment in the pile can be calculated directly by multiplying the bending strain by the product of Young's and the pile section modulus.



## INTRODUCTION

During the 1964 Niigata earthquake, many foundation piles of bridges and buildings were severely damaged by liquefaction-induced permanent ground displacement.<sup>1,2</sup> Detailed field investigations have been performed on the damage patterns of the piles and associated soil profiles.<sup>2,3</sup> Some investigations have been conducted to simulate the pile behavior during the lateral spreading and to study the mechanisms of damage.<sup>1,4</sup>

From a practical point of view, if we can estimate the ground displacement at which the pile under consideration will yield, or conversely, if we can judge whether the pile will be damaged or not at a given ground displacement, then this capability will help not only in the design of new pile foundations, but also in reducing damage to existing pile foundations. For this purpose, analytical studies were carried out to estimate the maximum bending moment induced in piles subjected to the lateral ground displacement caused by liquefaction. Numerical analyses were performed using a computer program "B-STRUCT," which was developed from a program originally designed for the analysis of buried pipelines.<sup>5</sup> The computer code is based on the finite element method which takes into account the geometric nonlinearity and material nonlinearities of the pile and soil.

Analytical results are summarized in three parts. First, analytical results are presented for a pile with a fixed-end condition, representing a pile rigidly embedded in the underlying soil. The fixed-end condition yields a maximum bending moment. The effect of pile embedment in nonliquefiable soil is discussed next. Bending moment reductions due to pile embedment as a function of the relative pile-soil stiffness are expressed. Finally, the effect of soil nonlinearity is discussed. Soil nonlinearity was modeled by spring-slider elements using bilinear force-displacement relationships. The piles were assumed to be constructed of linear elastic material.

## ANALYTICAL MODEL

Figure 1 shows the soil-pile system with various geometric parameters that were used to organize the analytical study. The water table marks the top of the liquefiable stratum of thickness,  $h_L$ , above which is a nonliquefiable soil cover. The pile is embedded a depth,  $l_b$ , into nonliquefiable soil. A pile length,  $l$ , spans the distance between the pile cap near the surface and the basal layer.

The interaction between the pile and adjacent soil was simulated by means of the finite element configuration shown in Figure 1. Beam elements with linear elastic and geometric nonlinear properties were used to represent the pile, and the soil reaction was modeled by means of spring-slider elements. The spacing of the spring-slider elements was chosen to conform with the minimum dimension required for beam on elastic foundation analysis.<sup>6</sup> Soil displacements were the specified input parameters, applied in a series of load increments until the final magnitude of maximum horizontal displacement,  $d_h$ , was

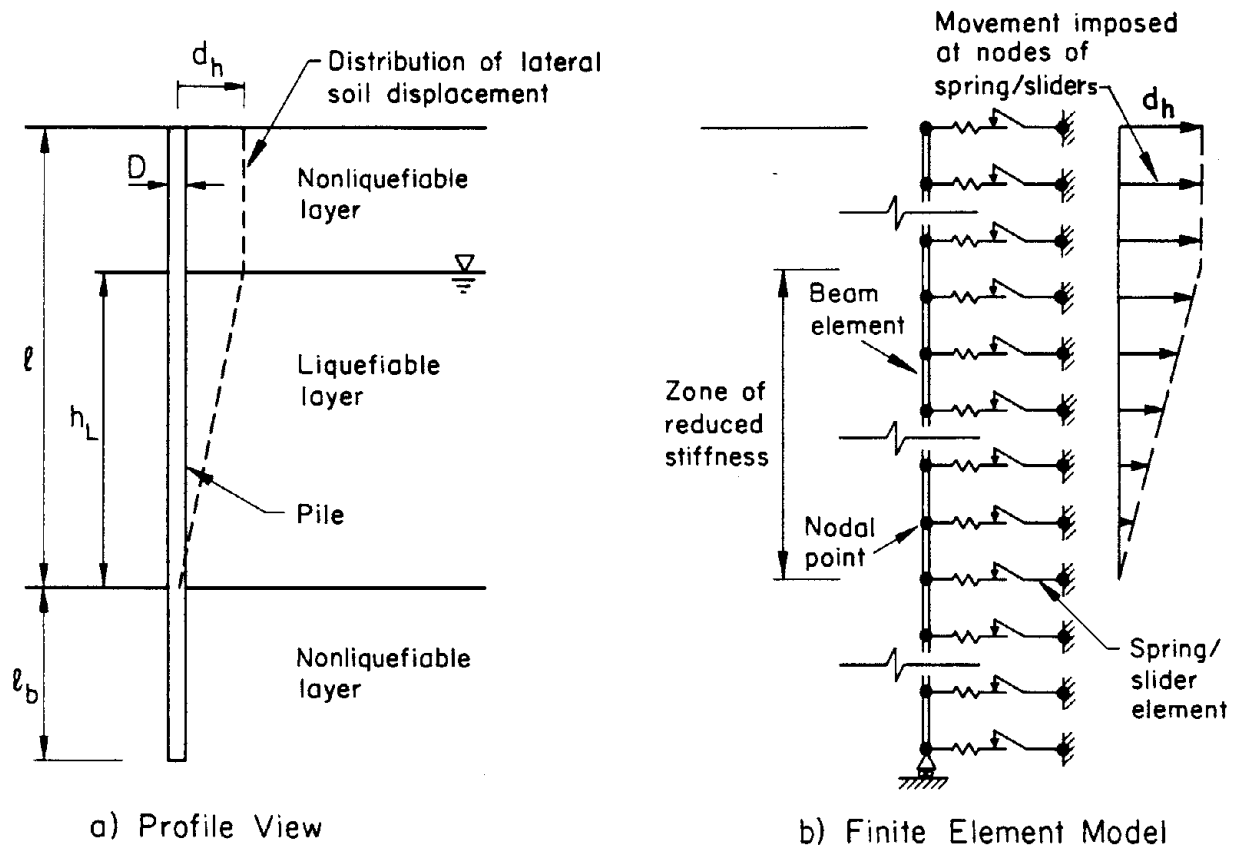


Figure 1. Profile of Pile and Soil-Structure Interaction Model for Lateral Spreading

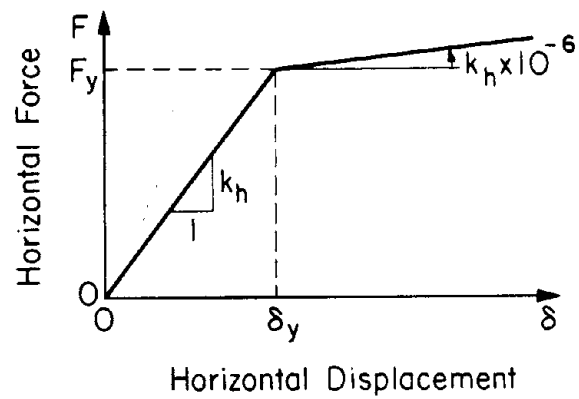


Figure 2. Force-Displacement Model for Pile-Soil Interaction

achieved.

A relatively simple model for the horizontal force-displacement relationship between pile and soil was adopted in this study, based on the coefficient of horizontal subgrade reaction proposed by Terzaghi<sup>7</sup> and the lateral bearing capacity factors proposed by Hansen.<sup>8</sup> Given that liquefaction and lateral spreading involve reductions in soil stiffness which are both complex and poorly understood, it was deemed appropriate to use a simple formulation. Such modeling clarifies pile performance at a level of precision more than adequate to comply with the variations and uncertainties related to soil liquefaction in the field.

The bilinear force-displacement relationship used to model the pile-soil interaction is shown in Figure 2. The soil yield force,  $F_y$ , at a nodal point of the finite element model was determined by the following equation

$$F_y = \sigma_z' N_q DL \quad (1)$$

where  $\sigma_z'$  is the effective stress at the point,  $N_q$  is the dimensionless coefficient proposed by Hansen<sup>8</sup> for pile foundations in sand,  $D$  is the pile diameter, and  $L$  is the sum of the half lengths of two joining beam elements at the nodal point. The yield displacement,  $\delta_y$ , was determined by dividing the yield force by the soil spring stiffnesses,  $k_h$ . The spring stiffnesses were determined by multiplying the coefficient of horizontal subgrade reaction and  $DL$ .

The coefficient of horizontal subgrade reaction,  $k_h$ , is given by

$$k_h = n_h \frac{z}{D} \quad (2)$$

in which  $n_h$  is the constant of horizontal subgrade reaction,  $z$  is the depth to the section of the pile of interest, and  $D$  is pile diameter. Values of  $n_h$  are a function of the effective soil unit weight, and values of  $k_h$  are a function of the effective vertical stress.

#### LINEAR ANALYSES

Linear analyses were performed, using only the coefficient of horizontal subgrade reaction,  $k_h$ , to represent pile-soil interaction. Nonlinear analyses were performed next, and were used to modify the linear results. The progression from linear to nonlinear analysis permits the more complex nonlinear reactions to be evaluated in context of the simpler linear conditions. Moreover, the linear reference base provides dimensionless parameters which are useful for summarizing the analytical results.

The following parameters were introduced to summarize the results of the

study:

- (i) The maximum bending strain,  $M_{\max}/ES$ , which is the ratio of the maximum bending moment,  $M_{\max}$ , to the product of Young's modulus,  $E$ , and the section modulus,  $S$ , of the pile.
- (ii) The ratio of the thickness of the liquefiable layer,  $h_L$ , to the depth to the bearing stratum,  $\ell$ ,  $h_L/\ell$ .
- (iii) The lateral deformation,  $d_h/\ell$ .
- (iv) The dimensionless length of the pile above the base layer,  $\beta\ell$ .
- (v) The dimensionless depth of pile embedment in the base layer,  $\beta_b\ell_b$ .

Nondimensional parameters,  $\beta$  and  $\beta_b$ , are given by the following expressions

$$\beta = (k_h^S D/(4EI))^{-1/4} \quad (3)$$

$$\beta_b = (k_h^b D/(4EI))^{-1/4} \quad (4)$$

in which  $k_h^S$  and  $k_h^b$  are the coefficients of horizontal subgrade reaction of the surface layer and the base layer, respectively;  $D$  is the pile diameter, and  $EI$  is the flexural rigidity of the pile. Soil displacement was assumed to be constant within the surface nonliquefiable layer and to decrease linearly within the liquefiable layer.

Values of  $k_h$  represent soil before the onset of liquefaction. For the liquefiable layer,  $k_h$  was reduced by a factor of 50 to represent the reduction in soil stiffness which accompanies increased pore water pressure. A range of reduction factors was used in the nonlinear analyses to show how variations in reduced stiffness influence pile response for different ratios of liquefied soil thickness to depth to bearing stratum,  $h_L/\ell$ . To expedite the analyses, the weighted average value of  $k_h$  for a given soil profile was assumed to be constant throughout the upper soil layers.

#### PILES WITH FIXED-END CONDITIONS

Figure 3 shows the relationship between maximum bending strain in the pile,  $M_{\max}/ES$ , and lateral deformation,  $d_h/\ell$ , for linear analyses of piles fixed

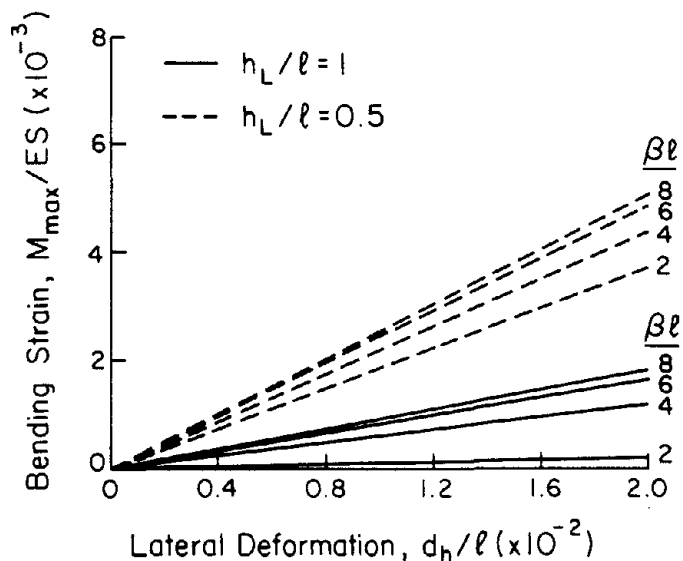


Figure 3. Pile Bending Strain as a Function of Lateral Deformation for Fixed-End Linear Analyses

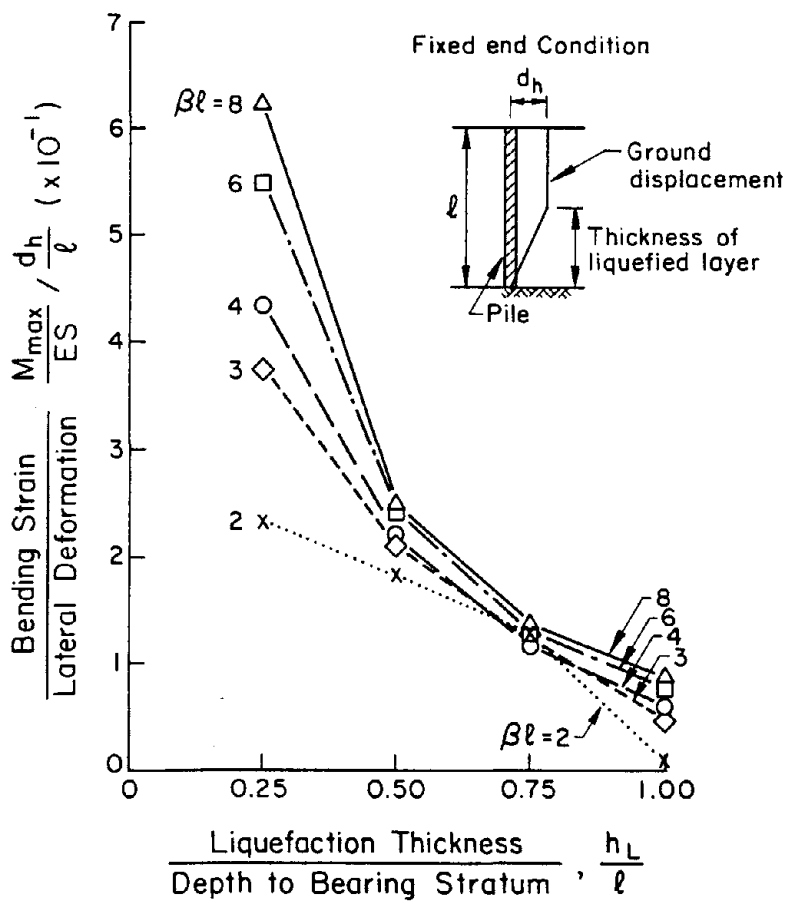


Figure 4. Bending Strain per Lateral Deformation as a Function of Subsurface Geometry

rigidly in the basal bearing stratum. In all analyses, the maximum bending moment was induced near the base of the pile. Two conditions, pertaining to  $h_L/l = 1.0$  and  $0.5$ , are illustrated in the figure for various pile-soil stiffnesses. The smaller  $h_L/l$  results in substantially increased bending strains at all values of  $\beta l$ .

The ratio of maximum bending strain to lateral deformation,  $(M_{\max}/ES)/(d_h/l)$ , versus the ratio of the thickness of the liquefiable layer to that of the entire upper layer,  $h_L/l$ , are summarized in Figure 4. Using this plot,  $M_{\max}$  can be estimated for a given magnitude of ground displacement,  $d_h$ . Conversely, when the allowable bending moment of a pile,  $M_{\max}$ , is given, the ultimate ground displacement at which the pile yields can be estimated.

The curve for  $\beta l = 2$  in this figure shows a different trend than the others because the pile is very stiff. A pile with  $\beta l < \pi$  often is treated in design for soil-structure interaction<sup>9</sup> as a relatively rigid member.

#### BASE EMBEDMENT EFFECTS

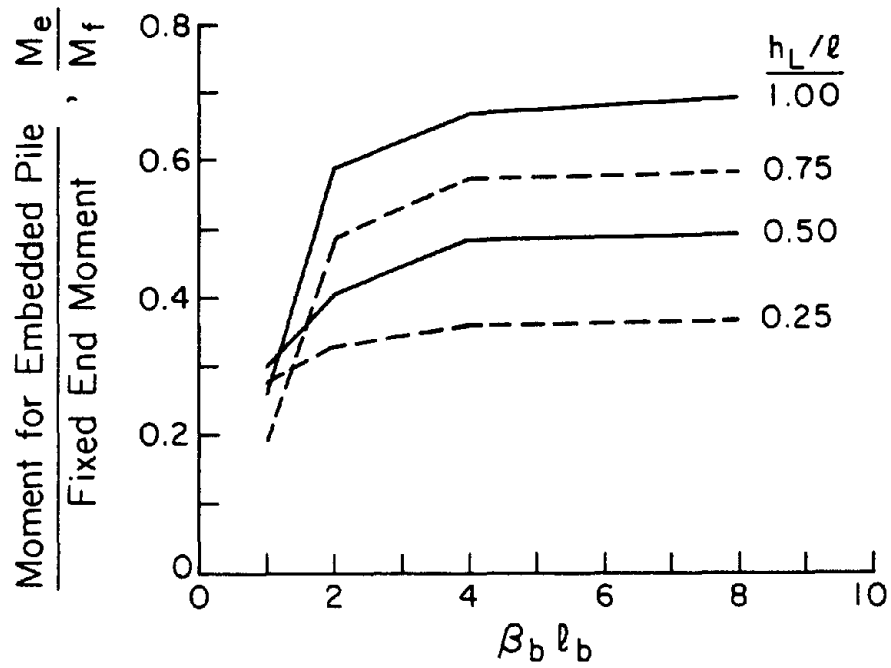
The maximum bending moment induced in the embedded pile,  $M_e$ , was obtained for four conditions in which  $\beta_b l_b$  was 1, 2, 4, and 8. The maximum bending moments,  $M_e$ , were divided by those obtained from the pile with fixed-end condition,  $M_f$ . The relationship between the ratios,  $M_e/M_f$  and  $\beta_b l_b$ , is shown in Figure 5 for the nondimensional parameters,  $h_L/l$ , of 0.25, 0.5, 0.75, and 1.0. Figure 5a is for the case of  $\beta l = 4$  and 5b for  $\beta l = 6$ .

The larger the value of  $\beta_b l_b$ , the deeper the embedment and/or the more flexible the pile. The ratio of  $M_e/M_f$ , which can be used as a reduction factor, increases as  $\beta_b l_b$  increases, but the factor becomes almost constant for  $\beta_b l_b \geq 4$ . The larger ratios of  $h_L/l$  give the larger factors,  $M_e/M_f$ , except at  $\beta_b l_b = 1$ . In all cases for  $\beta_b l_b \geq 2$ , the maximum bending moments were induced at the interface between the liquefiable layer and the nonliquefiable base layer. For the  $\beta_b l_b = 1$ , however, the maximum bending moments were induced at the interface between the surface nonliquefiable layer and the liquefiable layer for  $h_L/l = 0.5$  and  $0.25$ . This resulted in the variable trends of  $M_e/M_f$  for  $\beta_b l_b < 2$ .

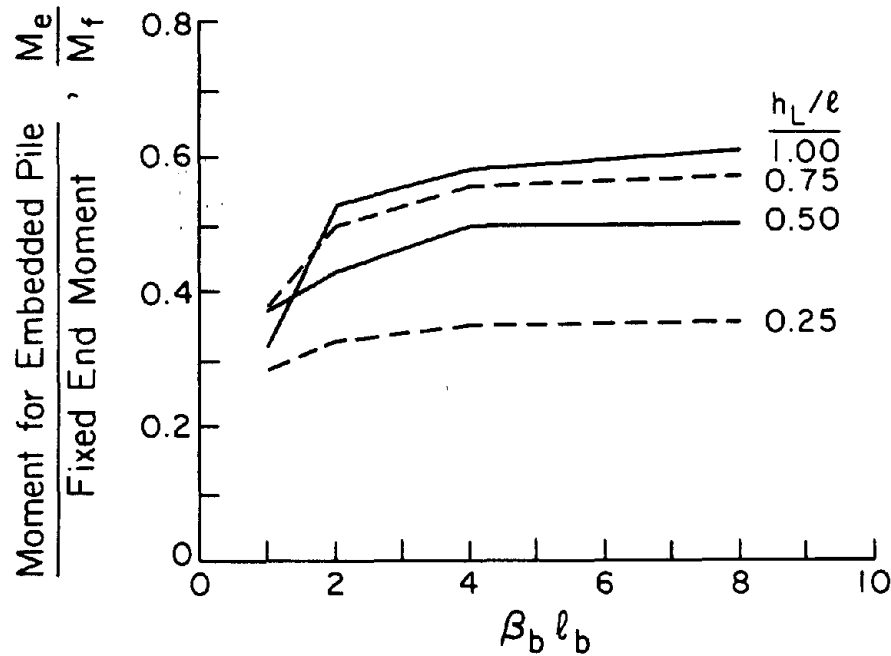
#### NONLINEAR ANALYSES

Nonlinear analyses were performed by applying the bilinear force-displacement relationship illustrated in Figure 2. For the liquefiable layer, the soil spring stiffness was reduced by lowering the yield force with the yield displacement unchanged. In determining  $N_q$ , the angle of shear resistance of the soil was assumed to be  $30^\circ$  for the liquefiable layer and  $40^\circ$  for the nonliquefiable layers.

Figure 6 compares the maximum bending strains obtained from linear soil (solid lines) and nonlinear soil (broken lines) conditions. The results were



a)  $\beta l = 4$



b)  $\beta l = 6$

Figure 5. Ratio of Maximum Moments for Embedded and Fixed-End Piles as a Function of Relative Pile Stiffness

obtained for  $\beta l = 4$  and  $\beta_b l_b = 2$ . The most pronounced effects of nonlinearity are experienced when  $h_L/l = 1.0$ . As the relative thickness of the intact upper layer increases (i.e., as  $h_L/l$  decreases), nonlinear effects diminish. For  $h_L/l \leq 0.75$ , there is little difference between the linear and nonlinear analyses over the range of lateral deformation studied.

It should be noted that the maximum bending strain is "saturated" for  $h_L/l = 1.0$  in nonlinear soil conditions. This "saturation" appears after the yielding of all soil springs, because the external forces due to ground deformation do not increase after the yielding.

The ratios of maximum nonlinear to linear bending moments,  $M_N/M_L$ , are shown in Figure 7. The ratios for  $h_L/l = 0.25, 0.5, \text{ and } 0.75$  are greater than 0.9 for  $d_h/l \leq 0.02$ . This means that nonlinear effects have a small influence on pile response when a nonliquefiable layer exists at the ground surface. On the other hand, a nonlinear soil reaction significantly affects the pile response when the whole surface layer liquefies. This implies that the spring stiffness will be a critical factor in the pile response when the whole surface layer liquefies.

Analyses were performed assuming five different spring stiffnesses for the liquefiable layer, i.e.,  $1/5, 1/10, 1/25, 1/50, \text{ and } 1/125$ , of the intact soil stiffness for three ratios of  $h_L/l = 1.0, 0.75, \text{ and } 0.5$ . To reduce the spring stiffness, the yield forces of the soil were divided by the factors of 5, 10, 25, 50, and 125 with the ultimate displacements unchanged.

The ratios of maximum nonlinear to linear bending moments,  $M_N/M_L$ , versus the lateral deformation,  $d_h/l$ , are shown in Figures 8a, b, and c. The embedment factor,  $\beta_b l_b$ , was assumed to be 2 in these analyses. From Figure 8a, for which the whole surface layer was assumed to be liquefied, it is clear that softening of the soil significantly affects the ratios of  $M_N/M_L$ . The soft soil drastically decreases the ratio of the maximum bending moments as the lateral deformation increases. In Figures 8a and b, there is a tendency for the moment ratios to decrease hyperbolically beyond a certain level of lateral deformation. This tendency is attributed to the existence of a "saturation" level for maximum bending strain. The maximum bending moment in the pile subjected to nonlinear soil reaction,  $M_N$ , is constant above a certain threshold, while the maximum bending moment of the pile within linear soil,  $M_L$ , increases proportionally with the lateral deformation.

For  $h_L/l = 0.5$ , where the bottom half of the surface layer was assumed to be liquefied, neither the material nonlinearity nor the soil softening is significant. The reductions of the maximum bending moment in this case are about 15% at a lateral deformation of 0.04. For  $h_L/l = 0.75$ , the reductions in linear bending moment are less than 10% below lateral deformations of about 0.025.

These results suggest that the existence of a nonliquefiable layer above a liquefiable layer holds the key to estimating maximum bending moment induced in the pile. When a relatively thick nonliquefiable layer ( $h_L/l \leq 0.75$ ) is above a liquefiable layer, neither material nonlinearity nor reductions of soil stiffness within the liquefiable layer significantly affects the results.



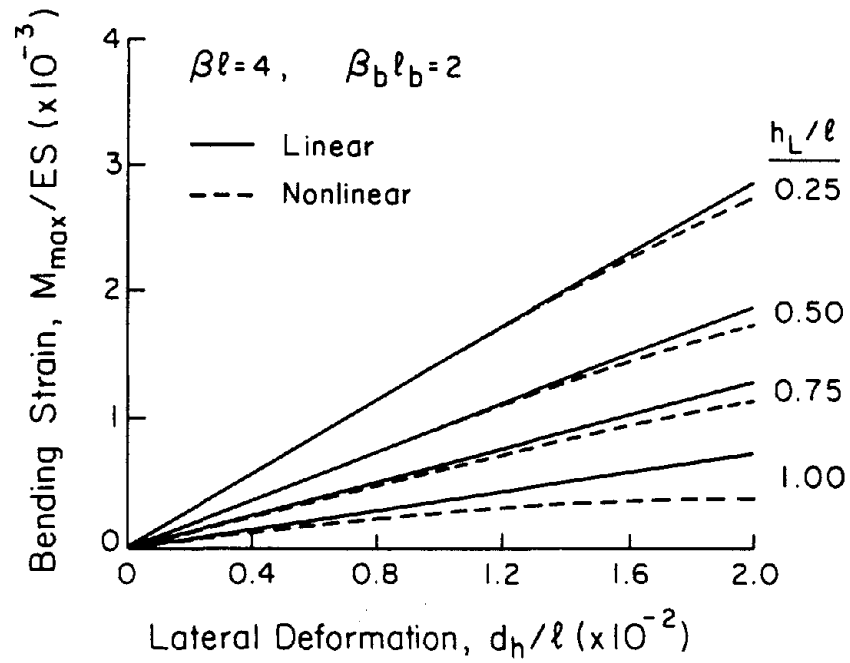


Figure 6. Comparisons of Bending Strains vs. Lateral Deformation for Nonlinear and Linear Analyses

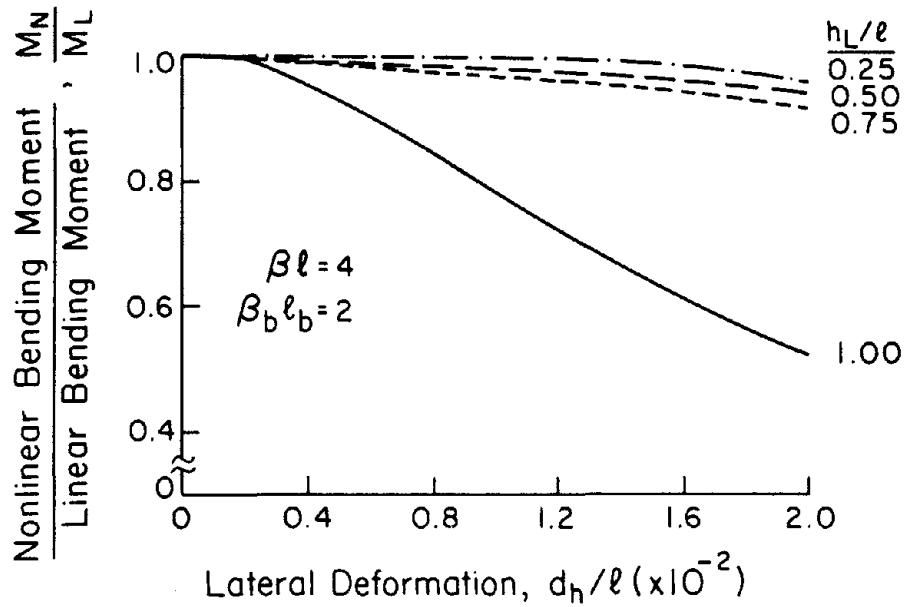


Figure 7. Ratio of Nonlinear to Linear Bending Strains as a Function of Lateral Deformation for Different Subsurface Geometries

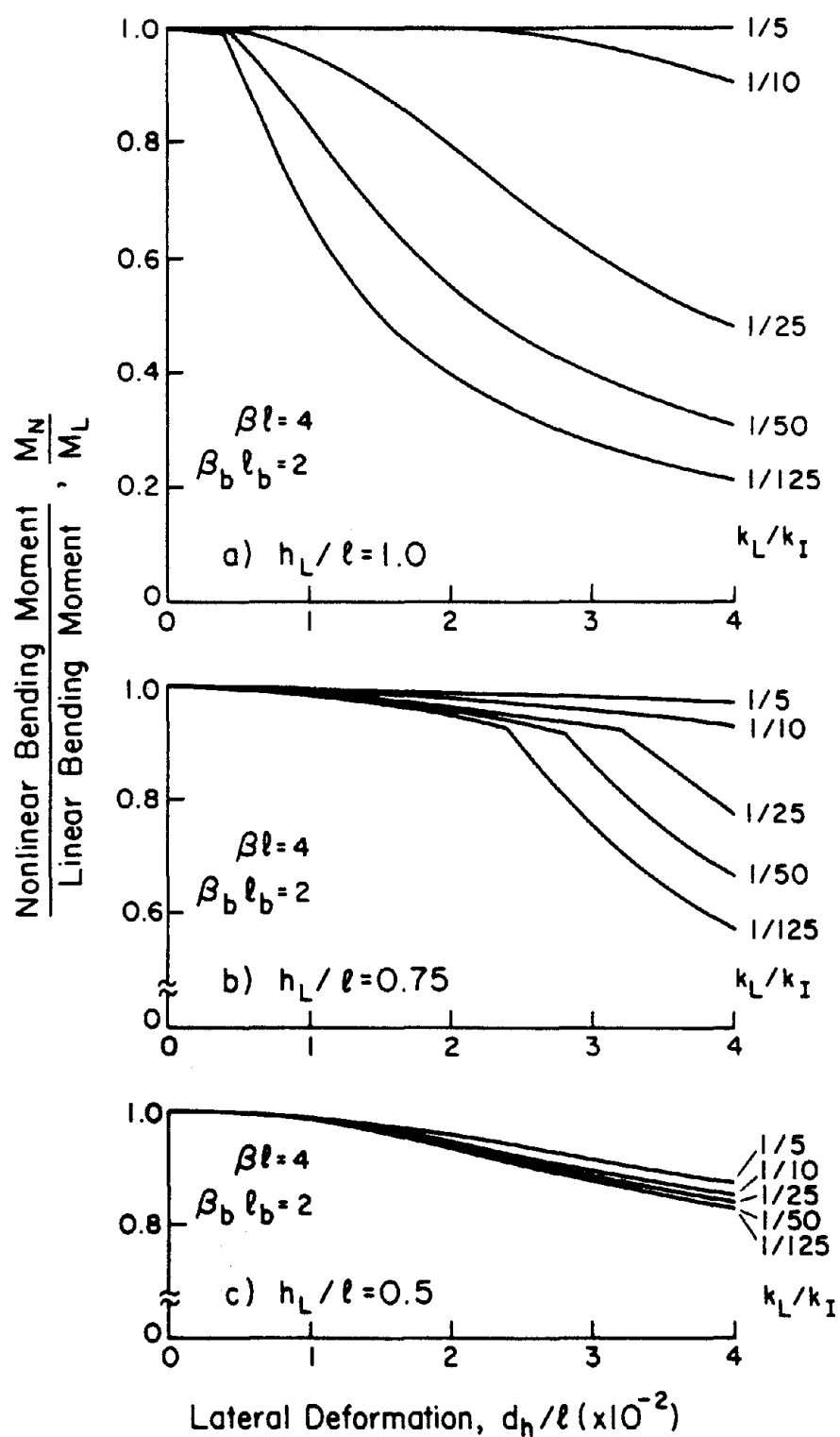


Figure 8. Ratio of Nonlinear to Linear Bending Moments as a Function of Lateral Deformation for Various Subsurface Geometries and Reductions in Soil Stiffness

A slightly conservative estimation of the maximum bending moment will be obtained from the linear analyses. For these conditions, the most important factor is the geometry of the subsurface layers and degree of fixity associated with pile embedment in the basal bearing stratum.

#### CONCLUDING REMARKS

Analyses of pile foundation response to lateral spreading reveals that the onset of pile damage is affected significantly by the existence of a nonliquefiable layer at the ground surface. An intact surface layer with thickness greater than about one-third that of the underlying liquefiable layer will have a dominant effect on pile performance, and cause bending failures at relatively low values of lateral deformation. For such conditions, neither the material nonlinearity nor the loss of soil stiffness significantly affects the maximum bending moment in the pile. This result has considerable practical value because it allows engineers to identify subsurface geometries for which linear models of soil-structure interaction can give good estimates of allowable deformation. These types of subsurface conditions pose the greatest threat to existing buildings. Large diameter relatively stiff caisson foundations would be required for new buildings to resist lateral soil forces under these circumstances. Alternatively, a more cost-effective solution might be found through various site improvement schemes.

When no intact soil or a very thin nonliquefiable layer at the ground surface is expected, the estimation of maximum bending moment is not simple. Substantially reduced bending moments are possible under these circumstances. The soil stiffness of the liquefiable layer must be chosen carefully for a reliable analysis because it significantly affects the pile response.

#### ACKNOWLEDGMENTS

The research on which this paper is based was sponsored by the National Center for Earthquake Engineering Research, Buffalo, NY, under Project Number 883014. The assistance of Professor M. Hamada of Tokai University is deeply appreciated.

#### REFERENCES

1. Hamada, M., S. Yasuda, R. Isoyama, and K. Emoto, "Study on Liquefaction-Induced Permanent Ground Displacements," Association for the Development of Earthquake Prediction, Tokyo, Nov. 1986.

2. Kawashima, K., K. Shimizu, S. Mori, M. Takagi, N. Suzuki, and S. Nakamura, "Analytical Studies on Damage to Bridges and Foundation Piles Caused by Liquefaction-Induced Permanent Ground Displacement," Proceedings, 1st Japan-U.S. Workshop on Liquefaction, Large Ground Deformations, and Their Effects on Lifeline Facilities, Tokyo, Nov. 1988, pp. 99-117.
3. Kawamura, S., T. Nishizawa, and H. Wada, "Damage to Piles Due to Liquefaction Found by Excavation Twenty Years After the Earthquake," Nikkei Architecture, 1985. (In Japanese.)
4. Stewart, H. E., F. Miura, and T. D. O'Rourke, "Pile Damage Due to Large Ground Displacement," Proceedings, 1st Japan-U.S. Workshop on Liquefaction, Large Ground Deformations, and Their Effects on Lifeline Facilities, Tokyo, Nov. 1988, pp. 173-182.
5. O'Rourke, T. D. and M. S. Tawfik, "Analysis of Pipelines Under Large Ground Deformations," Geotechnical Engineering Report 86-1, School of Civil and Environmental Engineering, Cornell University, Ithaca, NY, Mar. 1986.
6. Boresi, A.P., O. M. Sidebottom, and J. O. Smith, Advanced Mechanics of Materials, 3rd Ed., John Wiley and Sons, Inc., New York, 1978.
7. Terzaghi, K., "Evaluation of Coefficients of Subgrade Reaction," Geotechnique, Vol. 5, No. 4, 1955, pp. 297-326.
8. Hansen, J. B., "The Ultimate Resistance of Rigid Piles Against Transversal Forces," Bulletin 12, Danish Geotechnical Institute, Copenhagen, 1961, pp. 1-9.
9. Yokoyama, M., "Design for Pile Foundations and Its Application," San-kaido, 1978, p. 33. (In Japanese.)

# Seismic Stability of Waterfront Tied-Back Walls

by

**G. NEELAKANTAN\***, **MUNIRAM BUDHU\*\***,

*Department of Civil Engineering and Engineering Mechanics,*

*University of Arizona, Tucson, AZ-85721, U.S.A.*

and

**R. RICHARDS, Jr.\*\*\***

*Department of Civil Engineering,*

*State University of New York at Buffalo, NY-14260, U.S.A.*

## SUMMARY

Port and harbour facilities are important lifeline structures which have suffered severe damage during seismic events. Many of these facilities are constructed using tied-back walls for which there is generally no acceptable design methodology. We conducted an analytical study of tied-back walls subjected to seismic loads. The analysis is a pseudo-static limit equilibrium method wherein linear failure surfaces are assumed to develop on both the active and passive sides of the tied-back wall. The hydrodynamic pressures on both sides of the wall were assumed to be linearly distributed. We found that the depth of embedment required for a tied-back wall to sustain a given acceleration increases substantially if water is present. An examination of our predictions with a case study - Bulkhead No.4, Sendai Harbour, Japan, during the June 12, 1978 Miyagi-ken-Oki earthquake - shows that even if the anchor was initially adequately designed, for the reported design seismic coefficient of 0.1, the wall would have failed under the accelerations imposed by the Miyagi-ken-Oki earthquake, irrespective of the liquefaction of the subsoil.

\* Graduate Student

\*\* Associate Professor

\*\*\* Professor

## INTRODUCTION

The failures of retaining walls during seismic events are numerous and abound in the literature. These failures have not attracted similar magnitude of attention that have been and are paid to the failures of buildings. The fundamental reason, perhaps, for this is that often the failures of retaining walls do not result in any significant loss of lives. However, severe infrastructure damages, loss or destruction of lifeline facilities and economic set backs and hardships result from failures of retaining walls.

Port and harbour facilities and their associated infrastructures are good examples of lifeline systems which rely on the stability of retaining walls to survive seismic and other natural and man-made hazards. Many port and harbour facilities are constructed using tied-back (flexible) retaining walls. Several of these walls have failed during seismic events. Many of these failures have been attributed to the liquefaction of the soils. But, there are substantial records which indicate that some of these failures occur in soils that have not liquefied.

Research into seismic behavior and design of retaining walls was predominantly concerned with rigid gravity-retaining walls (Fig.1.) because of the heavy usage of this type of wall in bridge abutments and piers. A seismic design procedure based on a limited displacement approach was suggested by Richards and Elms (1979) and now widely used in engineering practice. It was shown by Richards and Elms (1979) that inertia effects play a very important role in the seismic stability of a gravity retaining wall. In a 'flexible' tied-back retaining wall (Fig.2.), typical of the type used in port and harbour facilities, inertial effects are likely to be unimportant. It seems, intuitively, that the passive pressures and as a consequence the depth of embedment, and the strength and stability of the anchor will control the stability of tied-back walls under static and seismic loads.

The purpose of our research study was to examine the behavior of model tied-back retaining walls so as to gain an insight into the performance of these walls under simulated seismic loadings and to validate/calibrate through shaking table experiments a pseudo-static limit analysis of this type of wall. Our efforts were directed at tied-back walls founded in dry cohesionless soils (Neelakantan et. al., 1988, 1989). In this contribution we extend the analysis to saturated cohesionless soils and consider the effects of water on both sides of the wall. We use use a

case study of a failure of a tied-back wall in Sendai Port, Japan, during the 1978 Miyagi-ken-Oki earthquake to evaluate the prediction of our analysis.

### SHEET PILE WALL SUBJECTED TO SEISMIC ACCELERATION

A sheet pile wall subjected to a horizontal acceleration component  $k_h g$  and a vertical acceleration component  $k_v g$  where  $k_h$  and  $k_v$  are the horizontal and vertical coefficients of accelerations and  $g$  is the acceleration due to gravity, is shown in Fig.3. The directions of  $k_h$  and  $k_v$  as shown in Fig.3. are taken as positive.

The net active lateral thrust on the wall due to the active fill is:

$$P_{AE} = \frac{1}{2} \gamma_b H_A^2 (1 - k_v) K_{AE} \quad (1)$$

where  $\gamma_b$  is the buoyant density and  $K_{AE}$ , the dynamic coefficient of active earth pressure, was derived by Mononobe-Okabe (1926, 1929) as :

$$K_{AE} = \frac{\cos^2(\phi_A - \theta)}{\cos \theta \cos(\delta_A + \theta) \left[ 1 + \sqrt{\frac{\sin(\phi_A + \delta_A) \sin(\phi_A - \theta - \iota_A)}{\cos(\delta_A + \theta) \cos(\iota_A)}} \right]^2} \quad (2)$$

where :

$\theta = \arctan\left(\frac{k_h}{1 - k_v}\right)$ ,  $\gamma_b$  = the buoyant unit weight of the soil,  $H_A$  = height of the active wedge,  $\phi_A$  = angle of internal friction of the soil on the active side,  $\delta_A$  = angle of friction between wall and the soil on the active side and  $\iota_A$  = slope of the ground surface behind the wall.

Similarly the net passive lateral thrust due to the soil is :

$$P_{PE} = \frac{1}{2} \gamma_b D^2 (1 - k_v) K_{PE} \quad (3)$$

where  $K_{PE}$ , the dynamic coefficient of passive earth pressure, is :

$$K_{PE} = \frac{\cos^2(\phi_P - \theta)}{\cos \theta \cos(\delta_P + \theta) \left[ 1 - \sqrt{\frac{\sin(\phi_P + \delta_P) \sin(\phi_P - \theta + \iota_P)}{\cos(\delta_P + \theta) \cos(\iota_P)}} \right]^2} \quad (4)$$

where :

$D$  = depth of embedment,  $\phi_P$  = angle of internal friction of the soil on the passive side,  $\delta_P$  = angle of friction between wall and the soil on the passive side and  $\iota_P$  = slope of the ground surface in front of the wall on the passive side.

The static components of earth pressure resultants for a uniform soil act at one third the depth of the soil from the bottom of the wall. The points of application of the additional dynamic components of the earth pressure resultants are not well established. Seed and Whitman (1970) have shown, from tests on gravity walls, that the location of the additional dynamic component of the active earth pressure resultant increases as earthquake effects become significant. A theoretical analysis done by Wood (1973) for an assumed elastic soil indicated that the resultant of the dynamic earth pressure acted at mid-height of the wall. In the present analysis, it is assumed that the additional dynamic component of the active earth pressure resultant acts at  $H_A/2$ . Neelakantan et. al. (1988, 1989) have shown theoretically that the additional dynamic component of the passive earth pressure resultant should, for practical purposes, be taken to act at one third the depth of the soil from the bottom of the wall on the passive side.

Fig.4. shows the forces and the point of action during a seismic event for a sheet pile wall. In this figure,  $P'_{AE}$  and  $P'_{PE}$  are the dynamic components of  $P_{AE}$  and  $P_{PE}$  respectively, and hence :

$$P'_{AE} = P_{AE} - P_A \quad (5)$$

and

$$P'_{PE} = P_P - P_{PE} \quad (6)$$

The earthquake induces additional stresses (hydrodynamic stresses) on the wall due to the presence of water. The hydrodynamic stress distribution is very complex and a simple approach is adopted here. For the purpose of our analysis, we simplify the problem by considering the hydrodynamic stresses to vary linearly with depth and we assume that the hydrodynamic stress resultant acts at mid-height of the wall. We neglect the effects of energy reflections within the saturated soil mass and we assume that the additional pore water pressure that builds up in the soil due to the seismic loading dissipates instantaneously. We also assume, for simplicity, that the hydrodynamic stresses only affects the dynamic active pressures and thus neglect any sloshing which are likely to occur in front of the wall.

By considering the free body diagram of the wall (Fig.4.) and considering failure to occur by rotation of the wall about the top (anchor), the overturning moment,  $M_O$ , is :

$$M_O = P'_{AE} \cos(\delta_A) \frac{(H_A)}{2} + P_A \cos(\delta_A) \left(\frac{2}{3} H_A\right) + \frac{1}{2} \Delta F_W H_A \quad (7)$$



where  $\Delta F_W$ , the additional hydrodynamic stress resultant on the active side, is :

$$\Delta F_W = \frac{1}{2} k_h \gamma_w H_A^2 \quad (8)$$

Consideration of the forces on the passive side yields the restraining moment capacity :

$$M_R = P_P \cos(\delta_P) \left( H_A - \frac{D}{3} \right) - P'_{PE} \cos(\delta_P) \left( H_A - \frac{H_P}{3} \right) \quad (9)$$

and thus the factor of safety of the system against failure by rotation about the top is :

$$F = \frac{M_R}{M_O} \quad (10)$$

The retaining wall system will begin to rotate about the top, hence begin to fail, when the value of  $F$  in equation (10) reduces to 1.0. The acceleration ratio  $\tan \theta$  ( $= \frac{k_h}{1-k_v}$ ) at failure ( $F = 1.0$ ) will be called the critical acceleration ratio  $\tan \theta^*$ . The solution of equation (10) for a given factor of safety will yield the depth of embedment for various design acceleration ratios ( $\frac{k_h}{1-k_v}$ ).

## ANALYTICAL RESULTS

Wall Friction In our study of the seismic behavior of flexible retaining walls supporting dry cohesionless soil, we have established the importance of passive wall friction when addressing the seismic stability of these structures (Neelakantan et. al., 1988, 1989). Mobilization of interface friction on the passive side of the wall enhances the seismic stability of flexible retaining walls. In the present analysis, we assume that the presence of water deters the complete mobilization of wall friction on the passive side. We have neither found any evidence in the literature nor conducted experiments with saturated sands to support this assumption. However, this assumption will lead to a conservative solution. Any wall friction that may be mobilized will retard failure.

Depth of Embedment The depth of embedment has a critical influence on the stability of a flexible retaining wall since these structures derive a large part of their stability from the passive resistance that develops in the embedded portion of the wall. In general an increase in the embedment depth ratio (D/H ratio) above the static condition ( $\tan \theta^* = 0$ ) significantly increases the sustainable value of  $\tan \theta^*$  (Neelakantan et. al., 1988, 1989).

In Fig.5, we examine the effects of water on both sides of the retaining wall at anchor level for a soil with an angle of internal friction of  $30^\circ$  and taking the wall-soil interface friction as zero. For a given acceleration ratio a much larger embedment depth ratio - when compared to a retaining wall supporting dry soil - is required to guard against failure. As an example, if the design acceleration ratio is 0.3, the limiting D/H required for a dry cohesionless soil is 0.69 which is slightly above the static case (when the design  $\tan \theta^* = 0$ ). However, if water is present on both sides of the wall at anchor depth, the D/H ratio required is 1.0, an increase of almost 45 percent.

Case Study : Bulkhead No. 4, Sendai Harbour, Japan The 1978 Miyagi-ken-Oki earthquake of magnitude 7.0 and of focal depth 30 km struck Honshu Island, Japan, on June 12, 1978. Several waterfront facilities located on this island have suffered severe damage. These waterfront structures were reported to be designed using a seismic coefficient of 0.1 (Werner, 1986). The peak horizontal and vertical ground accelerations recorded at Shiogama Port, located about 100 km from the earthquake epicenter, were 0.29g and 0.22g respectively.

Werner (1986), using finite element method, analysed Bulkhead No.4 at Sendai Port, Japan. This bulkhead comprised of sheetpile walls anchored using steel H-beams (Fig.6). The apron and pavements at this bulkhead suffered severe cracking and settlement. The site is shown in Fig.7. Werner (1986) concluded from his analysis that the failure of Bulkhead No.4 was due to soil liquefaction.

We will now examine the seismic stability of Bulkhead No.4. In our analysis we assume uniform cohesionless soils, and thus we simplify the soil profile by taking an average angle of internal friction of  $30^\circ$ . The following parameters were used in the analysis :  $\phi_A = \phi_P = 30^\circ$ ,  $\delta_A = \delta_P = 0^\circ$ ,  $D = 14\text{m}$ ,  $H = 11\text{m}$ ,  $\gamma = 2.0\text{t}/\text{m}^3$  and  $\gamma_w = 10\text{kN}/\text{m}^3$ . The factor of safety of Bulkhead No.4 under static conditions, against failure by rotation about the anchor is about 3.5. If water were absent (dry, cohesionless soil) the wall would fail, according to our analysis, at an acceleration ratio of 0.49 (Fig.5). Assuming the water level at the time of the earthquake to be at the same level as the anchor, we obtain from Fig.5 a failure acceleration ratio  $\tan \theta^* = 0.36$ . This predicted failure acceleration ratio is fortuitously nearly equal to the acceleration ratio recorded at Shiogama Harbour ( $\tan \theta^* = \frac{k_h}{1-k_v} = \frac{0.29}{1-0.22} = 0.37$ ) and used by Werner (1986) in his finite element analysis of Bulkhead No.4.

Our analysis, thus, shows that even if the anchor were adequately designed for a seismic coefficient of 0.1 (and we presumed it to be so), the bulkhead would have failed irrespective of any soil liquefaction. It seems plausible that the actual mode of failure of Bulkhead No.4 may be anchor failure, since the recorded damage - apron cracking and settlements - may be an indication of this failure mode.

### CONCLUSION

In this paper we have attempted to analyse the performance of a waterfront tied-back wall under seismic loads. We used a pseudo-static analysis to study the behavior of tied-back walls wherein water is present on both sides of the wall. In spite of the simple treatment of the hydrodynamic stresses, we found from examining the case history of Bulkhead No.4, Sendai Harbour, that this bulkhead would have failed irrespective of liquefaction of the soils.

### REFERENCES

1. N. Mononobe and H. Matsuo, 'On the Determination of Earth Pressures during Earthquakes', *Proc. World Engineering Conference*, Vol.9, 177-185 (1929).
2. S. Okabe, 'General Theory of Earth Pressures', *J. Jap. Soc. of Civil Engrs.*, Vol.12, No.1. (1926).
3. R. Richards and D. G. Elms, 'Seismic Behaviour of Gravity Retaining Walls', *J. Geotech. Engrg Div., Proc. ASCE*, Vol.105, No.GT4, 449-464 (1979).
4. H. B. Seed and R. V. Whitman, 'Design of Earth Retaining Structures for Dynamic Loads', *Lateral Stresses in the Ground and Design of Earth Retaining Structures*, *ASCE*, 103-147 (1970).
5. J. H. Wood, 'Earthquake-Induced Soil Pressures on Structures', *Report No. EERL 73-05*; Earthquake Engng. Res. Lab., Calif. Inst. of Tech., Pasadena, CA., 1973.
6. G. Neelakantan, M. Budhu and R. Richards, Jr, 'Stability of a Tied-Back Sheet Pile Wall Under Seismic Loading', *Proceedings*; First Japan-U.S. Workshop on Liquefaction, Large Ground Deformation and Their Effects on Lifeline Facilities, Tokyo, Japan, November 1988.
7. G. Neelakantan, M. Budhu and R. Richards, Jr, 'Behavior of Flexible Tied-Back Retaining Walls Under Seismic Loading', Report Submitted to the National Science Foundation, September 1989.

8. S. D. Werner, 'A case Study of the Behavior of Seaport Facilities During the 1978 Miyagi-Ken-Oki Earthquake', Lifeline Seismic Risk Analysis - Case Studies, Published by A.S.C.E., 1986.

#### APPENDIX I. - NOTATIONS

The following symbols are used in this paper:

$D$  = depth of embedment;

$H$  = height of the soil retained;

$H_A$  = height of the active wedge

$K_A$  = static coefficient of active earth pressure;

$K_{AE}$  = dynamic coefficient of active earth pressure;

$K_P$  = static coefficient of passive earth pressure;

$K_{PE}$  = dynamic coefficient of passive earth pressure;

$k_h$  = coefficient of horizontal acceleration;

$k_v$  = coefficient of vertical acceleration;

$P_A$  = Static component of active earth pressure resultant;

$P_{AE}$  = Active earth pressure resultant;

$P'_{AE}$  = Dynamic component of active earth pressure resultant;

$P_P$  = Static component of passive earth pressure resultant;

$P_{PE}$  = Passive earth pressure resultant;

$P'_{PE}$  = Dynamic component of active earth pressure resultant;

$\gamma$  = unit weight of soil;

$\gamma_b$  = buoyant unit weight of soil;

$\gamma_w$  = unit weight of water;

$\delta_A$  = wall friction on the active side;

$\delta_P$  = wall friction on the passive side;

$\iota_A$  = slope of the ground on the active side;

$\iota_P$  = slope of the ground on the passive side;

$\phi_A$  = angle of internal friction of the soil on the active side;

$\phi_P$  = angle of internal friction of the soil on the passive side;

$\theta = \arctan \left( \frac{k_h}{1-k_v} \right)$ ;

$\tan \theta^*$  = critical (failure) acceleration ratio and

$\Delta F_W$  = additional hydrodynamic stress resultant.

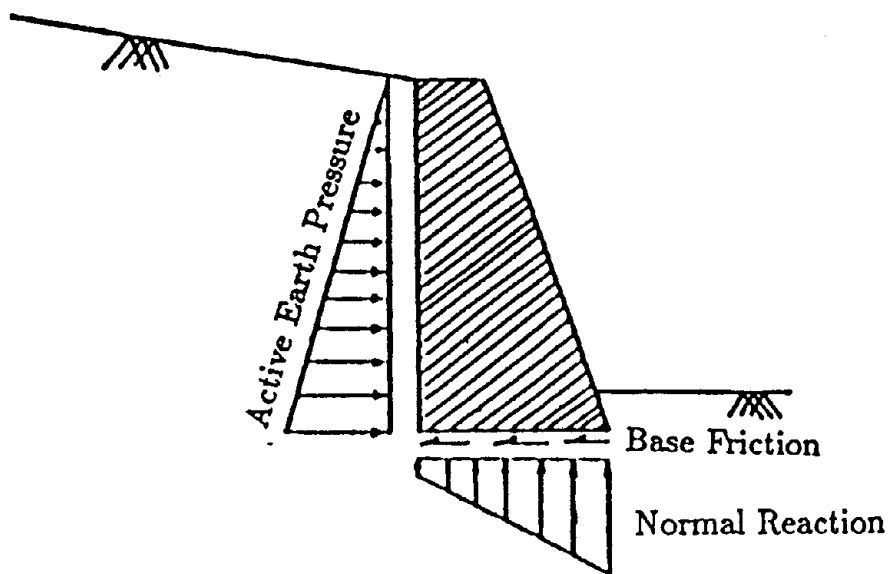


Fig. 1. - Gravity Retaining Wall

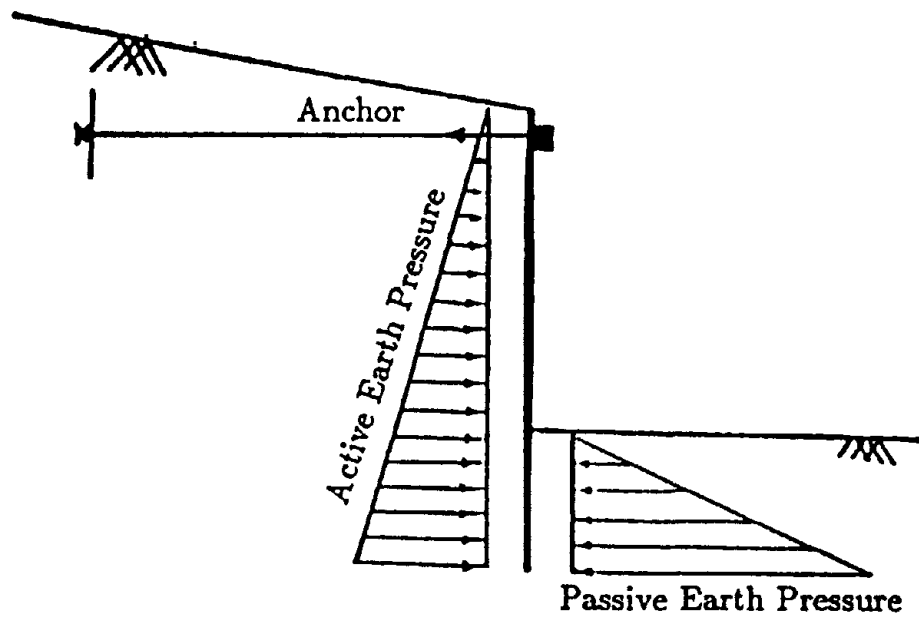


Fig. 2. - Flexible Tied-Back Retaining Wall

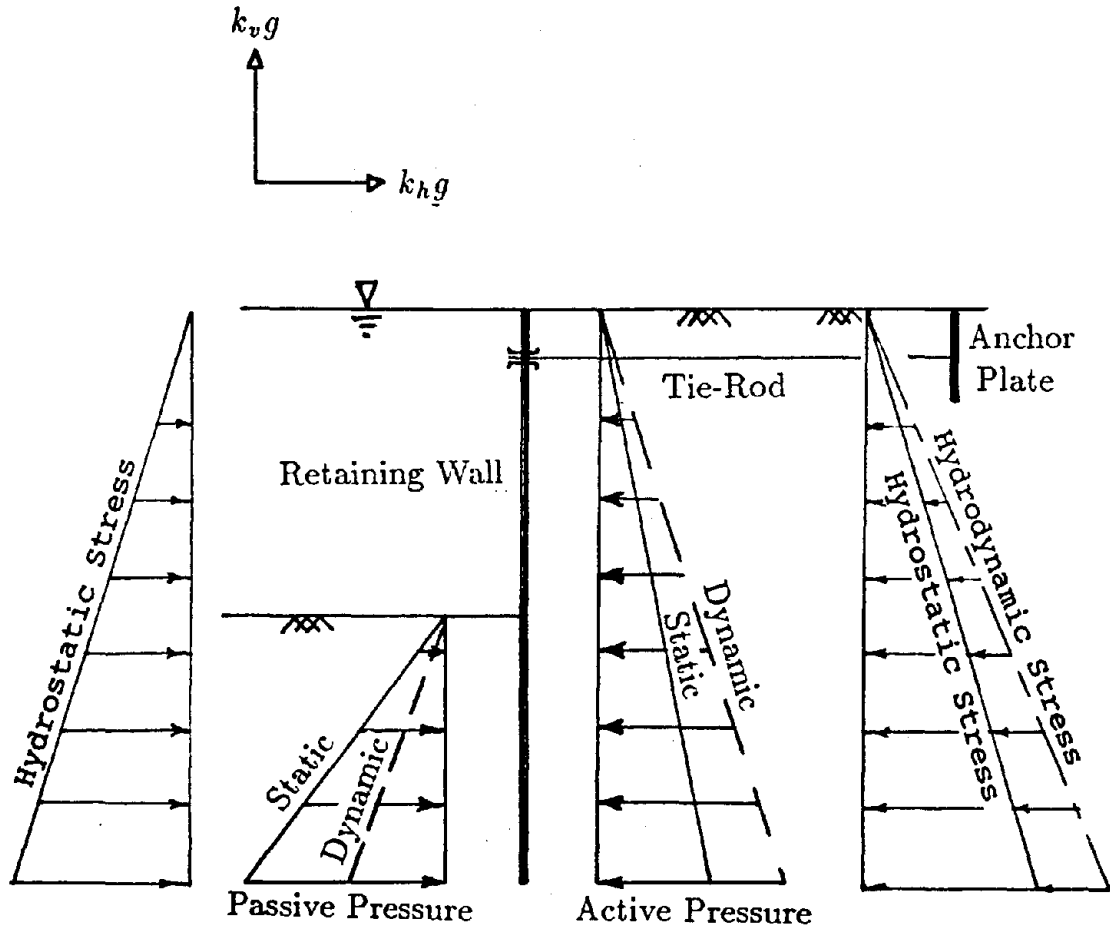


Fig. 3. - Water and Earth Pressures in a Tied-Back Wall System

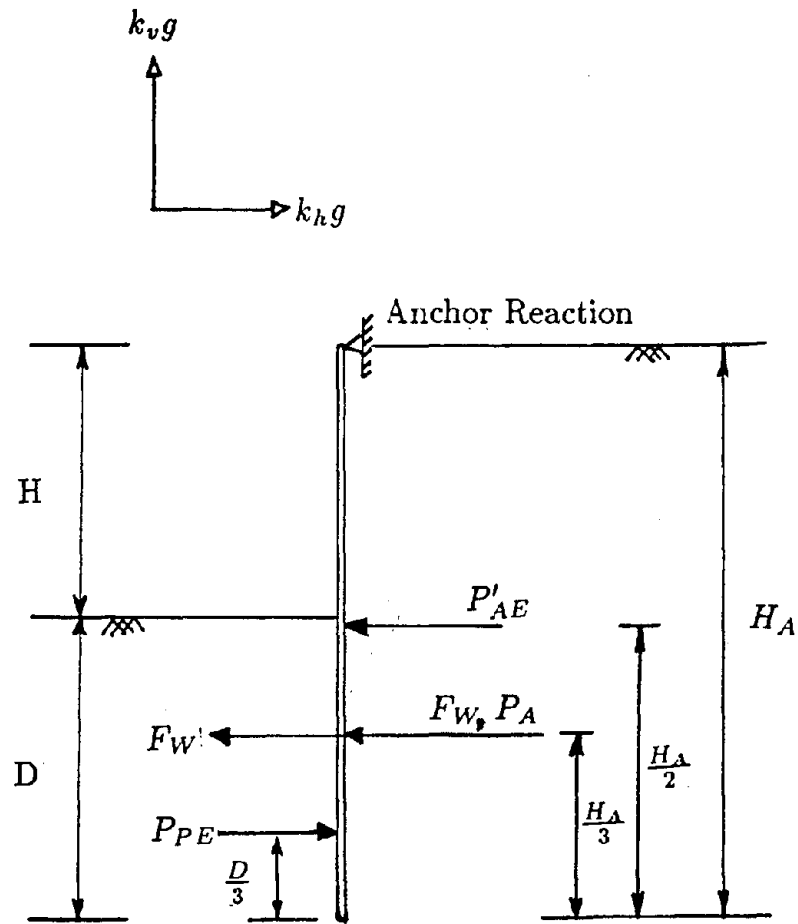


Fig. 4. - Stress Resultants Acting on a Tied-Back Wall

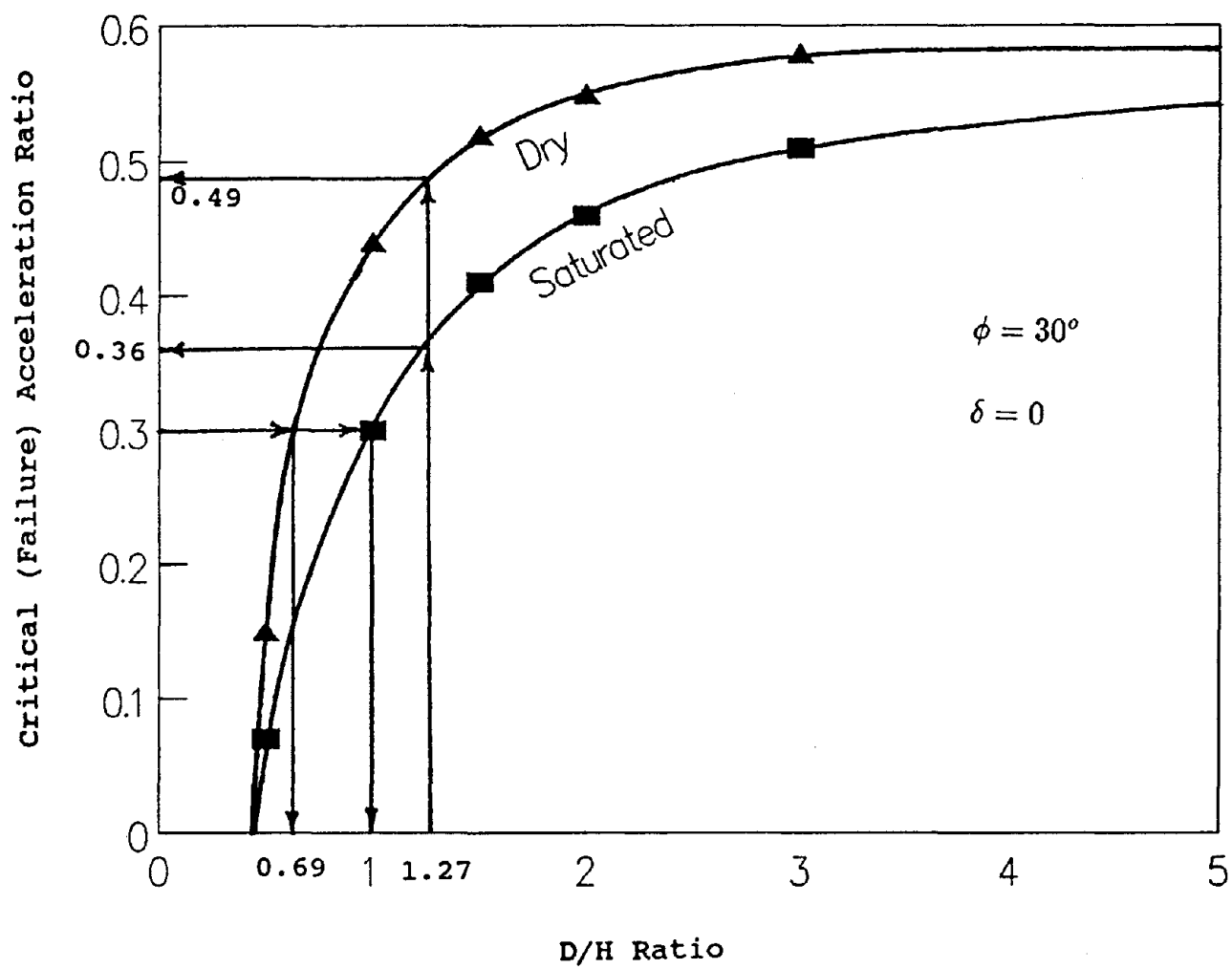


Fig. 5. - Effect of D/H ratio on the Critical (Failure) Acceleration Ratio



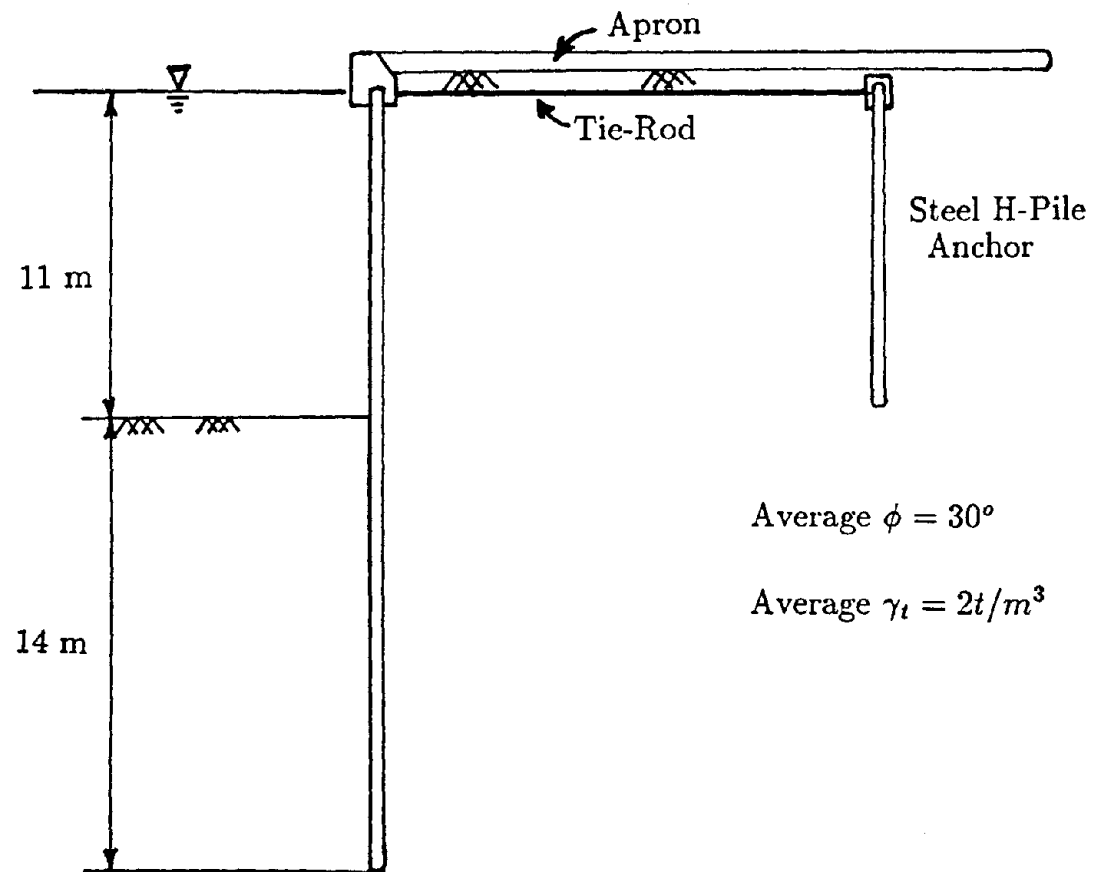


Fig. 6. - Configuration of Sheet-Pile Bulkhead No.4 at Sendai Port, Japan

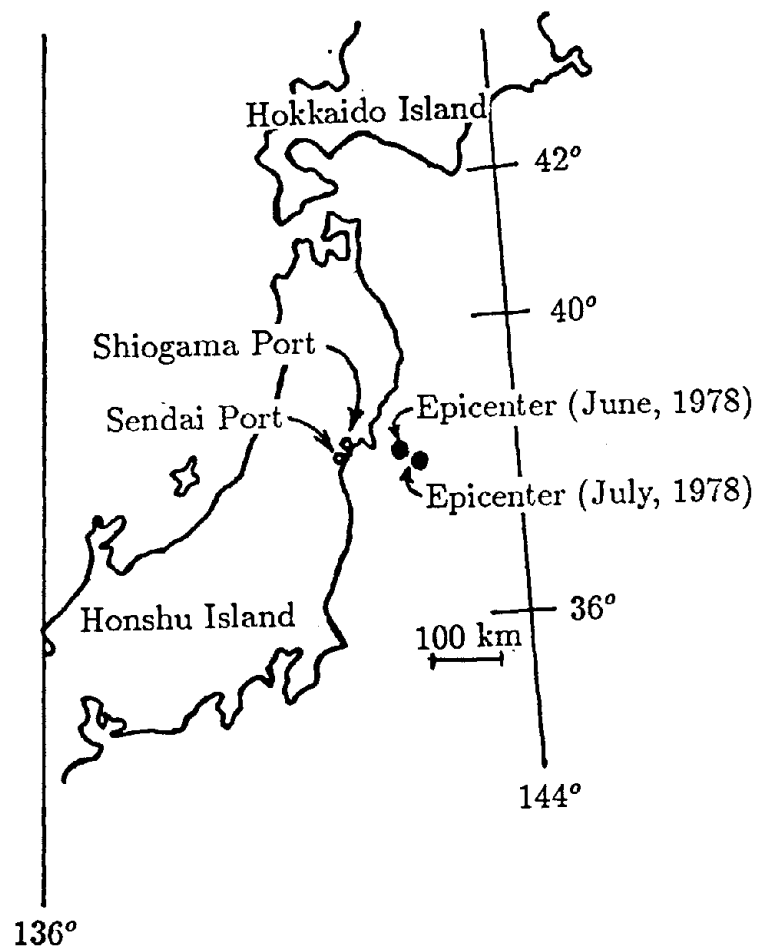


Fig. 7. - Map Showing Earthquake Epicenter and Harbour Locations

LIQUEFACTION ANALYSIS OF SEAWALL DURING 1983  
NIPPONKAI-CHUBU EARTHQUAKE

Y. Fujii

Office of Technical Development  
TAKENAKA Civil Engineering & Construction Co., Ltd.

M. Hatanaka & T. Shiomi

Chief Research Engineers  
TAKENAKA Technical Research Laboratory

and

Y. Tanaka  
Assistant Manager  
Office of Technical Development  
TAKENAKA Civil Engineering & Construction Co., Ltd.

ABSTRACT

Public facilities were damaged by the Nipponkai-Chubu Earthquake (Magnitude=7.7) on 26th of May in 1983. One of the damages was observed at Akita Port. Large residual displacement of the steel sheet pile wall and settlement of the ground induced by liquefaction were observed. In order to account for the damage done during the earthquake due to liquefaction, numerical simulation was conducted. The method of the numerical simulation used here was based on a two-phase dynamic nonlinear theory which took into account dissipation of excess pore water pressure as well as accumulation. The numerical results were compared with the values obtained from the observations. Bending moments of the sheet pile wall during the earthquake were also investigated. The result showed that the method of numerical simulation was capable to simulating the liquefaction phenomena for the seawall.

## INTRODUCTION

On the 26th of May in 1983, the Nipponkai-Chubu Earthquake with a magnitude of 7.7 struck off the shore of Akita Prefecture (Fig.1). Lifelines such as those for water supply and sewage sustained a great deal of damage within Noshiro city. In Akita Port the seawall at Ohama No. 2 Wharf suffered damage. A Large part of these extensive damages were induced by soil liquefaction. It is important for engineers to solve and/or predict this type of problem. In recent years, numerical methods to simulate soil liquefaction were proposed (Zienkiewicz et al., 1984 etc.). The structural damage caused by the soil liquefaction was simulated through the numerical study (Shiomi et al. 1988, Iai et al. 1988 etc.) In this paper, numerical simulation was made to simulate not only the soil liquefaction problem but also the damages, e.g. residual displacement. The numerical method used here was the nonlinear dynamic effective stress analysis program DIANA-J (Dynamic Interaction Approaches and Nonlinear Analysis-Japan) employing a two-dimensional finite element method (Zienkiewicz et al, 1984).

## DAMAGE OF THE SEAWALL

The seawall of Ohama No. 2 Wharf shown in Fig. 2 reported by Tsuchida et al., 1985, consists of the followings: i) sheet pile wall at the front, ii) steel pipe piles (Diameter=550mm, thickness=12mm, length=15m and center-to-center=2m installed at a place twenty meters behind the front of the sheet pile wall and iii) tierods (Diameter=55mm) connect these two types of piles. Behind the sheet piles, loose, fine sand is deposited on the sea bed to a height of 12 meters. Under the loose, fine sand layer, there is fine sand, the type of which is N-value of the standard penetration test ( $\bar{N}_{spt}$ ) > 20, and silty sand. The total length of the seawall is 235 meters. This seawall was extensively damaged by the earthquake shown in Fig. 2. The upper parts of the sheet piles of the seawall displaced 1.5 meters toward the sea in a horizontal direction. Furthermore, the phenomenon of sand boiling and extensive settlement was observed on the apron. Cracks and folding on the sheet piles were also observed at the place which was approximately 8 meters from the top of the apron.

## INITIAL STRESS ANALYSIS

The initial stress analysis was made using the two-dimensional finite element model which is shown in Fig. 3. In order to avoid the influence induced by the friction between the piles and the surrounding soil layer, joint elements were installed between the ground and both the sheet piles and the steel pipe piles.

Table 1 shows the material properties used in the initial stress analysis. The coefficient of permeability and internal friction angle of the fine sand were obtained from laboratory tests. Shear modulus was estimated from the  $\bar{N}_{spt}$ . Fig. 4 shows the static bending moment of the sheet piles which was

obtained from the analysis.

## LIQUEFACTION ANALYSIS

Fig. 5 shows two components of acceleration observed at the ground surface of the Akita port by Tsuchida et al. (1985). Due to the fact that this section (Fig. 2) has an angle of 33.4 degree at E-W component, input motion of the liquefaction analysis was obtained through compounding these two factors. Furthermore, the time history of acceleration at a depth of 26 meters was calculated through the one-dimensional multi-reflection theory. The analysis was started at 11.1 second, in which the main shock occurred between 13.1 and 24.2 seconds after the start of the recorded wave. Fig. 6 shows the time history of input acceleration.

Fig. 7 shows the numerical model for liquefaction analysis. The joint elements used in the initial stress analysis were removed. The soil constitutive model used in the analysis was Pastor-Zienkiewicz model (PZ model) (Pastor et al., 1986). Material properties of the PZ model used for the analysis were determined in order to meet the relationship between the cyclic stress ratio and the number of the cyclic load (Tsuchida et al., 1985) through conducting the local stress simulation of the triaxial test (Tanaka et al., 1987 and Shiomi, 1988). Table 2 illustrates the material properties used in the liquefaction analysis.

## RESULTS OF NUMERICAL SIMULATION

Fig. 8 illustrates the time histories of the horizontal response acceleration at the locations which were indicated in Fig. 7. Fig. 9 and 10 represent the time history of both the horizontal and the vertical displacements at the points of A, B, C and D. From these figures, it can be seen that the horizontal and vertical displacement are accumulated, and remain residual.

Fig. 11 illustrates the time history of the excess pore water pressure at the elements of E, F, G, H and I as indicated in Fig. 7. At the element of E, the excess pore water pressure is observed to have tendency to become negative. This is considered to be a result of cyclic mobility at this element. The element of H also has a tendency to do the same. However, it is found that the excess pore water pressure tends to accumulate at the element of H. On the other hand, at the location of I, it is found that there is a tendency for the excess pore water pressure to gradually generate. The excess pore water pressure at the final time of the numerical simulation is 40KPa, and the excess pore water pressure ratio is approximately 50% of the initial effective mean stress.

Fig. 12 shows the pattern of maximum response acceleration during the calculation. Fig. 13 shows the displacement pattern at the final time of the simulation (11.1 sec.). In Fig. 13, the fact that the seawall deforms in the direction of the sea and the ground is settled, can be clearly identified. The Tops of the sheet piles move 29 cm toward the sea in a horizontal direction. Maximum settlement of the ground surface at the apron between the sheet piles and the steel pipe piles is 11 cm.

Fig. 14 represents the bending moment of the sheet piles. Fig. 14(a) shows a bending moment at 11.1 seconds, and Fig. 14(b) shows a bending moment in which the initial bending moment is added to this. This value reaches a maximum degree at the place which is 8-11 meters away under the ground surface.

#### COMPARISON BETWEEN OBSERVATION AND NUMERICAL SIMULATION

After the earthquake, the tops of the sheet piles, which were located in front of the seawall, were observed to have moved 1.5 meters in a horizontal direction. In this study, displacement is calculated at 0.3 meters occurring during the analysis period. The settlement of the ground surface was observed to be approximately 1.4 meters. The calculated settlement is 0.1 meter. The result of the analysis expresses the state of the damage qualitatively. However, the amount of both the movement of the sheet pile tops and the settlement of the ground at the apron were smaller than the values obtained from the observations. It is considered that in this analysis, the calculation is not carried out to the extent in which the excess pore water pressure is perfectly dissipated. The place where cracks of the sheet piles occur correspondes quite closely to the place where the bending moment reaches its maximum value. Because the linear elements are used for the sheet piles, the phenomenon of rupture which exceeds the yield strength is not completely expressed. On the other hand, the generation process of the excess pore pressure is considered to be well represented qualitatively.

#### CONCLUDING REMARKS

The numerical simulation dealt with in this paper has clarified that the damage sustained at Akita Port in the Nipponkai-Chubu earthquake can be simulated to some extent by the employment of the dynamic nonlinear effective stress analysis program DIANA-J. Extension of the calculation time and estimation of the earth pressure of the ground behind the sheet pile wall, will be carried out in the future.

#### ACKNOWLEDGEMENT

The authors would like to express the appreciation to Dr. S. Iai of the Port and Harbour Research Institute, of the Ministry of Transport for their cooperation in supplying earthquake data and useful discussion about the analysis results.

#### REFERENCES

1. Report of Cooperative Research and Colaboration, Liquefaction and Large-

ground Deformation and their Effects on Lifeline Facilities (1988) in Japanese.

2. Tsuchida, H., Noda, S., Inatomi, T., Uwabe, T., Iai, S., Ohneda, H. and Toyama, S., Damage to Port Structure by the 1983 Nipponkai-Chubu Earthquake, Technical Note at the Port and Harbour Research Institute, No. 511 (1985) in Japanese.

3. Zienkiewicz, O.C. and Shiomi, T., Dynamic Behaviour of Saturated Porous Media: The Generalized Biot Formulation and its Numerical Solution, Int. Jour. of Numerical and Analytical Methods in Geomechanics, Vol. 8, p.71-96 (1984).

4. Shiomi, T., Tsukuni, S. and Tanaka, Y., A Simulation Study of Ground Liquefaction in a Soil-Structure Interaction Problem, 9WCEE (1988).

5. Iai, S., Damage to Port and Harbour Facility by Liquefaction, Proc. of 1st Japan-U.S. Workshop on Liquefaction, Large Ground Deformation and their Effects on Lifeline Facilities, p.185-192 (1988).

6. Imai, T., P- and S-wave Velocities of the Ground in Japan, Proc. of 9th Int. Conf. on SMFE, Vol. 2, p.257-260 (1977).

7. Pastor, M. and Zienkiewicz, O.C., A Generalized Plasticity, Hierarchical Model for Sand Under Monotonic and Cyclic Loading, Proc. of 2nd Int. Symp. on Numerical Models in Geomechanics, p.131-150 (1986).

8. Tanaka, Y., Shiomi, T. and Hirose, T., Simulation of Geotechnical Centrifuge Test by Two-phase FE Analysis, Int. Conf. on Computational Plasticity, Models, Software and Application (1987).

Table 1 Material Properties (Initial Stress Analysis)

## (a) Linear Material

Material Number	No.5 (Sea Water)
IPhase/2Phases	1Phase
Shear Modulus G (kPa)	$4.44 \times 10^{-9}$
Bulk Modulus K (kPa)	$2.22 \times 10^{-6}$
Poisson's Ratio $\nu$	0.499
Unit Weight of Water ( $t/m^3$ )	1.0
Porosity	1.0

## (b) Nonlinear Materials (Mohr-Coulomb Model)

Material Number	No.1 (Fine Sand)	No.2 (Fine Sand)	No.3 (Silty Sand)	No.4 (Fine Sand)
IPhase/2Phases	1Phase	1Phase	1Phase	1Phase
Shear Modulus G (kPa)	33800	33800	136000	213000
Bulk Modulus K (kPa)	73200	73200	295000	462000
Poisson's Ratio $\nu$	0.3	0.3	0.3	0.3
Mass Density of Soil ( $t/m^3$ )	2.7	0.7	1.03	1.16
Unit Weight of Water ( $t/m^3$ )	1.0	1.0	1.0	1.0
Porosity	0.4	0.5	0.4	0.35
Permeability (m/sec.)	$0.9 \times 10^{-3}$	$0.9 \times 10^{-3}$	$0.15 \times 10^{-6}$	$0.1 \times 10^{-3}$
Cohesion C (kPa)	0.01	0.01	49.0	0.01
Angle of Internal Friction $\phi$ (°)	37.9	37.9	15.0	42.6

## (c) Beam Elements

Material Number	No.6 (Sheet Pile)	No.7 (Steel Pile)	No.8 (Tierod)	No.9 (Sheet Pile)
Young's Modulus E (kPa)	$2.06 \times 10^8$	$2.06 \times 10^8$	$2.06 \times 10^8$	$2.06 \times 10^8$
Shear Modulus G (kPa)	$7.94 \times 10^7$	$7.94 \times 10^7$	$7.94 \times 10^7$	$7.94 \times 10^7$
Mass Density ( $t/m^3$ )	6.8	0.67	6.8	7.8
Geometrical Moment of Inertia ( $m^4$ )	$8.6 \times 10^{-4}$	$2.74 \times 10^{-4}$	$4.5 \times 10^{-7}$	$8.6 \times 10^{-4}$
Section Area ( $m^2$ )	0.0306	0.0203	0.00238	0.0306



Table 2 Material Properties (Liquefaction Analysis)

## (a) Linear Material

Material Number	No.5 (Sea Water)
1Phase/2Phases	1Phase
Shear Modulus $G$ (kPa)	$4.44 \times 10^{-9}$
Bulk Modulus $K$ (kPa)	$2.22 \times 10^{-6}$
Poisson's Ratio $\nu$	0.499
Unit Weight of Water ( $t/m^3$ )	1.0
Porosity	1.0

## (b) Nonlinear Materials (PZ Model)

Material Number	No.1 (Fine Sand)	No.2 (Fine Sand)	No.3 (Silty Sand)	No.4 (Fine Sand)
1Phase/2Phases	2Phases	2Phases	2Phases	2Phases
Shear Modulus $G$ (kPa)	33800	33800	136000	213000
Bulk Modulus $K$ (kPa)	73200	73200	295000	462000
Poisson's Ratio $\nu$	0.30	0.30	0.30	0.30
Mass Density of Soil ( $t/m^3$ )	2.7	2.7	2.7	2.7
Unit Weight of Water ( $t/m^3$ )	1.0	1.0	1.0	1.0
Porosity	0.4	0.5	0.40	0.35
Permeability (m/sec.)	$0.9 \times 10^{-3}$	$0.9 \times 10^{-3}$	$0.15 \times 10^{-6}$	$0.1 \times 10^{-3}$
Angle of Internal Friction $\phi$ (°)	37.9	37.9	39.1	42.6
$M_r$	0.60	0.60	0.85	1.089
$\alpha_r$	0.635	0.635	1.14	1.653
$M_g$	1.20	1.20	1.31	1.361
$\alpha_g$	0.35	0.35	0.35	0.35
$\beta_0$	4	4	4	4
$\beta_1$	0.2	0.2	0.2	0.2
$H_0$	15	15	17.5	20
$H_{u0}$	0.5	0.5	0.65	0.8
$\tau_u$	3	3	5	7
$\tau$	2	2	4	6

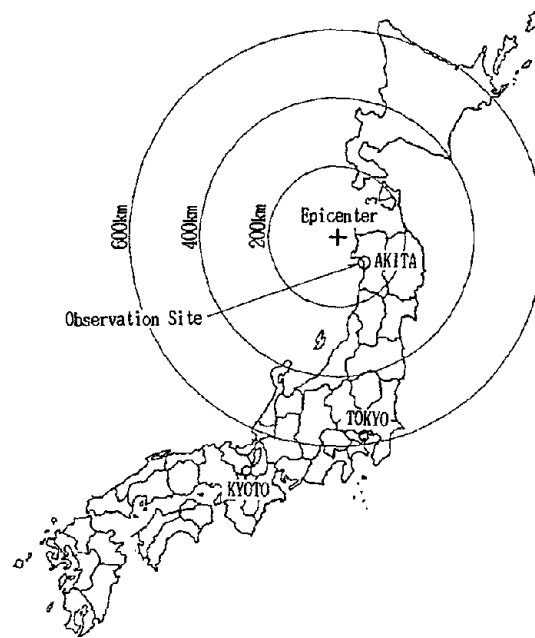


Fig.-1 Epicenter of the earthquake and observation site

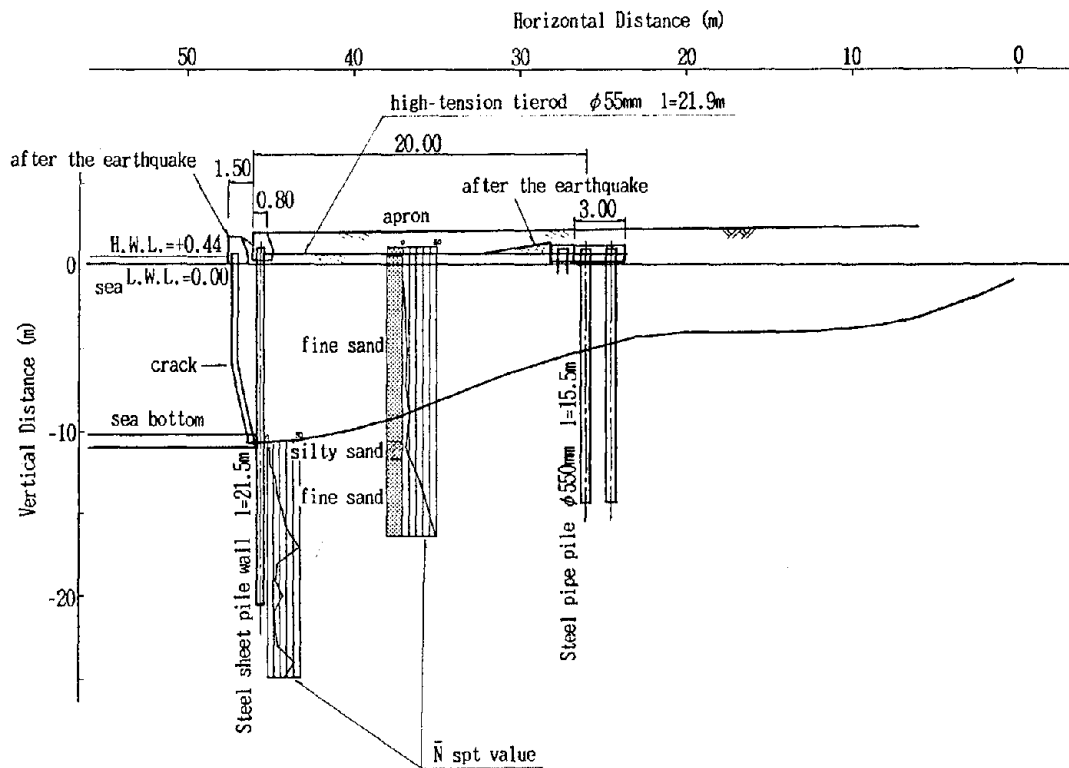


Fig.2 Typical section of Ohama-10m No.2 Wharf in Akita Port after the earthquake (Tsuchida et al., 1985)

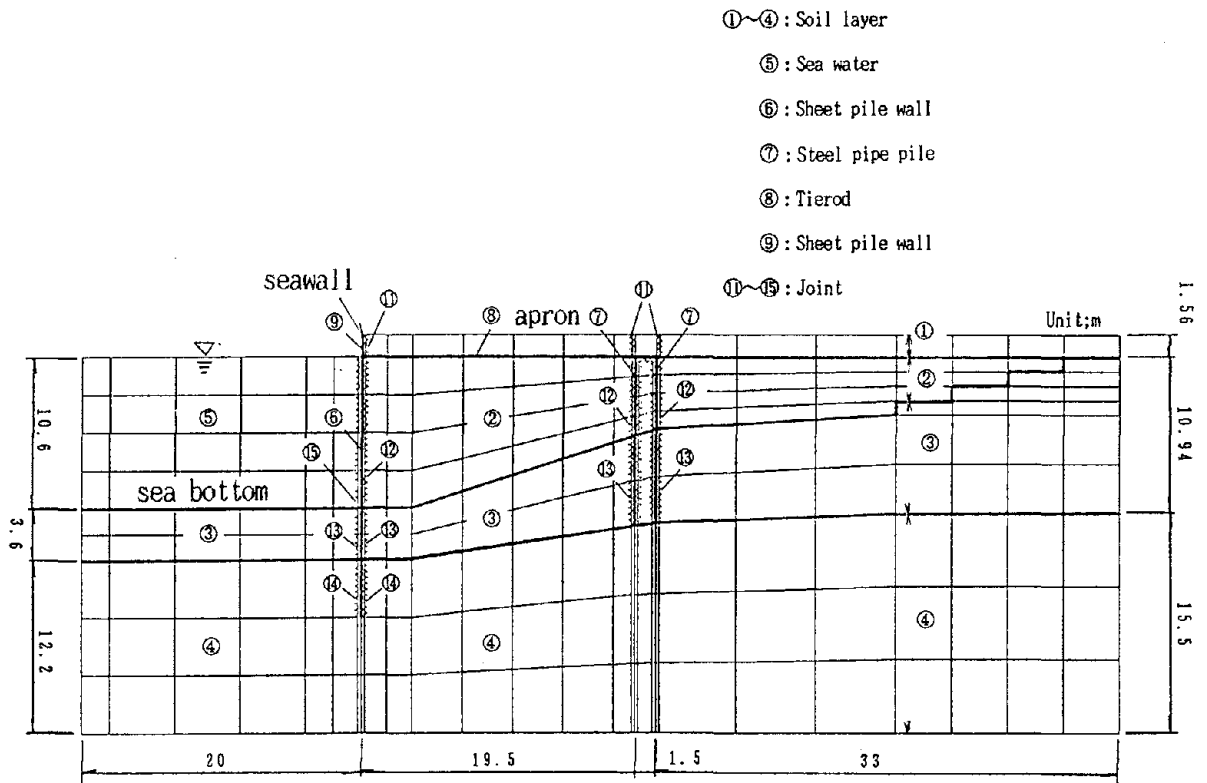


Fig. 3 Finite Element Model (initial stress analysis)

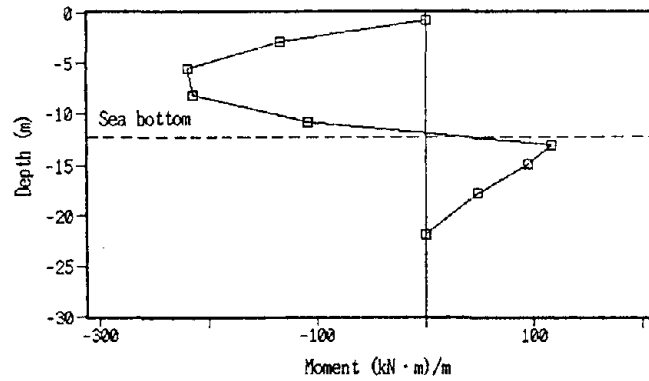


Fig. 4 Distribution of bending moment of steel pile (Initial stress analysis)

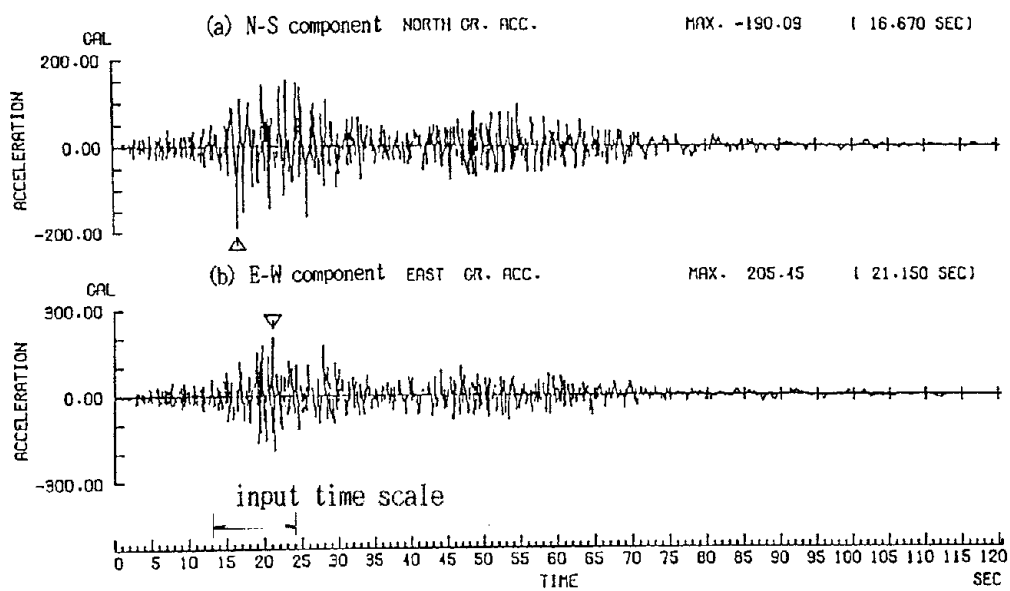


Fig.5 Recorded acceleration (Tsuchida et al.,1985)

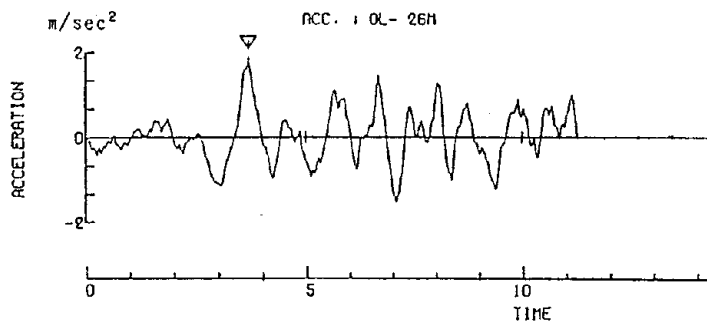


Fig.6 Input motion at G.L. -26m

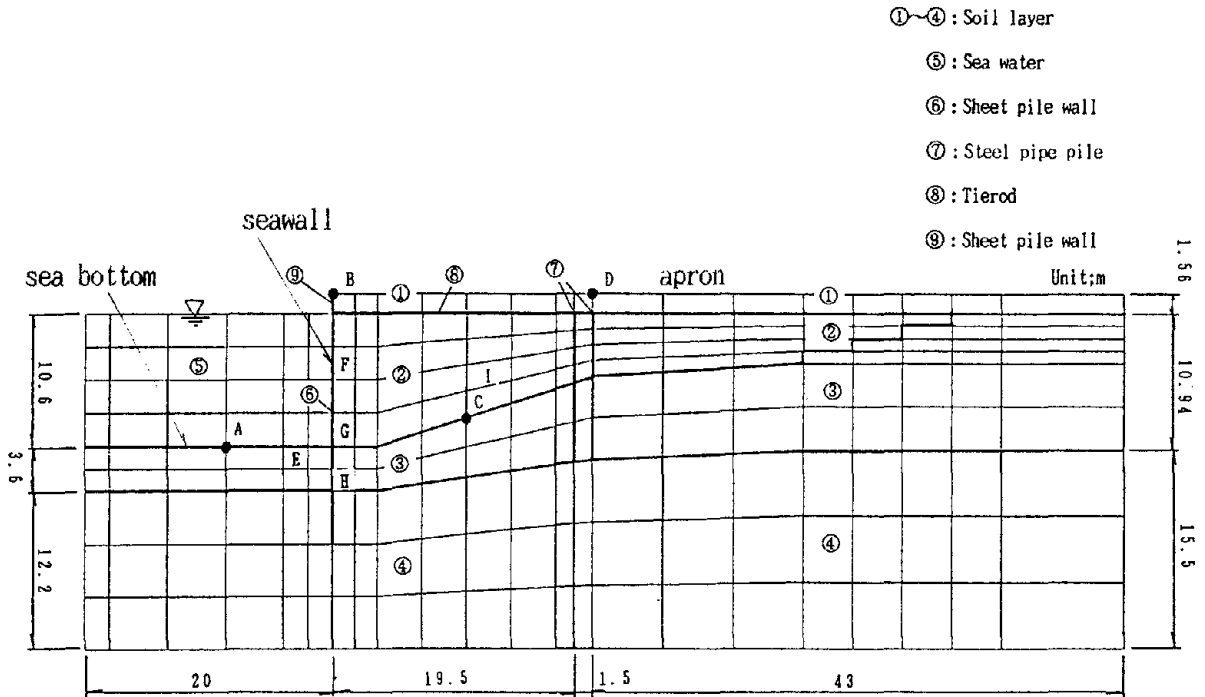


Fig.7 Finite Element Model (Nonlinear dynamic analysis)

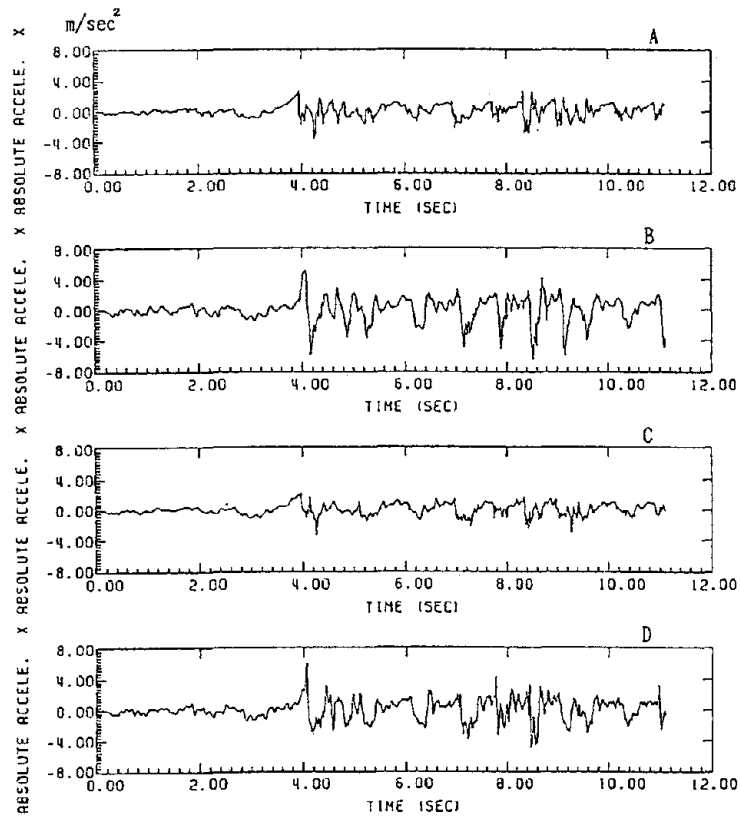


Fig. 8 Time history of horizontal acceleration

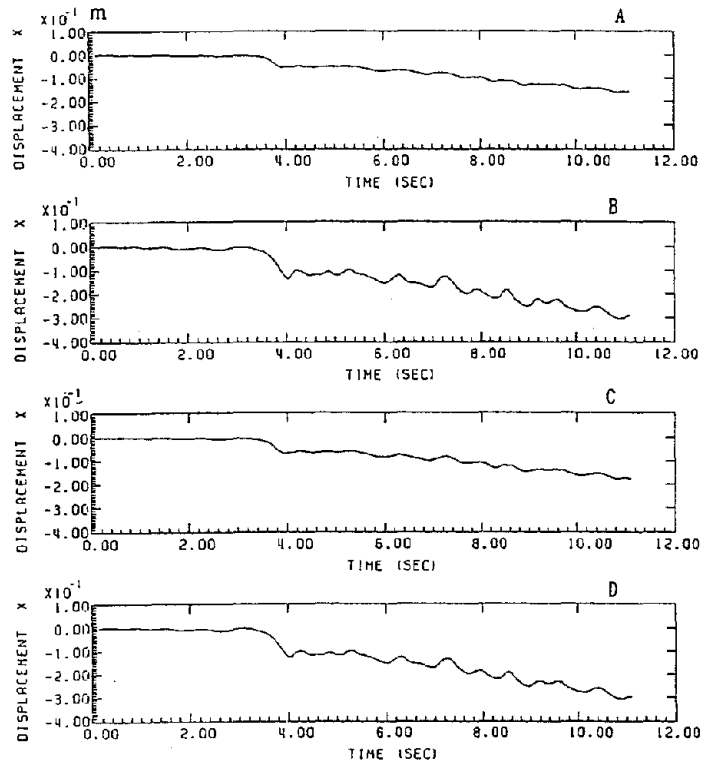


Fig. 9 Time history of horizontal displacement

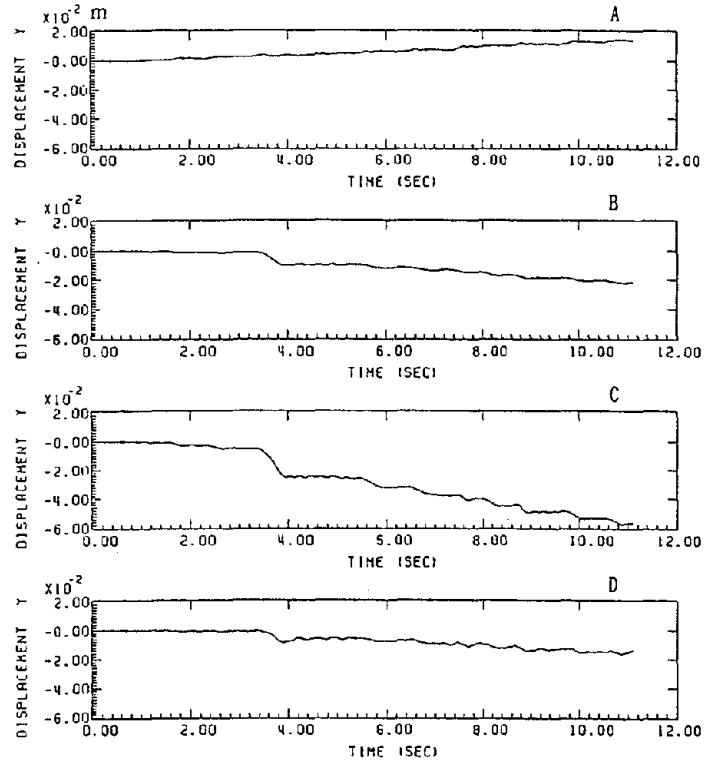


Fig. 10 Time history of vertical displacement

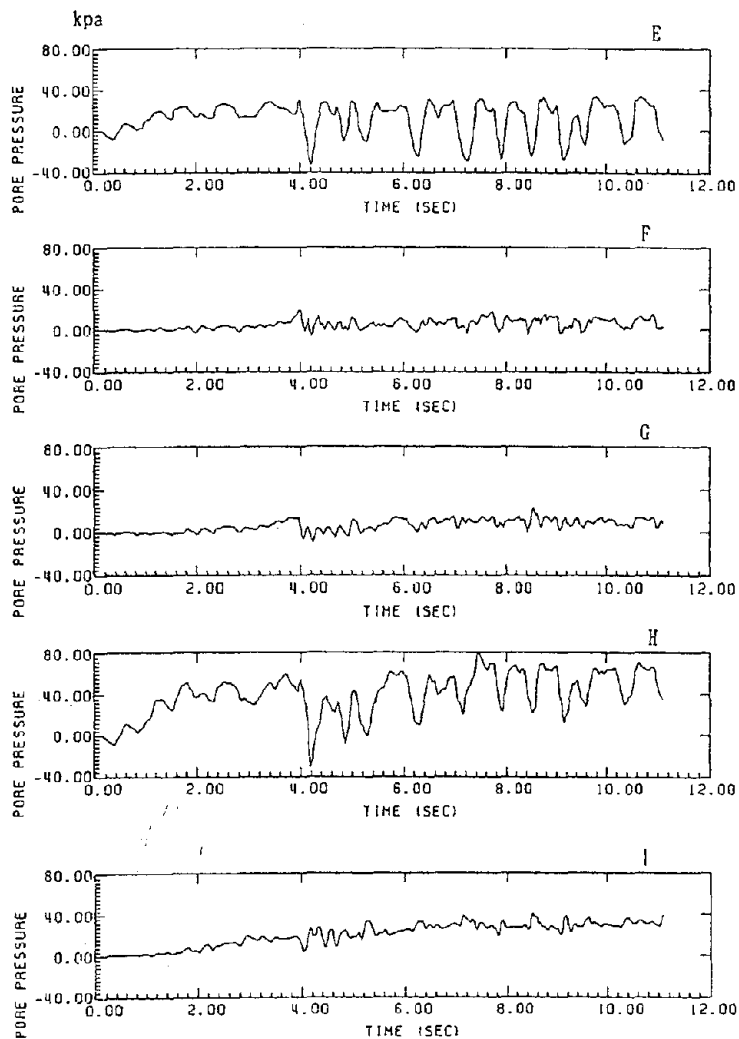
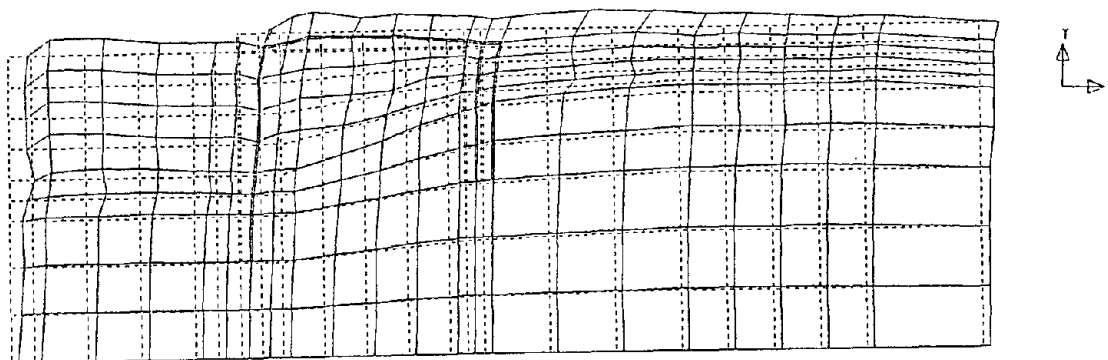
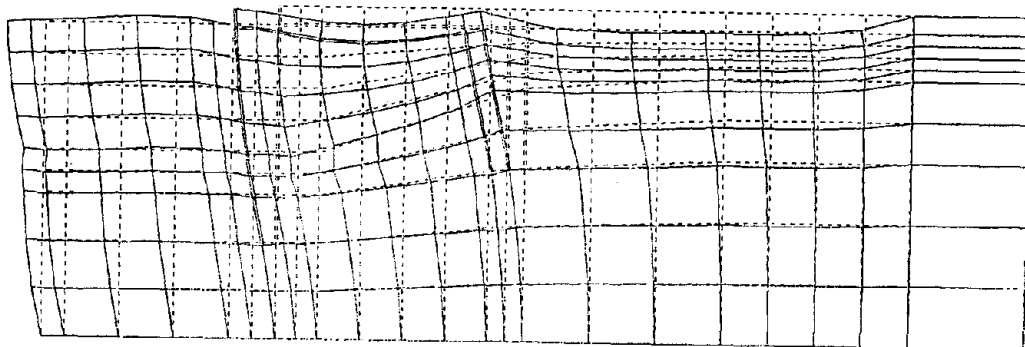


Fig. 11 Time history of excess pore water pressure



MAX. ACC. SCALE :  $\text{---} 8.40 \text{ m/sec}^2$

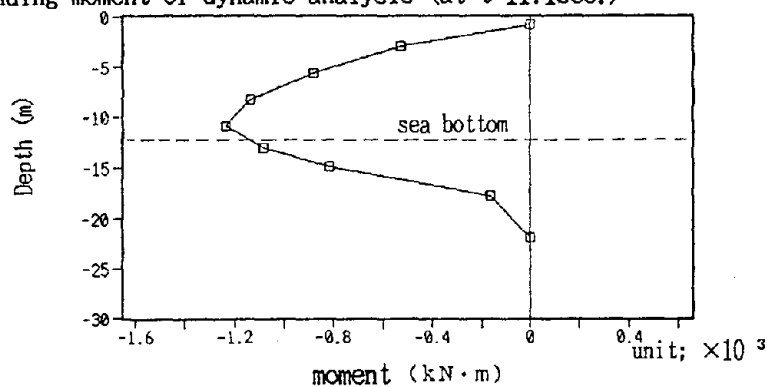
Fig.12 Pattern of maximum response acceleration



SCALE : 1 / 400  
DISP. SCALE :  $\rightarrow 2.99E-01$

Fig.13 Displacement pattern at 11.1 seconds

(a) Bending moment of dynamic analysis (at t=11.1sec.)



(b) Bending moment of dynamic analysis plus initial stress analysis

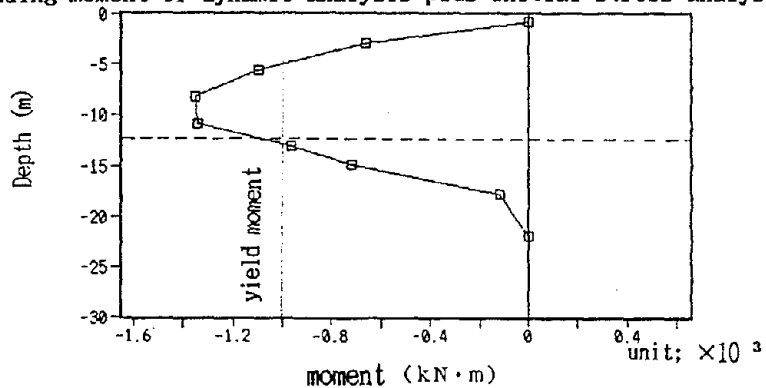


Fig. 14 Bending moment of sheet pile wall



# APPROXIMATE ANALYSIS PROCEDURES FOR PERMANENT GROUND DEFORMATION EFFECTS ON BURIED PIPELINES

Michael J. O'Rourke

Professor of Civil Engineering  
Rensselaer Polytechnic Institute

## ABSTRACT

Approximate analysis procedures for the effects Permanent Ground Deformation (PGD) on continuous buried steel pipelines are presented. The analysis is restricted to transverse PGD (ground motion perpendicular to the pipeline axis) with no abrupt ground displacement at the margins of the lateral spread. The assumed failure mechanism is local compressional buckling of the thin wall pipe. Failure diagrams for mild steel pipe are presented as functions of  $\delta$ , the amount of PGD movement and  $L$ , the spatial extent of the lateral spread zone.

## INTRODUCTION

In the past, earthquakes have caused damage to buried pipelines. The damage mechanisms have been permanent ground deformation (PGD) due to faulting, landslides, liquefaction or seismic settlements, and seismic wave propagation. An excellent summary of buried pipeline damage due to 18 North American earthquakes is given by O'Rourke, Grigoriu and Khater (1). They observe, for example, that approximately 50 percent of all pipeline breaks from the 1906 San Francisco earthquake occurred within one city block of zones of lateral spreading due to liquefaction. The remaining 50 percent of the breaks occurred outside the lateral spreading zones where wave propagation was the prominent damage mechanism.

As far as materials are concerned, modern continuous steel pipelines have performed well in past earthquakes. These pipelines typically have continuous circumferential electric arc welds. However, continuous steel pipelines constructed prior to 1940 have not fared as well. In these pre-modern pipelines, damage typically occurs at the welded joints. Other areas susceptible to damage are those previously weakened by corrosion.

The effects of PGD on buried pipelines has been the subject of recent research activity. Suzuki, Arata and Suzuki (2) have presented results from a non-linear finite element code LINE-FLEX. Similarly, O'Rourke and Lane (3) show results from a parametric study using the UNIPIP computer program.

In this paper, an approximate analytical procedure for the effects of PGD on modern continuous buried steel pipelines is presented. Transverse PGD (ground motion perpendicular to the pipeline axis) with no abrupt ground displacement at the margins of the lateral spread is considered.

Such an analytical procedure is considered useful in that it is applicable to the design office environment and also provides a physical foundation for interpreting parametric studies based on various computer codes.

Figure 1 shows a continuous pipeline subject to transverse PGD with no abrupt displacement at the margins. The PGD is characterized by the maximum amount of ground movement  $\delta$  as well as the length  $L$  over which the movement occurs.

As a first approximation one can model the pipeline as a fixed-fixed beam with a span  $L$ . The resulting pipeline behavior is primarily a function of the span. For large spans, more than about 60 ft. for the pipe considered herein, the pipeline is flexible and moves with the soil. That is the lateral displacement of the pipeline at point A would be only slightly less than  $\delta$ . In other words the flexible pipeline is subject to an imposed displacement. For such a flexible pipe subject to a given amount of ground movement, the longer the span the better. For short spans, less than about 60 ft. for the pipes considered herein, the pipeline is stiff and the soil would flow over and under the pipeline. This soil movement would "load" the pipeline but result in pipeline displacement at Pt. A substantially less than  $\delta$ . For such a stiff pipe subject to load, the shorter the span the better. These two pipeline behavior modes (i.e. flexible pipe or stiff pipe) are used herein to establish failure diagrams for modern mild steel pipe with a well-defined yield stress of  $F_y = 36$  ksi. Pipe diameters ( $\phi$ ) of 20 and 40 inches as well as wall thickness ( $t$ ) of 1/4 and 1/2 inch are considered.

For modern welded steel pipelines, the compressive stress due to bending at the margin of the PGD (that is, at the ends of the fixed-fixed beam) is critical for both flexible and stiff pipe. Failure is assumed to occur if the net compressive stress exceeds the local buckling stress for the pipeline.

### LOCAL BUCKLING STRESS

As noted by Schilling (4), the critical compressive stress for local buckling of an unpressurized thin circular cylinder in air is

$$f_{cr} = a \cdot c \cdot E \cdot t/r \quad (1)$$

where  $t$  is the wall thickness,  $r$  is the pipeline radius,  $E$  is Youngs Modulus,  $c$  is a local buckling imperfection parameter and  $a$  is a plasticity reduction factor. The local buckling imperfection parameter  $c$  range from 0.40 to 0.50 for the radius to thickness ratios  $r/t$  ranging from 80 to 20 respectively.

The plasticity reduction factor is defined as

$$a = 1.10 \sqrt{\frac{E_s \cdot E_t}{E^2}} \quad (2)$$

where  $E_s$  and  $E_t$  are the secant and tangent modulus for the level of stress in question.

Since the plasticity reduction factor is a function of the level of stress, an iterative procedure must, in general, be used to solve for the critical buckling stress. If one models steel as a Ramberg–Osgood material with shape parameter  $n$  and secant stress  $f_{0.7}$  corresponding to the intersection of the stress–strain curve and the  $0.7E$  secant line, the secant and tangent moduli at a level of stress  $f$  are given by the ratios

$$\frac{E}{E_s} = 1 + \frac{3}{7} \left[ \frac{f}{f_{0.7}} \right]^{n-1} \quad (3)$$

and

$$\frac{E}{E_t} = 1 + \frac{3n}{7} \left[ \frac{f}{f_{0.7}} \right]^{n-1} \quad (4)$$

Modeling mild steel with a well defined yield stress = 36 ksi as a Ramberg–Osgood material with a shape parameter  $n = 100$  and secant stress  $f_{0.7} = 36$  ksi, the local building stress  $f_{cr}$  is essentially 36 ksi for the two diameters and two wall thicknesses considered.

Internal pressure has the effect of increasing the local buckling stress. Harris et al. (5) show that for moderate values of the normalized internal pressure  $\rho(r/t)^2/E$ , the percentage increase in the local buckling stress for a unstiffened circular cylinder is linearly proportional to the normalized internal pressure. Specifically, the percentage increase in buckling stress is zero for zero internal pressure and is about 61% for a normalized internal pressure = 0.169 and above. For the pipelines considered herein, the increase in local buckling stress can be shown to be less than 10% for internal gage pressures of 150 psi or less. The increase in local buckling stress due to internal pressure is conservatively neglected in this analysis.

### FLEXIBLE PIPELINES

As mentioned previously, for large spans the pipeline is flexible and closely follows the ground displacement. For the purpose of establishing failure criterion for this case, it will be conservatively assumed that the pipeline displacement exactly matches the ground displacement. The assumed displacement pattern for the soil and for a flexible pipeline is

$$y(x) = \frac{\delta}{2} \left[ 1 - \cos 2\pi x/L \right] \quad (5)$$

where  $x$  is the coordinate along the pipeline axis. This displacement pattern induces flexural bending in the pipelines as well as axial tension due to the change in arc length. Failure occurs when the net compressive stress (flexural bending minus axial tension) equals the local buckling stress for the pipe.

### Flexural Bending Stress

The pipeline curvature due to the assumed displacement pattern in Eq. (5) is

$$\frac{d^2y}{dx^2} = \frac{\delta}{2} \left[ \frac{2\pi}{L} \right]^2 \cos 2\pi x/L \quad (6)$$

and the maximum moment at the margins and center becomes

$$M_{\max} = EI \frac{\delta}{2} \left[ \frac{2\pi}{L} \right]^2 \quad (7)$$

The resulting maximum bending stress for flexible pipe is then given by

$$f_{bf} = \frac{E\delta\phi}{4} \left[ \frac{2\pi}{L} \right]^2 \quad (8)$$

when  $\phi$  is the pipeline diameter.

### Axial Tension Stress

The arc length  $L_{\text{arc}}$  of the pipeline is given by the standard relationship

$$L_{\text{arc}} = \int_0^L \sqrt{1 + \left[ \frac{dy}{dx} \right]^2} dx \quad (9)$$

For the assumed pipeline displacement in Eq. (5), it can be shown that this expression is equivalent to

$$L_{\text{arc}} = \sqrt{1 + \left[ \frac{\delta\pi}{L} \right]^2} \int_0^L \sqrt{1 + \frac{(\delta\pi/L)^2 \sin^2 \frac{2\pi x}{L}}{1 + (\delta\pi/L)^2}} dx \quad (10)$$

Making the substitution  $\Theta = 2\pi x/L$ . The arc length becomes

$$L_{\text{arc}} = \frac{L}{2\pi} \sqrt{1 + \left[ \frac{\delta\pi}{L} \right]^2} \int_0^{2\pi} \sqrt{1 - k^2 \sin^2 \Theta} d\Theta \quad (11)$$

when  $k^2 = \frac{1}{1 + \left[ \frac{L}{\pi \delta} \right]^2}$ . Note that the relationship in Eq. (11) is simply a constant times the complete elliptical integral of the second kind. The axial tension strain  $\epsilon_a$  due to arc length effects is given by

$$\epsilon_a = \frac{L_{\text{arc}} - L}{L} \quad (12)$$

Table 1 presents the arc length axial strain from Eq's. (11) and (12) as a function of the  $\delta/L$  ratio. As one might expect, the axial tension strain is an increasing function of the  $\delta/L$  ratio.

For mild steel with a linear stress-strain relationship up to the local buckling stress, the axial stress,  $f_a$ , due to arc length effects is the strain given in Eq. (12) times the Modulus of Elasticity  $E$

$$f_a = E \left[ \frac{L_{\text{arc}} - L}{L} \right] \quad (13)$$

### Critical Length for Flexible Pipe

As mentioned previously, a flexible pipeline would survive a given amount of PGD  $\delta$  if the span  $L$  is sufficiently long. The critical length for flexible pipe  $L_f$  (i.e. survival for  $L > L_f$ ) is that length for which the next compressive stress equals the local building stress, that is

$$f_{bf} - f_a = f_{cr} \quad (14)$$

where  $f_{bf}$  is the maximum bending stress for flexible pipe given by Eq. (8),  $f_a$  is the axial tension due to arc length effects given by Eq. (13) for a steel with a linear stress-strain relation, and  $f_{cr}$  is the local buckling stress given by Eq. (1). For the mild steel considered herein,  $f_{cr} = 36$  ksi. However, the axial stress due to arc length effects is a function of the  $\delta/L$  ratio (as shown in Table 1), and the bending stress for flexible pipe is a function of the pipe diameter  $\phi$ , the amount of PGD  $\delta$ , and the spatial extent of the lateral spread zone  $L$ .

Using an iterative procedure, the critical length for flexible pipe  $L_f$  for both pipe diameter considered was evaluated for various values of  $\delta$ , the amount of PGD. These values of  $L_f$  are shown in Table 2. Note that  $L_f$  is an increasing function as of  $\delta$  as one would expect. In addition the axial stress due to arc length effects can be substantial for large values of  $\delta$  and small diameter pipe. For example, for 2.0 ft. of PGD, the axial stress due to arc length effects is 13.6 ksi for the 20 in. diameter pipe. This contradicts the observation by Suzuki, Arata and Suzuki (2) that the axial strains are small compared to the bending strains.

## STIFF PIPELINES

As mentioned previously, for short spans the pipeline is stiff and the soil flows over and around the pipeline. For this stiff pipeline case, the pipeline displacements are substantially less than those of the soil and the pipe is "loaded" by the resulting soil-structure interaction forces. Failure occurs when the compressive bending stresses exceed the local buckling stress. It can be shown that the axial stresses due to arc length effects are small since pipe displacements are small for this stiff pipeline case.

### Soil-Structure Interaction Force

The force on a pipeline due to soil flowing over and around it is needed to evaluate the behavior of stiff pipelines. Laboratory tests by Trautmann and O'Rourke (6) show a curvilinear load deformation relationship. Herein, the load deformation relationship is approximated by the elasto-plastic relationship shown in Figure 2. Note that the normalized lateral force per unit length  $F_1/\gamma\phi H$ , where  $\gamma$  is the soil density and  $H$  is the depth to the bottom of the pipe, is a function of the normalized relative displacement  $Y/\phi$  and the  $H/\phi$  ratio. For an assumed cover of 3 ft. (depth to top of the pipe), the  $H/\phi$  ratios of interest are 2.8 for the 20 in. diameter pipe and 1.9 for the 40 in. diameter.

Also note that the full lateral load, that is the flat plastic portion of the load deformation relationship is mobilized at fairly small values of the normalized relative displacement. That is the lateral force per unit length for the 20 in. diameter pipe is  $6\gamma\phi H$  for relative displacements of 3 in. or larger, while for the 40 in. pipe  $F_1 = 5\gamma\phi H$  for relative displacements of 4 in. or larger.

### Critical Length for Stiff Pipe

As mentioned previously, a stiff pipeline would survive a given amount of PGD  $\delta$  if the span or spatial extent of the lateral spread zone  $L$  is sufficiently short. The critical length for stiff pipe  $L_s$  (i.e. survival for  $L < L_s$ ) is that length for which the flexural bending stress  $f_{bs}$  equals the local buckling stress.

$$f_{bs} = f_{cr} \quad (15)$$

Note that the axial tension stress due to arc length effects is quite small and conservatively neglect in the evaluation of  $L_s$ .

The flexural bending stress for stiff pipe  $f_{bs}$  is evaluated herein by considering a fixed-fixed beam subject to a uniform load per unit length  $F_1$  and a soil density of 110 pcf. Utilizing the flat plastic portion of Fig. 2,  $F_1 = 6\gamma\phi H$  for the 20 in. pipe and  $5\gamma\phi H$  for 40 in. pipe.

The bending moment of the margins of the lateral spread is

$$M = \frac{F_1 L^2}{12} \quad (16)$$

and the bending stress for stiff pipe  $f_{bs}$  is

$$f_{bs} = \frac{M}{S} = \frac{F_1 L^2}{3\pi t \phi^2} \quad (17)$$

Hence the critical length for stiff pipe becomes

$$L_s = \phi \sqrt{\frac{3\pi t f_{cr}}{F_1}} \quad (18)$$

The critical length  $L_s$  for mild steel with a straight line stress strain curve and  $f_{cr} = 36$  ksi is presented in Table 3 for the two pipe diameters and wall thicknesses considered. This critical length for stiff pipe is applicable for ground displacement large enough to mobilize the full soil-structure interaction force (i.e.,  $6\gamma\phi H$  for 20 inch pipe). That is, the  $L_s$  values in Table 3 apply for PGD  $\delta$  of roughly 3 inches or larger for 20 inch diameter pipe and roughly 4 inches or larger for 40 inch diameter pipe. For smaller  $\delta$ ,  $F_1$  decreases and the critical length for stiff pipe increases rapidly with small decreases in  $\delta$ .

### FAILURE DIAGRAM

The critical length for flexible pipe (survival for  $L > L_f$ ) in Table 2 and the critical length for stiff pipe (survival for  $L < L_s$ ) in Table 3 is combined to form the PGD failure diagram in Figure 3. The curve shows the combinations of PGD movement  $\delta$  and spatial extent or width of the lateral spread zone  $L$  which leads to failure of mild steel pipe. As an example, a 40 inch diameter pipe with 1/4 inch wall thickness would survive a PGD movement of 1.5 feet if the spatial extent of the lateral spread was greater than 185 ft. or less than 31.2 feet.

### CONCLUSIONS

An approximate analytical procedure for the effects of Permanent Ground Deformation (PGD) on continuous buried pipe was developed. The analysis was restricted to transverse PGD (ground motion perpendicular to the pipe axis) with no abrupt displacement at the margins of the lateral spread zone. Mild steel with linear stress-strain behavior up to a well defined yield stress of 36 ksi was considered. Flexural stresses and axial stresses due to arc length changes were evaluated and compared to a failure stress corresponding to local buckling of the thin wall pipe.

A failure diagram was developed which contains two bounds. For a given amount of PGD movement, it was shown that the pipe survives if the width or spatial extent of

the lateral spread zone is larger than  $L_f$  or less than  $L_s$ . For widths larger than  $L_f$  the pipe is flexible enough to conform to the imposed ground movement. For widths less than  $L_s$ , the pipe is strong enough to resist the load imposed by the soil flowing over and under the pipe.

The analytical procedure is relatively straightforward and hence potentially suitable for the design office environment. In addition it provides a physical foundation for interpreting parametric studies of various computer codes.

### ACKNOWLEDGEMENTS

The work presented herein was supported by the National Science Foundation's National Center for Earthquake Engineering Research (NCEER). This support is gratefully acknowledged. However the findings and conclusions are the author's alone and do not necessarily reflect the views of NSF or NCEER.

### REFERENCES

1. O'Rourke, T., Grigoriu, M., and Khater, M., (1985) "Seismic Response of Buried Pipeline; A State-of-the-Art Review", in Decade of Progress in Pressure Vessel Technology-1985, C. Sundararajan ed., American Society of Mechanical Engineering.
2. Suzuki, N., Arata, O., and Suzuki, I., (1988) "Parametric Study of Deformation Analysis of Welded Pipeline Subject to Liquefaction-Induced Permanent Ground Deformation" Proc 1st Japan-U.S. Workshop on Liquefaction, Large Ground Deformation and their Effects on Lifeline Facilities, Tokyo.
3. O'Rourke, T., and Lane, P., (1989), Liquefaction Hazards and their Effects on Buried Pipelines" Tech. Report NCEER-89-0007, National Center for Earthquake Engineering Research.
4. Schilling, C., (1965) "Buckling Strength of Circular Tubes," Journal of Structural Div., ASCE, Vol. 91, No. ST5, Oct., pp. 325-348.
5. Harris, L., Sver, H., Skene, W., and Benjamin, R., (1957), "The Stability of Thin-Walled Unstiffened Circular Cylinders Under Axial Compression Including the Effects of Internal Pressure," Journal of Aeronautical Sciences, Vol. 24, No. 8, Aug., pp. 587-596.
6. Trautmann, C. and O'Rourke, T., (1983), "Load-Deformation Characteristics of Pipe Affected by Permanent Earthquake Ground Movements," Proc. Inter. Symposium on Lifeline Earthquake Engineering, ASME.



$\delta/L$	$\epsilon_a$
1/25	0.0038
1/50	0.00097
1/75	0.000376
1/100	0.000173
1/150	0.000089
1/200	0.0000367

Table 1. Arc Length Axial Strain for Various  $\delta/L$  Ratios

PGD Displacement $\delta$ (ft.)	Critical Length for Flexible Pipe $L_f$ (ft.)	
	$\phi = 20''$	$\phi = 40''$
0.25	56.4	80.3
0.50	78.7	112
1.0	109	156
2.0	138	215
3.0	150	253

Table 2. Critical Length for Flexible Pipe as a Function of the Amount of PGD

Pipe Diameter $\phi$ (in.)	Wall Thickness $t$ (in.)	Critical Length for Stiff Pipe $L_s$ (ft.)
20	1/4	23.5
20	1/2	33.2
40	1/4	31.2
40	1/2	44.1

Table 3. Critical Length for Stiff Pipe

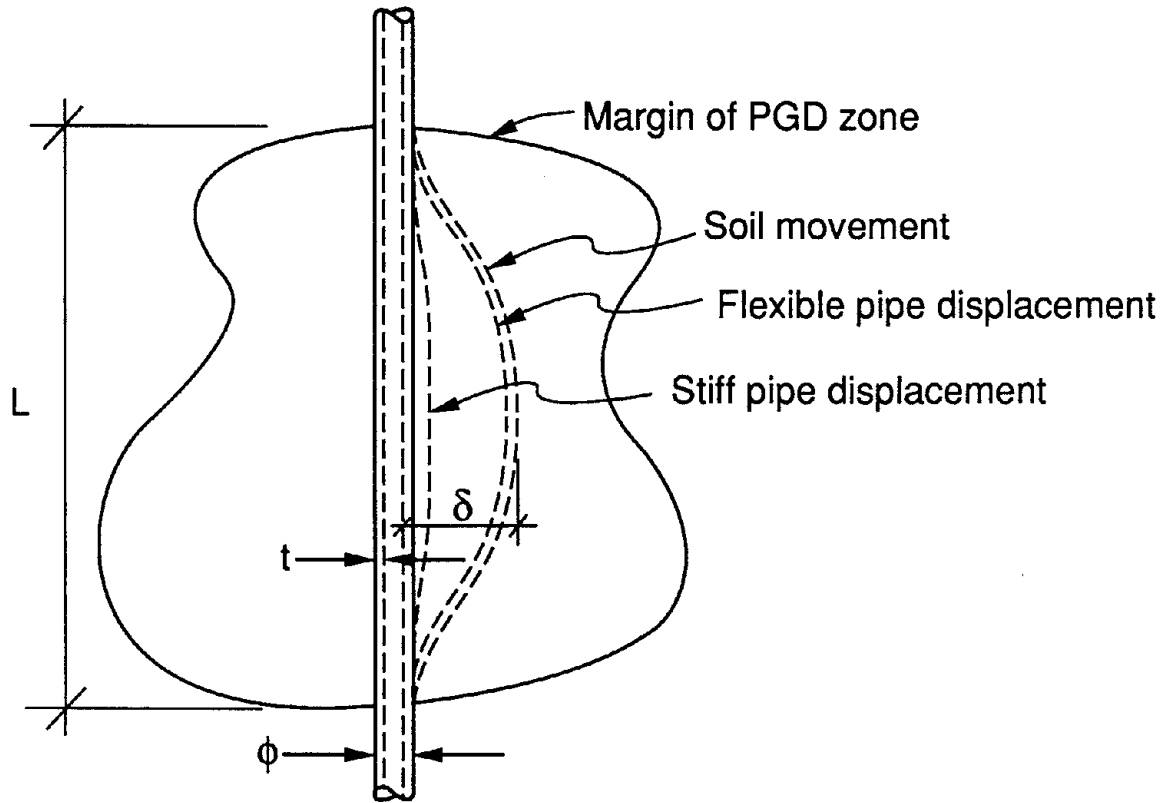


Figure 1. Pipeline Subject to Transverse PGD

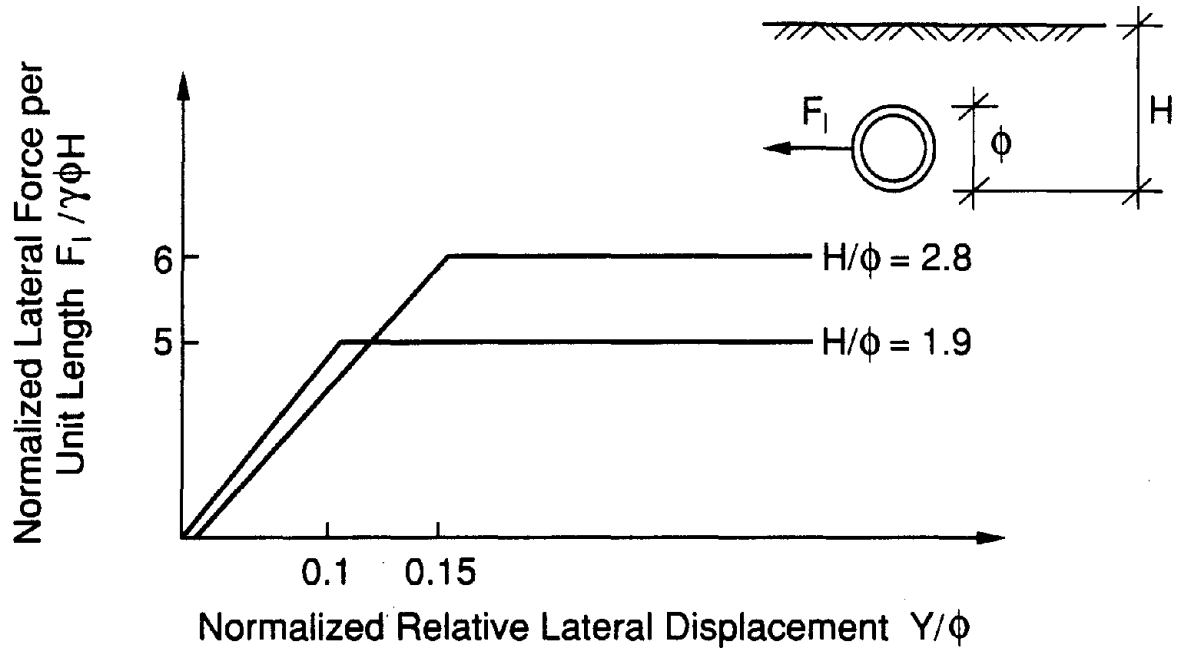


Figure 2. Assumed Soil-Structure Interaction Relationship for Stiff Pipelines

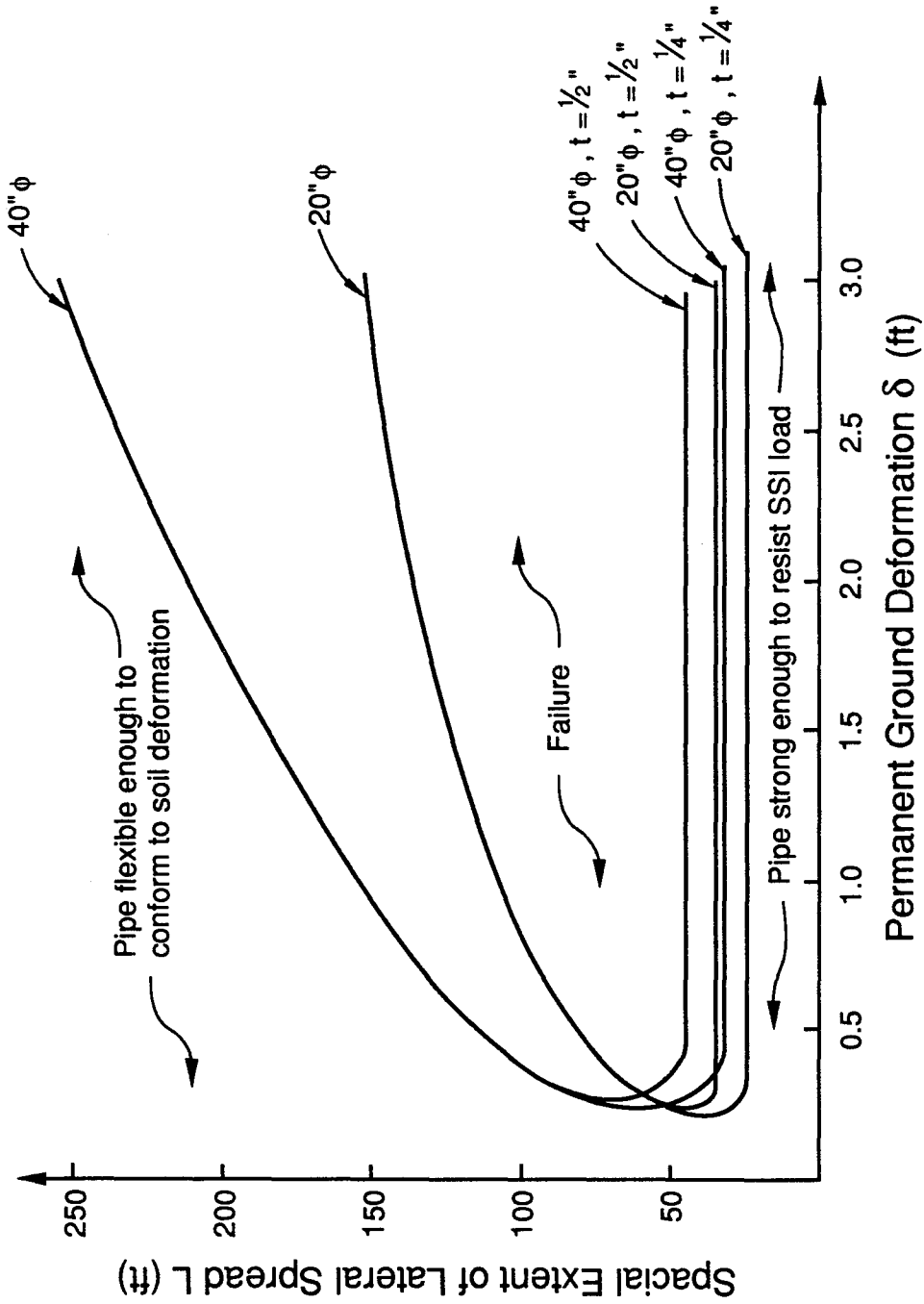


Figure 3. Failure Diagram for Mild Steel Pipe.

PARAMETRIC STUDY ON FLEXIBILITY OF BURIED PIPELINE  
SUBJECT TO LARGE GROUND DISPLACEMENT

Takashi KOBAYASHI<sup>1)</sup> Hiroyuki NAKANE<sup>2)</sup>  
Nobuhisa SUZUKI<sup>3)</sup> and Masami ISHIKAWA<sup>4)</sup>

- 1) Pipeline Department, Tokyo Gas Co., Ltd.
- 2) Pipeline Planning and Administration Department, Tokyo Gas Co., Ltd.
- 3) Engineering Research Center, NKK Corporation
- 4) Gas Industries Department, NKK Corporation

ABSTRACT

The purpose of this parametric study is to investigate the characteristics of a buried pipeline deformation caused by liquefaction-induced large ground displacement. The deformation analyses of the buried pipeline were performed with a nonlinear finite element computer code assuming several patterns of the ground displacement.

The calculated results made it clear that the maximum strain induced in the pipeline was susceptible to the width of the ground displacement and occurred at a certain width of ground displacement.

## INTRODUCTION

Liquefaction-induced large ground displacements are being focused as one of the most significant cause of damages to the buried pipelines. Actually in a liquefiable zone, the damages to the buried pipelines due to the past earthquakes give some evidence of large deformations of pipes. Hence, when we design earthquake-resistant pipeline with liquefaction considered, it is basic and important matter that the piping system has enough ability to endure the ground displacements due to high ductility of the material.

It is commonly recognized that steel pipe has high ductility, toughness and plastic creep capacity. Consequently, the pipe does not immediately break when the stress exceeds the yield point. For this reason, steel pipe has been widely adopted as a buried pipeline material. Steel pipe has such excellent characteristics that it may endure liquefaction-induced large ground displacement.

In this paper, we analyze steel pipeline deformation subject to large ground displacement. Using a nonlinear finite element computer code, we investigated the character of plastic behavior beyond the yield point. We further examined the displacement behavior of buried pipeline affected by the distribution form of ground displacement.

The subject of analysis is mainly buried straight pipeline comprised of steel pipe (JIS STPY41) whose outside diameter is 406.4 mm and wall thickness is 7.9 mm. The analysis was performed considering the nonlinear character of both steel and soil.

## DEFINITION OF GROUND DISPLACEMENT DISTRIBUTION

The mode classification of input ground displacement model has been suggested by author<sup>1)</sup>, but it is still unsatisfactory for evaluating the ground displacement distribution form quantitatively.

Hence, in this analysis, we assumed the ground displacement distribution model as shown in Figure 1, where the vector of ground displacement is a normal angle to the axis of the pipeline. We also assumed the magnitude of the liquefaction-induced ground displacement by equation (1).<sup>2)</sup>

$$D = D_{\max} \cdot \cos^n (\pi x / L) \quad (1)$$

D: the magnitude of the ground displacement  
 D<sub>max</sub>: the maximum ground displacement  
 n: the shape parameter for the distribution of the ground displacement  
 L: the width of the ground displacement

The ground displacement distribution defined by equation (1) is axi-symmetric and can be versatile to represent various configurations by changing the shape parameter (n).

In this analysis, the parameters are chosen as: n = 0, 1, 2, 4,  
 L = 5, 10, 13, 15, 20, 30, 40 (m)      D<sub>max</sub> = 0 ~ 2 (m).

## NONLINEAR FINITE ELEMENT ANALYSIS

In this study, the subject of analysis is mainly the welded steel pipe 400A (outside diameter 406.4 mm, wall thickness 7.9 mm). We also, however, partly analyzed steel pipes 200A (outside diameter 216.3 mm, wall thickness 5.8 mm) and 600A (outside diameter 609.6 mm, wall thickness 9.5 mm).

We assumed that the material character of steel pipe is bilinear as shown in Figures 2 and 3. The soil spring characteristic that acts on the pipelines diminishes with ground liquefaction. This phenomenon is confirmed by interior oscillation test, but the rate of diminution changes depending on the degree of ground liquefaction. At the point of full liquefaction, the rate of diminution is about 1/10 of the original level<sup>3)</sup>. However, it is difficult to evaluate the degree of practical liquefaction, therefore we do not consider the diminution of the soil spring characteristic on the safe side. Hence, we assumed the soil spring characteristic as shown in Figure 4 (for longitudinal direction) and 5 (for lateral direction)<sup>4)</sup>.

### CALCULATED RESULTS OF PARAMETRIC STUDY

#### Shape parameter(n) for the distribution of ground displacement

The relationship between the maximum ground displacement  $D_{max}$  and the peak tensile strain  $\epsilon_{peak}$  is shown in Figure 6. When  $n = 0, 1$  and  $2$ , the  $\epsilon_{peak}$  increases in proportion to the increase of  $D_{max}$  and reaches the highest point of  $\epsilon_{peak}$  at  $D_{max} = 70$  cm to  $80$  cm. After that, the  $\epsilon_{peak}$  gradually diminishes and becomes a constant value at  $D_{max} = 200$  cm. In this case, the  $\epsilon_{peak}$  is always large when  $n = 2$ . The  $\epsilon_{peak}$  reaches a maximum value 1.6% at the point  $D_{max} = 80$  cm.

On the other hand, the  $\epsilon_{peak}$  for  $n = 4$  increases with the increase of  $D_{max}$  and reaches 1.0% at  $D_{max} = 50$  cm. After this, the  $\epsilon_{peak}$  remains constant for a time. The  $\epsilon_{peak}$  again begins to increase at  $D_{max} = 100$  cm and gradually approaches the maximum value of  $n = 2$ . At  $D_{max} = 200$  cm, the maximum value of the  $\epsilon_{peak}$  is 1.56%.

The parametric study on the effect of  $n$  made it clear that  $n = 2$  gives the maximum strain in the range where  $D_{max}$  is less than 200 cm.

#### Width of ground displacement (L)

The width of ground displacement  $L = 5, 10, 13, 15, 20, 30$  and  $40$  cm are chosen for the parametric study. Figure 7 represents the relationship between the maximum displacement  $D_{max}$  and the peak tensile strain  $\epsilon_{peak}$ . When  $L = 5$  m and  $L = 10$  m, the  $\epsilon_{peak}$  increases with the increase of  $D_{max}$  up to  $D_{max} = 10$  cm and  $70$  cm. After that, the  $\epsilon_{peak}$  reaches the saturation point and becomes a constant value. Incidentally, the maximum value of the  $\epsilon_{peak}$  for  $L = 5$  m is 0.13% and it remains in the elastic range.

When  $L = 13$  m and  $L = 15$  m, the  $\epsilon_{peak}$  increases with the increase of  $D_{max}$ . At the range where  $D_{max}$  is small, the  $\epsilon_{peak}$  shows the same tendency as when  $L = 10$  m.

The  $\epsilon_{\text{peak}}$  reaches a maximum value at the point  $D_{\text{max}} = 70$  cm to 80 cm and the  $\epsilon_{\text{peak}}$  for  $L = 13$  m shows the maximum value 1.6%. After that point, the  $\epsilon_{\text{peak}}$  gradually diminishes and in the range where  $D_{\text{max}}$  exceeds 150 cm, the  $\epsilon_{\text{peak}}$  reaches the saturation point and shows a constant value.

When  $L = 20$  m and  $L = 30$  m, the  $\epsilon_{\text{peak}}$  increases with the increase of  $D_{\text{max}}$  and the  $\epsilon_{\text{peak}}$  is maximum at the point  $D_{\text{max}} = 150$  cm. However, the rate of increase of the  $\epsilon_{\text{peak}}$  to  $D_{\text{max}}$  and the value of the  $\epsilon_{\text{peak}}$  is smaller than when  $L = 10$  m, 13 m and 15 m.

The  $\epsilon_{\text{peak}}$  for  $L = 40$  m increases monotonously up to  $D_{\text{max}} = 200$  cm, but the rate of increase of the  $\epsilon_{\text{peak}}$  to  $D_{\text{max}}$  is still smaller than when  $L = 20$  m and 30 m.

Accordingly,  $L = 13$  m gives the maximum strain 1.6% in the range where  $D_{\text{max}}$  is less than 200 cm. As  $L$  becomes greater, the rate of increase of the  $\epsilon_{\text{peak}}$  to  $D_{\text{max}}$  is smaller and the strain shifts within a low level.

Further, the calculated results of steel pipes 200A and 600A are shown in Figure 8 and 9. According to these figures, it is recognized that  $L = 8$  m for 200A and  $L = 19$  m for 600A give the maximum strain.

The "L" that gives the maximum strain of steel pipes 200A, 400A and 600A is shown in Table 1. The "C" in Table 1 indicates the characteristic length that is calculated from differential equation (2) of the elastic beam supported on elastic foundations<sup>5</sup>).

$$EI \frac{d^4 y}{dx^4} = -qD \quad (2)$$

$$\gamma = 3 \sqrt{\frac{qD}{EI}} \quad (3)$$

$$C = 1/\gamma = 3 \sqrt{\frac{EI}{qD}} \quad (4)$$

The relationship between  $L/C$  and peak tensile strain  $\epsilon_{\text{peak}}$  is shown in Figure 10.

Table 1 and Figure 10 indicate that the  $\epsilon_{\text{peak}}$  reaches a maximum value at a certain value of  $L/C$  ( $L/C = 1.60$  to  $1.67$ ). This suggests that it is effective to introduce the characteristic length  $C$  as a fundamental parameter.

#### CALCULATED RESULTS OF PIPELINE DEFORMATION

According to Figure 7, the patterns of pipeline deformation can be classified as four types depending on the width of ground displacement  $L$  ( $L = 5$  to  $10$  m,  $L = 13$  to  $15$  m,  $L = 20$  to  $30$  m and  $L = 40$  m).



L = 10 m

Ground displacement distribution input, pipeline displacement, ground reaction and strain distribution are shown in Figures 11 to 14. Furthermore, Figure 15 represents the model illustrative of the pipeline deformation.

The ground reaction at the region of (A) and (B) in Figure 15 are  $q = 1.88 \text{ kgf/cm}^2$ , and  $q = -1.88 \text{ kgf/cm}^2$ , respectively. This means that the ground reaction reaches its maximum strength. Hence, this deformation pattern looks to be equivalent to the model of a uniformly loaded beam subjected to maximum ground strength as its load.

Figures 11 and 12 indicate that when the maximum ground displacement  $D_{\max}$  is 80 cm, the maximum displacement of pipeline  $\delta_{\max}$  remains 37 cm ( $\delta_{\max}/D_{\max} = 0.46$ ). This indication means that a sliding of the ground must have occurred along the pipeline.

The strain distribution is shown in Figure 14. The peak strain  $\epsilon_{\text{peak}}$  always occurs at the maximum ground displacement input point. Despite the increase of  $D_{\max}$ , this tendency did not change.

L = 13 m

Ground displacement distribution input, pipeline displacement, ground reaction and strain distribution are shown in Figures 16 to 19. This deformation pattern is approximately the same as the pattern when  $L = 13 \text{ m}$ .

Figures 16 and 17 indicate that when the maximum ground displacement  $D_{\max}$  is 150 cm, the maximum displacement of the pipeline  $\delta_{\max}$  is 74 cm ( $\delta_{\max}/D_{\max} = 0.49$ ). Hence, a sliding of the ground must have occurred along the pipeline.

The strain distribution is shown in Figure 19. The peak strain  $\epsilon_{\text{peak}}$  occurs at the maximum ground displacement input point in the region (A) in Figure 15. However, the value of the strain diminishes at the point where  $D_{\max}$  exceeds 80 cm. On the other hand, the strain at the region (B) in Figure 15 gradually increases.

L = 30 m

Ground displacement distribution input, pipeline displacement, ground reaction and strain distribution are shown in Figures 20 to 23.

Figures 20 and 21 indicate that when the maximum ground displacement  $D_{\max}$  is 150 cm, the maximum displacement of pipeline  $\delta_{\max}$  is 149 cm ( $\delta_{\max}/D_{\max} = 0.99$ ). Hence, it is obvious that the pipeline deformation is following the ground movement. The ground reaction is distributed as shown in Figure 22. Although part of the ground reaches its maximum strength, most of the ground remains in an elastic range. Hence, it is obvious that a sliding of the ground must not have occurred along the pipeline.

In this case, the pipeline deformation pattern that is following the ground movement approximates the model of shear deformation as shown in Figure 24.

Strain distribution is shown in Figure 23. The peak strain  $\epsilon_{\text{peak}}$  occurs at the region (B) as shown in Figure 24. The strain at the region (A) as shown in Figure 24 increases with the increase of  $D_{\text{max}}$  and gradually approaches the strain level at the region (B).

$L = 40 \text{ m}$

Ground displacement distribution input, pipeline displacement, ground reaction distribution, and strain distribution are shown in Figures 25 to 28.

In this case, a similar tendency to  $L = 30 \text{ m}$  is observed. According to the strain distribution as shown in Figure 28, the strain at the region (A) and (B) in Figure 24 is the same level, respectively. Hence, this pipeline deformation pattern is still more similar to the model of shear deformation than when  $L = 30 \text{ m}$ .

The calculated results of pipeline deformation are as follows. When  $L$  is small, the pipeline deformation pattern is equivalent to the model of a uniformly loaded beam subjected to maximum ground strength as its load.

On the other hand, when  $L$  is large, the pipeline behaves similarly to the shear deformation model.

#### CONCLUSION

A parametric study of deformation analyses of a 400A steel pipeline subject to large ground displacement was performed. The followings can be concluded from calculated results.

- (1) Concerning the shape parameter for the distribution of the ground displacement ( $n$ ),  $n = 2$  gives the maximum strain of the pipeline in the range where the maximum ground displacement ( $D_{\text{max}}$ ) is less than 200 cm.
- (2) Concerning the width of the ground displacement ( $L$ ),  $L = 13 \text{ m}$  gives the maximum strain of the pipeline in the range where  $D_{\text{max}}$  is less than 200 cm. Furthermore, the similar tendency are observed for 200A and 400A.
- (3) Regarding the pipeline deformation behavior, when  $L$  is small, the pipeline deformation pattern looks to be equivalent to the model of a uniformly loaded beam subjected to maximum strength as its load. On the other hand, when  $L$  becomes large, the pipeline tends to behave similarly to the shear deformation model.

#### ACKNOWLEDGEMENT

The authors wish to acknowledge the invaluable assistance of Mr. Shinichi Suzuki of the Tokyo Giko Company in doing calculations and preparing figures.

## REFERENCES

- 1) T. Kobayashi, "Recommended Practice for Earthquake Resistant Design of Gas Pipelines Considering Liquefaction, First Japan-US Workshop", ADEP/NCEER (1988).
- 2) N. Suzuki, O. Arata and I. Suzuki, "Parametric Study on Deformation Analysis of Welded Pipelines Subject to Liquefaction-Induced Permanent Ground Displacement", First Japan-US Workshop", ADEP/NCEER (1988).
- 3) Susumu Yasuda, Kimimasa Saito and Nobuhisa Suzuki "Restraint of Liquefied Ground on Buried Pipelines", Collection of Papers Published in 19th Meeting of Earthquake Engineering, pp. 189-192, 1987.
- 4) Japan Gas Association, "Earthquake Resistant Design Code for Gas Pipeline", (1982).
- 5) N. Suzuki, "Dimensionless Representation for Nonlinear Flexural Behavior of Buried Pipeline", First Japan-US Workshop, ADEP/NCEER (1988).

Table 1. L where peak is maximum

Diameter	L (cm)	L/C
200A	800	1.67
400A	1300	1.60
600A	1900	1.67

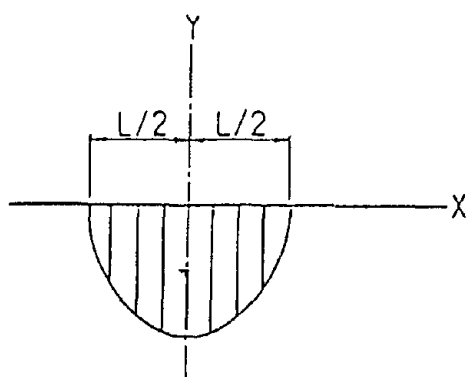


Figure 1. Ground displacement distribution model

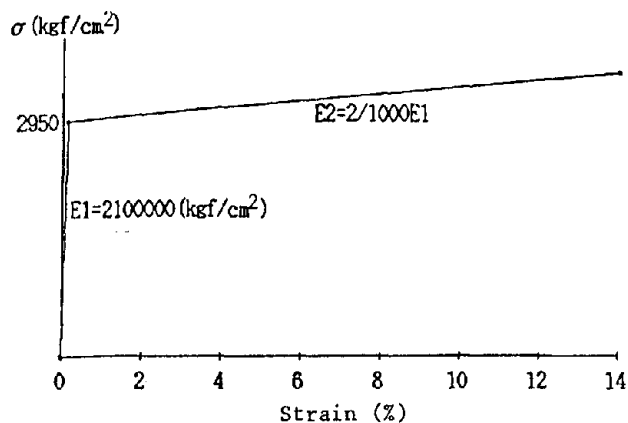


Figure 2. Material character of steel pipe (stress-strain relationship)

200A :  $M_y=579970$  (kgf · cm)  
 400A :  $M_y=2851175$  (kgf · cm)  
 600A :  $M_y=7804815$  (kgf · cm)

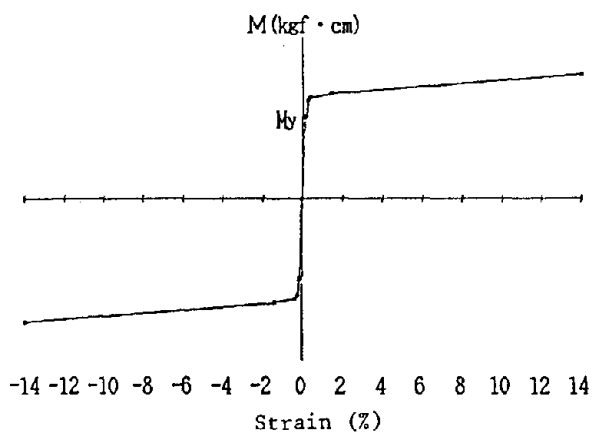


Figure 3. Material character of steel pipe (moment-strain relationship)

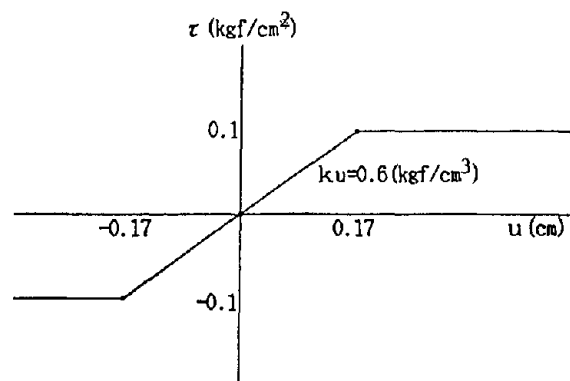


Figure 4. Non-linear soil spring (for longitudinal direction)

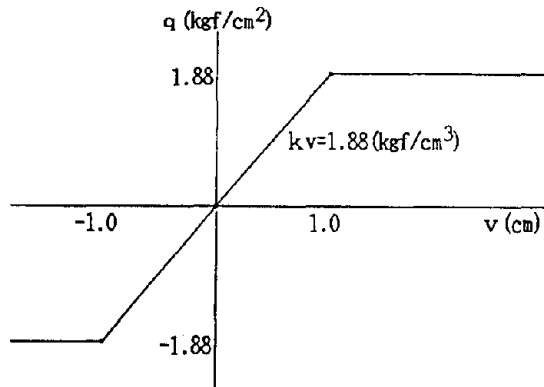


Figure 5. Non-linear soil spring (for lateral direction)

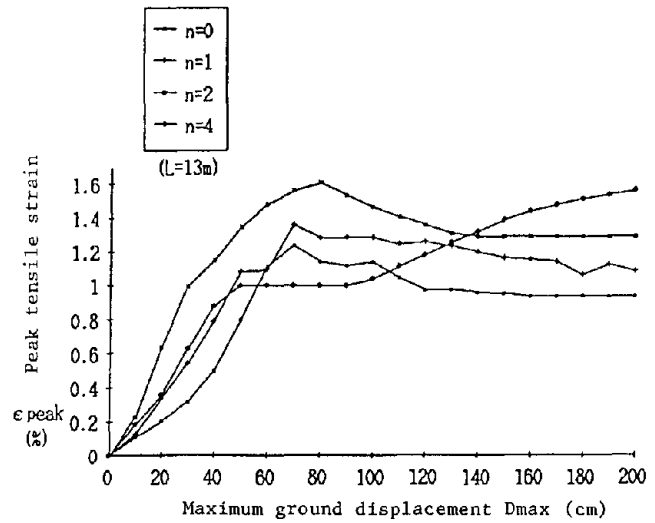


Figure 6. Relationship between maximum ground displacement and peak tensile strain

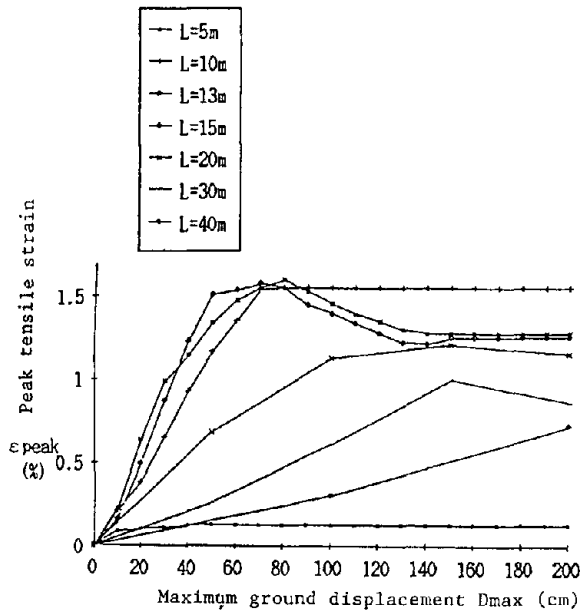


Figure 7. Relationship between maximum ground displacement and peak tensile strain (400A)

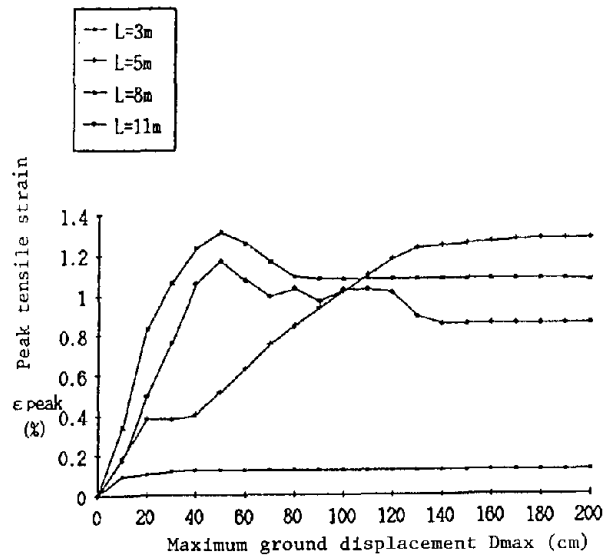


Figure 8. Relationship between maximum ground displacement and peak tensile strain (200A)

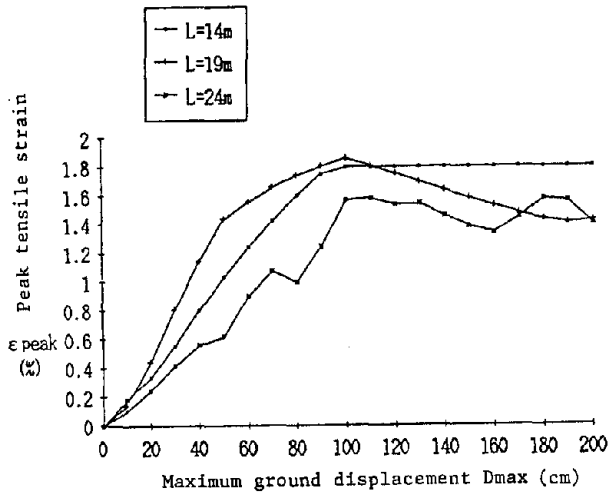


Figure 9. Relationship between maximum ground displacement and peak tensile strain (600A)

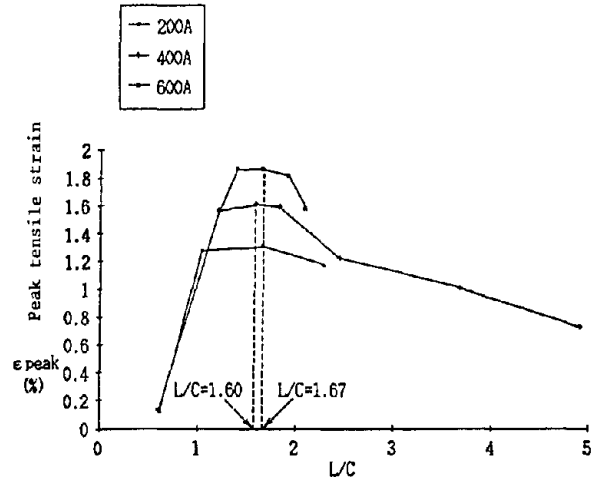


Figure 10. Relationship between  $L/C$  and peak tensile strain

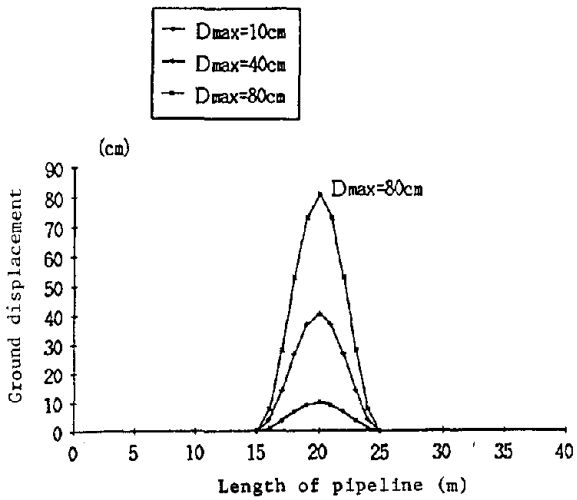


Figure 11. Ground displacement distribution input

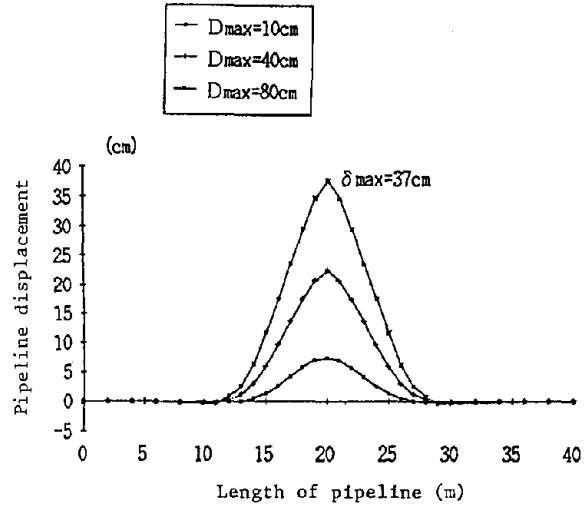


Figure 12. Pipeline displacement distribution

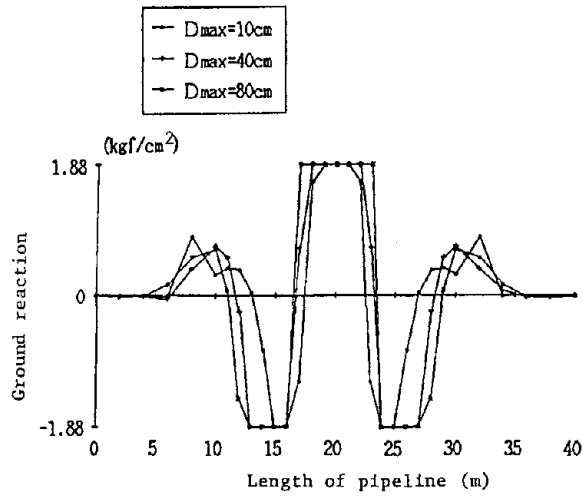


Figure 13. Ground reaction

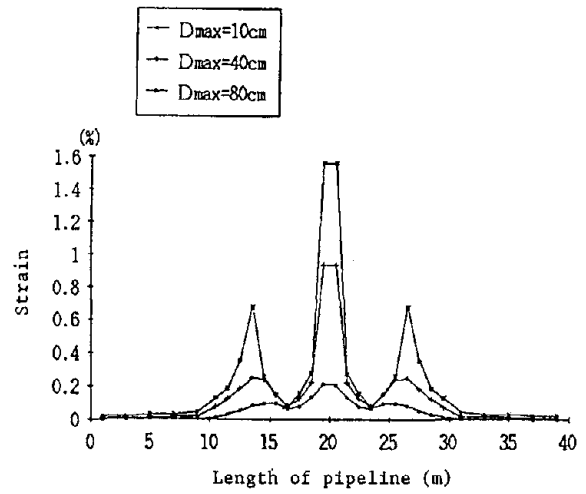


Figure 14. Strain distribution

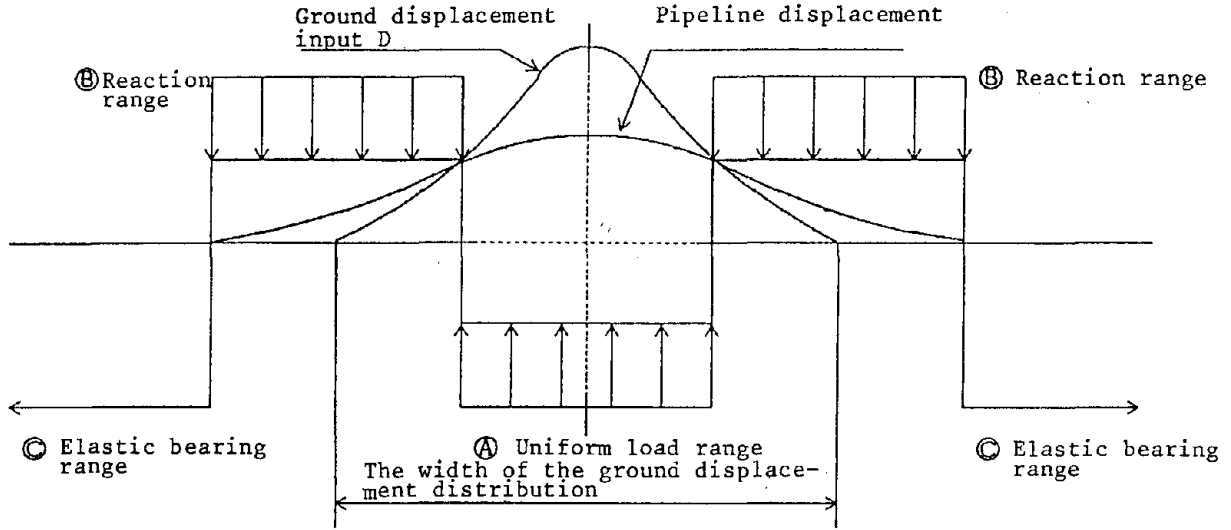


Figure 15. Uniformly loaded model

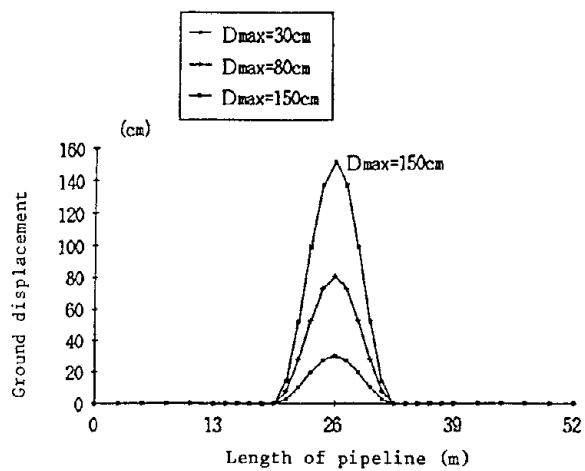


Figure 16. Ground displacement distribution input

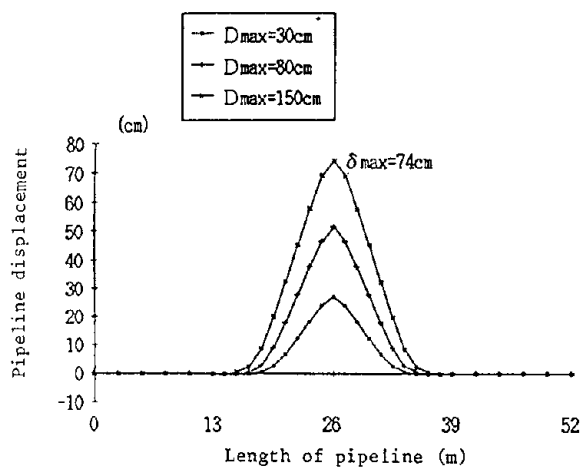


Figure 17. Pipeline displacement

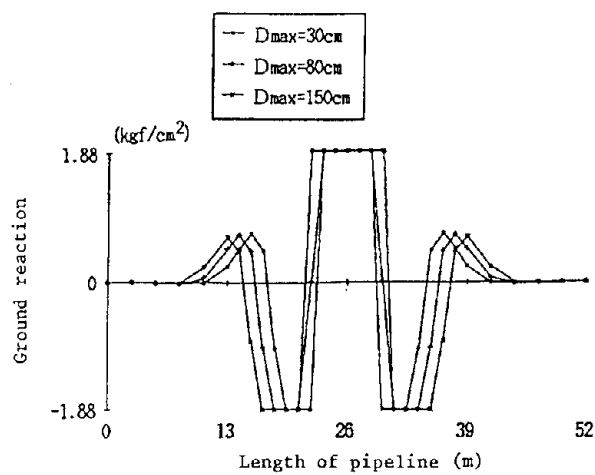


Figure 18. Ground reaction pipeline

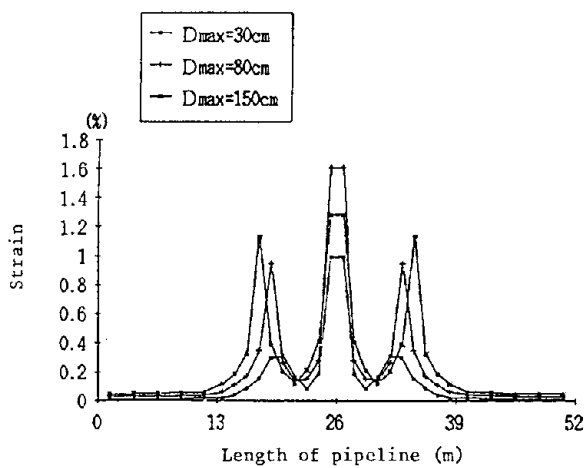


Figure 19. Strain distribution



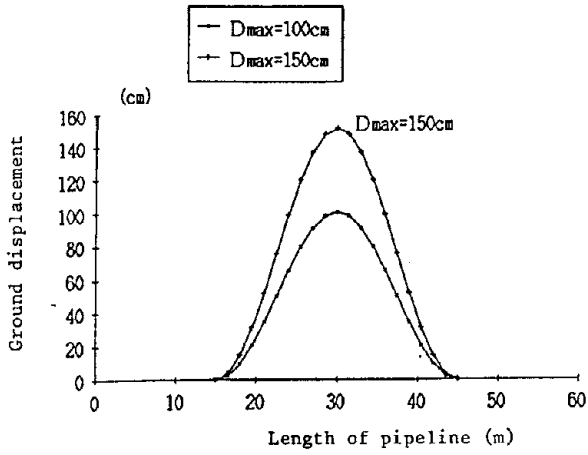


Figure 20. Ground displacement distribution input

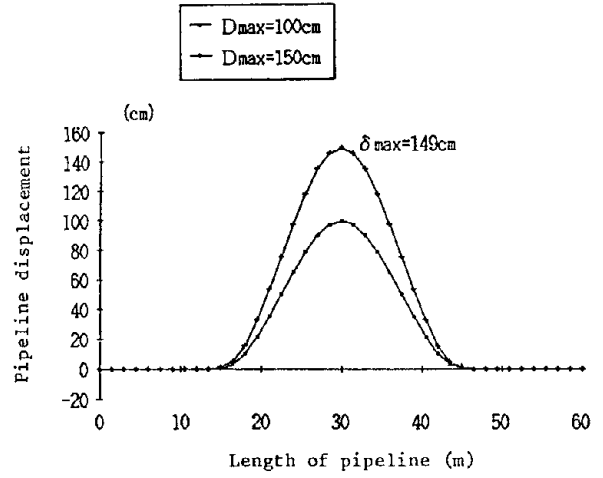


Figure 21. Pipeline displacement

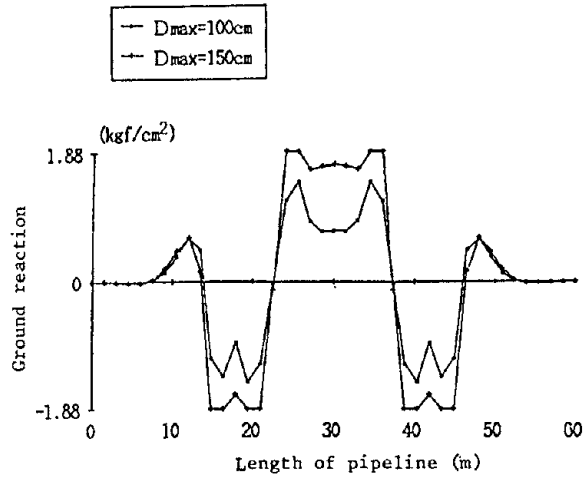


Figure 22. Ground reaction

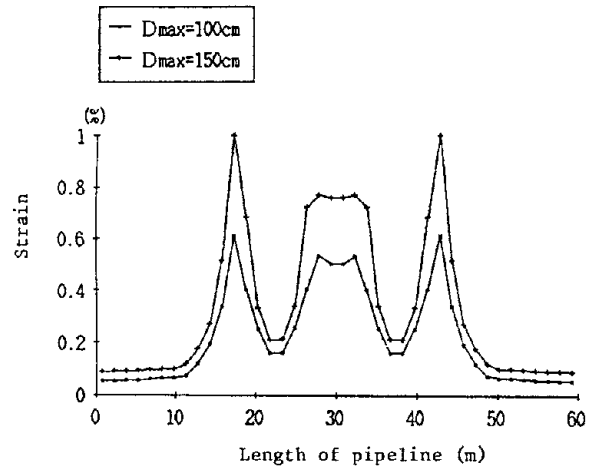


Figure 23. Strain distribution

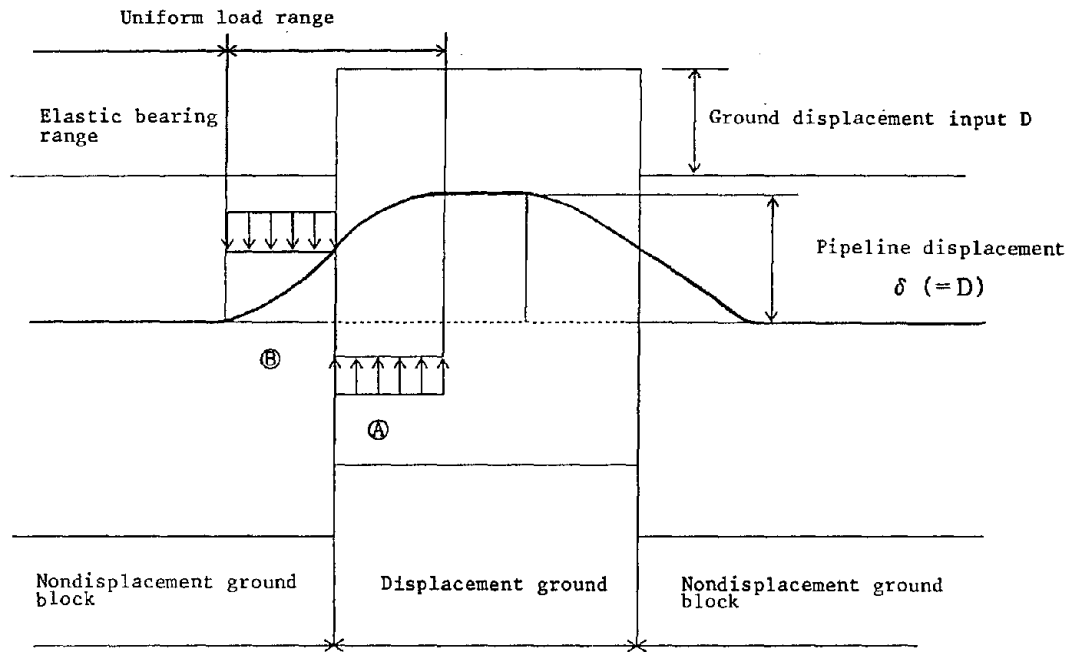


Figure 24. Shear deformation model

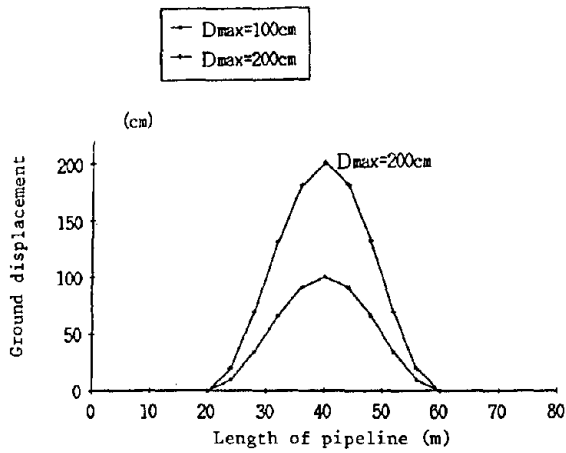


Figure 25. Ground displacement distribution input

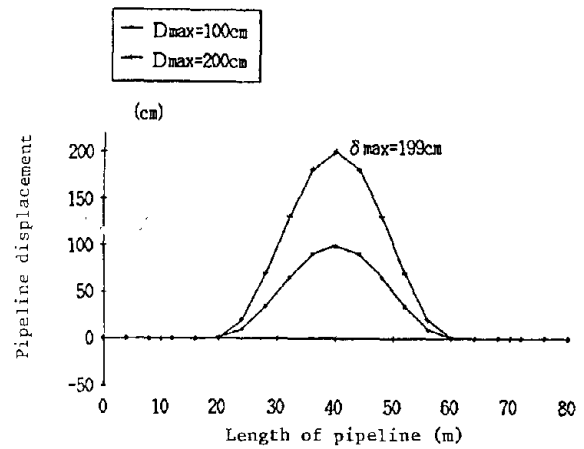


Figure 26. Pipeline displacement

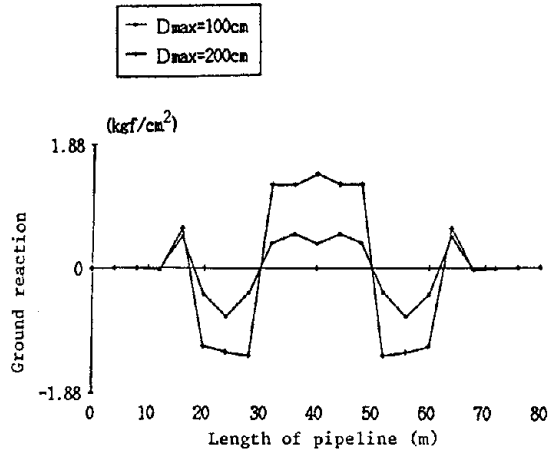


Figure 27. Ground reaction distribution

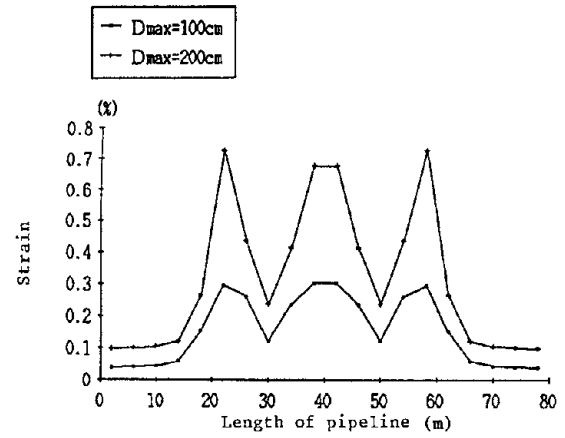


Figure 28. Strain distribution

**RELIEVING SEISMIC STRESSES LOCKED IN GAS PIPELINES**

J. D. Mc Norgan

Staff Supervisor - Pipeline Design  
Southern California Gas Company

**ABSTRACT**

When buried gas pipelines are displaced across fault ruptures, resulting stresses can present operational and regulatory problems. Locked-in stresses can range in value from minor to significant. Analytical and physical investigations are used to assess prevailing conditions. Procedures and remedial measures are developed to remove adverse stresses and potential hazards. Recommendations are made for future studies.

## INTRODUCTION

On October 15, 1979, a magnitude 6.6 earthquake struck near the city of El Centro in California's Imperial Valley. This earthquake was followed by 30 aftershocks, with eight having magnitudes of 5 or higher. The ground rupture extended for 19 miles and crossed three of Southern California Gas Company's high pressure gas pipelines. These pipelines were two supply lines running south along Dogwood Road and a 4-inch line running east just north of Highway 80, feeding Holtville.

Although these lines had not ruptured, they were located in areas where the ground had suffered permanent lateral displacements of up to 12 inches. Since this ground faulting could have a significant effect on the buried pipelines at the crossings, Southern California Gas Company (SoCalGas) decided to conduct a post-earthquake investigation of the condition of these pipelines and make any necessary repairs. This paper describes some of the operations experienced in conducting the investigation and removing the potentially adverse conditions which were found.

### Preliminary Investigations

The first excavation was made four miles east of El Centro where there was about 12 inches of right lateral movement visible on the ground surface. The 4-inch line was exposed by ditching with a backhoe for a length of approximately 32 feet. It was noted that the pipe had a definite offset in a horizontal plane. A string line was laid out parallel to the pipeline and measurements were taken of the distance from the centerline of the pipe to the string at intervals of two feet. The length of the open ditch was increased on both ends. During this operation, the offset in the 4-inch pipe was noted to be decreasing. After a total length of 72 feet had been exposed the offset no longer decreased. A second set of offset measurements was made and recorded. The offset measurements for both excavated conditions are presented on Figure 1.

An inspection of the physical condition of the pipe was then made. It was noted that the pipe wrap at the fault crossing had soil between it and the pipe. The wrap was removed and the pipe was visually inspected. The pipe was found to be intact, with no evidence of damage. The exposed pipe was rewrapped and then backfilled.

The second excavation was on Dogwood Road approximately six miles north of El Centro. At this location, the fault trace appeared to have split into two segments separated by 770 feet with the larger or more prominent trace south of the smaller one. The fault rupture had a 6-inch right lateral offset and a 4-inch

vertical displacement, with the southerly section higher than the northerly one. The 10-inch gas line in the west side of Dogwood Road (Line 6001) was exposed in a short bellhole at the southern fault trace. The southerly section of the pipe was found to be displaced laterally 2-3/4 inches to the west. The bellhole was increased in length by trenching both to the north and south to determine if there were any other displacements in the pipeline. When the exposed length of pipe was approximately 36 feet in length, the lateral displacement of the line began to increase. Trenching was stopped at this point to prevent additional movement and possible damage.

A second trench was dug north of the first one, after leaving a soil plug of approximately 20 feet between the excavations. When this second trench was about 52 feet long, the previously straight section of the pipe began to deflect horizontally to the east. The center offset, as measured, was 10 inches. A third trench was then excavated, beginning 20 feet south of the initial excavation. In this instance, the previously straight pipe began to deflect laterally when this trench was about 60 feet long. Maximum offset was 7 inches to the east.

The north and south trenches and most of the central trench were then backfilled. The two 20-foot long soil plugs next were excavated. No significant change in the offset of the pipe at the fault crossing was noted. All exposed pipe was then backfilled to conclude this part of the field investigation.

Preliminary evaluation of this data indicated that the 4-inch line to Holtville was exposed to lateral forces sufficient to cause local yielding of the pipe at the fault. The reduction of total offset at this location indicated that the tensile stresses in the pipe were eliminated when the additional length of the pipe was exposed and no additional corrective measures were required. The conditions prevailing at the 10-inch line suggested that a different corrective plan would be required.

The 10-inch line had been displaced laterally and had deformed as a column in a buckling mode. The forces necessary to cause buckling in a restrained pipe column were calculated. Table 1 shows the relationship between column length, the compressive force and the axial stress for a 10-inch pipe column having a wall thickness of 0.188 inches.

From data in Table 1, it appeared that the pipeline was experiencing compressive forces in the range of 200 to 250 kips. This could have a significant impact on any operations involving the removal of a pipe segment. Of interest was how much the pipe might move when cut. Since the pipeline had three feet of well compacted sandy soil cover, it was estimated that it would have frictional resistance of 500 pounds per lineal foot. This would result in axial compression of about six inches, if the pipe were stressed to its SMYS of 42,000 psi.

SoCalGas decided that the large compressive forces present in these lines should be removed to restore the regulatory required integrity of the pipelines. Also, we believed that data should be gathered during the removal to determine the magnitude of the stresses removed and to generate usable guidelines to determine the need for future removals.

### **Stress Removal**

Following the decision to remove the pipe sections having the adverse stresses, a complex series of events were set in motion. Lines 6000 and 6001 transport the entire gas supply to our Imperial Valley district. For a planned major interruption, such as this, we notify our high volume customers, the Road Department, the Sheriff's Department, the Fire Department, the adjacent property owners, and all others who are likely to be impacted. Since these lines operate at up to 1,000 psi pressure, we elected to use a transmission pipeline crew for the cutting and welding operations rather than a distribution service crew, since they are best qualified in arc welding on high pressure pipelines.

Although we have standard procedures covering the removal of pipe sections under fire controlled conditions, for each job a separate, detailed plan is prepared. The plan for this project identified all personnel assigned, their responsibilities, the time of each event, and all the material and equipment normally required including that needed for potential emergencies. The preparatory steps called for identification of all customer taps or services and a load study to ensure that customer needs would be met. Next came the lubrication and servicing of block valves to ensure they would hold pressure when the line was blown down.

The 10-inch pipeline was blown down to low pressure. Flagmen and barricades were deployed at the site and a 20-foot long bellhole was dug at the fault crossing. Two-inch diameter fire control stacks were welded on each side of the planned cutout. Survey control points were then installed at the southerly end of the bellhole in order to measure pipe movement.

After all preparations had been completed, a cutting torch was clamped to the pipe and cutting began. When the pipe had been slowly cut from the 12 o'clock position, easterly to the 4 o'clock position, the pipe suddenly broke, thrusting itself laterally a distance of 4 to 6 inches. A planned second cut was made intending to remove the damaged section of pipe. When this cut was completed, however, the pipeline was still locked in a highly compressive state. A third and fourth cut were made, which then permitted the three sections to be removed. The exposed ends of the pipeline were temporarily sealed with canvas.

The pipe had not moved sufficiently to account for all the assumed locked-in strain. Also, since the pipeline segments were not in alignment, it was necessary to strip the line of backfill sufficiently to provide the flexibility necessary to make a tie-in weld. Trenching was begun along the pipe. As the trenching progressed away from the bellhole, the pipe continued to grow toward the center of the hole. Pipe stripping was stopped after 200 feet had been exposed because there was enough flexibility to align the pipe ends and there was no additional growth. The total growth was 4-3/4 inches. A 10-foot segment of pipe was then welded in to reconnect the pipeline segments.

## Conclusions

We have concluded that ground displacements at a fault crossing can cause residual stresses in a pipeline, even though the pipe yields and is permanently deformed. These stresses can cause significant unplanned pipe movements, especially if a pipe section is cut out.

From an operational stand point, compressive forces in a pipeline present greater concerns than tensile forces. The presence of compressive forces can be determined by excavating a length sufficient to cause lateral displacement in a pipe buckling mode.

Excessive tensile forces in a pipeline can be eliminated without cutting the line by stripping an adequate length of pipe. It is believed that removal of excessive compressive stresses can only be done by removing a section of pipe and then causing the pipe to grow in length to relieve the stresses.

The frictional forces between pipe and soil and the axial forces acting on the pipe are the primary factors in determining the pipe stresses and how much of the pipe must be stripped to relieve adverse stresses. Engineering guidelines need to be developed to determine these axial forces in pipelines, as well as the frictional forces resulting from the interaction of various pipe surfaces or coatings and soils and their degree of compaction.



TABLE 1

<u>L (ft.)</u>	<u>Force (kips)</u>	<u>Stress (ksi)</u>
40	447	72
42	406	65
44	370	59
46	338	54
48	311	50
50	286	46
52	265	42
54	246	39
56	228	37
58	213	34
60	199	32

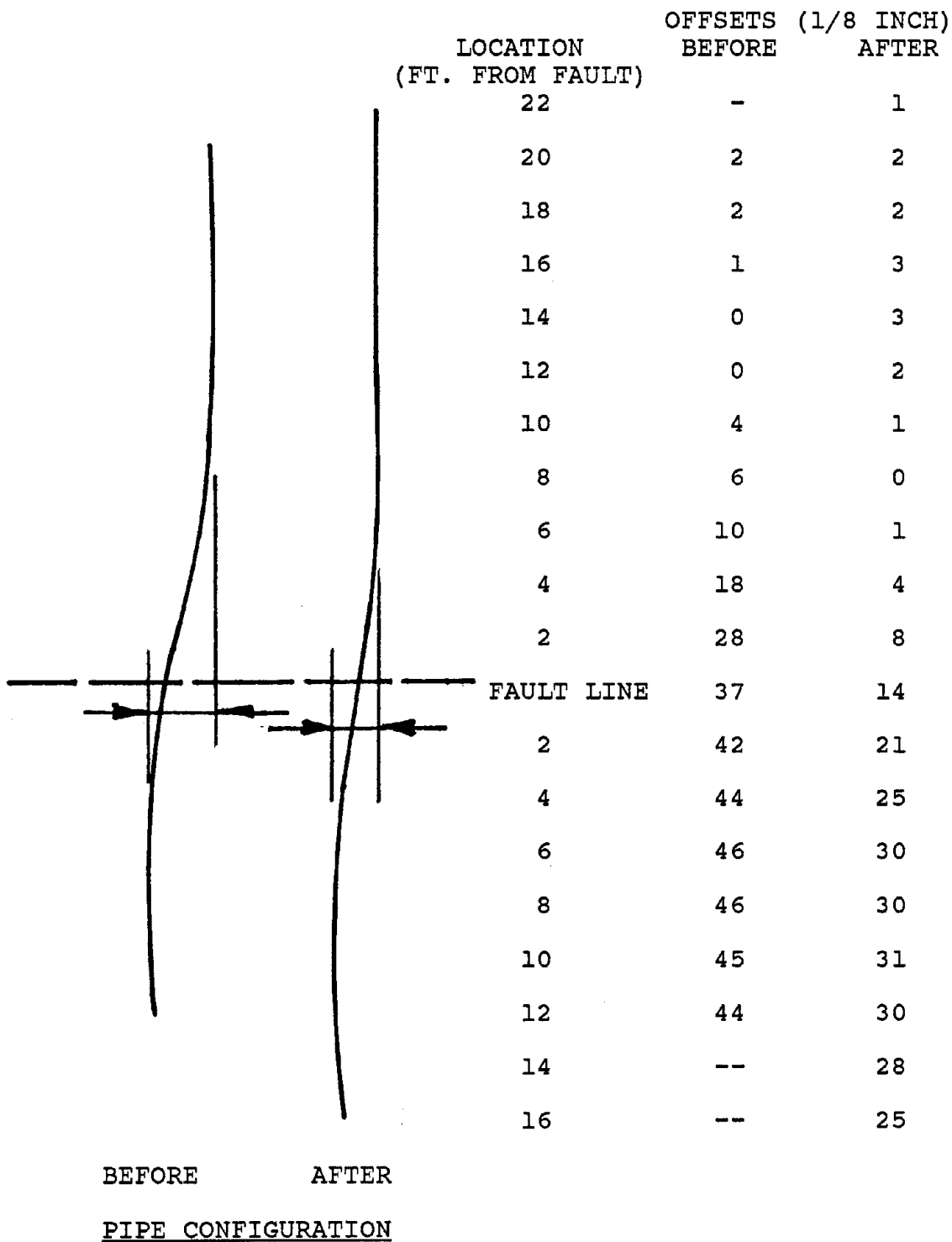


FIGURE 1.

EFFECTS OF LARGE GROUND DEFORMATION  
ON  
BURIED WATER PIPES OF POWER PLANT

Hideyo Suzuki<sup>(\*)</sup>, Masayuki Satoh<sup>(\*\*)</sup> and Shiro Fukui<sup>(\*\*)</sup>

(\*) Tokyo Electric Power Co., Inc.

(\*\*) Tokyo Electric Power Services Co., Ltd.

ABSTRACT

Investigated in this report are relationships between large ground deformation and damaged features of buried circulating water pipes and boiler water pipe of the Niigata Thermal Power Plant during the 1964 Niigata Earthquake. Further, the liquefaction potential of the plant site is estimated based on in-situ bore hole data and relationships between calculated PLs and the large ground displacements are investigated. Through the investigation, it is indicated that the permanent ground displacement becomes large with the increase of liquefaction index and that most of the features of the observed damage is related to the permanent ground displacement not only qualitatively but also quantitatively.

## INTRODUCTION

The authors have been studying the damage features of buried pipes during earthquakes and the relationship between observed damage and large ground deformation induced by liquefaction. The major objective of the study is to investigate the relationships among permanent ground deformation, type and magnitude of damages, soil profile and soil properties, liquefaction potential and so on.

In this report, the permanent ground displacement and the observed damage of circulating water pipes and a boiler water pipe of a thermal power plant in the event of the 1964 Niigata earthquake are first described. Then, the data of permanent ground deformation collected by aerial photos and confirmed by precise drawing of the plant are compared with quantitative and qualitative data of damaged pipes.

The authors used the permanent ground deformation collected by Professor Hamada. The data was obtained quantitatively in form of relative displacements by using the aerial photos taken before and after the earthquake.

### USED DATA OF PERMANENT GROUND DISPLACEMENT

Some useful common targets to measure the relative ground displacement along the pipes before and after the earthquake had been masked in the photos taken before the earthquake by several temporal stock yards of soil surrounding the route of the pipes, because the site work was continuing for constructing the another unit besides the unit already in operation. Those targets which had been masked by the above temporal site works were indicated on the precise drawings compiled soon after the completion of the construction work.

Additional common targets were also selected out of both the drawings and the aerial photos in order to investigate the relative permanent ground displacement before and after the earthquake.

### OUTLINE OF BURIED PIPES AND DAMAGE FEATURES

After the last report ( Ref. 2 ), some damage data were supplemented by measuring the amount of pull-out, dislocation or horizontal movement from photos taken during the repair works, in addition to the data obtained from design document survey.

The layout of the plant site and the routes of the circulating water pipes and the boiler water pipe are shown in Figure 1. The outline of the structure of each pipe and damage features are described below.

### Circulating Water Pipes

The head race pipes between the inlet structure and the power plant are ductile cast iron pipes; the total length is 1,140 m with unit length<sub>3</sub> of 6.0/4.9 m and the inside diameter of 1.50 m, and the design flow is 22 m<sup>3</sup>/s. The major portion of the pipes were buried and were supported by piles and concrete structures at the joints as shown in Figure 2. An overhead crossing was provided the intersection with the rail road by a four-spanned warren truss bridge of 160 m in length. At the other crossings under roads, reinforced concrete culverts were used as shown in Figure 3. All of the joints were facilitated with mechanical joints as shown in Figure 4.

The tail race pipes between the power plant and an outlet structure use the same ductile cast iron pipes as the head race pipes; the total length is 1,050 m with unit length of 6.0/4.0 m and the inside diameter of 1.50 m. The major portion of the pipes was buried. For the portion of 50 m in length from the outlet structure, the pipe was installed on the ground. At the crossings under the roads and the rail road, the culverts of reinforced concrete were used. As for the tail race pipes, the mat foundation of reinforced concrete was prepared within the area where the soil had not sufficient strength. All joints were facilitated with mechanical joints.

The damage features of both head race and tail race of circulating water pipe system are as follows.

Cracks and settlements of the ground were found along the whole length of the pipe system. At the ground surface near the inlet structure, the settlement was measured as about 2 m, and up to the portion of about 120 m from the inlet structure the pipe was found to be displaced horizontally by maximum 1.0m and many joints opened. The overhead crossing bridge itself showed no damage, however the pipe mounted on the bridge was observed as movement by 2 cm along the axis of the bridge, which was measured by the scratches left on the bridge. In the tail race section, some "pull-out" were found. At the location around 70 m from Rinkoh Bridge, the horizontal movement of the pipe of 0.90 m and the settlement of 0.20 were found. In the section near the outlet structure, where the pipes were placed on the ground, the horizontal movement of the pipes of about 0.6m were found. With these movements, many joints showed openings with/without dislocation.

### Boiler Water Pipe

Boiler water pipe system consisted of the inlet structure located at upstream about 9 km from the estuary, the sedimentation pond near the inlet on Agano River, the pumping station and the pipe line of cast iron of about 12 km in length with 300 mm diameter. Most portions of the pipe were buried being connected by mechanical joints at the ends of unit pipes.

Along the whole length of the pipe, the ground showed settlements and horizontal movements which might have caused many openings at the joints of the pipe, although these unit pipes themselves showed no damages except few bend pipes.

In addition to the above pipe line, the feed water pipe for the boiler as denoted "boiler water pipe" in Figure 1 passing through the power plant site was also investigated on the damage, of which some damage data and soil layer profile data existed and a lot of ground displacement vectors have been obtained.

### INVESTIGATION ON LIQUEFACTION

Locations of boring points along the circulating water pipes and boiler water pipe are shown by the numbers from 1 through 12 in Figure 1. The four typical soil profiles of them are shown in Figure 5. Bore holes from No. 1 through No. 9, which were measured about three years before the earthquake, are located along the circulating water pipes, and No.9 through No. 10 along the boiler water pipe. As are shown in these soil layer profiles, the surface layer within the depth to 20 m from the ground surface, which are usually considered to be a liquefiable zone, consists generally of medium to fine sand if the thin layers of silt distributed partially were neglected.

Using these profiles of each boring hole, Factor of Liquefaction Resistance ( FL ) and Index of Liquefaction Potential( PL ) were calculated (Ref. 5). According to the ground conditions described in the reconnaissance report (Ref.1), the ground surface are roughly flat, EL. +3m, and the ground water level was usually kept at around the sea level.

Some examples of FL and PL values obtained from the bore holes Nos. 1, 4, 9 and 12 are shown in Figure 5. The estimated peak ground acceleration at the ground surface used in the calculation is 159 gals, which was observed at Kawagishi-cho apartment house, 4 km to the south-west of the power plant. Further, the peak ground acceleration of 200 gals was also used for the purpose of comparison.

According to the resulted FLs and PLs, the soils around the bore holes Nos.1 and 2 near Shinano River region of the head race pipe, and at Nos. 8 and 9 near the tail race pipes and boiler water pipe are considered very vulnerable to be liquefied. On the other hand, the soils around Nos. 3 to 7, and Nos.10 to 11 near the power house have higher SPT( N )-values, resulting to give relatively high FL and low PL values.

The relationships of the permanent ground displacement versus the thickness of liquefied layer, and permanent ground displacements versus PL values are shown in Figures 6 through 9. In these figures, the permanent ground displacements are defined as the averaged and maximum values of permanent displacements, respectively, observed within the circles of 50 m radii having their centers at each boring points. Although the observed devia-

tion of the data are somewhat large, these relations show the tendency that as the thickness of liquefied layer and PL values become large, the averaged and maximum permanent ground displacements also become large.

#### COMPARISON WITH DAMAGES OF PIPES AND PERMANENT GROUND DEFORMATION

The permanent ground displacement vectors measured along the axis of the circulating water pipes and the boiler water pipe are as shown in Figure 10 and 11. In these figures, damage features of pipes are also described. The relations between the permanent ground displacement vectors and damage features are described below for each of the above pipe systems.

##### Circulating Water Pipes

[ Note ; Area numbers as below are concerned in Figs. 10 and 11. ]

[ Area 1 ] At the joint between the inlet structure and the head race pipes, the pull-out of 4 to 9 cm was observed as is shown in Photo 1 and the relative displacement of the ground, which seems to have affected as tensile force to the joint, agrees with the damage feature of the pipe. This amount of the pull-out is considered to be rather small, if compared with the ground deformation of 75 cm.

[ Area 2 ] As shown in Photo 2, the horizontal movement of 118 cm at the pipe was observed which agrees with the permanent ground displacement in both the direction and amount.

[ Area 3 ] The pull-out of 2cm was observed at the joint. In this area compressive deformation is considered to have occurred from the data of permanent ground displacements. Using these data, the damage feature of the pipe can not be explained.

[ Area 4 ] The pull-out of about 2cm was observed at the joint. This phenomenon is also unable to be explained by the ground deformation.

[ Area 5 ] The horizontal movement of 92 cm at the pipe was observed as shown in Photo 3, which agrees with the ground deformation in both the direction and amount.

[ Area 6 ] As shown in Photo 4 the opening of the joint was observed possibly due to the horizontal movement of the pipe. This is considered to have occurred due to the horizontal ground movement of the upstream area as evident from Photo 3.

[ Area 7 ] As shown in Photo 5, the horizontal movement of 60cm occurred at the pipe, and the direction of the movement is almost the same as that of the ground deformation. But the amount of the horizontal movement of the pipes is much smaller than the ground deformation.

[ Area 8 ] At the joint between the tail race pipe and the outlet structure, both the pull-out of 10 to 45 cm and dislocation of 25 cm have occurred as shown in Photo 6.

According to the ground deformation data, pull-outs, dislocations or lateral movements other than stated above might have possibly occurred somewhere else at these pipes, however we could not have identified any damage other than those described above from the reconnaissance reports (Ref. 1).

As mentioned above, the horizontal movements of the pipe in the transverse direction to the pipe axis can be explained well by the ground deformation surrounding the pipe. However, the damage of the pipe in the axial direction, in particular the amount of the pull-out at the joints, are not always explained well by the ground deformation data. The reason why the amount of pull-out was much smaller than the ground displacement may be attributed to low resistance of the axial direction.

### Boiler Water Pipe

[ Area 1 ] As shown in Photo 7, the pull-out was observed at the joint, but no quantitative description was left in the past report. The damage feature of the pipe shows inconsistency, comparing the ground displacement vectors of this portion.

[ Area 2 ] As shown in Photo 8 and 9, horizontal movement of the pipe occurred and pull-out at the joint occurred, but no quantitative description is left. Although the estimated amount of the pull-out is about 20 cm from the evidence in the photographs, this amount cannot be supported by the ground data because of lack of the targets near the area in the aerial photos.

[ Area 3 ] The bend of the pipe was damaged. According to the report, some cracks along the curved axis have appeared. This might be attributed to the ground deformation which acted to cause widening of the bend.

[ Area 4 ] As shown in Photo 10, the pull-out occurred at the joint. The amount of the pull-out was shown as 50 cm from the photo. It is estimated that the pull-out was due to the perpendicular displacement of about 2 m at the northern part and pulling direction of axial displacements of about 80 cm at the southern part as shown in Figure 11, if wider region is concerned.

### CONCLUSIONS

Based upon the damage feature of the buried circulating water pipes and the boiler water pipe and the permanent ground deformation data of the thermal



power plant which were measured by aerial photos and reconnaissance reports at the time of the 1964 Niigata Earthquake, and the boring data of the soil along the pipes, the relationship between damage feature and ground deformation were studied.

From the study, the followings can be concluded;

1) Using the boring data along the buried pipes, the thickness of liquefied layer and Index of Liquefaction Potential ( PL ) were calculated. According to the results, there is the tendency that as the thickness of liquefied layer or PL become large, the permanent deformation also becomes large.

2) As the results of the examination of the relationship between the damage of the circulating water pipes and the associated ground deformation, the ground displacement was found to some extent capable to explain the horizontal movement of pipes both qualitatively and quantitatively. However, the phenomena observed along the pipe axis, such as pull-out at the joint, can not be well explained; the amount of the pull-out is much smaller than that of the ground deformation. As the reasons of this discrepancy, the possibility of slippage between the pipe and the surrounding soil may be considered.

3) As for the boiler water pipe, neither a quantitative nor a qualitative study on the relationships between ground deformation and damage feature of the pipe were possible, because even the description of the damage feature was unclear and no quantitative damage data was reported.

#### ACKNOWLEDGMENTS

The authors wish to express their sincere thanks to Professor K. Kubo and Professor M. Hamada for their advice and encouragement for this study. And, fruitful discussion and helpful assistance given by many engineers from Tohoku, Chubu and Kansai Electric Power Companies are highly appreciated.

## REFERENCES

- 1) Japan Society of Civil Engineers : Report on The 1964 Niigata Earthquake, 1966 (in Japanese).
- 2) H. Suzuki : Damage to Buried Pipes Caused by Large Ground Displacement, Proc. 1st Japan-U.S. Workshop on Liquefaction, Large Ground Deformation and Their Effects on Lifeline Facilities, November 1988, Tokyo, Japan, pp 127-132.
- 3) M. Hamada, S. Yasuda, R. Isoyama and K. Emoto : Study on Liquefaction Induced Permanent Ground Displacements, Association for the Development of Earthquake Prediction, November 1968, Tokyo, Japan.
- 4) M. Hamada, S. Yasuda, R. Isoyama and K. Emoto : Observation of Permanent Ground Displacements Induced by Soil Liquefaction, Proc. JSCE, No.336/III-6, Dec., 1986, pp211-220.
- 5) T. Iwasaki, et al. : A Practical Method for Assessing Soil Liquefaction Potential Based on Case Studies at Various Sites in Japan, Proceedings of 5th Japan Earthquake Engineering Symposium, 1978, Tokyo, Japan (in Japanese).

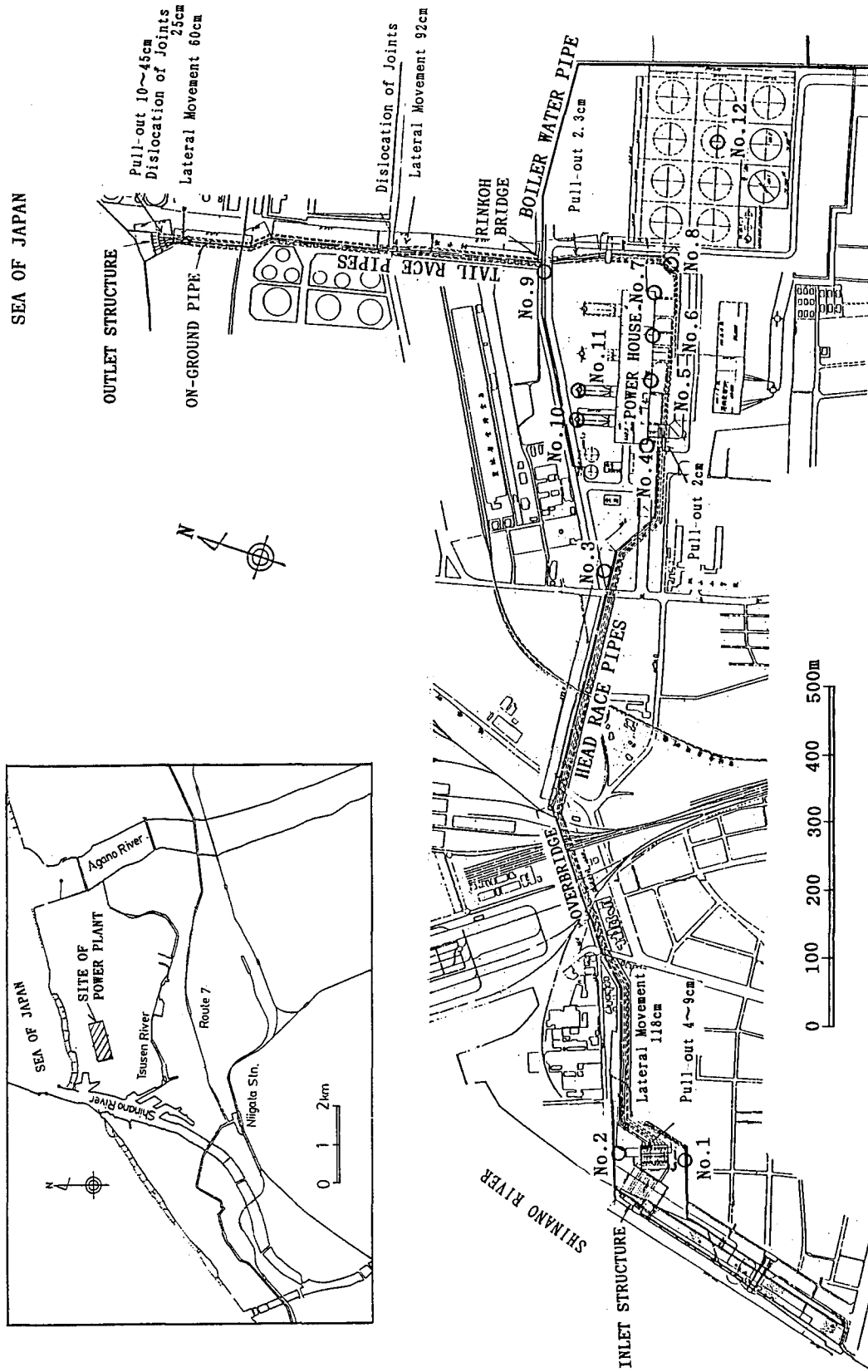


Figure 1 Routes of Circulation Water Pipes and Boiler Water Pipe, and Location of Exploration Bore Hole

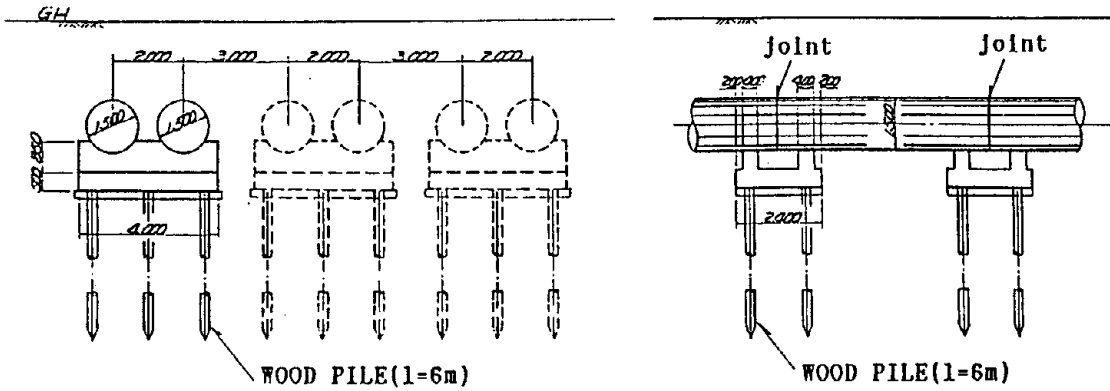


Figure 2 Major Part of Circulation Water Pipes

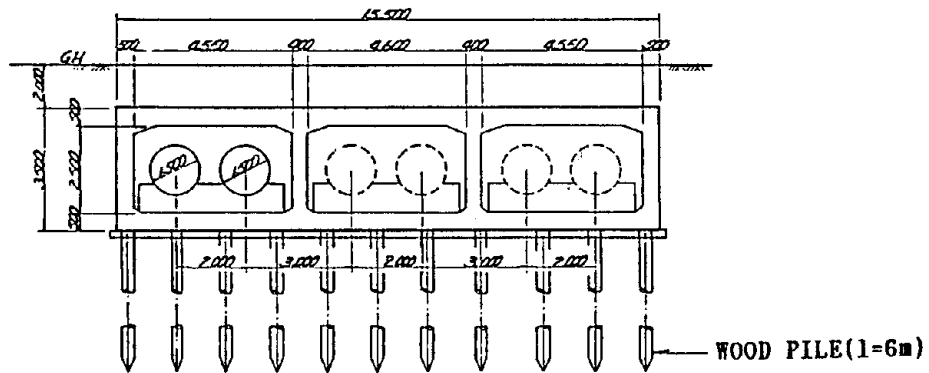


Figure 3 Under Road Crossing Part of Circulation Water Pipes

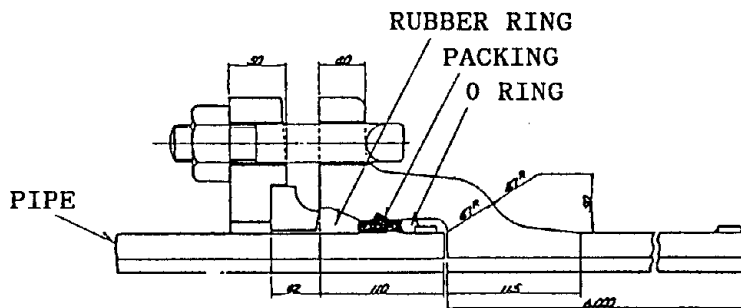


Figure 4 Mechanical Joint of Circulation Water Pipes

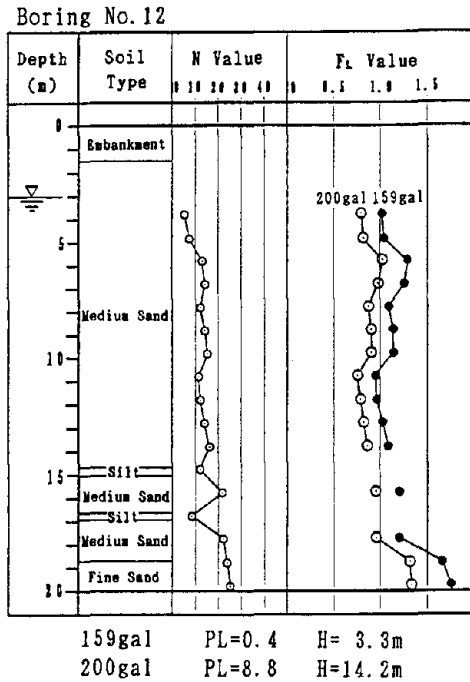
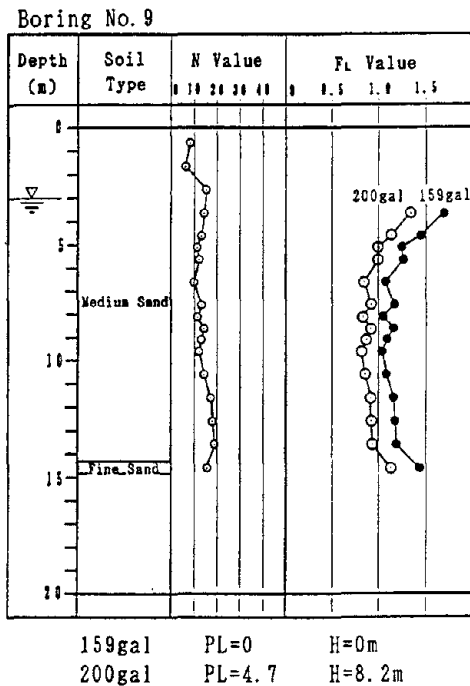
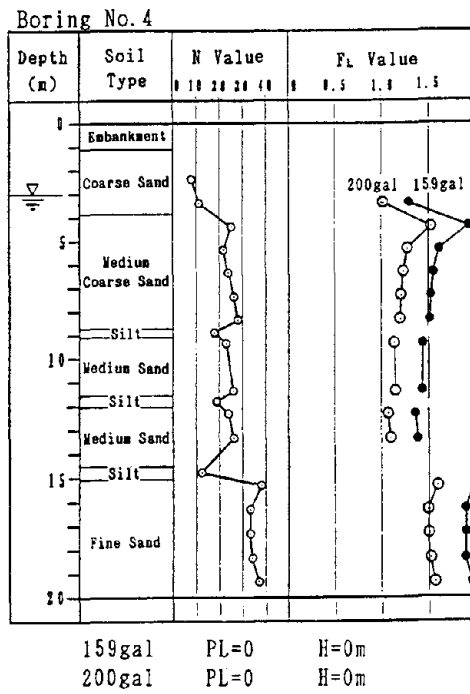
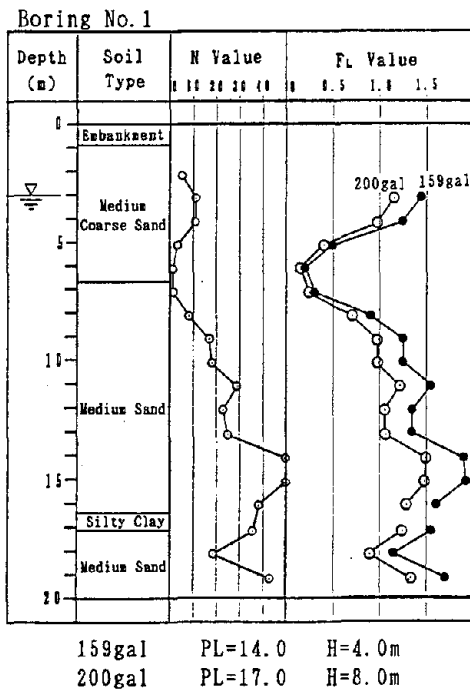


Figure 5 Typical Soil Profiles and Calculated FL, PL and Thickness of Liquefied Layer(H)

Note : Boring numbers are indicated in Figure 1.

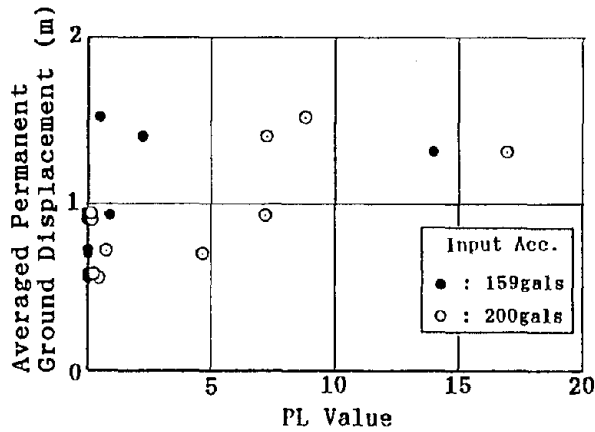


Figure 6 Relationship between PL value and Averaged Value of Permanent Ground Displacements

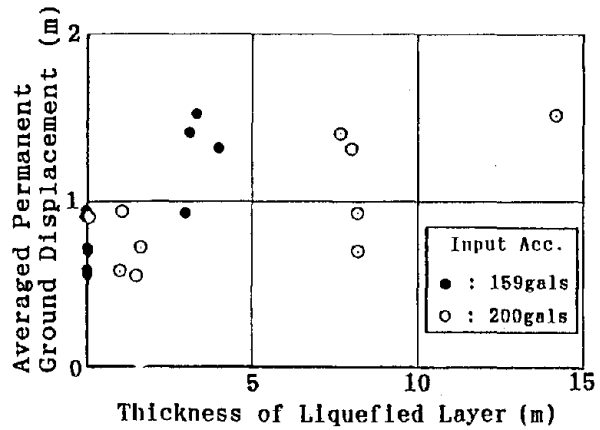


Figure 7 Relationship between Thickness of Liquefied Layer and Averaged Value of Permanent Ground Displacements

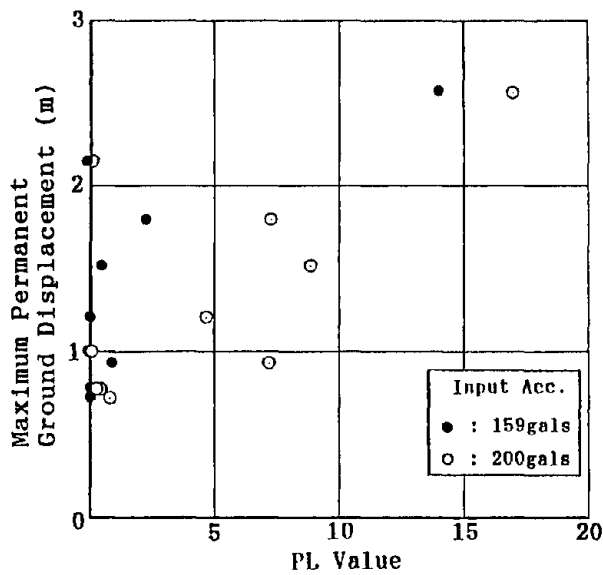


Figure 8 Relationship Between PL Value and Maximum Value of Permanent Ground Displacements

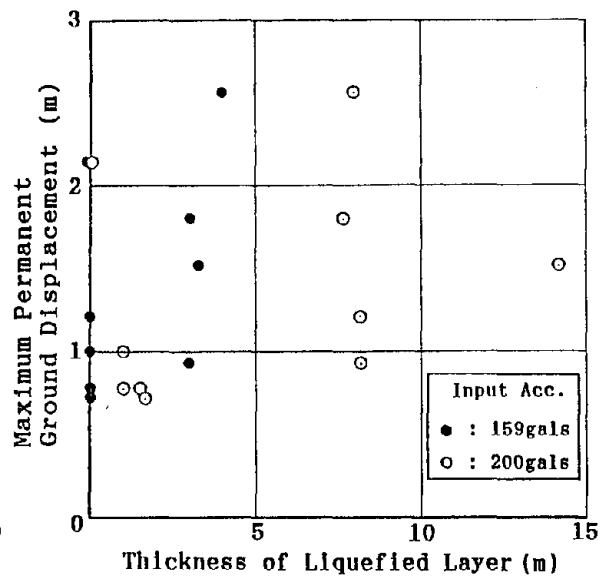


Figure 9 Relationship between Thickness of Liquefied Layer and Maximum Value of Permanent Ground Displacements

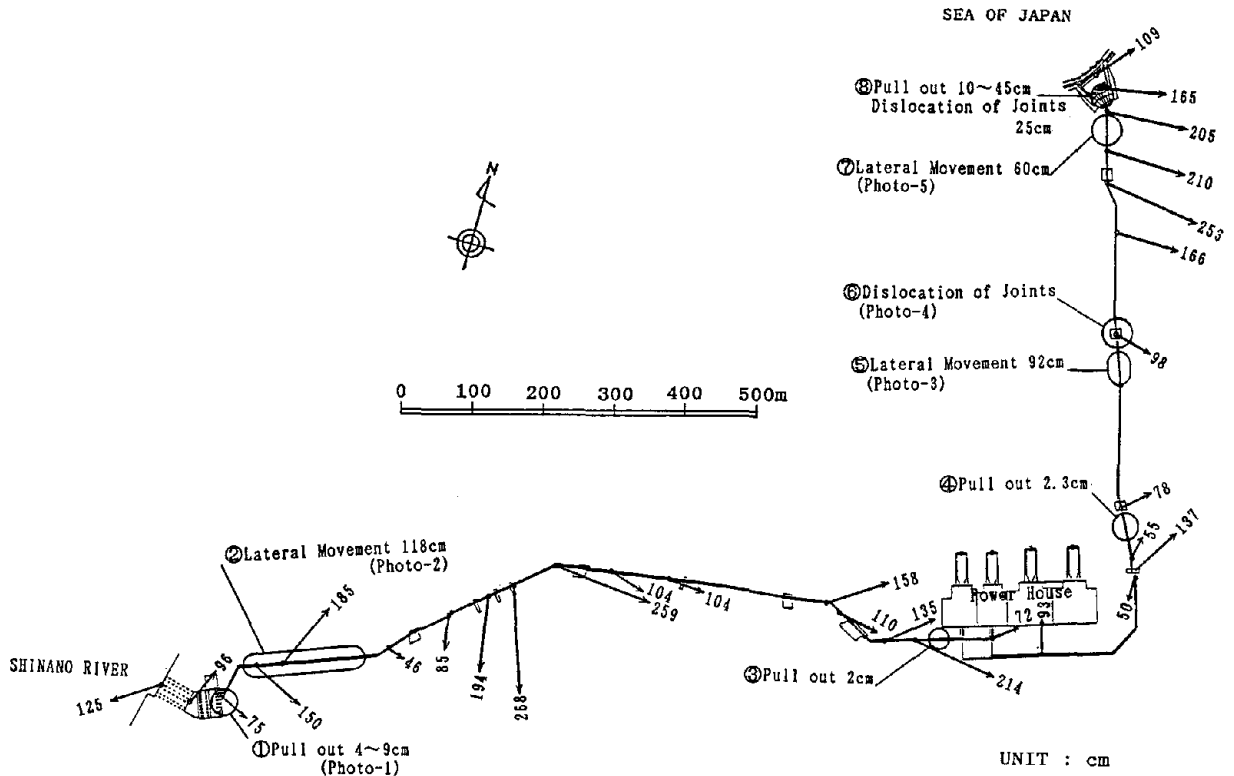


Figure 10 Permanent Ground Displacement Vectors Measured along Circulation Water Pipes and Damage Features of Pipes

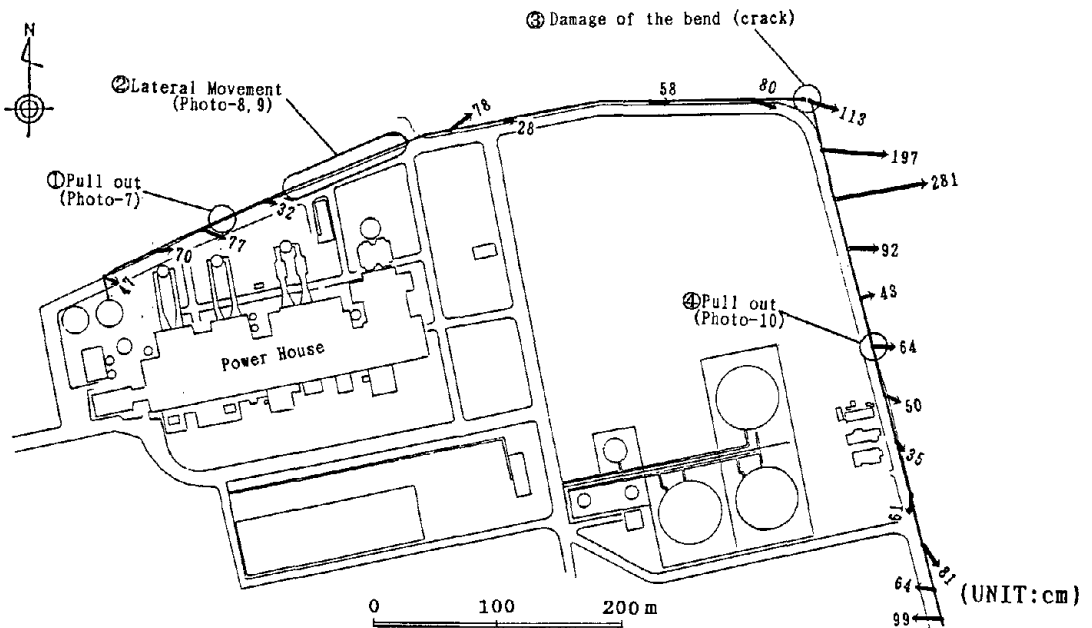


Figure 11 Permanent Ground Displacement Vectors Measured along Boiler Water Pipe and Damage



Photo 1 Pull-out at Joint of Head Race Pipe in Area ①



Photo 2 Horizontal Movement of Head Race Pipes in Area ②



Photo 3 Horizontal Movement of Tail Race Pipes in Area ⑤

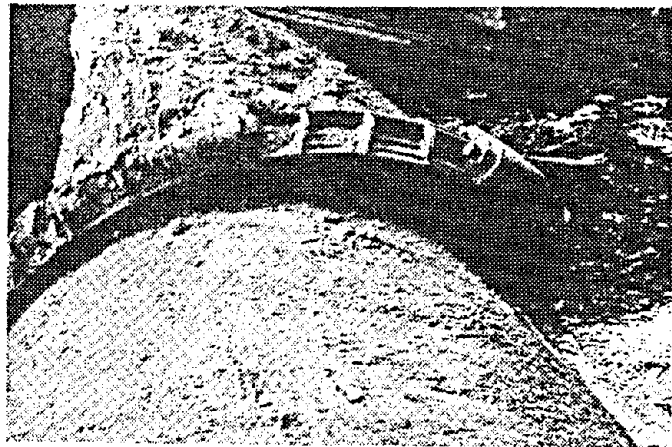


Photo 4 Dislocation at Joint of Tail Race Pipe in Area ⑥





Photo 5 Horizontal Movement of  
Tail Race Pipes in Area ⑦ (On-ground Pipes)



Photo 6 Pull-out and Dislocation at Joint  
of Tail Race Pipes in Area ⑧

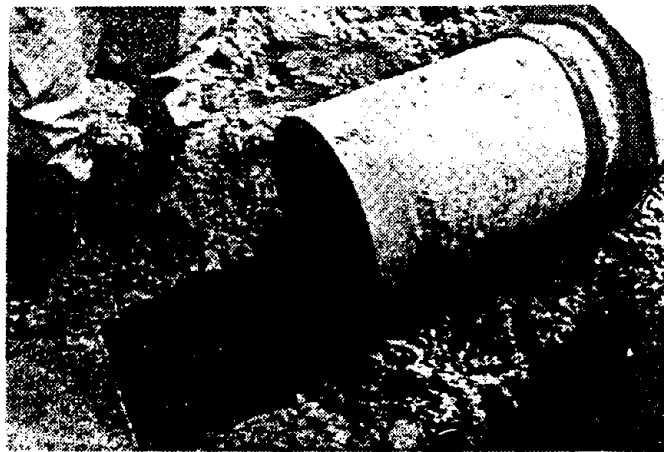


Photo 7 Pull-out at Joint of  
Boiler Water Pipe in Area ①

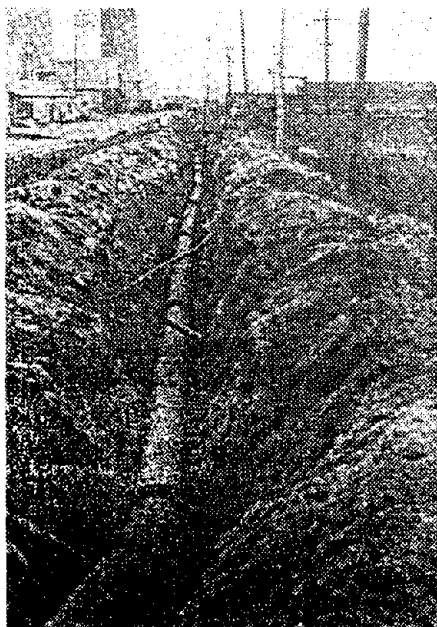


Photo 8 Horizontal Movement of  
Boiler Water Pipe in Area ②

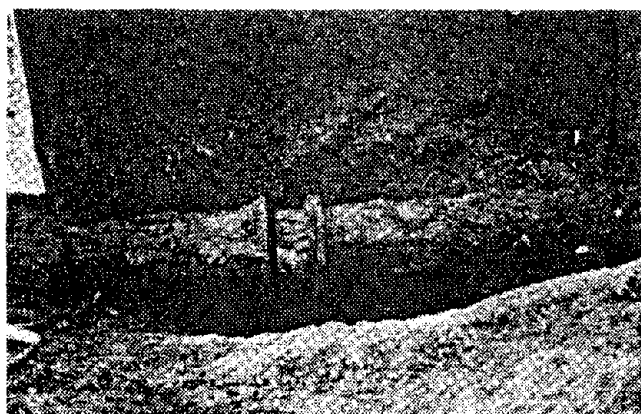


Photo 9 Pull-out at Joint of  
Boiler Water Pipe in Area ②

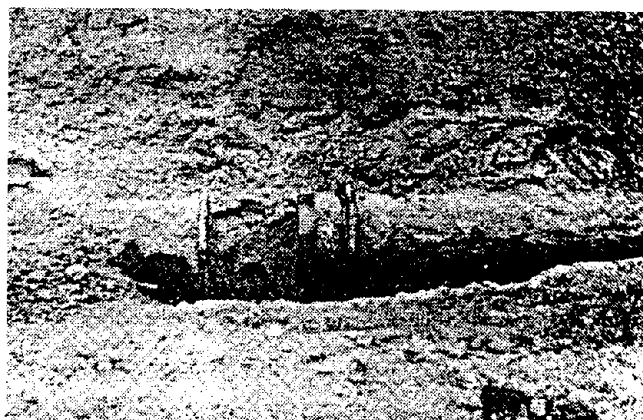


Photo 10 Pull-out at Joint of  
Boiler Water Pipe in Area ④

## **EFFECTS OF LIQUEFACTION-INDUCED GROUND MOVEMENT ON PIPELINE**

Masakatsu MIYAJIMA\* and Masaru KITAURA\*\*

- \* Assistant Professor  
Department of Civil Engineering, Kanazawa University
- \*\* Professor  
Department of Civil Engineering, Kanazawa University

### **ABSTRACT**

The present paper discusses the response of pipelines subjected to liquefaction-induced permanent ground deformation and the subsequent failure of pipelines. Initially here, effects of permanent ground deformation on pipelines are investigated by using earthquake damage data and model experiments are conducted. Next, response simulations of the buried pipelines, continuous welded steel pipelines and jointed ductile iron pipelines, are carried out. We clarify the influential factors of the permanent ground displacement to pipelines' damage.

## INTRODUCTION

Past severe earthquakes reveal that soil liquefaction is one of the most crucial geotechnical hazards during an earthquake, for example, the 1964 Niigata Earthquake in Japan, 1971 San Fernando Earthquake in U.S.A. and the 1983 Nipponkai-Chubu Earthquake in Japan. Liquefaction caused heavy damages to the various type of structures due to loss of bearing capacity, buoyancy effects and subsidence. On the other hand, other liquefaction hazard was pointed out by Hamada et al. recently <sup>1),2)</sup>. It is a permanent ground displacement induced by liquefaction. Using aerial photographs taken before and just after the earthquakes, Hamada et al. measured the permanent ground displacement following the 1964 Niigata Earthquake and the 1983 Nipponkai-Chubu Earthquake. According to their findings, the maximum detected permanent ground displacement was more than 8 m along the Shinano river in Niigata City and more than 5 m in Noshiro City <sup>1)</sup>. They also analyzed the quantitative correlations of the magnitude of the permanent ground displacement with the degree of damage to pipelines <sup>2), 3)</sup>. O'Rourke and Tawfik investigated pipeline response to permanent ground displacement near the Upper Van Norman Reservoir after the 1971 San Fernando Earthquake and related the damage to the patterns of permanent ground movement <sup>4)</sup>. These results indicated that buried pipelines were vulnerable to permanent ground deformation. Furthermore, Yasuda et al. carried out model experiments considering the characteristics of permanent ground displacement and discussed the causes of permanent ground displacement <sup>5)</sup>. Some research work on the effects of permanent ground displacement on civil engineering structures has been undertaken in recent years <sup>6)-8)</sup>. Little work has been done on the response of pipelines subjected to permanent ground deformation so far, however.

The purposes of the present paper are to clarify the response of pipelines subjected to liquefaction-induced permanent ground displacement and to discuss the subsequent failure of pipelines. In the following chapters, liquefaction effects, especially permanent ground deformation, on the pipelines' damage are investigated by using the earthquake damage data during the 1983 Nipponkai-Chubu Earthquake and characteristics of permanent ground displacement are discussed based on the results of model experiments. Moreover, response simulations are conducted by using a modified transfer matrix method and failures of pipelines due to liquefaction-induced permanent ground deformation are discussed. In this paper, a "damage" refers to one specific site of damage in a pipeline. Therefore, "number of damages" refers to the number of sites of damage in the piping under discussion.

### DAMAGE TO BURIED PIPELINE DUE TO PERMANENT GROUND MOVEMENT DURING THE 1983 NIPPONKAI-CHUBU EARTHQUAKE

The relationship between pipe damage and permanent ground displacement induced by liquefaction is investigated by using the earthquake damage data during the 1983 Nipponkai-Chubu Earthquake indicated by Hamada et al.<sup>1)</sup> in this chapter. Table 1 shows the total number of pipe damages in Noshiro City ( $\alpha$ ), the number of pipe damages in areas where permanent ground displacement occurred ( $\beta$ ) and the ratio between them ( $\beta/\alpha$ ). The failure modes in this table are in accordance with those in Fig. 1. It is evident from this table that more than 30 percent of the total number of damages to ACP(asbestos cement pipe) and VP(polyvinyl chloride pipe), and about 20 percent of that to CIP(cast iron pipe) and DCIP(ductile cast iron pipe), are caused in the areas where permanent ground displacement occurred.

Fig. 2 indicates the relationship between horizontal permanent ground displacement and the number of pipe damages. This figure suggests that many damages were caused at sites where permanent ground displacement was greater than about 1 m. However, in order to discuss the

relationship between pipe damage and permanent ground displacement, it is more pertinent to observe ground strain around the buried pipelines than to observe absolute displacement. Therefore, the average ground strains for longitudinal and transverse directions of a pipe axis are evaluated using two vectors of the permanent ground displacements near the site of pipe damage. Figs. 3 and 4 indicate the relationship between the average ground strain and number of pipe damages, for longitudinal and transverse directions to the pipe axis, respectively. The minus values in Fig. 3 indicates a tensile strain. It can be seen from these figures that the pipe damages could be caused by an average ground strain as low as 1 percent or less. The failure modes A and B correspond with the failure due to tensile and compressive forces, respectively, as illustrated in Fig. 1. The failure modes in Fig. 3, however, do not agree with those; i.e. both modes A and B can be shown in tension and compression strain regions. This fact may be explained by following points. Since the ground movement during an earthquake is variable, it is insufficient to merely observe the residual ground deformation after an earthquake in order to discuss the relationship between the pipe damage and ground strains. Furthermore, the pipe damage may be influenced by a greater local ground strain than that evaluated in the present study.

### EXPERIMENTS ON CHARACTERISTICS OF PERMANENT GROUND MOVEMENT

The distribution of permanent ground displacement along pipelines and magnification of the displacement are crucial factors in analysis of pipeline response. According to a distribution map of permanent ground displacement resulting from the 1964 Niigata Earthquake and the 1983 Nipponkai-Chubu Earthquake indicated by Hamada et al. <sup>1)</sup>, the distribution of permanent ground displacement is affected by local ground conditions such as the slope of the ground surface, the depth of the liquefied ground layer, etc <sup>2)</sup>. In this chapter, model experiments are carried out to understand the characteristics of the permanent ground displacement.

The diagram of the experimental apparatus is shown in Fig. 5. The sand box was 500 mm in width, 1500 mm in length and 350 mm in height. The model sand deposit had a slope of 2 % to 6 %. The sand deposit was made from loose saturated sand, whose physical properties are shown in Table 2. Since the sand stratum was constructed in water in these experiments, whole sand stratum was saturated and the ground water table depth did not vary for each case. Therefore the effects of the ground water table depth were negligible in these experiments. Forty six pins were installed at the surface of the sand stratum to measure horizontal deformation of the ground surface. The deformation of the ground surface during excitation was measured by means of a video camera. Pore pressure transducers were buried to a depth of 5 cm to measure an excess pore water pressure in the loose sand stratum and in the more dense one. The model sand stratum was vibrated by a harmonic wave with 5 Hz. Target acceleration of the table was 100 gal and it took about 5 seconds for the table to reach the given acceleration. The duration of the test was 30 seconds.

Fig. 6 shows the time histories of input acceleration, excess pore water pressure at the loose sand stratum (WP 1) and displacement at point 7 which is shown in Fig. 8 as described later. It is evident from this figure that the model ground deformed in high excess pore water pressure, that is, in a completely liquefied condition. Fig. 7 shows distribution of the permanent ground displacement. It is interesting to note that the ground displacement in the middle of the loose sand stratum was greater than that at the sides and the dense sand stratum did not deform. Since the wall of the sand box was against deformation of the sand stratum, the ground displacement in the loose sand stratum near the wall was also little. Therefore, the experiments carried out in the present study corresponded with the permanent ground displacement when liquefaction uniformly occurred in a certain area, which was enclosed with the dense sand stratum and two walls of the sand box in this experiment. Fig. 8 reflects a distribution of residual permanent ground

displacement at the middle of the ground surface, shown inside of the dashed area in Fig. 5. In this figure, the open circles indicate the initial sites of the pins and the solid circles, squares and triangles show the residual displacement of the pins for each case. This figure suggests that the shape of the distribution of the permanent ground displacement is approximately a sinusoidal curve. Furthermore, the maximum value of the permanent ground displacement is affected by the width of the loose sand deposit,  $W$ . Fig. 9 shows the relationship between the width of the loose sand stratum and the maximum value of the permanent ground displacement. The maximum value seems to be directly proportional to the width of the loose sand deposit.

Hamada et al. proposed a formula for estimating the magnitude of ground displacement by using the data obtained from the 1964 Niigata, the 1971 San Fernando, and the 1983 Nipponkai-Chubu Earthquakes<sup>2)</sup>. In this formula, the ground slope and thickness of the liquefied layer were taken into consideration. The experimental results mentioned above, however, suggest that the width of permanent ground displacement is one of the influential factors determining the magnitude of the ground displacements. Evaluation of the extent of liquefiable areas induced by earthquakes is indispensable for predicting the width of permanent ground displacement. Although several practical methods to evaluate the liquefaction potential of a soil deposit subjected to earthquake loading have been developed<sup>9)-13)</sup>, little work has been done on evaluation of the extent of liquefiable areas. Therefore, methods must be sought for predicting the extent of liquefiable areas in the future.

## SIMULATION OF PIPELINES' RESPONSE DUE TO PERMANENT GROUND MOVEMENT INDUCED BY SOIL LIQUEFACTION

### Analytical Models

The distribution of the permanent ground displacement can be assumed to be a sinusoidal curve as mentioned in the previous chapter. Although the results of the experiments indicated one of the displacement patterns which depend on the several ground conditions, this pattern is considered as the basic pattern of the ground displacement. It is because this pattern appears when liquefaction uniformly occurred in the loose sand stratum on smooth slope of the non-liquefied ground. The displacement pattern in this case is modeled as shown in Fig. 10. The basic differential equations governing the motion of a buried pipe can be established as follows:

$$EI \frac{d^4 v_1}{dx^4} + K_1 v_1 = K_1 d \left(1 - \sin \frac{\pi x}{2l}\right) \quad (0 < x < l) \quad (1)$$

$$EI \frac{d^4 v_2}{dx^4} + K_2 v_2 = 0 \quad (x \geq l) \quad (2)$$

where  $E$  = Young's modulus of the pipe material,  $I$  = area moment of inertia of the pipe,  $v_1, v_2$  = displacement of pipeline at each zone,  $K_1, K_2$  = equivalent soil spring constants for deformed ground and non-deformed ground, in which non-linear characteristics are taken into consideration<sup>14)</sup>.  $d$  = the maximum magnitude of the permanent ground displacement and  $l$  = half of extent of the permanent ground displacement along the pipeline, that is,  $2l = W$ . Subscripts 1 and 2 respectively correspond to the two sections shown in Fig. 10. The response of continuous welded steel pipelines and jointed ductile iron pipelines are simulated by using modified transfer matrix method<sup>15)</sup> herein. The dimensions of the pipelines list in Table 3. Fig. 11 shows the analytical model of jointed pipelines used in the present study. The jointed pipelines are assumed here to be connected by springs for rotational and translational movements at the joints.

### Application of Simulation Models to Continuous Welded Steel Pipelines

Figs. 12 and 13 show the results of the response simulations. These figures display the relationship between the maximum bending stress and the width of the liquefied zone. Fig. 12 expresses the results for the non-liquefied superficial layer deformation, that is,  $K_1/K_2 = 1.0$ . It can be seen from Fig. 12 that the maximum bending stress increases with a decrease in the width of the deformed ground. These values are much greater than the bending strength of 4200 kgf/cm<sup>2</sup>. Therefore the probability of failure is very high in this case. Fig. 13 shows the results for  $10^{-3}$  of the ratio of the equivalent soil spring constant,  $K_1/K_2$ . The maximum bending stress is smaller than that in Fig. 12 and the tendency of lesser pipe response with increasing width of deformed ground as shown in Fig. 12 does not appear in Fig. 13. In other words, the maximum bending stress for the width of liquefaction zone of 20 m is smaller than that for 40 m. This can be explained in terms of the slippage between the pipelines and liquefied sand.

The equivalent soil spring constant for liquefiable ground depends on the degree of liquefaction of the soil. Yoshida et al. carried out experiments using a model pile in the liquefied ground and indicated that the coefficient of subgrade reaction on pile decreased to 1 percent or more of that in the non-liquefied ground<sup>16</sup>). Yasuda et al. conducted experiments using sand box and steel pipe, and concluded that critical shearing force and equivalent soil spring constant in the liquefied ground became less than 10 percent of those in the non-liquefied ground<sup>17</sup>). Takada et al., after conducting model experiments to obtain the equivalent soil spring constant on the pipeline in the liquefied ground, pointed out that the ratio of 1/1000 to 1/3000 seems to be an appropriate value adopted for the buried pipeline subjected to liquefaction<sup>18</sup>). The authors also conducted experiments using steel pipeline and investigated the equivalent soil spring constant in relation to the degree of liquefaction<sup>19</sup>). Although some experimental results are revealed above, accumulation of experimental data under various condition is inevitable before these values are used in the earthquake resistant design. Therefore, the equivalent soil spring constant is regarded as a variable in the present study.

Figs. 14 and 15 express the relationships between the maximum bending stress and the ratio of the equivalent soil spring constant. Fig. 14 shows the response of pipelines for 1 m of the maximum magnitude of the permanent ground displacement and Fig. 15 reflects that for 40 m of the width of deformed ground. It can be seen from these figures that the maximum bending stress increases with an increase in the ratio of the equivalent soil spring constant, that is, a decrease in the degree of liquefaction. In other words, the probability of pipe failure is high for the deformation of the non-liquefied superficial layer above the liquefied layer. Generally speaking, the greater the degree of liquefaction is, the greater the magnitude of permanent ground displacement. Therefore, the failure of pipes could occur with even a relatively small ratio of the equivalent soil spring constant, that is, with great degree of liquefaction.

### Application of Simulation Models to Jointed Ductile Iron Pipelines

Figs. 16 and 17 show the results of the response simulations. These figures display the relationships between the maximum displacement angle at a joint and the width of the liquefied zone. Fig. 17 expresses the results for the non-liquefied superficial layer deformation, that is,  $K_1/K_2 = 1.0$ . It can be seen from Fig. 16 that the maximum displacement angle at a joint increases with a decrease in the width of the deformed ground. This tendency is identical to the results as shown in Fig. 12. Since the allowable value for displacement angle at a joint is 7°, failure at a joint can be caused by greater than 3 m permanent ground displacement in a width of the

liquefied zone less than 80 m. Pipe failure could also be caused by permanent ground displacement less than 1 m in a width of liquefied zone less than 20 m. Fig. 17 shows the results for  $10^{-3}$  of the ratio of the equivalent soil spring constant. The maximum displacement angle at a joint is smaller than that in Fig. 16, however, the tendency of lesser pipe response with increasing width of deformed ground is similar.

Figs. 18 and 19 express the relationships between the maximum displacement angle at a joint and the ratio of the equivalent soil spring constant. Fig. 18 shows the response of pipelines for 1 m of the maximum magnitude of permanent ground displacement and Fig. 19 reflects that for 40 m of the width of deformed ground. It can be seen from these figures that the maximum displacement angle at a joint decreases with a decrease in the ratio of the equivalent soil spring constant, that is, with an increase of the degree of liquefaction. The failure of pipes at a joint could occur with even a relatively small ratio of the equivalent soil spring constant, that is, with great degree of liquefaction because of great permanent ground displacement.

The above results obtained by the response simulation seem to show that the probability of failure is high for a relatively narrow width of the deformed non-liquefied superficial layer above the liquefied ground. However, we do not take into consideration the relationship between the magnitude of the maximum ground displacement and the width of deformed ground in these examples. It is a crucial point to clarify the relationship between the magnitude of permanent ground displacement, the degree of liquefaction and the width of deformed ground quantitatively in the future.

### CONCLUDING REMARKS

Conclusions obtained from the present study are summarized as follows:

(1) Many pipe damages occurred at sites where the permanent ground displacement was greater than 1 m. Moreover, the pipe damage could be caused even by an average ground strain of less than 1 percent.

(2) The tensile and compressive failure modes of the pipelines at joints do not always agree with the direction of the permanent ground displacement. Since the ground movement during an earthquake is variable, it is insufficient to observe the residual ground deformation after an earthquake in order to assess pipe damage.

(3) The shape of the distribution of the permanent ground displacement perpendicular to the slope of ground can be assumed to be a sinusoidal curve in the model experiments. The relationship between the maximum ground displacement and width of the permanent ground displacement is indicated based on the experimental results. The findings suggest that the width of the liquefied area is one of the most influential factors determining the magnitude of the ground displacements.

(4) The maximum bending stress of continuous steel pipelines subjected to permanent ground displacement increases with a decrease in the width of the deformed ground, however, the slippage between the pipelines and liquefied soil reduces the bending stress.

(5) The results of the response simulation for jointed pipelines suggest that the probability of failure at a joint is high in areas where the deformed non-liquefied superficial layer above liquefied ground is less than 80 m in width for the maximum permanent displacement greater than 1 m.

(6) The relationship between the magnitude of permanent ground displacement, the degree of liquefaction and the width of deformed ground is one of the crucial points for evaluating the failure of pipelines subjected to permanent ground displacement.

(7) It is crucial to predict liquefaction potential and generation of ground deformation in an extent smaller than 100 m for evaluating the pipelines' failure induced by permanent ground displacement.



Finally, we focused on only the response of the main distribution pipelines for water service with 400 mm nominal diameter to understand the response characteristics of the pipelines in this study, however, dimensionless parameters should be introduced to discuss the results quantitatively in the future analysis. Although the method for evaluation of pipeline response to permanent ground displacement induced by liquefaction was established in the present study, future study on the mechanisms of generation of permanent ground displacement is needed in order to clarify the effects of permanent ground displacement on pipelines.

### ACKNOWLEDGEMENT

This study is supported in part by the Kajima Foundation's Research Grant. The calculation was performed by FACOM F-170 computer at the Information Processing Center, Kanazawa University.

### REFERENCES

- 1) Hamada, M., Yasuda, S., Isoyama, R. and Emoto, K.: Observation of Permanent Ground Displacements Induced by Soil Liquefaction, Proceedings of Japan Soc. Civil Eng., No. 376, pp. 211-220, 1986 (in Japanese).
- 2) Hamada, M., Yasuda, S., Isoyama, R. and Emoto, K.: Study on Liquefaction-Induced Permanent Ground Displacements and Earthquake Damage, Proceedings of Japan Soc. Civil Eng., No. 376, pp. 221-229, 1986 (in Japanese).
- 3) Hamada, M.: Damage to Buried Pipes and Foundation Piles Due to Liquefaction-Induced Ground Displacement, Proceedings of the 1989 ASME Pressure Vessels and Piping Conference, PVP-Vol. 162, pp. 1-5, 1989.
- 4) O'Rourke, T. D. and Tawfik, M. S.: Effects of Lateral Spreading on Buried Pipelines During the 1971 San Fernando Earthquake, Earthquake Behavior and Safety of Oil and Gas Storage Facilities, Buried Pipelines and Equipment, PVP-Vol. 77, ASME, pp. 124-132, 1983.
- 5) Yasuda, S., Tada, H., Fukusaki, S., Nakashima, R. and Yamamoto, Y.: Shaking Table Test of Liquefaction Induced Permanent Ground Displacement, Proceedings of the 22nd Japan National Conference on Soil Mech. and Found. Eng., pp. 731-734, 1987 (in Japanese).
- 6) Kobayashi, H., Yoshida, N. and Nakamura S.: Investigation of Damage to Pile Foundations During 1964 Niigata Earthquake, Proceedings of the 20th JSCE Earthquake Engineering Symposium-1989, pp. 21-24, 1989 (in Japanese).
- 7) Mori, S., Shimizu, K., Suzuki, N., Takagi, M. and Nakamura, S.: Damage to Pile Foundations Caused by Liquefaction-Induced Permanent Ground Displacement and Its Analysis, Proceedings of the 20th JSCE Earthquake Engineering Symposium-1989, pp. 25-28, 1989 (in Japanese).
- 8) Kawashima, K., Sugita, H., Kano, N., Isoyama, R. and Taguchi, Y.: Relationship Between Damage to Sewerage and Permanent Ground Displacement -in Case of Noshiro City During 1983 Nipponkai-Chubu Earthquake-, Proceedings of the 20th JSCE Earthquake Engineering Symposium-1989, pp. 273-276, 1989 (in Japanese).
- 9) Seed, H. B. and Idriss, I. M. : Simplified Procedure for Evaluating Soil Liquefaction Potential, Proceedings of ASCE, Vol. 97, No. SM9, pp. 1249-1273, 1971.
- 10) Tatsuoka, F., Iwasaki, T., Tokida, K., Yasuda, S., Hirose, M., Imai, T. and Koh-no, M.: Standard Penetration Tests and Soil Liquefaction Potential Evaluation, Soils and Foundations, Japan Soc. Soil Mecha. Founda. Eng., Vol. 20, No. 4. pp. 95-111, 1980.
- 11) Seed, H. B., Idriss, I. M. and Arango, I.: Evaluation of Liquefaction Potential Using Field Performance Data, Proceedings of ASCE, Vol. 109, No. GE3, pp. 458-482, 1983.
- 12) Tokimatsu, K. and Yoshimi, Y.: Empirical Correlation of Soil Liquefaction Based on SPT N-value and fines content, Soils and Foundations, Japan Soc. Soil Mecha. Founda. Eng., Vol. 23, No. 4. pp. 56-74, 1983.

- 13) Shibata, T. and Teeparaksa, W.: Evaluation of Liquefaction Potentials of Soils Using Cone Penetration Tests, *Soils and Foundations*, Japan Soc. Soil Mecha. Founda. Eng., Vol. 28, No. 2, pp. 49-60, 1988.
- 14) Japan Gas Association: Recommended Practice for Earthquake Resistant Design of Gas Pipelines, pp. 177-182, 1982 (in Japanese).
- 15) Nakamura, H.: A Modified Transfer Matrix Method with Improved Round off Errors, *Proceedings of Japan Soc. Civil Eng.*, No. 289, pp. 43-53, 1979 (in Japanese).
- 16) Yoshida, T. and Uematsu, M.: Dynamic Behavior of a Pile in Liquefaction Sand, *Proceedings of the 5th Japan Earthquake Engineering Symposium-1978*, pp. 657-663, 1987 (in Japanese).
- 17) Yasuda, S., Saito, K. and Suzuki, N.: Soil Spring Constant on Pipe in Liquefied Ground, *Proceedings of the 19th JSCE Earthquake Engineering Symposium-1987*, pp. 189-192, 1987 (in Japanese).
- 18) Takada, S., Tanabe, K., Yamajyo, K. and Katagiri, S.: Liquefaction Analysis for Buried Pipelines, *Proceedings of the 3rd International Conference on Soil Dynamics and Earthquake Engineering*, 1987.
- 19) Miyajima, M. and Kitaura, M.: Experiments on Restoring Force Characteristics of Pipe-Liquefied Layer System, *Memoirs of the Faculty of Technology, Kanazawa University*, Vol. 22, No. 1, pp. 11-20, 1989.

**Table 1** Number of damages due to permanent ground displacement in Noshiro City.

Pipe type		Failure mode					Total
		A	B	C	D	E	
ACP	(B)	4	7	37	1	38	87
	(α)	15	12	98	4	94	223
	(B)/(α)	0.27	0.58	0.38	0.25	0.40	0.39
VP	(B)	1	0	1	68	3	73
	(α)	4	6	1	189	10	210
	(B)/(α)	0.25	0	1.00	0.36	0.33	0.35
CIP	(B)	-	-	1	-	3	4
	(α)	-	-	1	-	22	23
	(B)/(α)	-	-	1.00	-	0.14	0.17
DCIP	(B)	-	-	0	-	1	1
	(α)	-	-	1	-	4	5
	(B)/(α)	-	-	0	-	0.25	0.20

(α): Total number of damages  
 (B): Number of damages due to permanent ground displacement

**Table 2** Physical properties of sand.

Specific gravity	2.67
Uniformity coefficient	2.96
Maximum void ratio	1.030
Minimum void ratio	0.721
50 percent diameter (mm)	0.2
Coefficient of permeability	0.0192
	(cm/s)

**Table 3** Dimensions of pipelines.

	SP	DCIP
Outer diameter (mm)	406.4	425.6
Thickness (mm)	6.0	8.5
Young's modulus (kgf/cm <sup>2</sup> )	2.1 x 10 <sup>6</sup>	1.6 x 10 <sup>6</sup>
Specific gravity	7.85	7.15

SP : Steel pipe  
 DCIP : Ductile cast iron pipe  
 ( 1kgf/cm<sup>2</sup> = 98kPa )

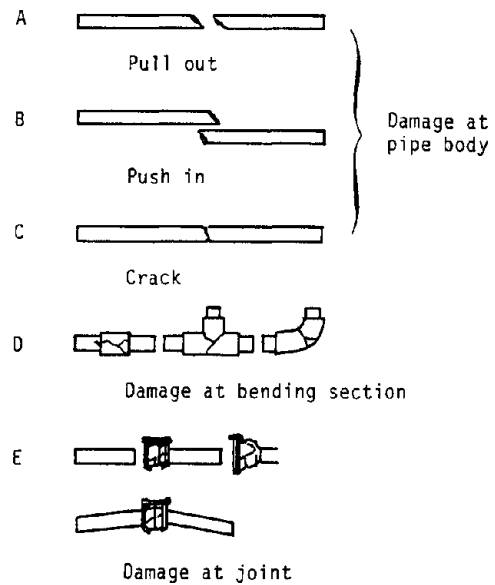


**Fig. 1** Failure modes of pipeline (from Noshiro City Gas and Waterworks Bureau, 1983).

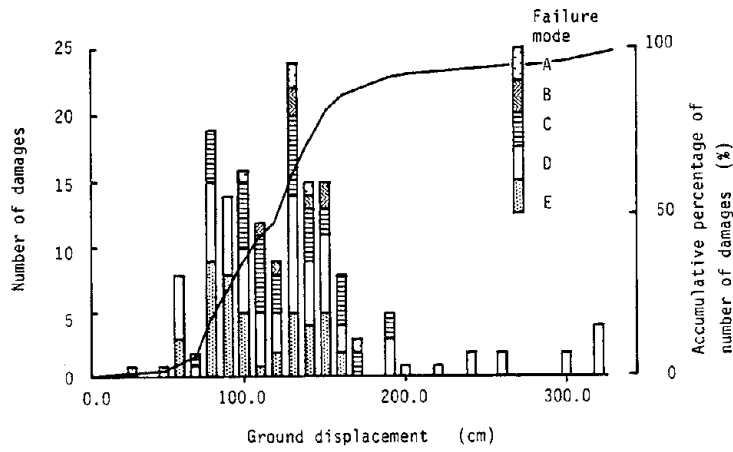


Fig. 2 Relationship between number of damages and permanent ground displacement .

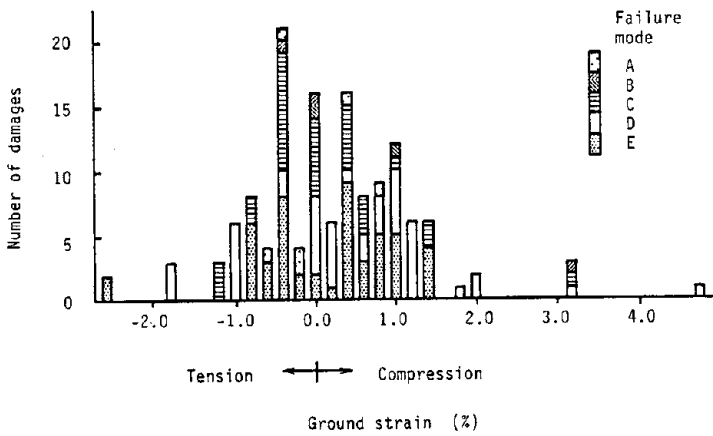


Fig. 3 Relationship between number of damages and average ground strain in longitudinal direction to the pipe axis .

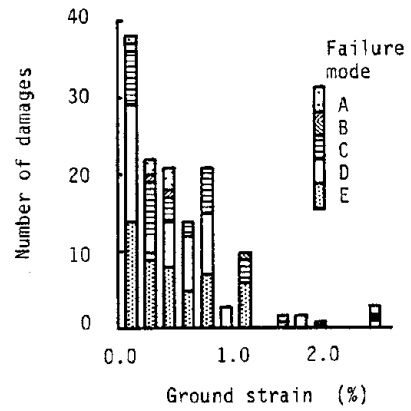


Fig. 4 Relationship between number of damages and average ground strain in transverse direction to the pipe axis .

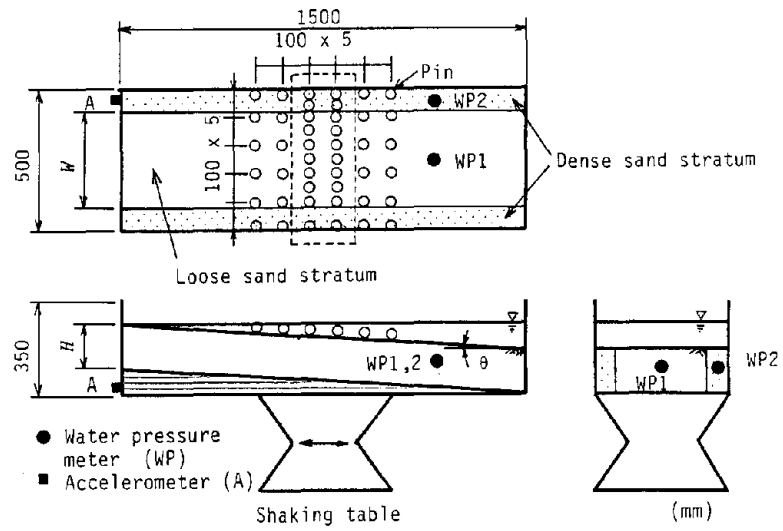


Fig. 5 General view of experimental apparatus.

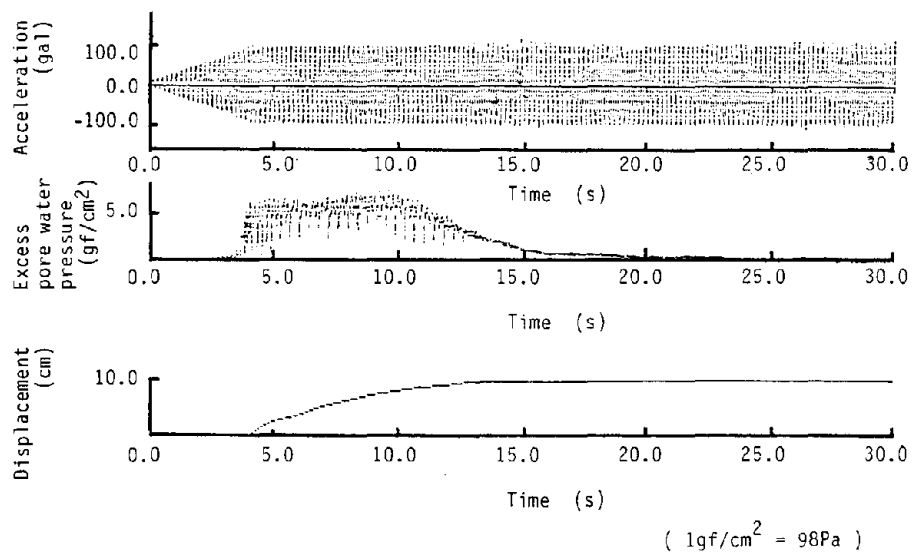


Fig. 6 Time histories of input acceleration, excess pore water pressure and permanent ground displacement at point 7.

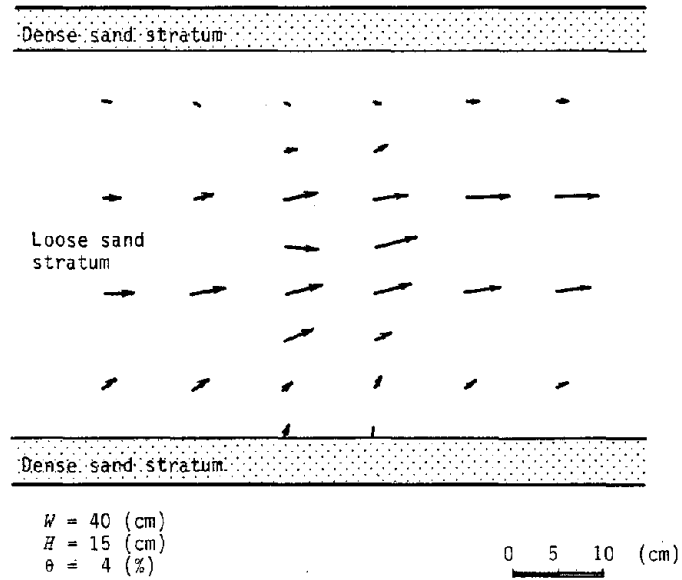


Fig. 7 Distribution of permanent ground displacement.

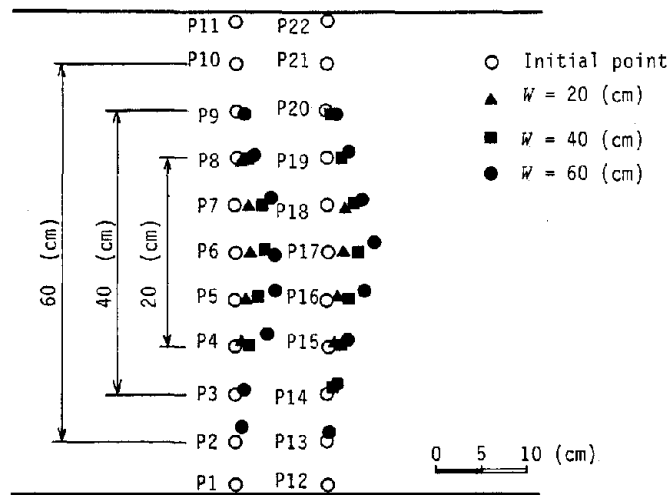


Fig. 8 Distribution of residual permanent ground displacement.

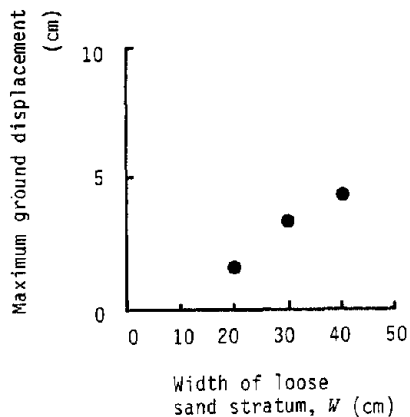


Fig. 9 Relationship between width of loose sand stratum and maximum ground displacement.

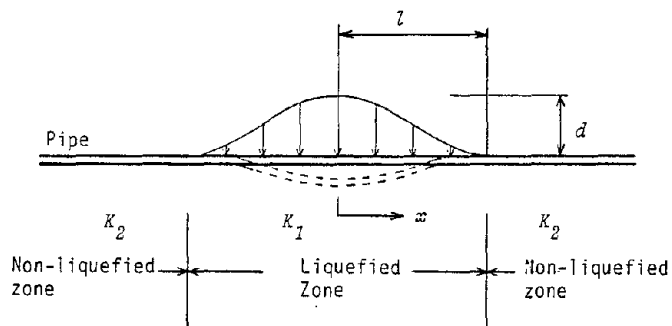


Fig. 10 Analytical model for permanent ground displacement (Plane figure).

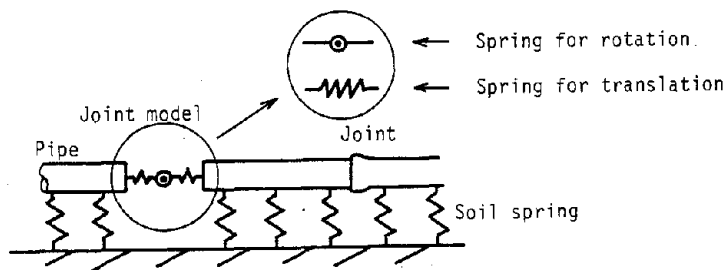


Fig. 11 Analytical model for jointed pipelines.

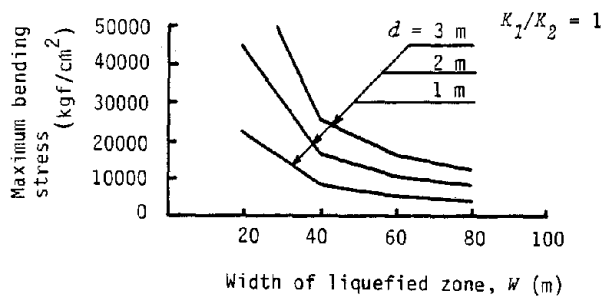


Fig. 12 Relationship between width of liquefied zone and maximum bending stress ( $K_1/K_2 = 1.0$ ).

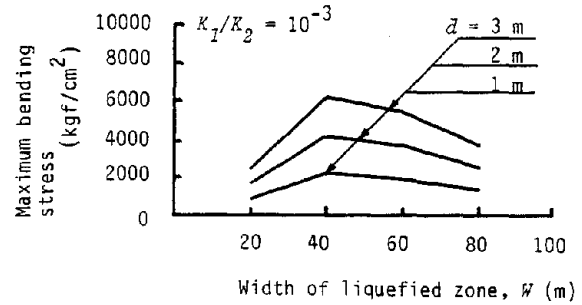


Fig. 13 Relationship between width of liquefied zone and maximum bending stress ( $K_1/K_2 = 10^{-3}$ ).

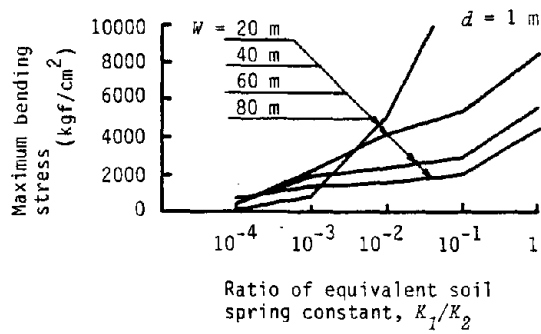


Fig. 14 Relationship between ratio of equivalent soil spring constant and maximum bending stress ( $d = 1$  m).

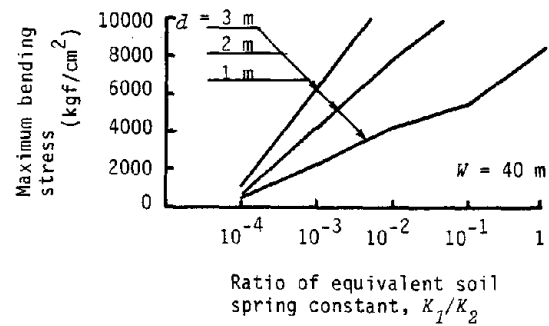


Fig. 15 Relationship between ratio of equivalent soil spring constant and maximum bending stress ( $W = 40$  m).



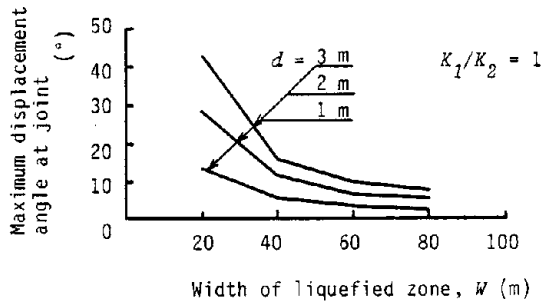


Fig. 16 Relationship between width of liquefied zone and maximum displacement angle at joint ( $K_1/K_2 = 1.0$ ).

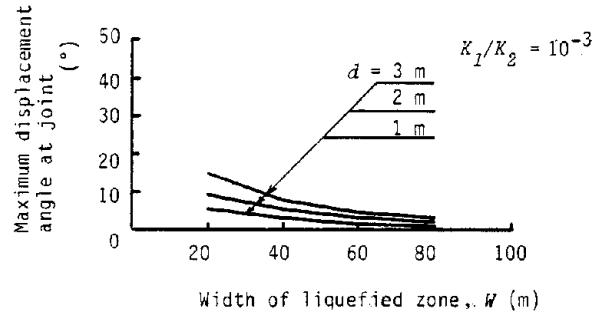


Fig. 17 Relationship between width of liquefied zone and maximum displacement angle at joint ( $K_1/K_2 = 10^{-3}$ ).

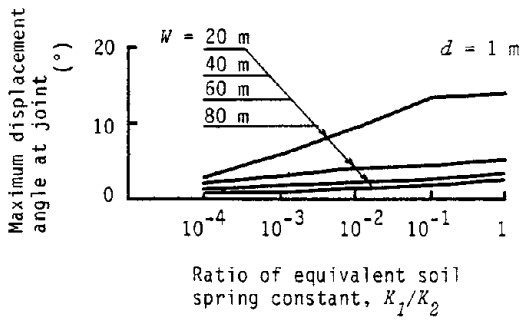


Fig. 18 Relationship between ratio of equivalent soil spring constant and maximum displacement angle at joint ( $d = 1\text{ m}$ ).

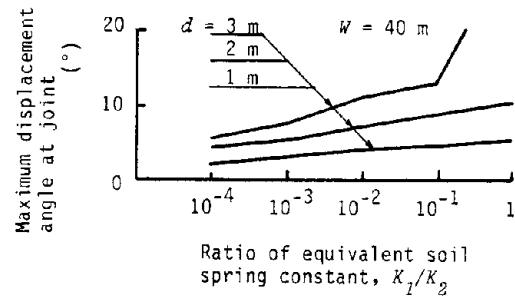


Fig. 19 Relationship between ratio of equivalent soil spring constant and maximum displacement angle at joint ( $W = 40\text{ m}$ ).

**ON BEAM MODE OF BUCKLING OF BURIED PIPELINES**

T. Ariman and B. J. Lee

College of Engineering and Applied Sciences  
University of Tulsa, Tulsa, Oklahoma 74104

**ABSTRACT**

Buried pipelines which lie on a base with localized imperfections are subject to compressive loading or displacements from the farfield. Pipelines in smaller diameters and shallow trenches tend to behave like beams. During the loading the pipe begins to lift upward and may buckle at a limit load which characterizes the beam type of buckling. In this paper beam mode of buckling of a buried pipeline is investigated. Results of a parametric study are obtained by a numerical method. A number of characteristic results for axial force vs uplifted length and on the effect of burial depth on limit load for three different soils are presented.

## INTRODUCTION

Earthquake behavior and safety of buried pipelines have attracted a great deal of attention in recent years [1-8]. Pipeline systems are generally built up over large geographical areas and therefore they are subjected to a variety of earthquake related hazards. Possible damage to buried pipelines could be due to permanent differential movements of ground by faulting, soil liquefaction, landslides, local compaction of ground and/or seismic waves, etc.

One of the most damaging effects on seismic activity on buried pipelines is buckling which falls into two categories. In a beam type of buckling, the pipe behaves basically as a beam and tends to bend itself out of the ground. Smaller diameter pipelines with shallow burial tend to behave like beams. The deformation in most of the cases reaches plastic stage; however, the pipe remains intact and continues to provide the service with no interruption. This type of failure is identified as "beam mode of buckling" [9-12]. It is suggested that in regions which may be subjected to large ground deformation this type of buckling may even be desirable because rupture, crushing, or breaking of the pipe can be avoided. The second type of possible buckling is the shell type which mostly occurs in large diameter pipelines with deep burial depth. It is usually associated with large local deformations (wrinkling), rupturing of the pipe and thus interruption of service. This type of buckling is named as "shell mode of buckling" [9-11]. In this paper beam mode of buckling is investigated and some representative results of a parametric study are presented.

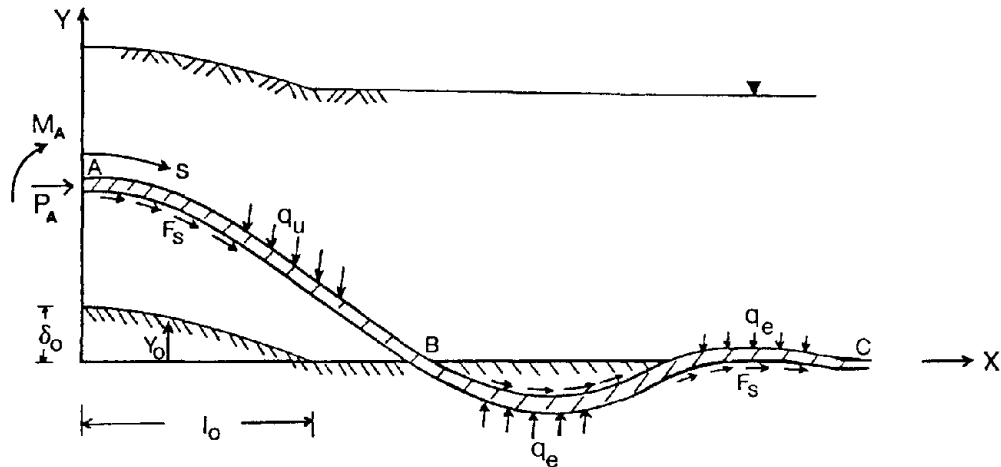
## BEAM MODE OF BUCKLING

The objective of this study is to deal with the beam type of buckling to improve the assumptions and remove the restrictions made in Ref. [11]. The buried pipelines, which lie on a base with localized imperfections such as bulges or hills, are subject to compressive loading or displacements from the far-field. The compression force is reduced by the frictional force before reaching the localized imperfection. During the loading process the pipe starts to lift upward and finally buckles at a limit load that characterizes the beam type of buckling. During uplifting, the pipe is subjected to certain uplift resistances from the soil which depends on the burial depth and soil properties.

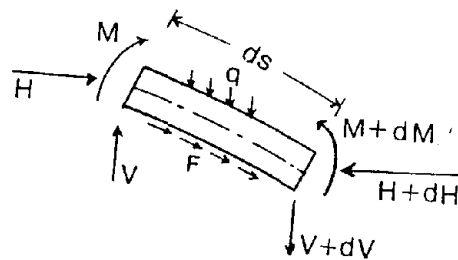
For the beam type of buckling in a previous publication, the pipe was modeled as a heavy beam on an imperfect, rigid or elastic foundation [11]. The large displacement response of the beam

under axial loading was found to be governed by a limit load which is imperfection-sensitive. The formulations of the theory in this work impose no restrictions on the size of displacements and rotations and hence make possible an analysis of the entire postbuckling range. It also combines the compressible nature of the member and an elasto-plastic moment-curvature relation and furthermore accounts for the effect of the soil medium.

### Governing Equations



a. Free Body Diagram



b. Elemental Equilibrium

Figure 1. One-half of a Buried Pipeline on a Locally Bulged Base.

Fig. 1a shows a buried pipeline lifted upward by a compressive axial force or displacement from the far-field, and the uplifting initiates at the zone of foundation imperfection. Due to the pipe sliding, the soil provides opposing frictional force  $F_s$ . The subgrade reaction on the pipe movement is applied differently for two sections: a non-linear uplift resistance on section AB,  $q_u$ ; and an elastic force on section BC,  $q_e$ , where the large deformation is not involved. The X-axis is taken along the

straight foundation and Y-axis is used to define the vertical displacement. The distance along the deformed line is  $s$ , and the angle of inclination is  $\theta$ .  $\delta_0$  and  $l_0$  are the amplitude and half length of the imperfection, respectively. Fig. 1b shows an infinitesimal beam element of length  $ds$  which carries a horizontal force  $H$ , a transverse force  $V$ , a bending couple  $M$ , foundation reactive force  $q$  ( $q_u$  or  $q_e$ ), and friction force  $F$  per unit of length. The exact differential equations can be derived based on the geometry and force equilibrium of the deformed element. These non-linear equations including the plastic effects are given as follows:

$$\frac{dM}{ds} = (1 + \epsilon_a) [V \cos \theta + H \sin \theta] \quad (1)$$

$$\frac{dV}{ds} = q - F_s (1 + \epsilon_a) \sin \theta \quad (2)$$

$$\frac{dH}{ds} = F_s (1 + \epsilon_a) \cos \theta \quad (3)$$

$$\frac{dX}{ds} = (1 + \epsilon_a) \cos \theta \quad (4)$$

$$\frac{dY}{ds} = - (1 + \epsilon_a) \sin \theta \quad (5)$$

$$M = \int_A \sigma_z Z dA \quad (6)$$

Where  $A$  is the cross-sectional area of the pipe;  $\epsilon_a$  is the axial strain in the beam section; and  $\sigma_z$  is the stress in the beam section at a distance  $Z$  from the centroidal axis.

For section AB, the non-linear soil force  $q_u$  in resisting the uplift movement of the pipe is given as

$$q_u = K_u (Y - Y_0) \quad (7)$$

Where  $Y_0$  is the magnitude of the imperfection at the location  $X$  and  $K_u$  is represented by a hyperbolic function [12]:

$$K_u = \frac{\gamma_s H_c D F'_{\max}}{Y'_f} \cdot \frac{1}{\alpha D + \frac{\beta}{Y'_f} (Y - Y_0)} \quad (8)$$

in which  $\gamma_s$  is the effective unit weight of soil;  $H_c$  represents depth from the ground surface to center of the pipeline;  $D$  is the external pipeline diameter;  $F'_{\max}$  and  $Y'_f$  are the non-dimensionalized maximum force and displacement, respectively; and  $\alpha$  and  $\beta$  represent curve - fitting coefficients. The values of  $F'_{\max}$ ,  $\gamma_s$ ,  $\alpha$  and  $\beta$  are obtained from experimental results [12] and are listed in Table 1. For relatively straight section BC, the intensity of the reaction force  $q_e$  at a point is assumed to be proportional to the deflection of the beam at that point, i.e.  $q_e = K_e (Y - Y_0)$ , and  $K_e$  is the soil stiffness.

$$K_e = 0.65 \left[ \frac{E_s D}{E I} \right]^{1/12} \cdot \frac{E_s}{1 - \mu_s^2} \quad (9)$$

where  $E_s$  is Young's modulus of the soil;  $E$  is Young's modulus of the pipe;  $I$  is the moment of inertia of the pipe section; and  $\mu_s$  represents Poisson's ratio for soil.

**Table 1. Material Properties and Force-Displacement Parameters**

	Sand	Loose	Medium	Dense		
$\gamma_s$		0.094	0.104	0.113		
$\phi$		31°	36°	44°		
$\alpha$		0.05	0.1	0.07		
$\beta$		0.95	0.9	0.93		
$H_c/D$	$F'_{\max}$	$Y_f/H_c$	$F'_{\max}$	$Y_f/H_c$	$F'_{\max}$	$Y_f/H_c$
1.5	1.3	0.0162	1.2	0.01	1.6	0.0088
4	2.0	0.0081	3.3	0.005	3.45	0.006
8	2.2	0.0039	5.3	0.012	7.2	0.0088
13	2.6	0.0028	8.0	N/A	11.3	N/A

As a result of pipe movements, longitudinal friction forces develop between the soil and pipe. The maximum axial soil force  $F_s$  per unit length of pipeline for a fully buried -line can be expressed as:

$$F_s = \frac{\pi D}{2} \gamma_s H_c (1 + K_0) \tan \phi_p \quad (10)$$

Where  $K_o$  is the coefficient of soil pressure at rest, approximately 0.5 for loose to moderately dense sand; and  $\phi_o$  is the interface angle of friction between soil and pipeline, approximately  $20^\circ$  for a smooth wall of steel buried in sand.

The long distances associated with buried pipeline systems greatly increase the likelihood of localized imperfection such as passing over small hills or locally bulged base and initial crookedness or ovalization of the pipe itself, etc. In this study, the imperfections are introduced into the supporting base in the form of the following for the amplitude and inclination respectively.

$$Y_o = \delta_o \left[ \frac{4X}{l_o} + 1 \right] \left[ \frac{X}{l_o} - 1 \right]^4 \quad X < l_o \quad (11)$$

$$\theta_o = - \text{Arctan} \left[ 20 \frac{\delta_o}{l_o^2} X \left[ \frac{X}{l_o} - 1 \right]^3 \right] \quad X < l_o \quad (12)$$

In the analysis, the pipeline is treated differently in three regions: an uplift region AB, a region with little deformations BC and a straight section from point C to the source where the axial force or displacement is induced. The section AB is subjected to the non-linear uplift resistance of the soil. The section BC is considered to be a beam on the elastic foundation. The straight section is assumed to remain straight and is not involved in the numerical analysis.

Due to the non-linear nature of the problem, a numerical solution that involves iterative improvements of initial guesses of the solution is required. A modified Newton-Raphson is used to obtain numerical results. Note that the iteration methods reduce the non-linear problem to the solution of a series of linear equations.

## RESULTS AND DISCUSSIONS

It has been recognized that for the perfect system there is no apparent bifurcation or limit point, and as the imperfection amplitude approaches zero asymptotically, the equilibrium axial load approaches infinity. A limit point is defined as the point on the equilibrium path at which the axial load is a relative maximum.

All cases herein are restricted to the foundation imperfections of the form given in Eqs. (11) and (12), and have the following system characteristics:

Pipe length for section AC (L) = 100 feet

Pipe diameter (D)	=	18	inches
Pipe thickness (t)	=	.562	inches
Young modulus of pipe (E)	=	$30 \times 10^3$	ksi
Yield stress of pipe ( $\sigma_y$ )	=	72	ksi

The material properties and force-displacement parameters for loose, medium and dense sands are given in Table 1. The half length of foundation imperfection is fixed at  $l_0 = 10$  feet so that an increase in the imperfection amplitude  $\delta_0$  represents an increase in the initial curvature of the foundation. The system for all cases is divided into 100 segments with 99 internal nodes.

Fig. 2 shows the axial load - vertical displacement curves for three values of imperfections ( $\delta_0/l_0 = 0.1, 0.2, 0.3$ ). Here,  $P_A/P_y$  denotes axial force  $P_A$  at point A nondimensionalized by the yield force  $P_y$  ( $P_y = \sigma_y A$ ,  $A$  is the pipe cross-sectional area) and  $Y_A$  the vertical displacement at point A. The results show that the overall response is quite sensitive to the magnitude of the imperfections, and a limit point at which pipe instability occurs characterizes the beam type of buckling. The slopes of the prebuckling paths are much steeper than those of the postbuckling paths. This indicates that a considerable loading is needed to buckle the pipe at a small displacement and afterward the unloading initiates accompanied by a substantial displacement. Also, at the onset of buckling, the slopes of the postbuckling paths decrease as the initial curvature of the foundation increases.

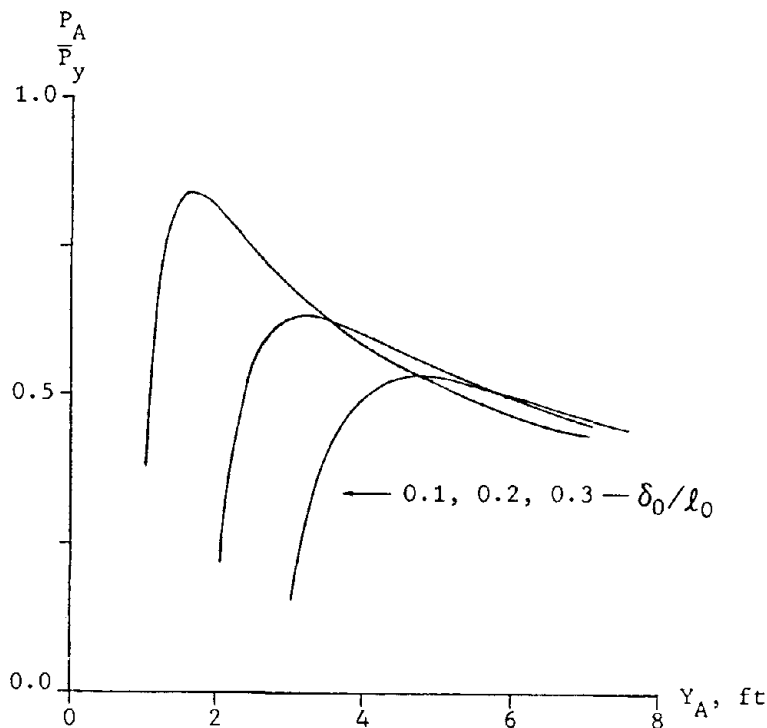
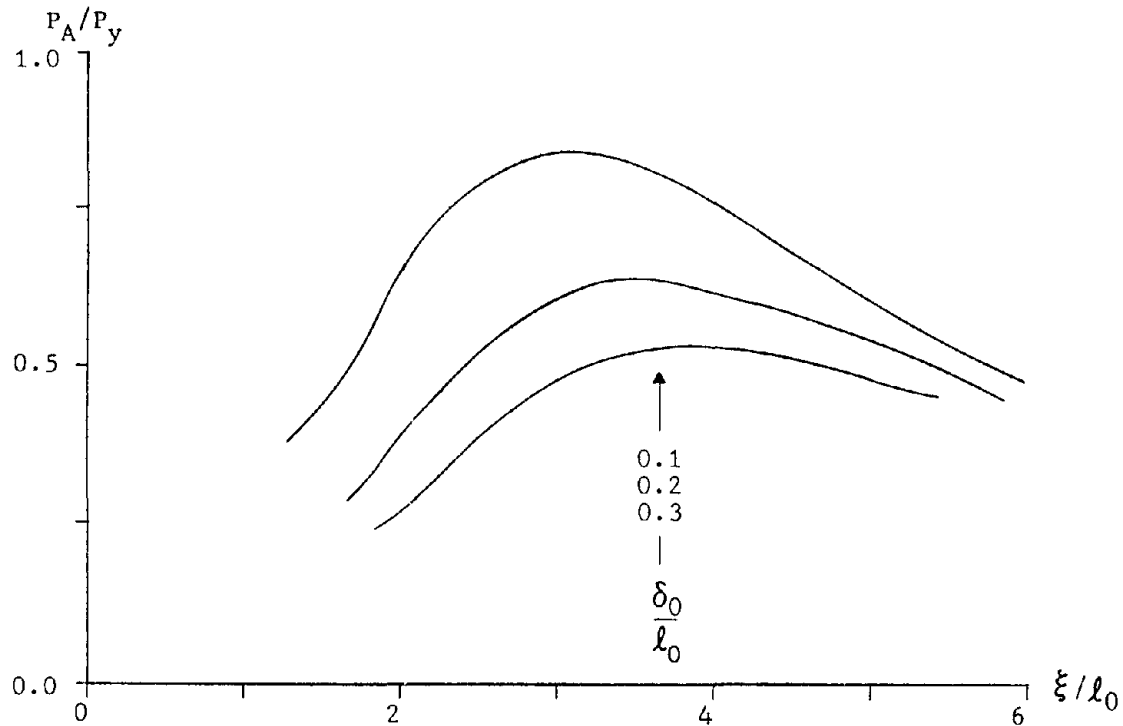


Figure 2. Limit Load vs. Crest Displacement

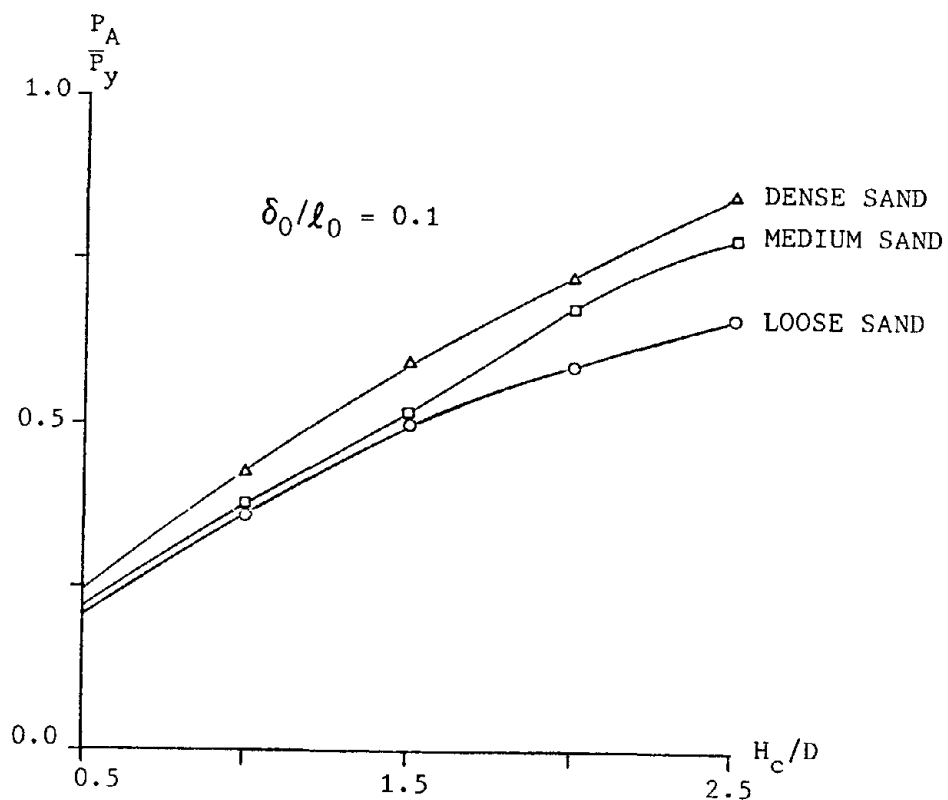




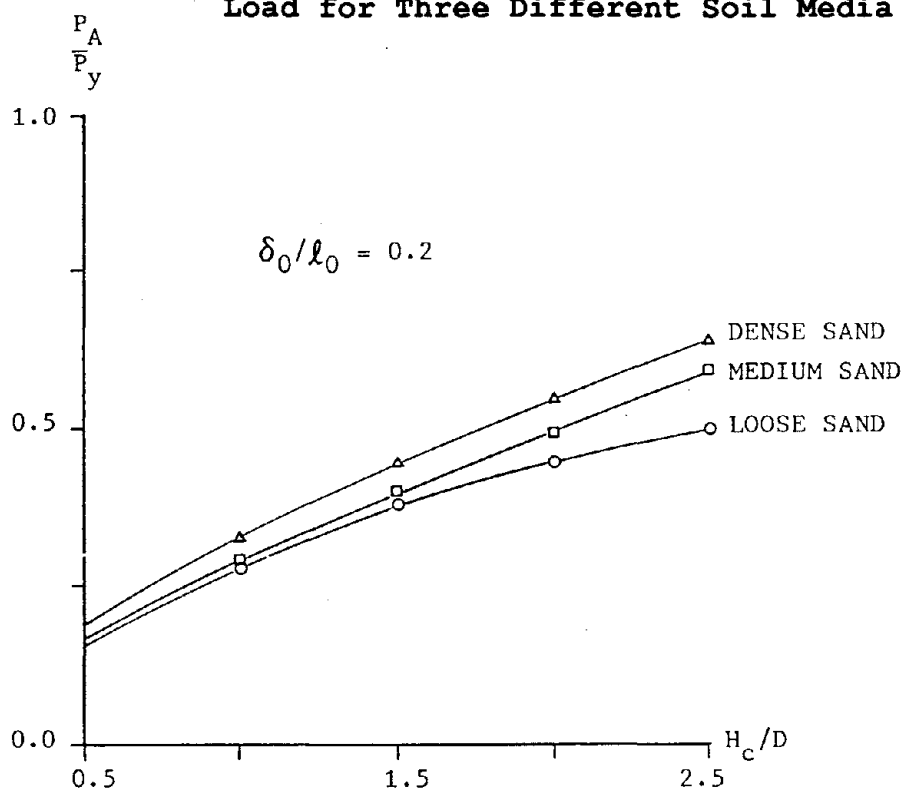
**Figure 3. Axial Force vs. Uplifted Length**

Fig. 3 shows the uplifted length  $\xi$  versus the axial force for three initial curvatures. The uplifted length at the limit point is somewhat longer for the large imperfection cases even though a smaller axial load is needed to buckle the pipe. Once the limit load is reached, the pipe lifts up at a rather fast pace that is usual to large imperfection cases. Determination of the length of the uplifted section of the pipeline could be important in the possible repair and replacement of the stated section in the case of an earthquake.

Figures 4-6 show the effects of the burial depth  $H_c$  that is nondimensionalized by dividing by the pipe diameter  $D$  on the limit load for loose, medium and dense sands for three foundation imperfections respectively. These case studies are used to show the important influences of nonlinear soil forces in resisting the uplift motion of the pipe on the critical load. It can be seen that an increase in either burial depth or soil density increases the soil resistances and thus leads to a higher buckling load. Also, as the burial depth decreases, the limit loads for three soil cases converge to the same value. Also, a preliminary study has shown that a moderate variation of the foundation modulus for section BC does not affect both the response and particularly the limit load much as long as there exists certain types of imperfections. This finding is consistent with the case studies for the pipes on the ground surface [11]. Therefore, the effects on the limit load would be mostly due to the soil uplift resistances in the section AB.



**Figure 4.** The Effect of Burial Depth on Limit Load for Three Different Soil Media



**Figure 5.** The Effect of Burial Depth on the Limit Load for Three Different Soil Media

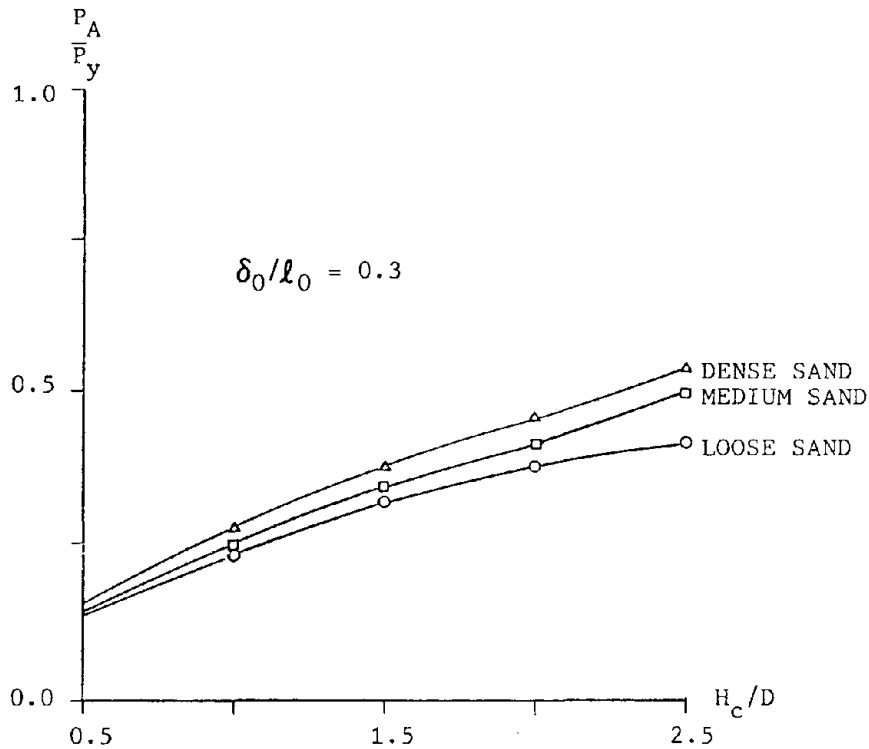


**Figure 6. The Effect of Burial Depth on Limit Load for Three Different Soil Media**

In all cases analyzed, the limit load does not exceed  $P_y$  and thus a simple elastic analysis is of availability. It is to be noted that if the imperfection gets less and approaches zero, the required buckling load may exceed  $P_y$  and the pipe would fail by plastic yielding, possibly subject to the shell type of buckling. Nevertheless, the present pipes tend to lift up and behave like a beam even well into the late postbuckling stage.

#### ACKNOWLEDGEMENTS

Research, from which this paper was developed, was sponsored by the National Center for Earthquake Engineering Research (NCEER) at the State University of New York, Buffalo, NY. The support and encouragement of NCEER are gratefully acknowledged. Thanks also are extended to N. Whipple for her expert help in the preparation of the manuscript.

**REFERENCES**

1. Ariman, T., "A Review of Buckling and Rupture Failures in Pipelines Due to Large Ground Deformations", Earthquake Behavior and Safety of Oil and Gas Storage Facilities, Buried Pipelines and Equipment, Edited by T. Ariman, PVP-77, ASME, 176-180, 1983.
2. Ariman, T., "Behavior of Pipelines Due to Large Ground Deformations", Proceedings of the 8th World Conference on Earthquake Engineering, 271-278, 1984.
3. Lee, L. H. N., Ariman, T., and Chen, C. C., "Elastic-Plastic Buckling of Buried Pipelines by Seismic Excitation", International Journal of Soil Dynamics and Earthquake Engineering, Vol. 3, No. 4, 168-173, 1984
4. O'Rourke, T. D. and Trautmann, C. H., "Analytical Modeling of Buried Pipeline Response to Permanent Earthquake Displacement", Geotechnical Engineering Report 80-4, July 1980.
5. O'Rourke, T. D. and Trautmann, C. H., "Buried Pipeline Response to Permanent Earthquake Ground Movements", ASME paper 80-C2/PVP-78, 1980.
6. Newmark, N. W. and Hall, W. J., "Pipeline Design to Resist Large Fault Displacement", Proc. U.S. National Conference on Earthquake Eng., Ann Arbor, MI, 416-425, 1975.
7. Kennedy, R. P., Chow, A. W., and Williamson, R. A., "Fault Movement Effects on Buried Oil Pipeline", Journal of Trans. Engr., ASCE, TE5, 617-633, 1977.
8. Wang, L.R.L., "Parametric Investigation of Buried Pipe Under Seismic Environments", Proc. of the 8th World Conf. of Earthquake Engr., San Francisco, Vol. VII, 483-490, 1984.
9. Lee, B. J. and Ariman, T., "Buckling of Buried Pipelines Crossing an Active Fault", Seismic Performance of Pipelines and Heavy Tanks, Edited by A. C. Singhal and T. Ariman, PVP-98-4, pp. 25-34, 1985.
10. Ariman, T., Lee, B. J., and Chen, G. Q., "Failure of Buried Pipelines Under Large Ground Deformations", Recent Advances in Lifeline Earthquake Engineering, Edited by T. Ariman et al, Computational Mechanics Publications, Southampton, UK, 1987.
11. Kyriakides, S., Yun, H. D., and Yew, C. H., "Buckling of Buried Pipelines Due to Large Ground Deformations", PVP-77

ASME, Edited by T. Ariman, 140-150, 1983.

12. Trautmann, C. H. and O'Rourke, T. D., "Behavior of Pipe in Dry Sand Under Lateral and Uplift Loading", Geotechnical Engineering Report 83-7, May 1983.
13. Eisenstat, S. C., Schultz, M. H., and Sherman, A. H., "Application of Sparse Matrix Methods to Partial Differential Equations", Proc. of AICA International Symposium on Computer Methods for Partial Differential Equations, Bethlehem, PA, 40-45, 1975.

**MODELING OF PERMANENT GROUND DEFORMATION FOR BURIED PIPELINES**

Nobuhisa SUZUKI

Engineering Research Center, NKK Corporation

Takashi KOBAYASHI

Pipeline Department, Tokyo Gas Co., Ltd.

Hiroyuki NAKANE

Pipeline Planning and Administration Dept., Tokyo Gas Co., Ltd.

Masami ISHIKAWA

Gas Industries Department, NKK Corporation

**ABSTRACT**

Spatial distribution and modeling of liquefaction-induced permanent large ground displacement are presented on the basis of case history information of the 1964 Niigata Earthquake in a 1000m\*800m rectangular area. Ground deformation in the area of interest can be classified into stream-flow-like and vortex-like movement as a result of the spatial distribution analysis of the ground displacement vectors. The ground displacement patterns, which are peculiar to the modeling for the buried pipelines subject to axial or flexural deformation, are simply characterized by the length or the width of the patterns along the pipelines and their maximum displacement. The idealized ground displacement patterns and the results of quantitative analysis will be quite effective for the safety assessment and the seismic design of the pipelines buried in a liquefiable zone.

## INTRODUCTION

The liquefaction-induced permanent ground movement, which is related closely to soil layer profiles of the estimated liquefaction zone, is a significant parameter for the safety assessment of underground structures such as the buried pipelines and foundation piles (Refs.1-4).

As for the foundation piles, we can estimate the displacement pattern of the permanent ground movement along the foundation piles. It is because that collapse modes or damages to the piles have revealed some evidence with respect to the relationship between possible patterns of the ground displacement and the failure modes of the foundation piles. Actually nonlinear finite element analysis of the piles of the N-building in Niigata City have successfully predicted a trapezoidal or a triangular pattern of the ground displacement along the piles (Ref.5).

On the other hand, we have to estimate the spatial distribution of the ground displacement for the seismic design and deformation analysis of the buried pipelines. It may be more difficult than the case of foundation piles to perform the estimation as we have to deal with much more information over a wide area in which lifeline networks are extended. In fact, we have not developed appropriate methodology to know the spatial distribution of the ground displacement.

The objective in this paper is therefore to make an attempt to perform the modeling or idealization of the permanent ground deformation required for the buried pipelines through investigating the permanent ground displacement occurred during the 1964 Niigata Earthquake.

## LARGE GROUND DEFORMATION IN NIIGATA CITY

### Measured Ground Displacement in the Area of Interest

Figure 1 shows the 1000m\*800m rectangular area of interest in the south of which the Niigata Railway Station is located (Ref.1). The rectangular area

covers the center of Niigata City where lifeline network systems for gas and water distribution had been constructed before 1964.

Figure 2 represents the permanent ground displacement vectors occurred during the 1964 Niigata Earthquake, which displacement vectors were measured at many specified points on the ground such as manholes, the lower end of poles and corners of buildings. Other hand, we have omitted the other data measured at roof edges, fences and guard rails because they are not supposed to have behaved similarly to the ground movement. The area of interest illustrated in Fig.2 is discretized into regular squares every 50 meter length. The location of any square with arbitrary size can be identified by the coordinates at the left bottom and the top right using the row numbers from 1 through 21 and rank symbols from A through Q, respectively. For example, the entire area of interest can be represented by 1A and 21Q, and we hereinafter describe the area in this case as (1A,21Q).

### Calculated Ground Deformation

Figure 3 shows the calculated permanent ground displacement at every point of intersection. Displacement at the points of intersection was calculated by interpolation or extrapolation with a second order polynomial selecting more than four measured data adjacent to the corresponding point.

The calculated permanent ground displacement in the area of interest can be separated into two groups by a vertical line between the points 9A and 9Q. One of the groups of the displacement vectors corresponds to the left hand side area of (1A,9Q), and those of another group are involved in the area of (9A,21Q).

The displacement vectors of the upper squares in the left side region of the area of interest, which can be expressed as (1M,2Q), tend to direct towards the east. The vectors of the lower squares, on the other hand, direct towards the south and the other vectors in the intermediate region change gradually their directions towards the south. All the vectors seem to form stream-flow-like movement.

On the other hand, the displacement vectors in the right side of the area seem to make a maelstrom revolving in a counter clockwise direction around a



square of (14I,15J). Furthermore, we can find some vectors spreading outwards the maelstrom in the lower portion of the right side area (17A,21F).

Figure 4 is provided to express intelligibly the deformed configuration of the rectangular area, which configuration is illustrated by combining the adjacent displacement vectors shown in Fig.3. Figure 4 is therefore of great help to our comprehension with respect to the magnitudes of the ground distortion induced in every regular square, which may be related to the ground strain.

The large deformation in the squares of (13I,21K) is conspicuous among the permanent ground movement shown in Fig.4. In particular the square of (13I,14J) is subject to significant compressive deformation, and the squares of (15I,21K) undergo large shear deformation.

Figures 5 and 6 are provided for supplementary data for the permanent ground deformation. Figure 5 represents contour lines with 0.2 meter intervals for absolute values of the ground displacement. The maximum displacement of 2.63 meters can be observed at the top left of the rectangular area and the minimum displacement of 0.06 meters at the bottom right. Observing the entire area, the displacement from 1 to 2 meters is predominant in the figure.

Fig.6 expresses the contour lines with respect to the directions of the displacement vectors every 30 degree transformation. The contour lines in Fig.6 represents smooth changes in the direction in the left half of the entire area and the upper quarter in the right half of the entire area. On the contrary, we can observe high density of the contour lines near the center of the right half of the rectangular area which tendency means that there are sudden changes in the direction of the displacement vectors.

## **MODELING OF PERMANENT GROUND DEFORMATION**

### **Displacement Patterns for Buried Pipelines**

It is needless to say that the permanent ground displacement along the buried pipelines are the most important data for the deformation analysis of the

buried pipelines (Refs.2-4). It is possible for us to make an assumption of arbitrary geometry of the buried pipelines to obtain the ground displacement along the buried pipelines. However, we would like to investigate the ground displacement along the lines of the 50 meter squares as presented in Figs 3 and 4. We can regard the lines consist of mesh as a lifeline network system in this case.

The liquefaction-induced permanent ground displacement for straight pipelines can be idealized as Figs.7 and 8. Figure 7 shows the longitudinal displacement patterns of permanent ground deformation, which may result in the axial deformation of the buried pipelines. The upper pattern in Fig.7 may induce compressive deformation into the pipeline and the lower pattern tensile deformation. The axial deformation can be identified by the length of transition area  $L$  and the relative ground displacement  $D_{\max}$ .

While the buried pipelines may subject to flexural deformation under the displacement pattern shown in Fig.8, which corresponds to the lateral spread and the displacement vectors are normal to the pipe axis. The pattern of the lateral permanent ground displacement can be expressed by parameters of the width of the ground displacement  $W$  and the maximum ground displacement  $D_{\max}$ .

### **Longitudinal Displacement Pattern**

Figure 9 shows the ground displacement along the mesh lines, which is calculated from the vectors in Fig.4. We can extract the longitudinal ground displacement patterns illustrated in Fig.7 from Fig.9.

Figure 10 represents the results of the extraction, in which the horizontal axis expresses the length of transition zone  $L$  and the vertical axis the maximum relative ground displacement  $D_{\max}$ . The positive values of  $D_{\max}$  correspond to the tensile deformation of the pipeline and the negative values the compressive deformation, respectively. Furthermore, the white marks represent  $D_{\max}$  obtained on the horizontal mesh lines and the black marks correspond to the data on the vertical mesh lines.

Figure 10 clarifies a linear relationship between  $D_{\max}$  and  $L$  for the compressive axial deformation. On the other hand, we do not have enough data of the tensile axial deformation especially for larger values of  $L$ . However,

we can recognize the similar tendency to the compressive deformation.

### Lateral Displacement Pattern

Figure 11 shows the lateral permanent ground displacement over the entire rectangular area, which was obtained from the displacement illustrated in Fig.4. Figure 12 represents the relationship between the parameters of  $W$  and  $D_{\max}$ , which characterize the lateral spread of soils as illustrated in Fig.8.

The results show the maximum displacement  $D_{\max}$  are not so sensitive to the change of the width of the lateral spread  $W$ , however, a linear relationship can be recognized between the parameters  $W$  and  $D_{\max}$ .

### CONCLUSIONS

The permanent ground movement observed in the 1000m\*800m rectangular area in Niigata City were discussed on the basis of case history information of the 1964 Niigata Earthquake representing the contour lines of the displacement vector or the spatial distribution of the ground displacement vectors. Also the displacement patterns of the ground movement, which consisted of the longitudinal displacement and the lateral spreading, were investigated quantitatively. We consequently obtained the following conclusions.

Ground deformation in the area of interest can be classified into the stream-flow-like movement and the vortex-like movement as a result of the spatial distribution analysis of ground displacement vectors.

From the pattern analysis of the longitudinal and the lateral ground displacement pattern, the length of the displacement patterns of the permanent ground movement, that may effect on the deformation of the buried pipelines, may reach several hundred meters.

On the other hand, we have not been able to focus on the local deformation which width were less than 50 meters. The narrow width local ground deformation may be a significant effect on the nonlinear deformation of

relatively small diameter buried pipelines. However the local ground deformation with narrow width can not be required for the deformation analysis of large diameter buried pipelines, so that the idealized ground displacement presented in this paper are applicable to the safety assessment of larger diameter pipelines.

#### ACKNOWLEDGEMENTS

The authors would like to thank Mr.I.Kubo and Mrs.M.Nishigaki of the Japan Industrial Technology Co., Ltd. for their help in the preparation of this paper.

#### REFERENCES

1. Hamada, H., Yasuda, S., Isoyama., R. and Emoto, K., "Study on Liquefaction Induced Permanent Ground Displacements," ADEP, 1986, 87p.
2. Kobayashi, T., "Recommended Practice for the Earthquake-Resistant Design of Gas Pipelines, with Liquefaction Considered," Proc. of First Japan-the U.S. Workshop, 1988, pp.212-221.
3. O'Rourke, T.D., "Critical Aspects of Soil-Pipeline Interaction for Large Ground Deformation," Proc. of First Japan-the U.S. Wokshop, 1988, pp.118-126.
4. Suzuki, N., Arata, O. and Suzuki, I., "Parametric Study on Deformation Analysis Welded Pipeline Subject to Liquefaction-Induced Permanent Ground Displacement," Proc. of First Japan-the U.S. Workshop, 1988, pp.155-162.
5. Kawashima, K., Shimizu, K., Mori, S., Takagi, M., Suzuki, N. and Nakamura, S., "Analytical Studies on Damage to Bridges and Foundation Piles Caused by Liquefaction-Induced Permanent Ground Displacement," Proc. of First Japan-the U.S. Workshop, 1988, pp.99-117.

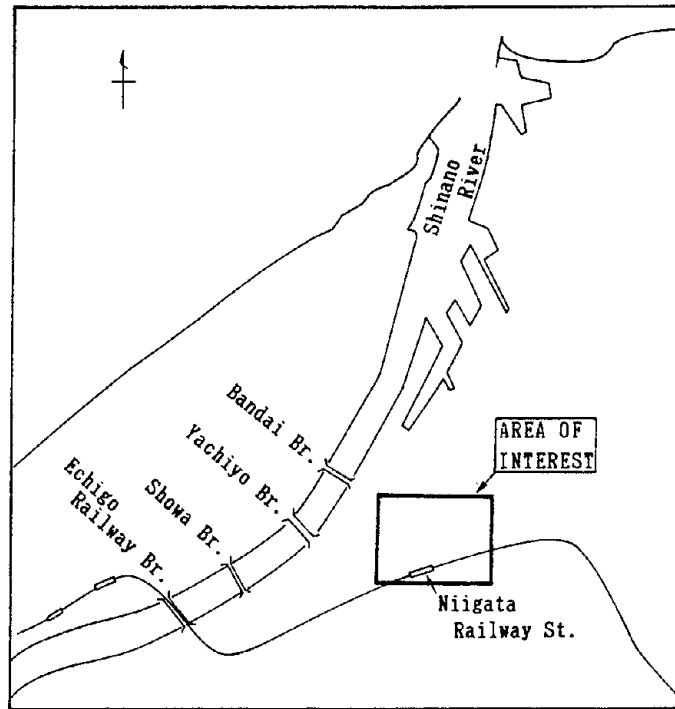


Figure 1 Niigata Area of Lateral Spreads during 1964 Niigata Earthquake

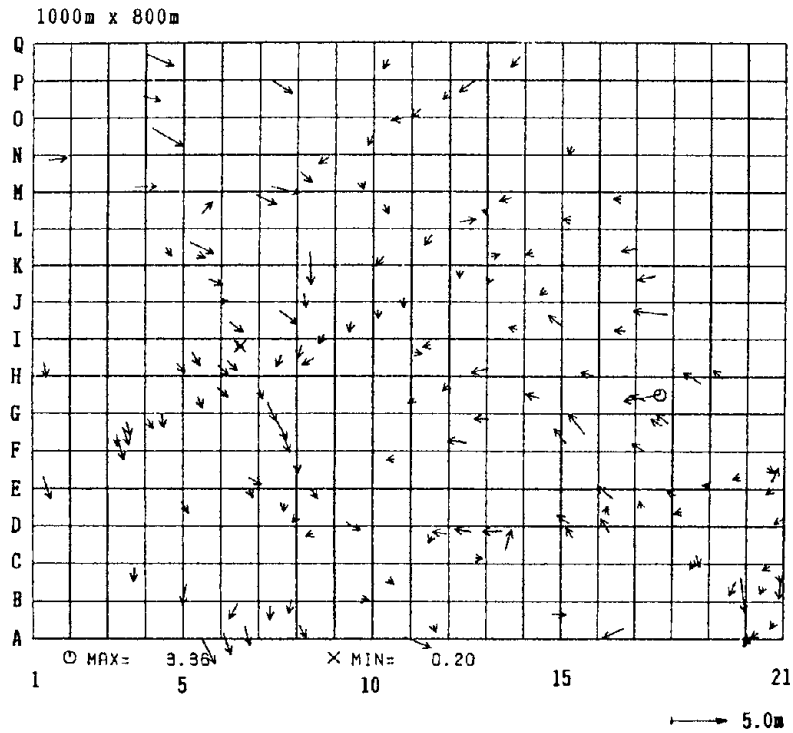


Figure 2 Measured Permanent Ground Displacements in Area of Interest

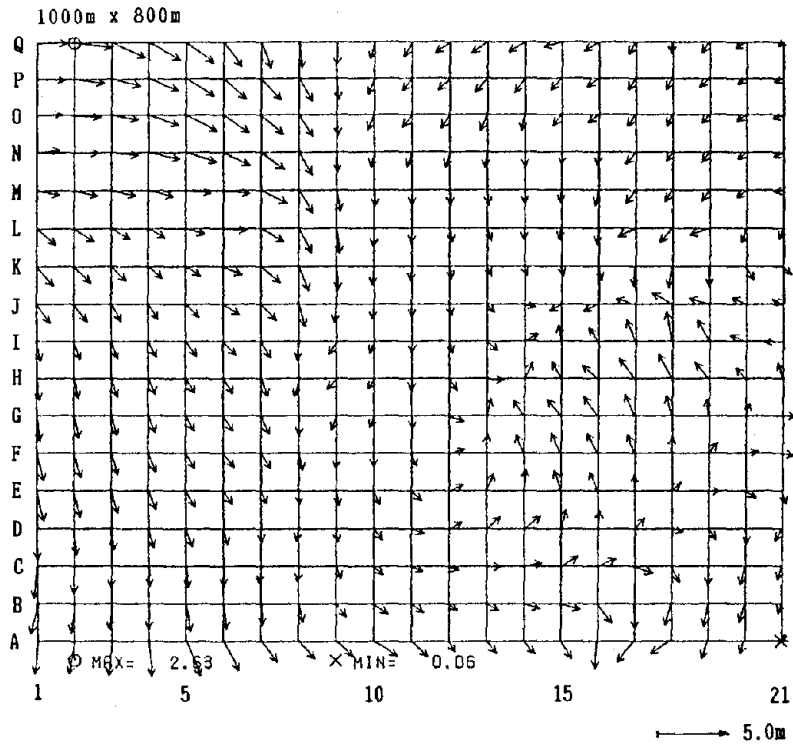


Figure 3 Calculated Displacement Vectors of P.G.D.

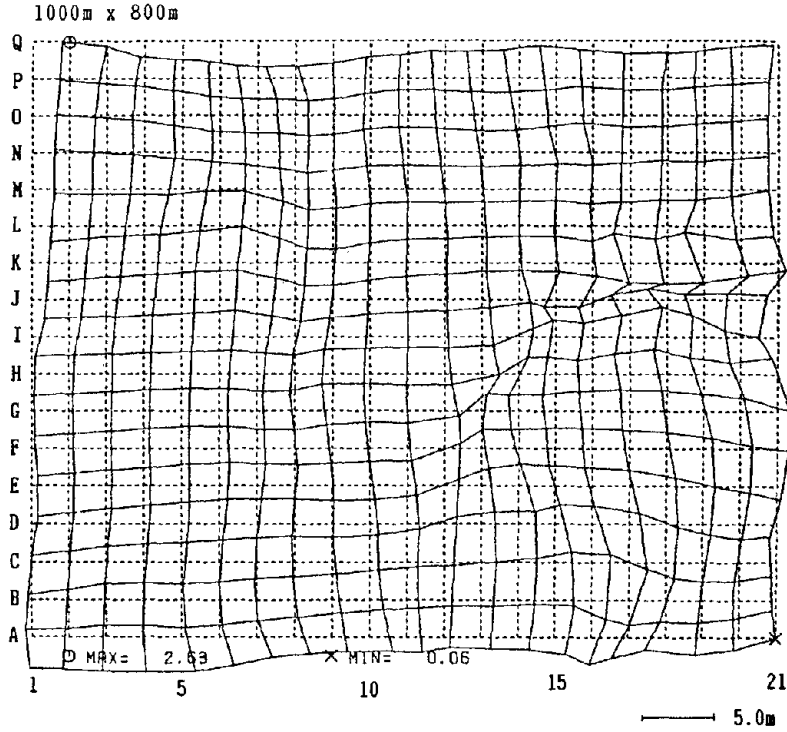


Figure 4 Calculated Permanent Ground Deformations

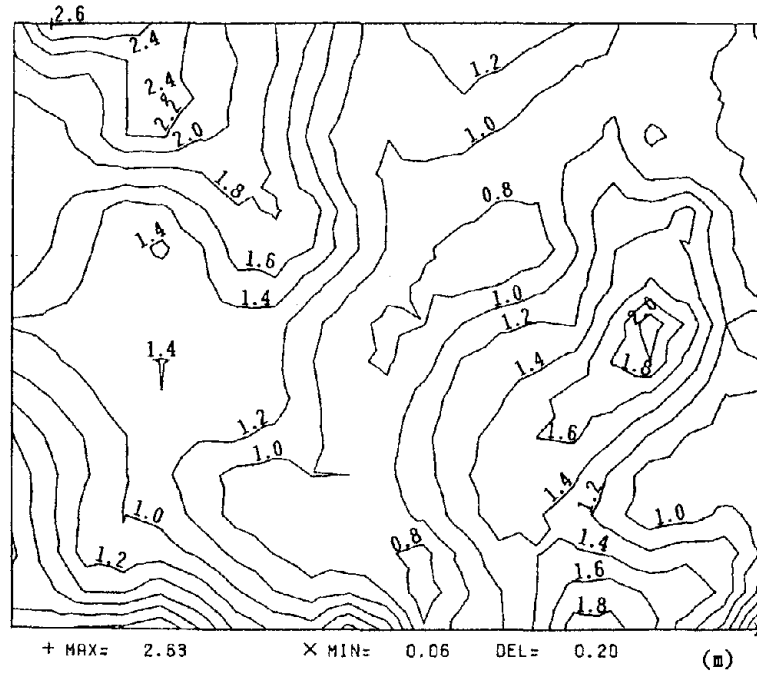


Figure 5 Contours for Magnitudes of Calculated Displacements of P.G.D.

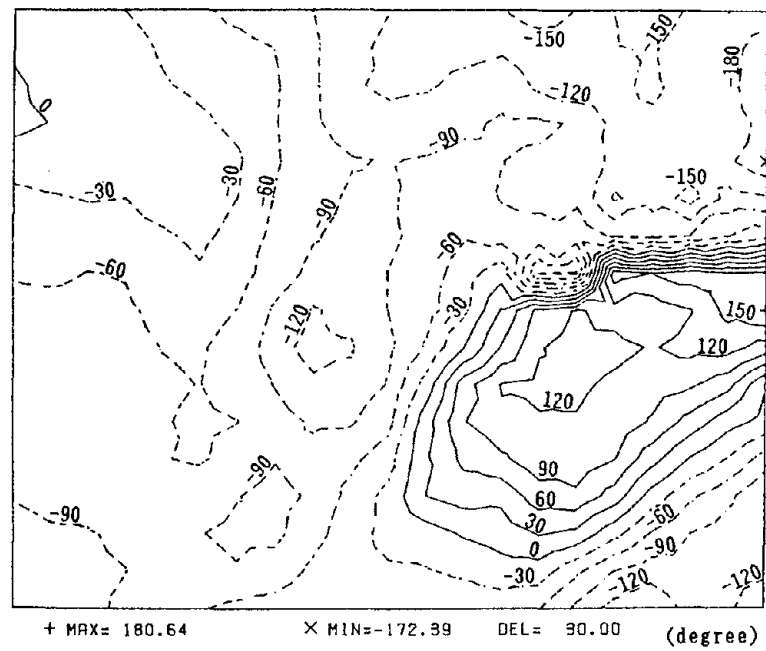


Figure 6 Contours for Angles of Calculated Displacements of P.G.D.

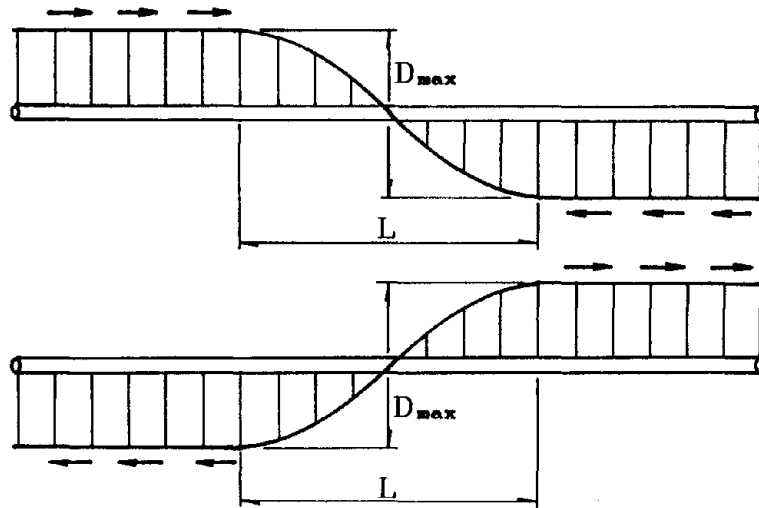


Figure 7 Parameters for Longitudinal Displacement Patterns

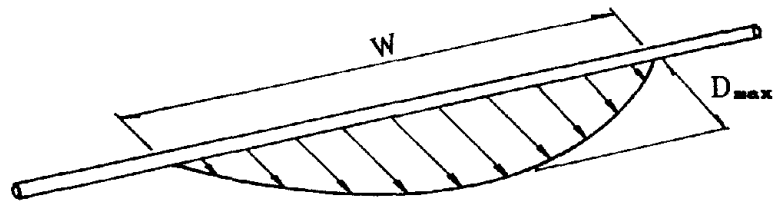


Figure 8 Parameters for Lateral Displacement Patterns



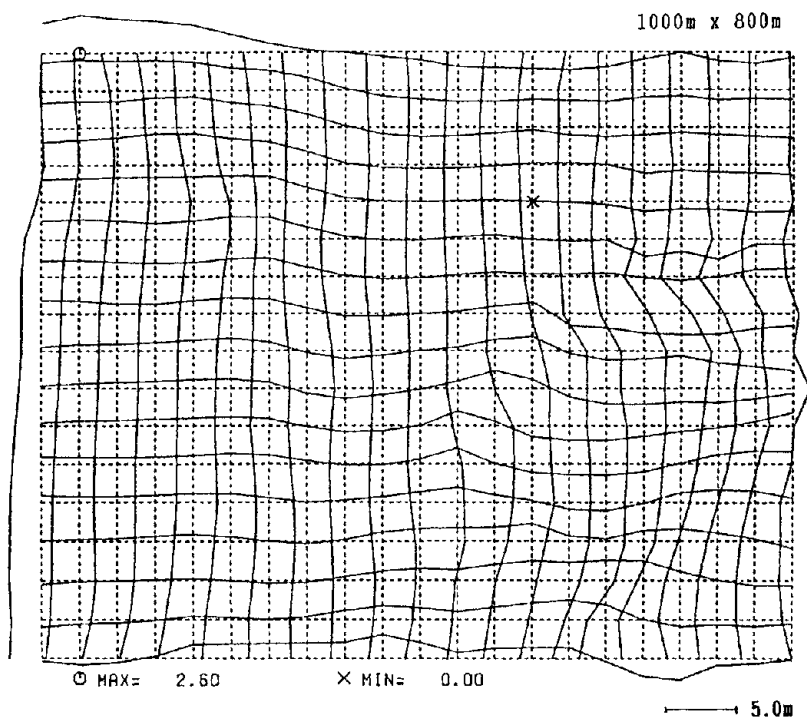


Figure 9 Longitudinal Displacements of P.G.D.

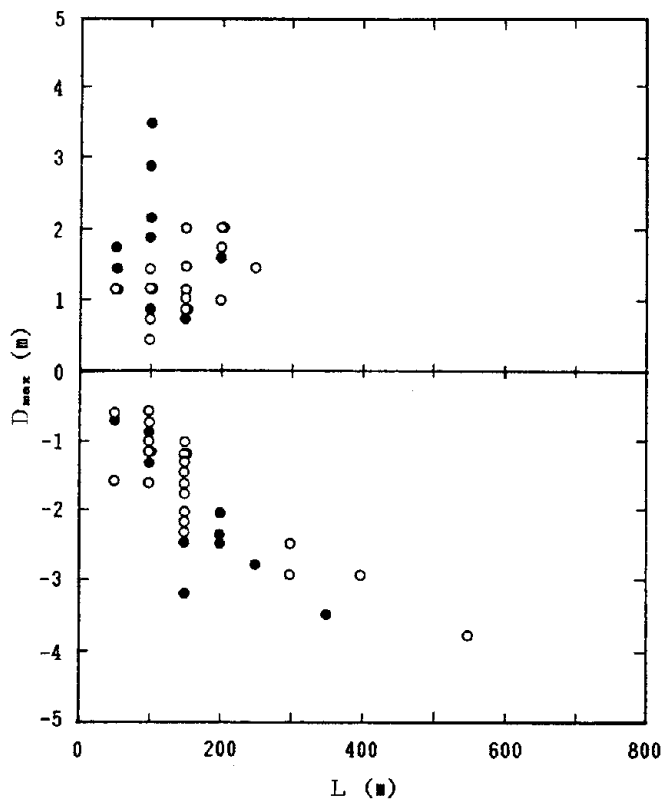


Figure 10  $D_{max}$  and L of Longitudinal Patterns of P.G.D.

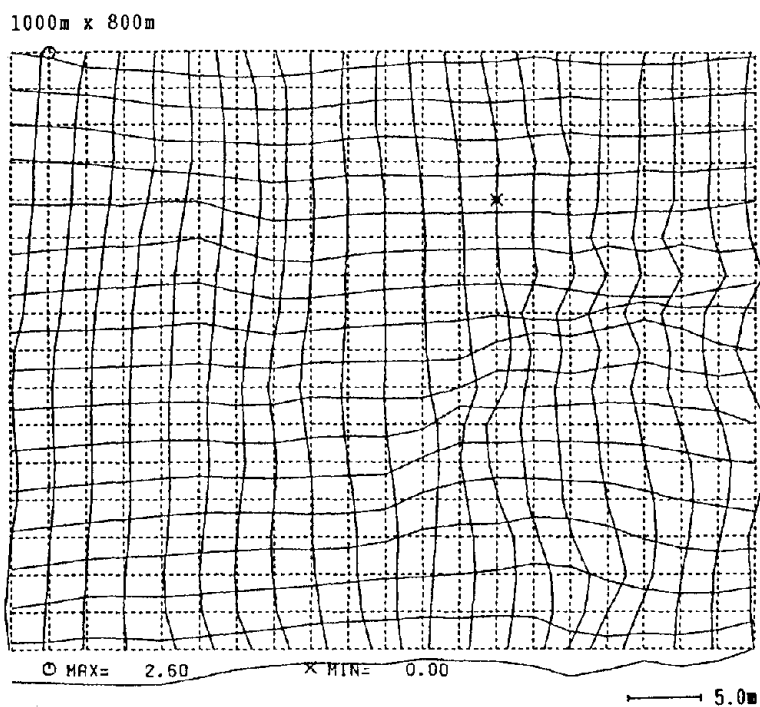


Figure 11 Lateral Displacements of P.G.D.

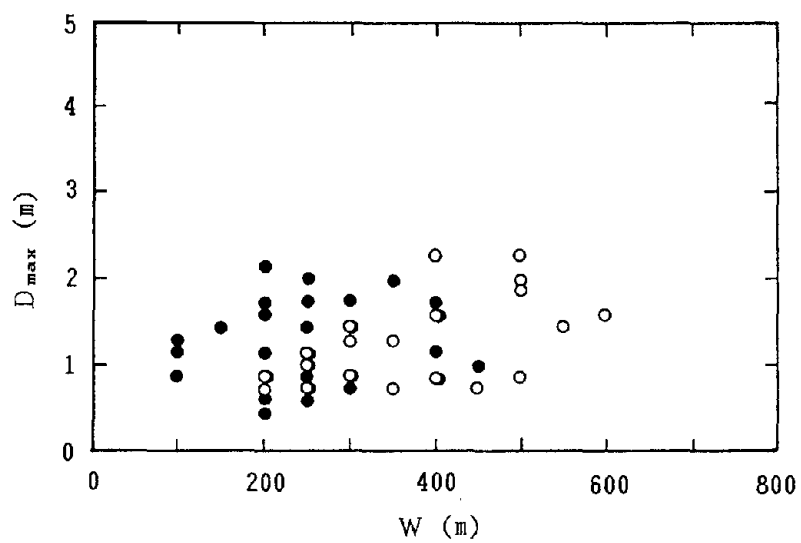


Figure 12 D<sub>max</sub> and W of Lateral Displacement Patterns of P.G.D.

**MODEL VIBRATION TEST OF FRAMED FOUNDATION-GROUND SYSTEMS  
DURING LIQUEFACTION**

Masaaki YOSHIKAWA <sup>1</sup> and Masanobu ARANO <sup>2</sup>

1. Earthquake Engineering Department, Tsukuba Research Institute, Okumura Corp., 387 Ohsuna, Tsukuba-shi, Ibaraki-ken, 300-33, Japan
2. ditto

**ABSTRACT**

Model vibration tests are performed to find out the effectiveness of the framed foundations for preventing liquefaction. In the fundamental study, loose saturated sand and model framed-foundations with different conditions were used in a flexible shear vessel attached to a shaking table. It was found out that the effect of the framed-foundation on the bearing capacity of the enclosed ground was higher under fixed tip condition than having a free tip. In practice, a series of model shaking tests were conducted to investigate the effectiveness of underground structure stabilization techniques during liquefaction. Surrounding a model underground structure with the fixed tip framed-foundation is found to be more effective than the one having used no stabilization technique. The authors conclude that the framed-foundation has effective resistance against liquefaction when the tip of the frame is fixed.

## INTRODUCTION

In 1964 Niigata earthquake, structures were collapsed due to permanent ground displacement of up to several meters caused by the liquefied ground. The horizontal displacements of the buildings which received a small damage in spite of severe damages of adjacent buildings, have been investigated by comparison of aerial photographs taken before and after the earthquake. Buildings that were supported by pile foundations or basements received smaller damage than those with surface footings. As reported in Ref. 1, Niigata City Hall was not so damaged such that it continued service. It was built on loose saturated sand and was designed against lateral movements by sheet piles that were much longer than those designed with non-liquefied ground. The ground enclosed by sheet piles might have prevented permanent ground displacement induced by liquefaction by adding stiffness to the sheet piles. Although the bearing capacity of the enclosed ground by such framings as interlocked steel piles or embedded walls have been verified by the model vibration tests (Refs. 2, 3, 4), there are not done so many studies on the effectiveness of the framed-foundation for preventing liquefaction.

In our study, the model vibration test is conducted to find out the effectiveness of the framed foundation in order to prevent liquefaction. In the fundamental step, framed-foundation models under different tip conditions in loose saturated sand were tested. It is found that the excessive pore pressure of enclosed ground, when the tip of the frame is fixed, reaches the maximum value slower than the ground outside of the frame, and that the effectiveness of the frame on the bearing capacity of the enclosed ground is higher under such a condition than the frame having a free tip.

For the practical testing, a model underground structure with framed-foundation was tested compared with the structure employing no stabilization technique. Surrounding the structure with crushed grain and framed-foundation was found to be effective against liquefaction.

## EXPERIMENTAL PROCEDURE WITH DIFFERENT TIP CONDITIONS

The real framed-foundation (30 m or 15 m height, 30 m length, 0.6 m width) is a hollow square having continuous walls. In the modeling a superstructure is treated as a virtual mass. Three framed scaled models under different tip condition are shown in Fig. 1.

### Ground Model and Similarity

The properties of the ground and the framed-foundation are tabulated in Table 1. The ground model material is a loose saturated sand having  $V_s$  equal to 70 m/s when  $D_r$  is 30% and is surrounded by the flexible shear vessel which is 0.8m, 2m, 2m in order to minimize the influences of finite boundaries. The framed-foundation models (1/50) are made from aluminum.

The model law and ratio of similarity (Ref. 5) used are tabulated in Table 2.

The models calculated from these scale factors are listed in Table 1.

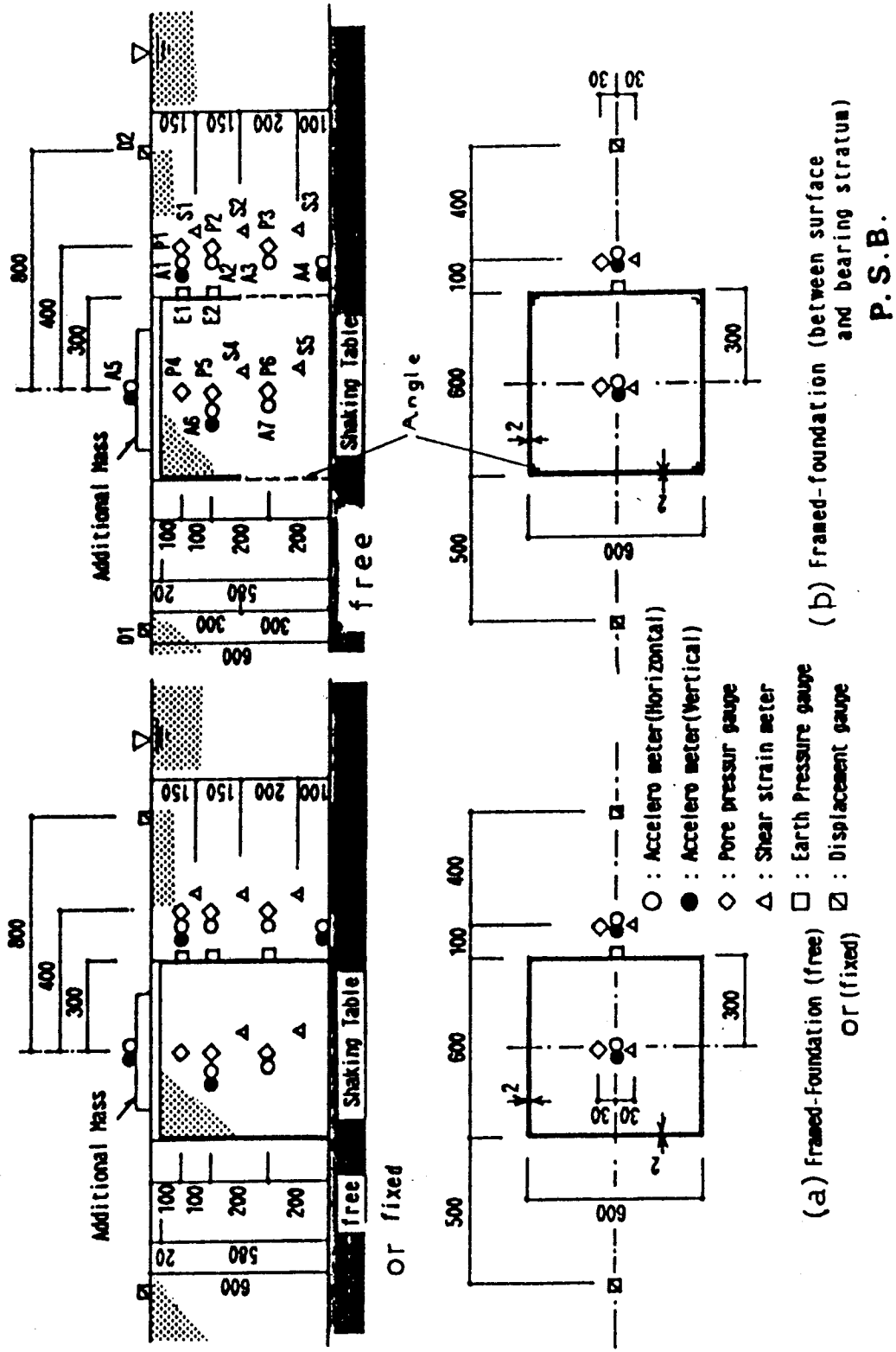


Fig. 1 Ground-Framed Foundation Model

**Table 1 Design Details of  
Prototype and Model**

Prototype	Model Aim
<b>FRAMED-FOUNDATION</b>	
In-situ concrete (unit: m)	Aluminum (cm)
Length 29	58
Width 0.6	0.1 (Execution 0.2)
Foundation 30,30,1	60,60,2
Structure 30,30,10	Additional mass
Density(g/cm <sup>3</sup> ) 2.4	2.7
<b>SOIL SYSTEM</b>	
Reclaimed sand	<b>SAND</b>
V <sub>s</sub> (m/s) 200	<u>Aim</u>   <u>Execution</u>
f <sub>g</sub> (Hz) 1.7	28   70
Depth(m) 30	12   10
	60(cm)
ρ <sub>d min, max</sub> (g/cm <sup>3</sup> )	1.5, 1.7
D <sub>50</sub> (mm)	0.46
U <sub>c</sub>	2.5
Poisson's ratio	0.45

**Table 2 Similarity and Scale  
Factor**

Function	Similitude	Scale Factor
Length	l <sub>m</sub> /l <sub>p</sub>	1/50
Stress	(ρ <sub>m</sub> /ρ <sub>p</sub> )(l <sub>m</sub> /l <sub>p</sub> )	1/50
Cohesion	(ρ <sub>m</sub> /ρ <sub>p</sub> )(l <sub>m</sub> /l <sub>p</sub> )	1/50
Time(Period)	(l <sub>m</sub> /l <sub>p</sub> ) <sup>1/2</sup>	1/7.1
Frequency	(l <sub>m</sub> /l <sub>p</sub> ) <sup>-1/2</sup>	7.1
Displacement	(l <sub>m</sub> /l <sub>p</sub> )	1/50
Velocity	(l <sub>m</sub> /l <sub>p</sub> ) <sup>1/2</sup>	1/7.1
Modulus	(ρ <sub>m</sub> /ρ <sub>p</sub> )(l <sub>m</sub> /l <sub>p</sub> )(ν <sub>m</sub> /ν <sub>p</sub> )	1/50
Mass Density	ρ <sub>m</sub> /ρ <sub>p</sub>	1
Acceleration	α <sub>m</sub> /α <sub>p</sub>	1
Internal Friction Angle	φ <sub>m</sub> /φ <sub>p</sub>	1
Damping	h <sub>m</sub> /h <sub>p</sub>	1
Constant		
Strain	ε <sub>m</sub> /ε <sub>p</sub>	1
Poisson's Ratio	ν <sub>m</sub> /ν <sub>p</sub>	1

suffix  
m:model  
p:prototype

Such variables as time and effective overburden pressure must be smaller than those of the prototype, because the small scaled model is tested in the same gravitational force field. In our past studies (Ref. 5), a new model ground material was developed which has superior reproductiveness of softening characteristics of ground, although the pore pressure can not be obtained because of the total stress. In this study, loose saturated sand is used to find out the effectiveness of liquefaction on a framed-foundation. When loose saturated sand is used as the model ground, the results of the model test emphasizes the progressive rise of pore pressures, and on the contrary hastens the dissipation of pore pressures because of the shallow depth compared with the real depth. Having selected suitable input motion (number of cycles of applied sinusoidal waves, frequency, acceleration amplitude), relative density of ground model and flexural rigidity of framed-foundation model, it is possible to obtain the emphasized liquefaction phenomena easily.

### Experimental Facility and Experiments

The shaking table (rated carrying weight 20 tf, max. accel. 3G) is shown in Fig. 2. It can simulate a three-dimensional motion as well as the triaxial rotations by developing the hydrostatic joint which enables to communicate smoothly to activating force by oil films. The measuring points where the micropickups were used were located at the ground surface and the ground (displacement gauge  $D_1 \sim D_2$ , accelerometer  $A_1 \sim A_7$ , pore pressure gauge  $P_1 \sim P_6$ , shear strain meter  $S_1 \sim S_3$ ), and the side of the frame (earth pressure gauge  $E_1 \sim E_3$ ) as shown in Fig. 1. Horizontal excitation of sinusoidal wave form up to 50 cycles with frequency equal to 15 Hz and maximum input acceleration of  $100 \text{ cm/s}^2$  were applied. The experiments were carried out for four cases, ground system without foundation (Ground), framed foundation-ground combined system fixed to the base (Fix), free to the base (Free) and penetrated between surface and bearing stratum (PSB). PSB may sink or overturn during liquefaction. Four slender piles made of aluminum (30.0 cm length, 2.5 cm width, 0.2 cm thickness) are used at the four tip corners to keep stable dynamically.

## DISCUSSION OF FUNDAMENTAL EXPERIMENTS

### Results of Ground System and Combined System

The time-response curves of the acceleration, the shear strain and the excessive pore pressure ( $u$ ) at the each depth of the ground are shown in Fig. 3. The time that  $u$  curve is paralleled to the time axis is shown as  $TP_{ih}$  ( $i=1, 3$ ) and the arrows. The time that  $u$  curves begin to decrease is put in parentheses. The liquefaction phenomena reaches from the surface ground to the inground, corresponding to the order of magnitude of  $u$  times,  $TP_{1h} < TP_{2h} < TP_{3h}$ . The ground in all layers becomes muddy after  $TP_{3h}$  passed. After keeping the muddy condition, the liquefaction stops from the inground to the surface ground. The time-response curves of the acceleration, the vibratory earth pressure, shear strain and  $u$  at the each depth of the framed foundation-ground are shown in Fig. 4 (a, b, c).

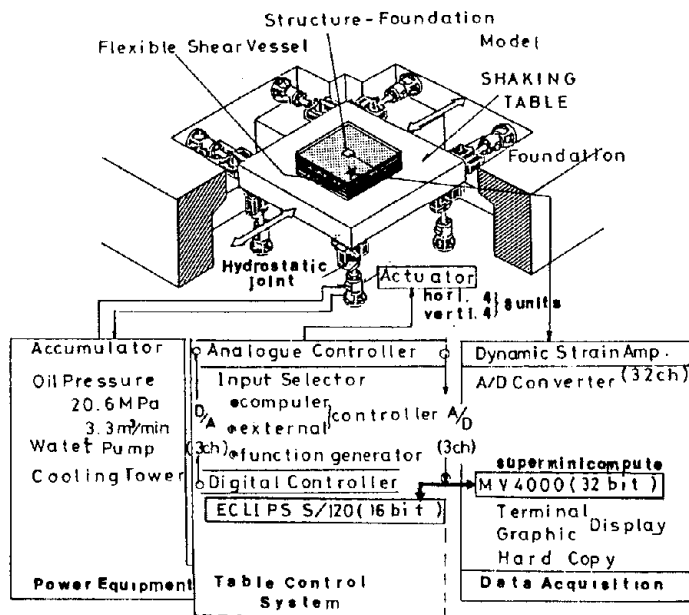


Fig. 2 3 Dimensional 6 Freedom Shaking Table

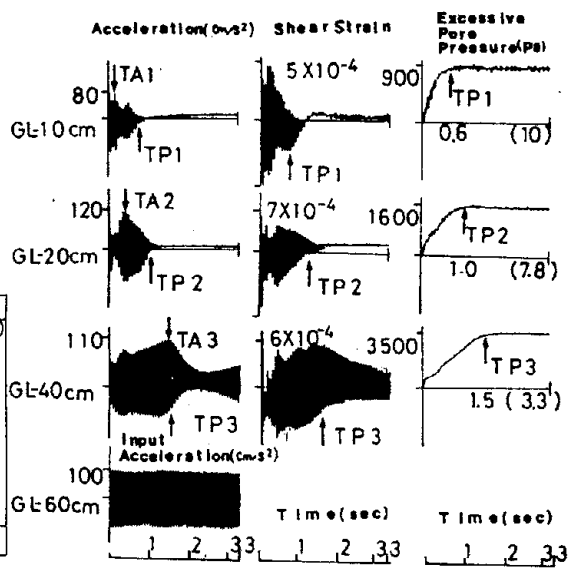


Fig. 3 Time-Response Curve of Ground (Horizontal, 15Hz, 100 cm/s²)

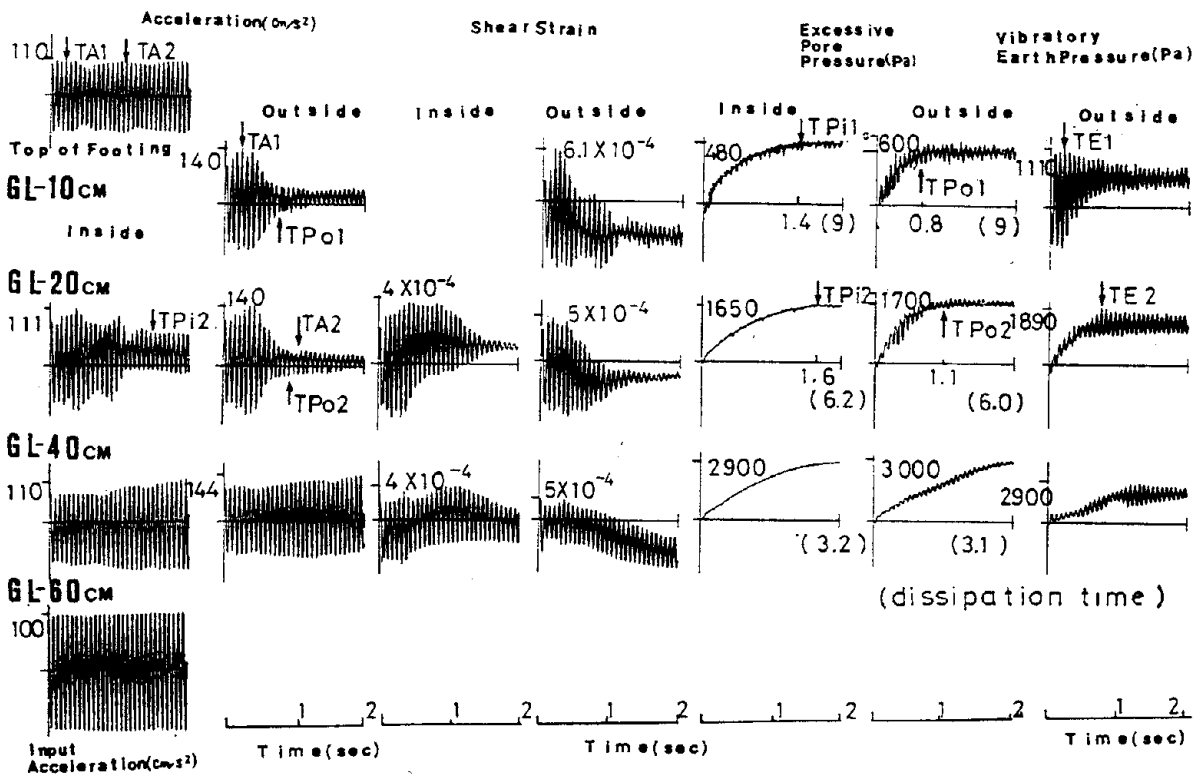


Fig. 4(a) Time-Response Curve of Ground-Framed-Foundation Fixed to the Base (Fix)



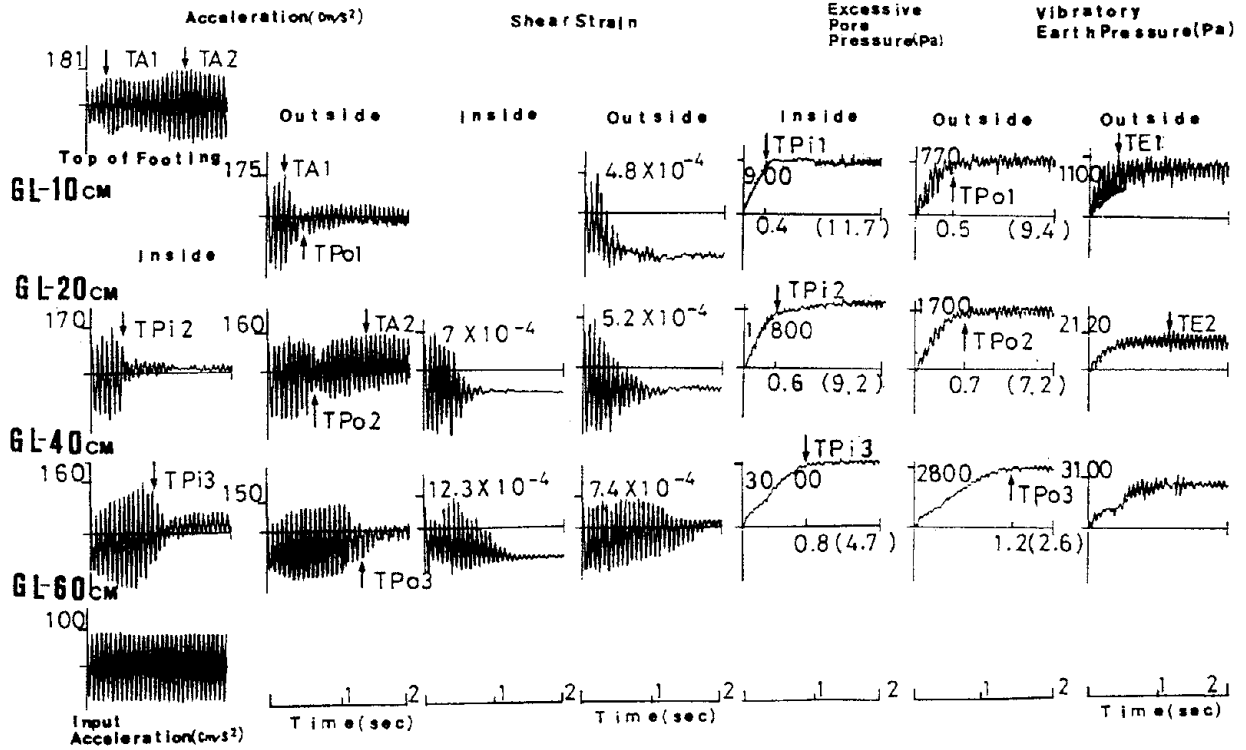


Fig. 4(b) Time-Response Curve of Ground-Framed-Foundation Free to the Base (Free)

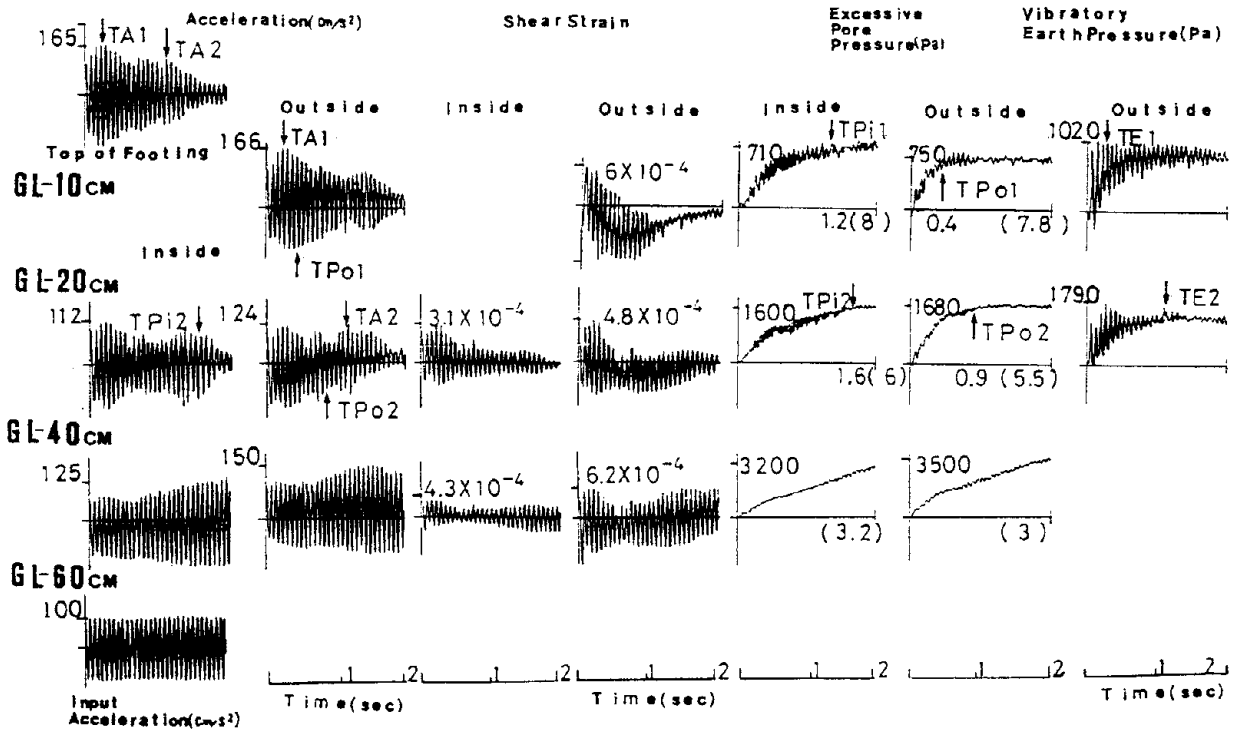
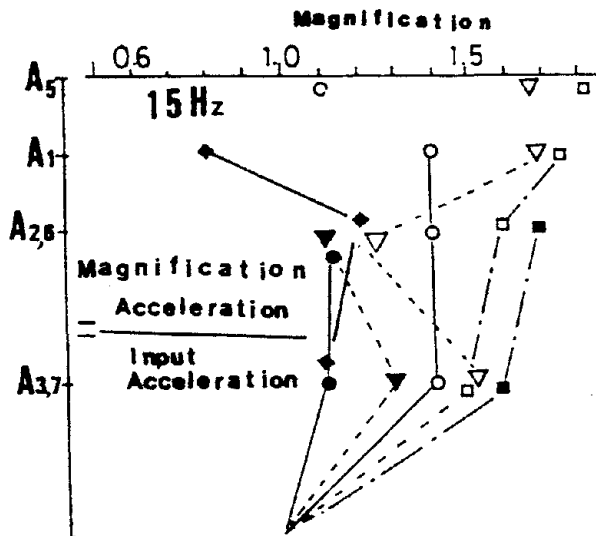


Fig. 4(c) Time-Response Curve of Ground-Framed-Foundation Penetrated between Surface and Bearing Stratum (PSB)

**Comparison of Maximum Response Value**

Maximum response acceleration and shear strain of Ground, Fix, Free and PSB are shown in Fig. 5 and Fig. 6 respectively.



**Fig. 5 Vertical distribution of Max. Response Acceleration**

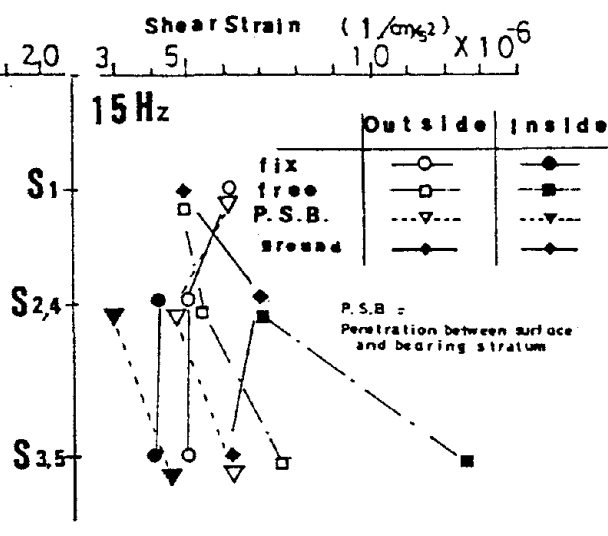


**Fig. 6 Vertical Distribution of Max. Response Shear Strain**

At both Fix and PSB, response values of inside ground are smaller than those of outside. On the contrary, at Free, values of inside are larger than those of outside. Times that  $u$  at each depth reaches to the max. value and starts to dissipate are shown in Fig. 7 respectively.

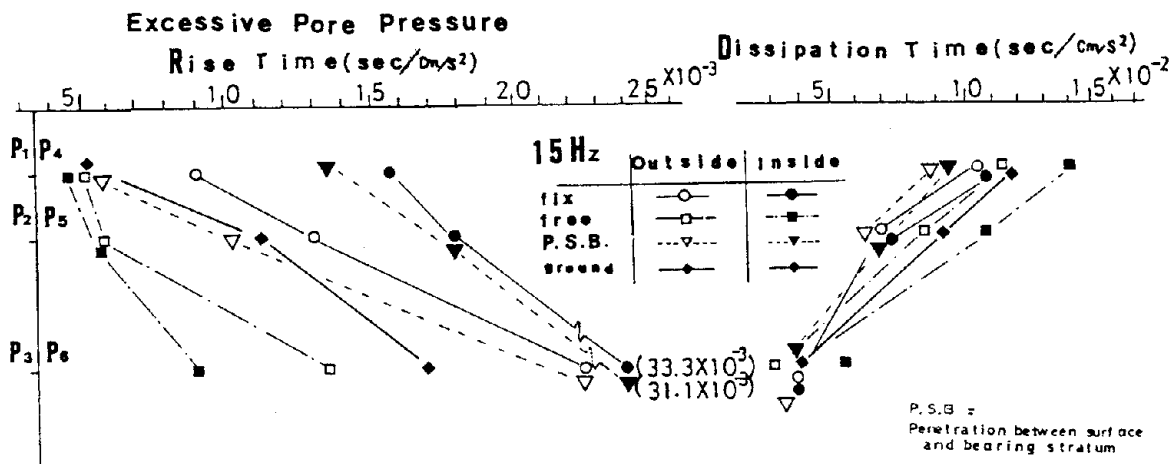


**Fig. 7 Vertical Distribution of Max. Response Excessive Pore Pressure (Rise and Dissipation)**

Times that  $u$  of both Fix and PSB reaches to the max. value are longer than those of ground without foundation. On the contrary times that  $u$  of both Fix and PSB starts to dissipate are shorter than those of ground. Times that  $u$  reaches to the max. value of the inside ground of Free are the shortest, and starts to dissipate are the longest of three types of framed-foundations respectively.

### Effectiveness of Framed Foundations

From Fig. 3 or Fig. 4, the response accel. and the shear strain of ground without foundation or Free at each layer reduce to zero as soon as  $u$  reaches to the effective overburden pressures. On the other hand, the response accel. and the shear strain of Fix or PSB are close to zero about one or two second late from TPon ( $n=1,2,3$ ) that  $u$  of the outside adjacent ground reach to the max. value. Fix in comparison of Free has the resistance strength due to the framed-foundation rigidity. On the other hand, the inside ground of Free are apt to liquefy due to the accumulation of reflective wave during the large displacement. PSB vibrates similar to the ground without foundation. Permanent settlements of the surface ground become smaller in the order Fix (5.2mm), Ground (5.6mm), PSB (6.2mm), Free (8.7mm) corresponding to the magnitude of horizontal displacement. Framed foundation under fixed tip condition is found to be more effective than that of Free or PBS. Next, a model framed foundation under fixed tip condition are shown as the stabilizing technique against liquefaction.

### PRACTICAL STUDY FOR EFFECTIVENESS

Underground structures such as manhole or culvert have a lower apparent specific gravity than the ground in the vicinity. The underground structure in the saturated sandy ground may float up straight or cant if the ground is susceptible to liquefaction during earthquake (Ref. 6). Framed foundation penetrated in the bearing stratum can be used for stabilizing technique against liquefaction. A real underground structure (2.0m height, 3.0m length, 2.0m width, apparent specific gravity 1.13) is buried 0.5m beneath the surface of a sandy ground. A model underground structure (MUS) with crushed grain and framed-foundation-ground ( $V_s$  50 cm/s in  $D_r$  40%) is attached on the shaking table in the 1/5 scale model as shown in Fig. 8.

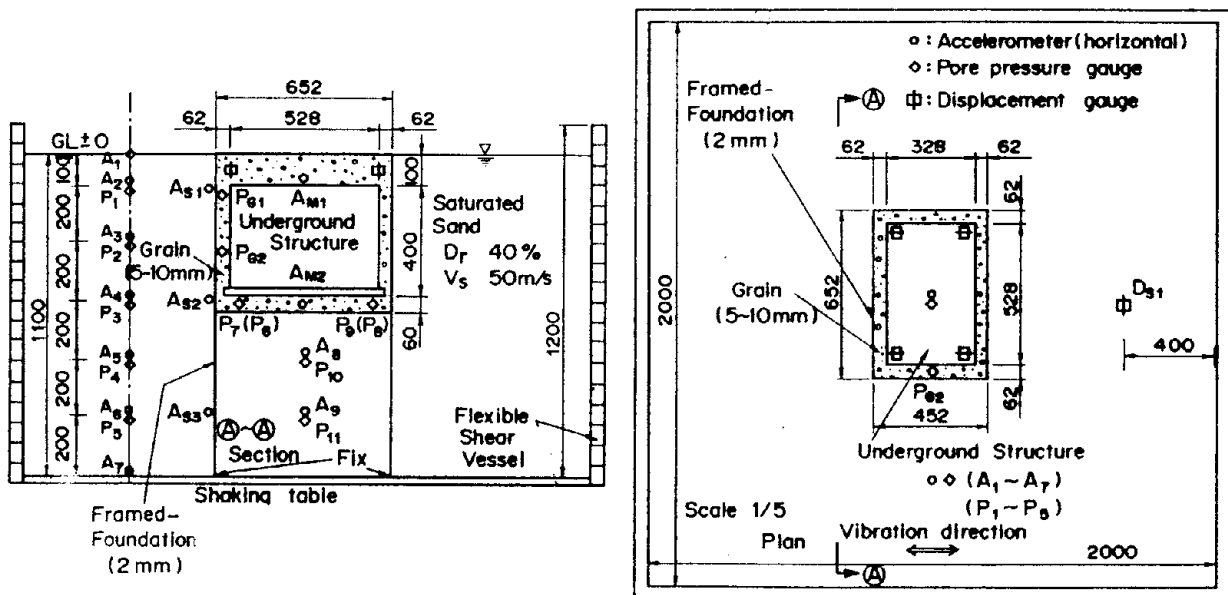


Fig. 8 Application for Framed-Foundation

Accelerometer  $A_1 \sim A_9$ ,  $AM_1 \sim AM_2$ ,  $AS_1 \sim AS_3$ , pore pressure gauge  $P_1 \sim P_{11}$ ,  $PG_1 \sim PG_2$  and displacement gauge  $DS_1 \sim DS_5$  were located around MUS.  $u$  at the each layer showed the complete liquefaction phenomena when number of cycles of applied sinusoidal waves were 20 in frequency 2Hz at acceleration amplitude  $220 \text{ cm/s}^2$ . To compare with the perfect liquefaction, input acceleration amplitude  $120 \text{ cm/s}^2$  at which  $u$  deep in the ground did not reach initial effective stress were added.

Three types of model tests were conducted, MUS employing no stabilization (Standard), MUS surrounded with crushed grain-ground combined system (crushed G), MUS with crushed grain and framed-foundation-ground combined system (framed-F).

### Results of Practical Experiment

$u$  of the surrounding ground in the depth from 1 second to the end vibration at 10 seconds is shown in Fig. 9 to investigate the degree of liquefaction.

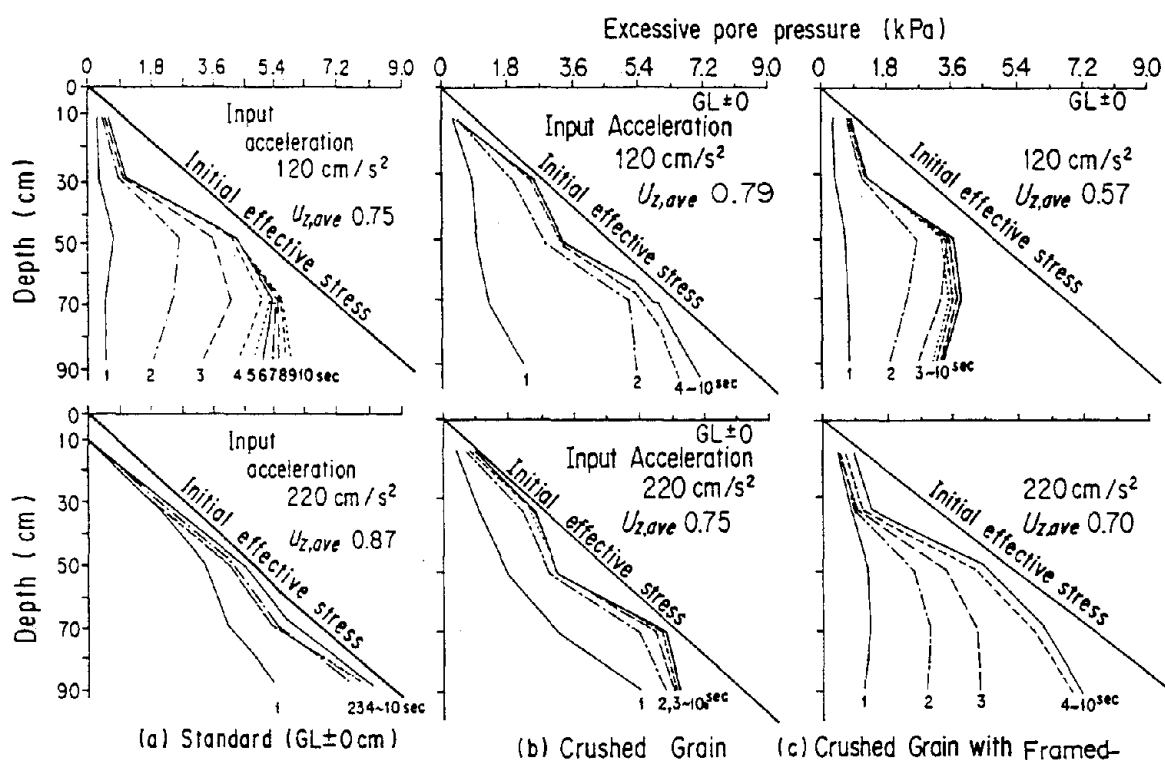
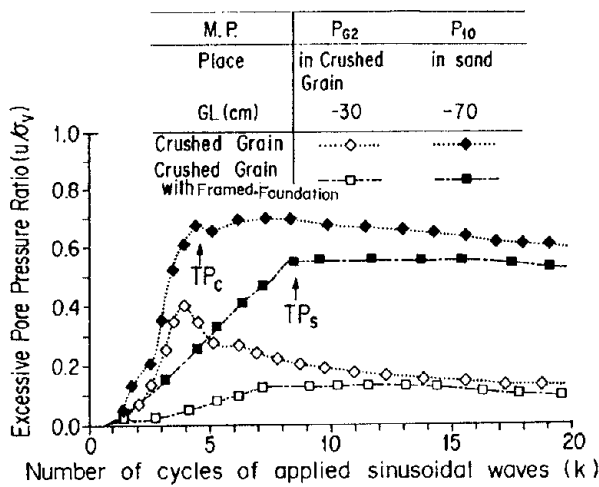
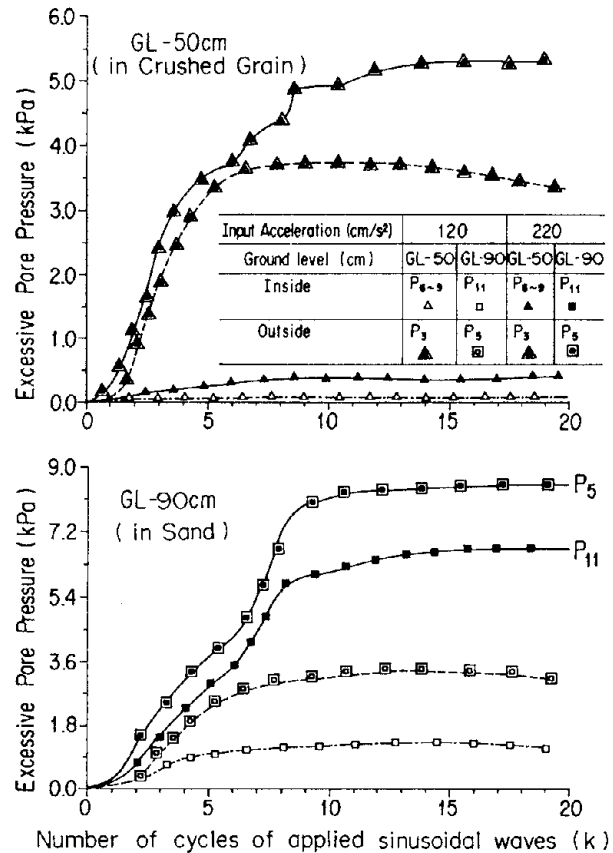


Fig. 9 Vertical Distribution of Excessive Pore Pressure ( $u$ )

A comparison of a rise time in  $u$  between crushed G ( $TP_C$ ) and framed-F ( $TP_S$ ) is shown in Fig. 10 where  $u/\sigma_v'$  was divided by the initial effective stress ( $\sigma_v'$ ) for generalization. A comparison of  $u$  between inside ( $P_6 \sim P_9, P_{11}$ ) and outside ( $P_3, P_5$ ) of framed-F is shown in Fig. 11.



**Fig. 10 Time-Response Curve of Excessive Pore Pressure (Crushed Grain and Crushed Grain with Framed-Foundation)**



**Fig.11 Time-Response Curve of Excessive Pore Pressure (Effectiveness of Framed-Foundation)**

**Discussion of Stabilizing Technique**

The reaching times to the initial effective stress line of both crushed G and framed-F were later than that of Standard from Fig. 9. The following formula is used to derive the max. value for the average  $u/\sigma_v'$  ( $u_{z,ave}$ ) which expresses the degree of liquefaction of the entire ground not a single measured point.

$$u_{z,ave} = \int_0^z u dz / \int_0^z \sigma_v' dz$$

The degree of liquefaction with three types derived with each measuring point matches that of value of  $u_{z,ave}$ .  $u_{z,ave}$  becomes smaller in the order Standard, crushed G, framed-F.  $u_{z,ave}$  is an index of the degree of liquefaction.  $TP_c$ , the time reaching to the max. value of crushed G is faster than  $TP_s$ , that of framed-F from Fig. 10. Max.  $u/\sigma_v'$  of crushed G is larger than that of framed-F. Framed-F is found to be more effective in dissipating the rise of  $u$  than crushed G.  $u$  of inside framed-F at the same depth is smaller than  $u$  of outside from Fig. 11. When the crushed grain and framed-foundation were used together, the restrained effect (or seismic or damping effect) was caused by the rigidity of the framed-foundation. Underground structure surrounded with crushed grain and framed-foundation was found to be effective against liquefaction.

## CONCLUSION

The important results obtained in this study on the liquefaction resistance of the framed-foundation are summarized as follows; (1) Times that excessive pore pressure of the fixed tip condition reaches to the maximum value are longer than those of ground without foundation. (2) Times that excessive pore pressure reaches to the maximum value of the inside ground of free tip condition are the shortest, and times that excessive pore pressure starts to dissipate are the longest of all. (3) Permanent settlements of surface ground become smaller in the order fix tip condition, penetrated between surface and bearing stratum, free tip condition corresponding to the magnitude of horizontal displacement. (4) Framed-foundation under fixed tip condition is found to be more effective than that of free or penetrated between surface and nearly stratum. (5) An index of the degree of liquefaction is expressed by the following equation.

$$u_{z,avê} = \int_0^z u dz / \int_0^z \sigma_v' dz$$

(6) Surrounding an underground structure with framed-foundation is found to be effective against liquefaction.

## ACKNOWLEDGMENTS

The authors express sincere thanks and appreciation to Mr. Toshihisa SHIMIZU of Technical Research Institute of OKUMURA Corporation for his invaluable assistance and to Mr. Koji YAGI and Mr. Hirokazu HATTORI of NTT Tsukuba Field Engineering Development Center for their earnest cooperation.

## REFERENCES

1. Architectural Institute of Japan, Investigative Report on Damaged Buildings in the 1964 Niigata Earthquake, page 550 (1964). (in Japanese)
2. YOSHIMI, Y. and TOKIMATSU, K., "Settlement of Buildings on Saturated Sand during Earthquakes," Soil and Foundation, JSSMFE, Vol.17, No.1, 23-38, 3, (1977).
3. ARAKAWA, T., KAWASHIMA, K., and MATSUMOTO, H., "Constraint Effect of Side Cell on Earthquake Resistance of Huge Artificial Island," Civil Engineering Journal, PWRI, Vol.26, No.4, 28-33, (1984). (in Japanese)
4. YOSHIKAWA, M. and ARANO, M., "Experimental Study on Framed-Foundation for Preventing Liquefaction," Proceedings of the 42nd Annual Conference of the JSCE, 1st, 868-869, 9, (1987). (in Japanese)
5. YOSHIKAWA, M., and ARANO, M., "Dynamic Behavior of a Model Pile Foundation-Ground Systems in the Liquefaction Process," Proceedings Vol.III, 9WCEE, III-599 - III-604, (1988).
6. YOSHIKAWA, M., NAKANO, M., HATTORI, H. and ARANO, M., "An Experimental Study on the Stabilizing Technique against Liquefaction - Manhole surrounded with Framed-Foundation -," Proceedings of the 43rd Annual Conference of the JSCE, 1st, 1124-1125, 10, (1988). (in Japanese)

# ASSESSMENT OF DAMAGE POTENTIAL AND EARTHQUAKE COUNTERMEASURES FOR LIFELINES

**Quantification of Severity Index Attenuation for the Eastern United**

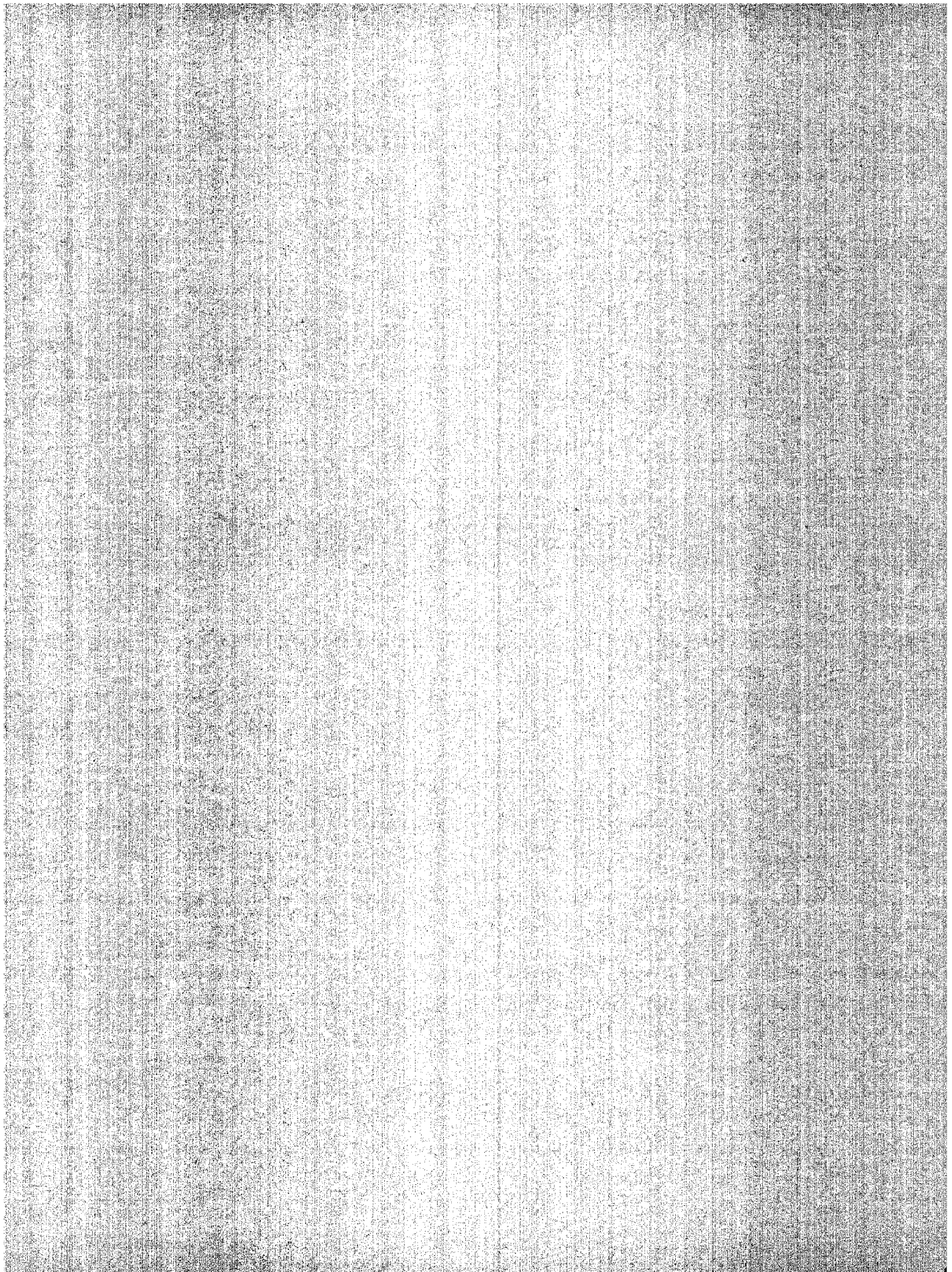
*T. L. Youd, D. M. Perkins, and W. G. Turner*

**Damage to and Disaster Mitigation for Civil Engineering Structure**

*M. Kawabe, Y. Nozawa, and S. Gotoh*

**Countermeasures to Mitigate Damage to Pipelines**

*M. Rosenberg and E. Richardson*





## LIQUEFACTION SEVERITY INDEX ATTENUATION FOR THE EASTERN UNITED STATES

T. Leslie YOUNG<sup>1</sup>, David M. PERKINS<sup>2</sup>, and William G. TURNER<sup>3</sup>

<sup>1</sup>Professor of Civil Engineering, Brigham Young University, Provo, Utah, USA

<sup>2</sup>Geophysist, U.S. Geological Survey, Golden, Colorado, USA

<sup>3</sup>Staff Engineer, Highland Soils Engineering, Inc., San Bernadino, Calif., USA

### ABSTRACT

To assess liquefaction severity index (LSI) attenuation in the eastern US, LSI values are estimated for several sites where effects of liquefaction were observed and described following earthquakes near New Madrid, Missouri (1811-12,  $M \sim 8.5$ ), Charleston, South Carolina (1886,  $M \sim 7.3$ ), and Sanguenay, Quebec, Canada (1988,  $M \sim 6$ ). These LSI estimates are plotted against horizontal distance from the seismic energy source to assess LSI attenuation. The data show that (1) log LSI attenuates approximately linearly with log distance, (2) earthquake magnitude and distance are primary parameters controlling LSI attenuation in the eastern US, which is consistent with data from the western US, and (3) LSI attenuates more slowly in the eastern US than in the western US, a result consistent with lower rates of attenuation of other earthquake parameters such as earthquake intensity, peak acceleration, and peak velocity.

### INTRODUCTION

Past studies have shown that ground displacement is the principal cause of liquefaction-induced earthquake damage. Pipelines, bridges and buildings have been particularly vulnerable to damage due to ground displacement. For example, every major pipeline break in the City of San Francisco during the 1906 earthquake occurred in zones of liquefaction-induced ground deformation (Youd and Hoose, 1978). Those breaks hampered efforts to fight the fire which caused about 85 percent of the total damage to that city. Liquefaction induced-lateral spreads damaged 266 highway and railway bridges to varying degrees, severely disrupting surface transportation in the affected region for many months following the 1964 Alaska earthquake (Youd, 1978). Ground displacements greater than a tenth of a meter caused serious damage to buildings during the 1964 Alaska, 1964 Niigata, Japan and many other earthquakes (Youd, 1989).

Because ground displacement is the major cause of liquefaction-induced earthquake damage, maps showing potential for ground displacement provide a useful vehicle for delineating liquefaction hazard. Maps showing ground displacement potential on gently sloping ground are particularly useful, because of the considerable development that has occurred and is occurring on that type of terrain. Lateral spreads are the predominant type of ground failure on gentle slopes; thus maps of lateral spread potential are particularly useful for hazard evaluation and mitigation.

### LIQUEFACTION SEVERITY INDEX

Youd and Perkins (1987) developed a technique for mapping potential for lateral spread displacement using a parameter termed liquefaction severity index (LSI). LSI is defined as the maximum lateral spread displacement in inches (millimeters divided by 25) that is likely to occur on gently sloping natural-deposits

that are highly susceptible to liquefaction. The highly susceptible materials considered include late Holocene floodplain and deltaic deposits containing substantial layers of saturated sandy sediment. The LSI scale is arbitrarily truncated at a value of 100 to provide a convenient scale ranging from 0 to 100. Although displacements greater than 2.5 m (100 in) are common in the near-field region of large earthquakes, such large displacements cause nearly total destruction and need not be further quantified for hazard studies. All displacements greater than 2.5 m are thus given an LSI value of 100. Table 1 gives criteria developed by Youd and Perkins for estimating LSI from ground displacements and other liquefaction effects.

Because maximum displacement is used to determine the LSI value for each locality, nearly all the ground displacements at any given locality are less than the LSI. Thus, the LSI provides a conservative estimate of maximum displacement. We estimate a 90 percent or greater probability of nonexceedance.

**TABLE 1.--QUALITATIVE ASSESSMENT OF ABUNDANCE AND GENERAL CHARACTER OF LIQUEFACTION EFFECTS AS A FUNCTION OF LSI FOR AREAS WITH WIDESPREAD LIQUEFIABLE DEPOSITS (AFTER YOOD AND PERKINS, 1987).**

LSI (1)	Abundance and General Character of Liquefaction Effects (2)
5	Very sparsely distributed minor ground effects include sand boils with sand aprons up to 0.5 m (1.5 ft) in diameter, minor ground fissures with openings up to a tenth of a meter wide, and ground settlements of up to 25 mm (1 in). Effects lie primarily in areas of recent deposition and shallow ground water table such as exposed stream beds, active flood plains, mud flats, shore lines, etc.
10	Sparsely distributed ground effects include sand boils with aprons up to 1 m (3 ft) in diameter, ground fissures with openings up to 0.3 m (1 ft) wide, and ground settlements of a few inches over loose deposits such as trenches or channels filled with loose sand. Slumps with up to a few tenths of a meter displacement are common along steep banks. Effects lie primarily in areas of recent deposition with a ground water table less than 3 m (10 ft) deep.
30	Generally sparse but locally abundant ground effects include sand boils with aprons up to 2 m (6 ft) diameter, ground fissures up to several tenths of a meter wide, some fences and roadways noticeably offset, sporadic ground settlements of as much 0.3 m (1 ft), and slumps with 0.3 m (1 ft) of displacements common along steep stream banks. Larger effects lie primarily in areas of recent deposition with a ground water table less than 3 m (10 ft) deep.
50	Abundant effects include sand boils with aprons up to 3 m (10 ft) in diameter that commonly coalesce into bands along fissures, fissures with widths up to 1.5 m (4.5 ft), fissures generally parallel or curve toward streams or depressions and commonly break in multiple strands, fences and roadways are offset or pulled apart as much as 1.5 m (4.5) in some places, ground settlements of more than 1 ft (0.3 m) occur locally, and slumps with a meter of displacement are common in steep stream banks.
70	Abundant effects include many large sand boils (some with aprons exceeding 6 m (20 ft) in diameter that commonly coalesce along fissures), long fissures parallel to rivers or shorelines usually in multiple strands with many openings as wide as 2 m (6 ft), many large slumps along streams and other steep banks, some intact masses of ground between fissures displaced a meter or two down gentle slopes, and frequent ground settlements of more than 0.3 m (1 ft).
90	Very abundant ground effects include numerous sand boils with large aprons, 30 percent or more of some areas covered with freshly deposited sand, many long fissures with multiple strands and openings as wide as two or more meters parallel streams and shore lines, intact masses of ground are commonly displaced more than two meters down gentle slopes, large slumps are common in stream and other steep banks, and ground settlements of more than 0.3 m (1 ft) are common.

Youd and Perkins assigned LSI values to several localities where liquefaction and lateral spreading occurred during past earthquakes in the western United States (US). Those values were correlated against earthquake magnitude ( $M_w$ ) and horizontal distance ( $R$ ) in kilometers from the seismic energy source. For western US earthquakes, the resultant empirical correlative equation is:

$$\log LSI = -3.49 - 1.86 \log R + 0.98M_w \quad (1)$$

Figure 1 shows LSI data and attenuation curves for the western US plotted on a graph of log LSI versus log R.

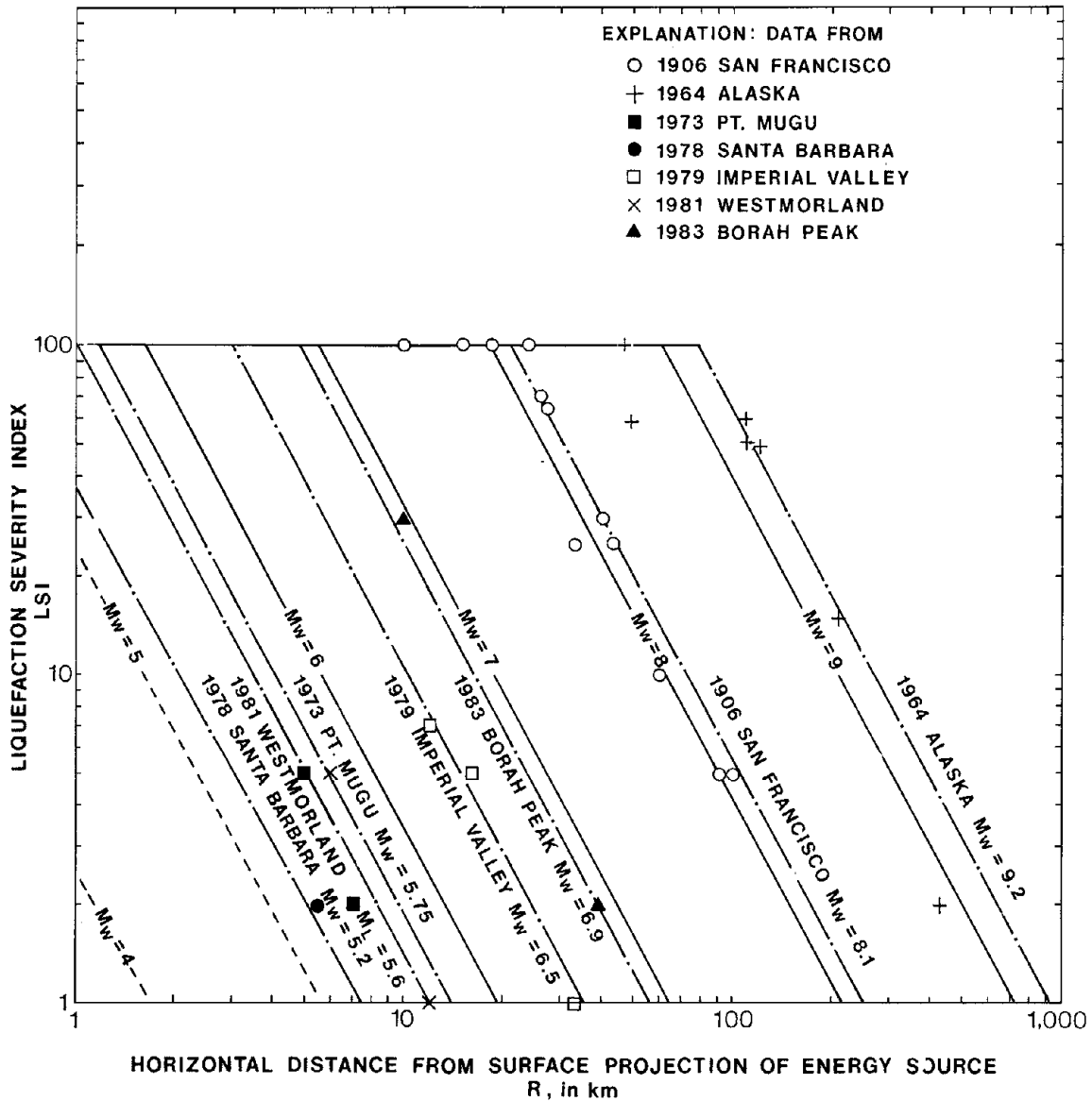
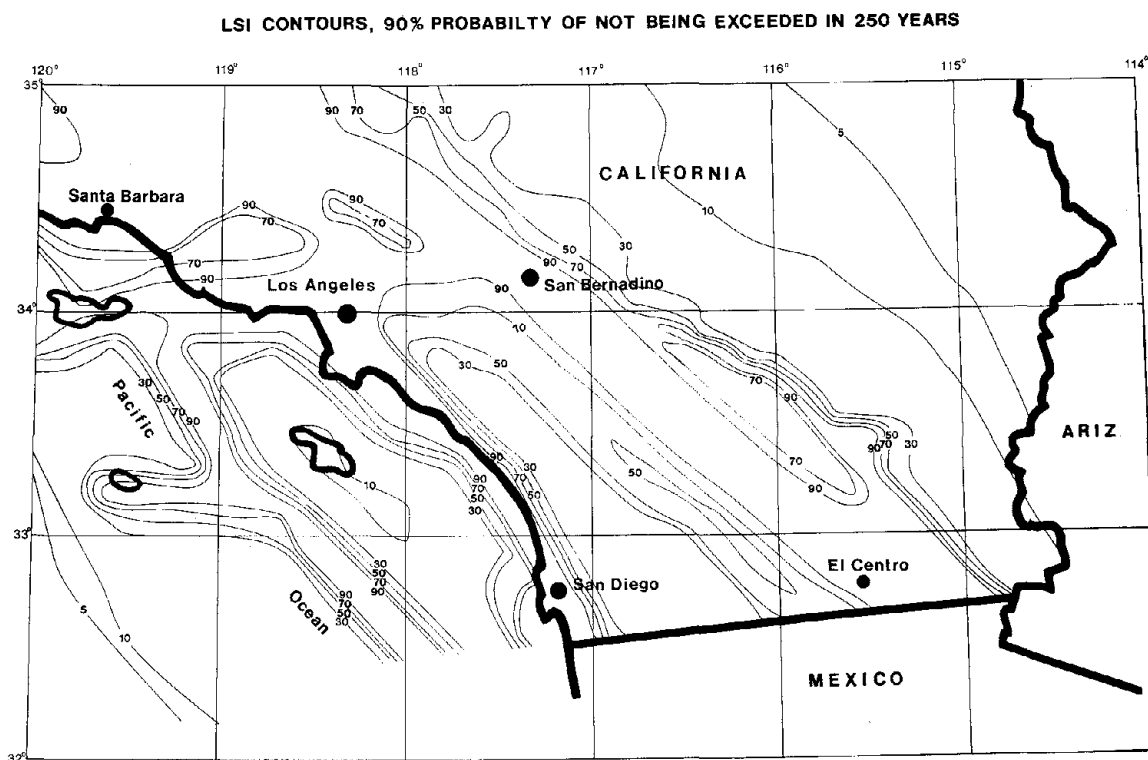


FIGURE 1.--LSI FROM SEVERAL WESTERN US EARTHQUAKES WITH ATTENUATION CURVES CALCULATED FROM EQUATION 1 (AFTER YUOD AND PERKINS, 1987)



**FIGURE 2.--LSI CONTOURS FOR SOUTHERN CALIFORNIA WITH 90 PERCENT PROBABILITY OF NOT BEING EXCEEDED IN 250 YEARS**

Youd and Perkins (1987) used seismic source zones prepared by Algermissen et al. (1980) along with Equation 1 as an LSI attenuation function in a standard seismic risk analysis to compile probabilistic LSI maps for southern California. One of those maps is reproduced in Figure 2. That map shows LSI contours with 90 percent probability of not being exceeded in a 250-year period. This map is an LSI opportunity map in that it shows maximum displacements that would be expected at any locality in the given exposure time assuming that each locality is underlain by gently-sloping, highly-liquefiable deposits. Clearly, every locality is not underlain by liquefiable sediment; thus, a second map, a liquefaction or lateral spread susceptibility map is required to complete the evaluation of ground failure hazard. The latter map requires delineation of local sedimentary units at a scale that can not be accurately depicted on a regional scale map, such as on the map shown in Figure 2. Additional research is needed to develop techniques for predicting ground displacement potential from liquefaction susceptibility maps of the types compiled to date.

Although regional LSI maps are not adequate for assessing absolute liquefaction hazard at a site, these maps are very useful for general hazard analyses. LSI values from a regional LSI map provide a generally conservative estimate of maximum lateral spread displacement that should occur on almost any type of deposit. (Displacements greater than the LSI could occur on some poorly compacted sandy artificial fills or embankments or on unusually sensitive natural deposits.) For example, at localities where ground displacements noted on an LSI map are smaller than those required to cause significant damage, about LSI = 4 or 100 mm for most structures (Youd, 1989), liquefaction hazard might be safely ignored, except for unusual site conditions such as an uncompacted artificial fill or for unusually sensitive structures. At localities where significant potential for damaging displacements is predicted, further study of the local geology and site conditions could be required or other mitigative measures taken.

The purpose of this project is to develop LSI maps for the eastern US. To compile those maps, LSI attenuation relationships are required for the eastern US. Because ground motions attenuate more slowly in the eastern US than in the west, LSI is also expected to attenuate more slowly in the east. To assess LSI attenuation in the east, we estimated LSI for several localities where liquefaction effects were observed and described following three major earthquakes. Those plots show that LSI attenuates with distance from the seismic energy source, but at a slower rate than in the western US. These plots provide a preliminary assessment of LSI attenuation in the eastern US.

### LSI DATA FOR EASTERN US EARTHQUAKES

Only a few earthquakes have occurred in the eastern US that have generated notable liquefaction effects and only fragmentary reports of those effects are available for most events. Sufficient data are available for three earthquakes to make estimates of LSI at several localities for each of these events. The earthquakes are the 1811-12 New Madrid, Missouri events ( $M_w$  about 8.5), the 1886 Charleston, South Carolina earthquake ( $M_w$  about 7.3) and the 1988 Sanguenay, Quebec, Canada earthquake ( $M_s$  about 6.0). The following paragraphs describe LSI evaluations for those events.

In assigning LSI at localities of reported liquefaction effects, the criteria noted in Table 1 were applied. There are, however, considerable ambiguities in the descriptions of some reported effects, as might be expected from antiquity and remoteness of at least the New Madrid event. Each of the descriptions were evaluated from three perspectives to give the most likely or best estimate of the LSI, the maximum probable LSI and the minimum probable LSI. In making these estimates the criteria of Table 1 were applied in the following hierarchical order: (1) Measured or estimated lateral ground displacements yield direct estimates of LSI, and any such information was given greatest importance. (2) Widths of fissures are also a function to horizontal ground displacement, but only provide an indirect estimate of displacement. Even where the widths of parallel fissures can be summed, there is still some uncertainty because walls of fissures may have collapsed leading to an overestimate of displacement, or the ground may have stretched as well as fracturing, leading to an under estimate. (3) Sand boils are common surface manifestations of liquefaction, but are not directly related to ground displacement. Thus, criteria in Table 1 that are based on the number and size of sand boil deposits are an indirect and rather imprecise measure of LSI. At many localities, however, sand boil deposits are the only or the most thoroughly described liquefaction effect and thus have considerable usefulness in estimating LSI from the written descriptions.

#### 1811-1812 New Madrid Earthquakes

During the winter of 1811-1812, the lower Mississippi River valley was shaken by some of the largest earthquakes that have occurred in the US during recorded history. The largest shocks were felt over a vast area extending as far east as New York, Boston and Quebec. The largest of the shocks had an estimated body-wave magnitude of 7.3, which is approximately equivalent to surface-wave magnitude of 8.6 (Nuttli, 1974; Street and Nuttli, 1984). Estimated moment magnitudes,  $M_w$ , for these events are about 8.5. These earthquakes generated large and numerous liquefaction effects including lateral spreads, ground subsidence, fissures, and sand boils. The largest and most pervasive liquefaction effects developed in a zone delineated by Fuller (1912) as "the area of principal disturbance characterized by general warping, ejections, fissuring, and severe landslides." That area is marked on Figure 3. Beyond the area of "principal disturbance," less severe liquefaction effects developed within a zone of "minor disturbance characterized by local fissuring, caving of stream banks, etc.," also plotted on Figure 3. Beyond that zone some additional sand boils and fissures were noted by several travelers passing through the area at the time of and shortly after the earthquake (Street and Nuttli, 1984).

For the New Madrid events, we placed the seismic energy source zone along the principal axis of the elliptical shaped area delineating the area of "principal disturbance." Based on a tabulation by Nuttli (1974, p. 529), we estimated that the length of the source zone for an  $m_b = 7.3$  earthquake should be about 65 km. We centered a line of that length on the principal axis of the elliptical area of principal disturbance to

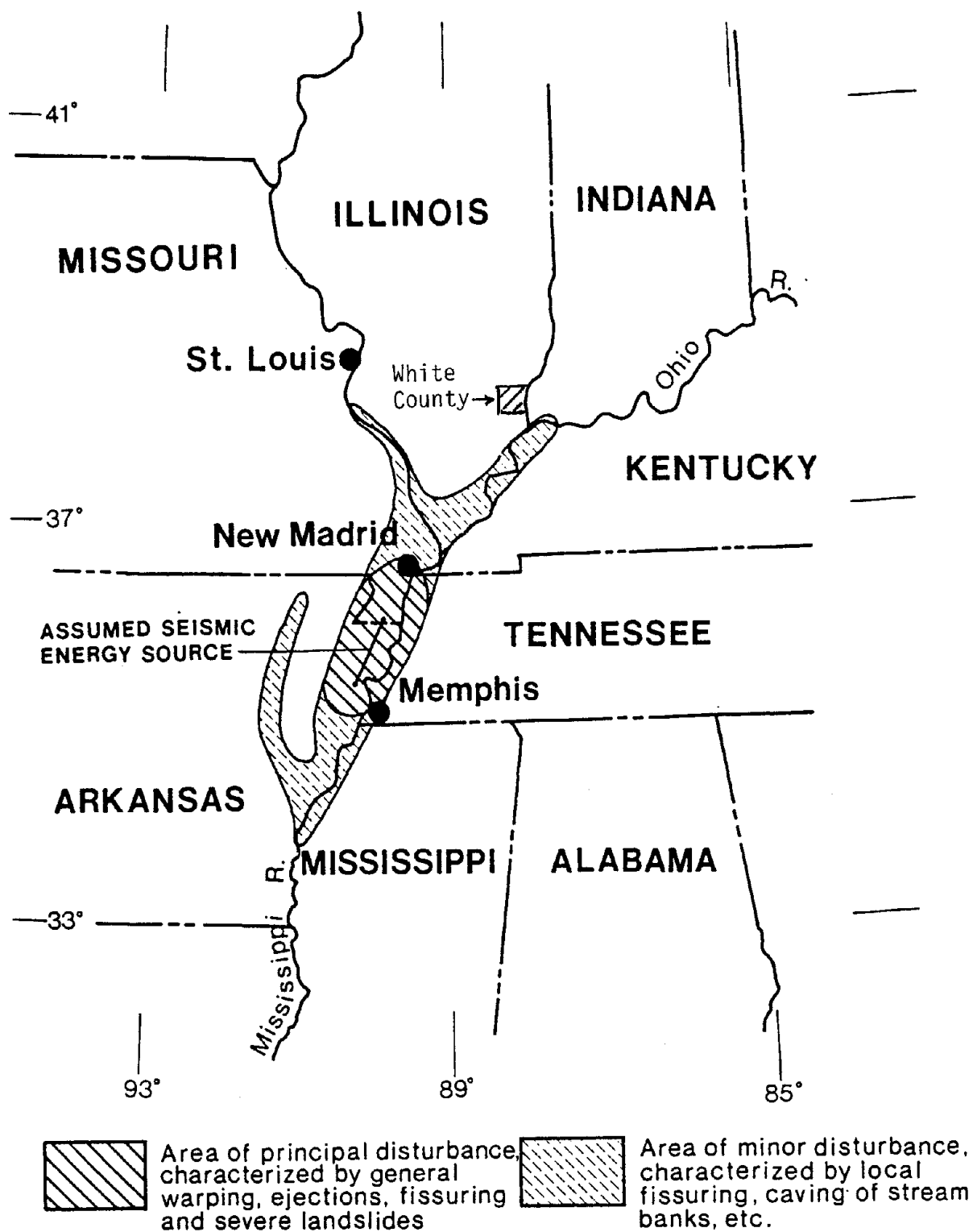


FIGURE 3.--AREAS OF PRINCIPAL AND MINOR DISTURBANCES AS IDENTIFIED BY FULLER (1912) FOR THE NEW MADRID EARTHQUAKES WITH ASSUMED SEISMIC ENERGY SOURCE ZONE NOTED ON MAP (AFTER TURNER, 1986)

approximately locate the seismic source zone. This placement is in general agreement with most estimates of the seismic source zone for those events. The 1811-1812 earthquake sequence included three events with estimated body-wave magnitudes between 7.0 and 7.3 (Street and Nuttli, 1984); thus, the composite source zone for the three events may have been somewhat longer than the zone marked on Figure 3. Because of this impreciseness of source zone, ranges are given for distances to some localities of liquefaction effects that are near the source zone.

Because of the considerable length of time before a thorough investigation was made of the New Madrid events, many liquefaction effects were destroyed or obliterated before detailed examinations were made. For example, even though considerable remnants of liquefaction effects remained when Fuller made his investigation of the area in the early 1900's, nearly 100 years after the earthquakes, he notes that overbank deposition and erosion due to flooding and meandering of the Mississippi and other rivers in the area had covered or removed many ground effects. This obliteration of fractures and sand boil deposits was greatest

TABLE 2.--ESTIMATED LSI FOR THE 1811-12 NEW MADRID EARTHQUAKES ( $M_w$  ABOUT 8.5)

SITE	DESCRIPTION	REFERENCE	DIST. km	ESTIMATED LSI		
				Max.	Best	Min.
Interior of zone of principal disturbance	Large fissure, sand boils and displaced ground, from approximately Marked Tree, Ark to New Madrid, Mo.	Fuller, 1912,	<50	100	100	100
Boundary of zone of principal disturbance	North of New Madrid, fissures 2 to 4 ft wide "the edges being marked with accumulations of sand and dark clayey shale." Very large sand boils also occurred in this area.	Fuller, 1912, p. 54, 82-83, and fig. 1	50-75	100	80	50
	South of Marked Tree, Ark., fissures 10 to 15 ft deep and 10 to 20 ft wide (most likely grabens).	Fuller, 1912, p. 56 and figs. 1 and 7				
Bound of zone of minor disturbance	"Stream banks were caved northward to Herculaneum, northeastward to Indiana, and southward to the Arkansas."	Fuller, 1912, p. 53	140	40	30	10
	"Less severe ground failure phenomena were observed along the Ohio river as far up river as a point somewhere between present day Henderson and Owensboro, Ky, and as far south along the Mississippi river as the mouth of the St. Francis river."	Street and Nuttli, 1984, p. 50				
Near St. Louis, Mo.	"O.W. Nuttli (oral comun.,) has found historical accounts that mention sand blow activity on the flood plain of the Mississippi River, near St. Louis."	Obermeier, 1988 p. 12	275	10	10	5
White County, Ill.	"Berry (1908) tells of sand blows and fissuring in White County, Illinois along the Wabash River."	Street and Nuttli, 1984, p. 45	250	20	10	5

near the rivers and thus particularly hampers our ability to assess LSI at localities beyond the area of principal disturbance, where ground effects were smaller and more concentrated near the river channels. Thus, the described effects represent only a small fraction of the entire array effects that were originally generated and the completeness of our LSI data set is likewise diminished.

Table 2 lists descriptions of liquefaction effects at various localities along with maximum, minimum, and best estimates of LSI for those places. The distance from the seismic source zone to each locality is also tabulated. Some additional information is given here to further amplify our estimates of LSI.

Within the interior of the area of principal disturbance, there are many descriptions of effects which indicate horizontal ground displacements in excess of 2.5 m. For example, Fuller (1912, p.56) describes fissures at a locality near the southern boundary of the area of principal disturbance as follows: "A mile and a half farther west, in Sec. 9, a series of northeast-southwest compound fissures of great size were observed. These are great canal-like depressions with flat bottoms and steep sides (higher even than the normal angle of repose) and so deep that a man on horseback is in some places unable to see over the top. It is probable that some of the depressions are from 10 to 15 feet [3 to 4.5 m] deep, and the bottoms are usually from 10 to 20 feet [3 to 6 m] in width." The ground effects described here, as at other localities with "compound fissures," are consistent with a lateral spread origin with lateral ground displacements in excess of 2.5 m. Similar features were observed near the northern bound of the area of principal disturbance.

The descriptions of sand boil deposits and fissures observed near St. Louis and in White County, Illinois are too brief to provide a conclusive estimate of LSI. The logic we used to assess LSI for these localities is as follows: Clearly there were some liquefaction effects at these sites. It is doubtful that such note would have been made if the effects were so minor as to be characterized by an LSI less than 5. Conversely, if these effects, particularly the fissures, had been of a width characterized by an LSI greater than 20, some additional note would likely have been made on their length or size as was done at many localities of larger effects. Because of the impreciseness of these descriptions, LSI can at best be estimated to the nearest multiple of 5 or 10. Thus, we gave values of 5, 10, or 20 for the minimum, best, and maximum estimates of LSI at these localities.

### **1886 Charleston, South Carolina Earthquake**

During the evening of August 31, 1886, a large earthquake struck an area northwest of Charleston, South Carolina. The earthquake was felt throughout nearly all of the US east of the Mississippi River. Nuttli (1983) estimated the body-wave and surface-wave magnitudes of the earthquake to be 6.6 and 7.5 respectively.

Numerous surface effects of liquefaction were observed in a area about 80 km in diameter centered on Charleston. Those effects were observed by several investigators whose descriptions have been compiled and evaluated in reports by Dutton (1890) and Peters and Hermann (1986).

Dutton identified two epicenters for the earthquake, each at the centers of subzones of more intense earthquake effects. Those epicenters are plotted on Figure 4 and a line connecting these two points is drawn as an approximate location of the zone of seismic energy release. This assumed source zone is consistent in length (20 to 30 km) and position with the generally accepted source zone for that earthquake.

Pertinent descriptions of the liquefaction effects at various localities are listed in Table 3 along with maximum, minimum, and best estimates of LSI, and the distance of the locality from the seismic source zone. Some additional information relative to the logic we used to assign LSI values is given below.

Ground displacements (as large as 8 ft 4 in (2.5 m)) and sand boils with extensive deposits as thick as 2 ft (0.6 m) were observed at Ten Mile Hill; these effects are large enough to be rated as LSI = 100 features. Dutton (1889, p. 312) marked Ten Mile Hill and several other places within the epicentral region with dark dots and described those sites as localities of "marked horizontal displacement." Although not clearly defined, displacements at some of the localities, such as Ten Mile Hill were as large as 2.5 m. From the few descriptions given for localities marked by dark dots, it appears that the larger of these displacements were generally greater than 1.5 m. We drew a bound around these darkened dots (Figure 4) and estimated that ground effects on this bound are representative of LSI 50 to 100 features.



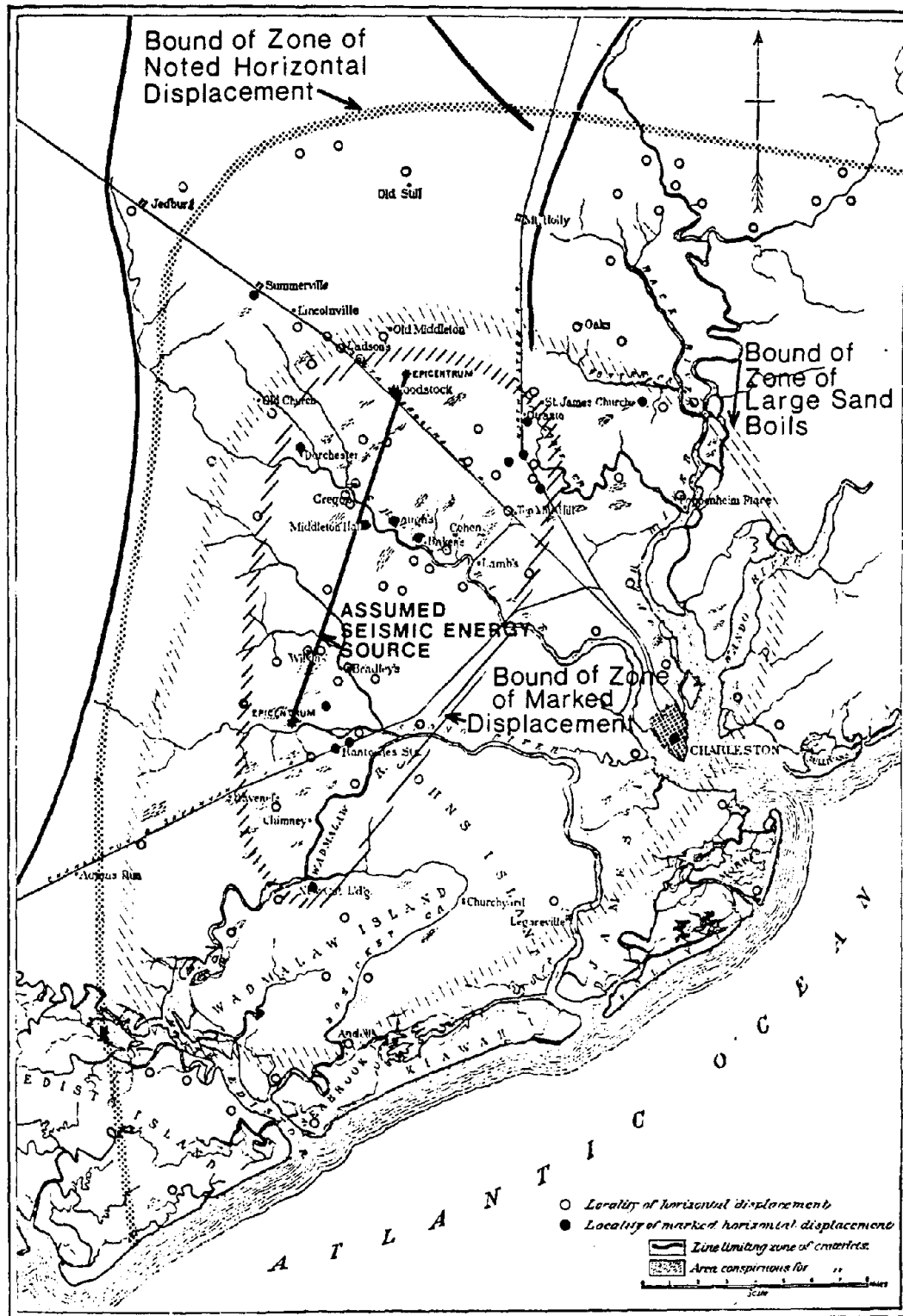


FIGURE 4.--LOCALITIES OF LIQUEFACTION EFFECTS NOTED BY DUTTON IN THE CHARLESTON, SOUTH CAROLINA REGION WITH ASSUMED SEISMIC SOURCE ZONE MARKED ON MAP (AFTER TURNER, 1986)

TABLE 3.--ESTIMATED LSI FOR THE 1886 CHARLESTON, SOUTH CAROLINA EARTHQUAKE

SITE	DESCRIPTION	REFERENCE	DIST. km	ESTIMATED LSI		
				Max.	Best	Min.
Mile 12 + 700, North Eastern Rail Road (Ten Mile Hill)	"Superstructure on embankment at point where trestle succeeds earthwork shifted 8 ft 4 inches to W. Embankment forced along azimuth down grade jamming south end of trestle,"	Peters and Hermann, 1986, p. 53.	8	100	100	100
Ten Mile Hill	"These craterlets seemed to reach their greatest development, both in size and number, near Ten-Mile Hill. Some of them were very large, one measuring 21 feet across. Many acres of ground were overflowed with the sand which was two feet or more in thickness near orifices."	Dutton, 1889, p. 284.	8	100	100	80
Most distant places of marked displacement	Map showing "localities of marked horizontal displacement." (Point at Charleston disregarded)	Dutton, 1889, pl. 27.	10	100	80	70
Most distant places of large sand boils	Map showing "areas conspicuous for craterlets."	Dutton, 1889, pl. 28	24	50	30	20
Most distant places of horizontal displ.	Map showing "localities of horizontal displacement."	Dutton, 1889, pl. 27	30	30	15	10
Bound sand boils noted by Dutton	Map showing "line limiting zone of craterlets."	Dutton, 1889, pl. 28	35	20	10	5
Georgetown, South Carolina	"Near the residence of Senator B.H. Williams was a sink of at least one foot in depth ... Three or four heaps of gray sand stood at irregular intervals on the edges of the sink. They were probably thrown up through the fissure by the internal convulsion."	Newspaper report (S.F. Obermeier, USGS, written comun.)	90	5	3	1

Dutton (1889, p. 318) also plotted localities of "areas conspicuous for craterlets [or sand boils]." These localities were sites of large and rather spectacular sand boils, some with craters several meters in diameter. We drew a bound around the localities so marked by Dutton (Figure 4) and estimated the LSI on that bound as follows. Although there is no direct relationship between sand boil activity and ground displacement, we estimated from the descriptions and the criteria given in Table 1 that the LSI on this bound ranged between 20 and 50.

Dutton (1889, p. 312) also plotted points on his maps noted as "locality of horizontal displacement." As shown on Figure 4, these sites generally lie well beyond the bound of "localities of marked horizontal displacement." We drew a bound around the "localities of horizontal displacement," and based on the few descriptions given estimate that displacements must have been as much as 250 mm and perhaps as great as 750 mm. These estimates give LSI values ranging from 10 to 30.

Dutton (1889, p. 318) also drew a bound on his map described as the "line limiting zone of craterlets [or sand boils]." From Table 1, we estimate that these sand boils were probably characteristic of LSI features in the 5 to 20 range to be so specifically noted.

A news paper article describing a more distant liquefaction feature was brought to our attention by Steve Obermeier (USGS, written communication). Based on the description of this feature as given in Table 3, and the fact that the reporter made a specific survey of the Georgetown area to find such features, we assigned an LSI value of 1 to 5 to this locality. Although the description is rather vague, clearly there was some ground effect associated with liquefaction, giving an LSI of at least 1 and no larger than 5. Additionally, based on the search that was made by the reporter, we conclude that no larger effects developed in the area and that this feature is a maximal liquefaction effect for that locality.

### 1988 Sanguenay, Quebec, Canada Earthquake

On November 25, 1988, a moderate magnitude earthquake struck the Parc Provincial des Laurentides about 40 km south of Chicoutimi, Quebec, Canada. The event, named the Sanguenay earthquake, has been assigned  $m_b$  and  $M$ , magnitudes of 5.9 and 6.0, respectively (Tuttle et al., 1989a; 1989b). That event generated minor liquefaction effects at several sites within a 55 km radius of the epicenter (Figure 5). For this analysis, we assumed the seismic energy source to be located directly beneath the epicenter, and measured horizontal distances from that point. For an  $M = 6$  event, the seismic source should have been several kilometers in extent and the source could have been a few kilometers from the epicenter. Thus, our source distances may be in error by a few kilometers.

Tuttle et al. (1989a) described several secondary ground effects generated by the 1988 Sanguenay earthquake. We used those descriptions, abstracted in Table 4, to assign LSI values for that event. No direct measurements of ground displacement were given, thus we used ground fissures and sand boil deposits, in that order of importance, to estimate LSI. No fissures with widths greater than 25 mm were reported on gently sloping ground. Thus, for nearly all of the sites, we assigned a minimum LSI of 1. Sand boil deposits were not very extensive at any of the sites, leading to maximum LSI values of 5 to 10. These values, along with distances from the seismic source, are listed in Table 4.

## ATTENUATION OF LSI IN THE EASTERN US

To assess LSI attenuation in the eastern US, LSI values listed in Tables 2, 3, and 4 were plotted against the respective estimated source distances. These results are shown on the log-log plot in Figure 6 along with best fit lines determined from least squares regression of the data. For comparison, we also plotted LSI that would be predicted for the western US using Equation 1. These plots show that LSI attenuates with distance in a consistent manner, that LSI is strongly a function of earthquake magnitude, and that LSI attenuates more slowly with distance in the eastern US than in the west. We have fit the data to log-linear equations similar in form to equation 1 and also to equations incorporating an anelastic attenuation function. Both equations provide reasonable fits to the data. We are now conducting additional analyses to determine best fits and to compare LSI attenuation functions with functions presently used to characterize attenuation of other earthquake parameters, such as maximum acceleration and velocity, and seismic energy.

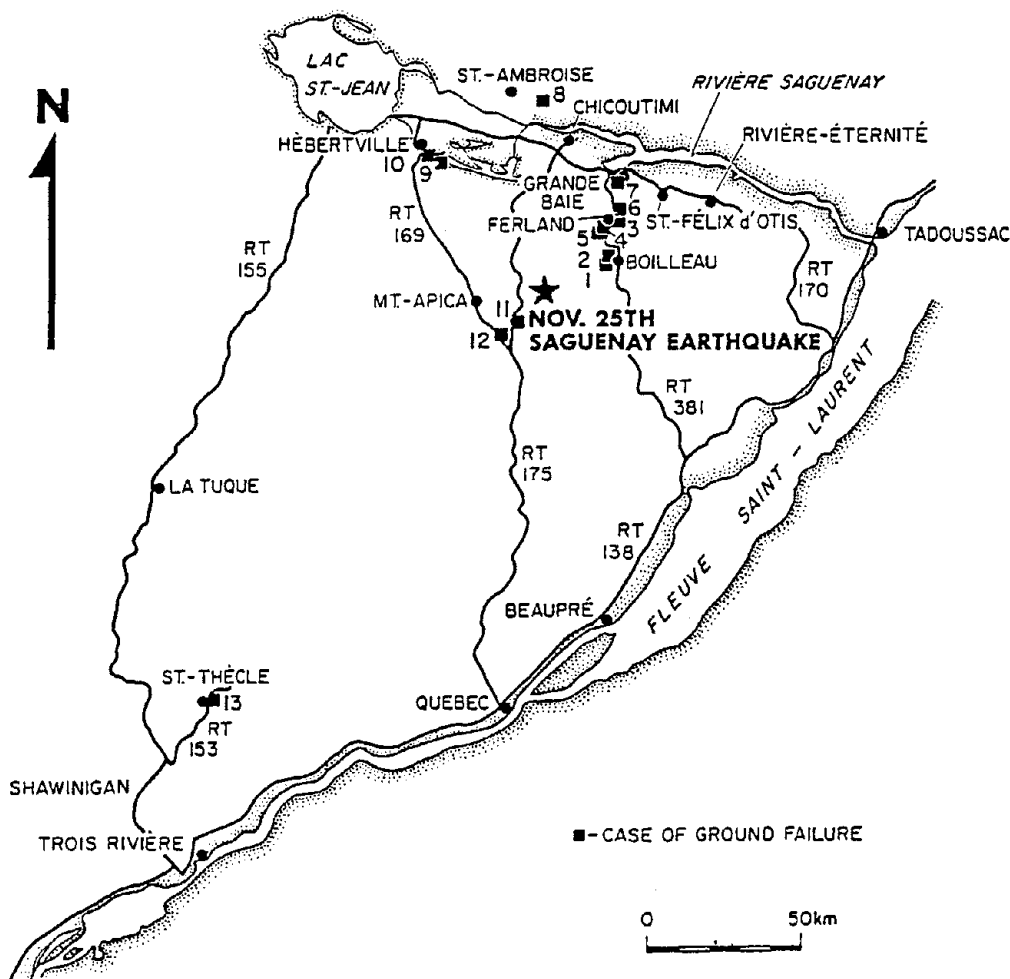


FIGURE 5.-- LOCATIONS OF GROUND FAILURES GENERATED BY THE 1988 SAGUENAY, QUEBEC, CANADA REPORTED BY TUTTLE ET AL. (1989a). MOST OF THE OBSERVED FAILURES WERE CONCENTRATED IN THE FERLAND-BOILLEAU VALLEY ABOUT 25 KM NORTHEAST OF THE EPICENTER (AFTER TUTTLE, ET AL., 1989a)

### CONCLUSIONS

Based on the data developed in Tables 2, 3, and 4, and plotted on Figure 5, we conclude the following:

1. LSI for eastern earthquakes attenuates with distance from the energy source with an exponential decay function similar in form to those developed for the western US.
2. Earthquake magnitude and distance from the seismic source are two primary parameters controlling the attenuation of LSI in the eastern US as well as in the west.
3. LSI attenuates more slowly in the eastern US than in the western US. This conclusion is consistent with the lower attenuation of other earthquake parameters such as intensity, acceleration, velocity, etc., in the eastern US.

TABLE 4.--ESTIMATES OF LSI FOR THE 1988 SANGUENAY EARTHQUAKE

SITE	DESCRIPTION	REFERENCE	DIST. km	ESTIMATED LSI		
				Max.	Best	Min.
Site 1	"A sand boil was observed [on the edge of a road] ... and many others ... on a nearby terrace within 15 m of the creek. The sand boils occurred at about 2 m spacings. ... The cones were 0.5 to 1 m in diameter"	Tuttle, et al., 1989, p. 5.	22	10	5	1
Site 2	"Two small sand boils were observed in a wet area ... A fissure at least 6 m in length had opened 8 cm about 1.5 m back from an old cut bank fluvial deposits."	Tuttle, et al., 1989, p. 5.	23	5	3	1
Site 4	"In a yard, ... a small fissure 1 cm wide and at least 0.6 m in length was observed ... Along the same trend and only 0.6 m away, a preexisting crack in the sidewalk had been widened by upward buckling. About 6 m to the south west of the fissure, a mound of very fine gray sand 0.5 to 1 m in diameter and 7.5 cm thick covered the grass. The sand mound reportedly formed during the earthquake. In addition, ... the residents claimed that large quantities of gray sand had come up in the creek ... as a result of the earthquake. ... [In the basement of the house,] the floor was separated from the base boards by about 1 cm and sand and water had entered the basement through this crack."	Tuttle, et al., 1989, p. 7.	27	5	3	1
Site 5	"A fissure about 10 m long and trending N1E was observed on the western side of the Rue Paquet. Very fine, gray sand was deposited along the fissure. The mound of sand was also 10 m in length, 2 m in width, and 3 cm thick adjacent to the fissure."	Tuttle, et al., 1989, p. 12.	23	5	3	1
Site 6	"Three fissures were observed ... [each] had a separation of about 8 mm. Two sand mounds reportedly formed ... One formed next to the creek ... and the other formed about 3 m from ... a small lake."	Tuttle, et al., 1989, p. 12.	34	4	2	1
Site 10	"A fissure approximately 20 m in length and with a separation of 8 to 16 mm formed 2 m from the waters edge. The crack was oriented parallel to the shore."	Tuttle, et al., 1989, p. 19	56	2	1	1

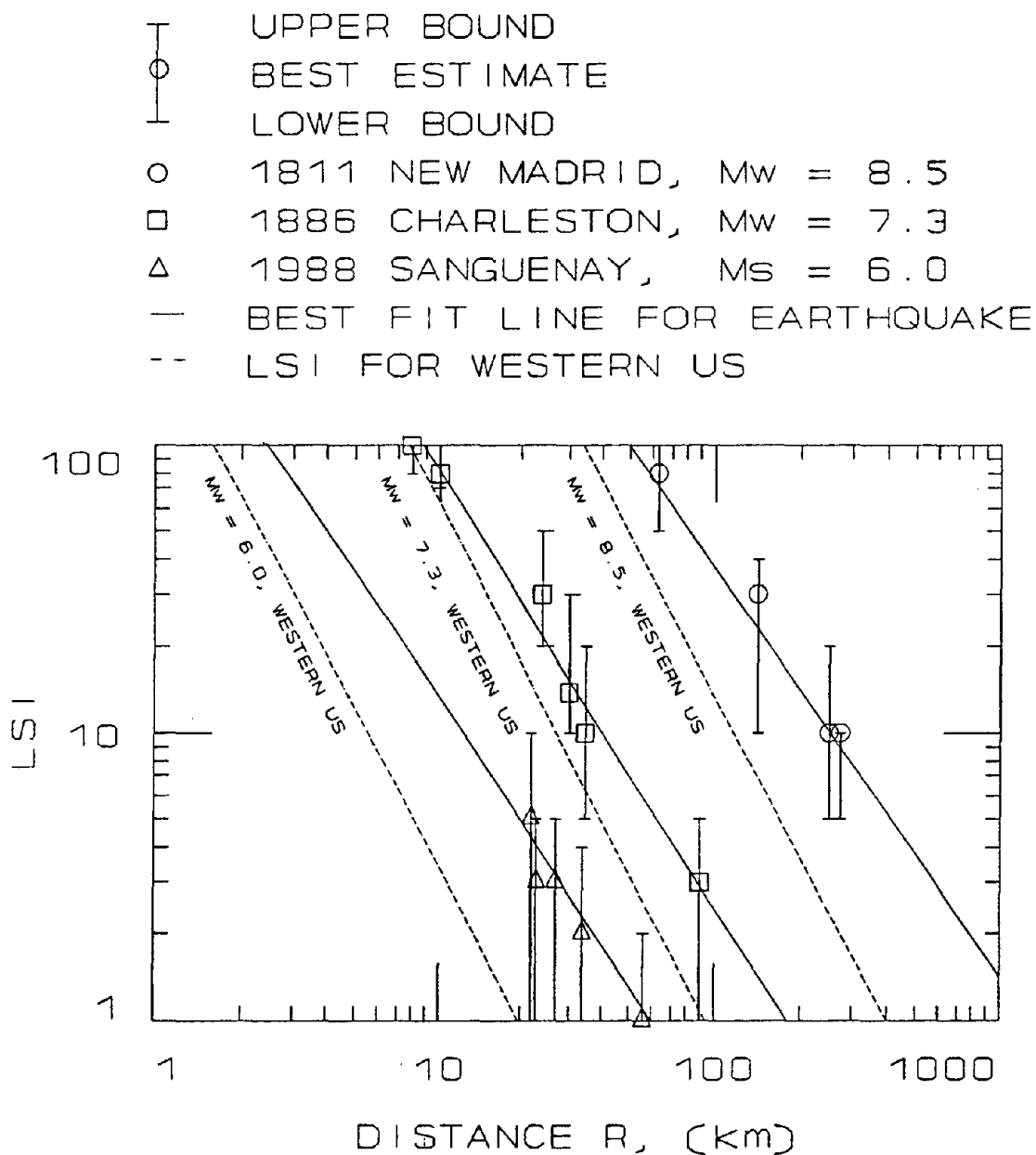


**FIGURE 5.--LSI VERSUS DISTANCE PLOTS FOR THREE EASTERN NORTH AMERICAN EARTHQUAKES WITH LEAST SQUARES BEST FIT LINES FOR EACH EARTHQUAKE PLUS LSI PREDICTED FOR THE WESTERN US FOR EQUIVALENT MAGNITUDE EARTHQUAKES FROM EQUATION 1**

## REFERENCES CITED

- Algermissen, S.T., Perkins, D.M., Thenhaus, P.C., Hanson, S.L., and Bender, G.L., 1982, Probabilistic estimates of maximum acceleration and velocity in rock in the contiguous United States: U.S. Geological Survey Open-File Report 82-1033, 99p.
- Dutton, C.E., 1889, The Charleston earthquake of August 31, 1886: U.S. Geological Survey, Ninth Annual Report, p. 207-528.
- Fuller, M.L., 1912, The New Madrid earthquake: U.S. Geological Survey Bulletin 494, 119 p.
- Nuttli, O.W., 1974, 1886 Charleston, South Carolina, earthquake revisited, *in* A Workshop on "The 1886 Charleston, south Carolina, Earthquake and Its Implications For Today:" U.S. Geological Survey, Proceedings of Conference XX, p. 44-50.
- Nuttli, O.W., 1983, Average Source-Parameters Relationships for Mid-Plate Earthquakes: Bulletin Seismological Society of America, v. 73, no. 2, p. 519-535.
- Peters, K.E., and Hermann, R.B., eds., 1986, First-hand observations of the Charleston earthquakes of August 31, 1886, and other earthquake materials: South Carolina Geological Survey, Bulletin 41, Columbia, S.C., 116 p.
- Street, R, and Nuttli, O.W., 1984, The Central Mississippi Valley earthquakes of 1811-1812, *in* Proceedings of the Symposium on "The New Madrid Seismic Zone:" U.S. Geological Survey, Open-File Report 84-770, p. 33-63.
- Turner, W.G., 1986, Computerized liquefaction mapping for the conterminous United States: unpublished MS thesis, Brigham Young University, Provo, Utah.
- Tuttle, M., Such, R., and Seeber, L., 1989a, Ground Failure Associate with the November 25th, 1988 Sanguenay Earthquake in Quebec Province, Canada: written report, Lamont-Doherty Geological Observatory of Columbia University, Palisades, N.Y.
- Tuttle, M., Seeber, L, and Jacob, K., 1989b, Earthquake-induced ground failure in northeastern North America: written report, Lamont-Doherty Geological Observatory of Columbia University, Palisades, N.Y.
- Youd, T. L., 1978, Major cause of earthquake damage is ground failure: Civil Engineering, v. 48, no. 4, p. 47-51.
- Youd, T.L., 1989, Ground failure damage to buildings during earthquakes, *in* Foundation Engineering Current Principles and Practices: American Society of Civil Engineers, v. 1, p. 758-770.
- Youd, T. L., and Hoose, S. N., 1978, Historic ground failures in northern California triggered by earthquakes: U. S. Geological Survey Prof. Paper 993, 177 p.
- Youd, T. L., and Perkins, D. M., 1987, Mapping of liquefaction severity index: Journal of Geotechnical Engineering, ASCE, vol. 113, no. 11, p. 1374-1392.

## LIQUEFACTION DISASTER MITIGATION FOR CIVIL ENGINEERING STRUCTURE IN JAPAN

Takahiro IWATATE<sup>1</sup>, Yoshiyuki NOZAWA<sup>2</sup>, and Shigeru GOTOH<sup>3</sup>

1. Central Research Institute of Electric Power Industry (EPRI), Japan
2. Engineering Research Center, The TOKYO Electric Power Co.;  
Inc., Japan
3. Institute of Technology, Shimizu, Corporation, Japan

### ABSTRACT

This paper presents the countermeasures on civil engineering structures against liquefaction which are currently proposed in Japan.

The basic consideration on countermeasure against liquefaction, the type and features of methods will be discussed, and moreover the effectiveness of the methods for countermeasure against liquefaction can be examined through the results of questionnaire on the execution performances of countermeasure.

The method of countermeasures are broadly classified into two types, according to the principle, one is that of preventing liquefaction and the other is that of improving structures themselves.

From the questionnaire of 41 execution performances of countermeasure against liquefaction, it is shown that most of these methods are aimed at preventing liquefaction of ground, and the methods aimed at improving structure itself are very few, and particularly, no sufficient evaluation is made on the effectiveness of prevention against permanent ground displacement, which is the target of the present study.

So, it will be necessary to clarify the extent and limit of effectiveness of each method against liquefaction and at the same time to examine an effective aseismic method against permanent ground displacement.



## INTRODUCTION

During the Niigata Earthquake, Nihonkai Chubu Earthquake, etc., conduits and manholes installed under the ground for water works, sewage systems, gas, telephone lines, etc., underground structures such as purification facilities, underground passages, etc., as well as bridge foundation, building foundation, and harbor structures such as bank-protection breakwaters, etc. suffered a serious damage owing to liquefaction of sandy ground.

To minimize damage to these civil engineering structures caused by liquefaction, therefore, it is necessary to study the development of methods for countermeasure against liquefaction, which can expect an aseismic effect on soft ground, as well as the effectiveness of countermeasure against permanent ground displacement, etc.

In this paper, with regard to methods for countermeasure against liquefaction, which are currently proposed, basic considerations the types and features of various methods as well as the results of questionnaire on execution performance of countermeasure against liquefaction will be discussed. (Ref. 1, 2, 3, 4)

### TYPES AND FEATURES OF METHODS FOR COUNTERMEASURE AGAINST LIQUEFACTION

Countermeasures against liquefaction can be broadly classified into the following two methods, and can also be classified according to the principle of countermeasure as follows.

- (1) Countermeasure which prevents the outbreak of liquefaction itself (Preventing Methods)
- (2) Countermeasure of improving structure itself which permits the outbreak of liquefaction but is intended not to impair the function of structures (Improving Structure Methods)

The types and features of methods for countermeasure against liquefaction are summarized in Table 1 for Preventing Methods and Table 2 for Improving Structure Methods.

The preventing methods include ① Compaction method, ② Replacement or Mixing treatment and Solidifying method, ③ Ground-water level reduction method, ④ Excess pore water pressure dissipation method, ⑤ Shearing deformation restraint method, etc.

The features of these preventing methods are described below.

- ① The compaction method, since its effectiveness was confirmed in the Niigata Earthquake (improved effectiveness was attained by the vibro-floatation method), has been widely applied based on the sand compaction pile method, etc. If compaction as deep as 10 to 20 m under the ground surface is desired, the sand compaction pile method,

vibro-floatation method or rod compaction method is appropriate. For surface compaction, the dynamic consolidation method or vibro-tamper method is suited. The compaction method can expect an effect of making the ground dense as well as an effect of reducing the shearing deformation owing to seismic motion.

However, when compacting the ground, many vibrations are generated. If there are structures in the neighborhood, therefore, the influence of vibrations on these structures comes into problem. Particularly, the dynamic consolidation method is low in construction cost but generates many vibrations, and is therefore suitable for execution of work in wider areas like reclaimed land than the ground around existing structures.

- ② The replacement or mixing treatment and solidifying method prevents the outbreak of liquefaction by excavating the soil layer which is liable to cause liquefaction and replacing it with other materials and mixing and impregnating cement into that soil layer. In the case of the replacement method, there are restrictions. For example, execution of work up to a deep position is difficult to carry out, while the mixing and impregnating method is generally high in construction cost. There is, however, an advantage that the mixing treatment method or chemical grouting method can be applied even in cases where methods for existing structures cannot be applied.
- ③ The ground-water level reduction method, as its feature, not only makes the surface's non-liquefied layer thick by placing the liquefaction layer under unsaturated condition but also increases the effective stress of soil deeper than the ground-water level, thereby increasing the strength against liquefaction. Although it is not a ground-water level reduction method, surface filling also gives a similar effect. However, these methods are liable to cause troubles. For example, if soft cohesive soil is present in a deep part, settlement due to consolidation breaks out at the same time and the ground-water level in the neighborhood is caused to decrease.
- ④ The excess pore water pressure dissipation method is a pipe drain method using porous pipes, in addition to a gravel drain method which used crushed stone as its material. Although some indoor and in-site experimental examples are reported, there are very few examples which have demonstrated its effectiveness. Although these methods are not intended to improve ground around drains, if excess pore water pressure begins to rise, they have effectiveness to immediately eliminate it, thus shortening the water pressure rise time and reducing the amount of rise. However, problems remain to be solved with respect to drainage resistance of drain, long-term clogging and settlement of ground owing to drainage.
- ⑤ The shear deformation restraint method prevents liquefaction by reducing the repeated shear stress which occurs owing to an earthquake and can also expect effectiveness which makes structures difficult to settle down even if liquefaction takes place. In this respect, therefore, the method is suited as a countermeasure against

liquefaction for existing structures.

The other hand, the improving structure methods include, ① Strengthen the foundation for direct-foundation structure, ② Increasing the number of piles and the stiffness of piles for pilefoundation structure, ③ Support with pile and sand bags and increasing the strength of the structure itself and the joint for underground structure, ④ Driving the sheet-piles or strengthen retaining work in the revetment for soil structure etc.

Thus, many proposals have been presented to prevent liquefaction, and each method varies with the types of structures and conditions of ground and has its own features in construction cost, workability, effectiveness, etc. In making actual application, therefore, it is necessary to select several possible methods based on the existing examples of countermeasures before starting the detail design of countermeasures and choose the most suitable method with sufficient consideration given to ground conditions, construction cost, work period, workability (including influence on surrounding environment and adjacent structures), economy, past results, reliability of effectiveness, etc.

The optimum method is not always limited to one method, but there is also a case where it is better to make combined use of 2 or 3 methods.

#### EXAMPLE OF EXECUTION PERFORMANCE OF COUNTERMEASURE AGAINST LIQUEFACTION

The Result of Case study of the execution performance of countermeasure against liquefaction through questionnaire.

Study was conducted on a total of 41 cases, which were classified by each method and summarized in Table 3.

When classified by principle, among methods for countermeasure against liquefaction, 23 cases (classification A) were mainly aimed at increasing density, including sand compaction pile method, dynamic consolidation method, vibro-rod method, etc., while 11 cases (classification B) were mainly aimed at dissipating pore water pressure, including crushed-stone drain method, drain pipe method, etc. These cases occupied a majority. Cases relating to countermeasures for structures included 1 case (classification D) of slurry wall method, 2 cases (classification F) of anti-floating method and 1 case (classification E) of displacement absorption by flexible joints. These cases were very few.

Besides, there were two cases (classifications C and G) where liquefaction was prevented by solidifying the ground as well as by replacing the ground.

From the results of the questionnaire, two typical examples of countermeasure by TEPCO and SHIMIZU corporation were shown in detail as follows.

#### Execution Performance of Countermeasure by TEPCO(Ref. 5)

The Vibro-rod method and the gravel drain method were applied for countermeasure of ground liquefaction of the site of TEPCO LNG fired thermal plant.

The outline of the countermeasure done at a site of TEPCO (Site A) is summarized in Table 4(a). Since this area had been reclaimed by unity sand, the probability of liquefaction was high as shown in Figure 1, 2.

Fundamentally the vibro-rod works was adopted, but for protecting the structure revetment from the vibration influence of vibro-rod works, the gravel drain method was adopted near the revetment.

Based on the result of the multi-reflection analysis whose maximum acceleration was 150 gal at the seismic bedrock, our prediction for liquefaction probability was calculated as shown in Figure 2 FL-value is the factor of liquefaction resistance. In this hatching area had the probability of liquefaction.

The width of countermeasure was decided by using the collapse angels of earth pressure as shown in Figure 3.

Also in Figure 1, the measuring points of excess pore water pressure are shown by open triangles. The measuring point of acceleration is near this area. Figure 4 shows the acceleration time histories of the ground motion and the time histories of the excess pore water pressure at 15m depth Chibaken Toho-oki earthquake of December 17, 1987. This earthquake's JMA magnitude was 6.7, and epicentral distance was about 80km. The maximum acceleration was 56 gal. Shown in this figure, the maximum value of the excess pore water pressure obtained at the non-countermeasure area is about three times as large as those of the countermeasure area.

In Figure 4 the accumulating and vanishing processes of the excess pore water pressure are not clear. But as shown in Figure 5 the other records obtained at another site of TEPCO (Site B), these processes appear for only 10 or less seconds. So it is easy to suppose that these processes are not shown clearly in Figure 4.

#### Execution Performance of Countermeasure by SHIMIZU Corporation

The sand compaction method was applied for countermeasure of ground liquefaction at new manufactory construction site as shown in Figure 6.

The outline of the countermeasure is summarized in Table 4(b).

At the Tokachi-oki earthquake, old manufactory which was countermeasured by Vibro-Floatation for soil liquefaction in this site found to be less damage where as most of the site was damaged.

However, in this case sand compaction pile method was applied to the new construction project because of its high reliability. A loose sand deposit was bedded at 5.5m in depth which would be liquefaction susceptible. The maximum ground surface acceleration observed adjacent to this site Tokachi-oki earthquake (225gal) was used at the design.

Sand compaction piles - 70cm in diameter, 5.5m in length - were set spacing of 1.5m in square. Countermeasure area covered the structure and extend to a same distance as the length of the sand compaction pile. Performance of the countermeasure was confirmed by the standard penetration test with increasing the soil selection density and N-Value shown in Figure 7. So far, real performance of the countermeasure has not been confirmed due to lack of a large earthquake.

### CONCLUSION

- (1) Methods for countermeasure against liquefaction can be broadly classified into a countermeasure against liquefaction itself (Preventing Methods) and a countermeasure which permits the outbreak of liquefaction but is intended not to impair the function of structures (Improving Structure Methods).
- (2) The countermeasure of preventing liquefaction comes in various method including the method of increasing density or increasing shear strength by solidifying, method of promoting early dissipation of excess pore water pressure, method of making it difficult to cause liquefaction by reducing the degree of saturation, etc., method of absorbing displacement owing to liquefaction, etc., and each method has attained respective achievements.
- (3) These methods vary with the types of structures, ground conditions and environmental conditions and have their own features in workability, effectiveness, etc.  
The present case study indicated that many methods of countermeasure against liquefaction are implemented according to the types of structures and ground conditions. However, most of methods for countermeasure against liquefaction consist of methods aimed at mainly increasing density, such as sand compaction method, dynamic consolidation method, vibro-rod method, etc. as well as methods aimed at dissipating pore water pressure, such as crushed stone drain method, drain pipe method, etc. Methods for countermeasure for structures to prevent permanent ground displacement and destruction of structures after liquefaction were very few.
- (4) In each method, its effectiveness, application limit, etc. are not clearly indicated owing to the lack of cases experiencing a strong earthquake. Particularly, no sufficient evaluation is made on the effectiveness of prevention against permanent ground displacement, which is the target of the present study, and there are many obscure points in this regard.
- (5) In the future, it will be necessary to carry forward study with respect to the extent of effectiveness of improved ground, the range of improvement, etc. and to promote improvement in economy of method of countermeasure against liquefaction and selection of the optimum method according to the importance of structures concerned, through

seismic observations, vibration tests and analyses using models, etc, and at the same time to examine an effective aseismic method against permanent ground displacement.

### ACKNOWLEDGMENTS

This research presented herein was supported by the Working-III Research Team of the Association for the Development of Earthquake Prediction (ADEP) of Japan.

The authors express sincere thanks and appreciation to Dr. Tsuneo KATAYAMA of professor of TOKYO University who is a leader of Working-III Research Team of ADEP and the researchers of Working-III Research Team of ADEP for their valuable support for this paper.

### REFERENCES

1. T. Iwatate and Y. Yoshii : Actual situation of damage caused by liquefaction to buried pipes and its countermeasure. Chapter II, Electric Power - Countermeasures against liquefaction of underground structures - Japan Science and Technology Association (in Japanese)
2. Y. Yoshimi : Soil Foundation Series ; Liquefaction of ground. Gihodo. (in Japanese)
3. N. Suematsu, Y. Yoshimi and Y. Sasaki : Liquefaction of ground ; Methods for mitigating damage caused by liquefaction. Society of Soil Engineers. (in Japanese)
4. T. Fujinami and T. Koyama : About countermeasures against liquefaction on underground transmission lines. Denryoku Doboku, N. 164, p.69-p.81, 1980. 1. (in Japanese)
5. T. Iwatate, K. Ohtomo, J. Tohma and S. Nozawa : Liquefaction disaster mitigation for underground structures. Proceedings of 1st Japan-U.S. Workshop on Liquefaction, Large Ground Deformation and Their Effects on Lifeline Facilities p.143-p.151, November 1988, Tokyo, Japan.

Table 1 Type and features of methods for countermeasure  
( countermeasure preventing ground liquefaction )  
(Part 1)

Classification by principle of countermeasure	Expected effectiveness of countermeasure	Applicability	Method	Applicable depth	Limit of effectiveness	Influence on surrounding environment	Past execution of work	Remarks
Compaction (increase in density)	The strength of ground is enhanced by increasing the density; however, like the sand compaction pile method which applies pressure in the horizontal direction, both density and confined stress (mean principal stress, strictly speaking) are caused to increase.	Most widely used as a countermeasure against liquefaction, and many methods are also proposed. It is necessary to thoroughly examine the features because improvable depth, limit of effectiveness and construction cost vary with methods. As vibration accompanies on the whole, it is necessary to pay attention environment.	Sand compaction pile	GL-45 approx.	N value: 25-30 approx.	Mainly based on vertical vibration ; exerting influence	◎	The use of gravel material permits dissipation of pore water pressure as well
			Vibro-flotation	GL-20 m approx.	N value: 15-20 approx.	Mainly based on horizontal vibration ; exerting no influence relatively	◎	The use of gravel material permits dissipation of pore water pressure as well
			Rod compaction	GL-20 m approx.	N value: 15-20 approx.	Mainly based on vertical vibration ; exerting influence relatively.	○	
			Dynamic consolidation	GL-10m approx.	N value: 15-20 approx.	Exerts influence owing to a large weight-drop impact force.	○	Compaction of not only a deep layer but also an extremely surface layer is possible.
			Vibro-tamper	GL-3m approx. Surface layer only	N value: 15 approx.	Mainly based on vertical vibration; exerting influence relatively	○	Suitable for surface-layer compaction. Widely used in compaction with other methods.
			Rolling compaction	20-30cm per layer. Shallower than ground water level	Relative density: 95% approx.	Exerts no influence relatively.	○	Effective in the case of backfilling or filling work.
			Group of piles	GL-10m approx.	Little confirmation has been made yet.	Exerts influence owing to vibration caused by pile driving.	△	Also provides a bearing effect by piles.
			Raw lime pile	GL-20m approx.	Little confirmation has been made yet.	Vibration is small, but there is influence by dust.	△	Compaction by water absorption and expansion of raw lime.

## (Part 2)

Classification by principle of countermeasure	Expected effectiveness of countermeasure	Applicability	Method	Applicable depth	Limit of effectiveness	Influence on surrounding environment	Past execution of work	Remarks
Replacement or mixing treatment and solidification	Increase in the strength of ground (replacement, mixing treatment and solidification). Improvement in permeability (crushed stone replacement)	As a countermeasure for the surface-layer section of ground the replacement method is frequently used also, in filling and quaywall, mixing treatment is frequently used. However, deep-layer mixing treatment takes time, and homogenization is generally difficult.	Replacement Surface-layer mixing treatment Deep-layer mixing treatment.	Gl-5m approx. Surface layer only. Gl-5m approx. Surface layer only. Gl-30m approx.	Effective, depending on material in the replacement section. Effective, depending on the amount of mixing Effective, depending on the amount of mixing Effective, depending on the amount of impregnation.	Minimum influence. Minimum influence. Minimum influence. Minimum influence.	◎ ○ ○ ○	The drainage effect permits a subsurface countermeasure in the neighborhood. It is necessary to pay attention to homogenization It is necessary to pay attention to homogenization Possible even with existing structures.
Lowering of ground-water level (lowering of the degree of saturation)	Prevents liquefaction by unsaturation (ground in the section higher than the ground-water level). Prevents liquefaction by increasing the effective restraint pressure (ground in the section lower than ground-water level).	The method using the drain ditch is inexpensive, but the water level generally does not go down very much. Other two methods permit to lower the water level considerably, but maintenance costs a lot. Applicable to existing structures in combined use with cut-off wall.	Drain ditch, drain pile Well point Deep well	Generally surface layer only, depending on cases. Possible to lower the water level by 0~5m approx. Possible to lower the water level by 13~20m approx.	More reliable in the section higher than the water level. More reliable in the section higher than the water level. More reliable in the section higher than the water level.	Minimum influence. Settlement of ground owing to a drop in waterlevel exerts influence. Settlement of ground owing to a drop in waterlevel exerts influence.	△ ○ △	Long-term running poses a problem. Long-term running poses a problem.
Dissipation of excess pore water pressure (drainage)	Reduction in the uplift by promoting the dissipation of excess water pressure makes the ground difficult to suffer liquefaction	Influence on the environment is small and some models are inexpensive, thus finding many uses.	Pile-type gravel drain Gravel drain in the underground structure backfilling section.	Gl-20m approx. Range of backfilling around structure	There are some problems in reliability, including permeability There are some problems in reliability, including permeability.	Minimum influence. Minimum influence.	◎ ◎	Put to use when influence on the environment comes into problem.
Restraint of shear deformation	Reduction in shear stress generated in the ground by restraining shear deformation during earthquake.	As construction cost is high, there are many cases where those installed for purposes are used.	Sheet-pile or underground continuous wall	Gl-10m approx.	Little confirmation has been made yet.	Vibration generated during sheet-pile driving exerts influence	△	

\* Revised and prepared with reference to literature 6)



Table 2 Type and features of methods for countermeasure  
(countermeasure improving structure itself)

Type of structure	Method for countermeasure	Expected effectiveness of countermeasure	Applicability	Past execution of work
Direct-foundation structure	Strengthen the foundation. (For example, install underground beams or reinforcing bars in strip footings.)	Even if ground suffers some differential settlement owing to liquefaction, it can withstand on the reinforced foundation.	Possible by some reinforcing work. But, settlement owing to sinking of the structure itself cannot be avoided.	Used in some structures, particularly finding uses in wooden houses in general as a countermeasure against liquefaction.
	Change to the pile foundation	The pile foundation can bear even if liquefaction takes place.	A different foundation form is applied.	Little used owing to expensive construction cost.
Pile-foundation structure	Increase the number of piles and the cross-section (stiffness) of piles.	As the horizontal resistance increases, horizontal displacement and stress which is generated in piles can be reduced.	As it is not a different foundation form, designing can be easily accomplished.	Widely used because the foundation form is not different and construction cost is low.
	Install oblique piles.	As the horizontal resistance increases, horizontal displacement and stress which is generated in piles can be reduced.	As it is not a different foundation form, designing can be easily accomplished. However, in cases where the angle of inclination is large, the bending stress which is constantly accompanied by a settlement due to consolidation may increase.	The foundation form remains the same and construction cost is low, but it is not generally used very much because it would be much simpler to change the number of piles. However, there are many results obtained in harbor facilities.
Underground structure	Increase the length of piles.	It is possible to increase the vertical bearing power.	As it is not a different foundation form, designing can be easily accomplished. However, effectiveness is small as to horizontal resistance.	Finding considerable uses with friction piles.
	Support with piles and sand bags.	Effective to restrain floating, settlement and lateral movement.	Applicability is good, posing little problem as to underground conduits and tunnels. However, sand bags can be used for underground conduits only.	Widely used because construction cost is not so high.
Soil structure	Increase the strength of the structure itself or joint or enhance deformation performance.	Even if the strain of ground increases owing to liquefaction, the structure may be designed to withstand it.	Only reinforcement may be applied. However, applicability is not clearly established in cases where the extent of liquefaction is severe and the strain is large.	Widely used because construction cost is not so high.
	In cases where liquefaction layers exist partially, apply suppression-filling or reduce the slope gradient. Drive sheet-piles or strengthen retaining work in the revetment.	The countermeasure makes it difficult to cause destruction even liquefaction takes place. Restrains the deformation of structures owing to liquefaction.	Only the shape may be slightly changed, but the effectiveness is not so large, and there is some safety factor. There is also a problem in acquiring land. It is considered very effective.	Widely used because of its simplicity. Reinforcing of retaining works is widely used because of its simplicity. Sheet-piles are frequently used in railway filling in particular.

Table 3 Example of methods for countermeasure against liquefaction (Part 1)

No	Classification	Name of method	Structure concerned	Location	Description	Presented by
1	A-SCP-1	S.C.P	Tank foundation ground	Coastal industrial zone	Prevention of liquefaction in buried soil layer	Tobishima Construction Co.
2	A-SCP-2	S.C.P and D.C	Tank foundation ground		D.C. improvement depth 3 ~ 6m, target $N \geq 15$	Kajima Construction Co.
3	A-SCP-3	S.C.P	Foundation ground of tank with filled-up bank for disaster prevention		Improvement of buried soil layer (6 ~ 8m, $N = 5$ )	Kajima Construction Co.
4	A-SCP-4	S.C.P	Foundation ground of underground LNG storage tank		Ground reclaimed with dredged sand, target $N \geq 15$	Kajima Construction Co.
5	A-SCP-5	S.C.P	Foundation ground of underground LNG storage tank	Sodegaura Plant, Tokyo Gas Co.	Prevention of liquefaction in buried soil layer, target $N \geq 15$	Tokyo Gas Co.
6	A-SCP-6	S.C.P	Factory foundation ground	Hachinohe, Aomori Pref.	Alluvial sand layer	Shimizu Construction Co.
7	A-SCP-7	S.C.P	Cooling intake pipeline		Reclaimed soil layer, $N = 5$	Tokyo Electric Power Co.
8	A-SCP-8	S.C.P	Filling for underground LNG storage tank		Reclaimed sand layer	Tokyo Electric Power Co.
9	A-SCP-9	S.C.P floating method	Crude-oil tank foundation	Seijo (Shikoku)	Ash and sand of G.L. -2 m ~ -10 m, $N = 2 \sim 10$ were improved to $N = 8 \sim 18$ .	Shikoku Electric Power Co.
10	A-SCP-10	Combined use of S.C.P. and G.D.	Pile foundation		S.C.P. is applied around pile foundation so that influence of lateral displacement during execution of work is avoided.	Kumagayagumi Co.
11	A-SCP-11	S.C.P	Circulating water channel (Pile foundation)		Improved width: 6 m from the end of structures; diameter: 700 mm; length: 10; pitch: 1.6 m; square arrangement	Sato Kogyo Co.
12	A-SCP-12	S.C.P	Common ditch		Improved range: 7 m from the end of structures; improved to depth of 10 m; diameter: 700 mm; length: 10 m; pitch: 1.7 m; square arrangement	Sato Kogyo Co.
13	A-SCP-13	S.C.P	Revetment		Improved range: 5.5 m from the end of structures; depth 8 m; diameter: 600 mm; length: 7.9~8.9 m; pitch: 2 m; square arrangement	Sato Kogyo Co.
14	A-SCP-14	S.C.P	Tank foundation		Improved range: 5 m from the end of structures; depth 8m; diameter: 800mm; length: 8 m; pitch: 1.8 m; square arrangement	Sato Kogyo Co.
15	A-DC-1	S.C.P. and D.C.	Tank foundation ground	Tomakomai	S.C.P. is applied after compacting the shallow-layer section (shallower than G.L. - 6 m) with D.C.	Shimizu Construction Co.
16	A-DC-2	D.C.	Tank foundation		Ground reclaimed with clay-mixed gravel; alluvium deposit; target: G.L. $N \geq 15$	Kajima Construction Co.
17	A-DC-3	D.C.	Foundation of main hall; foundation of various machines		Ground reclaimed with seabed sediments; G.L. 0 ~ 8 m, $N > 15$	Tohoku Electric Power Co.
18	A-DC-4	D.C.	Subbase-course reclamation work		Ground reclaimed with dredged sediments; target: $N = 10$ , $qc = 40 \text{ kgf/cm}$	Kajima Construction Co.
19	A-OFB-1	O.F.B	Tank foundation ground	Yatsushiro	Reclaimed land ( $N = 2 \sim 10$ )	Okumuragumi Co.
20	A-OFB-2	O.F.B	Powerplant	Sakaide	Reclaimed ground; sandy soil mixed with silty soil mass	Okumuragumi Co.
21	A-VR-1	Vibro-rod	LNG piping tunnel		Reclaimed sand layer	Tokyo Electric Power Co.
22	A-VF-1	Vibro-floatation method	Foundation ground of crude-oil tank, etc.	Niigata City	Typical example which shows the effectiveness of the compaction method. According to the thesis of Takashi Watanabe (1966).	CRIFPI
23	A-VF-2	Vibro-floatation method	Gate		Improved range: 3.8 m from the end of structures; depth: 5.6 m; diameter: 600 mm; length: 5.6 m; pitch: 1.2m; square arrangement	Sato Kogyo Co.
24	B-GD-1	G.D. (S.C.P)	Factory foundation ground	Miyazu, Kyoto	Gravel-mixed sandy ground; partially constructed with G.D. owing to noise and vibration problems.	Shimizu Construction Co., Ltd.
25	B-GD-2	G.D. (S.C.P.)	Box culvert	Tomakomai	The section which is liable to exert influence on existing structures is constructed with G.D.	Shimizu Construction Co., Ltd.

(Part 2)

No	Classification	Name of method	Structure concerned	Location	Description	Presented by
26	B-GD-3	G.D.	NTT-specification manhole	Past execution of work (Ogata-mura (1984))	A rise in pore water pressure is avoided to prevent the manhole from floating up.	NTT
27	B-GD-4	Crushed stone drain	Facilities of terminal treatment plant		Reclamation with surface layer of 12 m approx. and N value of less than 15, and fine sand layer on top of alluvium deposit; cylindrical drain	Tobishima Construction Co.
28	B-GD-5	Crushed stone pile drain	LNG piping tunnel		Cassion-type revetment; section adjacent to L-shaped revetment; cylindrical drain	Tokyo Electric Power Co.
29	B-GD-6	Crushed stone drain	L-shaped revetment		Uniform mountain sand. N = 7 ~ 10	Nippon Kokan
30	B-GD-7	Crushed stone drain	Circulating oil pump at thermal power plant		Piles of 400 mm in diameter are installed upto a depth of 10.5 m at pitchers of 2 m in the reclaimed sand layer and alluvial sand layer of the thermal power plant. The target is set at earthquakes of about M7.5, but there is no experience in suffering earthquakes.	Chubu Electric Power Co.
31	B-GD-8	Lining gravel drain	Underground transmission and distribution tunnel	Reclaimed land of Osaka Minami Port	Reclaimed sand layer on alluvial clay soil (layer thickness : about 15 m)	Kansai Electric Power Co.
32	B-GD-9	Crushed pile drain in combined use with steel sheet-piles	LNG gas conduit pipe		Owing to restriction by land, the improvement range was narrowed by driving sheet-piles.	Tokyo Electric Power Co.
33	B-GD-10	Crushed stone reclamation method	Underground transmission tunnel		Reclaimed sand layer (silty fine sand)	Tokyo Electric Power Co.
34	B-DP-1	Drain pile	Office building	Yashiro, Niigata Pref.	Alluvial sand layer 0 ~ 12 m is improved.	Taisei Construction Co.
35	C-1	Column-shaped solid body construction method	Building foundation ground		Gravel-mixed sand, silt, fine sand, sand; design method and design conditions; liquefaction layer is judged by Seed's method.	Kajima Construction Co.
36	C-2	Solidification method	Office building	In Kagoshima City	Alluvial Shirasu sand layer. N value is 5 or less up to G.L. - 15 m.	Takenaka Komuten Co.
37	D-1	Slurry wall Method	Factory facilities		Impermeable layer exists at G.L. - 16 m and deeper.	Taisei Construction Co.
38	E-1	Absorption of ground displacement by Polycron FRP flexible joints	Underground line and communication conduit		Possible to cope with floating due to liquefaction or displacement due to settlement of ground.	Kansai Electric Power Co.
39	F-1	Anti-floating pile work	Underground transmission tunnel		There is restriction by land owing to reclaimed sand layer and adjacent structures.	Tokyo Electric Power Co.
40	F-2	Anti-floating work (sand bag + sheet pile)	Buried pipe for underground transmission		There are restrictions with respect to alluvial sand layer, land and noise.	Tokyo Electric Power Co.
41	G-1	Excavation replacement	Tank foundation		Improved range: about 5 m from the end of structures; depth 2 m; judgement of effectiveness is made by flat-plate loading test.	Sato Kogyo Co.

Classification by principle of method : A (mainly by increase of density), B (mainly by dissipation of pore water pressure), C (mainly by solidification), D (mainly by lowering the degree of saturation), E (mainly by absorption of displacement), F (mainly by prevention of floating), G (mainly by replacement)

Explanation of abbreviations : S.C.P.: sand compaction pile method, D.C.: dynamic consolidation method; V.R.:vibro-rod method; G.D.: gravel drain method; D.P.: drain pile method  
O.F.B.: OKUMURA Foundation Betterment

Table 4-a Example of Execution Performance of Countermeasure by TBPCO

Reported from	Tokyo Electric Power Co.
Name of Method	Gravel Pile Drain ( No Ground Vibration )
Structure	LNG Conduit line (Pile Foundation)
Ground Condition	Reclaimed Sand ( $D_{50} = 0.3\text{mm}$ , Coefficient of uniformity: 2~7)
Construction Condition	Closed by Caisson Type Revetment and L-Type Revetment.
Reason for apply	In order to protect shore structure revetment from the vibration influence of vibro-rod work, gravel drain method was chosen for the portion near the revetment.
Design Condition	Input Acceleration of 150 gal at the Seismic bedrock (GL-50m) was applied for the design.
Expected Effect	Dissipating immediately excess pore water pressure.
Outline of works	Gravel pile of 1.0m in diameter were set spacing of 2.0m in triangle. (Fig.1)
Width of Countermeasure	Fig.3
Data and total value of works	1981. 3 ~ 1981. 7 Total Length 4500m (47m/day)
Evaluation of Countermeasure	In situ Vibration Tests Observations the accelerations and pore water pressure in improved and natural grounds during earthquake.
Seismic History	Chibaken Toho-oki earthquake of 17, 1987
Economic Evaluation	This method is comparatively 50% higher in cost than vibro-rod method, but is chosen to protect the shore structure revetment from the vibration influence of vibro-rod work.
Note	There are very few examples which have demonstrated it's effectiveness. The effectiveness protecting the ground settlement during liquefaction can not be examined.
Total Evaluation	For protecting the structure from the vibration influence of vibro-rod work, this method is effectiveness for countermeasure of ground liquefaction, but the effectiveness protecting the settlement and permanent ground displacement induced by the ground liquefaction can not be clarified. (Fig.4)

Table 4-b Example of Execution Performance of Countermeasure by SHIMIZU Corporation

Reported from	Shimizu Corporation
Name of Method	Sand Compaction Pile
Structures	Manufactory
Ground condition	Alluvial Sand
Construction condition	No Limitation
Reason for apply	The sand compaction pile method was applied because of its high reliability of ground liquefaction prevention.
Design conditions	The maximum ground surface acceleration measured at Ilatinohe on Tokachi-oki earthquake(225 gal) was applied to the design.
Expected effect	Increase soil relative density
Outline of works	Sand compaction piles of 70cm in diameter and 5.5m in length were set spacing of 1.5m in square. (Fig.6)
Area of countermeasure	Countermeasure covers the certain distance outside of structure as the length of the sand compaction pile.
Data and Total value of works	1974. 3~1974. 4 Total piles length is 3,644 m
Evaluation of countermeasure	Standard penetration tests. (Fig.7)
Seismic history	No large earthquake has been recorded after the countermeasure
Note	At Tokachi-oki earthquake, ground liquefaction was occurred around this site, but less liquefaction was found in the area where the Vibro-flotation was applied.
Total evaluation	This method is effective for countermeasure of Ground liquefactions, especially when noise and ground vibrations can be ignored.

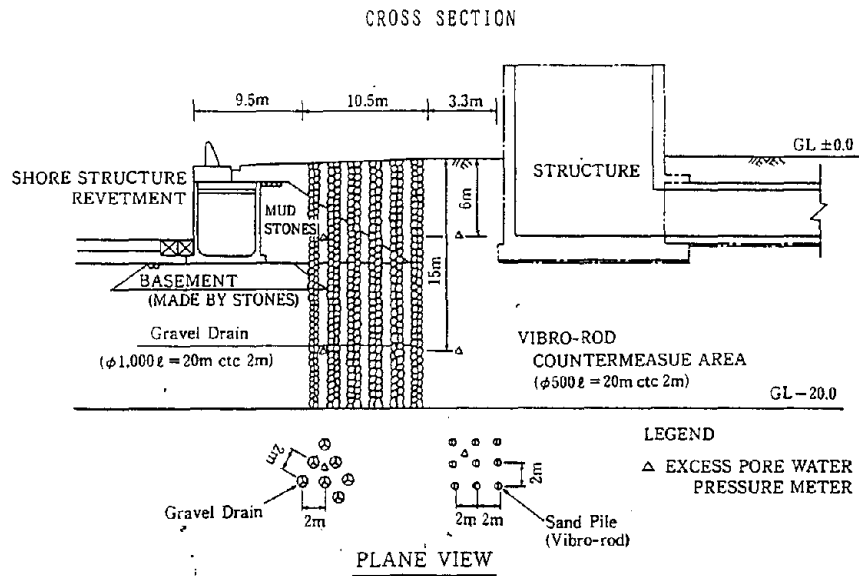


Figure 1 Outline of Countermeasure (Site A)

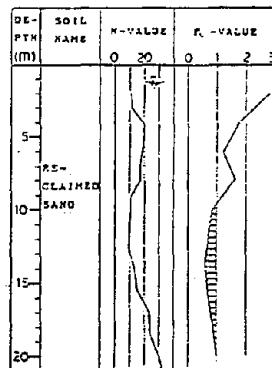


Figure 2 Geological Profile (Site A)

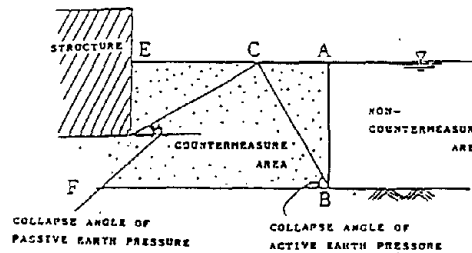


Figure 3 Width of Countermeasure

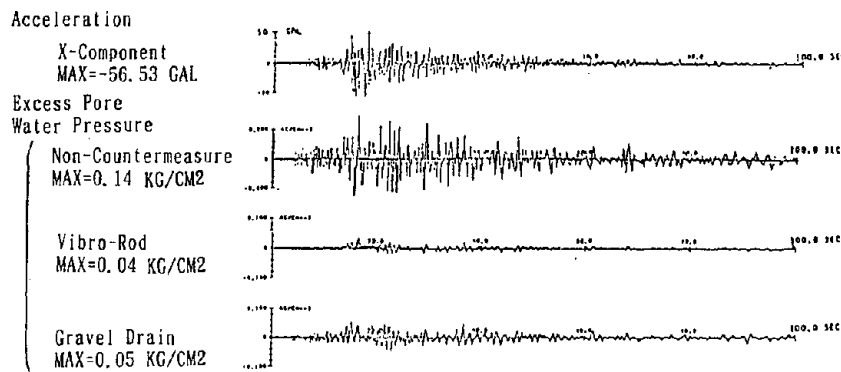


Figure 4 Example of Acceleration and Excess Pore Water Pressure Records (Site A, 1987, 12, 17)

Non-Countermeasure Area  
 ( $D_{50}=0.02\text{mm}$ ,  $\phi 74\mu$  Including 11%)

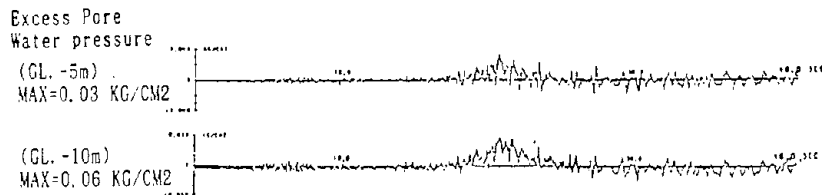
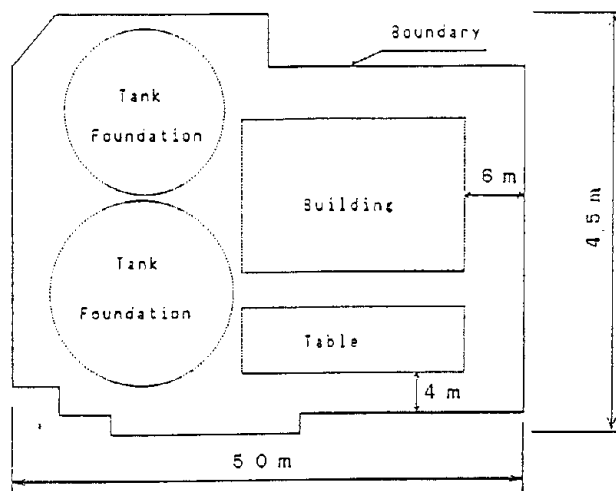


Figure 5 Example of Excess Pore Water Pressure Records Including The Clear Accumulating and Vanishing Processes (Site B, 1986.6.24)



Detail of Spacing

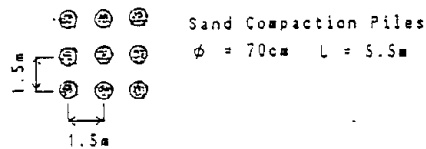
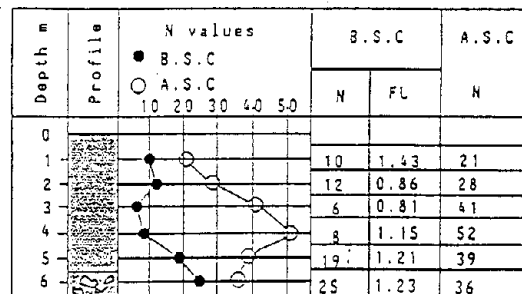


Figure 6 Plane View of The Countermeasure Area



B.S.C : Before Sand Compaction  
 A.S.C : After Sand Compaction

Figure 7 Soil Profile and Safety Factor of Liquefaction FL

## COUNTERMEASURES TO MITIGATE DAMAGE TO PIPELINES

Jeremy Isenberg  
Principal

Edward Richardson  
Associate

Weidlinger Associates  
4410 El Camino Real, Suite 110  
Los Altos, California 94022

### ABSTRACT

Fault offsets, lateral spreading due to liquefaction and other earthquake effects that result in localized soil deformation may damage pipelines if threshold levels of joint displacement and rotation are exceeded. The threat of damage increases with the magnitude of soil deformation and with the degree of localization. Damage is greater if the ductility of the pipe material or joint is small or if the direction of the pipe relative to the orientation of the deformed zone precludes ductile behavior (Ref 1).

Previous efforts to mitigate damage aim to address one or more of these factors. Such efforts have been partly guided by analytic models that are based on assumed modes of deformation and an assumed distribution of pipe-soil interface friction stress. These models are intuitively satisfying, have received wide peer review and have been used to design mitigation measures for important facilities, such as the Trans-Alaska pipeline. So far, no experimental validation is available to evaluate either the mitigation measures or the analytic models on which they are based. The main reason is that experiments in the laboratory require excessively large apparatus to prevent contamination by boundary effects; experiments in the field require opportunity such as that provided by the prediction project at Parkfield, CA (Refs. 2 and 3).

Future damage mitigation measures are likely to include increasing ductility while avoiding localized deformation. This can be done by putting the pipe into tension, by managing friction, by designing compliant joints and by using good welding practice. Lateral offsets may be accommodated by encasing the pipe in compliant material. Commercially available flexible joints for accommodating offsets are beginning to become available and appear to offer solutions for some cases.

## INTRODUCTION

Liquefaction, lateral spreading and surface expressions of fault movement pose major threats to pipelines. For example, lateral offsets of up to 20 ft. were considered in the design of the Trans-Alaska pipeline. Recently, there have been efforts to evaluate and improve the seismic performance of sewage and high pressure gas pipelines in urban areas crossed by fault zones. Ground rupture was considered in the design of an underwater sewer outfall that crosses the San Andreas fault (Ref. 4) and in a sewage tunnel that crosses the Newport-Inglewood fault zone in Los Angeles (Ref. 5). In addition to lateral offset, the effects of ground shaking due to wave propagation must be considered, as was done in the design of the Trans-Bay tunnel for BART (Ref. 6) in San Francisco.

## LATERAL OFFSETS

Figures 1a and 1b show a plan view of a pipeline which is subjected to lateral offset effects by a right lateral strike-slip fault at an angle  $\beta$ . The pipeline is oriented so that fault displacement,  $d_f$ , will cause tension in the buried pipeline. Newmark and Hall (Ref. 7) analyzed the pipeline deformation as an axisymmetric pattern of circular arcs, with each circular segment spanning the fault centerline and the location of an anchor point. The distance between the fault and the anchor point is known as the anchor length  $L_a$ . The anchor point is an effective anchor length beyond which there is no axial stress imposed in the pipeline due to fault movement. The analytical model developed by Kennedy et al (Ref. 8) accounts for the concentration of pipeline bending near the fault trace, increased frictional resistance between the pipe and soil in the zone of maximum bending and the nonlinear response of the pipeline steel to large tensile deformation. As illustrated in Figure 1c, the zone of increased frictional resistance is assumed to conform with the zone of pipeline curvature. These models and others, such as (Ref. 9) have been partially investigated under laboratory conditions, (Refs. 10 and 11), but cannot be studied fully in the laboratory on account of the difficulty in creating appropriate boundary conditions. One purpose of the pipeline experiment currently being conducted at Parkfield, CA (Ref. 3) is to observe bending and longitudinal strains due to lateral offsets under conditions of pipe-soil interface friction and end conditions that are typical of full size installations. The predicted recurrence of the 1966 Parkfield-Cholame earthquakes (Refs. 12 and 13) and the associated experiments (Ref. 2) provide an opportunity to study these assumptions.

## WAVE PROPAGATION EFFECTS

Figure 2 illustrates a pipeline subjected to an obliquely incident train of waves. The assumptions of analytic models to deal with this effect are completely different from those that treat lateral offset effects (Refs. 6,14-18). A common assumption of traveling wave models is that ground deformation is due to a wave train propagating with a predominant wave length and phase velocity and that the ground deformation is imposed on the pipeline. The dynamic pipe-soil interaction is assumed to be negligible. These assumptions have not been verified by measurements in US earthquakes. An experiment to investigate the relationship between ground shaking and the response of pipelines is being conducted in Tokyo at a site where surface rupture is not expected, (Ref. 19). A similar experiment designed to measure ground shaking effects on steel and cast iron water pipelines has been undertaken jointly by US and PRC investigators in China ( Ref. 26). In the pipeline experiment at Parkfield, CA, the deformation of the welded steel pipeline and the deformations of flexible joints in ductile iron pipelines will be observed during ground shaking from a relatively shallow-focus earthquake.



## LIQUEFACTION

Recently, a relationship was established between liquefaction-induced ground displacements in the 1983 Nihonkai-Chubu earthquake and the damage suffered by buried pipelines (Ref. 20). Areas of Noshiro City, where permanent ground displacements had been observed, were divided into 100 m square cells and the absolute amplitude of ground displacement was calculated. Similar estimates were made for regions of horizontal ground displacements, except that the unit of length was increased to 200 m. Damage rates for buried pipes in each zone were correlated with ground displacement taking into account type and size of pipes. Similar studies were performed for damage to gas pipes in Niigata due to the 1964 earthquake. It was concluded that damage to large diameter welded steel pipes in the Nihonkai-Chubu earthquake can be correlated with permanent ground displacement or ground strain; no correlation was found for small diameter pipes.

### Hazard Mitigation – An Overview

Two broad types of efforts to mitigate hazards or pipelines are being implemented. One is to adopt sound practices in the design and maintenance of new and replacement pipelines. For water transmission and distribution systems, these are outlined in the Advisory Notes on Seismic Design of Utility Lifelines (Ref. 21). These practices include identifying hazardous geological conditions, such as zones of potential liquefaction, lateral spreading and surface rupture. Additional seismological information needed to meet economic and public safety goals includes the return period of regional earthquakes and amount of ground movement as a function of earthquake magnitude and epicentral distance. A number of research efforts are aimed at developing engineering and economic models that support decision-making in regard to new construction, retrofit and maintenance. These include predictive models for response of pipelines when they are subjected to ground deformation, to liquefaction, to traveling wave effects and other seismic hazards.

The second type of effort is to design and construct pipes and joints that can accommodate ground movement without breaking or leaking. One strategy is to increase ductility while avoiding localized deformation. A way to accomplish this is to ensure, wherever possible, that the pipe is put into tension by the expected ground deformation. This step is feasible only in the few cases where the location and sense of the ground deformation are well-known, as at the crossing of a strike-slip fault such as the San Andreas. So long as the pipe is in tension, the possibility of using inelastic deformation to accommodate ground movement exists; if compressed, the pipe may buckle and fail in a manner which does not exploit its potential ductility. Proper selection of steel and good welding practice, including full penetration welds where possible, is required to realize the full potential for ductility of steel pipes. Design, manufacture and testing of compliant joints, which are discussed below, have recently been developed to the point where they are technically feasible for use in hazard mitigation. They are capable of sustaining internal pressure while undergoing rotation, torsion and extension. Models justifying their use on economic grounds are in their infancy, however. Another step, which seems intuitively beneficial, is corrosion control whereby the strength of the pipe is maintained over time. Some practices, such as wrapping pipe segments in sheets of polyvinyl, may have the collateral benefit of reducing pipe-soil interface friction; however, this has yet to be demonstrated.

## Example – Large Diameter Sewer Tunnel

Recently, a pipeline was designed as part of a project undertaken by the City of Los Angeles to replace an outdated and deteriorated sanitary sewer line (Ref 5). The tunnel is 12.64 km long and has inside diameters varying from 2.9 m to 3.75 m. Most of the tunnel is above groundwater level. For purposes of design, ground shaking was assumed to be characterized by peak horizontal acceleration of 0.3 g and a horizontal velocity of .31 m/sec. Shear wave velocities varied from 800 fps to 1,300 fps. Several known fault zones lie along the route, including several splays of the active Newport-Inglewood and the potentially active Overland Avenue and Charnock faults. It was estimated that an earthquake of moment magnitude  $M=6.5$  might occur every 800 years with 8 inches of horizontal displacement and that  $M=7$  might occur once in every 1,600 years with 18 inches of horizontal displacement. Vertical displacement is assumed to be one half of horizontal displacement.

Based on field work conducted under the project, a surface expression of the Newport-Inglewood fault zone about 160 feet wide was identified as requiring special pipeline design. Preliminary design studies recommended a solution involving a segmented pipe with specially designed joints. The entire reach of pipe within the fault zone is to be encased in a compliant cellular concrete or backpacking material. The procedures described in Ref. 1 were adopted to estimate the displacement transverse to the axis of the pipe that must be accommodated by the backpacking. The required thickness of backpacking,  $t$ , is

$$t = \frac{\delta_n}{2 \epsilon_a} \quad (1)$$

where

$$\delta_n = (\delta_y^2 + \delta_z^2)^{1/2} \quad (2)$$

and

$$\delta_y = \delta_n \cos \alpha \quad (3a)$$

$$\delta_z = \delta_n \cos \beta \quad (3b)$$

where  $\alpha$  and  $\beta$  are defined in Fig. 3.

The value of  $\epsilon_a$  is the lock up strain of the backpacking material; that is, the strain at which the voids are eliminated by crushing between the pipe and surrounding soil. It is assumed that crushing occurs only on one side of the pipe. Typical values might be  $\delta_n = 12$  inches and  $\epsilon_a = 0.6$ , which leads to a value of backpacking thickness of 10 inches. Thus, for the 160 feet of specially-designed pipe, the excavated diameter of the tunnel must be 20 inches more than the outside diameter of the pipe. Since the fault zone occurs near the terminus of the pipeline where the pipe diameter is about 150 inches, the total diameter would be increased by about 13 % to 170 inches.

In addition, the pipeline must be capable of sustaining an axial deformation of  $\delta_x$  and a rotation of  $\delta_r/2L$

where

$$\delta_x = \delta_{xh} + \delta_{xv} \quad (4)$$

and

$$\delta_{xh} = \delta_h \sin \alpha \quad (5a)$$

$$\delta_{xv} = \delta_v \sin \beta \quad (5b)$$

$$L = \frac{\delta_x}{2x} l \quad (\text{anchor length}) \quad (5c)$$

where

$$l = \text{length of a pipe segment}$$

$$x = \text{capacity of the joint in extension}$$

Since pipe segments are virtually rigid, the extension or compression must be provided by flexibility within joints. A pipe joint detail was designed to accommodate tension and compression for approximately 2 inches of axial displacement (including effects of rotation) per joint. Neoprene gasket seals were proposed that would prevent leakage while undergoing both axial deformation and rotation (Fig. 4).

No test data are available to evaluate the performance of this particular design. One of the desirable experiments would investigate combinations of rotation and extension under which performance is satisfactory. Envelope curves that define safe limits of rotation and extension for several types of joints are summarized in Ref. 22. An example of such a curve for a Dresser Industries Style 40 Long Coupling is given in Fig. 5.

## Example – San Fernando Water Pipeline

A design approach is developed in Ref. 23 which would allow ductile iron pipes with flexible joints to survive ground deformations such as occurred during the 1971 San Fernando earthquake at two specific locations. One of these was on Cometa Avenue, where about 4 feet of extension occurred in strike-slip accompanied by a small amount of dip-slip in a distance of about 47 feet. The other was on Harding Street, where dip-slip across 30 feet of disturbance caused 1.2 feet of compression. To this was added strike-slip leading to a total of 5.5 feet compression over 46 feet.

The usual type of rubber gasketed push-on joints cannot accommodate these deformations. Restrained push-on joints are available that use interlocking retainer glands or shear keys that eliminate the need for bolted-type harnesses. The former are less expensive and faster to assemble in the field. They are limited to end thrusts in tension of about 2 to 3 times the specified working pressure of the pipeline. In the present example, where greater joint flexibility and restrained axial strength are needed, ball joints of the type shown in Fig. 6a are available. Rotations of up to 15

degrees at each joint can be accommodated. By coupling these joints with restrained expansion-contraction sleeves (illustrated in Fig. 6b), narrow fault zones such as those at Harding St. and Cometa Ave. can be crossed safely. Further protection can be gained by increasing the anchor length. Multiple layers of loose polyethylene sleeving of the type that has been successfully used to protect ductile and cast iron pipes from corrosive soils may also be applied to reduce friction at the pipe-soil interface. As reported in Ref. 23, the 46 ft crossing of Harding Street would require 7 joints that could contract a total of 10 inches each; each joint would need to rotate about 3.3 degrees without buckling. At Cometa Avenue, slip joints that could extend 10 inches each would be satisfactory and four 9 ft. pipe lengths that would need to rotate about 5 degrees each. Ball joints would not be necessary in either crossing.

A critical assumption in estimating the number of joints is that the deformation is shared equally among them. Currently, no data are available to evaluate this assumption. One of the main purposes of emplacing ductile iron pipe segments with flexible joints in the Parkfield, CA, pipeline experiment is to provide such data.

### Example – Tokyo Gas Pipeline System

In contrast to the examples given above, Ref. 24 presents practical guidelines or standards which should be met in order to achieve satisfactory performance for a large, metropolitan gas pipeline system. The first step is to identify service areas for Tokyo Gas that are susceptible to liquefaction. The hazard is ranked for mesh zones 350 m x 250 m according to very high (PL > 15); high (5 < PL < 15); low (PL < 5) probabilities of liquefaction (PL). Soil layers judged susceptible to liquefaction are identified, and the permanent displacement at each site is calculated according to the expression proposed in Ref. 20 based on observations of the 1964 Niigata and 1983 Nihonkai-Chubu earthquakes.

$$D = .75 \times \sqrt{H} \times 3\sqrt{\theta} \quad (6)$$

where

D = Ground permanent displacement (m)

H = Liquefiable layer thickness (m)

$\theta$  = Maximum value (%) amount ground surface tilt, partial tilt and bottom tilt of liquefiable layer

The relative displacement under dynamic conditions is found by assuming a shear beam model in which the natural period is extended to account for liquefaction. Experiments were conducted to evaluate the loss of ground restraint and the soil reaction transverse to the pipe axis when liquefaction occurs. Based on this approach, the liquefaction hazard to pipelines was evaluated and compared with design criteria of the type found in ASME Sec III. For straight sections, allowable strains are 1.5% or  $\epsilon = 35t/D_m$ , whichever is less. Similar criteria are being evaluated for bent sections based on experiments. These procedures are currently being made available to design engineers.

## TECHNOLOGY OF FLEXIBLE JOINTS

The foregoing examples illustrate that reliable, easy to install, commercially manufactured flexible joints are central to damage mitigation strategies. To address this need, several pipe manufacturers in the US and Japan are currently developing and manufacturing such joints. One of these is the Ductile Iron Pipe Division of Kuboto, Ltd., whose S and SII joints are capable of accommodating expansion or contraction equal to 1% of the pipe length (ie, 2.4 inches for a 20 ft length of pipe) and 1.5 to 4 degrees of rotation. The allowable rotation varies inversely with pipe diameter. For cases requiring larger rotations, the DBJ type connection accommodates 15 degrees of rotation.

Another example of a flexible pipe joint (illustrated in Fig. 7) is manufactured by EBAA Iron Inc. under license from Suiken Co. of Japan. The expansion joint with rubber gasket has the capability to expand up to 12 inches but can undergo rotation only up to .29 degree. In order to accommodate larger rotations, a ball joint capable of rotation up to 15 degrees in any direction must be added to the assembly. Recently tests were conducted to investigate the performance of simple and compound joints under dynamic loading (Ref.25). Among the parameters reported are the energy dissipation for cyclic loading. Since the gaskets used are rubber, the rate dependence of transmitted forces and energy dissipation characteristics were expected.

A final example of a flexible pipe joint is illustrated in Figures 8-10 and is manufactured by US Pipe and Foundry Co. As shown in Fig. 10, two XTRA FLEX couplings can be used to accommodate rotations of up to 20 degrees each. The TR FLEX(a trademark of US Pipe and Foundry Co.) is a telescoping sleeve capable of accommodating axial elongation of up to two times the diameter of the pipe.

## CONCLUSIONS

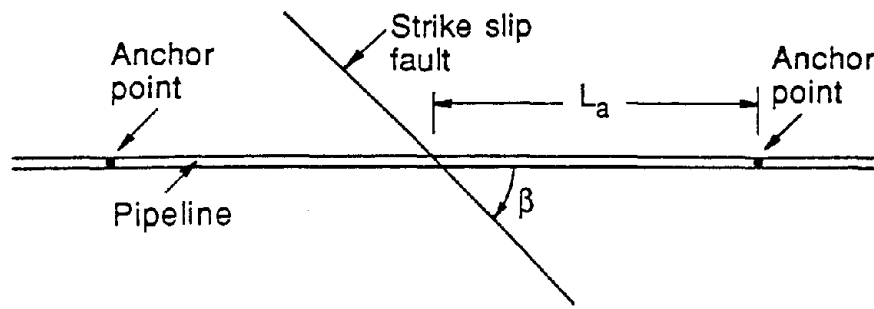
Due to increasing awareness of seismic hazards, engineers and pipeline manufacturers have developed ideas for accommodating large displacements and rotations which include flexible joints and compliant backpacking. Some hardware is commercially available. Successful design depends to a great extent on adequate geotechnical studies to define the location and extent of the earthquake hazard. Progress in geotechnical engineering which would permit quantitative estimates of displacements accompanying offsets or lateral spreading would motivate wider use of mitigation measures.

## REFERENCES

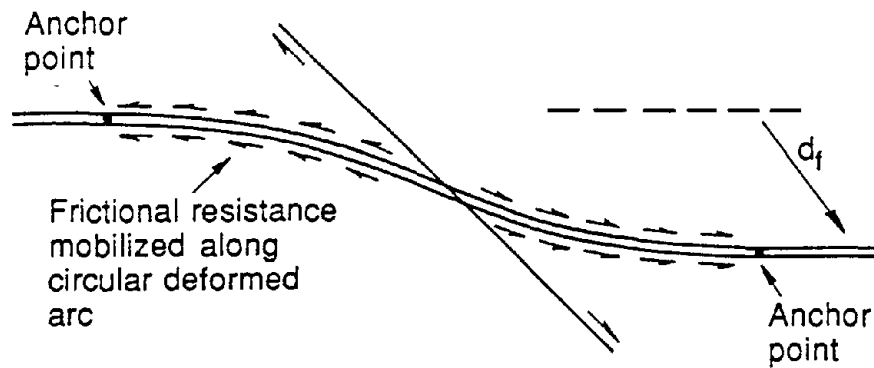
1. Nyman, D. J. (ed), "Guidelines for the Seismic Design of Oil and Gas Pipeline Systems," ASCE Technical on Lifeline Earthquake Engineering, ASCE, 1984
2. \_\_\_\_\_, "A Proposed Initiative for Capitalizing on the Parkfield, California Earthquake Prediction," Board of Earth Sciences, Commission of Physical Sciences, Mathematics and Resources, National Research Council, National Academy Press, Washington, DC, 1986
3. Isenberg, J., E. Richardson and T. D. O'Rourke "Experiment on Performance of Buried Pipelines Across San Andreas Fault," Technical Report NCEER-89-0005, Weidlinger Associates, March 10, 1989

4. Murphy, G. J., G. E. Hervert, Y. Eisenberg, and D. D. Treadwell, "Ocean Outfall Across the San Andreas Fault," Proceedings of the Second Specialty Conference of TCLEE, ASCE, Oakland, CA, Aug. 1981.
5. Desai, D.B., J. L. Merritt and B. Chang, "Shake to Survive Tunnel Design," Rapid Excavation and Tunneling Conference, Los Angeles, June 11-14, 1989
6. Kuesel, T. R., "Earthquake Design Criteria for Subways," Journal of the Structural Division, Proceedings ASCE, V 95, So. ST6, June 1969, p 1212-1231
7. Newmark, N.M. and W. J. Hall, "Pipeline Design to Resist Large Fault Displacement," Proceedings of the U.S. National Conf. on Earthquake Engineering, Ann Arbor, Michigan, 18-20 June 1975.
8. Kennedy, R.P, A.W. Chow and R.A. Williamson, "Fault Movement Effects on Buried Oil Pipelines," Journal of the Transportation Engineering Dev. Proc., ASCE, Vol. 103, 1977.
9. Wang, L. R-L, "Role and Development of Soil Parameters for Seismic Response of Buried Lifelines," Proc of the 4th National Congress on Pressure Vessel and Piping Technology, Earthquake Behavior and Safety of Oil and Gas Storage Facilities, Buried Pipelines and Equipment, ASME PVP77, Portland, Oregon, June 1983.
10. Takada, S. "Experimental Study on Mechanical Behavior of PVC Pipelines Subjected to Ground Subsidence," Proceedings of the 4th National Congress on Pressure Vessel and Piping Technology, Earthquake Behavior and Safety of Oil and Gas Storage Facilities, Buried Pipelines and Equipment, ASME PVP77, Portland, Oregon, June 1983.
11. Trautmann, C.H. and T. D. O'Rourke, "Load-Displacement Characteristics of A Buried Pipe Affected by Permanent Earthquake Ground Movements," Proceedings of the 4th National Congress on Pressure Vessel and Piping Technology, Earthquake Behavior and Safety of Oil and Gas Storage Facilities, Buried Pipelines and Equipment, ASME PVP77, Portland, Oregon, June 1983.
12. Brown, R. D. et al., "The Parkfield-Cholame California Earthquakes of June-August 1966--Surface Geologic Effects, Water Resources Aspects and Preliminary Seismic Data," US Geological Survey Professional Paper 579, US Government Printing Office, 1967
13. Bakun, W.H. and A. G. Lindh, "The Parkfield, California, Earthquake Prediction Experiment," Science 229, 1985, pp.619-624.
14. O'Rourke, M.J., G. Castro and I Hossain, "Horizontal Soil Strain Due to Seismic Waves," Journal of Geotechnical Eng., vol 110, No.9, Sept. 1984, p 1173-1187.
15. Shinozuka, M., R. Y. Tan and T. Koike, "Serviceability of Water Transmission Systems Under Seismic Risk," Proceedings of the 2nd Specialty Conference on the Technical Council on Lifeline Earthquake Eng., ASCE, Aug. 1981.
16. Shinozuka, M. and T. Koike, "Estimation of Structural Strains in Underground Lifeline Pipes," Technical Report No. NSF-PFR-78-15049-CU-4, Dept. of Civil Engineering and Engineering Mechanics, Columbia University, March 1979.

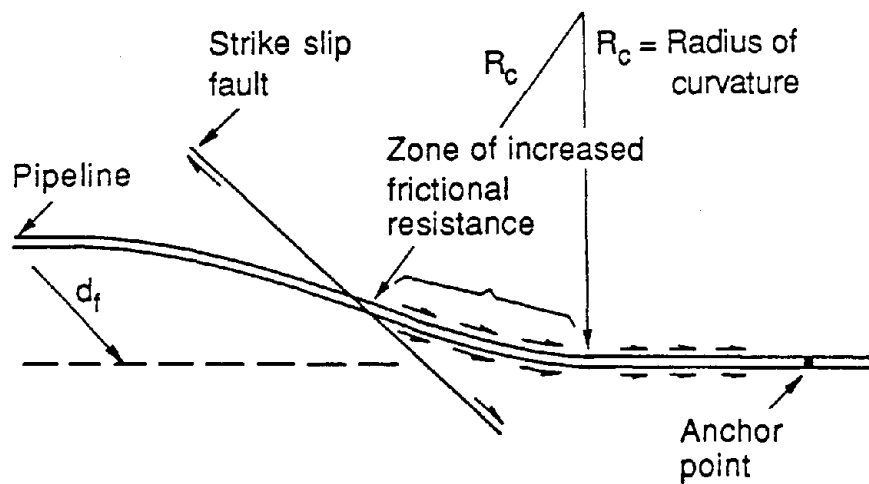
17. Datta, KS, A. H. Shah and N. El-Akily, "Dynamic Behavior of a Buried Pipe in a Seismic Environment," *J. of Applied Mechanics, Trans. ASME*, Vol. 49, 1982, p 141-148.
18. Iwasaki, T., "Earthquake Resistant Design of Underground Pipelines in Japan," *Proceedings of the US-Japan Workshop on Seismic Behavior of Buried Pipelines and Telecommunications Systems*, Tsukuba Science City, Japan, 5-7 December 1984.
19. Kawashima, K., Public Works Research Institute, Ministry of Construction, Government of Japan, Private Communication, 16 July 1987
20. Hamada, Masanori, "Damage to Buried Lifelines by Liquefaction-Induced Ground Displacement", Paper J-2, 3rd US-Japan Workshop on Earthquake Disaster Prevention for Lifeline Systems, Tsukuba Science City, Japan, May 11-13, 1989
21. \_\_\_\_\_, "Advisory Notes on Aseismic Design of Utility Lifelines" Technical Council on Lifeline Earthquake Engineering, ASCE, 1984
22. O'Rourke, T. D. and C.H. Trautmann, "Analytical Modeling of Buried Pipeline Response to Permanent Earthquake Displacements," *Geotechnical Engineering Report 80-4*, School of Civil and Environmental Engineering, Cornell University, July 1980
23. Ford, D. B., "Joint Design for Pipelines Subject to Large Ground Deformations," *Earthquake Behavior and Safety of Oil and Gas Storage Facilities, Buried Pipelines and Equipment*, 1983 International Symposium on Lifeline Earthquake Engineering. The 4th National Congress on Pressure Vessel and Piping Technology, ASME, Portland OR, June 1983
24. Nakane, Hiroyuki "Recommended Practice for Earthquake Resistant Design of Gas Pipelines Considering Liquefaction", Paper J-11, 3rd US-Japan Workshop on Earthquake Disaster Prevention for Lifeline Systems, Tsukuba Science City, Japan, May 11-13, 1989
25. Ishibashi, I., LRL Wang and H. Kennedy, Jr., "Energy Dissipation and Resistant Characteristics of A Flexible Pipe Joint," *PVP*, Honolulu, July, 1989.
26. Wang, LRL, H-P Sun and S-J Shen, "Field Investigations and Analysis of Buried Pipeline Under Various Seismic Environments," *Old Dominion University Report to National Science Foundation Under Grant ECE85-42982*, 1987.



(a) Before Fault Movement



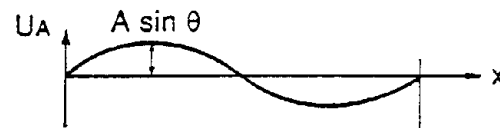
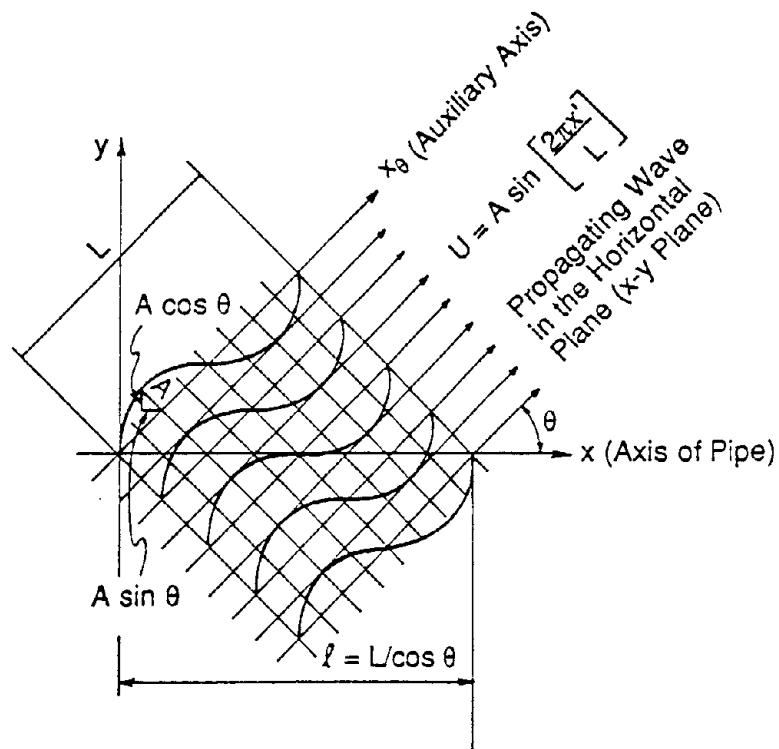
(b) After Fault Movement (Ref. 3)



(c) After Fault Movement (Ref. 4)

**Figure 1 Plan and Sectional Views of Continuous Pipeline Envisioned in Newmark-Hall Design Approach**





Axial Displacement  
(in x Direction)

$$\text{Displacement: } UA = A \sin \theta \cdot \sin \left[ \frac{2\pi \cos \theta}{L} \cdot x \right]$$

$$\text{Strain: } \frac{dUA}{dx} = \frac{2\pi A}{L} \sin \theta \cdot \cos \theta \cos \left[ \frac{2\pi \cos \theta}{L} x \right]$$



Transverse Displacement  
(in y - Direction)

$$\text{Displacement: } Ur = A \cos \theta \cdot \sin \left[ \frac{2\pi \cos \theta}{L} x \right]$$

$$\text{Curvature: } \varnothing = \frac{d^2 Ur}{dx^2} = \frac{-4\pi^2 A}{L^2} \cos^3 \theta \cdot \sin \left[ \frac{2\pi \cos \theta}{L} x \right]$$

**Figure 2 Model of Wave Propagation Effects for Pipeline Analysis (after Ref. 19)**

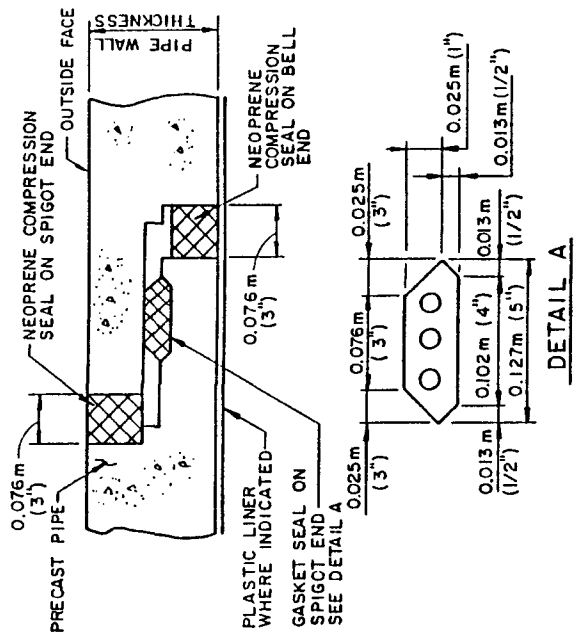


Figure 4 Proposed Pipe Joint to Accommodate Rotation and Axial Deformation (Ref. 5)

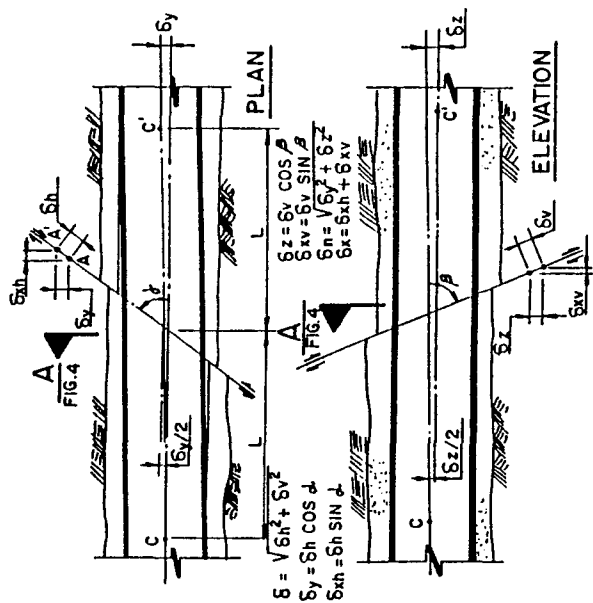


Figure 3 Plan and Elevation Views of a Pipeline Subjected to Strike and Dip-Slip (Ref. 5)

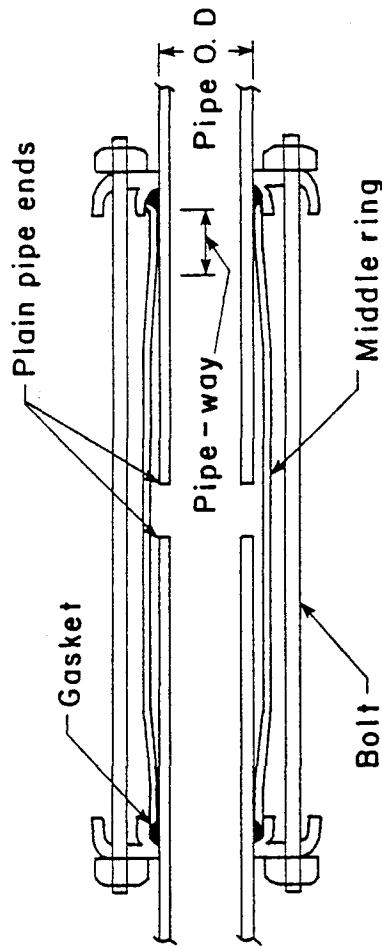
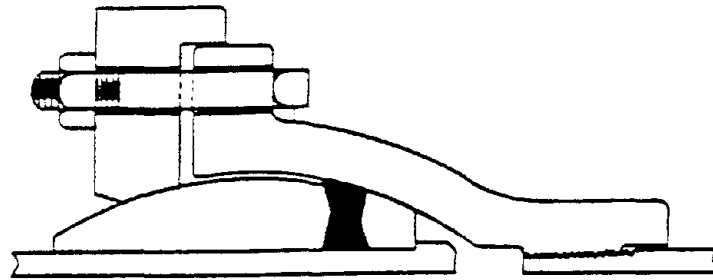
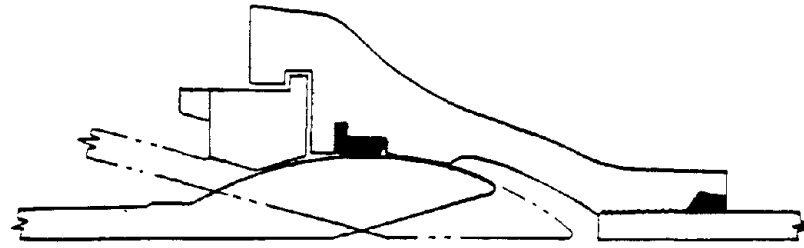
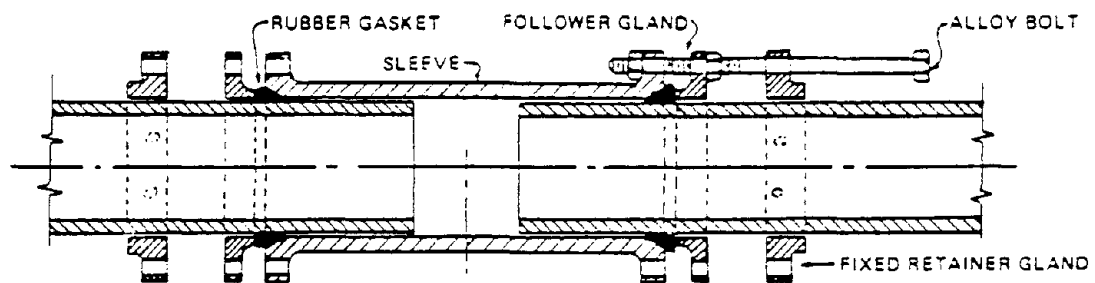


Figure 5 Dresser Industries Style 4D Long Coupling (Ref. 22)



(a) Ball Joints



(b) Restrained Expansion Joint

Figure 6 Separate Ball and Restrained Expansion Joints for Pipelines where Large Rotation (up to  $15^{\circ}$ ) Accompanies Extension or Compression (Ref. 23)

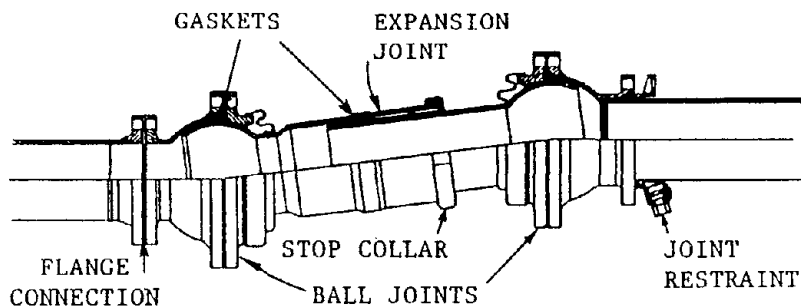


**Figure 7 Ductile Iron Pipe Joint to Accommodate Axial Deformation and Rotation, Available from EBAA Iron, Inc.**

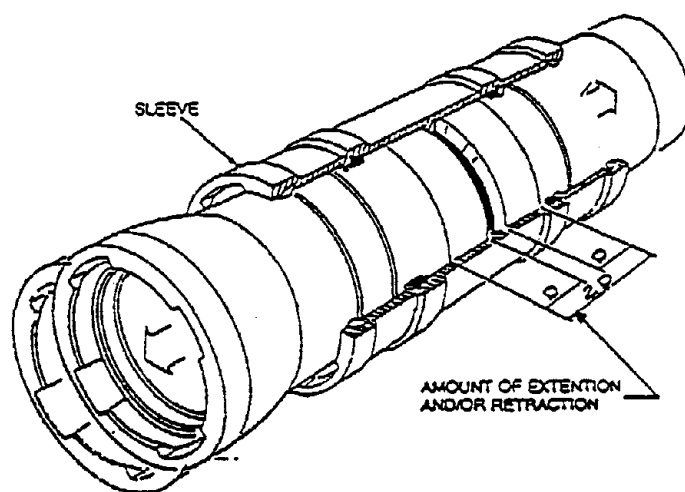


**Figure 8 TR FLEX<sup>(R)</sup> Telescoping Sleeve To Accommodate Axial Deformation, Available from US Pipe and Foundry Co.**

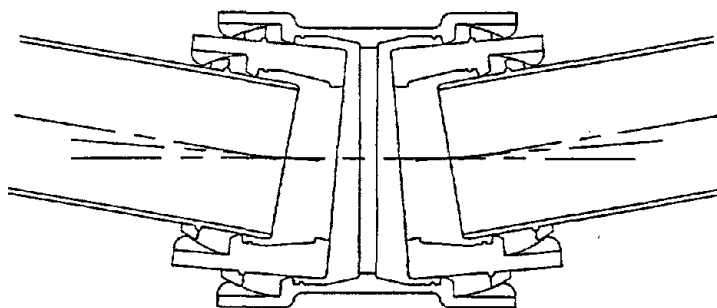


**Figure 9 XTRA FLEX Coupling to Accommodate Rotation, Available From US Pipe and Foundry Co.**

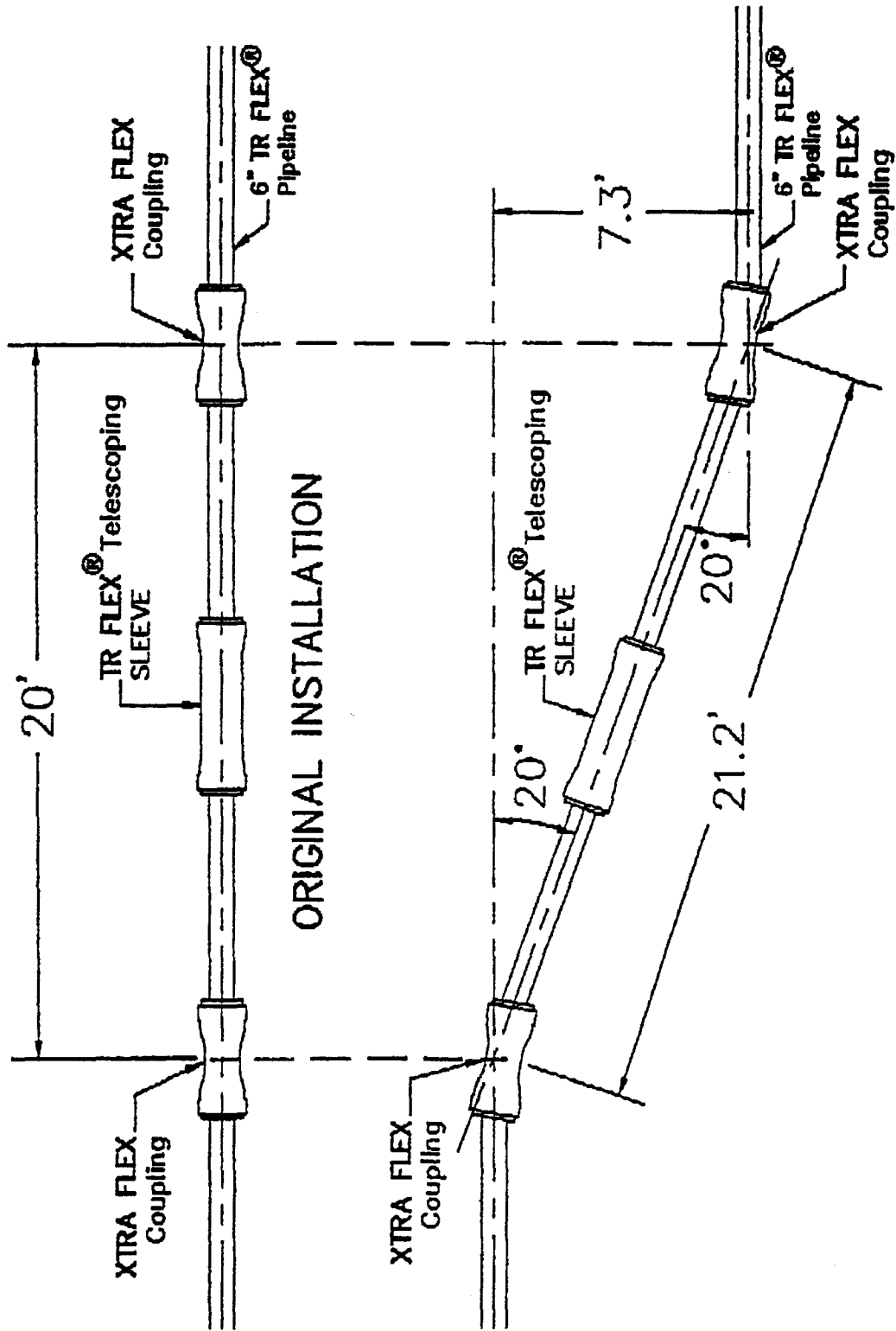
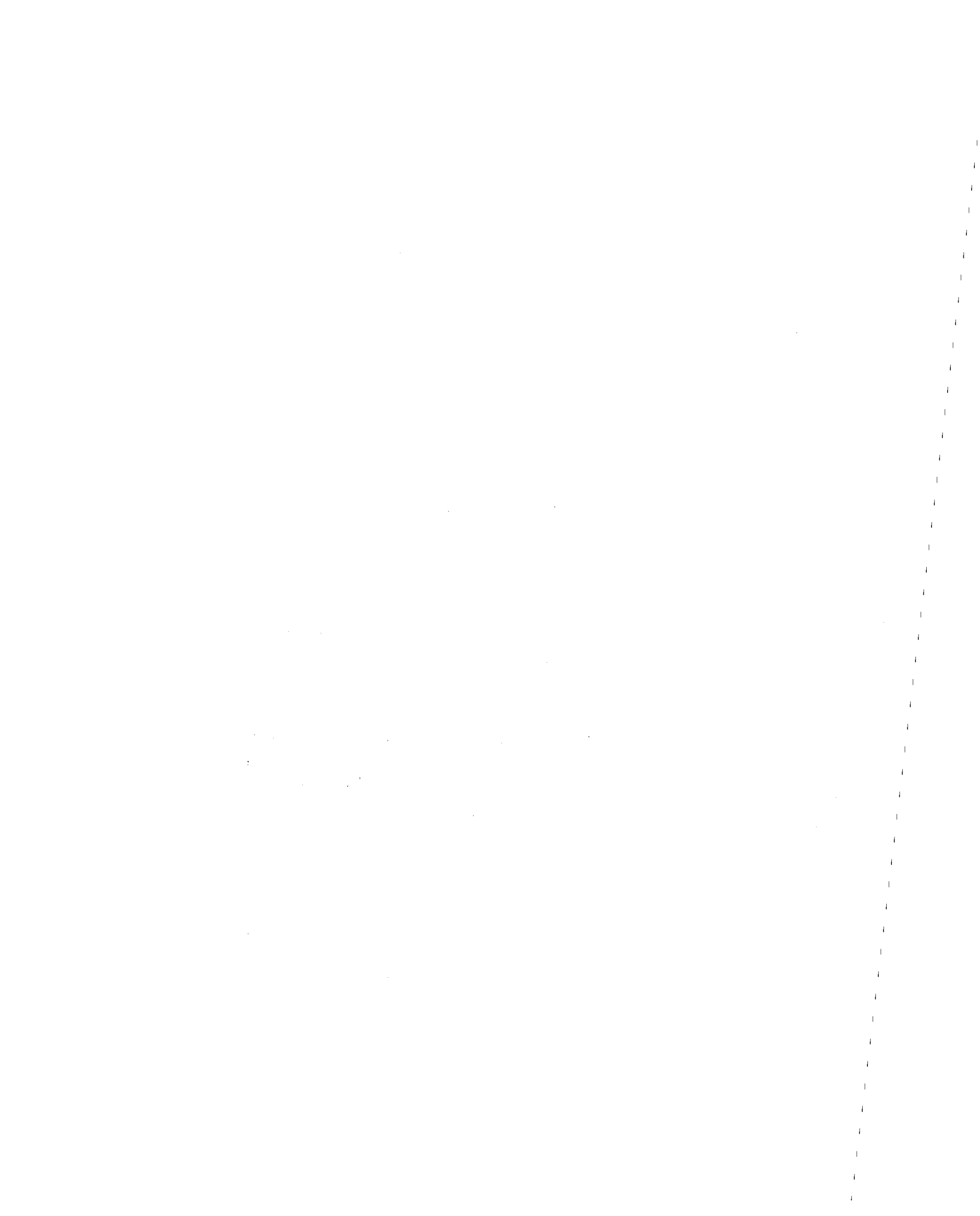
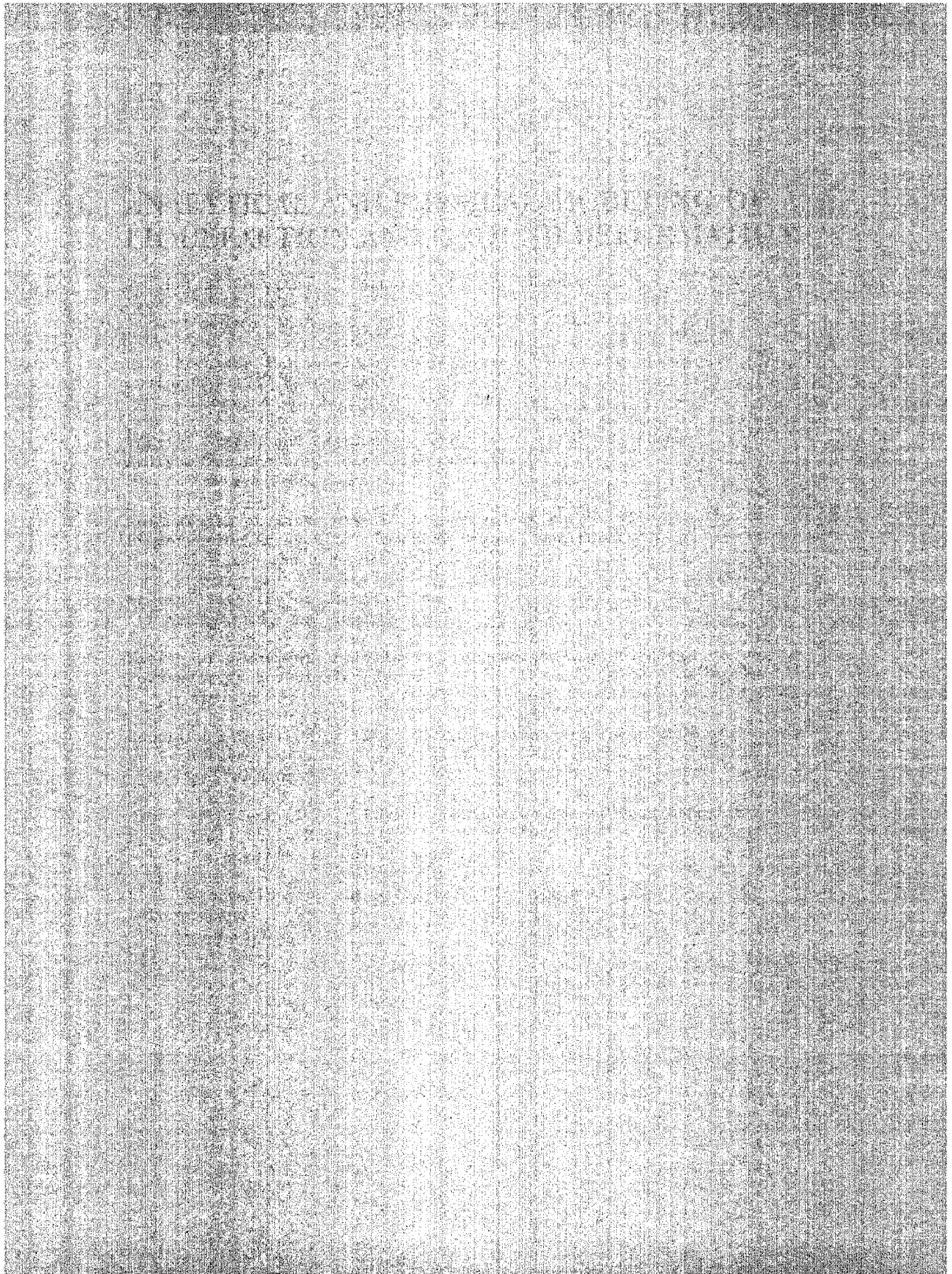


Figure 10 Installation after Substantial Soil Movement  
(US Pipe and Foundry Co.)



**READING GROUP SESSIONS**

482a





## WORKING GROUPS

On the third day of the workshop, participants divided into four groups with the charge to develop a "Technical Summary and Recommendations for Liquefaction, Large Ground Deformation and Their Effects on Lifelines". This document will establish a compact international overview of the subjects, and will provide guidance for researchers and practitioners interested in this field.

The following pages contain remarks to the working groups by Professor Shinozuka and summary statements by the groups regarding their objectives and plans.

REMARKS TO WORKING GROUPS  
by  
Professor M. Shinozuka  
Princeton University

The most important aspect of NCEER's research on lifeline facilities is the "systems approach". In our opinion, the systems approach as applied to a research effort such as this one is an approach where the goals of the research are achieved in the most cost-effective manner with the aid of interdisciplinary and multiprofessional interaction. In this connection, it is pointed out that the overall goals of NCEER's lifeline studies are to evaluate the seismic vulnerability of lifeline systems and recommend measures for mitigating the societal risk arising from the failure of lifeline systems due to earthquakes.

With this in mind, the technical summary and recommendations should provide answers to the following questions, among others:

- a. What is the specific purpose of your research?
- b. How does the result of your research fit the overall flow of research? What input do you need from other working groups? What output can you deliver that is usable by other working groups as input? Identify these other groups.
- c. What is the state-of-knowledge in each area of study?
- d. What is the degree of uncertainty associated with each body of knowledge?
- e. What are the items of future research to be carried out in order to reduce the degree of such uncertainty?

From the viewpoint of a systems approach, how well we can answer these and other questions and how well we can document them for future reference is indeed a key to the success not only of this workshop but also of the entire US-Japan Cooperative Research on Liquefaction, Large Ground Deformation and Their Effects on Lifeline Facilities.

**SECOND US-JAPAN WORKSHOP ON LIQUEFACTION, LARGE GROUND  
DEFORMATIONS AND THEIR EFFECTS ON LIFELINES**

**REPORT FROM WORKING GROUP NO. 1:  
EXPERIENCE DURING PAST EARTHQUAKES**

Working Group Members:

From Japan

Susumu Yasuda, Co-chairman  
Shiro Fukui  
Kenji Ishihara  
Ikuo Towhata  
Katsumi Shimizu  
Kazue Wakamatsu

From the United States

T. Leslie Youd, Co-chairman  
Thomas L. Holzer  
I.M. Idriss  
Bruce L. Roth  
Martitia Tuttle

INTRODUCTION

During the workshop, Working Group 1 reviewed progress in compiling case histories of liquefaction and large ground displacement, assessed the development of empirical criteria for predicting ground displacement, and considered future research needs and opportunities on this topic. The purposes of compiling and evaluating cases histories from past events are (1) to utilize past experience to improve our understanding of ground failure processes and factors that control those processes, (2) to develop a set of case histories to assist the development of analytical models for predicting ground displacement, (3) to provide sufficient data for the development of empirical criteria for predicting ground displacement, and (4) to provide well-documented case histories to be used in the verification of the models and criteria developed.

To accomplish these objectives, a coordinated US-Japan program is in progress to compile case histories of liquefaction-induced ground displacements for four Japanese earthquakes and four US earthquakes as listed in the following section. Data being compiled include surface displacements, site topography, soil stratigraphy and properties, ground water levels, and where possible ground motion data. A schedule has been set to complete the initial compilations by the end of 1989 and to publish a joint report containing the compiled case histories during the summer of 1990.

CASE HISTORY COMPILATIONS

The following are brief synopses of the case histories being compiled. Progress on most of these case histories were reported during the workshop.

1906 San Francisco earthquake,  $M_w = 8.1$ . The great 1906 San Francisco earthquake triggered liquefaction and ground displacement in three major zones in downtown San Francisco. Lateral spreads in those areas severed several major water mains cutting off delivery of water to a part of the city that was soon to be in flames. A thorough search has been made for reports and photographs that describe and illustrate the areas of ground failure. Measurements have been made from the photographs to determine amounts of ground displacement, and subsurface information has been collected from subsequent geotechnical investigations in the affected areas. These data, along with information on damage to pipelines and structures are being compiled into the final report which will be published in the joint report.

1923 Kanto earthquake,  $M = 7.9$ . The great 1923 Kanto earthquake killed an estimated 97,000 people and destroyed or badly damaged over 250,000 structures. An additional 447,000 structures were lost in the ensuing fires. Because of the extensive shaking and fire damage, little attention was given to liquefaction and ground displacement in the 1923 investigations and reconstruction. Liquefaction effects are now being compiled and studied through an examination of published damage reports and photographs taken after the 1923 event. Interviews with local residents who experienced the earthquake have also been conducted to gain additional information and locate areas of ground failure. Three areas of ground displacement have been identified for further study. Topographic and subsurface data are being collected and a report on these sites is in preparation.

1948 Fukui earthquake,  $M = 7.1$ . The Fukui earthquake caused extensive damage at various localities on the Fukui Plain including Fukui City. Liquefaction in the alluvial plane along the Kuzuryu River damaged foundations, bridges, embankments and houses. Vectors of ground displacement in areas of liquefaction have been constructed from photogrammetric measurements using pre- and post-earthquake aerial photographs. Interviews with local residents who witnessed the earthquake have produced additional information concerning the ground failures. Subsurface data is also being compiled from geotechnical investigations in the affected areas.

1964 Alaska earthquake,  $M_w = 9.2$ . Landslides and lateral spreads generated by the great Alaska earthquake of 1964 caused more than half the total damage inflicted by that event and severely disrupted lifelines including transportation routes and pipelines for many months. Investigations by geologists and engineers after the event documented ground displacements at several localities, particularly along the Alaska Railroad and in the communities of Anchorage and Valdez. To supplement those investigations and to provide topographic data, surveys were made of several key sites as part of the US-Japan joint project. Survey data is being analyzed and pre- and post-earthquake photography of Anchorage are being utilized to photogrammetrically determine additional displacements. Subsurface ground water and soil data are also being collected and compiled for publication in a final report.

1964 Niigata earthquake,  $M = 7.5$ . During the 1964 Niigata earthquake, spectacular and widespread liquefaction effects occurred in Niigata City and surrounding areas. Vectors of ground displacement in these areas have been determined from photogrammetric measurements on pre- and post-earthquake aerial photographs. Subsurface geotechnical data have been collected from past engineering investigations and supplemented by Swedish soundings to further define the subsurface stratigraphy and soil properties. Reports are being prepared to complete these studies.

1971 San Fernando earthquake,  $M = 6.5$ . During the 1971 San Fernando earthquake, large ground deformations occurred at the Joseph Jensen Filtration Plant along the west side of the Upper Van Norman Reservoir. Numerous soil borings were performed near the plant during plant design and several construction projects; these borings make this area one of the most densely probed localities of earthquake-induced ground displacement. Resurveys of reference points and photogrammetric analyses of aerial photographs taken before and after the earthquake provide a comprehensive view of lateral and vertical displacements at the site. Damage to pipelines and other constructed works at the site provide additional information on ground displacements and also provide well-documented relationships between ground displacement and consequent damage.

1979-87 Imperial Valley earthquakes  $M = 6.0-6.6$ . The Imperial Valley of southern California lies in one of the most seismically active areas of the United States. Liquefiable deposits are also common in that area making the valley a natural laboratory for the study of liquefaction. One locality, the Wildlife Site, has been instrumented to record ground motions above and below a liquefiable layer and pore-water pressures within the layer. The Superstition Hills earthquake of November 24, 1987 ( $M_w = 6.6$ ) excited that site and generated liquefaction with pore pressures rising to the total overburden pressure. These records are the first to track ground motions and pore pressures as complete liquefaction developed. Survey marks and a slope-indicator casing registered permanent ground displacements as great as 232 mm. At another locality, the Heber Road site, the 1979 Imperial Valley earthquake ( $M_w = 6.5$ ) shook three parallel deposits of silty sand with different geologic histories. Only one of the deposits liquefied and generated a lateral spread with up to 3 m of horizontal displacement.

#### EMPIRICAL CRITERIA FOR PREDICTING GROUND DISPLACEMENT

Many factors influence the development of liquefaction and ground displacement. These factors include intensity and duration of earthquake shaking, thickness and extent of the liquefiable layer, ground slope and nearness of a free face, depth of ground water, and density, grain-size distribution, packing and cementation of the granular sediment. Some preliminary evaluations have been made of these factors to develop empirical predictive criteria for ground displacement. Two empirical criteria have been proposed to date, the liquefaction severity index procedure developed by Youd and Perkins and an equation relating displacement to thickness of the liquefied layer and ground slope that has been proposed by Hamada et al.

Liquefaction severity index (LSI). Youd and Perkins developed criteria for estimating LSI from case histories of liquefaction-induced ground displacement in the western US. They define LSI as the maximum displacement of lateral spreads in millimeters divided by 25 at a locality. By evaluating LSI only on gently sloping late Holocene fluvial deposits such as floodplains and deltas, Youd and Perkins assume that all of the factors controlling ground displacement are held reasonably constant except the seismologic factors of intensity and duration of ground motion. They regressed LSI against magnitude,  $M_w$ , and distance from the energy source,  $R$ , and developed the following correlation:

$$\log \text{LSI} = - 3.49 - 1.86 \log R + 0.98 M_w \quad (1)$$

This equation does not incorporate specific site parameters, and thus is not valid for estimating site-specific displacements. The primary usefulness of equation 1 is to estimate the probable

maximum displacement that could occur at a locality as a consequence of liquefaction of gently-sloping highly-liquefiable sediment.

Equation of Hamada et al. From their studies of ground conditions and ground displacements at Niigata and Noshiro cities generated by the 1964 and 1983 earthquakes, respectively, Hamada et al. formulated the following empirical equation:

$$D = 0.75 H^{1/2} \theta^{1/3} \quad (2)$$

where D is displacement in meters, H is the thickness of the liquefied layer in meters, and  $\theta$  is the greater of the ground slope or the slope of the base of the liquefied layer, in percent. Note that the parameter H in equation 2, is a function of both subsurface site conditions and the intensity and duration of the earthquake motions.

Results published by Hamada et al. show that equation 2 predicts displacements at Niigata and Noshiro cities rather well, generally within minus 50 percent to plus 100 percent. Those localities were shaken by earthquakes with a narrow range of magnitudes (7.5 and 7.7, respectively) and peak accelerations (about 160 and 200 gal, respectively) and affected primarily clean medium- to coarse-grained sands. Further testing of this equation is required to evaluate its predictive capabilities for localities with different sizes of earthquakes, different soil conditions, etc.

Development of improved predictive criteria. Both Japanese and US investigators are continuing the evaluation of case history data being compiled to develop improved empirical criteria for predicting ground displacements.

## FUTURE RESEARCH NEEDS

The immediate research objective of the joint US-Japan effort is to complete the compilation and publish case histories for the eight earthquakes noted above. This publication should be available by late summer of 1990.

After the case histories are completed, evaluations should be made of the completeness of the data sets and the degrees of uncertainty in the data. Some known limitations and uncertainties are:

1. Only fragments of some important parameters are available, such as ground motion records. A notable exception is the Wildlife site where ground motions and pore-water pressures were recorded.
2. Some properties that are important to liquefaction evaluation have not been routinely measured and are not reported for all case histories. Examples are permeability and shear-wave velocity.
3. Statistical evaluations should be made of the data to evaluate the degree of uncertainty in the reported measurements.

Work is in progress in both the Japan and the US to analyze the compiled data in order to develop improved empirical predictive correlations. Analyses are also being made to develop and verify analytical predictive techniques (see report from Group 2). As part of these studies, ground-failure mechanisms and factors controlling ground displacement are being investigated.

It is very probable that more information will be required to adequately develop empirical criteria and validate analytical techniques. To accomplish this need, it is likely that selected case history sites will be identified for further investigation including more detailed subsurface investigation to provide the required information.

The present work has concentrated on sites where significant ground displacements have occurred. Some additional case histories may be needed at liquefaction sites where displacement did not occur. This information is required to verify non-displacement conditions.

Plans should be made to develop additional and improved case histories from liquefaction occurrences during future earthquakes. To accomplish this augmentation, the following suggestions might be considered.

1. Develop more instrument sites in liquefaction prone areas. Such sites might include devices for monitoring time histories of displacement as well as ground motions and pore pressures.
2. Monitored sites without expensive electrical instrumentation might also be considered. Such sites could be equipped with surveyed points and inclinometer casings to provide three dimensional delineation of ground displacements.
3. Pre-earthquake aerial photography might be taken of pertinent localities of probable liquefaction. The photographs should be at large scale and with sufficient ground control to facilitate accurate measurement of ground displacements.

SECOND US-JAPAN WORKSHOP ON LIQUEFACTION, LARGE GROUND  
DEFORMATIONS AND THEIR EFFECTS ON LIFELINES

REPORT FROM WORKING GROUP NO. 2:  
MODELING LARGE GROUND DEFORMATION

Working Group Members:

From Japan

Susumu Iai<sup>a</sup>  
Kin-Ichi Kasuda  
Masakatsu Miyajima  
Nozomu Yoshida<sup>a</sup>

From United States

Ricardo Dobry<sup>a</sup>  
Ahmed Elgamal  
Jean H. Prevost  
Harry E. Stewart<sup>a</sup>  
Mladen Vucetic

Other International

Juan Murria (Venezuela)  
Scott Steedman (U.K.)  
Harry Van der Graaf  
(Netherlands)

<sup>a</sup> - Group Leaders

INTRODUCTION

During the workshop, Working Group 2 met to review current progress and to define future directions and needs related to modeling of large ground deformations. The goal of this working group is to develop accepted site-specific analytical techniques to predict the value and spatial pattern of ground deformations for a given earthquake shaking. The decision was made that the modeling should concentrate on the effects of shaking in the absence of structures, i.e. the far field. Five key topical areas that will be addressed in the Guidelines were identified and discussed.

The first important topical area relevant to the development of sound analytical modeling must necessarily include a definition of the physical mechanisms responsible for permanent ground deformations. The mechanisms are mostly associated with gravity, although other contributing factors could be present. Mechanistic effects that play important roles include, but may not be limited to, gravity and seismic stresses per Newmark-type analyses, the effects of delayed deformations, the roles of subsurface flow and the redistribution of pore water pressures, and true inertial forces. The Guidelines will address the above mechanisms, with emphasis on the physics of liquefaction-induced ground deformations.

A second topical area relevant to accurate analytical modeling relates to specific site and earthquake parameters. These parameters must be measurable or at least realistically determined. Four groupings of site parameters were identified. The first group relates to earthquake shaking. The earthquake shaking must be quantified as to the level, frequency content and duration. The shape of the time record is an important factor as well, since unequal cyclic intensities affect the ground response. The second grouping of site parameters revolve around the specifics of surface and subsurface topography and slope, the thickness and depth of liquefiable layers, and the presence of other layered features. Although these parameters can be quantified readily, the importance of subtle differences and



features must be addressed. The third grouping of site and earthquake parameters relates to the other site properties not specifically addressed in the second grouping. These include the groundwater conditions, including both the location of the free surface and any subsurface flow conditions. Geologic features such as age, seismic history, cementation, stress history and initial stresses, and the effects of human activities are known to influence site response, but have not been fully quantified. The relative importance of all these factors needs to be understood so that site-specific differences in ground movement can be explained. The fourth grouping of site specific parameters consists of fundamental soil properties. In addition to simple descriptors such as grain size and unit weights, we must be able to account for the nonlinear cyclic stress-strain-strength properties, especially when dealing with large strains. Important properties necessary for accurate modeling also include hydraulic conductivity, compressibility, in-situ lateral stresses, and how these properties change during cyclic loading.

The third topical area identified during the Working Group session that will be included in the Guidelines is devoted to the general analytical methods that are available. Analytical methods for large ground deformation can be classified broadly into three groups: 1) two-phase effective stress, 2) total stress with reduced stiffness, and 3) displacement pattern or geometric methods. Within these broad categories there are several features that should be included in a comprehensive approach. These features relate to effects that can occur during the earthquake, such as sliding, and those that can occur following the motion. During the earthquake, effective stress methods may be more suitable, whereas effective stress based methods, equivalent elastic methods with reduced stiffness, or a continuity-mass balance approach may be used when looking at post-earthquake deformations. The Guidelines will address the requirements necessary for an ideal or high-quality analytical technique. The Guidelines should include a description of what methods are available currently, the limitations imposed by small deformation theory versus more complete large deformation formulations, the benefits of one-, two-, and three-dimensional formulations, and the benefits and drawbacks of more complex approaches. The reliability of current methods must be addressed, focusing on how models have been used in the past and how well they agree with case history results.

The fourth topical area that will be included in the Guidelines deals with the role of physical modeling. Physical modeling, such as done using a centrifuge or shake table, is important to help calibrate analytical techniques and validate analytical approaches, augment case history studies, and to define and identify displacement mechanisms not covered by current analysis procedures. The Guidelines will serve to define what is an acceptable physical model. Scale effects will be discussed in light of the combination of model scales and gravitational accelerations suitable for centrifuges and shake tables.

The fifth topical area for inclusion in the Guidelines deals with the utility of laboratory- and field-test-based soil properties. The important soil properties necessary for accurate modeling will be identified. Critical issues from a property standpoint are: 1) what are the important properties, 2) how do we obtain reliable values, 3) how do we account for the level of stress intensity for physical model testing, e.g., low stress level for shake table versus high stress level for centrifuge, and 4) how reliable are the properties determined either by laboratory or field methods.

In addition to the specific topical areas discussed above we plan to include sections that summarize the analytical contributions made by both the Japanese and

U.S. sides during the First and Second Workshops. These summaries will set the stage for where we are going based on what is available currently. The contributions supplied by Working Group 2 to the Guidelines will include recommendations for practicing engineers, recommendations for future research, and a consensual approach towards the development of rational analytical modeling techniques.

SECOND US-JAPAN WORKSHOP ON LIQUEFACTION, LARGE GROUND  
DEFORMATIONS AND THEIR EFFECTS ON LIFELINES

REPORT FROM WORKING GROUP NO. 3:  
EARTHQUAKE RESISTANT DESIGN

Working Group Members:

From Japan

M. Hamada<sup>a</sup>  
H. Suzuki<sup>a</sup>  
M. Sato  
T. Tazoh  
N. Suzuki  
T. Kobayashi  
S. Sato

From United States

M. O'Rourke<sup>a</sup>  
M. Shinozuka<sup>a</sup>  
T. Ariman  
M. Budhu  
G. Gazetas  
J. McNorgan  
F. Miura

<sup>a</sup> - Group Leaders

INTRODUCTION

The working group considered four facilities or subsystems which can be damaged by Permanent Ground Deformation: 1) Buried Pipelines, 2) Pile Foundations, 3) Quay Walls, and 4) Buried Tanks. For each facility, the working group attempted to identify the current state of knowledge and critical considerations which should be addressed in the Guidelines.

Buried Pipelines

The behavior of buried pipelines subject to Permanent Ground Deformation (PGD) is a function of the system type, and size and type of PGD movement. A segmented system such as water distribution piping responds differently than a continuous system such as welded steel gas transmission piping. Furthermore, a given system responds differently to transverse PGD (ground movement perpendicular to the pipeline axis) than to longitudinal PGD (ground movement parallel to the pipeline axis). Finally, the response of a given system to either transverse or longitudinal PGD is a function of both the amount of PGD as well as the width or spatial extent of the lateral spread zone.

The working group felt that the Guidelines should contain three sections on buried piping. The first section on Engineering Models and Analysis Techniques would address both numerical (Finite Element) methods as well as closed form solutions. The second section of Failure Criterion would cover available information on the joint displacement and/or rotation in segmented pipelines leading to leakage as well as the axial force and/or moment leading to crushing of the bell. For continuous pipelines, the maximum tensile strain and local buckling stress are of

primary interest. The second section would also cover conditions leading to slippage at the soil-pipe interface. The third section would cover Damage Probabilities.

#### Quay Walls

The working group felt that the Behavior and Design of Quay Walls portion would consist of four sections. The first section on Analysis and Engineering Models would cover both analytical and physical models. The second section on Material Properties and Failure would discuss pertinent soil properties and associated soil tests. Case histories of Niigata and other earthquakes are contemplated for the third section on Damage Probability. The fourth section will address Future developments.

#### Pile Foundations

It is proposed that this portion begin with a review of seismic loading of pile foundation. This review will cover kinematic loading of the pile due to wave propagation in the soil as well as inertial loading due to vibration of the supported mass. The final section will present analysis and observations of the effects of pore water pressure buildup and liquefaction-induced deformation on piles.

#### Tanks

Three sections entitled Analysis and Engineering Models, Material Properties and Failure, and Damage Probabilities covering buried tanks, semi-buried tanks and above ground tanks were proposed by the working group.

SECOND US-JAPAN WORKSHOP ON LIQUEFACTION, LARGE GROUND  
DEFORMATIONS AND THEIR EFFECTS ON LIFELINES

REPORT FROM WORKING GROUP NO. 4:  
EARTHQUAKE COUNTERMEASURES

Working Group Members:

From Japan

K. Kubo<sup>a</sup>  
T. Iwatate<sup>a</sup>  
M. Ishikawa  
S. Okada  
T. Meda

From United States

J. Isenberg<sup>a</sup>  
J. McNorgan  
G. Martin  
C. Scawthorn

<sup>a</sup> - Group Leaders

INTRODUCTION

Recommendations for earthquake countermeasures form an essential component of the proposed engineering guidelines for liquefaction, large ground deformations and their effects on lifelines. The overall goal of the Earthquake Countermeasures Group is to identify and summarize engineering means for improving the performance of lifelines in earthquakes and to identify cost effective approaches to underpin economic incentives for such countermeasures.

The success of mitigation measures depends on a thorough understanding of the related geotechnical hazards. The other working groups will provide background and guidance in this regard. The group documenting experience during previous earthquakes will summarize information on the type and origin of the geotechnical hazards related to liquefaction and large ground deformations and how conditions favoring these hazards may be recognized. The group addressing the modeling of large ground deformations will outline methods of making quantitative estimates of the hazards, for example, the amount of lateral spreading that may accompany liquefaction. Finally, the group addressing earthquake resistant design will provide criteria for new construction and retrofitting that will form the basis for recommended mitigation approaches the countermeasures group will summarize in the guidelines.

The scope of recommendations to be included in the guidelines will encompass definitions of the geotechnical hazards to lifelines and the type of structures and related range of countermeasures to be considered. With regard to hazards, emphasis will be placed on liquefaction-induced slope instability, lateral spreading, large differential ground deformations and settlement. We will also consider lateral offsets of the type accompanying strike slip fault movement. Structures to be considered will include pipelines (water, gas and oil); underground electrical transmission lines; telecommunications; storage tanks; tunnels and highway bridges.

The range of countermeasures to be considered will include ground strengthening by means of engineered construction, in-situ stabilization, dispersion of critical lifeline facilities, and emergency plans or operational solutions.

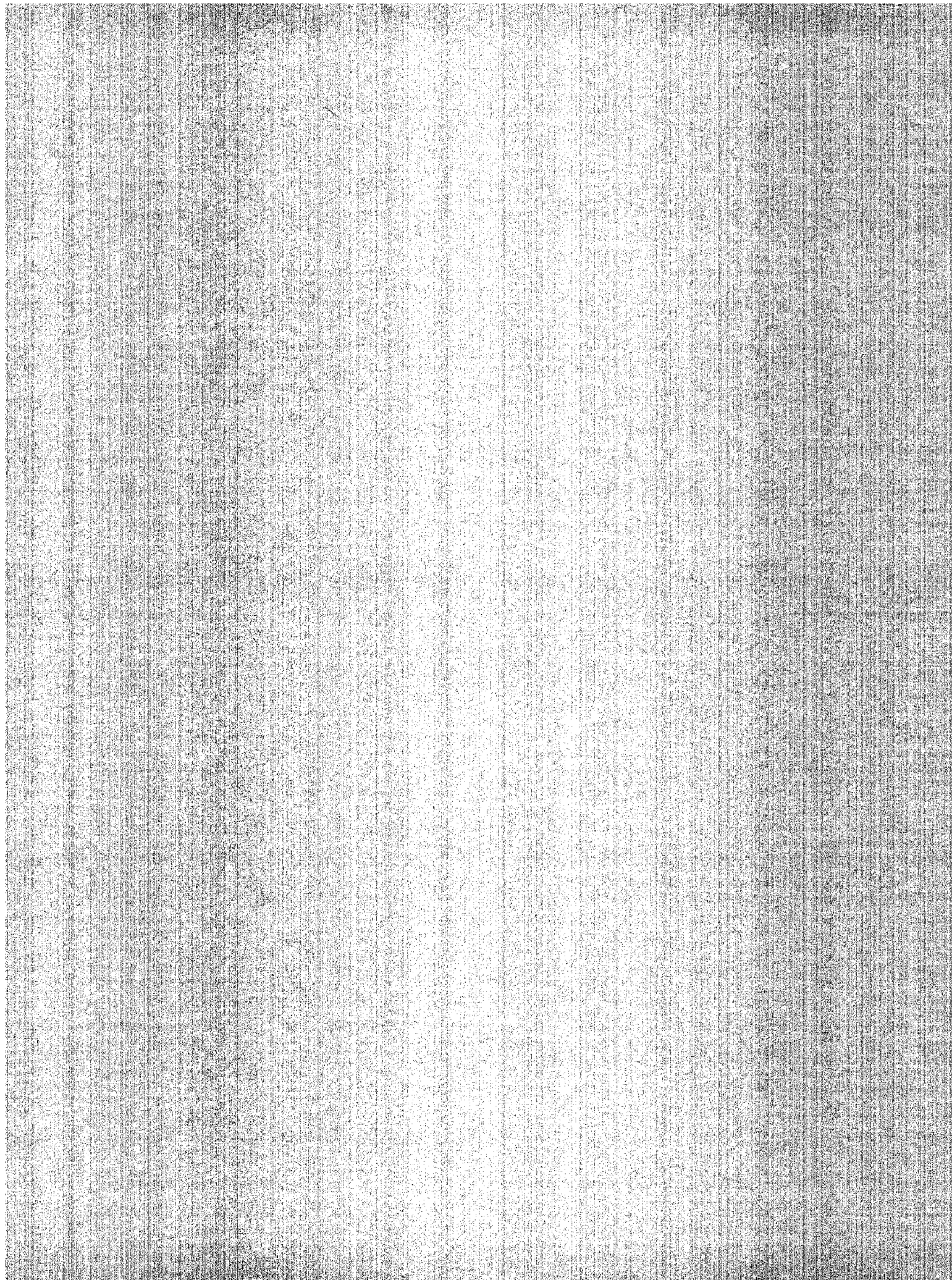
The current state-of-practice in hazard mitigation for lifelines will be summarized in the guidelines. Various mitigation methods, their applicability to soil conditions identified at a site, specific representative applications and relative costs of the various mitigation techniques will be addressed. Examples will be drawn from both U.S. and Japanese practice including related discussion on problems encountered and the overall success of the techniques deployed. The commentary will draw heavily on recently developed Japanese guidelines, for example, the criteria developed by the Tokyo Gas Company for the survival of gas pipelines in liquefiable soils.

An important facet of the guidelines will be the identification of incentives, particularly economic justifications for deploying countermeasures. Even though the technical means may exist for identifying hazards and improving performance, the economic rationale for investing in countermeasures needs to be convincingly defined. The basis for justification revolves around cost benefit and risk analyses which take into account the inherent uncertainties of the frequency and location of earthquakes, and the site conditions.

Finally, the guidelines will identify future research needs including testing and earthquake damage reconnaissance required to support the recommendations in the guidelines. The report will also evaluate whether the field is mature enough to warrant the development of manuals of practice or code related documents.

**REMARKS**

196a





## CLOSING REMARKS

by  
Professor K. Kubo

and  
Professor M. Shinozuka  
Princeton University

What we have achieved here in this workshop indeed represented a systems approach to the complex problems of liquefaction, large ground deformation and their effects on lifeline facilities. During the first two days, we have seen the presentation of more than thirty papers appropriate to the theme of this workshop. More importantly, these papers were selected for presentation on the basis of the overall goals of the US-Japan Cooperative Research so that they facilitate the working group discussions. In this regard, we are highly appreciative of Professors Hamada and T. O'Rourke's work being well done in this direction.

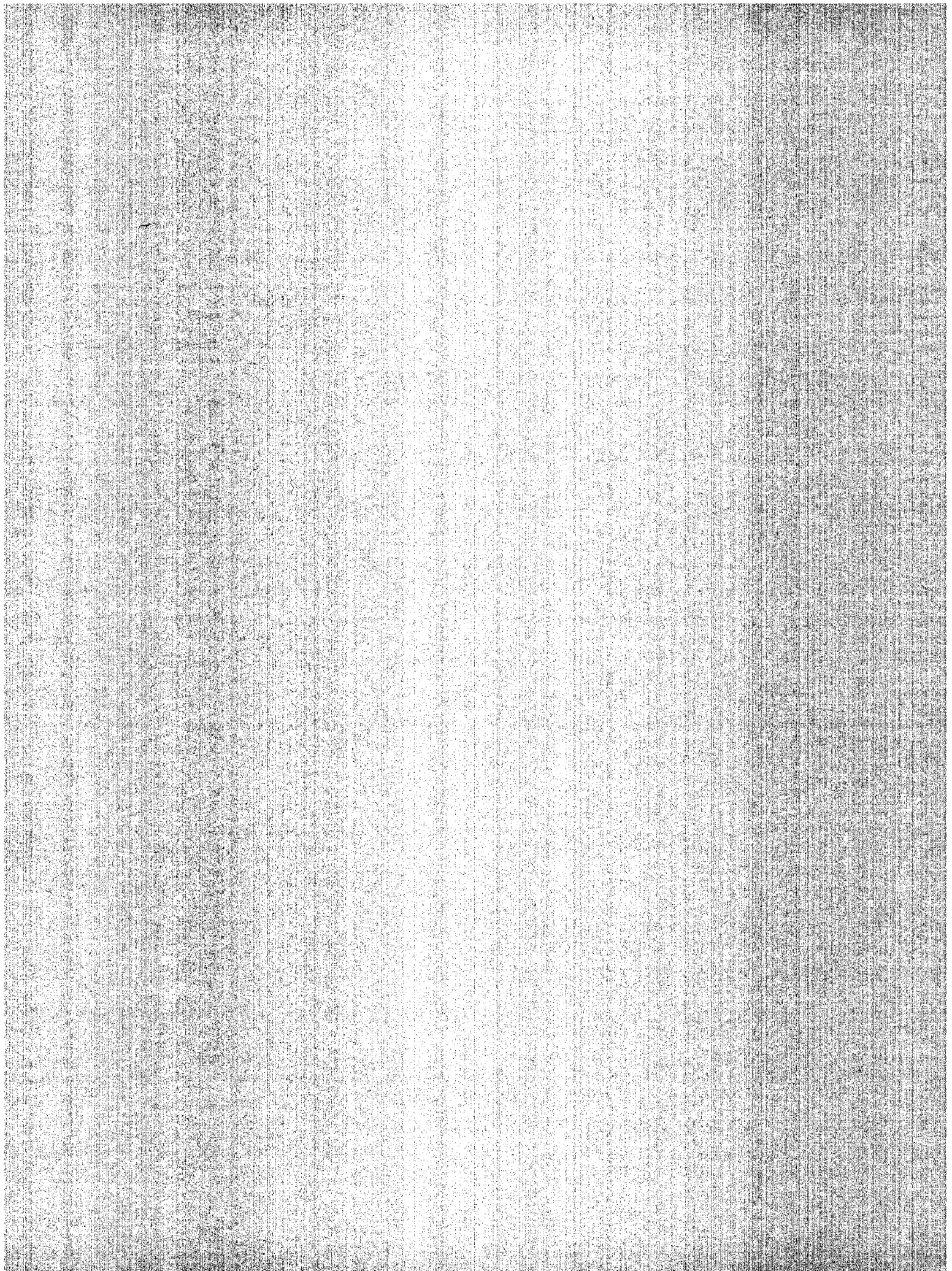
The four subject areas for group discussion, namely: a) case history studies, b) large ground motion modeling, c) earthquake-resistant design, and d) countermeasures were also appropriately chosen for the purpose of discussion. The Technical Summary and Recommendations that come out of these discussion groups will be quite useful, particularly in their final form, and will make an impact on engineering practice. I am particularly appreciative of the summary of Group 1 dealing with the uncertainty issue head-on. Very frankly, many things we do in this area sometimes appear to get lost under a mountain of uncertainties, although it is the nature of the beast we have to deal with. In this regard, Professor Kubo and I wish to request that the working groups, and particularly working group leaders, interact with each other in the process of information and data transfer from one group to another. For example, the large ground deformation modeling group should recognize the uncertainty involved in the information transferred from the case study group. In turn, the large ground deformation modeling group should provide the design group with input information with some assessment of the degree of uncertainty associated with it.

Related to the uncertainty issue is the fact that the entire phenomenon of liquefaction and large ground deformation is highly probabilistic. For example, the location, temporal and spatial frequency and size of lateral spreads that might be observed in an earthquake must be dealt with probabilistically in order to draw any reasonable conclusion when assessing the seismic reliability and risk of spatially extended lifeline system. In fact, it seems that, in order to develop procedures of seismic vulnerability evaluation of lifeline facilities usable for their designs, we must synthesize what we know under the probabilistic framework. Since this aspect does not appear to have come out explicitly during the working group discussions, it is urged that group leaders add their thoughts on this aspect in their final report.

Finally, we would like to thank the coordinators of this workshop, Professors Hamada and Tom O'Rourke, the leaders of the working groups, and all the participants for their efforts that made this workshop a success.



# WORLDWIDE PARTICIPANTS



## PARTICIPANTS

U.S. Participants

Mr. K. Adalier Rensselaer Polytechnic Inst.	Dr. S.C. Liu NSF
Dr. Teo Ariman University of Tulsa	Dr. Geoff Martin Earth Technology Corporation
Mr. Bijam Baziar Rensselaer Polytechnic Inst.	Mr. John D. McNorgan Southern California Gas Company
Dr. Ian Buckle NCEER	Dr. Fusa Miura Yamaguchi University (Visiting Professor at Cornell)
Dr. Muniram Budhu University of Arizona	Dr. Michael O'Rourke Rensselaer Polytechnic Inst.
Dr. Peter Cheng U.S. Information Center	Dr. Thomas O'Rourke Cornell University
Dr. Ricardo Dobry Rensselaer Polytechnic Inst.	Dr. Chaim Poran University of North Carolina
Dr. Ahmed Elgamal Rensselaer Polytechnic Inst.	Dr. Jean Prevost Princeton University
Dr. George Gazetas SUNY/Buffalo	Mr. Bruce Roth Cornell University
Dr. Michel Ghosn City College of NY	Dr. Charles Scawthorn EQE, Inc.
Dr. Thomas Holzer U.S. Geological Survey	Dr. Masanobu Shinozuka Princeton University
Mr. Ping Hsu General Hauling, Inc.	Dr. Harry E. Stewart Cornell University
Dr. I.M. Idriss University of California	Ms. Martitia Tuttle Lamont-Doherty Geological Observatory of Columbia U.
Dr. Jeremy Isenberg Weidlinger Assoc.	Dr. Mladen Vucetic University of California
Dr. Klaus Jacob Lamont-Doherty Geological Observatory of Columbia U.	Mr. Rihui Yang Cornell University
Ms. C. Keane Princeton U.	Dr. T. Leslie Youd Brigham Young University

Japanese Participants

Mr. Shiro Fukui  
Tokyo Electric Power Services  
Co., Inc.

Prof. Masanori Hamada  
Tokai University

Mr. Susumu Iai  
Port and Harbour Research Inst.  
Ministry of Transport

Prof. Kenji Ishihara  
University of Tokyo

Mr. Masami Ishikawa  
NKK Corporation

Mr. Takahiro Iwatate  
Institute of Electric Power  
Industry

Mr. Kin-ichi Kasuda  
Kumagai-Gumi Co., Ltd.

Mr. Koji Kitazawa  
Taisei Corporation

Mr. Takashi Kobayashi  
Tokyo Gas Co., Ltd.

Prof. Keizaburo Kubo  
University of Tokyo

Mr. Toshiro Maeda  
Taisei Corporation

Prof. Masakatsu Miyajima  
Kanazawa University

Mr. Keizo Ohtomo  
Central Research Institute of  
Electric Power Industry

Mr. Susumu Okada  
Kiso-Jiban Consultants Co., Ltd.

Mr. Masayuki Sato  
Tokyo Electric Power Services  
Co., Inc.

Mr. Seichi Sato  
Taisei Corporation

Mr. Katsumi Shimizu  
Shimizu Corporation

Mr. Hideyo Suzuki  
Tokyo Electric Power

Mr. Nobuhisa Suzuki  
NKK Corporation

Mr. Takashi Tazoh  
Shimizu Corporation

Prof. Ikuo Towhata  
University of Tokyo

Ms. Kazue Wakamatsu  
Waseda University

Prof. Susumu Yasuda  
Kyushu Institute of Technology

Mr. Nozomu Yoshida  
Sato Kogyo Co., Ltd.

Mr. Masaaki Yoshikawa  
Okumura Corporation

International Participants

Dr. J. Abi-Saab  
MARAVEN, S.A.  
Venezuela

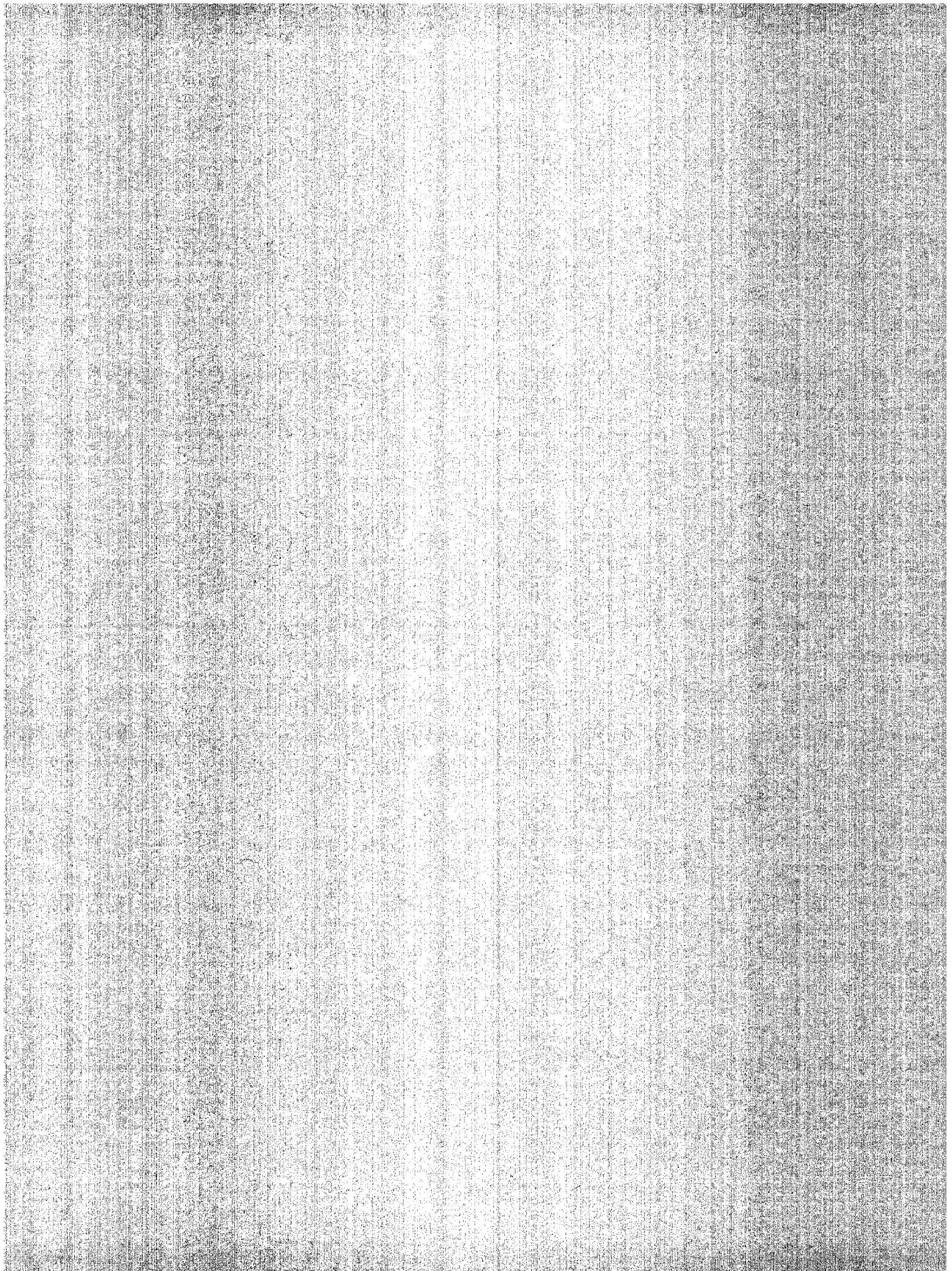
Dr. Juan Murria  
MARAVEN, S.A.  
Venezuela

Prof. Michael Pender  
University of Auckland  
New Zealand

Dr. R.S. Steedman  
Univ. of Cambridge

Mr. H.J. Van der Graaf  
Delft Geotechnics  
NETHERLANDS







**NATIONAL CENTER FOR EARTHQUAKE ENGINEERING RESEARCH  
LIST OF PUBLISHED TECHNICAL REPORTS**

The National Center for Earthquake Engineering Research (NCEER) publishes technical reports on a variety of subjects related to earthquake engineering written by authors funded through NCEER. These reports are available from both NCEER's Publications Department and the National Technical Information Service (NTIS). Requests for reports should be directed to the Publications Department, National Center for Earthquake Engineering Research, State University of New York at Buffalo, Red Jacket Quadrangle, Buffalo, New York 14261. Reports can also be requested through NTIS, 5285 Port Royal Road, Springfield, Virginia 22161. NTIS accession numbers are shown in parenthesis, if available.

- NCEER-87-0001 "First-Year Program in Research, Education and Technology Transfer," 3/5/87, (PB88-134275/AS).
- NCEER-87-0002 "Experimental Evaluation of Instantaneous Optimal Algorithms for Structural Control," by R.C. Lin, T.T. Soong and A.M. Reinhorn, 4/20/87, (PB88-134341/AS).
- NCEER-87-0003 "Experimentation Using the Earthquake Simulation Facilities at University at Buffalo," by A.M. Reinhorn and R.L. Ketter, to be published.
- NCEER-87-0004 "The System Characteristics and Performance of a Shaking Table," by J.S. Hwang, K.C. Chang and G.C. Lee, 6/1/87, (PB88-134259/AS). This report is available only through NTIS (see address given above).
- NCEER-87-0005 "A Finite Element Formulation for Nonlinear Viscoplastic Material Using a Q Model," by O. Gyebi and G. Dasgupta, 11/2/87, (PB88-213764/AS).
- NCEER-87-0006 "Symbolic Manipulation Program (SMP) - Algebraic Codes for Two and Three Dimensional Finite Element Formulations," by X. Lee and G. Dasgupta, 11/9/87, (PB88-219522/AS).
- NCEER-87-0007 "Instantaneous Optimal Control Laws for Tall Buildings Under Seismic Excitations," by J.N. Yang, A. Akbarpour and P. Ghaemmaghami, 6/10/87, (PB88-134333/AS).
- NCEER-87-0008 "IDARC: Inelastic Damage Analysis of Reinforced Concrete Frame - Shear-Wall Structures," by Y.J. Park, A.M. Reinhorn and S.K. Kunnath, 7/20/87, (PB88-134325/AS).
- NCEER-87-0009 "Liquefaction Potential for New York State: A Preliminary Report on Sites in Manhattan and Buffalo," by M. Budhu, V. Vijayakumar, R.F. Giese and L. Baumgras, 8/31/87, (PB88-163704/AS). This report is available only through NTIS (see address given above).
- NCEER-87-0010 "Vertical and Torsional Vibration of Foundations in Inhomogeneous Media," by A.S. Veletsos and K.W. Dotson, 6/1/87, (PB88-134291/AS).
- NCEER-87-0011 "Seismic Probabilistic Risk Assessment and Seismic Margins Studies for Nuclear Power Plants," by Howard H.M. Hwang, 6/15/87, (PB88-134267/AS). This report is available only through NTIS (see address given above).
- NCEER-87-0012 "Parametric Studies of Frequency Response of Secondary Systems Under Ground-Acceleration Excitations," by Y. Yong and Y.K. Lin, 6/10/87, (PB88-134309/AS).
- NCEER-87-0013 "Frequency Response of Secondary Systems Under Seismic Excitation," by J.A. HoLung, J. Cai and Y.K. Lin, 7/31/87, (PB88-134317/AS).
- NCEER-87-0014 "Modelling Earthquake Ground Motions in Seismically Active Regions Using Parametric Time Series Methods," by G.W. Ellis and A.S. Cakmak, 8/25/87, (PB88-134283/AS).
- NCEER-87-0015 "Detection and Assessment of Seismic Structural Damage," by E. DiPasquale and A.S. Cakmak, 8/25/87, (PB88-163712/AS).
- NCEER-87-0016 "Pipeline Experiment at Parkfield, California," by J. Isenberg and E. Richardson, 9/15/87, (PB88-163720/AS).

- NCEER-87-0017 "Digital Simulation of Seismic Ground Motion," by M. Shinozuka, G. Deodatis and T. Harada, 8/31/87, (PB88-155197/AS). This report is available only through NTIS (see address given above).
- NCEER-87-0018 "Practical Considerations for Structural Control: System Uncertainty, System Time Delay and Truncation of Small Control Forces," J.N. Yang and A. Akbarpour, 8/10/87, (PB88-163738/AS).
- NCEER-87-0019 "Modal Analysis of Nonclassically Damped Structural Systems Using Canonical Transformation," by J.N. Yang, S. Sarkani and F.X. Long, 9/27/87, (PB88-187851/AS).
- NCEER-87-0020 "A Nonstationary Solution in Random Vibration Theory," by J.R. Red-Horse and P.D. Spanos, 11/3/87, (PB88-163746/AS).
- NCEER-87-0021 "Horizontal Impedances for Radially Inhomogeneous Viscoelastic Soil Layers," by A.S. Veletsos and K.W. Dotson, 10/15/87, (PB88-150859/AS).
- NCEER-87-0022 "Seismic Damage Assessment of Reinforced Concrete Members," by Y.S. Chung, C. Meyer and M. Shinozuka, 10/9/87, (PB88-150867/AS). This report is available only through NTIS (see address given above).
- NCEER-87-0023 "Active Structural Control in Civil Engineering," by T.T. Soong, 11/11/87, (PB88-187778/AS).
- NCEER-87-0024 "Vertical and Torsional Impedances for Radially Inhomogeneous Viscoelastic Soil Layers," by K.W. Dotson and A.S. Veletsos, 12/87, (PB88-187786/AS).
- NCEER-87-0025 "Proceedings from the Symposium on Seismic Hazards, Ground Motions, Soil-Liquefaction and Engineering Practice in Eastern North America," October 20-22, 1987, edited by K.H. Jacob, 12/87, (PB88-188115/AS).
- NCEER-87-0026 "Report on the Whittier-Narrows, California, Earthquake of October 1, 1987," by J. Pantelic and A. Reinhorn, 11/87, (PB88-187752/AS). This report is available only through NTIS (see address given above).
- NCEER-87-0027 "Design of a Modular Program for Transient Nonlinear Analysis of Large 3-D Building Structures," by S. Srivastav and J.F. Abel, 12/30/87, (PB88-187950/AS).
- NCEER-87-0028 "Second-Year Program in Research, Education and Technology Transfer," 3/8/88, (PB88-219480/AS).
- NCEER-88-0001 "Workshop on Seismic Computer Analysis and Design of Buildings With Interactive Graphics," by W. McGuire, J.F. Abel and C.H. Conley, 1/18/88, (PB88-187760/AS).
- NCEER-88-0002 "Optimal Control of Nonlinear Flexible Structures," by J.N. Yang, F.X. Long and D. Wong, 1/22/88, (PB88-213772/AS).
- NCEER-88-0003 "Substructuring Techniques in the Time Domain for Primary-Secondary Structural Systems," by G.D. Manolis and G. Juhn, 2/10/88, (PB88-213780/AS).
- NCEER-88-0004 "Iterative Seismic Analysis of Primary-Secondary Systems," by A. Singhal, L.D. Lutes and P.D. Spanos, 2/23/88, (PB88-213798/AS).
- NCEER-88-0005 "Stochastic Finite Element Expansion for Random Media," by P.D. Spanos and R. Ghanem, 3/14/88, (PB88-213806/AS).
- NCEER-88-0006 "Combining Structural Optimization and Structural Control," by F.Y. Cheng and C.P. Pantelides, 1/10/88, (PB88-213814/AS).
- NCEER-88-0007 "Seismic Performance Assessment of Code-Designed Structures," by H.H.-M. Hwang, J.-W. Jaw and H.-J. Shau, 3/20/88, (PB88-219423/AS).

- NCEER-88-0008 "Reliability Analysis of Code-Designed Structures Under Natural Hazards," by H.H-M. Hwang, H. Ushiba and M. Shinozuka, 2/29/88, (PB88-229471/AS).
- NCEER-88-0009 "Seismic Fragility Analysis of Shear Wall Structures," by J-W Jaw and H.H-M. Hwang, 4/30/88, (PB89-102867/AS).
- NCEER-88-0010 "Base Isolation of a Multi-Story Building Under a Harmonic Ground Motion - A Comparison of Performances of Various Systems," by F-G Fan, G. Ahmadi and I.G. Tadjbakhsh, 5/18/88, (PB89-122238/AS).
- NCEER-88-0011 "Seismic Floor Response Spectra for a Combined System by Green's Functions," by F.M. Lavelle, L.A. Bergman and P.D. Spanos, 5/1/88, (PB89-102875/AS).
- NCEER-88-0012 "A New Solution Technique for Randomly Excited Hysteretic Structures," by G.Q. Cai and Y.K. Lin, 5/16/88, (PB89-102883/AS).
- NCEER-88-0013 "A Study of Radiation Damping and Soil-Structure Interaction Effects in the Centrifuge," by K. Weissman, supervised by J.H. Prevost, 5/24/88, (PB89-144703/AS).
- NCEER-88-0014 "Parameter Identification and Implementation of a Kinematic Plasticity Model for Frictional Soils," by J.H. Prevost and D.V. Griffiths, to be published.
- NCEER-88-0015 "Two- and Three- Dimensional Dynamic Finite Element Analyses of the Long Valley Dam," by D.V. Griffiths and J.H. Prevost, 6/17/88, (PB89-144711/AS).
- NCEER-88-0016 "Damage Assessment of Reinforced Concrete Structures in Eastern United States," by A.M. Reinhorn, M.J. Seidel, S.K. Kunnath and Y.J. Park, 6/15/88, (PB89-122220/AS).
- NCEER-88-0017 "Dynamic Compliance of Vertically Loaded Strip Foundations in Multilayered Viscoelastic Soils," by S. Ahmad and A.S.M. Israil, 6/17/88, (PB89-102891/AS).
- NCEER-88-0018 "An Experimental Study of Seismic Structural Response With Added Viscoelastic Dampers," by R.C. Lin, Z. Liang, T.T. Soong and R.H. Zhang, 6/30/88, (PB89-122212/AS).
- NCEER-88-0019 "Experimental Investigation of Primary - Secondary System Interaction," by G.D. Manolis, G. Juhn and A.M. Reinhorn, 5/27/88, (PB89-122204/AS).
- NCEER-88-0020 "A Response Spectrum Approach For Analysis of Nonclassically Damped Structures," by J.N. Yang, S. Sarkani and F.X. Long, 4/22/88, (PB89-102909/AS).
- NCEER-88-0021 "Seismic Interaction of Structures and Soils: Stochastic Approach," by A.S. Veletsos and A.M. Prasad, 7/21/88, (PB89-122196/AS).
- NCEER-88-0022 "Identification of the Serviceability Limit State and Detection of Seismic Structural Damage," by E. DiPasquale and A.S. Cakmak, 6/15/88, (PB89-122188/AS).
- NCEER-88-0023 "Multi-Hazard Risk Analysis: Case of a Simple Offshore Structure," by B.K. Bhartia and E.H. Vanmarcke, 7/21/88, (PB89-145213/AS).
- NCEER-88-0024 "Automated Seismic Design of Reinforced Concrete Buildings," by Y.S. Chung, C. Meyer and M. Shinozuka, 7/5/88, (PB89-122170/AS).
- NCEER-88-0025 "Experimental Study of Active Control of MDOF Structures Under Seismic Excitations," by L.L. Chung, R.C. Lin, T.T. Soong and A.M. Reinhorn, 7/10/88, (PB89-122600/AS).
- NCEER-88-0026 "Earthquake Simulation Tests of a Low-Rise Metal Structure," by J.S. Hwang, K.C. Chang, G.C. Lee and R.L. Ketter, 8/1/88, (PB89-102917/AS).
- NCEER-88-0027 "Systems Study of Urban Response and Reconstruction Due to Catastrophic Earthquakes," by F. Kozin and H.K. Zhou, 9/22/88.

- NCEER-88-0028 "Seismic Fragility Analysis of Plane Frame Structures," by H.H-M. Hwang and Y.K. Low, 7/31/88, (PB89-131445/AS).
- NCEER-88-0029 "Response Analysis of Stochastic Structures," by A. Kardara, C. Bucher and M. Shinozuka, 9/22/88, (PB89-174429/AS).
- NCEER-88-0030 "Nonnormal Accelerations Due to Yielding in a Primary Structure," by D.C.K. Chen and L.D. Lutes, 9/19/88, (PB89-131437/AS).
- NCEER-88-0031 "Design Approaches for Soil-Structure Interaction," by A.S. Veletsos, A.M. Prasad and Y. Tang, 12/30/88, (PB89-174437/AS).
- NCEER-88-0032 "A Re-evaluation of Design Spectra for Seismic Damage Control," by C.J. Turkstra and A.G. Tallin, 11/7/88, (PB89-145221/AS).
- NCEER-88-0033 "The Behavior and Design of Noncontact Lap Splices Subjected to Repeated Inelastic Tensile Loading," by V.E. Sagan, P. Gergely and R.N. White, 12/8/88, (PB89-163737/AS).
- NCEER-88-0034 "Seismic Response of Pile Foundations," by S.M. Mamoon, P.K. Banerjee and S. Ahmad, 11/1/88, (PB89-145239/AS).
- NCEER-88-0035 "Modeling of R/C Building Structures With Flexible Floor Diaphragms (IDARC2)," by A.M. Reinhorn, S.K. Kumath and N. Panahshahi, 9/7/88, (PB89-207153/AS).
- NCEER-88-0036 "Solution of the Dam-Reservoir Interaction Problem Using a Combination of FEM, BEM with Particular Integrals, Modal Analysis, and Substructuring," by C-S. Tsai, G.C. Lee and R.L. Ketter, 12/31/88, (PB89-207146/AS).
- NCEER-88-0037 "Optimal Placement of Actuators for Structural Control," by F.Y. Cheng and C.P. Pantelides, 8/15/88, (PB89-162846/AS).
- NCEER-88-0038 "Teflon Bearings in Aseismic Base Isolation: Experimental Studies and Mathematical Modeling," by A. Mokha, M.C. Constantinou and A.M. Reinhorn, 12/5/88, (PB89-218457/AS).
- NCEER-88-0039 "Seismic Behavior of Flat Slab High-Rise Buildings in the New York City Area," by P. Weidlinger and M. Ettouney, 10/15/88.
- NCEER-88-0040 "Evaluation of the Earthquake Resistance of Existing Buildings in New York City," by P. Weidlinger and M. Ettouney, 10/15/88, to be published.
- NCEER-88-0041 "Small-Scale Modeling Techniques for Reinforced Concrete Structures Subjected to Seismic Loads," by W. Kim, A. El-Attar and R.N. White, 11/22/88, (PB89-189625/AS).
- NCEER-88-0042 "Modeling Strong Ground Motion from Multiple Event Earthquakes," by G.W. Ellis and A.S. Cakmak, 10/15/88, (PB89-174445/AS).
- NCEER-88-0043 "Nonstationary Models of Seismic Ground Acceleration," by M. Grigoriu, S.E. Ruiz and E. Rosenblueth, 7/15/88, (PB89-189617/AS).
- NCEER-88-0044 "SARCF User's Guide: Seismic Analysis of Reinforced Concrete Frames," by Y.S. Chung, C. Meyer and M. Shinozuka, 11/9/88, (PB89-174452/AS).
- NCEER-88-0045 "First Expert Panel Meeting on Disaster Research and Planning," edited by J. Pantelic and J. Stoyale, 9/15/88, (PB89-174460/AS).
- NCEER-88-0046 "Preliminary Studies of the Effect of Degrading Infill Walls on the Nonlinear Seismic Response of Steel Frames," by C.Z. Chrysostomou, P. Gergely and J.F. Abel, 12/19/88, (PB89-208383/AS).

- NCEER-88-0047 "Reinforced Concrete Frame Component Testing Facility - Design, Construction, Instrumentation and Operation," by S.P. Pessiki, C. Conley, T. Bond, P. Gergely and R.N. White, 12/16/88, (PB89-174478/AS).
- NCEER-89-0001 "Effects of Protective Cushion and Soil Compliancy on the Response of Equipment Within a Seismically Excited Building," by J.A. HoLung, 2/16/89, (PB89-207179/AS).
- NCEER-89-0002 "Statistical Evaluation of Response Modification Factors for Reinforced Concrete Structures," by H.H-M. Hwang and J-W. Jaw, 2/17/89, (PB89-207187/AS).
- NCEER-89-0003 "Hysteretic Columns Under Random Excitation," by G-Q. Cai and Y.K. Lin, 1/9/89, (PB89-196513/AS).
- NCEER-89-0004 "Experimental Study of 'Elephant Foot Bulge' Instability of Thin-Walled Metal Tanks," by Z-H. Jia and R.L. Ketter, 2/22/89, (PB89-207195/AS).
- NCEER-89-0005 "Experiment on Performance of Buried Pipelines Across San Andreas Fault," by J. Isenberg, E. Richardson and T.D. O'Rourke, 3/10/89, (PB89-218440/AS).
- NCEER-89-0006 "A Knowledge-Based Approach to Structural Design of Earthquake-Resistant Buildings," by M. Subramani, P. Gergely, C.H. Conley, J.F. Abel and A.H. Zaghaw, 1/15/89, (PB89-218465/AS).
- NCEER-89-0007 "Liquefaction Hazards and Their Effects on Buried Pipelines," by T.D. O'Rourke and P.A. Lane, 2/1/89, (PB89-218481).
- NCEER-89-0008 "Fundamentals of System Identification in Structural Dynamics," by H. Imai, C-B. Yun, O. Maruyama and M. Shinozuka, 1/26/89, (PB89-207211/AS).
- NCEER-89-0009 "Effects of the 1985 Michoacan Earthquake on Water Systems and Other Buried Lifelines in Mexico," by A.G. Ayala and M.J. O'Rourke, 3/8/89, (PB89-207229/AS).
- NCEER-89-R010 "NCEER Bibliography of Earthquake Education Materials," by K.E.K. Ross, 3/10/89, (PB90-109901/AS).
- NCEER-89-0011 "Inelastic Three-Dimensional Response Analysis of Reinforced Concrete Building Structures (IDARC-3D), Part I - Modeling," by S.K. Kunnath and A.M. Reinhorn, 4/17/89, (PB90-114612/AS).
- NCEER-89-0012 "Recommended Modifications to ATC-14," by C.D. Poland and J.O. Malley, 4/12/89.
- NCEER-89-0013 "Repair and Strengthening of Beam-to-Column Connections Subjected to Earthquake Loading," by M. Corazao and A.J. Durrani, 2/28/89, (PB90-109885/AS).
- NCEER-89-0014 "Program EXKAL2 for Identification of Structural Dynamic Systems," by O. Maruyama, C-B. Yun, M. Hoshiya and M. Shinozuka, 5/19/89, (PB90-109877/AS).
- NCEER-89-0015 "Response of Frames With Bolted Semi-Rigid Connections, Part I - Experimental Study and Analytical Predictions," by P.J. DiCorso, A.M. Reinhorn, J.R. Dickerson, J.B. Radziminski and W.L. Harper, 6/1/89, to be published.
- NCEER-89-0016 "ARMA Monte Carlo Simulation in Probabilistic Structural Analysis," by P.D. Spanos and M.P. Mignolet, 7/10/89, (PB90-109893/AS).
- NCEER-89-0017 "Preliminary Proceedings of the Conference on Disaster Preparedness - The Place of Earthquake Education in Our Schools, July 9-11, 1989," 6/23/89, (PB90-108606/AS).
- NCEER-89-0018 "Multidimensional Models of Hysteretic Material Behavior for Vibration Analysis of Shape Memory Energy Absorbing Devices, by E.J. Graesser and F.A. Cozzarelli, 6/7/89.

- NCEER-89-0019 "Nonlinear Dynamic Analysis of Three-Dimensional Base Isolated Structures (3D-BASIS)," by S. Nagarajaiah, A.M. Reinhorn and M.C. Constantinou, 8/3/89.
- NCEER-89-0020 "Structural Control Considering Time-Rate of Control Forces and Control Rate Constraints," by F.Y. Cheng and C.P. Pantelides, 8/3/89.
- NCEER-89-0021 "Subsurface Conditions of Memphis and Shelby County," by K.W. Ng, T-S. Chang and H-H.M. Hwang, 7/26/89.
- NCEER-89-0022 "Seismic Wave Propagation Effects on Straight Jointed Buried Pipelines," by K. Elhmadi and M.J. O'Rourke, 8/24/89.
- NCEER-89-0023 "Workshop on Serviceability Analysis of Water Delivery Systems," edited by M. Grigoriu, 3/6/89.
- NCEER-89-0024 "Shaking Table Study of a 1/5 Scale Steel Frame Composed of Tapered Members," by K.C. Chang, J.S. Hwang and G.C. Lee, 9/18/89.
- NCEER-89-0025 "DYNA1D: A Computer Program for Nonlinear Seismic Site Response Analysis - Technical Documentation," by Jean H. Prevost, 9/14/89.
- NCEER-89-0026 "One-Quarter Scale Model Studies of Active Tendon Systems and Active Mass Dampers for Aseismic Protection," by A.M. Reinhorn, T.T. Soong, R.C. Lin, Y.P. Yang, Y. Fukao, H. Abe and M. Nakai, 9/15/89, to be published.
- NCEER-89-0027 "Scattering of Waves by Inclusions in a Nonhomogeneous Elastic Half Space Solved by Boundary Element Methods," by P.K. Hadley, A. Askar and A.S. Cakmak, 6/15/89.
- NCEER-89-0028 "Statistical Evaluation of Deflection Amplification Factors for Reinforced Concrete Structures," by H.H.M. Hwang, J-W. Jaw and A.L. Ch'ng, 8/31/89.
- NCEER-89-0029 "Bedrock Accelerations in Memphis Area Due to Large New Madrid Earthquakes," by H.H.M. Hwang, C.H.S. Chen and G. Yu 11/7/89.
- NCEER-89-0030 "Seismic Behavior and Response Sensitivity of Secondary Structural Systems," by Y.Q. Chen and T.T. Soong, 10/23/89.
- NCEER-89-0031 "Random Vibration and Reliability Analysis of Primary-Secondary Structural Systems," by Y. Ibrahim, M. Grigoriu and T.T. Soong, 11/10/89.
- NCEER-89-0032 "Proceedings from the Second U.S. - Japan Workshop on Liquefaction, Large Ground Deformation and Their Effects on Lifelines, September 26-29, 1989," Edited by T.D. O'Rourke and M. Hamada, 12/1/89.